To the Graduate Council:

I am submitting herewith a dissertation written by Brendan Richardson Bream entitled "Tectonic implications of para- and orthogneiss geochronology and geochemistry from the southern Appalachian crystalline core." I have examined the final electronic copy of this dissertation for form and content and recommend that it be accepted in partial fulfillment of the requirements for the degree of Doctor of Philosophy, with a major in Geology.

Robert D. Hatcher, Jr.
Major Professor

We have read this dissertation
and recommend its acceptance:

Calvin F. Miller

Lawrence A. Taylor

George K. Schweitzer

Acceptance for the Council:

Anne Mayhew
Vice Provost and
Dean of Graduate Studies

(Original signatures are on file with official student records.)

TECTONIC IMPLICATIONS OF PARA- AND ORTHOGNEISS GEOCHRONOLOGY AND GEOCHEMISTRY FROM THE SOUTHERN APPALACHIAN CRYSTALLINE CORE

A Dissertation
Presented for the
Doctor of Philosophy
Degree
The University of Tenessee, Knoxville

Brendan R. Bream
May 2003

Copyright © 2003 by Brendan Richardson Bream
All rights reserved

DEDICATION

This dissertation is dedicated to my wife and best friend,
Katy Bream,
whose limitless patience, support, and love made its completion possible.

ACKNOWLEDGMENTS

I would first like to thank my advisor, Dr. Robert D. Hatcher, Jr., for his guidance and the opportunity to work on this project. Dr. Calvin F. Miller, Vanderbilt University, is thanked for his enthusiasm and for serving as my off-campus advisor. My other committee members, Drs. Lawrence A Taylor and George K. Schweitzer, provided perceptive comments, patience, and a generous amount of time. Dr. Paul D. Fullagar, University of North Carolina—Chapel Hill, is gratefully acknowledged for his contribution of time, isotopic data, and insight with regard to this research. Analytical assistance at UCLA was provided by Chris Coath, Kevin McKeegan, and Mark Harrison. Analytical and interpretive assistance at the Stanford-USGS Micro Analysis Center SHRIMP RG facility was provided by Joe Wooden, Anders Meibom, Bob Jones, and Brad Ito. Allan Patchen facilitated development of the automated imaging technique for the University of Tennessee's electron microprobe.

A number of individuals have spent a considerable amount of time discussing this research (mostly in the field): Leonard Weiner, Carl Merschat, and Mark Carter (North Carolina Geological Survey); Butch Maybin (South Carolina Geological Survey); Jim Hibbard (North Carolina State University); Jack Garihan and Bill Ranson (Furman University). I thank these individuals, Calvin Miller, and especially Robert Hatcher, Jr. for emphasizing (and reminding me, when necessary, about) the importance of field work. Russ Mapes, Chuck Carrigan, Chris Thomas, and Susanne Meschter McDowell (past Vanderbilt University students) and Joe Hill, Scott Giorgis, Scott Williams, Sara Bier, Jay Kalbas, and Arthur Merschat (past and present UTK students) spent a significant amount of time in the field with me over the last six years.

This research would not have been possible without financial support from the National Science Foundation (grants EAR 98-14800 to R.D. Hatcher, Jr. and EAR 98-14801 to C.F. Miller) and the University of Tennessee Science Alliance Center of Excellence. Additionally, this work could not have been put into its proper context without the vast amount of information provided in numerous maps, including those in unpublished theses and dissertations. Collaborative research with M.K. Panigrahi (Indian Institute of Technology, Kharagpur) and Jack Callahan (Appalachian State University) broadened both my interests and experience. Finally, a debt of gratitude is owed to the members, unofficial and official, of the "Hatchery". Most notably, Nancy Meadows has provided gallons of fresh coffee, pounds of chocolate, engaging conversation, and reassurance throughout my six-plus year residency in Tennessee.

ABSTRACT

Sedimentary and metasedimentary rocks the southern Appalachian Blue Ridge and Inner Piedmont contain a valuable record of Late Proterozoic Laurentian margin evolution following the breakup of Rodinia. These paragneisses contain rift-and-drift facies cover rocks deposited unconformably on Grenville basement in the western and eastern Blue Ridge. Paleogeographic reconstructions and increasing amounts of geochronologic and isotopic data limit the derivation of most southern Appalachian crystalline core cover sequences to the Laurentian and/or west Gondwanan craton(s). Southern Appalachian crystalline core paragneiss samples have ε_{Nd} values between –8.5 and –2.0 at the time of deposition and contain abundant 1.1-1.25 Ga zircon cores with Grenville 1.0-1.1 Ga metamorphic rims. Less abundant detrital zircon core ages include pre-Grenvillian Middle Proterozoic 1.25-1.6 Ga, Early Proterozoic 1.6-2.1 Ga, and Late Archean 2.7-2.9 Ga sources. Blue Ridge Grenvillian basement has almost identical ε_{Nd} values and displays the same dominant magmatic core and metamorphic rim zircon ages. Based on these data, nonconformable basement-cover relationships, and crustal ages in eastern North America, we suggest that the extensive sedimentary packages in the southern Appalachian Blue Ridge and western Inner Piedmont are derived from Laurentia. Relatively high initial $^{87}Sr/^{86}Sr$ values between 0.707 and 0.723, Middle to Upper Proterozoic T_{DM} ages, high SiO_2 content, LREE enrichment, low chemical index of alteration values mostly between 41 and 66, and restricted Th/Sc and Zr/Sc values for Laurentian sedimentary and metasedimentary samples further support derivation from Grenvillian rocks like those exposed in the western Blue Ridge. ε_{Nd} values from Carolina terrane volcanic, plutonic, and volcaniclastic rocks are isotopically less evolved than southern Appalachian paragneisses and Blue Ridge Grenvillian basement easily separating this composite terrane from the mostly Laurentian terranes to the west. Neoproterozoic (~590 Ma), Ordovician (peaks at ~500 and ~485 Ma), and Silurian (peak at ~435 Ma), as well as Grenvillian and older, zircons in eastern Inner Piedmont paragneisses indicate that these rocks were deposited much later (late Silurian to Devonian) and could be entirely derived from a Panafrican source or possibly a mixture of Panafrican and recycled Laurentian margin assemblages.

Detrital zircons from the Middle Ordovician (475 Ma) Sevier Shale sample are Grenvillian (1.0 to 1.25 Ga), Middle Proterozoic (1.35 to 1.45 Ga), and Early Proterozoic (1.8 Ga). New U-Pb zircon ages for Ordovician metaplutonic units include the following: Dahlonega gold belt Cane Creek felsic gneiss (482 ± 4 Ma), western Inner

Piedmont Dysartsville Tonalite (468 ± 8 Ma), eastern Blue Ridge Kennesaw felsic gneiss (444 ± 11 Ma), western Inner Piedmont Lenoir Quarry Migmatite (450 ± 6 Ma inherited cores; 342 ± 5 Ma and 330 ± 6 Ma metamorphic overgrowths), western Inner Piedmont Poor Mountain Quartzite (metatuff?) (459 ± 4 Ma and 445 ± 4 Ma), western Inner Piedmont Toccoa granitoid (449 ± 4 Ma), and western Inner Piedmont Zirconia pegmatite (327 ± 2 Ma). T_{DM} ages between 1.2 and 2 Ga for the Cane Creek, Dysartsville, Kennesaw, and Toccoa granitoids indicate derivation from preexisting Grenvillian and possibly recycled older crust. High initial $^{87}Sr/^{86}Sr$ values for the Lenoir Quarry Migmatite and Cane Creek, Dysartsville, Kennesaw, and Toccoa granitoids also indicate derivation from preexisting continental crust. Major Laurentian margin depositional and orogenic events following the breakup of Rodinia and preceeding collision with Africa in the southern Appalachians are divisible into the following: Late Proterozoic to Early Cambrian, Middle Ordovician, Late Silurian, and Late Devonian to Early Carboniferous. Events of the Late Proterozoic to Early Cambrian include rift-related magmatism followed by Laurentian-derived rift-and-drift facies deposition. Middle Ordovician events related to island-arc accretion at the Laurentian margin include creation of the foreland Sevier basin, felsic magmatism, closure of a small ocean, eclogite formation in the eastern Blue Ridge, and granulite facies metamorphism in the central Blue Ridge. New detrital zircon evidence indicates that Late Silurian pelitic and psammitic material in the eastern Inner Piedmont was derived from both the Laurentian margin and Carolina terrane likely at the leading edge of the proximal Carolina terrane. Evidence of the Neoacadian orogenic event (Late Devonian to Early Carboniferous) includes a foreland clastic wedge, pervasive magmatism (in the eastern Inner Piedmont and eastern Blue Ridge), and penetrative deformation and metamorphism. These new data together with field relationships justifies revision of the tectonostratigrahic terranes in the southern Appalachians southeast of the western Blue Ridge into the Cartoogechaye and Cowrock (higher thrust sheets of the central Blue Ridge), Dahlonega gold belt, Tugaloo (eastern Blue Ridge and western Inner Piedmont), Cat Square (eastern Inner Piedmont), and exotic Carolina terranes is justified.

PREFACE

This dissertation presents a portion of the results derived from collaborative research with students and faculty at several universities. The primary objective of my research was to address the provenance of metasedimentary units in the southern Appalachian crystalline core. This work was possible due to the availability of islands of detailed geologic mapping and several complementary studies focused on southern Appalachian Grenville basement, Paleozoic granitoids, and Ordovician mafic-ultramafic complexes.

This dissertation is presented as several independent parts representing published and soon to be submitted manuscripts. Part I, accepted for publication, presents new detrital zircon and Nd isotopic data for southern Appalachian crystalline core paragneisses. Part II presents a revised Paleozoic tectonic synthesis that incorporates existing data with new granitoid geochronologic, foreland detrital zircon, Nd and Sr isotopic, and whole-rock geochemical data. Parts III and IV are contributions published in the 2002 Carolina Geological Society guidebook for a field trip that focused on recent detailed mapping in the South and Brushy Mountains in the North Carolina Inner Piedmont. Part V is an excerpt from a submitted manuscript, which addresses the timing and petrogenesis of two Archean granitoids that host a copper-molybdenum deposit in central India.

Appendix I consists of topographic maps with sample locations for most samples discussed in Parts I and II. Appendix II is U-Pb ion microprobe detrital zircon data collected at Stanford University (a complete dataset for all UCLA and Stanford data is available as a data repository from the Geological Society of America). Appendix III contains all whole-rock elemental data collected for this research.

TABLE OF CONTENTS

I. Detrital zircon ages and Nd isotopic data from the southern Appalachian crystalline core, GA-SC-NC-TN: New provenance constraints for Laurentian margin paragneisses 1
ABSTRACT 2
INTRODUCTION 3
GEOLOGIC SETTING 4
SAMPLES 7
ANALYTICAL METHODS 13
RESULTS 16
APPALACHIAN CRUSTAL AFFINITY 20
DISCUSSION 26
SUMMARY 29
ACKNOWLEDGEMENTS 30
REFERENCES CITED 30

II. Southern Appalachian Paleozoic orogenesis revised: Geochemical, isotopic, and geochronologic constraints for Neoproterozoic to mid-Paleozoic depositional, magmatic, and tectonic processes 40
ABSTRACT 41
INTRODUCTION 42
GEOLOGIC SETTING 46
SAMPLES 50
ANALYTICAL METHODS 58
RESULTS 60
SOUTHERN APPALACHIAN CRYSTALLINE CORE TECTONIC BOUNDARIES AND TERRANES 91
SYNTHESIS OF MAJOR PALEOZOIC DEPOSITIONAL AND OROGENIC EVENTS IN THE SOUTHERN APPALACHIANS 100
DISCUSSION 105
CONCLUSIONS 106
REFERENCES CITED 107

III. The southern Appalachian Inner Piedmont: New perspectives based on recent detailed geologic mapping, Nd isotopic evidence, and zircon geochronlogy 122
INTRODUCTION 123
GEOLOGIC SETTING AND PREVIOUS WORK 126
NEW PERSPECTIVES ON OLD PROBLEMS 136
ACKNOWLEDGEMENTS 152
REFERENCES CITED 153

IV. Inner Piedmont stratigraphy, metamorphism, and deformation in the Marion-South Mountains area, Noth Carolina 165
ABSTRACT 166
INTRODUCTION 167
GEOLOGIC SETTING 170
ROCK UNITS 172
METAMORPHISM 208
STRUCTURAL GEOLOGY 214
SUMMARY 231
ACKNOWLEDGEMENTS 231
REFERENCES CITED 232

V. Ion microprobe age of Malanjkhand granitoids, Central India 239
INTRODUCTION 240
SHRIMP RG METHODOLOGY 240
ZIRCON U-Pb DATING 243
CONCLUSIONS 246
REFERENCES CITED 249

APPENDIX 251
Appendix I. 252
Appendix II. 280
Appendix III. 289
VITA 296

LIST OF FIGURES

Part I

Figure 1: Tectonic map of the southern Appalachians 5
Figure 2: Geologic map of a portion of the southern Appalachians with sample locations 9
Figure 3: Cathodoluminescence (CL) and backscattered electron (BSE) images of analyzed detrital zircons 15
Figure 4: Epsilon Nd evolution over time for the metasedimentary samples compared with data from Blue Ridge basement, Chopawamsic and Milton terranes, and Carolina Terrane 18
Figure 5: Summed probability plots for detrital zircons 21

Part II

Figure 1: Lithotectonic divisions of the southern Appalachians 44
Figure 2: Tectonic map of a portion of the southern Appalachians with sample locations 47
Figure 3: Concordia plots of ^{204}Pb-corrected data 65
Figure 4: Summed probability plot of data from Sevier Shale zircons 67
Figure 5: Summed probability plot of data from Poor Mountain Quartzite zircons 71
Figure 6: Summed probability plot of zircon rim analyses 72
Figure 7: ε_{Nd} evolution with time compared to metasedimentary data, black lines,of .. Bream et al. (in press) 76
Figure 8: ε_{Nd} vs. Sr/Sr at 550, 475, and 420 Ma 78
Figure 9: Element variance for (meta)sedimentary sample data normalized to North .. American shale composite (NASC) 81
Figure 10: Chondrite normalized REE plot of (meta)sedimentary data. 83
Figure 11: Tectonic discriminant plots for (meta)sedimentary data 89
Figure 12: Chondrite normalized REE plot of granitoid data 92
Figure 13: Element variance for granitoid data normalized to primitive mantle 92
Figure 14: Tectonic discriminant plot for granitoids after Pearce et al. (1984) 93

Part III

Figure 1: Tectonic map of the southern Appalachians 125
Figure 2: Metamorphic isograd map of North Carolina, South Carolina, and part of east Tennessee 130
Figure 3: Epsilon Nd evolution over time for metasedimentary samples compared with data from Blue Ridge basement, Carolina terrane, and Chopawamsic-Milton terranes 138
Figure 4: Summed probability plots of detrital zircon data for the tectonic divisions .. shown in Figure 1 140

Figure 5: Summed probability plots of detrital zircon data for the tectonic divisions .. shown in Figure 1 and proposed divisions of Hatcher (this guidebook) for .. divisions southeast of the Hayesville fault 141

Part IV

Figure 1: Tectonic map of the southern Appalachians 169
Figure 2: Geologic map of the Marion-South Mountains area 171
Figure 3: Western Inner Piedmont generalized stratigraphy with major faults 173
Figure 4: Photograph and photomicrographs of Tallulah Falls Formation 176
Figure 5: Quartz-feldspar-mica ternary diagram comparing the composition of the upper Tallulah Falls Formation, lower Tallulah Falls Formation, and Poor Mountain Quartzite 178
Figure 6: Photograph and photomicrographs of Tallulah Falls Formation garnet-mica schist 179
Figure 7: Photomicrographs of the unit at the contact between the upper Tallulah Falls Formation and the Poor Mountain Amphibolite 181
Figure 8: Photograph and photomicrographs of Poor Mountain Amphibolite 185
Figure 9: Ortho- and para-amphibolite discriminant diagram comparing amphibolites and amphibole gneisses of the Poor Mountain Formation, Tallulah Falls Formation, and Dysartsville Tonalite 187
Figure 10: AFM diagram comparing amphibolites and amphibole gneisses of the Poor Mountain Formation, Tallulah Falls Formation, and Dysartsville Tonalite .. 188
Figure 11: Plots of wt % Al_2O_3 versus normative plagioclase composition (P=100*An/(An+Ab)) comparing amphibolites and amphibole gneisses of the Poor Mountain Formation, Tallulah Falls Formation, and Dysartsville Tonalite 189
Figure 12: Photomicrograph of Poor Mountain Quartzite 190
Figure 13: Major element discrimination diagram for distinguishing ortho- and ..... paragneisses in metamorphic terranes 192
Figure 14: Photographs and photomicrographs of the Dysartsville Tonalite 194
Figure 15: Anorthite (An)-Orthoclase (Or)-Albite (Ab) normative feldspar ternary .... diagram 196
Figure 16: IUGS modal classification of granitoid units of the western Inner Piedmont 198
Figure 17: Photographs and photomicrographs of the Henderson Gneiss 199
Figure 18: Photographs and photomicrograph of eastern Inner Piedmont sillimanite schist 201
Figure 19: Photograph and photomicrograph of eastern Inner Piedmont meta-graywacke 202
Figure 20: IUGS modal classification of Toluca Granite and Walker Top Granite 204
Figure 21: Photograph and photomicrograph of the Toluca Granite 205
Figure 22: Major element discrimination diagram distinguishing ortho- and paragneisses in metamorphic terranes 206
Figure 23: Photograph and photomicrograph of Walker Top Granite 207

Figure 24: Domain map for a portion of the North Carolina Inner Piedmont 217
Figure 25: Lower hemisphere, equal-area contoured diagrams of poles to foliation for the Marion-South Mountains area 220
Figure 26: Lower hemisphere, equal-area contoured diagrams of lineations and directions of regional scale sheath fold axes in the Marion-South Mountains area 221
Figure 27: Lower hemisphere, equal-area contoured diagrams of fold axes in the area 224
Figure 28: Cross sections 227

Part V

Figure 1: Regional geologic maps of the Malanjkhand area 241
Figure 2: Images of representative zircon grains from the grey and pink granites 245
Figure 3: Tera-Wasserburg concordia diagrams, conventional concordia diagrams, and summed probability plots of SHRIMP RG data for the pink and grey granites 248

LIST OF TABLES

Part I
Table 1: Samples with stratigraphic association and coordinates 10
Table 2: Sm-Nd isotopic data 19

Part II
Table 1: Sample location and formation association 51
Table 2: U-Pb IMP zircon data 61
Table 3: Pooled $^{206}Pb^*/^{238}U$ and Concordia ages for magmatic and suspected magmatic samples 64
Table 4: Sm-Nd concentrations and isotopic data 74
Table 5: Rb-Sr concentrations and isotopic data 75
Table 6: Whole-rock oxide weight percents with chemical indices of alteration (CIA) for (meta)sedimentary samples 79
Table 7: Whole-rock trace element concentrations and ratios for (meta)sedimentary .. samples 87
Table 8: Whole-rock element granitoid chemistry with normative mineralogy 90
Table 9: Whole-rock trace element concentrations for granitoid samples 90

Part III
Table 1: Sample locations with formations keyed to Figure 1 51

Part IV
Table 1: Pressure and temperature estimates from a garnet amphibolite sample and ... several pelitic schist samples from the Marion-South Mountains area 213
Table 2: Deformational framework and related events for the Inner Piedmont, North . Carolina 216

Part V
Table 1: Ion microprobe (SHRIMP RG) data for zircons from the grey and pink grantites 244
Table 2: Summary of zircon ages 247

PART I

Detrital zircon ages and Nd isotopic data from the southern Appalachian crystalline core, GA-SC-NC-TN: New provenance constraints for Laurentian margin paragneisses

This chapter was accepted for publication in a Geological Society of American Special Paper/Memoir and is scheduled for printing in late 2003 or early 2004. My co-authors are Robert D. Hatcher, Jr., Calvin F. Miller, and Paul D. Fullagar:

> Bream, B.R., Hatcher, R.D., Jr., Miller, C.F., Fullagar, P.D., *in press*, Detrital zircon ages and Nd isotopic data from the southern Appalachian crystalline core, GA-SC-NC-TN: New provenance constraints for Laurentian margin paragneisses, *in* Tollo, R.P., Corriveau, L., McLelland, J., and Bartholomew, M.J., eds., Proterozoic evolution of the Grenville orogen in North America: Boulder, Colorado, Geological Society of America Special Paper (or Memoir).

My contributions to this paper are: (1) most of the writing, (2) sample collection and sample preparation, (3) collection of the ion microprobe data, and (4) integration of the isotopic data collected by P.D. Fullagar. The use of "we" and "our" in the text refers to the co-authors and myself.

ABSTRACT

Sedimentary and metasedimentary rocks within the southern Appalachian Blue Ridge and Inner Piedmont contain a valuable record of Late Proterozoic Laurentian margin evolution following the breakup of Rodinia. Paleogeographic reconstructions and increasing amounts of geochronologic and isotopic data limit the derivation of these paragneisses to the Laurentian and/or west Gondwanan craton(s). Southern Appalachian crystalline core paragneiss samples have ε_{Nd} values between –8.5 and –2.0 at the time of deposition and contain abundant 1.1-1.25 Ga zircon cores with Grenville 1.0-1.1 Ga metamorphic rims. Less abundant detrital zircons are pre-Grenvillian Middle Proterozoic 1.25-1.6 Ga, Early Proterozoic 1.6-2.1 Ga, and Late Archean 2.7-2.9 Ga. Blue Ridge Grenvillian basement has almost identical ε_{Nd} values and displays the same dominant magmatic core and metamorphic rim zircon ages. Based on our data, nonconformable basement-cover relationships, and crustal ages in eastern North America, we contend that the extensive sedimentary packages in the southern Appalachian Blue Ridge and western Inner Piedmont are derived from Laurentia. ε_{Nd}

values from Carolina terrane volcanic, plutonic, and volcaniclastic rocks are isotopically less evolved than southern Appalachian paragneisses and Blue Ridge Grenvillian basement easily separating this composite terrane from the mostly Laurentian terranes to the west. Neoproterozoic and Ordovician, as well as Grenvillian, zircons in central Inner Piedmont paragneisses indicate that these samples were deposited much later and could be entirely derived from a Panafrican source or possibly a mixture of Panafrican and recycled Laurentian margin assemblages.

INTRODUCTION

The immense dimensions of the Grenvillian orogen that assembled Rodinia is confirmed by the widespread distribution of Grenvillian belts on numerous pre-Grenvillian cratonic margins (e.g., Hoffman, 1991). Although the existence and Late Proterozoic breakup of the Rodinian supercontinent is virtually indisputable, many details concerning the evolution of the southern Laurentian margin remain controversial and problematic. Sedimentary fill in the rift basins along the eastern Laurentian margin and western Iapetus ocean was deposited nonconformably on Grenvillian and likely pre-Grenvillian crust that forms the pree-Paleozoic basement of the southern Appalachians. In these sedimentary sequences is a record of the rift-to-drift transition (Wehr and Glover, 1985; Simpson and Sundberg, 1987; Williams and Hiscott, 1987; Simpson and Eriksson, 1989; Thomas, 1991) and later overprinting by Paleozoic orogenies. A complex rift history is verified by reconstructions of the margin (e.g., Rast and Kohles, 1986; Bartholomew, 1992), basement-cover sequence relationships (e.g., Hatcher et al., this volume), and polyphase rifting (Badger and Sinha, 1988; Aleinikoff et al., 1995; Brewer and Thomas, 2000; Cawood et al., 2001). Deposition of extensive rift fill, in places well over 1000 m thick, along most of the southern Laurentian margin was coeval with a latest Neoproterozoic-Early Cambrian rifting event. Continued rifting,

accompanied by deposition of drift facies across the margin, facilitated the development of a true passive margin. There is general agreement regarding Laurentian derivation of the western Blue Ridge rift-to-drift sedimentary packages. The paucity of more internal paragneiss isotopic and geochronologic data combined with the polydeformed and metamorphosed nature of the crystalline core, however, has resulted in the characterization of the internal high-grade lithotectonic packages as "disrupted" (Horton et al., 1989) and "problematic" (Goldsmith and Secor, 1993) terranes. New detrital zircon U-Pb ages and Sm-Nd data obtained from Blue Ridge and Inner Piedmont metapsammitic and metapelitic samples place previously unavailable limits on the provenance of the southern Laurentian margin deposits.

GEOLOGIC SETTING

Appalachian marginal terranes are exposed along the length of the orogen as continuous and discontinuous elongate curvilinear belts from Alabama to Newfoundland (Williams, 1978), and are separated by major, mostly orogen-scale, faults (Fig. 1). Both suspect and exotic accreted terranes of the southern Appalachians contain sedimentary sequences deposited in a variety of settings on a range of basements. Western Blue Ridge rift facies sedimentary and volcanic rocks were unconformably deposited on rifted Grenvillian basement include the Ocoee Supergroup and the Mt. Rogers Formation, Grandfather Mountain, and Mechum River Formations. The widely distributed eastern Blue Ridge-western Inner Piedmont Tallulah Falls-Ashe-Sandy Springs-Emuckfaw Formation was deposited on small Grenvillian continental fragments and possibly oceanic crust. Paragneisses of the Hayesville-Soque River and Chunky Gal-Shope Fork thrust sheets, herein referred to as the central Blue Ridge, and Dahlonega gold belt were deposited as immature siliciclastic sediments either intruded by, deposited on, or possibly intercalated with Ordovician mafic assemblages of oceanic and/or volcanic arc/back-arc

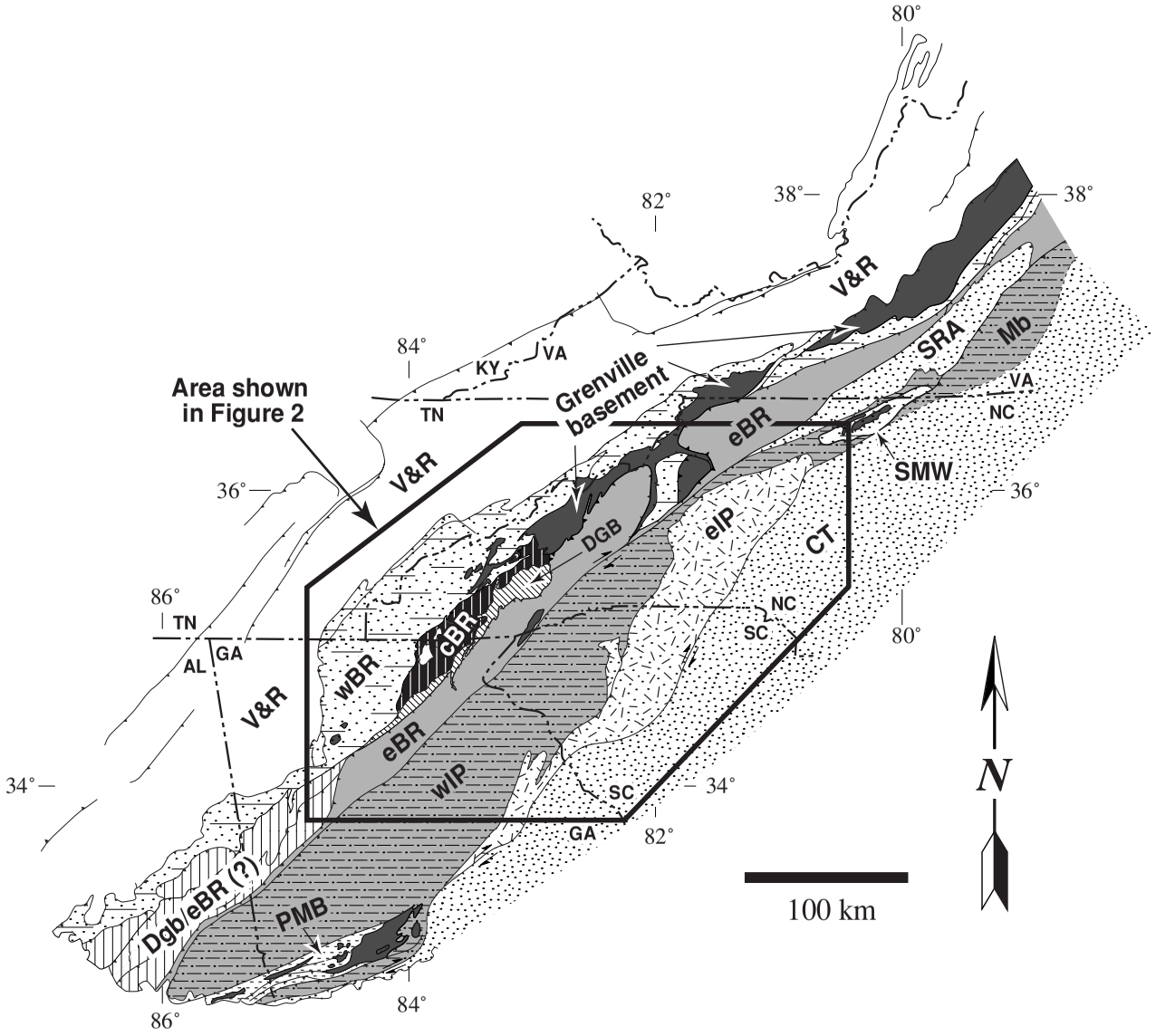

Figure 1. Tectonic map of the southern Appalachians modified from Hatcher et al. (1990). c&eIP-central and eastern Inner Piedmont; cBR-central Blue Ridge; DGB-Dahlonega gold belt; eBR-eastern Blue Ridge; PMB-Pine Mountain Block; SMW-Sauratown Mountains window; SRA-Smith River Allochthon; V&R-Valley and Ridge; wBR-western Blue Ridge; wIP-western Inner Piedmont. See Table 1 for sample coordinates.

affinities (Spell and Norrell, 1990; Berger et al., 2001; Thomas et al., 2001; Settles et al., 2001). The Sauratown Mountains, Grandfather Mountain, and Pine Mountain windows expose several internal Grenvillian basement granitoids and their associated cover sequences (Fig. 1). Basement-cover relationships and lithologic features similar to those found in the western Blue Ridge have been documented in Pine Mountain window (e.g., Schamel et al., 1980; Sears et al., 1981; Kish et al., 1985; Steltenpohl, 1988) and Sauratown Mountains window (McConnell, 1988; Walker et al., 1989) cover sequences. Recent ion microprobe zircon U-Pb geochronologic data reveal suggest an Amazonian source for cover sequence samples from the Pine Mountain window (Steltenpohl et al., this volume).

Several crustal fragments of Laurentian affinity formed during rifting; some were preserved as massifs in the southern Appalachian Blue Ridge (e.g., Toxaway dome), while others were transported and ultimately accreted as exotic terranes onto other cratons (Dalla Salda et al., 1992; Dalziel et al., 1994; Keppie et al., 1996; Thomas and Astini, 1996; Cawood et al., 2001). Southern Appalachian Grenvillian basement massifs can be classified based on structural position within the orogen; external massifs were transported in thrust sheets over the Laurentian margin whereas internal massifs are located beneath major detachments and are exposed in windows (Hatcher, 1984). Western Blue Ridge external basement massifs are distributed within the internal portion of the terrane as a linear outcrop belt along the Blue Ridge Front adjacent to the Valley and Ridge and in the Grandfather Mountain window. Eastern Blue Ridge internal massifs are much smaller, occurring mostly as complexly folded structures (Hatcher et al., this volume).

Rift-related magmatic rocks provide constraints on the timing of Rodinian rifting; unfortunately, western Iapetus geochronologic and paleomagnetic data for these rocks are sparse. Data for the southern Appalachians are limited to Neoproterozoic ages ranging

from 730 to 760 Ma for the Bakersville dike swarm (Goldberg et al., 1986; Ownby et al., this volume), Crossnore complex plutons (Su et al., 1994), and Mount Rogers metarhyolite (Aleinikoff et al., 1995). Rift-related magmatic rocks in the adjacent central Appalachians, however, include the Catoctin Formation metarhyolite dated at 572 ± 5 and 564 ± 9 Ma (Aleinikoff et al., 1995) and the Robertson River suite dated at 702-735 Ma (Tollo and Aleinikoff, 1996). The two age groups for rift-related magmatism in the Appalachians are interpreted to represent an earlier failed event and a younger successful event that created and opened the Iapetus ocean (Badger and Sinha, 1988; Aleinikoff et al., 1995; Brewer and Thomas, 2000). Cawood et al. (2001) also proposed that the younger event is divisible into two distinct phases: the first, ~570 Ma, opened the Iapetus ocean and the second, ~540-535 Ma, evolved into the passive margin after fragmentation of much of the southern Laurentian margin, probably again reflecting the rift-to-drift transition (e.g., Wehr and Glover, 1985; Williams and Hiscott, 1987). It was in these complex latest Neoproterozoic to Early Cambrian rift basins, and in nearly coeval to time-transgressive distal slope-rise to ocean floor environments, that southern Appalachian crystalline core paragneisses were deposited.

SAMPLES

Samples were collected using several criteria including quality of mapping and documented tectonic or stratigraphic significance of individual units. Sampling was biased toward metapsammite lithologies that were expected to contain sufficient detrital zircons and other heavy minerals. Fresh unaltered material, representative of each unit or lithology, was collected. We here present new U-Pb detrital zircon ages and Sm-Nd whole-rock isotopic data for 20 metasedimentary samples from the southern Appalachian Blue Ridge and Inner Piedmont. The Paleozoic metamorphic grade of these samples ranges from subgreenschist in the westernmost Blue Ridge to middle and upper

amphibolite facies in the eastern Blue Ridge and Inner Piedmont (see Fig. 2 and Table 1 for sample localities).

Western Blue Ridge samples

Samples from the western Blue Ridge are from Ocoee Supergroup rift facies. The basal rift facies nonconformably overlie Grenville basement in the western Blue Ridge (King et al., 1958). One sample is from the Snowbird Group, the oldest Ocoee Supergroup unit, one is from the Great Smoky Group, and two are from the Walden Creek Group, the youngest unit in the Ocoee Supergroup. The Longarm Quartzite is predominantly feldspathic sandstone that ranges from <100 to 1,000 m thick in the middle of the Snowbird Group (Montes and Hatcher, 1999). The sample is from the Pigeon River Gorge in North Carolina at the westbound rest area on Interstate 40. Upper Ocoee Supergroup rift samples include a medium- to coarse-grained sandstone sample with small conglomeratic interlayers located in the uppermost Dean Formation (Great Smoky Group) on TN 68 southeast of Tellico Plains. Calcareous fine-grained Sandsuck Formation (Walden Creek Group) sandstone was collected at Springtown area Starr Mountain, Tennessee. A matrix-supported polymictic conglomerate from the Sandsuck Formation (Walden Creek Group) was also sampled at Chilhowee Dam on U.S. 129 in southeastern Tennessee. This conglomerate contains large (up to 0.5 m) rounded clasts of mostly milky quartz with subordinate amounts of quartzite, limestone, dolostone, quartz-epidote (from veins) rare granitoid, and black mud (now slate) in a dominantly medium-grained siliciclastic matrix. Attempts were made during sample preparation to isolate matrix material.

Central Blue Ridge sample

One sample of metasandstone from the central Blue Ridge—Coleman River Formation of Hatcher (1979)—was collected on U.S. 76 west of Clayton, Georgia, less

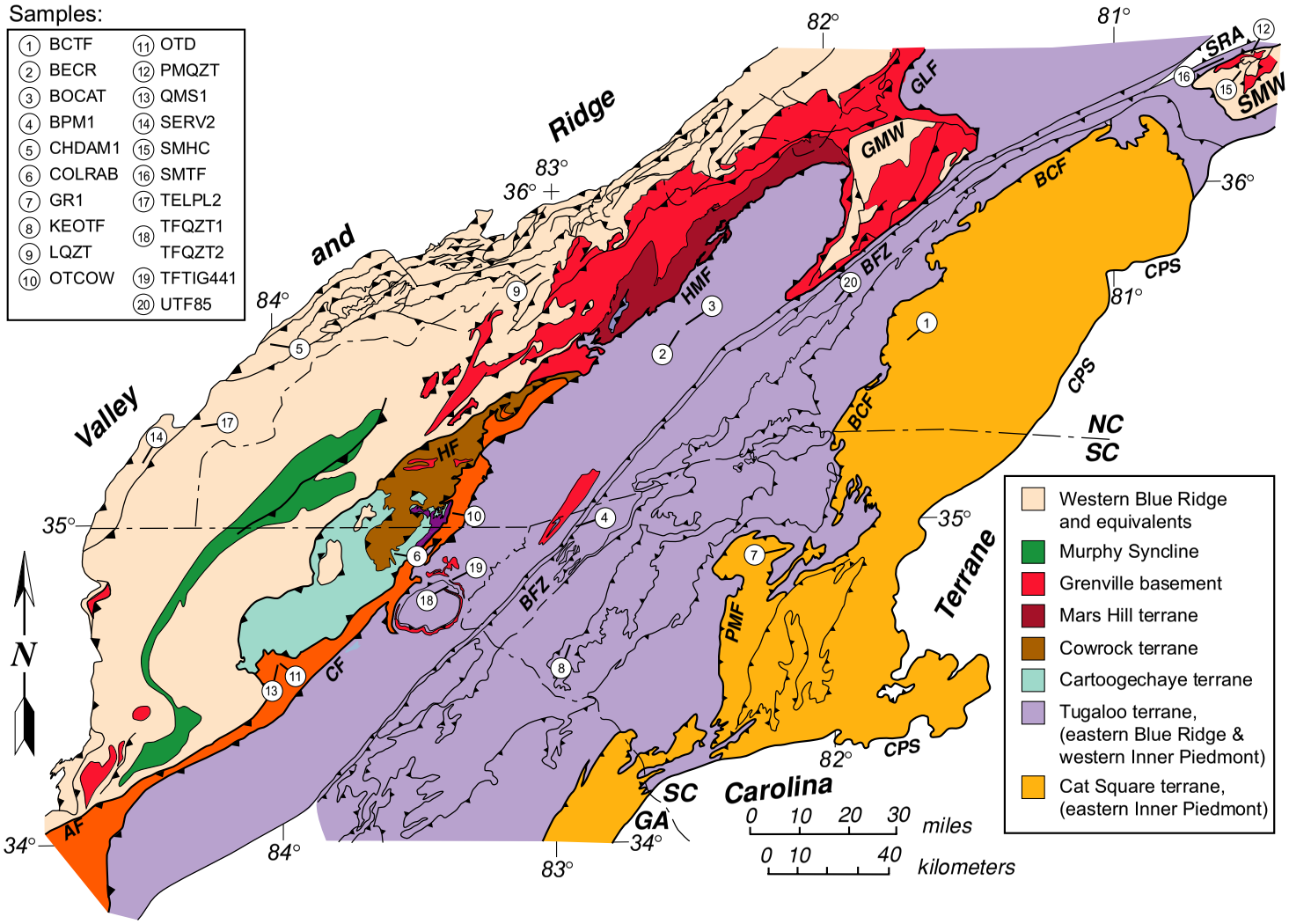

Figure 2. Geologic map of a portion of the southern Appalachians with sample locations. AF-Allatoona fault; BCF-Brindle Creek fault; BFZ-Brevard fault zone; CF-Chattahoochee fault; GLF-Gossan Lead fault; GMW-Grandfather Mountain window; HF-Hayesville fault; HMF- Holland Mountain fault; PMF-Paris Mountain fauls; SMW-Wauratown Mountains window; SRA-Smith River allochthon. Modified from Hatcher (2002, in press).

Table 1. Samples with stratigraphic association and coordinates.

Sample	Figure 2 Location	Formation or unit name	7.5-minute quadrangle	County (State)	Latitude (°N)	Longitude (°W)
western Blue Ridge						
CHDAM1	5	Walden Creek Group (Ocoee Supergroup)	Tallassee	Blount (TN)	35.548	84.050
LQZT	9	Longarm Quartzite, Snowbird Group (Ocoee Supergroup)	Cove Creek Gap	Haywood (NC)	35.702	83.040
SERV2	14	Sandsuck Formation, Walden Creek Group (Ocoee Supergroup)	McFarland	Polk (TN)	35.248	84.444
TELPL2	17	Dean Formation, Great Smoky Group (Ocoee Supergroup)	Tellico Plains	Monroe (TN)	35.336	84.296
central Blue Ridge						
COLRAB	6	Coleman River Formation	Hightower Bald	Rabun (GA)	34.908	83.612
Dahlonega gold belt						
OTCOW	10	Otto Formation	Prentiss	Macon (NC)	35.060	83.453
OTD	11	Otto Formation	Campbell Mountain	Lumpkin (GA)	34.560	84.074
QMS1	13	Otto Formation	Campbell Mountain	Lumpkin (GA)	34.533	84.018
eastern Blue Ridge						
BECR	2	Tallulah Falls Formation-Ashe Formation (metagraywacke member)	Dunsmore Mountain	Buncombe (NC)	35.454	82.661
BOCAT	3	Tallulah Falls Formation-Ashe Formation (metagraywacke member)	Asheville	Buncombe (NC)	35.600	82.538
TFQZT1	18	Tallulah Falls Formation (quartzite member)	Tiger	Rabun (GA)	34.817	83.424
TFQZT2	18	Tallulah Falls Formation (quartzite member)	Tallulah Falls	Rabun (GA)	34.736	83.391
TFTIG441	19	Tallulah Falls Formation-Ashe Formation (metagraywacke member)	Tiger	Rabun (GA)	34.838	83.422
Sauratown Mountains window						
SMHC	15	Hogan Creek Formation	Siloam	Surry (NC)	36.271	80.602
PMQZT	12	Pilot Mountain Quartzite	Pinnacle	Surry (NC)	36.344	80.482
western Inner Piedmont						
BPM1	4	Chauga River Formation (Brevard-Poor Mountain Transitional member)	Salem	Oconee (SC)	34.916	82.914
KEOTF	8	Tallulah Falls Formation-Ashe Formation (aluminous schist member)	Seneca	Oconee (SC)	34.696	82.879
SMTF	16	Tallulah Falls Formation-Ashe Formation (metagraywacke member)	Copeland	Surry (NC)	36.275	80.732
UTF85	20	Tallulah Falls Formation-Ashe Formation (metagraywacke member)	Marion East	McDowell (NC)	35.644	81.987
eastern Inner Piedmont						
BCTF	1	metagraywacke biotite-gneiss not presently assigned to a formation	Benn Knob	Rutherford (NC)	35.539	81.702
GR1	7	metagraywacke biotite-gneiss not presently assigned to a formation	Greer	Spartanburg (SC)	34.917	82.139

NAD27 CONUS coordinates

than 1 km east of the Rabun-Towns county line. This unit is the most widely distributed of the Coweeta Group, making up most of the Hayesville-Soque River thrust sheet (Cowrock terrane of Hatcher et al., this volume).

Dahlonega gold belt samples

Three samples were collected from the Otto Formation in the Dahlonega gold belt, a unit consisting of intercalated metapelite and metasandstone (Hatcher, 1988). One sample locality is in the Coweeta Hydrologic Laboratory at Otto, North Carolina, in the footwall of the Shope Fork thrust. Two samples are from the footwall of the Hayesville-Soque River thrust fault in the Allatoona thrust sheet ~2.5 km west and ~7 km west-northwest of Dahlonega, Georgia in the Campbell Mountain 7.5-minute quadrangle.

Eastern Blue Ridge and western Inner Piedmont samples

Six samples of Tallulah Falls-Ashe Formation were collectedfrom the Eastern Blue Ridge and western Inner Piedmont (Tugaloo terrane of Hatcher et al., this volume). Eastern Blue Ridge Tallulah Falls-Ashe Formation was sampled at a roadcut through Beaucatcher Mountain in Asheville (NC); ~200 m north of Bent Creek Gap in the Bent Creek Experimental Forest ~15 km southwest of Asheville, North Carolina on the Blue Ridge Parkway (locality is same as sample ts-500 of Merschat and Carter, 2002); and from the north flank of the Tallulah Falls dome on U.S. 23-441 ~5 km south-southwest of Clayton, Georgia. The western Inner Piedmont Tallulah Falls-Ashe Formation was sampled in the Forbush thrust (Heyn, 1984) in a railroad cut on the Yadkin River directly southwest the Sauratown Mountains window ~13 km east-northeast of Elkin-Jonesville, North Carolina. A second western Inner Piedmont sample was collected from a roadcut 150 m north of Exit 85 on Interstate 40 south of Marion, North Carolina. A third sample was collected on U.S. 76-123 in the Six Mile thrust sheet at Keowee, South Carolina. All of these samples contain middle to upper amphibolite facies mineral assemblages and

are dominantly one-mica (biotite up to 30%), one feldspar (plagioclase) metagraywackes. The other eastern Blue Ridge sample locality is the Tallulah Falls Quartzite sampled on U.S. 23-441 at Wiley, Georgia; this sample is medium-grained, locally conglomeratic (vein quartz and both plagioclase and K-feldspar clasts), quartzite located within the Tallulah Falls dome, and at this locality contains upright graded beds (Fritz et al., 1989). The remaining sample locality is on South Carolina State Highway 11 where it crosses Lake Keowee (west side), in the westernmost Inner Piedmont (Hatcher and Acker, 1984). This sample consists of metasiltstone with mica-fish and thin metagraywacke interlayers, the Brevard-Poor Mountain transitional member of Hatcher's (1969, 2002) Chauga River Formation.

Sauratown Mountains window samples

Both the Hogan Creek Formation and Pilot Mountain Quartzite were sampled in the Sauratown Mountains window. The Hogan Creek Formation consists of metasandstone, pelitic schist, and minor marble in nonconformable contact with Grenville basement orthogneisses of the outer window (Hatcher et al., 1988). The sample is from an abandoned quarry on the Yadkin River ~4 km upstream from Siloam, North Carolina. The Pilot Mountain Quartzite overlies the Sauratown Formation, informally named by Heyn (1984) and formally named by Horton and McConnell (1991), and is also in nonconformable contact with Grenville basement. The Pilot Mountain Quartzite is a well-sorted quartz arenite that preserves primary sedimentary structures (Walker et al., 1989). The Pilot Mountain Quartzite and Sauratown Formation are restricted to the inner Sauratown Mountains window.

Eastern Inner Piedmont samples

The eastern Inner Piedmont samples are metagraywackes from a metapelite-dominated unit (Hatcher and Bream, 2002). The eastern Inner Piedmont samples are not

currently assigned to a recognized stratigraphy. One sample was collected ~9 km west-northwest of Casar, North Carolina in Brier Creek and the other sample was collected ~2.5 km south of Duncan, South Carolina near the Duncan Correctional Center.

ANALYTICAL METHODS

Whole-rock powders were prepared in an alumina ceramic mill and shatterbox from representative material collected in the field. The samples were cut into thin slabs on a trim saw, rinsed with isopropyl alcohol and deionized water, broken up by hand, and then ground to a fine powder. Sm and Nd isotopic data were determined in the Department of Geological Sciences, University of North Carolina at Chapel Hill using a Micromass VG Sector 54 thermal ionization mass spectrometer using the same analytical technique as outlined in Fullagar et al. (1997).

Fresh, representative samples (4-5 kg) of each rock unit were collected and standard mineral separation techniques were employed to isolate the heaviest nonferromagnetic phases. Attempts to split samples into coarse- and fine-grained fractions were made difficult by overall sample hardness; consequently, separates from the coarser-grained western Blue Ridge Sandsuck Formation conglomerate was obtained from a mixture of clast and matrix fragments despite efforts to sample the matrix. A minimum of 60-70 zircon grains per sample were hand-picked, mounted in epoxy with zircon standard AS3 or AS57 (1099 Ma; Paces and Miller, 1993) and/or R33 (419 Ma; Stanford USGS Micro Analysis Center), and polished to the approximate center of average-size grains. Zoning and inclusions were identified from cathodoluminescence (CL) images obtained for each grain and, in most cases, grains were also photographed with a combination of transmitted and reflected light to augment surface and internal feature identification. Sensitive high-resolution ion microprobe (IMP) data were collected during two sessions at the University of California Los Angeles using the Cameca IMS-1270 and during four

sessions at Stanford University using the SHRIMP-RG (sensitive high-resolution ion microprobe reverse geometry) over two years.

Routine analytical techniques and operating conditions for IMP zircon analyses were followed (e.g., Quidelleur et al., 1997, for the Cameca IMS-1270 technique; Bacon et al., 2000, for SHRIMP RG technique) and are briefly summarized here. The primary ion beam produced ~1 μm deep and up to ~25 μm by ~30 μm wide analytical pits in the zircons (smaller beam sizes, down to ~10 μm, were used for some UCLA data). Before each analysis, the primary beam was used to remove the gold coat and surface contamination on the targeted spot. IMP sessions at UCLA employed fifteen mass peak scans for each spot. The number of scans was reduced to five, with only a slight decrease in precision in part due to a larger primary beam, for the Stanford IMP sessions to increase the total number of analyses per sample. Sample isotopic counts were referenced to counts on a zircon standard (AS3 or AS57) [R33 was also used during some Stanford sessions], which was analyzed approximately every fifth analysis. Most unknown analyses contained minor amounts of common Pb corresponding to modest common Pb corrections. Most analyses were corrected for common Pb using a ^{204}Pb correction. A ^{208}Pb correction was applied to some UCLA data with ^{208}Pb/^{204}Pb values<200 and low Th/U ratios (see data reduction in Carrigan et al., in press). Analyzed grains were reimaged (backscattered electron and CL) with a Cameca SX-50 electron microprobe at the University of Tennessee–Knoxville to confirm the location and dimensions of IMP analytical spots (Fig. 3).

Analyses with ^{206}Pb*/^{238}U and ^{207}Pb*/^{206}Pb* ages that differed by more than 10 percent were excluded from the probability plots in order to increase the likelihood that the summed probabilities represent accurate ages; similar studies used comparable values (e.g., Mueller et al., 1992; Cawood and Nemchin, 2001; DeGraff-Surpless et al., 2002). We excluded Paleozoic rim data and constructed summed probability plots of remaining

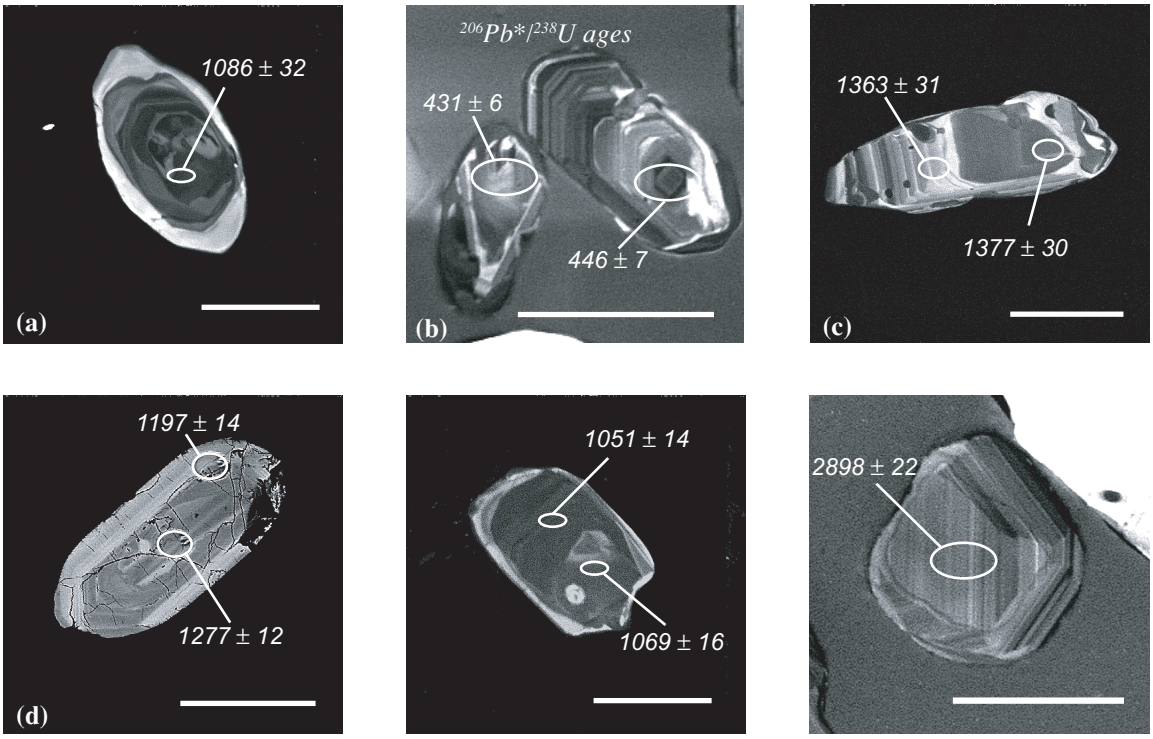

Figure 3. Cathodoluminescence (CL) and backscattered electron (BSE) images of analyzed detrital zircons. Unless otherwise noted, ages are $^{207}Pb^*/^{206}Pb^*$ in Ma with 1σ errors. (a) Eastern Blue Ridge Tallulah Falls sample (CL; sample TFTIG441). (b) Eastern Inner Piedmont metagraywacke (CL; sample GR1). (c) Tallulah Falls Formation (CL; sample SMTF). (d) Sauratown Mountains window Hogan Creek Formation (BSE; sample SMHC). (e) Western Inner Piedmont Tallulah Falls Formation (CL; sample UTF85). (f) Dahlonega gold belt Otto Formation (CL; sample QMS1). NOTE: Spot locations for (b) and (f) are approximate. Scale bar is 100 μm.

core and non-Paleozoic rim data using $^{206}Pb^*/^{238}U$ ages for analyses up to 1.6 Ga and $^{207}Pb/^{206}Pb$ for analyses older than 1.6 Ga. Summed probability curves for the $^{207}Pb^*/^{206}Pb^*$ ages are also provided for reference. Approximately 20 percent, up to 53 percent, of the analyses for each group were eliminated by exclusion of data with $^{206}Pb^*/^{238}U$ and $^{207}Pb^*/^{206}Pb^*$ ages that differed by more than 10 percent. As expected due to the reduced sensitivity of $^{207}Pb^*/^{206}Pb^*$ ages for young zircons, most excluded analyses were Late Proterozoic and Paleozoic; although, a Middle Proterozoic component with >10% age discrepancies was noted in several samples. The choice of 1.6 Ga is arbitrary —Cawood and Nemchin (2001) selected 1.5 Ga —but convenient because of the small number of analyses at or near this age. Statistically, it is possible that some zircon age ranges within individual samples were not identified (Dodson et al., 1988); therefore our data are better suited for evaluation based on positive rather than negative results (i.e., the presence of an age is more reliable than its absence). Data were pooled into summed probability plots for each sampled tectonic division.

RESULTS

The goal of this research was to address provenance constraints based on new detrital zircon ages and Nd isotopic data for samples from each of the major southern Appalachian tectonic divisions west of the central Piedmont suture and southeast of the Blue Ridge front (Fig. 1, Fig. 2). Isotopic and geochronologic data for metasedimentary rocks must be interpreted together with structural and stratigraphic constraints provided by field observations and detailed mapping. Despite a number of published detrital heavy mineral suite studies (e.g., Carroll et al., 1957; Hadley, 1970), similar studies in the southern Appalachians are sparse. Our results necessitate reevaluation of the provenance and crustal affinity of the terranes from which the samples were derived.

Whole-rock Sm-Nd data

A modest but increasing amount of Nd isotopic data now exist for crystalline rocks (mainly granitoids) of the Blue Ridge, Inner Piedmont, and Carolina terrane (Fig. 4). Data from the metasedimentary rocks of the Blue Ridge and Inner Piedmont (Table 2) have T_{DM} ages ranging from 1.2 to 1.9 Ga and e_{Nd} values around the time of deposition (~600 Ma) between –2.1 to –8.5, clearly overlapping Grenville basement data of Carrigan et al. (in press) and Hatcher et al. (this volume). The data also partially overlap with the field defined for older more isotopically evolved Mars Hill terrane (Bartholomew and Lewis, 1988, 1992) samples (Carrigan et al., in press; Ownby et al., this volume). There appears to be little correlation of sample isotopic maturity with terrane or distance from the Laurentian margin but notably the oldest T_{DM} ages are from the Sauratown Mountains window and Dahlonega gold belt. Based on these data, the sediments could have been derived from a combination of more isotopically evolved (relative to the Grenville basement exposed in the southern Appalachians) source(s) and less evolved juvenile crustal source(s); or, more likely, derived directly from rocks of similar age and isotopic maturity to the Grenville basement of the Blue Ridge and Sauratown Mountains window. Data from Chopawamsic and Milton terrane para- and orthogneisses (Wortman et al., 1996; Coler et al., 2000) also overlap the field for southern Appalachian Grenville basement whereas Nd data (mostly metaigneous) from the Kings Mountain, Charlotte, Milton, Carolina slate, Raleigh, Kiokee, and eastern slate belts of the Carolina terrane favor the generation of Paleozoic magmas from juvenile isotopically depleted crust with a minor contribution (possibly increasing with time) from older more evolved crust (Fig. 4)(Samson et al., 1995; Fullagar et al., 1997). Late Proterozoic sources, increasing with distance from the western-eastern Blue Ridge boundary, are noted for Paleozoic granitoids of the southern Appalachian Blue Ridge, Inner Piedmont, and Carolina terrane (Fullagar et al., 1997); this relationship suggests

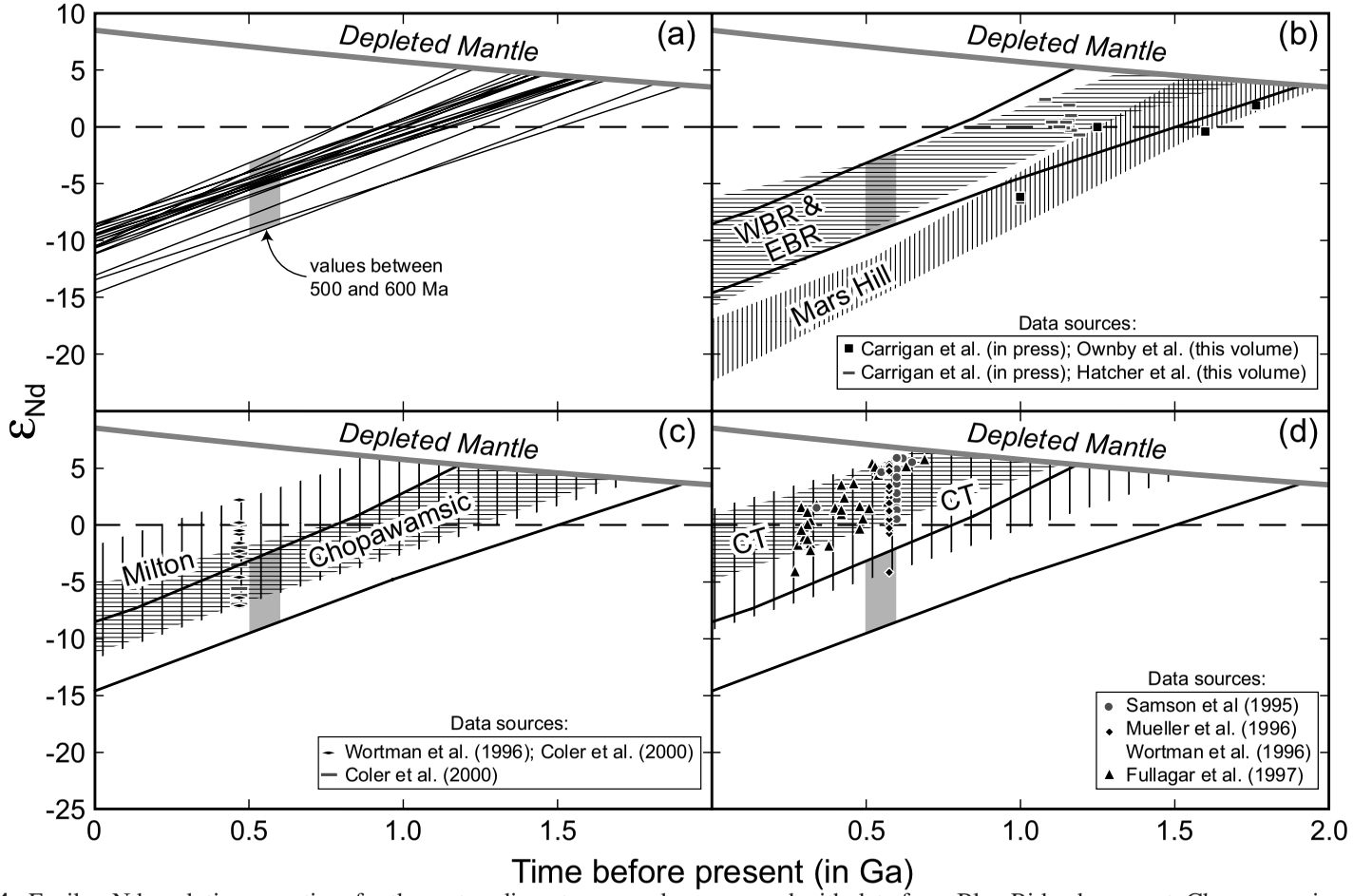

Figure 4. Epsilon Nd evolution over time for the metasedimentary samples compared with data from Blue Ridge basement, Chopawomsic and Milton terranes, and Carolina terrane. (a) Metasedimentary sample data presented here showing evolution from present to intersection with the depleted mantle. The outlined field is the range of values between 500 and 600 Ma. (b) Metasedimentary data field with western and eastern Blue Ridge Grenvillian basement (WBR & EBR; horizontal lines) and Mars Hill terrane (vertical lines) data. (c) Metasedimentary data field with Chopawamsic (horizontal lines) and Milton belt (vertical lines) data. (d) Metasedimentary data field with Carolina terrane data (CT). Note evolution lines in (b-d) are defined by upper and lower boundaries of data in (a), symbols represent values at the estimated time of crystallization and/or deposition, data with $^{147}Sm/^{144}Nd$ >0.15 were excluded, and depleted mantle curve from DePaolo (1981).

Table 2. Sm-Nd isotopic data.

Sample	Figure 2 Location	Sm (ppm)	Nd (ppm)	$^{147}Sm/^{144}Nd$	$^{143}Nd/^{144}Nd$ ($\pm 2\sigma$)†	ε_{Nd} (at present)	ε_{Nd} (at 600 Ma)	T_{DM} (Ga)
western Blue Ridge								
CHDAM1	5	3.82	21.92	0.10775	0.512093 (04)	-10.6	-3.8	1.37
LQZT	9	3.30	18.71	0.10914	0.512067 (10)	-11.1	-4.4	1.42
SERV2	14	5.66	29.72	0.11783	0.512120 (05)	-10.1	-4.1	1.46
TELPL2	17	7.46	39.57	0.11668	0.512150 (05)	-9.5	-3.4	1.40
central Blue Ridge								
COLRAB	6	5.41	26.57	0.12594	0.512121 (05)	-10.1	-4.7	1.60
Dahlonega gold belt								
OTCOW	10	8.93	44.75	0.12356	0.512195 (06)	-8.6	-3.0	1.43
OTD	11	7.62	37.48	0.12575	0.512200 (05)	-8.5	-3.1	1.46
QMS1	13	4.30	21.03	0.12660	0.511948 (03)	-13.5	-8.1	1.91
eastern Blue Ridge								
BECR	2	9.63	47.07	0.12665	0.512146 (06)	-9.6	-4.2	1.57
BOCAT	3	5.14	24.38	0.13050	0.512171 (04)	-9.1	-4.0	1.59
SMTF	16	10.52	52.66	0.12370	0.512091 (07)	-10.7	-5.1	1.61
TFQZT1	18	9.70	55.61	0.10795	0.512184 (03)	-8.9	-2.1	1.24
TFQZT2	18	3.68	19.79	0.11505	0.512100 (07)	-10.5	-4.2	1.45
Sauratown Mountains window								
SMHC	15	4.46	23.55	0.11720	0.511888 (06)	-14.6	-8.5	1.82
PMQZT	12	5.21	27.18	0.11854	0.512064 (06)	-11.2	-5.2	1.56
western Inner Piedmont								
BPM1	4	8.37	41.23	0.12570	0.512134 (07)	-9.8	-4.4	1.57
KEOTF	8	8.38	39.95	0.12986	0.512185 (05)	-8.8	-3.7	1.56
TFTIG441	19	6.92	32.29	0.13260	0.512152 (05)	-9.5	-4.6	1.67
UTF85	20	11.40	58.35	0.12092	0.512155 (05)	-9.4	-3.6	1.46
central Inner Piedmont								
BCTF	1	4.80	32.12	0.09238	0.512097 (04)	-10.6	-2.6	1.19
GR1	7	6.73	36.45	0.11430	0.511968 (05)	-13.1	-6.8	1.64

(i) Initial values.

T_{DM} age calculated according to DePaolo (1981), using $^{147}Sm/^{144}Nd = 0.1967$ and $^{143}Nd/^{144}Nd = 0.512638$ for present day Bulk Earth values.

$\varepsilon_{Nd} = [\{[^{143}Nd/^{144}Nd]_{Sample} - [^{143}Nd/^{144}Nd]_{Bulk\ Earth}\}/\{[^{143}Nd/^{144}Nd]_{Bulk\ Earth}\} \times 10^4$. Bulk Earth: $^{143}Nd/^{144}Nd = 0.512638$ present day, $^{143}Nd/^{144}Nd = 0.511864$ at 600 Ma.

$^{143}Nd/^{144}Nd$ measured ratios normalized to $^{146}Nd/^{144}Nd = 0.7219$

†2σ errors are reported as last two significant digits.

that magma generation during Paleozoic orogenesis involved larger amounts of juvenile crust away from the Laurentian margin (Fullagar, 2002).

Detrital zircon data

The summed probabilities for pooled samples (Fig. 5) should be viewed as "relative" abundances because of differences in number and types of samples, number of individual analyses for each division, separation and analytical bias, multiple analyses of grains with unique ages, and the consolidation of samples into their respective tectonic terranes. Most detrital grains contain brightly luminescent (in CL) interior zones with oscillatory zoning and relatively unzoned thin darker rims. Summed probability plots illustrate the ubiquitous nature of Grenvillian magmatic (~1000-1250 Ma) and metamorphic (~950-1000 Ma) ages in detrital zircons. A pre-Grenvillian component is also present in all southern Appalachian crystalline core terrane summed probability plots. Recognized pre-Grenvillian ages are early Middle Proterozoic (1.25-1.6 Ga), Early Proterozoic (1.6-2.1 Ga), and Late Archean (2.7-2.9 Ga). Absence of grains between 2.0 to 2.6 Ga was noted in almost all samples. Except for the eastern Blue Ridge and Sauratown Mountains window, Early Proterozoic zircons occur in each of the terranes. Late Archean zircons were identified in the central Blue Ridge, Dahlonega gold belt, and central Inner Piedmont samples. Post-Grenvillian detrital zircons are also present in samples from the Dahlonega gold belt, eastern Blue Ridge, western Inner Piedmont, and eastern Inner Piedmont. These ages are Late Proterozoic and early Paleozoic (central Inner Piedmont only) for detrital components.

APPALACHIAN CRUSTAL AFFINITY

Determining crustal affinities for basement and unmetamorphosed, often fossiliferous, sedimentary rocks is more straightforward than identifying clear evidence of crustal affinity for penetratively deformed and metamorphosed sedimentary rocks, like

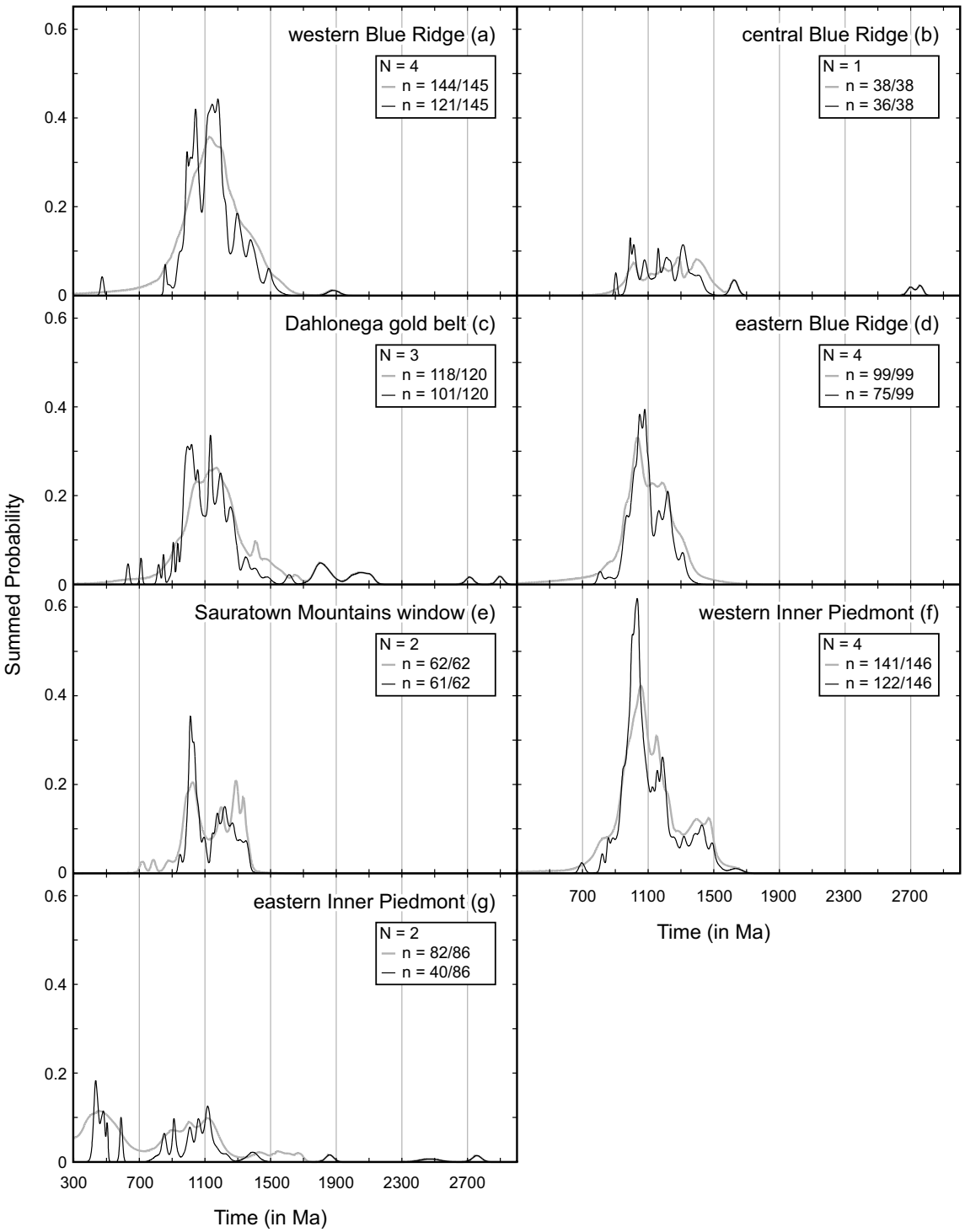

Figure 5. Summed probability plots for detrital zircon data. Thicker gray lines are $^{207}Pb^*/^{206}Pb^*$ ages and thinner black lines are $^{206}Pb^*/^{238}U$ ages for analyses with $^{207}Pb^*/^{206}Pb^*$ ages <1.6 Ga and $^{207}Pb^*/^{206}Pb^*$ ages for analyses with $^{207}Pb^*/^{206}Pb^*$ ages >1.6 Ga. (a) Western Blue Ridge samples. (b) Central Blue Ridge samples. (c) Dahlonega gold belt samples. (d) Eastern Blue Ridge samples. (e) Sauratown Mountains window samples. (f) Western Inner Piedmont samples. (g) Eastern Inner Piedmont samples. Note that N refers to the number of samples from each terrane, n refers to the number of analyses plotted over the total number of analyses, and that all plots are at the same scale.

those found in the southern Appalachian crystalline core. The predominance of 1.0-1.25 Ga detrital zircon ages strongly suggests that these terranes were all near a Grenvillian source, consistent with the nonconformable nature of most basement-cover contacts in the Blue Ridge and Sauratown Mountains window. These Grenvillian ages, however, have limited use when taken alone for establishing distinct source(s) because of the almost ubiquitous presence of Grenvillian belts on the margins of pre-Grenvillian cratons that were near or adjacent to the Laurentian margin during the initial rifting stages (e.g., Hoffman, 1991; Rogers, 1996; Dalziel, 1997).

Gondwanan connections

Early workers positioned the west African craton near or adjacent to the Appalachian segment of Laurentia prior to the breakup of Rodinia (Bird and Dewey, 1970; Hatcher, 1978). More recent work has presented convincing evidence that west Gondwanan cratons of South America (Amazonia, Rio de la Plata) were juxtaposed with the southeastern Laurentian margin (Dalziel, 1991; Hoffman, 1991). The exact positions and relative movements of the west Gondwanan Amazonia, Rio de la Plata, Congo, and Kalahari cratons relative to Laurentia are variably portrayed in different paleogeographic reconstructions. In most reconstructions, however, the Amazonia and Rio de la Plata cratons appear as the conjugate margin to Laurentia (e.g., Hoffman, 1991; Dalziel, 1992, 1997; Cawood et al., 2001; Payolla et al., 2002). The Congo craton has also been placed opposite the Amazonia craton near the southern Laurentian margin (Hoffman, 1991). Although very distal, Dalziel et al. (2000) suggested the Kalahari craton may have been close to central Texas at ~1100 Ma. Each of these cratons thus represents a potential source for distal Late Proterozoic to early Paleozoic sediments of the southern Appalachian eastern Blue Ridge and Inner Piedmont. The Argentine Precordillera and adjacent Sierra de Pie de Palo is generally accepted as a transported Laurentian fragment

(e.g., Borrello, 1971; Ramos et al., 1986; Astini et al., 1995; Ramos et al., 1998; Vujovich and Kay, 1998; Thomas and Astini, 1999; Casquet et al., 2001); other candidates for transported Laurentian fragments include the South American Chilenia and Cuyania terranes, Oaxacan terrane of Mexico, and possibly the northern Appalachians Dashwoods block (e.g., Keppie and Ortega-Gutiérrez, 1999; Keppie and Ramos, 1999; Cawood et al., 2001). Paleozoic transfer of peri-Gondwanan terranes (e.g., Avalonian-Carolina terrane) onto the Laurentian margin is also widely documented (e.g., Secor et al., 1983; Hatcher, 1989; Keppie and Ramos, 1999). Although the exact provenance of these smaller far-traveled crustal fragments is debatable, their present-day distribution is evidence for the complex rifting and subsequent plate interactions at the Laurentian margin.

An exotic origin for the internal eastern Laurentian terranes (e.g., Jefferson terrane of Horton et al., 1989) is frequently proposed to model of subduction and accretionary wedge development at the margin (e.g., Abbott and Raymond, 1984; Rankin et al., 1989). In such models, rocks in the ultramafic and metamorphosed basalt/gabbro-bearing wedge(s) are considered exotic and are separated from the Laurentian margin by a series of Paleozoic faults interpreted to represent the suture and subduction zone locus (e.g., Hatcher, 1978, 1987; Rankin, 1994). Based on correlations with the Late Proterozoic-Cambrian Potomac orogeny in the central Appalachians, Hibbard and Samson (1995) proposed that portions of the southern Appalachian marginal terranes record tectonothermal histories that predate Laurentian passive margin development, possibly developing in a peri-Gondwanan setting. Correlation of magmatic and tectonic events has also been used to link the Laurentian margin with South America (Dalla Salda et al., 1992; Keppie and Ramos, 1999). In particular, comparisons of the Pampean (530-510 Ma), Famatinian (490-470 Ma), and Achalian (403-382 Ma) magmatic pulses in the southern Sierras Pampeanas (Argentina) revealed similarities to Laurentian margin

magmatic activity, thus supporting the possibility that Laurentia and western Gondwana collided ~470 Ma producing magmas along the margins of both cratons (Stuart-Smith et al., 1999). This latter possibility would then require that subsequent Paleozoic orogenies (late Taconian, Acadian, and Alleghanian) be intracratonic (originally suggested by Bird and Dewey, 1970), unless an as yet undocumented rifting event also occurred.

North American detrital zircon ages directly cited as supporting Gondwanan affinity include: (1) combinations of 570 Ma, 1,500-1,550 Ma, 2,600-2,750 Ma, and absence of 1,000-1,150 Ma zircons from the eastern New England Appalachians (Karabinos and Gromet, 1993); (2) combinations of 515-635 Ma, abundant 1,967-2,282 Ma, and ~2,700 Ma zircons for a Florida basement sandstone (Mueller et al., 1994); (3) combination of ~550-700 Ma arc magmatism with ~1,000-1,300 Ma and 1,500-1,550 Ma zircons from the Avalon terrane in Nova Scotia (Keppie et al., 1998); (4) presence of ~550-700 Ma, 2,000-2,200 Ma and minor components of ~1,000, 1,200, and 1,800 Ma zircons in samples from the late Paleozoic Magdalen basin near the Avalon and Meguma terranes in the Canadian Appalachians (Murphy and Hamilton, 2000); and (5) presence of Neoproterozoic ages and 1,100-1,800 Ma with increased contributions of 1,800-2,500 Ma and Archean ages over time for younger Carolina terrane samples (Samson et al., 2001). Based on the presence of 2,200-2,400 Ma and ~1,400 Ma detrital zircons in the Pine Mountain window of Alabama, Heatherington et al. (1997) and Steltenpohl et al. (2001, this volume) suggested that the Hollis Quartzite may be derived from west Gondwana and that the mixture of Laurentian (or South American Rondonian province) and probable Gondwanan detrital zircons favored deposition of the Hollis Quartzite, roughly coeval with the separation of the Pine Mountain crustal block from Gondwana. Each of these studies noted the presence of Late Proterozoic to Early Cambrian and Archean detrital grains with varying, but minor Early and Middle Proterozoic components with the notable exception of the Hollis Quartzite.

Laurentian connections

A Laurentian connection for the entire metasedimentary package northwest of the Carolina terrane was proposed in the depositional model of Hatcher (1978), wherein the western Blue Ridge and eastern Blue Ridge sedimentary packages were related as facies equivalents within an ocean basin that developed between the Laurentian margin and a rifted fragment of continental basement. In this model, western Inner Piedmont paragneisses were deposited on the eastern margin of the rifted continental basement block. Detailed field work in the eastern Blue Ridge and western Inner Piedmont has correlated stratigraphic sequences across the Brevard fault zone that separates these divisions (e.g., Heyn, 1984; Hopson and Hatcher, 1988) and identified nonconformable or locally faulted basement-cover contacts around the small massifs of the eastern Blue Ridge (Hatcher et al., this volume). These relationships and our new data suggest that eastern Blue Ridge-western Inner Piedmont paragneisses are correlative, and/or perhaps time transgressive equivalents, to the western Blue Ridge cover sequences that are known to unconformably overlie Grenville basement. Recently published Nd and inherited zircon data demonstrate that Ordovician arc rocks of the Chopawamsic and Milton terranes (Coler et al., 2000) are isotopically more evolved than Gondwanan-affinity arcs (Nance and Murphy, 1994; Samson et al., 1995) and show remarkable similarities with recognized Laurentian arc terranes (e.g., Bronson Hill anticlinorium), Blue Ridge Grenvillian basement, and Blue Ridge-western Inner Piedmont paragneisses (Fig. 3). Detrital zircons from Newfoundland Humber zone rift-facies, drift-facies, and foreland basin samples are interpreted to represent material derived from the Superior craton, Early Proterozoic and Grenvillian orogenic belts, and Neoproterozoic rift-related magmatic rocks (Cawood and Nemchin, 2001). Detrital zircon age studies in younger central and northern Appalachian Paleozoic foreland sedimentary sequences also favor derivation from Laurentia (Gray and Zeitler, 1997; McLennan et al., 2001) and suggest that the

source becomes younger and more restricted over time.

DISCUSSION

Although whole-rock Nd isotopic data and detrital zircon ages can provide important information concerning the evolution of metasedimentary rocks, a surprisingly limited amount of these data exist for the southern Appalachians. Three crustal affinities appear to be possible for the southern Appalachian Blue Ridge and Inner Piedmont metasedimentary samples: (1) Laurentian derivation; (2) west Gondwanan derivation; or (3) a combination of Laurentian and west Gondwanan derivation. The data shown in Figures 4 and 5 taken alone do not preclude any of the aforementioned scenarios. Our data differ from similar studies in the southern Appalachians (e.g., Heatherington et al.,1997; Miller et al., 2000; Steltenpohl et al., 2001, this volume), however, because of the presence of an Early Proterozoic component, albeit minor, for most of the southern Appalachian divisions. Based on the occurrence of the major age ranges of our data, the source(s) must include Grenvillian rocks and 1,250-1,400 Ma components for all of the sampled terranes. Additionally, most of the divisions also contain varying amounts of 1,350-1,500 Ma ages. Archean source(s) are required for the zircon suites in the central Blue Ridge, Dahlonega gold belt, and central Inner Piedmont. The Dahlonega gold belt also contains an appreciable component of ~1,600-2,100 Ma ages, which is not nearly as abundant in the other divisions (limited to single analyses in the western Blue Ridge and central Inner Piedmont). Notably, two grains from the Dahlonega gold belt are between 2,000 and 2,100 Ma, an age range not abundant in the Laurentian craton. Based on the presence of Ordovician detrital zircons in the central Inner Piedmont samples, deposition in this terrane is younger (late Silurian to Devonian) and likely deposited between the proximal Laurentian margin and approaching peri-Gondwanan terranes.

Some have contended that the entire package of rocks from the Valley and Ridge

and western Blue Ridge boundary to the southeastern boundary of the Inner Piedmont is Laurentian (e.g., Hatcher, 1978, 1987, 1989); others, however, have proposed that all of the rocks east of the Allatoona-Hayesville-Holland Mountain-Gossan Lead fault are exotic (e.g., Rankin et al., 1989; Hibbard and Samson, 1995) to North America. Our data, as well as data from the Chopawamsic and Milton terranes (Coler et al., 2000), suggest that these terranes were either built on or interacted with Mesoproterozoic crust. Southern Appalachian basement rocks are mostly Grenvillian (Carrigan et al., in press; Hatcher et al., this volume); studies in the Mars Hill terrane in the western Blue Ridge, however, have identified older whole-rock isotopic components (Monrad and Gulley, 1983; Sinha et al., 1996; Carrigan et al., in press; Ownby et al., this volume) and pre-Grenvillian zircons with an abundant 1,200-1,300 Ma component and lesser amounts of 1,400-1,500 Ma; 1,600-1,900 Ma; and 2,700 Ma ages (Fullagar and Gulley, 1999; Ownby et al., 2002; Carrigan et al., in press; Ownby et al., this volume). Consequently, basement rocks of the Blue Ridge or their eroded and/or subsurface equivalents are the best candidates for the abundant Grenvillian detrital zircons and lesser amounts of some Middle and Early Proterozoic detrital zircons. The combination of 1.3-1.5 Ga and Grenvillian detrital zircons is readily explained by a mid-continent granite-rhyolite source with transport through or along the eroding Grenville orogen.

Our samples are largely dominated by zircons in the ~900-1,400 Ma range and roughly resemble the detrital zircon data for Paleozoic sediments in the northern Appalachian foreland (Middle Ordovician Austin Glen Member of the Normanskill Formation and Lower Silurian Shawangunk Formation; Gray and Zeitler, 1997; McLennan et al., 2001) and Newfoundland Humber Zone basal sedimentary units (Bradore and Summerside Formations; Cawood and Nemchin, 2001). They contrast markedly with northern Appalachian and Florida basement samples that are largely devoid of Grenvillian detrital zircons (Karabinos and Gromet, 1993; Mueller et al., 1994;

Murphy and Hamilton, 2000; Samson et al., 2001). Except for the eastern Inner Piedmont, our data essentially lack the Late Proterozoic-Early Cambrian component of the Gondwanan terranes and show a reasonable overlap with the age distributions constructed for the southern Grenville by Cawood and Nemchin (2001 and references therein). The post-Grenvillian detrital zircon ages could represent sediment input from one or more of the following: pan-African crustal fragments (e.g., Carolina terrane), Amazonian Brasiliano detritus (Keppie et al., 1998), late Neoproterozoic rift-related igneous rocks (e.g., Crossnore plutons or Catoctin Formation equivalents; Cawood and Nemchin, 2001), or Ordovician magmatic rocks (eastern Inner Piedmont only). Detrital zircon data for the Dahlonega gold belt and the single central Blue Ridge sample are distinct due to an Archean component in each and an early Middle Proterozoic age population in the Dahlonega gold belt. Dahlonega gold belt samples represent the best candidates for a mixed Laurentian and Gondwanan affinity; however, this is difficult to explain since these terranes are structurally beneath the eastern Blue Ridge and western Inner Piedmont which are most likely derived from Laurentia. One possibility is that the sediments of the Dahlonega gold belt and associated Ordovician arcs are younger than the surrounding sediments of the Chattahoochee and Hayesville-Soque River thrust sheets and reflect a different sediment transport direction and/or sources not exposed during initial rifting.

Surface geologic data from carbonate horses in the Brevard fault zone (Hatcher et al., 1973), matching Valley and Ridge reflector characteristics with those beneath the Brevard fault zone (Clark et al., 1978), and regional seismic reflection data (Cook et al., 1980; Costain et al., 1989) from the Inner Piedmont of Georgia and South Carolina place the crystalline thrust sheets of the eastern Blue Ridge and Inner Piedmont above Valley and Ridge carbonate and clastic rocks. Seismic data from the Pine Mountain block and vicinity (Nelson et al., 1987) provide evidence of Valley and Ridge-type rocks on

basement to the northwestern edge of the block. The early accretion of an exotic Pine Mountain block to the Laurentian margin with its Grenville basement and Paleozoic clastic-carbonate cover, followed by the development of high and low temperature Alleghanian shear zones (Steltenpohl et al., 1992; Student and Sinha, 1992; Steltenpohl and Kunk, 1993) and final detachment along the master Appalachian décollement beneath the window is compatible with the available data (Hooper and Hatcher, 1988; McBride et al., 2001).

SUMMARY

Laurentian crustal affinity is favored here for paragneisses in the southern Appalachian Blue Ridge and western Inner Piedmont. This proposal is based on: the presence and availability of eastern North America cratonic and basement material with the same ages found in southern Appalachian detrital zircons; favorable overlap of Nd isotopic values for southern Appalachian metasedimentary rocks and Grenvillian basement, and the paucity of distinctly Gondwanan (2.0-2.4 Ga) detrital zircons. Laurentian provenance requires that the Iapetus ocean basin was isolated from west Gondwana from the time of Rodinian rifting until the Middle Ordovician, sources include early Middle Proterozoic rocks from the mid-continent granite-rhyolite province or less likely the Mars Hill terrane, that the Pine Mountain block is either entirely exotic (inclusive of the Grenville basement) or represents a significantly further traveled fragment of Laurentia, and that the eastern Blue Ridge and western Inner Piedmont paragneisses are time-transgressive or rift facies equivalents of the western Blue Ridge paragneisses.Gondwanan affinity requires that these sediments were deposited proximal to a Grenville belt in western Gondwana. A mixed provenance is plausible for the Dahlonega gold belt but creates significant tectonic and depositional issues due its location between and beneath terranes that have connections to Laurentia.

ACKNOWLEDGMENTS

Chris Coath, Kevin McKeegan, and Mark Harrison provided invaluable assistance with the UCLA IMP. Joe Wooden and Anders Meibom provided operational, in addition to interpretive, assistance with the Stanford University IMP. Members of the North Carolina Geological Survey (Leonard Weiner, Carl Merschat, and Mark Carter) and South Carolina Geological Survey (Butch Maybin) are gratefully acknowledged for accompanying the authors on many of our sampling trips and for numerous conversations in the field regarding this work. NSF grants EAR-9814800 to R.D. Hatcher and EAR-9814801 to C.F. Miller funded this research. Review and comments by Mark Steltenpohl and Stephen Kish improved the focus and quality of this manuscript.

REFERENCES CITED

Abbott, R.N., Jr., and Raymond, L.A., 1984, The Ashe metamorphic suite, northwest North Carolina: Metamorphism and observations on geologic history: American Journal of Science, v. 284, p. 350-375.

Aleinikoff, J.N., Zartman, R.E., Walter, M., Rankin, D.W., Lyttle, P.T., and Burton, W.C., 1995, U-Pb ages of metarhyolites of the Catoctin and Mount Rogers Formations, central and southern Appalachians: Evidence for two phases of Iapetian rifting: American Journal of Science, v. 295, p. 428-454.

Astini, R.A., Benedetto, J.L., and Vaccari, N.E., 1995, The early Paleozoic evolution of the Argentine Precordillera as a Laurentian rifted, drifted and collided terrane: A geodynamic model: Geological Society of America Bulletin, v. 107, p. 253-273.

Bacon, C.R., Persing, H.M., Wooden, J.L., and Ireland, T.R., 2000, Late Pleistocene granodiorite beneath Crater Lake caldera, Oregon, dated by ion microprobe: Geology, v. 28, p. 467-470.

Badger, R.L., and Sinha, A.K., 1988, Age and Sr isotopic signature of the Catoctin volcanic province: Implications for subcrustal mantle evolution: Geology, v. 16, p. 692-695.

Bartholomew, M.J., 1992, Structural characteristics of the Late Proterozoic (post-Grenville) continental margin of the Laurentian craton, *in* Bartholomew, M.J., Hyndman, D.W., Mogk, D.W., and Mason, R., eds., Basement Tectonics 8: Characterization and comparison of ancient and Mesozoic continental margins—Proceedings of the 8th international conference on basement tectonics: Dordrecht,

The Netherlands, Kluwer Academic Publishers, p. 443-467.
Bartholomew, M.J., and Lewis, S.E., 1988, Peregrination of Middle Proterozoic massifs and terranes within the Appalachian Orogen, Eastern U.S.A., *in* Martinez-Garcia, E., ed., Geology of the Iberian Massif with communications presented at the International Conference on Iberian terranes and their regional correlation: Trabajos de Geologia, University of Oviedo, Spain, v. 17, p. 155-165.
Bartholomew, M.J., and Lewis, S.E., 1992, Appalachian Grenville masifs: Pre-Appalachian translational tectonics, *in* Mason, R., ed., Basement Tectonics 7—Proceedings of the seventh International conference: Dordrecht, The Netherlands, Kluwer Academic Publishers, p. 363-374.
Berger, S., Cochrane, D., Simons, K., Savov, I., Ryan, J.G., and Peterson, V.L., 2001, Insights from rare earth elements into the genesis of the Buck Creek complex, Clay County, NC: Southeastern Geology, v. 40, p. 201-212.
Bird, J.M., and Dewey, J.F., 1970, Lithosphere plate: Continental margin tectonics and the evolution of the Appalachian orogen: Geological Society of America Bulletin, v. 81, p. 1031-1060.
Borrello, A.V., 1971, The Cambrian of South America, *in* Holland, D.H., ed., Cambrian of the New World: London, New York, Wiley-Intersicence, p. 385-438.
Brewer, M.C., and Thomas, W.A., 2000, Stratigraphic evidence for Neoproterozoic-Cambrian two-phase rifting of southern Laurentia: Southeastern Geology, v. 39, p. 91-106.
Carrigan, C.W., Miller, C.F., Fullagar, P.D., Hatcher, R.D., Jr., Bream, B.R., and Coath, C.D., in press, Ion microprobe age and geochemistry of southern Appalachian basement, with implications for Proterozoic and Paleozoic reconstructions: Precambrian Research.
Carroll, D., Neuman, R.B., and Jaffe, H.W., 1957, Heavy minerals in arenaceous beds in parts of the Ocoee Series, Great Smoky Mountains, Tennessee: American Journal of Science, v. 255, p. 175-193.
Casquet, C., Baldo, E., Pankhurst, R.J., Rapela, C.W., Galindo, C., Fanning, C.M., and Saavedra, J., 2001, Involvement of the Argentine Precordillera terrane in the Famatinian mobile belt: U-Pb SHRIMP and metamorphic evidence from the Sierra de Pie de Palo: Geology, v. 29, p. 703-706.
Cawood, P.A., and Nemchin, A.A., 2001, Paleogeographic development of the east Laurentian margin: Constraints from U-Pb dating of detrital zircons in the Newfoundland Appalachians: Geological Society of America Bulletin, v. 113, p. 1234-1246.
Cawood, P.A., McCausland, P.J.A., and Dunning, G.R., 2001, Opening Iapetus: Constraints from the Laurentian margin in Newfoundland: Geological Society of America Bulletin, v. 113, p. 443-453.
Clark, H.B., Costain, J.K., and Glover, L., III, 1978, Structural and seismic reflection studies of the Brevard ductile deformation zone near Rosman, North Carolina: American Journal of Science, v. 278, p. 419-441.
Coler D.G., Wortman, G.L., Samson, S.D., Hibbard, J.P., and Stern, R., 2000, U-Pb

geochronologic, Nd isotopic, and geochemical evidence for the correlation of the Chopawamsic and Milton terranes, Piedmont zone, southern Appalachian orogen: Journal of Geology, v. 108, p. 363-380.
Cook, F.A., Brown, L.D., and Oliver, J.E., 1980, The southern Appalachians and the growth of continents: Scientific American, v. 243, p. 156-168.
Costain, J.K., Hatcher, R.D., Jr., and Çoruh, C., 1989, Appalachian ultradeep core hole (ADCOH) project site investigation regional seismic lines and geologic interpretation, Plate 8 in Bally, A.W., and Palmer, A.R., eds., The geology of North America: An overview, The geology of North America, v. A, and *in* Hatcher, R. D., Jr., Thomas, W. A., and Viele, G. W., eds., The Appalachian-Ouachita orogen in the United States: Boulder, Colorado, Geological Society of America, The Geology of North America, v. F2.
Dalla Salda, L.H., Cingolani, C., and Varela, R., 1992, Early Paleozoic orogenic belt of the Andes in southwestern South America: Result of Laurentia-Gondwana collision: Geology, v. 20, p. 617-620.
Dalziel, I.W.D., 1991, Pacific margins of Laurentia and East Antarctica-Australia as a conjugate rift pair: Evidence and implications from an Eocambrian supercontinent: Geology, v. 19, p. 598-601.
Dalziel, I.W.D., 1992, On the organization of American plates in the Neoproterozoic and the breakout of Laurentia: GSA Today, v. 2, p. 237-241.
Dalziel, I.W.D., 1997, Neoproterozoic-Paleozoic geography and tectonics: Review, hypothesis, environmental speculation: Geological Society of America Bulletin, v. 109, p. 16-42.
Dalziel, I.W.D., Dalla Salda, L.H., and Gahagan, L.M., 1994, Paleozoic Laurentia-Gondwana interaction and the origin of the Appalachian-Andean mountain system: Geological Society of America Bulletin, v. 106, p. 243-252.
Dalziel, I.W.D., Mosher, S., and Gahagan, L.M., 2000, Laurentia-Kalahari collision and the assembly of Rodinia: Journal of Geology, v. 108, p. 499-513.
Degraff-Surpless, K., Graham, S.A., Wooden, J.L., and McWilliams, M.O., 2002, Detrital zircon provenance analysis of the Great Valley Group, California: Evolution of an arc-forearc system: Geological Society of America Bulletin, v. 114, p. 1564-1580.
DePaolo, D., 1981, Neodymium isotopes in the Colorado Front Range and crust-mantle evolution in the Proterozoic: Nature, v. 291, p. 193-196.
Dodson, M.H., Compston, W., Williams, I.S., and Wilson, J.F., 1988, A search for ancient detrital zircons in Zimbabwean sediments: Journal of the Geological Society, London, v. 145, p. 977-983.
Fritz, W. J., Hatcher, R. D., Jr., and Hopson, J. L., ed., 1989, Geology of the eastern Blue Ridge of northeast Georgia and the adjacent Carolinas: Georgia Geological Society Guidebooks, v. 9, 199 p.
Fullagar, P.D., 2002, Evidence for Early Mesoproterozoic (and older?) crust in the southern and central Appalachians of North America: Gondwana Research, v. 5, p. 197-203.

Fullagar, P.D., and Gulley, G.L., Jr., 1999, Pre-Grenville uranium-lead zircon age for the Carvers Gap Gneiss in the western Blue Ridge of North Carolina-Tennessee: Geological Society of America Abstracts with Programs, 31, no. 3, p. 16.

Fullagar, P.D., Goldberg, S.A., and Butler, J.R., 1997, Nd and Sr isotopic characterization of crystalline rocks from the southern Appalachian Piedmont and Blue Ridge, North and South Carolina: *in* Sinha, A. K., Whalen, J. B., and Hogan, J. P., eds., The Nature of Magmatism in the Appalachian Orogen: Boulder Colorado, Geological Society of America Memoir 191 p. 165-179.

Goldberg, S.A., Butler, J.R., and Fullagar, P.D., 1986, The Bakersville dike swarm: Geochronology and petrogenesis of Late Proterozoic basaltic magmatism in the southern Appalachian Blue Ridge: American Journal of Science, v. 286, p. 403-430.

Goldsmith, R., and Secor, D.T., Jr., 1993, Proterozoic rocks of accreted terranes in the eastern United states, *in* Reed, J.C., Jr., Bickford, M.E., Jr., Houston, R.S., Link, P.K., Rankin, D.W., Sims, P.K., and Van Schmus, W.R., eds., Precambrian: Conterminous United States: Boulder, Colorado, Geological Society of America, The Geology of North America, v. C-2, p. 422-439.

Gray, M.B., and Zeitler, P.K., 1997, Comparison of clastic wedge provenance in the Appalachian foreland using U/Pb ages of detrital zircons: Tectonics, v. 16, p. 151-160.

Hadley, J.B., 1970, The Ocoee Series and its possible correlatives, *in* Fisher, G.W., Pettijohn, F.P., Reed, J.C., Jr., and Weaver, K.N., eds., Studies of Appalachian geology: Central and southern: New York, John Wiley and Sons, p. 247-260.

Hatcher, R.D., Jr., 1969, Stratigraphy, petrology and structure of the low rank belt and part of the Blue Ridge of northwesternmost South Carolina: South Carolina Division of Geology, Geologic Notes, v. 13, p. 105-141.

Hatcher, R.D., Jr., 1978, Tectonics of the western Piedmont and Blue Ridge, southern Appalachians: Review and speculation: American Journal of Science, v. 278, p. 276-304.

Hatcher, R.D., Jr., 1979, The Coweeta Group and Coweeta syncline: major feature of the North Carolina-Georgia Blue Ridge: Southeastern Geology, v. 21, no. 1, p. 17-29.

Hatcher, R.D., Jr., 1984, Southern and central Appalachian basement massifs, *in* Bartholomew, M.J., ed., The Grenville event in the Appalachians and related topics: Boulder, Colorado, Geological Society of America Special Paper 194, p. 149-153.

Hatcher, R.D., Jr., 1987, Tectonics of the southern and central Appalachian internides: Annual Review of Earth and Planetary Science, v. 15, p. 337-362.

Hatcher, R.D., Jr., 1988, Bedrock geology and regional geologic setting of Coweeta Hydrologic Laboratory in the eastern Blue Ridge, with some discussion of Quaternary deposits and structural controls of topography, *in* Swank, W. T., and Crossley, D. A., Jr., eds., Coweeta Symposium Volume 66: New York, Springer-Verlag, p. 81-92.

Hatcher, R.D., Jr., 1989, Tectonic synthesis of the U.S. Appalachians, Chapter 14, *in* Hatcher, R.D., Jr., Thomas, W.A., and Viele, G.W., eds., The Appalachian-Ouachita orogen in the United States: Boulder, Colorado, Geological Society of America, The

Geology of North America, v. F-2, p. 511-535.
Hatcher, R.D., Jr., and Acker, L.L., 1984, Geology of the Salem quadrangle, South Carolina: South Carolina Geological Survey MS-26, 23 p., 1:24,000 scale.
Hatcher, R.D., Jr., and Bream, B.R., eds., 2002, Inner Piedmont tectonics focused mostly on detailed studies in the South Mountains and the southern Brushy Mountains, North Carolina: Carolina Geological Society Guidebook, North Carolina Geological Survey, 145 p.
Hatcher, R. D., Jr., Price, V., Jr., and Snipes, D.S., 1973, Analysis of chemical and paleotemperature data from selected carbonate rocks of the southern Appalachians: Southeastern Geology, v. 15, p. 55-70.
Hatcher, R.D., Jr., Osberg, P.H., Drake, A.A., Jr., Robinson, P., and Thomas, W.A., 1990, Tectonic map of the U.S. Appalachians, *in* Hatcher, R.D., Jr., Thomas, W.A., and Viele, G.W., eds., The Appalachian-Ouachita orogen in the United States: Boulder, Colorado, Geological Society of America, The Geology of North America, v. GNA-F-2.
Hatcher, R.D., Jr., Hooper, R.J., McConnell, K.I., Heyn, T., and Costello, J.O., 1988, Geometric and time relationships between thrusts in the crystalline southern Appalachians, *in* Mitra, G. and Wojtal, S., eds., Appalachian thrusting: Geological Society of America Special Paper 222, p. 185-196.
Heatherington, A.L., Steltenpohl, M.G., Yokel, L.S., and Mueller, P.A., 1997, Ages of detrital zircons from the Pine Mountain and Inner Piedmont terranes and the Valley and Ridge Province; implications for Neoproterozoic tectonics of the southern Laurentian margin: Geological Society of America Abstracts with Programs, v. 29, no. 6, p. 432.
Heyn, T., 1984, Stratigraphic and structural relationships along the southwestern flank of the Sauratown Mountains anticlinorium (unpublished M.S. thesis): Columbia, University of South Carolina, 192 p.
Hibbard, J.P., and Samson, S.D., 1995, Orogenesis exotic to the Iapetan cycle in the southern Appalachians, *in* Hibbard, J.P., van Staal, C.R., and Cawood, P.A., eds., Current perspectives in the Appalachian-Caledonian orogen: Geological Society of Canada Special Paper 41, p. 191-205.
Hoffman, P.F., 1991, Did the breakout of Laurentia turn Gondwanaland inside-out?: Science, v. 252, p. 1409-1412.
Hooper, R.J., and Hatcher, R.D., Jr., 1988, Pine Mountain terrane, a complex window in the Georgia and Alabama Piedmont: Evidence from the eastern termination: Geology, v. 16, p. 307-310.
Hopson, J.L., and Hatcher, R.D., Jr., 1988, Structural and stratigraphic setting of the Alto allochthon, northeast Georgia: Geological Society of America Bulletin, v. 100, p. 339-350.
Horton, J.W., Jr., and McConnell, K.I., 1991, The western Piedmont, *in* Horton, J.W., Jr., and Zullo, V.A., eds., The Geology of the Carolinas: Knoxville, Tennessee, The University of Tennessee Press, p. 36-58.
Horton, J.W., Jr., Drake, A.A., Jr., and Rankin, D.W., 1989, Tectonostratigraphic terranes

and their Paleozoic boundaries in the central and southern Appalachians, *in* Dallmeyer, R.D., ed., Terranes in the Circum-Atlantic Paleozoic orogens: Geological Society of America Special Paper 230, p. 213-245.

Karabinos, P., and Gromet, P., 1993, Application of single-grain zircon evaporation analyses to detrital grain studies and age discrimination in igneous suites: Geochimica et Cosmochimica Acta, v. 57, p. 4257-4267.

Keppie, J.D., and Ortega-Gutiérrez, F., 1999, Middle American Precambrian basement: A missing piece of the reconstructed 1-Ga orogen, *in* Ramos, V.A., and Keppie, J.D., eds., Laurentia-Gondwana connections before Pangea: Geological Society of America Special Paper 336, p. 199-210.

Keppie, J.D., and Ramos, V.A., 1999, Odyssey of terranes in the Iapetus and Rheic oceans during the Paleozoic, *in* Ramos, V.A., and Keppie, J.D., eds., Laurentia-Gondwana connections before Pangea: Boulder, Colorado, Geological Society of America Special Paper 336, p. 267-276..

Keppie, J.D., Dostal, J., Murphy, J.B., and Nance, R.D., 1996, Terrane transfer between eastern Laurentia and western Gondwana in the early Paleozoic: Constraints on global reconstructions, *in* Nance R.D., and Thompson, M.D., eds., Avalonian and related peri-Gondwanan terranes of the Circum-North Atlantic: Boulder, Colorado, Geological Society of America Special Paper 301, p. 369-380.

Keppie, J.D., Davis, D.W., and Krogh, T.E., 1998, U-Pb geochronological constraints on Precambrian stratified units in the Avalon composite terrane of Nova Scotia, Canada: tectonic implications: Canadian Journal of Earth Sciences, v. 35, p. 222-236.

King, P.B., Hadley, J.B., Neuman, R.B., and Hamilton, W., 1958, Stratigraphy of Ocoee series, Great Smoky Mountains, Tennessee and North Carolina: Geological Society of America Bulletin, v. 69, p. 947-966.

Kish, S.A., Hanley, T.B., and Schamel, S., eds., 1985, Geology of the southwestern Piedmont of Georgia: Geological Society of America Annual Meeting, Field Trip Guide, 47 p.

McBride, J.H., Hatcher, R.D., Jr., and Stephenson, W.J., 2001, Toward reconciliation of seismic reflection and field geologic mapping from the Pine Mountain Belt; preliminary results: Geological Society of America Abstracts with Programs, v. 33, no. 2, p. 74.

McConnell, K.I., 1988, Geology of the Sauratown Mountains anticlinorium: Vienna and Pinnacle 7.5 minute quadrangles, *in* Hatcher, R.D., Jr., ed., Structure of the Sauratown Mountains window, North Carolina: Raleigh, North Carolina, North Carolina Geological Survey, Carolina Geological Society field trip guidebook, p. 51-66.

McLennan, S.M., Bock, B., Compston, W., Hemming, S.R., and McDaniel, D.K., 2001, Detrital zircon geochronology of Taconian and Acadian foreland sedimentary rocks in New England: Journal of Sedimentary Research, v. 71, p. 305-317.

Merschat, C.E., and Carter, M.W., 2002, Bedrock geologic map of the Bent Creek Research and Demonstration Forest, Southern Research Station, USDA Forest Service, including the North Carolina Arboretum and a portion of the Blue Ridge

Parkway: North Carolina Geological Survey Geologic Map Series-9, 1:12,000 scale.
Miller, C.F., Hatcher, R.D., Jr., Ayers, J.C., Coath, C.D., and Harrison, T.M., 2000, Age and zircon inheritance of eastern Blue Ridge plutons, southwestern North Carolina and northeastern Georgia, with implications for magma history and evolution of the southern Appalachian orogen: American Journal of Science, v. 300, p. 142-172.
Monrad, J.R., and Gulley, G.L., 1983, Age and P-T conditions during metamorphism of granulite-facies gneisses, Roan Mountain, NC-TN, *in* Lewis, S.E., ed., Geological investigations in the Blue Ridge of northwestern North Carolina: Carolina Geological Society Field Trip Guidebook, p. 41-51.
Montes, C., and Hatcher, R.D., Jr., 1999, Documenting Late Proterozoic rifting in the Ocoee basin, western Blue Ridge, North Carolina: Southeastern Geology, v. 39, p. 37-50.
Mueller, P.A., Wooden, J.L., and Nutman, A.P., 1992, 3.96 Ga zircons from an Archean quartzite, Beartooth Mountains, Montana: Geology, v. 20, p. 327-330.
Mueller, P.A., Heatherinton, A.L., Wooden, J.L., Shuster, R.D., Nutman, A.P., and Williams, I.S., 1994, Precambrian zircons from the Florida basement: A Gondwanan connection: Geology, v. 22, p. 119-122.
Mueller, P.A., Kozuch, M., Heatherington, A.L., Wooden, J.L., Offield, T.W., Koeppen, R.P., Klein, T.L., and Nutman, A.P., 1996, Evidence for Mesoproterozoic basement in the Carolina terrane and speculations on its origin, *in* Nance, R.D., and Thompson, M.D., eds., Avalonian and related peri-Gondwanan terranes of the Circum-North Atlantic: Boulder, Colorado, Geological Society of America Special Paper 304, p. 207-217.
Murphy, J.B., and Hamilton, M.A., 2000, Orogenesis and basin development: U-Pb detrital zircon age constraints on evolution of the late Paleozoic St. Marys basin, Central mainland Nova Scotia: Journal of Geology, v. 108, p. 53-71.
Nance, R.D., and Murphy, J.B., 1994, Contrasting basement isotopic signatures and the palinspastic restoration of peripheral orogens: Example from the Neoproterozoic Avalonian-Cadomian belt: Geology, v. 22, p. 617-620.
Nelson, A.E., and Gillon, K.A., 1985, Stratigraphic nomenclature in the Richard Russell and Helen thrust sheet, north Georgia, *in* Contributions to Stratigraphy, 1984: U.S. Geological Survey Bulletin No. 1605-A, p. A59-A62.
Nelson, K.D., Arnow, M., Giguere, M., and Schamel, S., 1987, Normal-fault boundary of an Appalachian basement massif: Results of COCORP profiling across the Pine Mountain Belt in western Georgia: Geology, v. 15, p. 832-836.
Paces, J.B., and Miller, J.D., 1993, Precise U-Pb age of Duluth complex and related mafic intrusions, northeastern Minnesota: Geochronological insights into physical, petrogenetic, paleomagnetic, and tectonomagmatic processes associated with the 1.1 Ga Mid-Continent rift system: Journal of Geophysical Research, v. 98, p. 13997-14103.
Payolla, B.L., Bettencourt, J.S., Kozuch, M., Leite, W.B., Fetter, A.H., and Van Schmus, W.R., 2002, Geological evolution of the basement rocks in the east-central part of the Rondônia Tin Province, SW Amazonian craton, Brazil: U-Pb and Sm-Nd

isotopic constraints: Precambrian Research, v. 119, p. 141-169.
Quidelleur, X., Grove, M., Lovera, O.M., Harrison, T.M., Yin, A., and Ryerson, F.J., 1997, Thermal evolution and slip history of the Renbu Zedong thrust, southeastern Tibet: Journal of Geophysical Research, v. 102, p. 2659-2679.
Ramos, V.A., Jordan, T.E., Allmendinger, R.W., Mpodozis, C., Kay, S.M., Cortes, M., and Palma, M., 1986, Paleozoic terranes of the central Argentine-Chilean Andes: Tectonics, v. 5, p. 855-880.
Ramos, V.A., Dallmeyer, R.D., and Vujovich, G., 1998, Time constraints on the early Palaeozoic docking of the Precordillera, central Argentina, *in* Pankhurst, R.J., and Rapela, C.W., eds., The proto-Andean margin of Gondwana: London, Geological Society Special Publication 142, p. 143-158.
Rankin, D.W., 1994, Continental margin of the eastern United States: Past and present, *in* Speed, R.C., ed., Phanerozoic Evolution of North American continent-ocean transitions: Boulder, Colorado, Geological Society of America, DNAG Continent-Ocean Transect Volume, p. 129-218.
Rankin, D.W., Drake, A.A., Glover, L., III, Goldsmith, R., Hall, L.M., Murray, D.P., Ratcliffe, N.M., Read, J.F., Secor, D.T., Jr., and Stanley, R.S., 1989, Pre-orogenic terranes, *in* Hatcher, R.D., Jr., Thomas, W.A., and Viele, G.W., eds., The Appalachian-Ouachita orogen in the United States: Boulder, Colorado, Geological Society of America, The Geology of North America, v. F-2, p. 7-100.
Rast, N., and Kohles, K.M., 1986, The origin of the Ocoee Supergroup: American Journal of Science, v. 286, p. 593-616.
Rogers, J.J.W., 1996, A history of the continents in the past three billion years: Journal of Geology, v. 104, p. 91-107.
Samson, S.D., Hibbard, J.P., and Wortman, G.L., 1995, Nd isotopic evidence for juvenile crust in the Carolina terrane, southern Appalachians: Contributions to Mineralogy and Petrology, v. 121, p. 171-184.
Samson, S.D., Secor, D.T., and Hamilton, M.A., 2001, Wandering Carolina: Tracking exotic terranes with detrital zircons: Geological Society of America Abstracts with Programs, v. 33, no. 6, p. 263.
Schamel, S., Hanley, T.B., and Sears, J.W., 1980, Geology of the Pine Mountain window and adjacent terranes in the Piedmont province of Alabama and Georgia: Geological Society of America, Southeastern Section Meeting Guidebook, 69 p.
Sears, J.W., Cook, R.B., and Brown, D.E., 1981, Tectonic evolution of the western part of the Pine Mountain window and adjacent Inner Piedmont province, in Sears, J.W., ed., Contrasts in tectonic style between the Inner Piedmont terrane and the Pine Mountain window: Alabama Geological society 18th Annual Field Trip Guidebook, p. 1-13.
Secor, D.T., Samson, S.L., Snoke, A.W., and Palmer, A.R., 1983, Confirmation of the Carolina slate belt as an exotic terrane: Science, v. 221, p. 649-651.
Settles, D.J., Bream, B.R., and Hatcher, R.D., Jr., 2001, The Sally Free mafic complex and associated mafic rocks of the Dahlonega gold belt: Evidence of Ordovician arc volcanism and intrusion northwest of Dahlonega, Georgia: Geological Society of

America Abstracts with Programs, v. 33, no. 6, p. 262.
Simpson, E.L., and Eriksson, K.A., 1989, Sedimentology of the Unicoi Formation in southern and central Virginia; evidence for late Proterozoic to Early Cambrian rift-to-passive margin transition: Geological Society of America Bulletin, v. 101, p. 42-54.
Simpson, E.L., and Sundberg, F.A., 1987, Early Cambrian age for synrift deposits of the Chilhowee Group of southwestern Virginia: Geology, v. 15, p. 123-126.
Sinha, A.K., Hogan, J.P., and Parks, J., 1996, Lead isotope mapping of crustal reservoirs within the Grenville superterrane: I. Central and southern Appalachians, American Geophysical Union Monograph 95, p. 293-305.
Spell, T.L., and Norrell, G.T., 1990, The Ropes Creek assemblage: Petrology, geochemistry, and tectnoic setting of an ophiolitic thrust sheet in the southern Appalachians: American Journal of Science, v. 290, p. 811-842.
Steltenpohl, M.G., 1992, The Pine Mountain window of Alabama; basement-cover evolution in the southernmost exposed Appalachians, *in* Bartholomew, M.J., Hyndman, D.W., Mogk, D.W., and Mason, R., eds., Basement Tectonics 8: Characterization and comparison of ancient and Mesozoic continental margins—Proceedings of the 8th International Conference on Basement Tectonics, 1988: Dordrecht, The Netherlands, Kluwer Academic Publishers p. 491-501.
Steltenpohl, M.G., and Kunk, M.J., 1993, $^{40}Ar/^{39}Ar$ thermochronology and Alleghanian development of the southernmost Appalachian Piedmont, Alabama and Southwest Georgia: Geological Society of America Bulletin, v. 105, p. 819-833.
Steltenphol, M.G., Goldberg, S.A., Hanley, T.B., and Kunk, M.J., 1992, Alleghanian development of the Goat Rock fault zone, southernmost Appalachians: Temporal compatibility with the master decollement: Geology, v. 20, p. 845-848.
Steltenpohl, M.G., Heatherington, A.L., and Mueller, P.A., 2001, Our current understanding of the Grenville event in the southernmost Appalachians, Pine Mountain window, Alabama: Geological Society of America Abstracts with Programs, v. 33, no. 6, p. 29.
Stuart-Smith, P.G., Miró, R., Sims, J.P., Pieters, P.E., Lyons, P., Camacho, A., Skirrow, R.G., and Black, L.P., 1999, Uranium-lead dating of felsic magmatic cycles in the southern Sierras Pampeanas, Argentina: Implications for the tectonic development of the proto-Andean Gondwana margin, *in* Ramos, V.A., and Keppie, J.D., eds., Laurentia-Gondwana connections before Pangea: Boulder, Colorado, Geological Society of America Special Paper 336, p. 87-112.
Student, J.J., and Sinha, A.K., 1992, Carboniferous U-Pb ages of zircons from the Box Ankle and Ocmulgee faults, central Georgia: Implications for accretionary models: Geological Society of America Abstracts with Programs, v. 24, no. 2, p. 69.
Su, Q., Goldberg, S.A., and Fullagar, P.D., 1994, Precise U-Pb zircon ages of Neoproterozoic plutons in the southern Appalachian Blue Ridge and their implications for the rifting of Laurentia: Precambrian Research, v. 68, p. 81-95.
Thomas, W.A., 1991, The Appalachian-Ouachita rifted margin of southeastern North America: Geological Society of America Bulletin, v. 103, p. 415-431.

Thomas, W.A., and Astini, R.A., 1996, The Argentine Precordillera; a traveler from the Ouachita Embayment of North American Laurentia: Science, v. 273, p. 752-757.
Thomas, W.A., and Astini, R.A., 1999, Simple-shear conjugate rift margins of the Argentine Precordillera and the Ouachita embayment of Laurentia: Geological Society of America Bulletin, v. 111, p. 1069-1079.
Thomas, C.W., Miller, C.F., Bream, B.R., and Fullagar, P.D., 2001, Origins of mafic-ultramafic complexes of the eastern Blue Ridge, southern Appalachians: Geochronologic and geochemical constraints: Geological Society of America Abstracts with Programs, v. 33, no. 2, p. 66.
Tollo, R.P., and Aleinikoff, J.N., 1996, Petrology and U-Pb geochronology of the Robertson River igneous suite, Blue Ridge Province, Virginia; evidence for multistage magmatism associated with an early episode of Laurentian rifting: American Journal of Science, v. 296, p. 1045-1090.
Vujovich, G.I., and Kay, S.M., 1998, A Laurentian? Grenville-age oceanic arc/back-arc terrane in the Sierra de Pie de Palo, Western Sierra Papeanas, Argentina, *in* Pankhurst, R.J., and Rapela, C.W., eds., The proto-Andean margin of Gondwana: London, Geological Society Special Publication 142, p. 159-179.
Walker, D., Driese, S.G., and Hatcher, R.D., Jr., 1989, Paleotectonic significance of the quartzite of the Sauratown Mountains window, North Carolina: Geology, v. 17, p. 913-917.
Wehr, F., and Glover, L., III, 1985, Stratigraphy and tectonics of the Virginia-North Carolina Blue Ridge; evolution of a late Proterozoic-early Paleozoic hinge zone: Geological Society of America Bulletin, v. 96, p. 285-295.
Williams, H., 1978, Tectonic lithofacies map of the Appalachian orogen: St. John's Memorial University of Newfoundland, Map no. 1, scale 1:1,000,000.
Williams, H., and Hiscott, R.N., 1987, Definition of the Iapetus rift-drift transition in western Newfoundland: Geology, v. 15, p. 1044-1047.
Wortman, G.L., Samson, S.D., and Hibbard, J.P., 1996, Discrimination of the Milton belt and the Carolina terrane in the southern Appalachians: A Nd isotopic approach: Journal of Geology, v. 104, p. 239-247.

PART II

Southern Appalachian Paleozoic orogenesis revised: Geochemical, isotopic, and geochronologic constraints for Neoproterozoic to mid-Paleozoic depositional, magmatic, and tectonic processes

This chapter is a synthesis paper anticipated for submission to a scientific journal. The authors will be Brendan R. Bream, Robert D. Hatcher, Jr., Calvin F. Miller, and Paul D. Fullagar. My contributions to this paper are: (1) most of the writing, (2) sample collection and sample preparation, (3) collection of the ion microprobe data, and (4) integration of the isotopic data collected by P.D. Fullagar. The use of "we" and "our" in the text refers to the co-authors and myself.

ABSTRACT

Southern Appalachian crystalline core paragneisses contain rift and drift facies cover rocks, deposited unconformably on Grenville basement in the western Blue Ridge. These sediments were entirely derived from Laurentia except in the eastern Inner Piedmont, Carolina terrane, and Pine Mountain window. Relatively high initial $^{87}Sr/^{86}Sr$ values between 0.707 and 0.723, Middle to Upper Proterozoic T_{DM} ages, high SiO_2 content, LREE enrichment, low chemical index of alteration values mostly between 41 and 66, and restricted Th/Sc and Zr/Sc values for Laurentian sedimentary and metasedimentary samples further support derivation from Grenvillian rocks like those exposed in the western Blue Ridge. Detrital zircons from the Middle Ordovician (475 Ma) Sevier Shale sample are Grenvillian (1.0 to 1.25 Ga), Middle Proterozoic (1.35 to 1.45 Ga), and Early Proterozoic (1.8 Ga). New U-Pb zircon ages for Ordovician metaplutonic units include the following: Dahlonega gold belt Cane Creek felsic gneiss (482 ± 4 Ma), western Inner Piedmont Dysartsville Tonalite (468 ± 8 Ma), eastern Blue Ridge Kennesaw granitoid (444 ± 11 Ma), western Inner Piedmont Lenoir Quarry Migmatite (450 ± 6 Ma inherited cores; 342 ± 5 Ma and 330 ± 6 Ma metamorphic overgrowths), western Inner Piedmont Poor Mountain Quartzite (459 ± 4 Ma and 445 ± 4 Ma), western Inner Piedmont Toccoa granitoid (449 ± 4 Ma), and western Inner Piedmont Zirconia pegmatite (327 ± 2 Ma). T_{DM} ages between 1.2 and 2 Ga for the Cane Creek, Dysartsville, Kennesaw, and Toccoa granitoids indicate derivation from preexisting Grenvillian and possibly older crust. High initial $_{87}Sr/_{86}Sr$ values for the

Lenoir Quarry Migmatite and Cane Creek, Dysartsville, Kennesaw, and Toccoa granitoids also indicate derivation from preexisting crust. Major Laurentian margin depositional and orogenic events following the breakup of Rodinia and preceeding collision with Africa in the southern Appalachians are divisible into the following: Late Proterozoic to Early Cambrian, Middle Ordovician, Late Silurian, and Late Devonian to Early Carboniferous. Events of the Late Proterozoic to Early Cambrian include rift-related magmatism followed by Laurentian-derived rift and drift facies deposition. Middle Ordovician events related to island arc accretion at the Laurentian margin include creation of the foreland Sevier basin, felsic magmatism, closure of a small ocean, eclogite formation in the eastern Blue Ridge, and granulite facies metamorphism in the central Blue Ridge. New detrital zircon evidence indicates that Late Silurian pelitic and psammitic material in the eastern Inner Piedmont was derived from both the Laurentian margin and Carolina terrane likely at the leading edge of the proximal Carolina terrane. Evidence of the Neoacadian orogenic event (Late Devonian to Early Carboniferous) includes a foreland clastic wedge, pervasive magmatism, and penetrative deformation and metamorphism. Based on these new data and integration with field relationships, revised division of the southern Appalachian crystalline core southeast of the western Blue Ridge into the Cartoogechaye and Cowrock (higher thrust sheets of the central Blue Ridge), Dahlonega gold belt, Tugaloo (eastern Blue Ridge and western Inner Piedmont), Cat Square (eastern Inner Piedmont), and exotic Carolina terranes is justified.

INTRODUCTION

The Appalachian orogen extends from Newfoundland to Alabama and is largely the product of Late Neoproterozoic-Early Cambrian opening and Ordovician to Devonian closing of the Iapetus ocean followed by Carboniferous-Permian closing of the Theic-Rheic ocean. Numerous depositional, magmatic, metamorphic, and deformational events

constructed the southern Appalachian lithotectonic assemblage (Fig. 1). Blue Ridge basement includes igneous and sedimentary rocks deposited, intruded, and metamorphosed during or slightly preceding the Grenville orogeny (e.g., Bartholomew and Lewis, 1984; Ownby et al., in press). The Grenville age of these rocks remains largely undisputed but several have suggested that southern Appalachian Proterozoic basement (or portions thereof) may be allochthonous relative to Laurentian Grenvillian rocks (e.g., Bartholomew and Lewis, 1992; Dalziel et al., 1994; Sinha and McLelland, 1999; Loewy et al., 2002; Carrigan et al., in press; Ownby et al., in press). Despite this possibility, there is little evidence for a large component of non-Laurentian material in all but the most outboard southern Appalachian sedimentary/metasedimentary sequences (e.g., Bream et al., in press; Steltenpohl et al., in press).

Blue Ridge Grenvillian basement is nonconformably overlain by Late Proterozoic (e.g., Grandfather Mountain and Mount Rogers Formations, Snowbird Group, Catoctin Formation) and Paleozoic (e.g., Chilhowee Group) sedimentary and volcanic sequences. Deposition of these thick dominantly sedimentary packages occurred during and mostly following breakup of Rodinia, the timing of which is delimited between 572 and 560 Ma for the central Appalachian Catoctin Formation (Badger and Sinha, 1988; Aleinikoff et al., 1995). An earlier (730 to 760 Ma) unsuccessful Neoproterozoic rifting event has also been documented in the Appalachians (Goldberg et al., 1986; Su et al., 1994; Aleinikoff et al., 1995; Cawood et al., 2001). Deposition of eastern Blue Ridge and western Inner Piedmont metasedimentary sequences is roughly coeval with deposition of more proximal drift facies. Reports by Unrug and Unrug (1990) and Unrug et al. (2000) of Silurian and possibly younger fossils in the Walden Creek Group (Ocoee Supergroup), raises possibilities that complicate existing Ocoee basin depositional concepts (e.g., Rast and Kohles, 1986). If correct, these ages require the Walden Creek Group and part of the upper Great Smoky Group be deposited after the Chilhowee Group rift-to-drift facies and

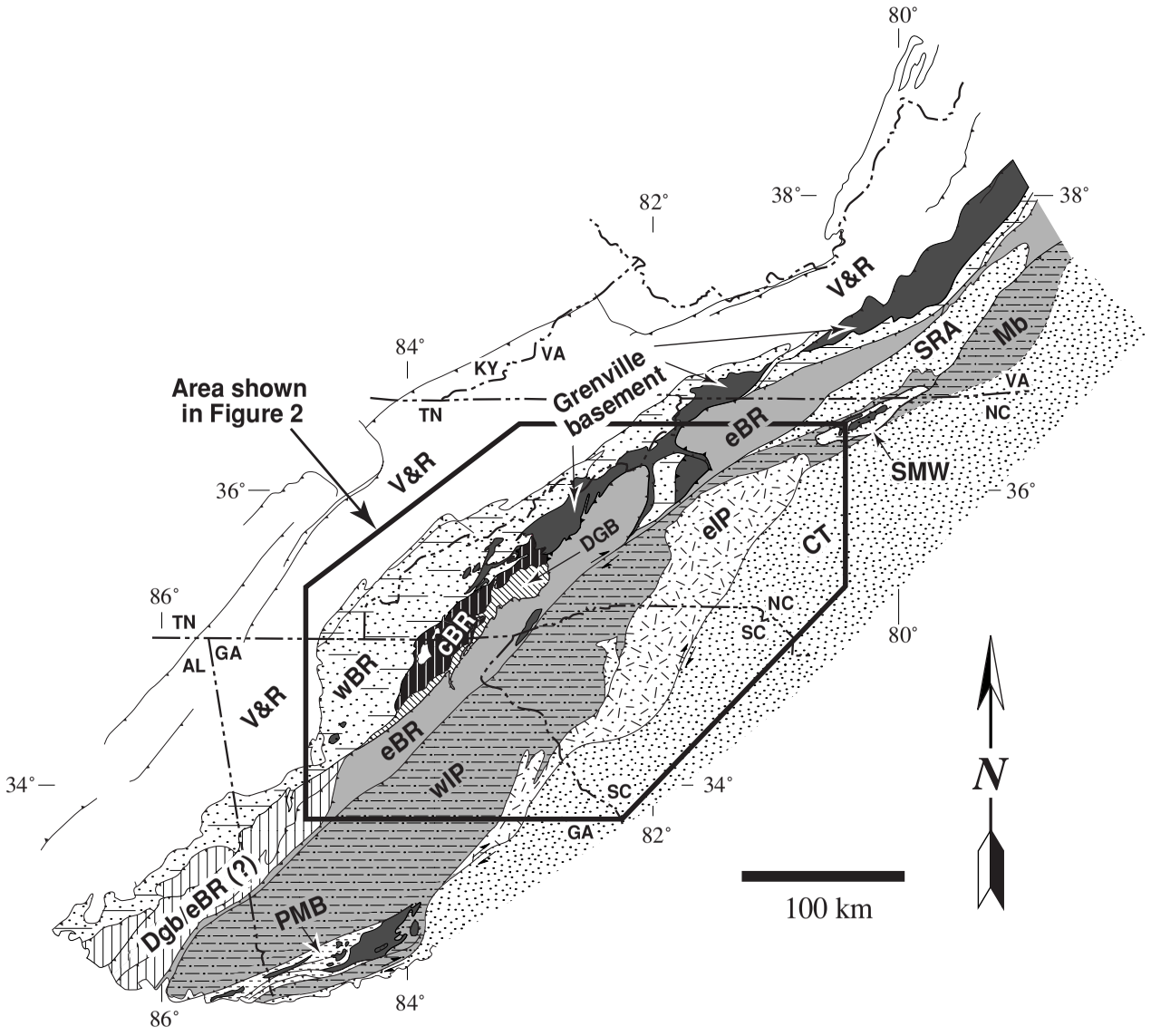

Figure 1. Lithotectonic divisions of the southern Appalachians. Modified from Hatcher et al. (1990). eIP-central and eastern Inner Piedmont; cBR-central Blue Ridge; CT-Carolina terrane; Dgb/DGB-Dahlonega gold belt; eBR-eastern Blue Ridge; Mb-Milton belt; PMB-Pine Mountain Block; SMW-Sauratown Mountains window; SRA-Smith River Allochthon; V&R-Valley and Ridge; wBR-western Blue Ridge; wIP-western Inner Piedmont.

that western Blue Ridge deformation and metamorphism in these units is later than the Taconic and Neoacadian orogenies. Some of the Unrug et al. (2000) sample localities (e.g., Servilla quarry) occur in mapped lower Sandsuck Formation (Walden Creek Group) carbonate that is repeated by a minor fault, but is otherwise in sequence beneath the Chilhowee Group (Carter, 1994; Carter et al., 1995).

Following the breakup of Rodinia, several Paleozoic orogenic events occurred at the margin of eastern North America (present coordinates). Delimiting the timing of these events has led to numerous tectonic scenarios for development of the southern Appalachians (e.g., Brown, 1970; Hatcher, 1987, 1989; Dalla Salda et al., 1992a, 1992b; Hibbard et al., 2002). The tectonic setting, extent, and timing of the Acadian and Neoacadian event(s) remain particularly unconstrained. Most workers have supported Ordovician (Taconic) accretion, metamorphism, and deformation of suspect terranes northwest of the Carolina terrane (e.g., Williams and Hatcher, 1982; Horton et al., 1989), in addition to Ordovician accretion of the Carolina composite terrane (e.g., Vick et al., 1987; Hibbard, 2000). Recent monazite and zircon rim geochronologic data (e.g., Dennis and Wright, 1997; Carrigan et al., 2001), however, suggest a major thermal event ~350 Ma and are cited in support of Devonian (Acadian) accretion of the Carolina terrane (e.g., Hatcher et al., 1999) as proposed earlier (e.g., Hatcher, 1987, 1989).

Our objectives here are to: (1) present new southern Appalachian geochronologic, Nd and Sr isotopic, and geochemical data that will help to constrain many of the uncertainties listed above; (2) compare these data with those from similar studies in this and other parts of the Appalachians, including data from Proterozoic basement, detrital zircons, and Paleozoic plutons; and (3) present an updated Paleozoic model for southern Appalachian orogenesis.

GEOLOGIC SETTING

The crystalline core, consisting of the rited margin, several suspect terranes, and at least two confirmed exotic terranes, comprises most of the southern Appalachians (Figs. 1 and 2). Metamorphism here, rare fossils, and a paucity of modern geochemical and geochronologic data have to date provided only loose constraints on crustal affinity (mostly for assemblages southeast of the Allatoona-Hayesville-Gossan Lead fault). Although Valley and Ridge fossil and stratigraphic records provide a fundamental timeframe for deposition and deformation, crystalline core rocks west of the Carolina terrane are nonfossiliferous and polydeformed. Neoproterozoic to early Paleozoic sedimentary sequences were deposited in a passive margin setting following the successful opening of the Iapetus ocean. Synrift sediments were variably and nonconformably distributed over Grenvillian basement near the margin in a complex series of rift basins (e.g., Thomas, 1991). Proximal to distal rift facies are present in the southern Appalachian Blue Ridge and western Inner Piedmont. These sequences include the Ocoee Supergroup which is largely devoid of volcanic and volcaniclastic rocks, and the Mount Rogers, Grandfather Mountain, Catoctin, and Mechum River Formations that contain rift-related volcanic and volcaniclastic rocks (e.g., Hatcher, 1989; Rankin et al., 1989). Rift sequence thicknesses may locally exceed 10 km (King et al., 1958; Thomas, 1991). The Lower Cambrian Chilhowee Group was deposited both conformably above these rift sediments and and unconformably on Grenvillian basement (e.g., King, 1970; Rankin, 1970). Transition from rift-to-drift sedimentation is preserved in either the upper (Williams and Hiscott, 1987) or lower (Thomas, 1991) Chilhowee Group. Up section from the Chilhowee into the Lower Ordovician is a transgressive sequence of carbonate (Shady Dolomite) then fine-grained siliciclastics that become carbonate to the east (Lower Cambrian Rome Formation and western Middle to Upper Cambrian Conasauga Group) overlain by some 900 m of carbonates (e.g., Upper Cambrian-Lower Ordovician

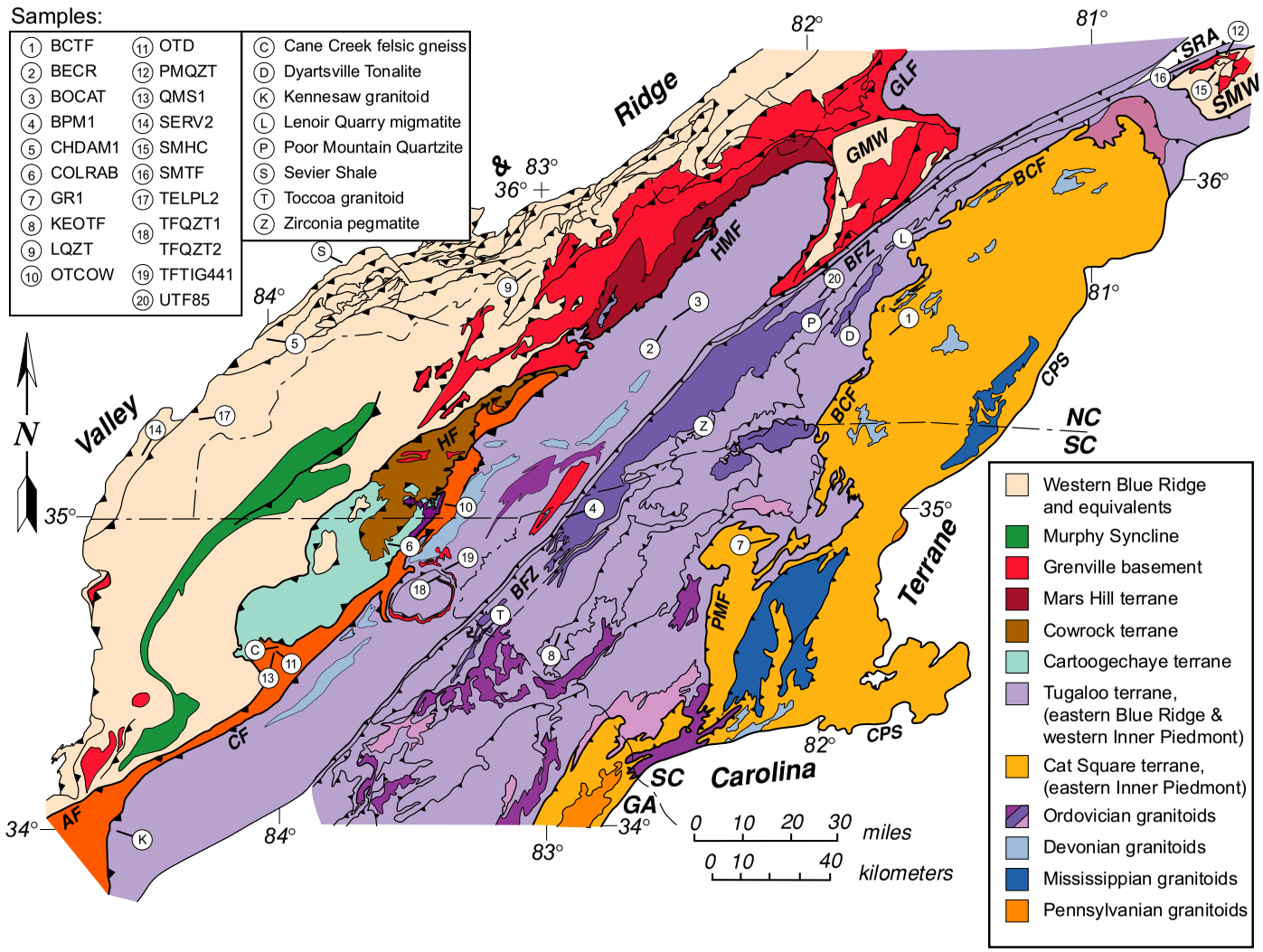

Figure 2. Tectonic map of a portion of the southern Appalachians with sample locations. AF-Allatoona fault; BCF-Brindle Creek fault; BFZ-Brevard fault zone; CF-Chattahoochee fault; CPS-Central Piedmont Suture; HF-Hayesville fault; HMF-Holland Mountain fault; GLF-Gossan Lead fault; PMF-Paris Mountain fault; SMW-Sauratown Mountains window; SRA-Smith River Allochthon. From Hatcher, 2002 and Hatcher et al., in press).

Knox Group). The Middle Ordovician unconformity was succeeded initially by renewed carbonate deposition followed by the diachronous arrival of (e.g., Shanmugam and Lash, 1982) siliciclastics shed from the emerging Taconic highlands. Middle Ordovician foreland siliciclastic sources were located to the east and southeast in most of the central and southern Appalachians (e.g., Shanmugam and Walker, 1978; Shanmugam and Lash, 1982; Drake et al., 1989). In the southern Appalachians, rapid deposition during the Middle Ordovician occurred in the Sevier foreland basin that developed in response to tectonic subsidence (e.g., Walker et al., 1983). Paleogeographic reconstructions for most of the Sevier basin favor early, easterly derivation of clastic turbidite material that followed tectonic uplift related to thrust loading in the source region and westward subsidence followed by basin maturation resulting from tectonic quiescence (Shanmugam and Walker, 1980; Quinlan and Beaumont, 1983). Water depth in the Sevier foreland basin reached a maximum of 800 m with greater than 2500 m of shales and sandstone (Shanmugam and Walker, 1978). The Sevier clastic wedge is comparable with the younger Llandeilo-Caradoc-Ashgill and Llandovery Maritinsburg-Juniata-Tuscarora clastic wedge (greater than 4000 m in the Martinsburg alone: Drake and Epstein, 1967) that occurs predominantly in the central Appalachians but rests atop the Sevier wedge in northeastern Tennessee (Drake et al., 1989). Clastic wedges with an eastern source were also deposited in the Appalachian foreland during the Acadian (Catskill, central Appalachians) and Alleghanian (Appalachian basin, southern and central Appalachians) orogenies.

Older plutonic and metamorphic ages from more internal portions of the southern Appalachians fall between 450 and 480 Ma (Drake et al., 1989). Newer U-Pb zircon data confirm that eastern Blue Ridge and western Inner Piedmont plutons were emplaced within this time frame (Ranson et al., 1999; Vinson, 1999; C.F. Miller et al., 2000; Meschter et al., 2002) and that granulite metamorphism occurred near 470 Ma (Moecher

and Miller, 2000; Moecher et al., in review) in the central Blue Ridge. Eclogite formation in the eastern Blue Ridge also occured in this timeframe at ~460 Ma (B.V. Miller et al., 2000; Stewart and Miller, 2001). Mafic and ultramafic rocks of the Dahlonega gold belt also have Ordovician ages (Thomas, 2001). Eastern Blue Ridge and eastern Inner Piedmont Acadian and Neoacadian granitoids are mostly Late Devonian to Early Carboniferous, 375 to 325 Ma (C.F. Miller et al., 2000; Mapes, 2002). New evidence suggests that one or more widespread thermal-metamorphic events took place between 360 and 320 Ma (Dennis and Wright, 1997; Bream et al., 2000; Mirante and Patino-Douce, 2000; Carrigan et al., 2001; Kohn, 2001; Mirante, 2001; Kalbas et al., 2002). The Neoacadian event(s) is/are largely restricted to the eastern Inner Piedmont and Carolina terrane.

Deformation in the southern and central Appalachian foreland occurred during the Alleghanian orogeny by thin-skinned, west-vergent thrusting of unmetamorphosed Paleozoic sedimentary rocks when Gondwanaland collided with Laurentia pushed in front of the crustal Blue Ridge-Piedmont megathrust sheet. Earlier thrusts in the crystalline core are likewise relatively thin, have a range of displacements, and ultimately are thrust over western Blue Ridge Laurentian basement and cover sequences; timing of thrust emplacement, however, is significantly more difficult to resolve. As in other high-grade terranes, rocks of the southern Appalachian crystalline core were intensely deformed and transposed during peak metamorphic deformational events. Metamorphic grade in the crystalline core reaches granulite facies but is middle to upper amphibolite facies kyanite- to sillimanite-grade assemblages are most common (Butler, 1991). Despite the intense deformation and metamorphism, some primary igneous and sedimentary features (e.g., euhedral megacrysts, rare graded beds, compositional layering, and stratigraphic contacts) have survived.

SAMPLES

Fresh samples were collected at road outcrops, in quarries, and less often in streams. An effort was made to sample well-mapped sedimentary-metasedimentary units and plutons and, where possible, within recognized stratigraphic sequences (Table 1). Metasedimentary sample data used here were obtained from the same material and localities referenced by Bream (2002) and Bream et al. (in press). Metaigneous samples presented here represent previously undated Dahlonega gold belt, eastern Blue Ridge, and western Inner Piedmont units (Fig. 2, Table 1).

Sedimentary and metasedimentary

With the exception of the Sevier Shale, western Blue Ridge, and eastern Inner Piedmont samples, depositional timing of crystalline core samples remains loosely constrained. As previously discussed, successful rifting of Rodinia began with extrusion of the Catoctin Formation volcanic rocks. Based on this constraint and the possibility that successful rifting in the northern Appalachians may have occurred in two pulses, ~570 Ma and between 540 and 535 Ma (Cawood et al., 2001), we chose to estimate the time of deposition at 550 Ma for most samples; deposition was most likely time transgressive however, with deposition beginning around 565 Ma followed by successful rifting and progressively younger deposition eastward on younger oceanic, fragmented continental, or transitional crust. A time transgressive sequence favors early, 565-560 Ma, deposition of the Ocoee Supergroup in the western Blue Ridge followed by later in-sequence deposition into the Ordovician (in northeastern Tennessee, see Hardeman, 1966) and Cambrian, 550-520, Ma deposition of the Tallulah Falls-Ashe Formation in the eastern Blue Ridge. Deposition of the western Inner Piedmont Chauga River Formation may be as young as 490 Ma (Tremadoc). Eastern Inner Piedmont (Cat Square terrane) deposition is constrained by the age of the youngest detrital components (~445 Ma and

Table 1. Sample location and formation association. Coordinates are NAD27 CONUS.

Sample	Figure 2 Location	Formation or unit name	7.5-minute quadrangle	County (State)	Latitude (°N)	Longitude (°W)
Valley and Ridge						
SEV	S	Sevier Shale	Kinzel Springs	Blount (TN)	35.735	83.822
western Blue Ridge						
CHDAM1	5	Walden Creek Group (Ocoee Supergroup)	Tallassee	Blount (TN)	35.548	84.050
LQZT	9	Longarm Quartzite, Snowbird Group (Ocoee Supergroup)	Cove Creek Gap	Haywood (NC)	35.702	83.040
SERV2	14	Sandsuck Formation, Walden Creek Group (Ocoee Supergroup)	McFarland	Polk (TN)	35.248	84.444
TELPL2	17	Dean Formation, Great Smoky Group (Ocoee Supergroup)	Tellico Plains	Monroe (TN)	35.336	84.296
central Blue Ridge						
COLRAB	6	Coleman River Formation	Hightower Bald	Rabun (GA)	34.908	83.612
Dahlonega gold belt						
OTCOW	10	Otto Formation	Prentiss	Macon (NC)	35.060	83.453
OTD	11	Otto Formation	Campbell Mountain	Lumpkin (GA)	34.560	84.074
QMS1	13	Otto Formation	Campbell Mountain	Lumpkin (GA)	34.533	84.018
WIMPY	C	Cane Creek Felsic Gneiss	Campbell Mountain	Lumpkin (GA)	34.576	84.017
eastern Blue Ridge						
BECR	2	Tallulah Falls Formation-Ashe Formation (metagraywacke member)	Dunsmore Mountain	Buncombe (NC)	35.454	82.661
BOCAT	3	Tallulah Falls Formation-Ashe Formation (metagraywacke member)	Asheville	Buncombe (NC)	35.600	82.538
KEN	K	Kennesaw granitoid	Kennesaw	Cobb (GA)	34.018	84.592
TFQZT1	18	Tallulah Falls Formation (quartzite member)	Tiger	Rabun (GA)	34.817	83.424
TFQZT2	18	Tallulah Falls Formation (quartzite member)	Tallulah Falls	Rabun (GA)	34.736	83.391
TFTIG441	19	Tallulah Falls Formation-Ashe Formation (metagraywacke member)	Tiger	Rabun (GA)	34.838	83.422
Sauratown Mountains window						
SMHC	15	Hogan Creek Formation	Siloam	Surry (NC)	36.271	80.602
PMQZT	12	Pilot Mountain Quartzite	Pinnacle	Surry (NC)	36.344	80.482
western Inner Piedmont						
BPM1	4	Chauga River Formation (Brevard-Poor Mountain Transitional member)	Salem	Oconee (SC)	34.916	82.914
VM1782	D	Dysartsville Tonalite	Glenwood	McDowell (NC)	35.549	81.962
KEOTF	8	Tallulah Falls Formation-Ashe Formation (aluminous schist member)	Seneca	Oconee (SC)	34.696	82.879
LVQ1	L	Lenoir Quarry migmatite	Kings Creek	Caldwell (NC)	35.931	81.479
POMTN	P	Poor Mountain Quartzite	Glenwood	McDowell (NC)	35.605	81.955
SMTF	16	Tallulah Falls Formation-Ashe Formation (metagraywacke member)	Copeland	Surry (NC)	36.275	80.732
TOC	T	Toccoa granitoid	Toccoa	Stephens (GA)	Hanson aggreg. quarry	
UTF85	20	Tallulah Falls Formation-Ashe Formation (metagraywacke member)	Marion East	McDowell (NC)	35.644	81.987
ZIRCONIA	Z	Zirconia Pegmatite	Zirconia	Henderson (NC)	35.233	82.446
eastern Inner Piedmont						
BCTF	1	metagraywacke not presently assigned to a formation	Benn Knob	Rutherford (NC)	35.539	81.702
GR1	7	metagraywacke not presently assigned to a formation	Greer	Spartanburg (SC)	34.917	82.139

NAD27 CONUS coordinates

~425 Ma; Bream et al., in press), and the age of the Toluca Granite, ~380 Ma (Mapes, 2002). Toluca Granite bodies occur as small deformed stocks and isolated pods throughout much of the eastern Inner Piedmont. They are likely catazonal plutons because they are concordant and lack contact aureoles like most Inner Piedmont plutons. Deposition of eastern Inner Piedmont psammitic and pelitic material is estimated at 420 Ma, thus providing enough time for burial to depths of sillimanite grade P-T conditions and in-situ melting to produce catazonal plutons. Sample descriptions for metasedimentary units of the Blue Ridge, Dahlonega gold belt, Sauratown Mountains window, and Inner Piedmont are slightly modified from Bream et al. (in press).

Valley and Ridge

One Middle Ordovician Sevier Shale sample was collected in the Tennessee Valley and Ridge from the immediate footwall of the Great Smoky fault (frontal Blue Ridge boundary) (Fig. 2). The sample locality is just northwest of Walland, TN on U.S. 321 in the Guess Creek fault hanging wall, a fault block that was unexposed prior to excavation of the roadcut. Maximum formation thickness NW of this locality is ~700 m (2,100 ft) (Neuman, 1955). Nearby and at the sample locality, this unit consists of cm-scale turbiditic siltstone and calcareous shale with minor calcareous sandstone, some conglomerate (Keith, 1895; Rodgers, 1953; Neuman, 1955; Larson et al., 1989). The time of deposition of this sample is determined as early Llanvirn by graptolites identified from in the *Nemagraptus gracilis* Zone or uppermost *Glyptograptus teretiusculus* Zone (Larson et al., 1989), indicating deposition just above the Middle Ordovician unconformity. This corresponds to a time of deposition of 475 Ma (Drake et al., 1989).

Western Blue Ridge

Samples from the western Blue Ridge are from Ocoee Supergroup rift facies. The basal rift facies nonconformably overlie Grenville basement in the western Blue Ridge (King et al., 1958). One sample is from the Snowbird Group, the oldest Ocoee

Supergroup unit, one is from the Great Smoky Group, and two are from the Walden Creek Group, the youngest unit in the Ocoee Supergroup. The Longarm Quartzite is predominantly feldspathic sandstone that ranges from <100 to 1,000 m thick in the middle of the Snowbird Group (Montes and Hatcher, 1999). The sample is from the Pigeon River Gorge in North Carolina at the westbound rest area on Interstate 40. Upper Ocoee Supergroup rift samples include a medium- to coarse-grained sandstone sample with small conglomeratic interlayers located in the uppermost Dean Formation (Great Smoky Group) on TN 68 southeast of Tellico Plains. Calcareous fine-grained Sandsuck Formation (Walden Creek Group) sandstone was collected at Springtown, TN southeast of Starr Mountain. A matrix-supported polymictic conglomerate from the Sandsuck Formation (Walden Creek Group) was also sampled at Chilhowee Dam on U.S. 129 in southeastern Tennessee. This conglomerate contains large (up to 0.5 m) rounded clasts of mostly milky quartz with subordinate amounts of quartzite, limestone, dolostone, quartz-epidote (from veins) rare granitoid, and black mud (now slate) in a dominantly medium-grained quartz-dominant siliciclastic matrix. Attempts were made during sample preparation to isolate matrix material.

Central Blue Ridge (Cowrock Terrane)

One sample of metasandstone from the central Blue Ridge—Coleman River Formation of Hatcher (1979)—was collected on U.S. 76 west of Clayton, Georgia, less than 1 km east of the Rabun-Towns county line. This unit is the most widely distributed of the Coweeta Group, making up most of the Hayesville-Soque River thrust sheet (Cowrock terrane of Hatcher et al., in press). The coleman River Formation (Hatcher, 1979, 1980) sample was collected on U.S. 76 in northern Georgia. Sampled material is coarsely layered (up to meters thick), well-foliated, migmatitic, fine- to medium-grained metasandstone. It also contains metapelite, calc-silicate, and amphibolite.

Dahlonega gold belt

Three samples were collected from the Otto Formation in the Dahlonega gold belt, a unit consisting of intercalated metapelite and metasandstone (Hatcher, 1988). One sample locality is in the Coweeta Hydrologic Laboratory at Otto, North Carolina, in the footwall of the Shope Fork thrust. Two samples are from the footwall of the Hayesville-Soque River thrust fault in the Allatoona thrust sheet ~2.5 km west and ~7 km west-northwest of Dahlonega, Georgia in the Campbell Mountain 7.5-minute quadrangle. The Otto Formation near Dahlonega, GA (Settles, 2002) has also been mapped as the Helen Member of the Canton Formation by German (1985) and Helen Group by Nelson and Gillon (1985) and Nelson (1991).

Sauratown Mountains window

Both the Hogan Creek Formation and Pilot Mountain Quartzite were sampled in the Sauratown Mountains window. The Hogan Creek Formation consists of metasandstone, pelitic schist, and minor marble in nonconformable contact with Grenville basement orthogneisses of the outer window (Hatcher et al., 1988). The sample is from an abandoned quarry on the Yadkin River ~4 km upstream from Siloam, North Carolina. The Pilot Mountain Quartzite overlies the Sauratown Formation, informally named by Heyn (1984) and formally named by Horton and McConnell (1991), and is also in nonconformable contact with Grenville basement. The Pilot Mountain Quartzite is a well-sorted quartz arenite that preserves primary sedimentary structures (Walker et al., 1989). The Pilot Mountain Quartzite and Sauratown Formation are restricted to the Sauratown Mountains inner window.

Eastern Blue Ridge and western Inner Piedmont (Tugaloo Terrane)

Six samples of Tallulah Falls-Ashe Formation were collected from the Eastern Blue Ridge and western Inner Piedmont (Tugaloo terrane of Hatcher et al., in press). Eastern Blue Ridge Tallulah Falls-Ashe Formation was sampled at a roadcut through

Beaucatcher Mountain in Asheville (NC); ~200 m north of Bent Creek Gap in the Bent Creek Experimental Forest ~15 km southwest of Asheville, North Carolina on the Blue Ridge Parkway (locality is same as sample ts-500 of Merschat and Carter, 2002); and from the north flank of the Tallulah Falls dome on U.S. 23-441 ~5 km south-southwest of Clayton, Georgia. The western Inner Piedmont Tallulah Falls-Ashe Formation was sampled in the Forbush thrust sheet (Heyn, 1984) in a railroad cut on the Yadkin River west the Sauratown Mountains window ~13 km east-northeast of Elkin-Jonesville, North Carolina. A second western Inner Piedmont sample was collected from a roadcut 150 m north of Exit 85 on Interstate 40 south of Marion, North Carolina. A third sample was collected on U.S. 76-123 in the Six Mile thrust sheet at Keowee, South Carolina. All of these samples contain middle to upper amphibolite facies mineral assemblages and are dominantly one-mica (biotite up to 30%), one feldspar (plagioclase) metagraywackes or sillimanite-garnet gneiss (Keowee, South Carolina).

The Tallulah Falls Quartzite was also sampled on U.S. 23-441 at Wiley, Georgia; this sample is medium-grained, locally conglomeratic (vein quartz and both plagioclase and K-feldspar clasts), quartzite located within the Tallulah Falls dome, and at this locality contains upright graded beds (Fritz et al., 1989). The remaining Inner Piedmont sample locality is on South Carolina State Highway 11 where it crosses Lake Keowee (west side), in the westernmost Inner Piedmont (Hatcher and Acker, 1984). This sample consists of metasiltstone with mica-fish and thin metagraywacke interlayers, the Brevard-Poor Mountain transitional member of the Chauga River Formation (Hatcher, 1969, 2002).

Eastern Inner Piedmont (Cat Square Terrane)

The central Inner Piedmont samples are metagraywackes from a metapelite-dominated unit (Hatcher and Bream, 2002). The central Inner Piedmont samples are not currently assigned to a recognized stratigraphy. One sample was collected ~9 km west-

northwest of Casar, North Carolina in Brier Creek and the other sample was collected ~2.5 km south of Duncan, South Carolina near the Duncan Correctional Center. These lithologic units, teh easternmost Inner Piedmont metasedimentary units, are not presently assigned to a recognized stratigraphy (Bier et al., 2002; Merschat and Kalbas, 2002).

Metaigneous Rocks

Cane Creek Felsic Gneiss

This unit is part of the Sally Free mafic complex (Settles et al., 2001; Settles, 2002) located in the Dahlonega gold belt of Georgia. Other units of the Sally Free mafic complex include: hornblende gneiss-metagabbro-amphibolite; amphibolite; and intermediate gneiss. Cane Creek felsic gneiss is foliated, strongly lineated, medium- to coarse-grained, and is locally mylonitic. The sample locality is approximately 2 km south of the Hayesville-Soque River.

Dysartsville Tonalite

The Dysartsville Tonalite of the western North Carolina Inner Piedmont (Bream, 2002) was originally named the Dysartsville pluton by Goldsmith et al. (1988). Several mafic and ultramafic bodies are present in the Dysartsville Tonalite. The Dysartsville Tonalite is massive to foliated, fine- to medium-grained, leucocratic, and contains both granoblastic and lepidoblastic textures.

Kennesaw Granitoid

The Kennesaw granitoid unit is part of the Laura Lake mafic-ultramafic complex in Georgia (McConnell and Abrams, 1984). This unit lies immediately southeast of the Chattahoochee fault, but faults have been mapped near the southeast edge of the Laura Lake mafic complex (V. J. Hurst, unpublished mapping) thus raising the possibility that Laura Lake complex is in a window and linked with Dahlonega gold belt complexes (J. O. Costello, pers. comm.).

Lenoir Quarry Migmatite

The Lenoir Quarry migmatite is an intermediate to mafic assemblage containing medium- to coarse-grained rocks in the immediate footwall of the Brindle Creek fault at the southeastern edge of the western Inner Piedmont (Merschat and Kalbas, 2002; Kalbas, 2003). This unit is intensely migmatitic and although heterogeneous consists mostly of hornblende-biotite metagranodiorite, amphibolite, and leucogranitoid. A sample of more leucocratic material was collected at the type locality from the Kings Creek 7.5-minute quadrangle in the Vulcan Materials Company, Lenoir Quarry.

Poor Mountain Quartzite (metatuff member?)

The Poor Mountain Formation of the western Inner Piedmont (Hatcher, 1969) is dominated by a basal amphibolite and amphibolite gneiss unit that grades up into a quartzofeldspathic unit, the Poor Mountain Quartzite (and marble in South Carolina). Trace element chemistry, summarized by Hatcher (2002), strongly suggests an oceanic setting, likely mafic volcanic arc or MORB, for the Poor Mountain Amphibolite (Davis, 1993; Yanagihara, 1994; Bream, 1999; Kalbas, 2003). The Poor Mountain Quartzite is a feldspathic micaceous quartzite that is interlayered with lower Poor Mountain Formation laminated amphibolite. The collected sample is from the upper unit and was collected in the North Carolina Inner Piedmont. Based on new data presented here, the sample is interpreted to have a felsic volcanic or volcaniclastic protolith with a western Inner Piedmont source.

Toccoa Granitoid

Rocks exposed in the Toccoa, GA aggregate quarry are dominantly fine- to medium-grained leucocratic granitoid. This is part of a suite of western Inner Piedmont Ordovician granitoid plutons that occurs from NE Georgia to NW North Carolina, and includes the Dysartsville Tonalite.

Zirconia Pegmatite

Syenitic pegmatite at the Freeman Mine (Zirconia, North Carolina) is located in the western Inner Piedmont, approximately 20-30 m thick, greater than 65 m in length, and deeply weathered (Olson, 1952). Zircon grains obtained from the Freeman Mine dump are large (up to several cm) and either highly fluorescent or poorly fluorescent in shortwave UV light (Callahan et al., 2002). Eight poorly fluorescent and seven highly fluorescent ~0.5 cm zircon grains were obtained from the mine dump for U-Pb dating.

ANALYTICAL METHODS

Ion Microprobe

Sensitive high-resolution ion microprobe (IMP) data presented here were collected during one session at the University of California Los Angeles using the Cameca IMS-1270 and during four sessions at Stanford University using the SHRIMP-RG (sensitive high-resolution ion microprobe reverse geometry). Routing zircon analytical procedures were followed during each session (e.g., Quidelleur et al., 1997, for the Cameca IMS-1270; Bacon et al., 2000, for the SHRIMP-RG). Fresh sample material was collected and processed using standard mineral separation techniques to concentrate heavy nonferromagnetic phases. At least 30 grains (60 for the Sevier Shale sample) grains were handpicked, and mounted in epoxy with zircon standard AS3 (SHRIMP-RG) or AS57 (Cameca IMS-1270)(1099 Ma; Paces and Miller, 1993). Kennesaw, Zirconia, and Sevier Shale zircons were also mounted with zircon standard R33 (419 Ma; SUMAC facility at Stanford University). Stanford data were also referenced to U standard SL13 (238 ppm). The mounts were polished to the approximate center of average-size grains and imaged with a scanning electron microscope (SEM) or electron microprobe (EMP) equipped with a cathodoluminescence (CL) detector. Most samples were photographed with a combination of transmitted and reflected light to identify surface and internal features. All data were corrected for common Pb with a minor ^{204}Pb correction). Comparable

results were produced at both labs using a smaller beam size (down to ~10 μm) and 15 mass peak cycles at UCLA and a larger beam size (~25 μm by 30 μm) and 5 mass peak cycles at Stanford University.

Analytical results for the Dysartsville Tonalite (sample VM1782) were regressed using ZIPS (version 2.4) software provided by the National Ion Microprobe Facility at UCLA (written by C. Coath). Most data obtained at Stanford University were regressed with PRAWN (version 6.5.5) and Lead (version 6.5.5) software (Australian National University) provided by the SUMAC facility at Stanford University. SQUID software (version 1.02; written by K. Ludwig, 2001b) was used for Kennesaw granitoid, Zirconia pegmatite, and a subset of Sevier Shale zircons which were referenced to zircon standard R33 at Stanford University. Standard concordia plots and discordia lines were constructed using Isoplot/Ex (version 2.49) written by K. Ludwig (1991; 2001a). Reported concordia ages, which provide a measure of concordance and utilize both $^{206}Pb^*/^{238}U$ and $^{207}Pb^*/^{235}U$ (* denotes radiogenic component) values simultaneously (Ludwig, 1998), were determined with decay constant errors (Ludwig, 2000) using Isoplot/Ex. Younger outliers, reflecting Pb-loss or core and rim overlap, were removed in some samples to obtain the reported $^{206}Pb^*/^{238}U$ and concordia ages. For most samples, it was necessary to remove reversely discordant or younger (interpreted to represent Pb-loss or core-rim overlap) analyses, and in a few instances older, $^{206}Pb^*/^{238}U$ ages from the pooled analyses to obtain reasonable MSWDs and probabilities of concordance.

Whole-rock elemental and isotopic analyses

Representative fresh material was cut into thin slabs on a trim saw, washed with isopropyl alcohol and deionized water, broken by hand into small pieces, and then powdered in a shatterbox with an alumina ceramic mill. Sample splits of the powders were analyzed by Activation Laboratories Ltd. (Ancaster, Ontario, Canada) using a

combination of: x-ray fluorescence (XRF); inductively coupled plasma optical emission spectrometry (ICP-OES); inductively coupled plasma mass spectrometry (ICP-MS); near-total digestion ICP-MS; and instrumental neutron activation analysis (INAA). Sm-Nd and Rb-Sr whole-rock isotopic data were also obtained from sample splits of the powders used for whole-rock analyses. Isotopic analyses were made at the Department of Geological Sciences, University of North Carolina Chapel Hill, using a VG (Micromass) Sector 54 thermal ionization mass spectrometer, following the Sm-Nd analytical techniques of Fullagar et al. (1997) and the Rb-Sr analytical techniques of Fullagar and Butler (1979) and Kish (1983).

RESULTS

Zircon Geochronology

Analytical data for zircon geochronology are presented in Table 2. The preferred magmatic age for (meta)igneous units is provided in Table 3 with statistics related to the pooled $^{206}Pb^*/^{238}U$ and concordia ages. Metamorphic ages include data not presented in Bream et al. (in press) for several samples. Most data are concordant (Fig. 3a-h).

Detrital

Detrital zircon data for all samples exclusive of the Sevier Shale are presented in Bream et al. (in press). Sevier Shale detrital zircons (21 of 24 analyses) contain distinctive Grenvillian (1.0 to 1.25 Ga), and pre-Grenvillian components. Pre-Grenvillian ages are dominantly Middle Proterozoic with peaks at ~1.35 and 1.45 Ga, although one Early Proterozoic grain with a $^{207}Pb^*/^{206}Pb^*$ age of 1.8 Ga was also identified (Fig. 4; Table 2). Errors associated with ages for this sample are suitable for determination of distinct detrital components (1 sigma errors for all analyses fall between 10 and 70 Ma for $^{206}Pb^*/^{238}U$ ages and between 25 and 300 Ma for $^{207}Pb^*/^{206}Pb^*$ ages). Three zircons plotted were too reversely discordant to be considered reliable; but the

Table 2. U-Pb IMP zircon data. M-metamorphic. IC-inherited core. M-C-rim and core overlap. (sq)-data regressed with SQUID software.

Analysis		U	Th		$^{204}Pb/$			Total								Radiogenic Ratios[1]								error	Ages (in Ma)[1]						
								$^{238}U/$		$^{207}Pb/$		$^{207}Pb/$		$^{206}Pb/$		$^{238}U/$		$^{207}Pb/$		$^{207}Pb/$		$^{206}Pb/$			$^{206}Pb/$		$^{207}Pb/$		$^{207}Pb/$		%
Label	Zone	(in ppm)		Th/U	^{206}Pb	± 1σ	f206%[2]	^{206}Pb	± 1σ	^{206}Pb	± 1σ	^{235}U	± 1σ	^{238}U	± 1σ	^{206}Pb	± 1σ	^{206}Pb	± 1σ	^{235}U	± 1σ	^{238}U	± 1σ	corr.	^{238}U	± 1σ	^{235}U	± 1σ	^{206}Pb	± 1σ	Conc [3]
SEV-1.1		179.4	170.8	0.95	0.000165	0.000142	0.0028	5.13	0.13	0.0874	0.0026	2.348	0.097	0.195	0.005	5.14	0.13	0.0851	0.0034	2.279	0.114	0.194	0.005	0.692	1145	26	1206	36	1317	80	87
SEV-2.1		133.9	119.2	0.89	0.000206	0.000146	0.0035	5.69	0.12	0.0723	0.0028	1.751	0.082	0.176	0.004	5.71	0.12	0.0693	0.0036	1.674	0.099	0.175	0.004	0.576	1040	21	999	38	909	112	114
SEV-3.1		201.1	63.3	0.31	0.000343	0.000172	0.0058	5.42	0.07	0.0797	0.0014	2.029	0.046	0.185	0.002	5.45	0.07	0.0748	0.0030	1.893	0.083	0.184	0.002	0.523	1086	13	1079	30	1063	83	102
SEV-4.1		481.6	318.4	0.66	0.000240	0.000064	0.0040	5.13	0.05	0.0914	0.0011	2.458	0.039	0.195	0.002	5.15	0.05	0.0881	0.0015	2.358	0.047	0.194	0.002	0.722	1144	9	1230	14	1384	33	83
†SEV-5.1		111.3	71.1	0.64	0.000974	0.000495	0.0174	11.40	0.30	0.0585	0.0036	0.707	0.049	0.088	0.002	11.60	0.32	0.0440	0.0086	0.523	0.105	0.086	0.002	0.140	533	14	427	73	0	0	--
SEV-6.1		61.4	25.7	0.42	<0.000001	0.000133	<0.0001	5.52	0.12	0.0757	0.0040	1.891	0.111	0.181	0.004	5.51	0.12	0.0778	0.0045	1.947	0.123	0.181	0.004	0.550	1075	21	1097	43	1142	118	94
SEV-7.1		139.9	82.9	0.59	0.000061	0.000153	0.0010	5.49	0.12	0.0815	0.0031	2.048	0.096	0.182	0.004	5.50	0.13	0.0807	0.0039	2.024	0.114	0.182	0.004	0.651	1078	23	1124	39	1213	99	89
SEV-8.1		90.7	62.4	0.69	0.000232	0.000351	0.0039	5.17	0.13	0.0869	0.0033	2.318	0.113	0.193	0.005	5.19	0.14	0.0836	0.0064	2.222	0.187	0.193	0.005	0.314	1136	28	1188	61	1284	157	88
†SEV-9.1		272.9	152.2	0.56	0.000919	0.000343	0.0165	12.30	0.31	0.0615	0.0022	0.689	0.032	0.081	0.002	12.51	0.32	0.0479	0.0058	0.528	0.067	0.080	0.002	0.091	496	12	430	46	95	266	523
SEV-10.1		156.1	77.9	0.50	0.000338	0.000153	0.0056	4.79	0.10	0.0902	0.0032	2.596	0.112	0.209	0.004	4.82	0.10	0.0854	0.0040	2.446	0.131	0.208	0.004	0.523	1216	23	1256	39	1326	93	92
SEV-11.1		140.4	57.0	0.41	0.000010	<0.000001	0.0002	3.95	0.09	0.0931	0.0024	3.248	0.116	0.253	0.005	3.95	0.09	0.0929	0.0024	3.242	0.116	0.253	0.005	0.729	1454	28	1467	28	1486	49	98
SEV-12.1		62.3	36.5	0.59	0.000141	0.000207	0.0023	4.36	0.10	0.0871	0.0024	2.757	0.106	0.230	0.005	4.37	0.10	0.0851	0.0040	2.688	0.149	0.229	0.005	0.519	1330	28	1325	42	1318	95	101
SEV-13.1		326.1	104.3	0.32	0.000065	0.000063	0.0011	5.08	0.06	0.0801	0.0014	2.175	0.049	0.197	0.002	5.08	0.06	0.0792	0.0017	2.148	0.056	0.197	0.002	0.811	1157	13	1164	18	1177	44	98
SEV-14.1		39.0	20.5	0.53	0.000105	0.000091	0.0018	4.93	0.18	0.0870	0.0042	2.433	0.156	0.203	0.007	4.94	0.18	0.0855	0.0045	2.388	0.161	0.203	0.007	0.348	1189	40	1239	49	1327	105	90
SEV-1 (sq)		91.7	39.3	0.43	0.000352	0.000251	0.6314	4.25	0.17	0.0932	0.0030					4.28	0.17	0.0883	0.0047	2.845	0.189	0.234	0.009	0.605	1355	49			1388	101	98
SEV-2 (sq)		57.0	15.0	0.26	<0.000001	<0.000001	0.0000	3.14	0.13	0.1101	0.0038					3.14	0.13	0.1101	0.0038	4.832	0.261	0.318	0.013	0.762	1782	64			1801	64	99
SEV-3 (sq)		295.5	75.0	0.25	0.000166	0.000076	0.2971	3.91	0.15	0.0969	0.0015					3.92	0.15	0.0946	0.0018	3.324	0.142	0.255	0.010	0.891	1463	50			1520	36	96
SEV-4 (sq)		59.7	25.3	0.42	<0.000001	<0.000001	0.0000	4.15	0.17	0.0875	0.0030					4.15	0.17	0.0875	0.0030	2.909	0.152	0.241	0.010	0.764	1393	50			1371	65	102
SEV-5 (sq)		105.2	81.3	0.77	<0.000001	<0.000001	0.0000	5.50	0.22	0.0801	0.0029					5.50	0.22	0.0801	0.0029	2.011	0.108	0.182	0.007	0.739	1078	39			1200	71	90
SEV-6 (sq)		112.9	55.4	0.49	<0.000001	<0.000001	0.0000	5.88	0.23	0.0710	0.0023					5.88	0.23	0.0710	0.0023	1.666	0.086	0.170	0.007	0.770	1013	37			958	67	106
†SEV-7 (sq)		47.9	17.9	0.37	0.000586	0.000374	1.0514	6.21	0.27	0.0688	0.0037					6.27	0.28	0.0603	0.0066	1.325	0.157	0.159	0.007	0.372	953	39			614	237	155
SEV-8 (sq)		467.2	131.8	0.28	<0.000001	<0.000001	0.0000	4.69	0.18	0.0880	0.0012					4.69	0.18	0.0880	0.0012	2.587	0.103	0.213	0.008	0.938	1246	43			1383	27	90
SEV-9 (sq)		65.2	34.4	0.53	0.001360	0.000355	2.4409	4.22	0.17	0.1001	0.0032					4.32	0.18	0.0809	0.0062	2.582	0.224	0.231	0.010	0.476	1342	50			1220	150	110
SEV-10 (sq)		247.0	97.2	0.39	0.002558	0.000484	4.5918	4.98	0.19	0.1256	0.0027					5.22	0.20	0.0899	0.0078	2.376	0.227	0.192	0.008	0.410	1130	41			1423	166	79
LVQ1-1.1	IC	604.2	381.4	0.63	0.000181	0.000056	0.0033	14.25	0.42	0.0575	0.0014	0.556	0.022	0.070	0.002	14.30	0.42	0.0548	0.0016	0.528	0.023	0.070	0.002	0.639	436	12	431	16	404	67	108
LVQ1-2.1	M	1544.4	52.7	0.03	0.000010	0.000000	0.0002	18.40	0.14	0.0524	0.0008	0.393	0.007	0.054	0.000	18.40	0.14	0.0523	0.0008	0.392	0.007	0.054	0.000	0.872	341	3	336	5	298	35	114
LVQ1-3.1	IC	205.1	97.5	0.48	0.000160	0.000106	0.0029	13.28	0.25	0.0573	0.0030	0.595	0.035	0.075	0.001	13.32	0.25	0.0550	0.0034	0.569	0.038	0.075	0.001	0.547	467	8	457	25	411	147	114
LVQ1-3.2	M	1712.5	65.5	0.04	0.000033	0.000025	0.0006	18.36	0.23	0.0531	0.0008	0.399	0.008	0.054	0.001	18.37	0.23	0.0526	0.0009	0.395	0.009	0.054	0.001	0.850	342	4	338	6	312	38	110
LVQ1-4.1	M	892.7	29.8	0.03	0.000087	0.000043	0.0016	17.46	0.19	0.0520	0.0013	0.411	0.011	0.057	0.001	17.48	0.19	0.0507	0.0015	0.400	0.013	0.057	0.001	0.761	359	4	342	9	227	67	158
LVQ1-5.1	M	3522.7	191.9	0.05	0.000018	0.000014	0.0003	18.87	0.39	0.0522	0.0006	0.382	0.010	0.053	0.001	18.88	0.39	0.0520	0.0007	0.380	0.010	0.053	0.001	0.936	333	7	327	7	284	30	117
LVQ1-6.1	IC	139.5	62.0	0.44	0.000413	0.000227	0.0075	13.87	0.77	0.0567	0.0030	0.564	0.046	0.072	0.004	13.97	0.77	0.0507	0.0047	0.500	0.057	0.072	0.004	0.483	446	24	412	39	225	221	198
LVQ1-7.1†	IC	300.5	263.6	0.88	0.000010	0.000000	0.0002	15.07	0.44	0.0559	0.0025	0.511	0.029	0.066	0.002	15.07	0.44	0.0557	0.0025	0.510	0.029	0.066	0.002	0.698	414	12	418	20	442	104	94
LVQ1-10.1†	IC	210.6	89.1	0.42	<0.000001	--	<0.0001	11.74	0.51	0.0497	0.0022	0.584	0.039	0.085	0.004	11.73	0.51	0.0504	0.0023	0.593	0.039	0.085	0.004	0.642	527	22	472	25	214	108	246
LVQ1-10.2	M	2344.9	43.9	0.02	0.000009	0.000008	0.0002	19.14	0.13	0.0524	0.0004	0.378	0.004	0.052	0.000	19.14	0.13	0.0523	0.0004	0.377	0.004	0.052	0.000	0.924	328	2	325	3	299	18	110
LVQ1-11.1	IC	247.4	105.6	0.43	0.000095	0.000106	0.0017	13.77	0.21	0.0585	0.0011	0.585	0.015	0.073	0.001	13.80	0.21	0.0571	0.0020	0.570	0.023	0.072	0.001	0.607	451	7	458	15	495	79	91
LVQ1-11.2	M	1323.5	55.1	0.04	<0.000001	--	<0.0001	17.93	0.38	0.0526	0.0006	0.404	0.010	0.056	0.001	17.92	0.38	0.0529	0.0007	0.407	0.011	0.056	0.001	0.854	350	7	347	8	324	31	108
LVQ1-12.1	IC	217.2	158.6	0.73	0.000074	0.000068	0.0013	14.08	0.21	0.0561	0.0012	0.549	0.015	0.071	0.001	14.10	0.21	0.0550	0.0016	0.538	0.019	0.071	0.001	0.682	442	6	437	12	411	67	108
LVQ1-13.1	IC	256.3	159.2	0.62	0.000080	0.000211	0.0014	13.72	0.17	0.0543	0.0022	0.546	0.024	0.073	0.001	13.74	0.18	0.0532	0.0040	0.534	0.041	0.073	0.001	0.403	453	6	434	28	336	178	135
LVQ1-13.2	M	857.1	22.1	0.03	0.000041	0.000048	0.0008	16.72	0.16	0.0536	0.0009	0.442	0.009	0.060	0.001	16.73	0.16	0.0530	0.0012	0.437	0.011	0.060	0.001	0.664	374	4	368	8	327	52	114
LVQ1-14.1	M	12298.0	334.7	0.03	0.000005	0.000008	0.0001	17.30	0.17	0.0525	0.0003	0.418	0.005	0.058	0.001	17.31	0.17	0.0524	0.0003	0.418	0.005	0.058	0.001	0.890	362	3	354	3	305	12	119
LVQ1-15.1†	IC	253.4	96.0	0.38	0.000010	0.000000	0.0002	14.78	0.38	0.0527	0.0023	0.491	0.026	0.068	0.002	14.79	0.38	0.0525	0.0023	0.490	0.026	0.068	0.002	0.597	422	10	405	18	309	103	137
LVQ1-15.2	M	834.1	425.0	0.51	0.000178	0.000052	0.0032	13.54	0.09	0.0553	0.0014	0.563	0.015	0.074	0.001	13.58	0.09	0.0527	0.0016	0.535	0.017	0.074	0.001	0.669	458	3	435	11	314	72	146
LVQ1-16.1	M	1547.4	158.3	0.10	0.000046	0.000044	0.0008	18.84	0.16	0.0547	0.0008	0.401	0.007	0.053	0.000	18.86	0.16	0.0541	0.0011	0.395	0.009	0.053	0.000	0.850	333	3	338	6	374	44	89
LVQ1-17.1†	IC	286.8	142.1	0.50	0.000081	0.000092	0.0015	13.25	0.17	0.0543	0.0018	0.565	0.020	0.075	0.001	13.27	0.17	0.0531	0.0023	0.552	0.026	0.075	0.001	0.636	468	6	446	17	334	100	140
LVQ1-18.1	M	700.6	20.4	0.03	0.000070	0.000112	0.0013	16.11	0.20	0.0528	0.0007	0.452	0.009	0.062	0.001	16.13	0.20	0.0518	0.0019	0.442	0.018	0.062	0.001	0.805	388	5	372	13	275	86	141
LVQ1-18.2	IC	188.4	55.7	0.30	0.000046	0.000092	0.0008	14.74	0.62	0.0538	0.0015	0.504	0.027	0.068	0.003	14.75	0.62	0.0532	0.0021	0.497	0.031	0.068	0.003	0.450	423	17	410	21	336	92	126
LVQ1-19.1	M?	1092.6	721.3	0.66	0.000145	0.000049	0.0027	29.23	0.42	0.0535	0.0009	0.252	0.006	0.034	0.000	29.31	0.42	0.0513	0.0012	0.242	0.007	0.034	0.000	0.662	216	3	220	6	256	55	84
LVQ1-20.1	M	858.9	34.4	0.04	0.000010	0.000000	0.0002	19.05	0.23	0.0528	0.0012	0.382	0.010	0.052	0.001	19.06	0.23	0.0526	0.0012	0.381	0.010	0.052	0.001	0.817	330	4	328	7	312	51	106
LVQ1-21.1	M	3827.5	372.8	0.10	0.000012	0.000007	0.0002	18.75	0.28	0.0526	0.0004	0.387	0.007	0.053	0.001	18.75	0.28	0.0524	0.0004	0.385	0.007	0.053	0.001	0.955	335	5	331	5	303	17	111
SBHI2-1	M	56.8	120.6	2.12	<0.000001	--	<0.0001	18.90	0.55	0.0569	0.0054					18.90	0.55	0.0569	0.0054	0.415	0.041	0.053	0.002	0.295	332	9			487	208	68
3HI-1	M	1722.9	4968.4	2.88	<0.000001	--	<0.0001	19.51	0.16	0.0540	0.0010					19.51	0.16	0.0540	0.0010	0.382	0.008	0.051	0.000	0.396	322	3			373	42	87
3HI-2	M	511.5	3093.4	6.05	<0.000001	--	<0.0001	19.19	0.19	0.0519	0.0018					19.19	0.19	0.0519	0.0018	0.373	0.013	0.052	0.001	0.280	328	3			280	79	117
1LO1-1.1	M	884.7	629.1	0.71	0.000108	0.000069	0.1962	19.44	0.15	0.0550	0.0014					19.48	0.15	0.0534	0.0017	0.378	0.013	0.051	0.000	0.233	323	2			345	74	94
1HI1-1.1	M	1744.2	137.2	0.08	<0.000001	--	<0.0001	19.27	0.12	0.0532	0.0009					19.27	0.12	0.0532	0.0009	0.380	0.007	0.052	0.000	0.321	326	2			336	40	97
1HI1-1.2	M	968.7	581.1	0.60	<0.000001	--	<0.0001	18.85	0.17	0.0514	0.0013					18.85	0.17	0.0514	0.0013	0.376	0.010	0.053	0.000	0.327	333	3			260	59	128
1LO1-1.2†	M	2182.2	43.6	0.02	<0.000001	--	<0.0001	18.81	0.09	0.0541	0.0010					18.81	0.09	0.0541	0.0010	0.396	0.008	0.053	0.000	0.257	334	2			374	42	89
LO4-1.1	M	712.7	1200.8	1.68	<0.000001	--	<0.0001	19.22	0.16	0.0535	0.0015					19.22	0.16	0.0535	0.0015	0.384	0.011	0.052	0.000	0.283	327	3			350	64	93
LO4-1.2	M	636.2	4410.7	6.93	<0.000001	--	<0.0001	19.16	0.17	0.0524	0.0016					19.16	0.17	0.0524	0.0016	0.377	0.012	0.052	0.000	0.283	328	3			302	68	108
LO3-1	M	550.5	105.9	0.19	<0.000001	--	<0.0001	19.12	0.18	0.0543	0.0017					19.12	0.18	0.0543	0.0017	0.391	0.013	0.052	0.000	0.287	329	3			383	71	86
LO3-2†	M	179.5	804.4	4.48	<0.000001	--	<0.0001	19.50	0.33	0.0457	0.0029					19.50	0.33	0.0457	0.0029	0.323	0.021	0.051	0.001	0.251	322	5			-19	155	--
KEN1-1		241.7	91.9	0.38	<0.000001	--	<0.0001	14.45	0.65	0.0553	0.0023					14.45	0.65	0.0553	0.0023	0.528	0.032	0.069	0.003	0.731	431	19			425	94	102
KEN1-12		405.4	239.6	0.59	<0.000001	--	<0.0001	14.18	0.55	0.0568	0.0017					14.18	0.55	0.0568	0.0017	0.553	0.027	0.071	0.003	0.786	439	16			485	67	91

Table 2. *continued*

Analysis Label	Zone	U (in ppm)	Th (in ppm)	Th/U	$^{204}Pb/^{206}Pb$	± 1σ	f206%[2]	Total $^{238}U/^{206}Pb$	± 1σ	$^{207}Pb/^{206}Pb$	± 1σ	$^{207}Pb/^{235}U$	± 1σ	$^{206}Pb/^{238}U$	± 1σ	Radiogenic Ratios[1] $^{238}U/^{206}Pb$	± 1σ	$^{207}Pb/^{206}Pb$	± 1σ	$^{207}Pb/^{235}U$	± 1σ	$^{206}Pb/^{238}U$	± 1σ	error corr.	Ages (in Ma)[1] $^{206}Pb/^{238}U$	± 1σ	$^{207}Pb/^{235}U$	± 1σ	$^{207}Pb/^{206}Pb$	± 1σ	% Conc [3]
KEN1-3		3594.2	3532.4	0.98	<0.000001	--	<0.0001	13.83	0.64	0.0557	0.0006					13.83	0.64	0.0557	0.0006	0.556	0.026	0.072	0.003	0.977	450	20			441	23	102
KEN1-4		184.0	60.0	0.33	<0.000001	--	<0.0001	14.57	0.58	0.0538	0.0026					14.57	0.58	0.0538	0.0026	0.510	0.032	0.069	0.003	0.635	428	16			364	109	117
KEN1-5		421.3	246.3	0.58	<0.000001	--	<0.0001	12.71	0.49	0.0538	0.0016					12.71	0.49	0.0538	0.0016	0.584	0.029	0.079	0.003	0.786	488	18			363	69	135
KEN1-6		274.9	97.1	0.35	<0.000001	--	<0.0001	14.04	0.55	0.0555	0.0024					14.04	0.55	0.0555	0.0024	0.545	0.032	0.071	0.003	0.669	443	17			434	98	102
KEN1-7		570.4	509.9	0.89	<0.000001	--	<0.0001	15.24	0.58	0.0554	0.0017					15.24	0.58	0.0554	0.0017	0.501	0.025	0.066	0.003	0.782	410	15			428	68	96
KEN1-8		273.5	86.0	0.31	<0.000001	--	<0.0001	13.69	0.53	0.0524	0.0023					13.69	0.53	0.0524	0.0023	0.528	0.031	0.073	0.003	0.667	454	17			302	99	150
KEN1-8B		266.6	86.5	0.32	<0.000001	--	<0.0001	13.75	0.61	0.0516	0.0022					13.75	0.61	0.0516	0.0022	0.518	0.032	0.073	0.003	0.717	452	19			269	99	168
KEN1-9		442.0	123.7	0.28	0.000645	0.000328	1.1611	13.84	0.53	0.0560	0.0017					14.01	0.54	0.0465	0.0052	0.458	0.054	0.071	0.003	0.327	445	17			23	269	1923
KEN1-10		386.7	145.6	0.38	<0.000001	--	<0.0001	13.94	0.55	0.0551	0.0018					13.94	0.55	0.0551	0.0018	0.545	0.028	0.072	0.003	0.767	447	17			418	73	107
KEN1-11		426.7	233.7	0.55	<0.000001	--	<0.0001	13.68	0.56	0.0564	0.0016					13.68	0.56	0.0564	0.0016	0.568	0.028	0.073	0.003	0.824	455	18			466	62	98
WIMPY-1.1		338.8	129.7	0.38	0.000039	0.000038	0.0007	12.89	0.18	0.0573	0.0011	0.612	0.015	0.078	0.001	12.90	0.18	0.0567	0.0012	0.606	0.016	0.078	0.001	0.819	481	6	481	10	479	48	100
WIMPY-2.1		147.7	51.6	0.35	0.000010	<0.000001	0.0002	12.90	0.16	0.0581	0.0022	0.621	0.026	0.078	0.001	12.90	0.16	0.0579	0.0022	0.619	0.026	0.078	0.001	0.273	481	6	489	16	527	87	91
WIMPY-3.1		406.3	157.3	0.39	0.000025	0.000037	0.0005	12.94	0.22	0.0563	0.0011	0.600	0.017	0.077	0.001	12.94	0.22	0.0559	0.0013	0.596	0.018	0.077	0.001	0.827	480	8	475	11	450	51	107
WIMPY-4.1		236.6	84.9	0.36	0.000010	<0.000001	0.0002	12.79	0.14	0.0563	0.0024	0.607	0.027	0.078	0.001	12.79	0.14	0.0562	0.0024	0.605	0.027	0.078	0.001	0.745	485	5	481	17	459	96	106
WIMPY-5.1†		412.5	71.3	0.17	0.000122	0.000069	0.0022	13.24	0.20	0.0562	0.0015	0.586	0.019	0.076	0.001	13.27	0.20	0.0545	0.0019	0.566	0.022	0.075	0.001	0.755	469	7	455	14	390	79	120
WIMPY-6.1		208.0	68.1	0.33	0.000031	0.000060	0.0006	12.92	0.19	0.0583	0.0022	0.622	0.026	0.077	0.001	12.93	0.19	0.0579	0.0024	0.617	0.028	0.077	0.001	0.793	480	7	488	18	524	93	92
WIMPY-7.1		80.4	25.2	0.31	0.000077	0.000151	0.0014	13.11	0.26	0.0583	0.0027	0.613	0.032	0.076	0.001	13.13	0.26	0.0572	0.0036	0.601	0.041	0.076	0.002	0.625	473	9	478	26	499	145	95
WIMPY-8.1		172.3	80.1	0.46	0.000070	0.000049	0.0013	12.87	0.19	0.0590	0.0021	0.632	0.026	0.078	0.001	12.88	0.19	0.0580	0.0023	0.621	0.027	0.078	0.001	0.637	482	7	490	17	530	87	91
WIMPY-9.1		540.2	277.8	0.51	0.000010	0.000007	0.0002	12.87	0.09	0.0572	0.0007	0.612	0.009	0.078	0.001	12.87	0.09	0.0570	0.0007	0.611	0.009	0.078	0.001	0.883	482	3	484	6	492	28	98
WIMPY-10.1		197.4	63.9	0.32	0.000010	0.000019	0.0002	12.73	0.16	0.0565	0.0012	0.612	0.015	0.079	0.001	12.73	0.16	0.0564	0.0012	0.611	0.016	0.079	0.001	0.765	488	6	484	10	467	48	104
POMTN--1.1†		335.9	230.6	0.69	0.000010	<0.000001	0.0002	12.98	0.13	0.0564	0.0010	0.599	0.013	0.077	0.001	12.98	0.13	0.0563	0.0010	0.597	0.013	0.077	0.001	0.416	478	5	476	8	462	40	103
POMTN--2.1†		661.2	517.8	0.78	0.000016	0.000023	0.0003	12.90	0.22	0.0542	0.0009	0.579	0.014	0.078	0.001	12.91	0.22	0.0539	0.0009	0.576	0.015	0.077	0.001	0.826	481	8	462	10	368	40	131
POMTN--3.1†		790.0	1023.9	1.30	0.000010	0.000019	0.0002	13.27	0.07	0.0548	0.0005	0.569	0.007	0.075	0.000	13.28	0.07	0.0546	0.0006	0.567	0.007	0.075	0.000	0.857	468	3	456	5	397	25	118
POMTN--4.1†		399.3	236.3	0.59	0.000075	0.000073	0.0014	13.09	0.12	0.0555	0.0019	0.585	0.021	0.076	0.001	13.11	0.12	0.0544	0.0022	0.572	0.024	0.076	0.001	0.749	474	4	459	16	388	92	122
POMTN--5.1†		473.5	331.6	0.70	0.000029	0.000027	0.0005	13.59	0.14	0.0545	0.0012	0.552	0.014	0.074	0.001	13.60	0.14	0.0540	0.0013	0.548	0.015	0.074	0.001	0.807	457	5	444	10	373	55	123
POMTN-6.1		462.9	286.9	0.62	0.000010	<0.000001	0.0002	13.54	0.13	0.0562	0.0009	0.573	0.011	0.074	0.001	13.54	0.13	0.0561	0.0009	0.571	0.011	0.074	0.001	0.799	459	4	459	7	455	34	101
POMTN-7.1		318.7	213.4	0.67	0.000048	0.000111	0.0009	13.75	0.37	0.0558	0.0020	0.560	0.026	0.073	0.002	13.76	0.37	0.0551	0.0026	0.552	0.032	0.073	0.002	0.657	452	12	447	21	417	110	108
POMTN-8.1		427.2	327.3	0.77	0.000014	0.000028	0.0003	14.04	0.12	0.0562	0.0007	0.552	0.009	0.071	0.001	14.04	0.12	0.0560	0.0009	0.550	0.010	0.071	0.001	0.779	443	4	445	7	454	34	98
POMTN-9.1		689.6	590.3	0.86	0.000009	0.000018	0.0002	13.81	0.09	0.0554	0.0006	0.553	0.008	0.072	0.000	13.81	0.09	0.0552	0.0007	0.551	0.008	0.072	0.000	0.810	451	3	446	5	421	27	107
POMTN-10.1†		502.8	382.2	0.76	0.000075	0.000099	0.0014	14.44	0.53	0.0558	0.0017	0.533	0.027	0.069	0.003	14.46	0.53	0.0547	0.0023	0.522	0.031	0.069	0.003	0.835	431	15	426	21	400	98	108
POMTN-11.1†		413.6	307.6	0.74	0.000033	0.000030	0.0006	13.55	0.09	0.0548	0.0008	0.557	0.010	0.074	0.001	13.55	0.09	0.0543	0.0009	0.552	0.011	0.074	0.001	0.778	459	3	446	7	382	39	120
POMTN-12.1		516.8	347.4	0.67	0.000021	0.000040	0.0004	14.02	0.15	0.0554	0.0009	0.545	0.011	0.071	0.001	14.03	0.15	0.0551	0.0011	0.542	0.013	0.071	0.001	0.751	444	4	440	8	416	44	107
POMTN-13.1†		330.2	173.8	0.53	0.000010	<0.000001	0.0002	13.45	0.13	0.0541	0.0011	0.554	0.013	0.074	0.001	13.45	0.13	0.0539	0.0011	0.553	0.013	0.074	0.001	0.729	462	4	447	8	367	45	126
POMTN-14.1		520.9	392.7	0.75	0.000022	0.000033	0.0004	13.98	0.14	0.0563	0.0010	0.555	0.012	0.072	0.001	13.99	0.14	0.0560	0.0012	0.552	0.013	0.071	0.001	0.776	445	4	446	9	452	46	98
POMTN-15.1		437.8	322.3	0.74	0.000010	0.000000	0.0002	13.55	0.16	0.0561	0.0009	0.571	0.012	0.074	0.001	13.55	0.16	0.0560	0.0009	0.569	0.012	0.074	0.001	0.813	459	5	458	8	451	35	102
POMTN-16.1†		390.4	246.7	0.63	0.000010	<0.000001	0.0002	13.32	0.14	0.0541	0.0010	0.560	0.013	0.075	0.001	13.33	0.14	0.0539	0.0010	0.558	0.012	0.075	0.001	0.775	466	5	450	8	368	42	127
POMTN-17.1†		282.0	171.2	0.61	0.000035	0.000042	0.0006	14.23	0.23	0.0592	0.0018	0.573	0.021	0.070	0.001	14.24	0.23	0.0587	0.0019	0.568	0.022	0.070	0.001	0.660	437	7	457	14	554	72	79
POMTN-18.1		365.1	232.0	0.64	0.000035	0.000032	0.0006	13.95	0.16	0.0548	0.0012	0.541	0.014	0.072	0.001	13.96	0.16	0.0543	0.0013	0.536	0.015	0.072	0.001	0.768	446	5	436	10	382	53	117
POMTN-19.1	M	1820.8	1101.1	0.60	0.000282	0.000074	0.0051	16.12	0.49	0.0572	0.0007	0.490	0.017	0.062	0.002	16.20	0.49	0.0531	0.0013	0.452	0.019	0.062	0.002	0.755	386	11	379	13	333	58	116
POMTN-20.1		534.7	402.2	0.75	0.000010	<0.000001	0.0002	13.59	0.11	0.0566	0.0007	0.574	0.009	0.074	0.001	13.59	0.11	0.0564	0.0007	0.573	0.009	0.074	0.001	0.838	458	4	460	6	470	29	97
POMTN-21.1		392.3	277.6	0.71	0.000021	0.000041	0.0004	13.50	0.14	0.0560	0.0008	0.572	0.011	0.074	0.001	13.50	0.14	0.0557	0.0010	0.568	0.013	0.074	0.001	0.745	461	5	457	8	439	42	105
TOC-1.1		1146.7	1138.6	0.99	0.000220	0.000184	0.0040	14.13	0.26	0.0621	0.0009	0.606	0.015	0.071	0.001	14.19	0.27	0.0589	0.0030	0.573	0.033	0.070	0.001	0.604	439	8	460	21	565	116	78
TOC-2.1		397.9	585.7	1.47	0.000114	0.000148	0.0021	13.78	0.22	0.0551	0.0012	0.552	0.016	0.073	0.001	13.81	0.22	0.0535	0.0026	0.534	0.029	0.072	0.001	0.426	451	7	434	19	348	115	129
TOC-3.1		1156.7	1777.9	1.54	0.000103	0.000135	0.0019	13.57	0.15	0.0574	0.0008	0.583	0.011	0.074	0.001	13.60	0.16	0.0559	0.0023	0.566	0.025	0.074	0.001	0.674	457	5	456	16	447	93	102
TOC-4.1		2215.0	1406.9	0.64	0.000026	0.000034	0.0005	13.62	0.12	0.0575	0.0007	0.582	0.009	0.073	0.001	13.63	0.12	0.0572	0.0009	0.578	0.011	0.073	0.001	0.845	456	4	463	7	498	33	92
TOC-5.1		637.7	689.1	1.08	0.000010	<0.000001	0.0002	14.43	0.22	0.0570	0.0015	0.545	0.017	0.069	0.001	14.43	0.22	0.0569	0.0015	0.544	0.017	0.069	0.001	0.725	432	6	441	11	487	58	89
TOC-6.1		1023.5	1845.7	1.80	0.000018	0.000038	0.0003	13.67	0.20	0.0564	0.0017	0.569	0.020	0.073	0.001	13.68	0.20	0.0562	0.0018	0.566	0.021	0.073	0.001	0.842	455	6	456	14	459	72	99
TOC-7.1		260.2	379.8	1.46	0.000010	0.000087	0.0002	13.81	0.34	0.0563	0.0025	0.562	0.030	0.072	0.002	13.81	0.34	0.0561	0.0029	0.560	0.033	0.072	0.002	0.539	451	11	452	22	457	117	99
TOC-8.1		1271.2	581.8	0.46	0.000010	0.000024	0.0002	13.86	0.28	0.0562	0.0013	0.559	0.018	0.072	0.001	13.86	0.28	0.0560	0.0014	0.557	0.019	0.072	0.001	0.714	449	9	450	12	453	55	99
TOC-9.1		325.3	327.1	1.01	0.000227	0.000393	0.0041	14.37	0.24	0.0597	0.0020	0.573	0.023	0.070	0.001	14.42	0.26	0.0564	0.0065	0.539	0.064	0.069	0.001	0.266	432	8	438	43	466	278	93
TOC-10.1		1781.1	753.5	0.42	0.000040	0.000026	0.0007	14.35	0.06	0.0568	0.0012	0.545	0.012	0.070	0.000	14.36	0.06	0.0562	0.0013	0.539	0.013	0.070	0.000	0.804	434	2	438	9	459	52	94
TOC-11.1		313.7	171.8	0.55	0.000104	0.000270	0.0019	13.99	0.27	0.0561	0.0026	0.552	0.029	0.071	0.001	14.02	0.28	0.0545	0.0050	0.536	0.051	0.071	0.001	0.341	444	9	436	34	393	218	113
TOC-12.1		301.9	384.2	1.27	<0.000001	0.000920	<0.0001	14.54	0.25	0.0556	0.0020	0.527	0.022	0.069	0.001	14.45	0.34	0.0607	0.0145	0.580	0.141	0.069	0.002	0.533	431	10	464	95	629	618	69
TOC-13.1		228.0	267.1	1.17	0.000439	0.000426	0.0079	14.48	0.31	0.0567	0.0020	0.540	0.023	0.069	0.002	14.60	0.34	0.0503	0.0070	0.475	0.068	0.069	0.002	0.289	427	10	395	48	208	294	205
TOC-14.1		458.6	544.9	1.19	0.000120	0.000153	0.0022	14.67	0.24	0.0591	0.0014	0.556	0.017	0.068	0.001	14.70	0.25	0.0574	0.0028	0.538	0.029	0.068	0.001	0.512	424	7	437	19	506	110	84
TOC-15.1		2900.9	2452.6	0.85	0.000021	0.000015	0.0004	14.06	0.20	0.0568	0.0005	0.557	0.010	0.071	0.001	14.07	0.20	0.0565	0.0006	0.554	0.010	0.071	0.001	0.913	443	6	448	7	472	22	94
TOC-16.1		545.5	845.2	1.55	0.000073	0.000089	0.0013	14.18	0.23	0.0572	0.0020	0.556	0.022	0.071	0.001	14.20	0.23	0.0561	0.0024	0.545	0.026	0.070	0.001	0.524	439	7	442	17	457	98	96

Table 2. *continued*

Analysis Label	Zone	U (in ppm)	Th (in ppm)	Th/U	$^{204}Pb/^{205}Pb$	± 1σ	f206%[2]	Total $^{238}U/^{206}Pb$	± 1σ	$^{207}Pb/^{206}Pb$	± 1σ	$^{207}Pb/^{235}U$	± 1σ	$^{206}Pb/^{238}U$	± 1σ	Radiogenic Ratios[1] $^{238}U/^{206}Pb$	± 1σ	$^{207}Pb/^{206}Pb$	± 1σ	$^{207}Pb/^{235}U$	± 1σ	$^{206}Pb/^{238}U$	± 1σ	error corr.	Ages (in Ma)[1] $^{206}Pb/^{238}U$	± 1σ	$^{207}Pb/^{235}U$	± 1σ	$^{207}Pb/^{206}Pb$	± 1σ	% Conc [3]
Dgn_25_sp1					0.000461	0.000126	0.75			0.0551	0.0014	0.575	0.019	0.076	0.001			0.0484	0.0023	0.501	0.027	0.075	0.001	0.452	467	9	412	18	119	114	391
Dgn_26_sp1					0.000252	0.000121	0.41			0.0575	0.0017	0.611	0.027	0.077	0.002			0.0538	0.0024	0.570	0.032	0.077	0.002	0.609	477	14	458	21	364	102	131
Dgn_24_sp1					0.000233	0.000173	0.38			0.0661	0.0021	0.709	0.038	0.078	0.003			0.0627	0.0033	0.670	0.047	0.077	0.003	0.670	481	19	521	28	700	110	69
Dgn_22_sp1					0.000179	0.000197	0.29			0.0599	0.0037	0.590	0.044	0.071	0.003			0.0573	0.0046	0.563	0.052	0.071	0.003	0.494	443	17	453	34	504	178	88
Dgn_19_sp1					0.000009	0.000016	0.02			0.0572	0.0014	0.589	0.021	0.075	0.002			0.0571	0.0014	0.588	0.021	0.075	0.002	0.737	465	9	470	14	494	55	94
Dgn_7_sp1					0.000091	0.000065	0.15			0.0591	0.0015	0.615	0.020	0.075	0.002			0.0578	0.0018	0.601	0.022	0.075	0.002	0.544	468	10	478	14	523	67	90
Dgn_8_sp1†					0.000981	0.000321	1.59			0.0610	0.0016	0.602	0.025	0.072	0.002			0.0467	0.0050	0.453	0.053	0.070	0.002	0.434	439	12	380	37	32	259	1353
Dgn_7_sp2					0.000493	0.000285	0.80			0.0620	0.0023	0.645	0.022	0.075	0.003			0.0548	0.0047	0.566	0.050	0.075	0.003	0.306	465	20	455	33	405	193	115
Dgn_6_sp1†	M-C				0.000725	0.000314	1.17			0.0656	0.0027	0.600	0.036	0.066	0.002			0.0551	0.0053	0.498	0.055	0.066	0.002	0.544	410	13	411	37	414	215	99
Dgn_6_sp2					0.000429	0.000175	0.70			0.0615	0.0019	0.652	0.024	0.077	0.002			0.0553	0.0031	0.582	0.037	0.076	0.002	0.440	474	12	466	24	423	127	112
Dgn_10_sp1	M				0.000096	0.000036	0.16			0.0541	0.0006	0.389	0.007	0.052	0.001			0.0527	0.0008	0.379	0.008	0.052	0.001	0.712	328	4	326	6	315	33	104
Dgn_3_sp1					0.000453	0.000143	0.73			0.0592	0.0013	0.641	0.024	0.078	0.002			0.0526	0.0024	0.565	0.033	0.078	0.002	0.615	484	13	455	21	313	106	155
Dgn_8_sp2	M				0.000635	0.000124	1.03			0.0555	0.0008	0.428	0.009	0.056	0.001			0.0462	0.0020	0.353	0.017	0.055	0.001	0.465	347	5	307	13	7	104	5082
Dgn_13_sp1†	M-C				0.000119	0.000062	0.19			0.0567	0.0011	0.535	0.011	0.068	0.001			0.0550	0.0015	0.518	0.014	0.068	0.001	0.355	426	7	424	10	412	59	104
Dgn_5_sp1					0.000042	0.000042	0.07			0.0561	0.0010	0.586	0.020	0.076	0.002			0.0555	0.0012	0.579	0.021	0.076	0.002	0.809	471	12	464	14	430	48	109
Dgn_9_sp1					0.000195	0.000102	0.32			0.0570	0.0015	0.583	0.019	0.074	0.001			0.0541	0.0021	0.553	0.025	0.074	0.001	0.460	461	9	447	16	377	89	122

Notes: (1) Common Pb corrected using measured ^{204}Pb.

(2) f206% denotes the percentage of ^{206}Pb that is common Pb.

(3) % Conc. = [($^{206}Pb/^{238}U$ Age)/($^{207}Pb/^{206}Pb$ Age)] * 100, where values > 100% are reversely discordant and values< 100% are normally discordant.

† Data points excluded from ages and probability plots.

M = Metamorphic overgrowth, C = Magmatic core, IC = Inherited core

Table 3. Pooled $^{206}Pb^*/^{238}U$ and Concordia ages for magmatic and suspected magmatic samples. MSWD-mean square of the weighted deviate.

	Cane Creek felsic gneiss (WIMPY)	Dysartsville Tonalite (VM1782)	Kennesaw granitoid (KEN)	Lenoir Quarry migmatite cores (LVQ1)	Poor Mountain metatuff (?) (POMTN) all cores	Poor Mountain metatuff (?) (POMTN) older and younger clusters		Toccoa granitoid (TOC)	Zirconia pegmatite
	n = 9/10	n = 10/14	n = 11/12	n = 7/11	n = 10/20	n = 5/10	n = 4/10	n = 11/16	n = 9/11
$^{206}Pb^*/^{238}U$ Age	482 ± 4	468 ± 8	444 ± 11	450 ± 6	451 ± 3	459 ± 4	444 ± 4	449 ± 4	327 ± 2
MSWD	0.31	0.54	1.35	1.74	2.66	0.14	0.09	1.74	1.48
Concordia Age[3]	482 ± 4	468 ± 8	442 ± 10	449 ± 6[4]	452 ± 4[4]	459 ± 4	445 ± 4	449 ± 4	327 ± 2
equivalence	0.41 (0.98)	0.90 (0.58)	1.02 (0.43)	1.15 (0.32)	1.7 (0.03)	0.98 (0.24)	0.62 (0.72)	1.17 (0.27)	1.00 (0.45)
concordance	0.03 (0.86)	0.47 (0.49)	0.90 (0.34)	1.5 (0.22)	1.4 (0.24)	0.013 (0.91)	0.49 (0.48)	2.6 (0.11)	0.17 (0.68)
equiv. & conc.	0.39 (0.99)	0.87 (0.62)	1.01 (0.44)	1.18(0.29)	1.7 (0.03)	0.22 (0.992)	0.60 (0.76)	1.2 (0.20)	0.95 (0.51)

Probabilities in parentheses for Concordia age MSWDs.

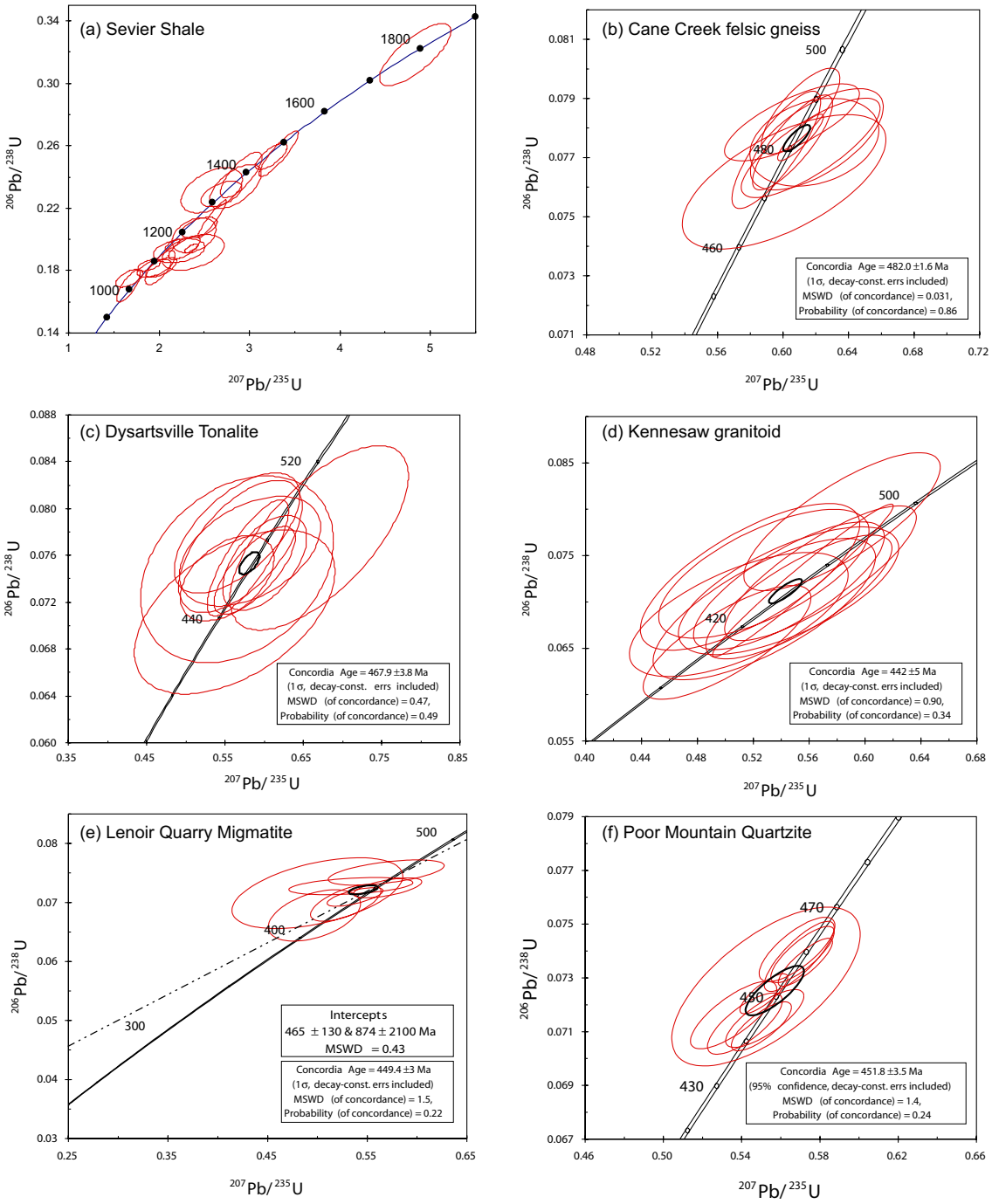

Figure 3. Concordia plots of ^{204}Pb-corrected data. (a) Sevier Shale. (b) Cane Creek felsic gneiss. (c) Dysartsville Tonalite. (d) Kennesaw granitoid. (e) Lenoir Quarry Migmatite cores. (f) Poor Mountain Quartzite. (g) Poor Mountain Quartzite older analyses. (h) Poor Mountain Quartzite younger analyses. (i) Toccoa granitoid. (j) Zirconia pegmatite. Note that ellipses are one sigma error and black ellipses are Concordia age.

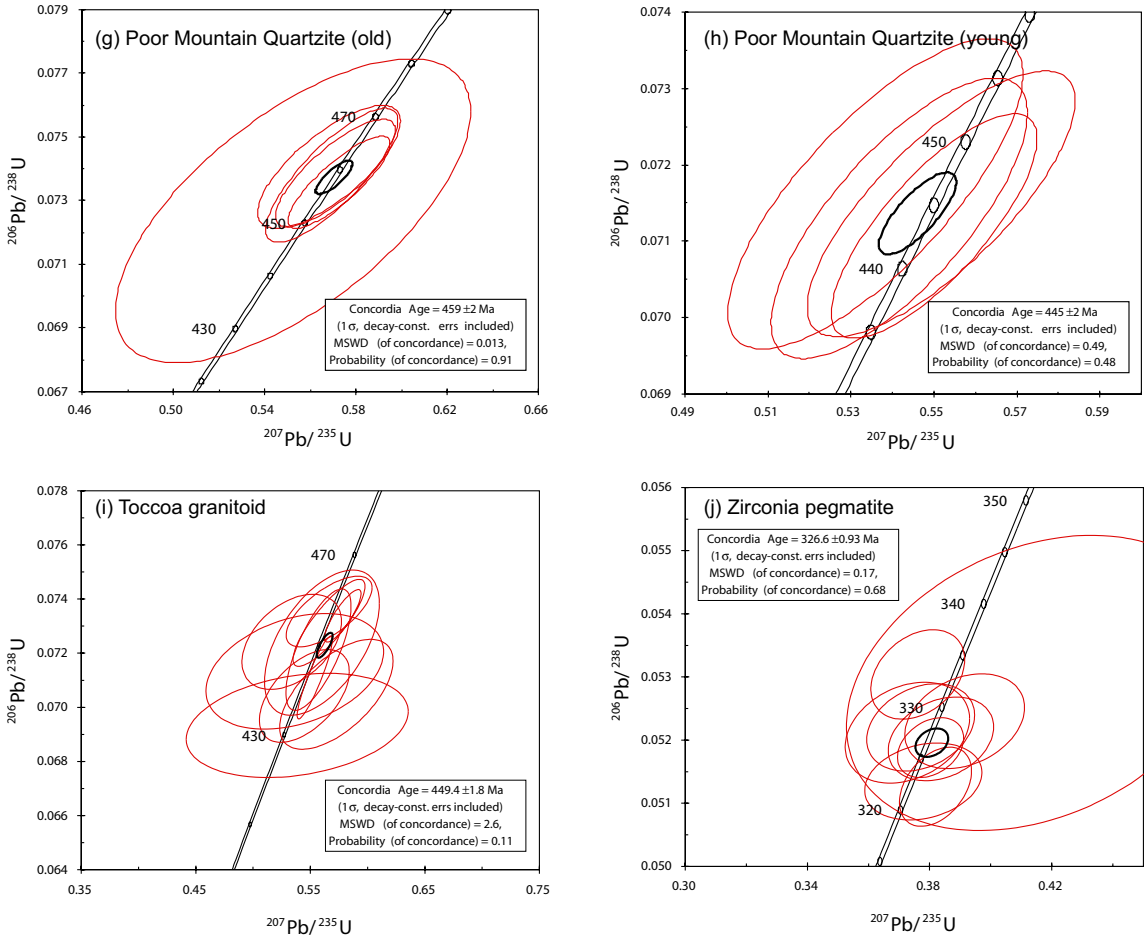

Figure 3. *continued*

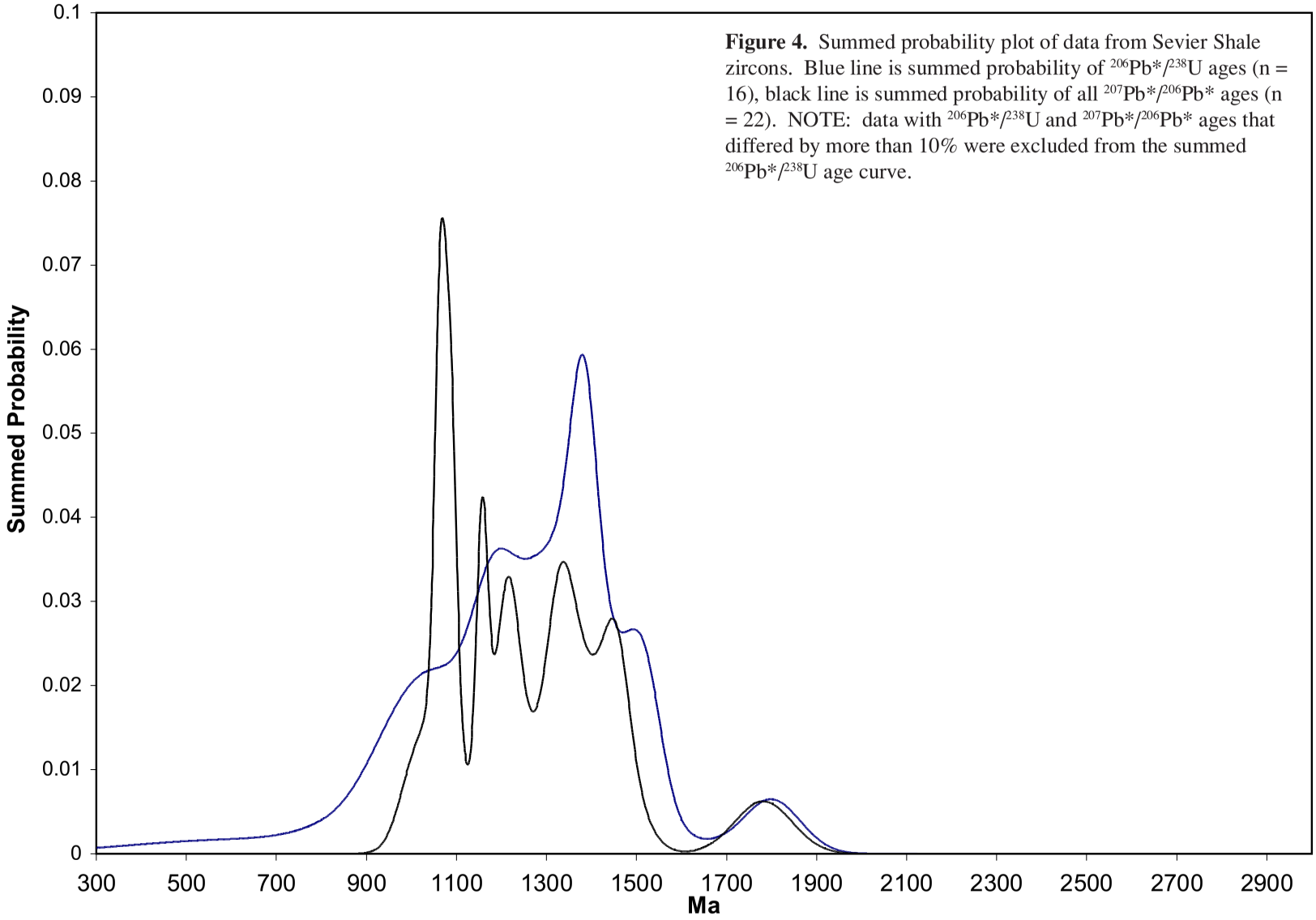

Figure 4. Summed probability plot of data from Sevier Shale zircons. Blue line is summed probability of $^{206}Pb^*/^{238}U$ ages (n = 16), black line is summed probability of all $^{207}Pb^*/^{206}Pb^*$ ages (n = 22). NOTE: data with $^{206}Pb^*/^{238}U$ and $^{207}Pb^*/^{206}Pb^*$ ages that differed by more than 10% were excluded from the summed $^{206}Pb^*/^{238}U$ age curve.

$^{206}Pb^*/^{238}U$ ages are Early Paleozoic for two analyses and ~950 Ma for one of the analyses.

Magmatic

Zircons analyzed from magmatic or suspect magmatic samples lack Grenvillian or older inheritance. Most grains exhibit magmatic zoning and are sub- to euhedral. Metamorphic overgrowths are generally rare (or poorly developed) with the notable exception of Lenoir Quarry migmatite grains (and eastern Inner Piedmont paragneiss samples discussed below).

Cane Creek Felsic Gneiss

Ion microprobe data, concordia diagrams, and a preliminary discussion of the results for this sample are also reported in Settles (2002). Analytical data for this sample are remarkably concordant and yield $^{206}Pb^*/^{238}U$ and concordia ages of 482 ± 4 Ma with the removal of a single discordant analysis.

Dysartsville Tonalite

Two analyses that overlapped core and rim zones and two reversely discordant analyses were removed from the pooled age determination. Pooled analyses for ten of fourteen magmatic zone analyses yielded $^{206}Pb^*/^{238}U$ and concordia ages of 468 ± 8 Ma. Several analyses are slightly to completely reversely discordant resulting in the reversely discordant concordia age. Two rim analyses were obtained on zircons from this sample yielding $^{206}Pb^*/^{238}U$ ages of 328 ± 8 and 347 ± 10 Ma, but the latter analysis is reversely discordant.

Kennesaw Granitoid

Pooled $^{206}Pb^*/^{238}U$ ages for all twelve analyses of zircons from this sample yield an age of 444 ± 10 Ma. Removal of one reversely discordant analysis results in a $^{206}Pb/^{238}U$ age of 444 ± 11 Ma and a concordia age of 442 ± 10 Ma.

Lenoir Quarry Migmatite

Ion microprobe data, concordia diagrams, and a discussion of this sample also appear in Kalbas (2003). Concordia diagrams have been replotted with discordia and concordia ages here. Eleven inherited zircon cores from this sample yielded $^{206}Pb/^{238}U$ ages ranging from 414 to 527 Ma. Removal of two reversely discordant and two younger (Pb-loss?) analyses yielded a pooled $^{206}Pb^*/^{238}U$ age of 450 ± 6 Ma. The concordia age for these seven analyses is 449 ± 6 Ma and the discordia line plotted for intersects the concordia line at 465 Ma. Twelve overgrowths on the zircons from this sample yielded $^{206}Pb^*/^{238}U$ ages ranging from 328 to 388 Ma when one young and one old outlier were excluded. The pooled $^{206}Pb^*/^{238}U$ age for the twelve thick (up to 50 μm wide) overgrowths is 344 ± 2 Ma (2σ error, MSWD = 2.6, n = 12). Summed probability plots of the overgrowth data suggest that two episodes of overgrowth may have occurred at 342 ± 5 Ma (2σ error, MSWD = 0.70, n = 3) and 330 ± 6 Ma (2σ error, MSWD = 0.79, n = 5). Based on the limited number of analyses it remains possible that the overgrowths in this sample developed at the same time; published U-Pb zircon rim and monazite studies, however, have reported comparable peaks (e.g., Dennis and Wright, 1997). Using both TIMS and Nd isotopic data, Hacker et al. (1998) interpreted a similar spread in SHRIMP ages to represent to be the result of older peak metamorphic and younger retrogressive growth. The Ordovician ages are interpreted here as the product of primary crystallization in the Poor Mountain Formation protolith.

Poor Mountain Quartzite (metatuff?) Member

$^{206}Pb^*/^{238}U$ ages for this sample range from Early Ordovician (~480 Ma) to Early Silurian (~430 Ma) with summed probability peaks at ~445 and ~460 Ma (Fig. 5). Removal of discordant data and outliers resulted in pooled $^{206}Pb^*/^{238}U$ and concordia ages of ~450 Ma with unreasonable MSWD's (2.66 for pooled $^{206}Pb/^{238}U$ ages) and probabilities (below 0.05 for concordia age equivalence and concordance). The

determined ages for data subsets yield 459 ± 4 and 445 ± 4 Ma ages. Based on these data it is doubtful that this sample contains zircons of a single age unless the cluster at 445 is interpreted to represent Pb-loss. It is important to note that it is unlikely that this sample contains abundant, or possibly any, Proterozoic zircons thus favoring a western Inner Piedmont source (magmatic or sedimentary). A single rim $^{206}Pb^*/^{238}U$ age of 386 ± 22 Ma (2σ error) was also obtained.

Toccoa Granitoid

$^{206}Pb^*/^{238}U$ ages for this sample range from 425 to 460 Ma. Removal of five younger analyses that might reflect Pb-loss resulted in a pooled $^{206}Pb/^{238}U$ and concordia age of 449 ± 4 Ma. Several analyses show slight normal discordance resulting in the low probability of concordance for the concordia age. A discordia line through all data has an upper intercept of 478 Ma.

Zirconia Pegmatite

Despite the large size (up to a cm) and multiple types of zoning present in the Zirconia pegmatite zircons, the ages are remarkably uniform. These grains have a wide range of U and Th concentrations, between 50 and 2200 ppm U and 40 and 5000 ppm Th with Th/U ratios from 0.02 to approximately 7. Removal of an analysis with the highest U concentration and lowest Th concentration of the group and a reversely discordant analyses resulted in pooled $^{206}Pb/^{238}U$ and concordia ages of 327 ± 2 Ma. The small error is attributed to the relatively high concentration of U in these zircons that resulted in significantly improved counts.

Metamorphic

Zircon overgrowths are most conspicuous on zircons from the Inner Piedmont, contain significantly more U and less Th (Table 2), and range in age between ~330 Ma to ~365 Ma (Fig. 6). Three peaks are discernable on summed probability plots when core-

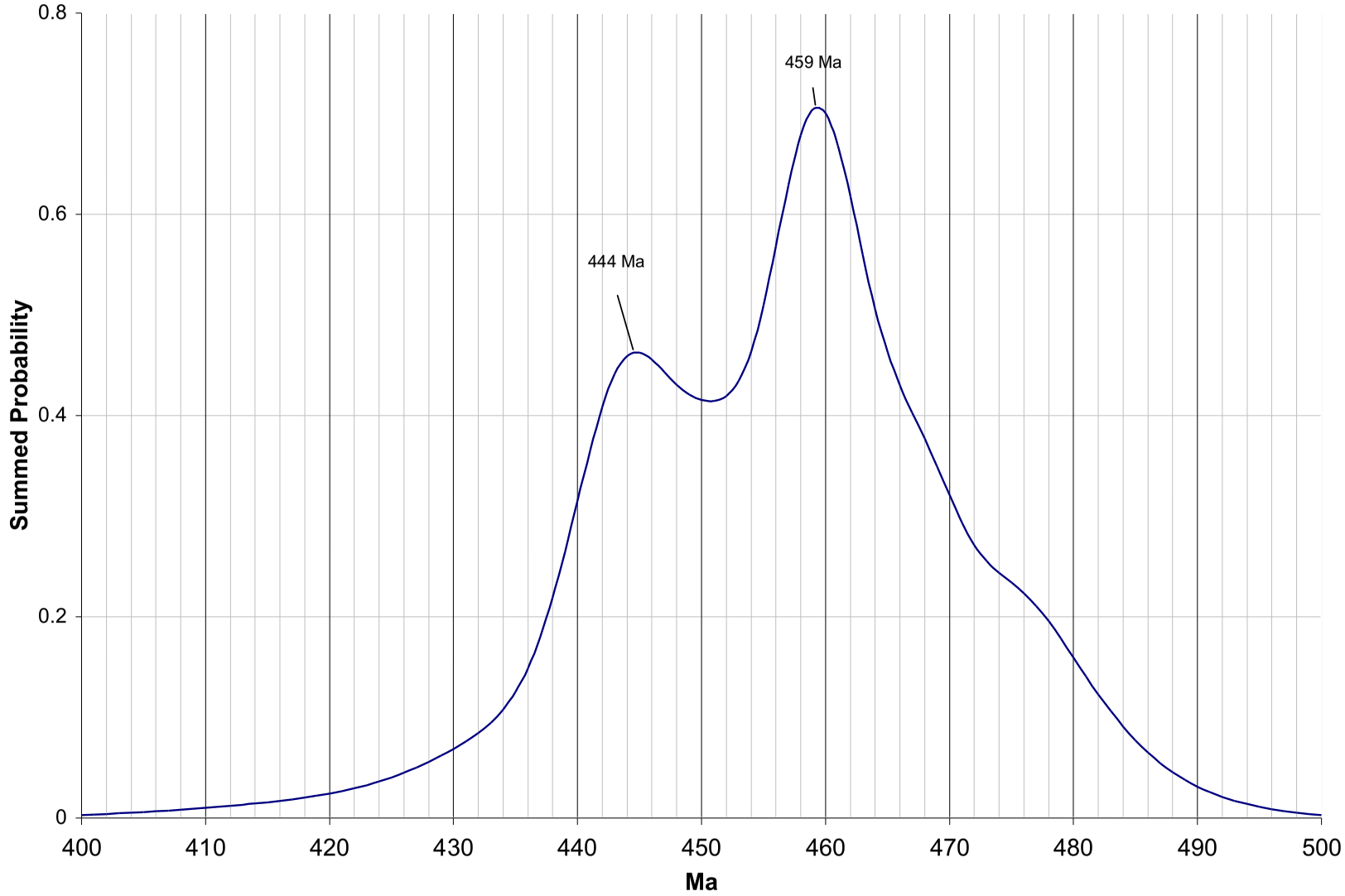

Figure 5. Summed probability plot of data from Poor Mountain Quartzite zircons.

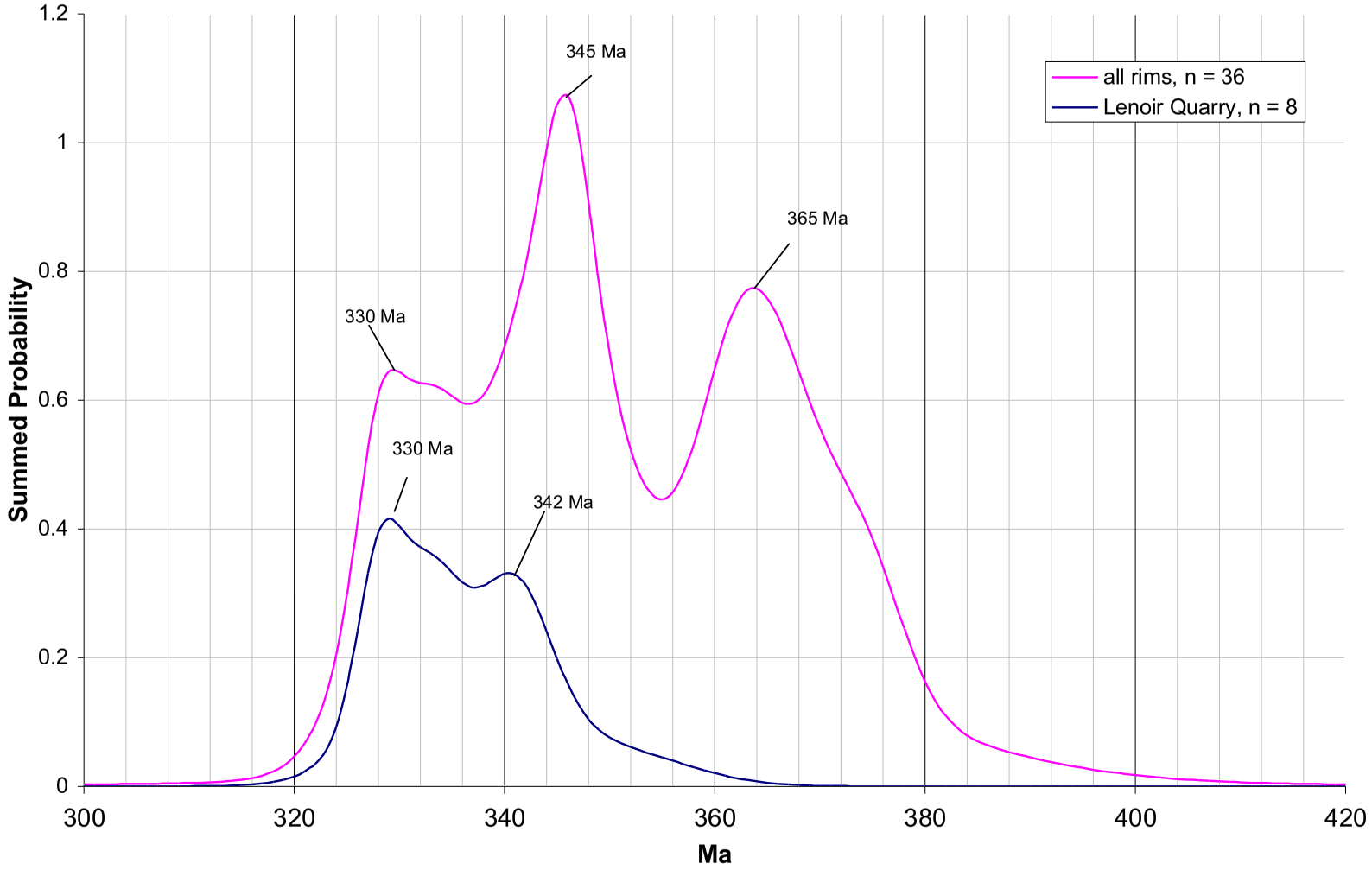

Figure 6. Summed probability plot of zircon rim analyses. Note that data from the Lenoir Quarry migmatite is included with "all rims."

rim overlap analyses are removed. These peaks are 330, 345, and 365 Ma for 36 analyses. Rims were analyzed in almost every Inner Piedmont sample but only one eastern Blue Ridge Ridge sample. Two analyses interpreted as core-rim overlaps, were identified in grains from the Dahlonega gold belt and the Poor Mountain Quartzite.

Whole-rock Sm-Nd and Rb-Sr data

Sm-Nd and Rb-Sr data and ages are provided in Tables 4 and 5, respectively. Sm-Nd data for sedimentary and metasedimentary samples, except for the Sevier Shale sample presented here, are reported in Bream et al. (in press).

Sedimentary and metasedimentary

Evolution of ε_{Nd} with time for the Sevier Shale sample plots toward the lower end of data from Bream et al. (in press) for (meta)sedimentary samples from the adjacent Blue Ridge and distal (relative to the foreland) Inner Piedmont (Fig. 7). This sample yielded very low ε_{Nd} values (-15.2 at 0 Ma and –10.8 at 475 Ma) suggesting that it was derived from a more evolved, and perhaps partially eroded, part of the adjacent western Blue Ridge. When plotted against data of Blue Ridge Proterozoic basement, the Sevier Shale is more compatible with data from the Mars Hill terrane (Carrigan et al., in press; Ownby et al., in press). Alternatively, the Sevier Shale may also be derived from more isotopically mature metasedimentary rocks than were sampled by Bream et al. (in press). Despite possible Sr mobility, relatively high initial $^{87}Sr/^{86}Sr$ values and Middle to Upper Proterozoic T_{DM} ages for almost all samples suggest derivation from Proterozoic rocks similar to Blue Ridge basement.

Metaigneous

T_{DM} values for Cane Creek, Dysartsville, Kennesaw, and Toccoa granitoids suggest derivation from preexisting Grenvillian and older crust (T_{DM} between 1.2 and 2 Ga) (Table 4) with most samples plotting near or slightly more positive than fields for

Table 4. Sm-Nd concentrations and isotopic data.

Unit or Formation	Sample ID†	Age‡ (in Ma)	Sm (ppm)	Nd (ppm)	$^{147}Sm/^{144}Nd$	$^{143}Nd/^{144}Nd$§ (± 2σ)	$\varepsilon_{Nd}^{(0)}$#	$\varepsilon_{Nd}^{(t)}$#	T_{DM}†† (in Ga)
sedimentary									
Sevier Shale	SEV (V&R)	475	1.07	5.36	0.12333	0.511858 (7)	-15.2	-10.8	2.00
(meta) igneous									
Cane Creek felsic gneiss	WIMPY (Dgb)	482	2.43	12.08	0.12449	0.512215 (3)	-8.2	-3.8	1.41
Dysartsville Tonalite	VM1782 (wIP)	468	0.91	3.36	0.16810	0.512458 (7)	-3.5	-1.8	1.95
Kennesaw granitoid	KEN (eBR)	444	3.04	14.10	0.13351	0.512307 (7)	-6.5	-2.9	1.39
Lenoir Quarry migmatite	LVQ1 (wIP)	450	1.39	8.22	0.10458	0.512371 (9)	-5.2	0.1	0.94
Poor Mountain Quartzite	POMTN (wIP)	451	2.29	5.30	0.26740	0.512853 (3)	4.2	0.1	-- ‡‡
Toccoa granitoid	TOC1 (wIP)	449	4.70	22.78	0.12763	0.512376 (4)	-5.1	-1.2	1.18

† Dgb = Dahlonega gold belt, V&R = Valley and Ridge, wIP = western Inner Piedmont.

‡ Age is the preferred depositional or magmatic age as summarized in Table 3 and text.

§ $^{143}Nd/^{144}Nd$ measured ratios normalized to $^{146}Nd/^{144}Nd = 0.7219$, 2σ errors reported to the last significant digit.

$\varepsilon_{Nd}^{(t)} = \{[(^{143}Nd/^{144}Nd)_{Sample}^{(t)} - (^{143}Nd/^{144}Nd)_{Bulk\ Earth}^{(t)}] / (^{143}Nd/^{144}Nd)_{Bulk\ Earth}^{(t)}\} \times 10^4$. $\varepsilon_{Nd}^{(0)}$ = at present day, $\varepsilon_{Nd}^{(t)}$ = at time of crystallization or deposition. Bulk Earth present day parameters: $^{143}Nd/^{144}Nd = 0.512638$, $^{147}Sm/^{144}Nd = 0.1967$.

†† T_{DM} age calculated according to DePaolo (1981), $\varepsilon_{Nd} = 0.25T^2 - 3T + 8.5$.

‡‡ T_{DM} unreliable due to high $^{147}Sm/^{144}Nd$ value.

Table 5. Rb-Sr concentrations and isotopic data.

	Unit or Formation	Sample ID†	Age‡ (in Ma)	Rb (ppm)	Sr (ppm)	$^{87}Rb/^{86}Sr$	$^{87}Sr/^{86}Sr^{(0)}$§ (± 2σ)	$^{87}Sr/^{86}Sr^{(t)}$
(meta) sedimentary	-not assigned-	BCTF (eIP)	420	115.7	447.6	0.748	0.713477 (08)	0.709003
	Tallulah Falls Fm.	BECR (eBR)	~550	74.6	140.7	1.539	0.731331 (10)	0.719266
	Tallulah Falls Fm.	BOCAT (eBR)	~550	36.6	170.3	0.623	0.721219 (12)	0.716337
	Chauga River Fm.	BPM1 (wIP)	~550	97.8	190.8	1.485	0.724504 (13)	0.712864
	Coleman River Fm.	COLRAB (cBR)	~550	13.5	228.4	0.171	0.721700 (10)	0.720357
	-not assigned-	GR1 (eIP)	420	169.0	217.7	2.251	0.725620 (10)	0.712156
	Tallulah Falls Fm.	KEOTF (wIP)	~550	103.3	208.0	1.438	0.722353 (10)	0.711078
	Snowbird Gp.	LQZT (wBR)	~550	95.4	64.1	4.325	0.753174 (09)	0.719264
	Otto Fm.	OTCOW (Dgb)	~550	101.1	288.3	1.016	0.723334 (10)	0.715370
	Otto Fm.	OTD (Dgb)	~550	105.2	127.6	2.390	0.730408 (10)	0.711667
	Pilot Mountain Quartzite	PMQZT (SMW)	~550	18.6	10.2	5.284	0.748500 (08)	0.707070
	Otto Fm.	QMS1 (Dgb)	~550	84.7	101.2	2.428	0.732666 (13)	0.713632
	Walden Creek Gp.	SERV2 (wBR)	~550	68.1	185.9	1.061	0.721833 (13)	0.713513
	Sevier Shale	SEV (V&R)	475	5.6	291.1	0.055	0.710025 (09)	0.709651
	Hogan Creek Fm.	SM-HC (SMW)	~550	15.9	72.2	0.639	0.727186 (10)	0.722176
	Tallulah Falls Fm.	SM-TF (eBR)	~550	81.9	109.0	2.177	0.725869 (10)	0.708800
	Walden Creek Gp.	TELP2 (wBR)	~550	77.2	68.0	3.294	0.739895 (10)	0.714065
	Tallulah Falls Fm.	TFQZT1 (eBR)	~550	191.5	172.1	3.231	0.744100 (10)	0.718770
	Tallulah Falls Fm.	TFQZT2 (eBR)	~550	76.2	100.9	2.192	0.736784 (10)	0.719595
	Tallulah Falls Fm.	TFTIG441 (eBR)	~550	11.3	109.7	0.300	0.725726 (12)	0.723376
	Tallulah Falls Fm.	UTF85 (wIP)	~550	105.0	285.1	1.066	0.720680 (10)	0.712319
(meta) igneous	Kennesaw granitoid	KEN (eBR)	444	51.0	296.5	0.498	0.709710 (09)	0.706560
	Lenoir Quarry Migmatite	LVQ1 (wIP)	450	44.1	128.0	0.997	0.711732 (09)	0.705343
	Poor Mountain Quartzite	POMTN (wIP)	451	5.6	3.4	4.821	0.735803 (13)	0.704829
	Toccoa granitoid	TOC1 (wIP)	449	89.7	88.1	2.952	0.725962 (06)	0.707080
	Dysartsville Tonalite	VM1782 (wIP)	468	31.4	126.4	0.720	0.711463 (09)	0.706664
	Cane Creek felsic gneiss	WIMPY (Dgb)	482	56.1	84.5	1.925	0.721034 (10)	0.707815

† Dgb = Dahlonega gold belt, cBR = central Blue Ridge, eBR = eastern Blue Ridge, eIP = eastern Inner Piedmont, SMW = Sauratown Mountains Window, V&R = Valley and Ridge, wBR = western Blue Ridge, wIP = western Inner Piedmont.

‡ Age is the preferred depositional or magmatic age as summarized in the text and Table 3.

§ $^{87}Sr/^{86}Sr$ measured ratios normalized to $^{86}Sr/^{88}Sr = 0.1194$, 2σ errors are reported as last two significant digits.

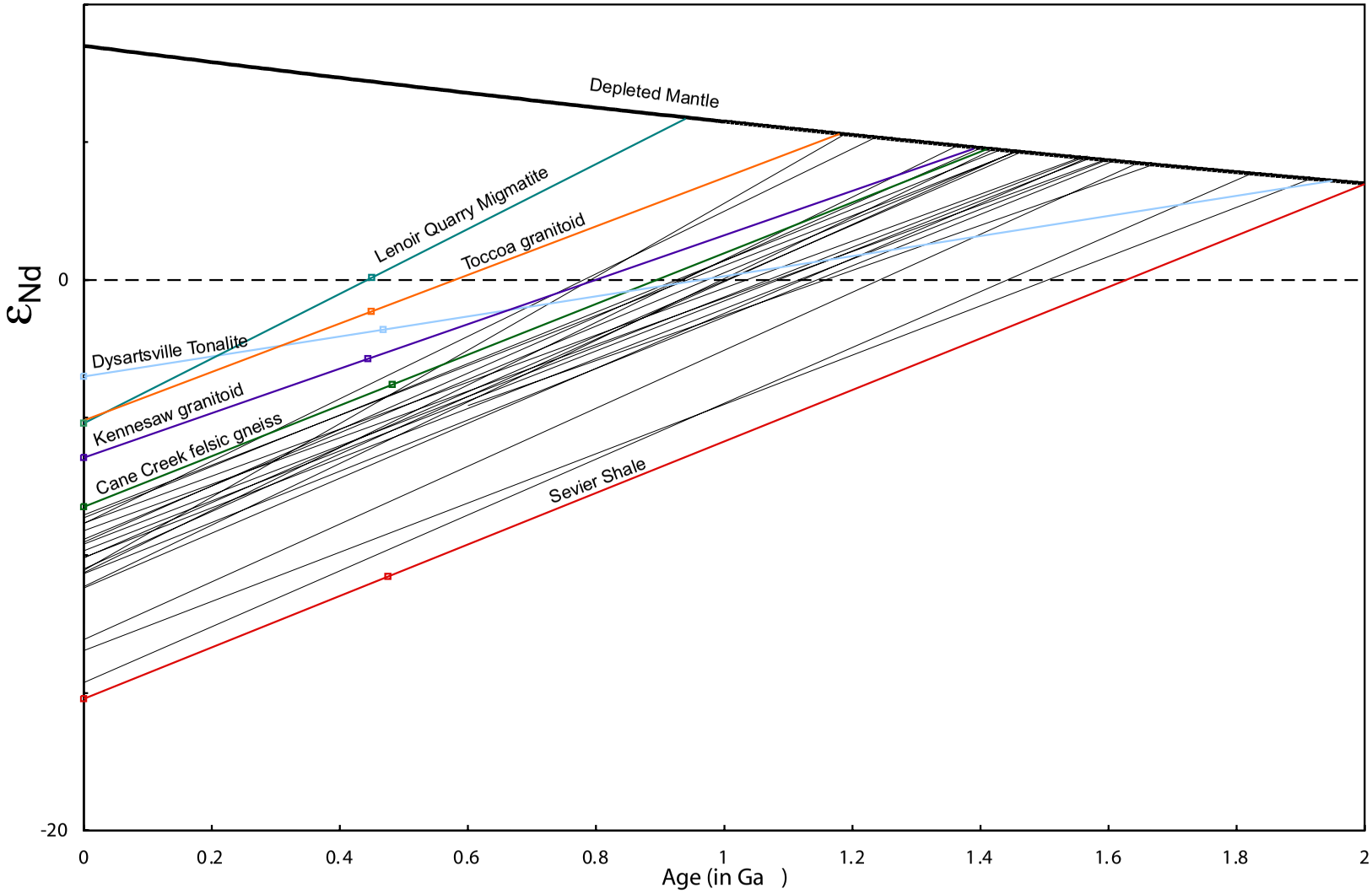

Figure 7. ε_{Nd} evolution with time compared to metasedimentary data, black lines, of Bream et al. (in press).

Grenvillian basement at the time of crystallization (Carrigan et al., in press; Hatcher et al., in press; Ownby et al., in press) (Fig. 7). The Lenoir Quarry Migmatite sample yielded the youngest T_{DM} age of ~1.0 Ga, but is comparable to T_{DM} ages reported for western Inner Piedmont plutons (Fullagar et al., 1997; Vinson, 1999). Poor Mountain Quartzite $^{147}Sm/^{144}Sm$ was too high (0.26740) to produce a meaningfull T_{DM} age. Interestingly, both the Cane Creek and Kennesaw samples have the most negative present-day ε_{Nd} values, -8.2 and -6.5 respectively. Initial $^{87}Sr/^{86}Sr$ values for all samples suggest derivation from older continental crustal sources with the possible exception of the Poor Mountain Quartzite (metatuff?) in agreement with the T_{DM} ages (Fig. 8). Other workers have reported similar results for southern Appalachian plutons (e.g., Fullagar et al., 1997).

Whole-rock geochemistry

Sedimentary and metasedimentary

Most samples have high SiO_2 (60-90%), and large ranges of Al_2O_3 (1-18%), Na_2O (0.05-4.2), and K_2O (0.2-6.3) (Table 6). The degree of weathering in sedimentary samples is estimated using the chemical index of alteration (CIA; CIA = $[(Al_2O_3)/(CaO + Na_2O + K_2O + Al_2O_3)] *100$; Nesbitt and Young, 1982). Expected values for idealized rock types are as follows: fresh basalts (30-45), granites and granodiorites (45-55), average shales (70-75) (Nesbitt and Young, 1982). With the exception of the Sevier Shale (CIA = 2) and the Pilot Mountain Quartzite (CIA = 75), the samples have CIA values ranging from 41 to 66 (Table 6) suggesting minor to moderate weathering. The low CIA in the Sevier Shale is due to the high CaO content, 41%, of the sample and the high CIA value for the Pilot Mountain Quartzite sample, a quartz arenite, results from low concentrations of CaO, Na_2O, and K_2O. High SiO_2, moderate weathering, and the somewhat coarse-grained nature of most samples are compatible with the interpreted

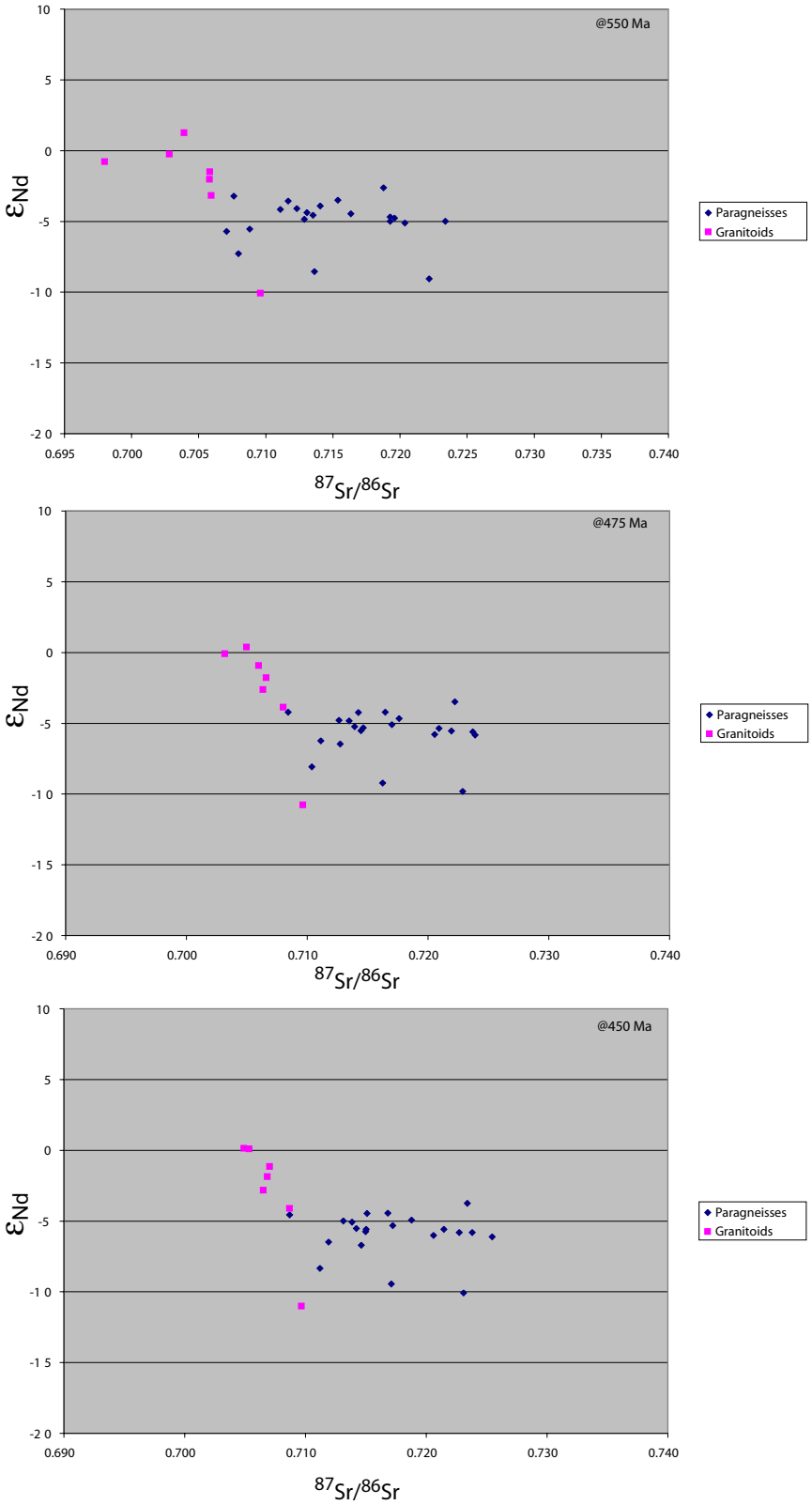

Figure 8. ε_{Nd} vs. Sr/Sr at 550, 475, and 420 Ma.

Table 6. Whole-rock oxide weight percents with chemical indices of alteration (CIA) for (meta)sedimentary samples. nd-below detection limit.

Unit or Formation[†]		-na-	TF Fm	TF Fm	CR Fm	CR Fm	WC Gp	-na-	TF Fm	S Gp	O Fm	O Fm	PM Qtz	O Fm	WC Gp	S Sh	HC Fm	TF Fm	WC Gp	TF Fm	TF Fm	TF Fm	TF Fm
Sample ID		BCTF	BECR	BOCAT	BPM1	COLRAB	CHDAM	GR1	KEOTF	LQZT	OTCOW	OTD	PMQZT	QMS1	SERV2	SEV	SM-HC	SM-TF	TELP2	TFQZT1	TFQZT2	TFTIG441	UTF85
Tectonic belt[‡]		(eIP)	(eBR)	(eBR)	(wIP)	(cBR)	(wBR)	(eIP)	(wIP)	(wBR)	(Dgb)	(Dgb)	(SMW)	(Dgb)	(wBR)	(V&R)	(SMW)	(eBR)	(wBR)	(eBR)	(eBR)	(eBR)	(wIP)
Detection Limit[#]																							
SiO_2	0.01 %	65.67	71.34	77.15	68.30	72.61	75.93	64.08	66.65	89.18	61.36	65.20	95.71	77.44	79.77	20.62	68.19	63.73	69.76	71.50	88.98	68.76	65.82
Al_2O_3	0.01 %	17.70	12.37	10.85	14.09	11.40	7.36	14.87	15.26	5.69	14.56	15.56	2.80	10.35	6.54	1.27	12.68	15.46	14.71	13.30	5.05	13.28	15.62
Fe_2O_3	0.01 %	4.02	5.33	3.57	6.08	4.28	4.17	6.05	5.89	0.45	9.84	6.27	0.27	4.14	1.98	0.55	7.69	5.40	4.58	3.54	0.96	5.50	6.29
MnO	0.01 %	0.03	0.09	0.08	0.09	0.22	0.089	0.07	0.09	nd	0.07	0.09	nd	0.05	0.05	0.02	0.18	0.10	0.03	0.03	0.01	0.08	0.10
MgO	0.01 %	1.62	1.79	1.18	1.58	0.83	0.9	4.27	1.76	0.10	2.71	2.14	0.09	1.23	0.61	1.74	1.93	2.11	1.06	0.96	0.27	2.51	1.92
CaO	0.01 %	3.20	1.92	1.27	1.96	7.65	2.74	3.89	2.15	0.02	2.53	2.25	nd	0.71	2.36	41.49	2.17	1.57	1.03	0.80	0.19	3.30	2.70
Na_2O	0.01 %	4.19	3.22	3.26	2.38	0.83	1.17	1.65	2.65	0.47	2.50	2.45	0.05	1.61	1.27	0.41	2.23	2.60	1.91	2.26	0.52	2.35	3.37
K_2O	0.01 %	2.01	2.02	1.24	3.03	0.37	2.4	2.98	3.12	3.63	2.89	3.37	0.80	2.17	2.84	0.19	2.07	4.12	2.26	6.31	3.08	2.51	2.32
TiO_2	0.005 %	0.595	0.803	0.714	0.925	0.801	0.531	0.816	0.922	0.067	1.821	0.954	0.175	0.820	0.701	0.051	0.901	0.809	1.194	0.669	0.542	0.874	0.692
P_2O_5	0.01 %	0.11	0.16	0.10	0.17	0.20	0.12	0.16	0.17	0.04	0.22	0.16	0.03	0.15	0.08	0.04	0.05	0.18	0.16	0.15	0.03	0.20	0.22
LOI	0.01 %	1.14	0.94	0.88	1.60	1.14	4.97	1.38	1.84	0.52	1.55	1.72	0.55	1.65	4.05	34.13	0.68	2.48	3.05	0.78	0.53	0.85	1.18
TOTAL	%	100.29	99.98	100.29	100.20	100.34	100.39	100.21	100.50	100.17	100.06	100.17	100.47	100.32	100.25	100.49	98.77	98.56	99.75	100.30	100.17	100.22	100.24
CIA		54	53	55	57	44	42	53	57	55	55	57	75	62	41	2	56	57	66	53	53	51	55

[†] -na- = not assigned, TF Fm = Tallulah Falls Fm., CR Fm = Coleman River Fm., WC Gp = Walden Creek Gp., S Gp = Snowbird Gp., O Fm = Otto Fm., PM Qtz = Pilot Mountain Quartzite, S Sh = Sevier Shale, HC Fm = Hogan Creek Fm.

[‡] Dgb = Dahlonega gold belt, cBR = central Blue Ridge, eBR = eastern Blue Ridge, EIP = eastern Inner Piedmont, V&R = Valley and Ridge, SMW = Sauratown Mountains window, wBR = western Blue Ridge, wIP = western Inner Piedmont.

[#] CIA = $Al_2O_3/[Al_2O_3 + K_2O + Na_2O + CaO]$ *100 using molecular proportions (Nesbitt and Young, 1982).

rifted margin depositional setting.

Multielement plots normalized to the North American shale composite (NASC: Gromet et al., 1984) show more spread in the more mobile and less compatible elements (during Paleozoic metamorphism) and restricted ranges, near NASC values, for less mobile and more compatible elements (Fig. 9). The largest variations are present in the Sevier Shale, western Blue Ridge, and Sauratown Mountains window sample composite plot. This is attributed to the variety of lithologies sampled here which include a quartz arenite, conglomerate, feldspathic sandstone, and calcareous siltstone. The remaining sample groupings for the central Blue Ridge, eastern Blue Ridge, western Inner Piedmont, and eastern Inner Piedmont show remarkably similar elemental trends. Almost all samples show minimal to no enrichment in these elements with depletion in Mn and Cs relative to NASC.

Rare earth elemental concentrations in sedimentary and metasedimentary rocks provide an average value of the source rock(s) (e.g., Taylor et al., 1986) and remain largely unaltered by sedimentary and metamorphic processes (e.g., Fleet, 1984; Muecke et al., 1979). Thus, the REE trends in southern Appalachian (meta)sedimentary samples provide important information about the rocks from which they were derived. Most samples show moderate to pronounced negative Eu anomalies (Eu/Eu* = 0.5-0.9) and LREE-enrichment (La_N/Yb_N = 5-27, with most between 5 and 9) similar to trends for Blue Ridge Grenvillian samples (Fig. 10). One eastern Inner Piedmont sample, BCTF, showed a postive Eu anomaly (Eu/Eu* = 1.3) and the greatest LREE (La_N/Yb_N = 27).

Trace element ratios most useful for assessing the sedimentary characteristics of siliciclastics are Th/Sc, Zr/Sc, La/Sc, Co/Th, Cr/Th, Cr/V, and V/Ni (McLennan et al., 1983, 1990; Taylor and McLennan, 1985; Wronkiewicz and Condie, 1990; Cullers, 1994). The Th, Sc, and Zr concentrations provide an estimate of chemical differentiation in source material and sedimentary recycling/sorting because Th is incompatible in

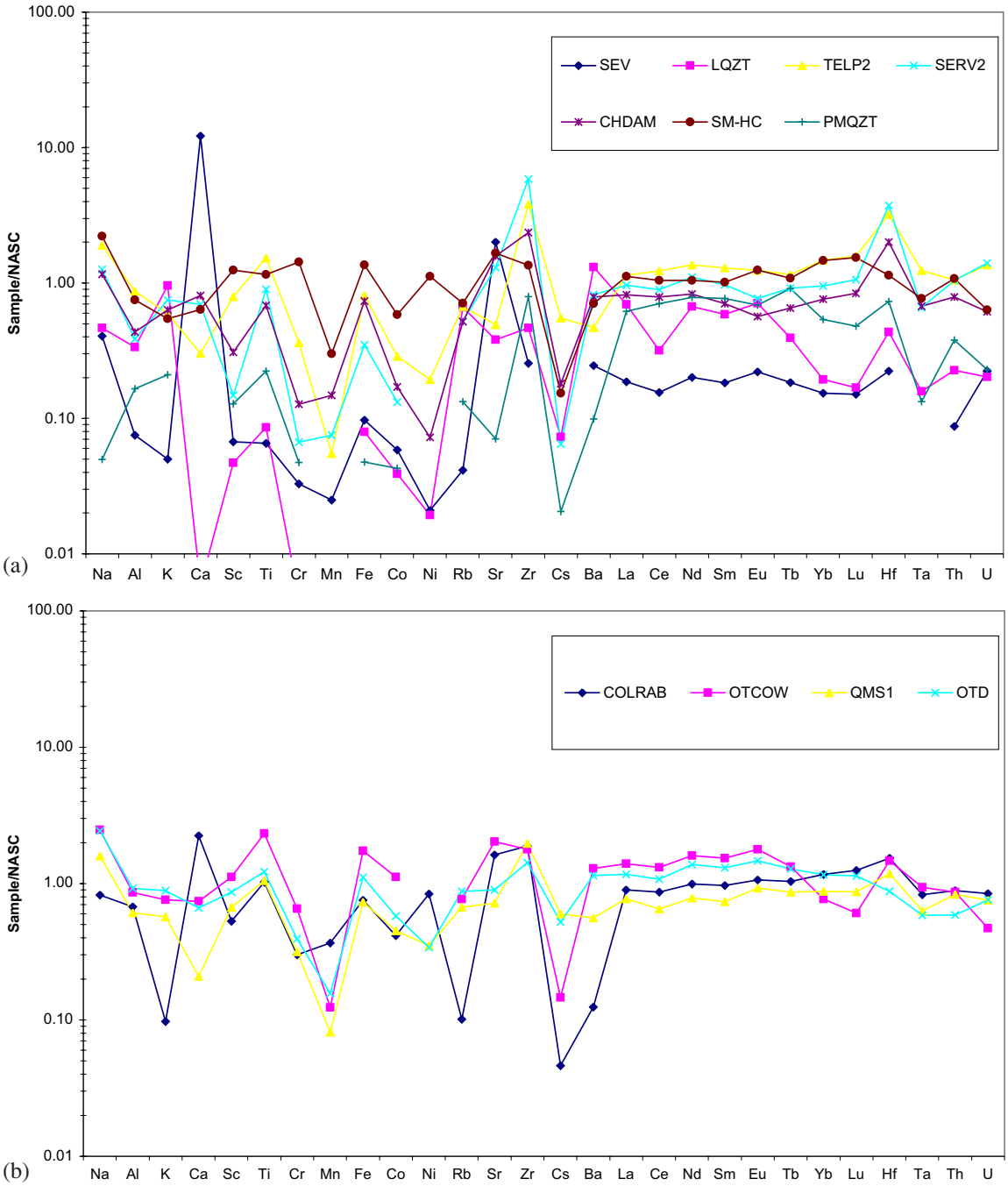

Figure 9. Element variance for (meta)sedimentary sample data normalized to North American shale composite (NASC; Gromet et al., 1984). (a) Sevier Shale (Valley and Ridge), western Blue Ridge, and Sauratown Mountains window. (b) Central Blue Ridge. (c) Eastern Blue Ridge and western Inner Piedmont. (d) Eastern Inner Piedmont.

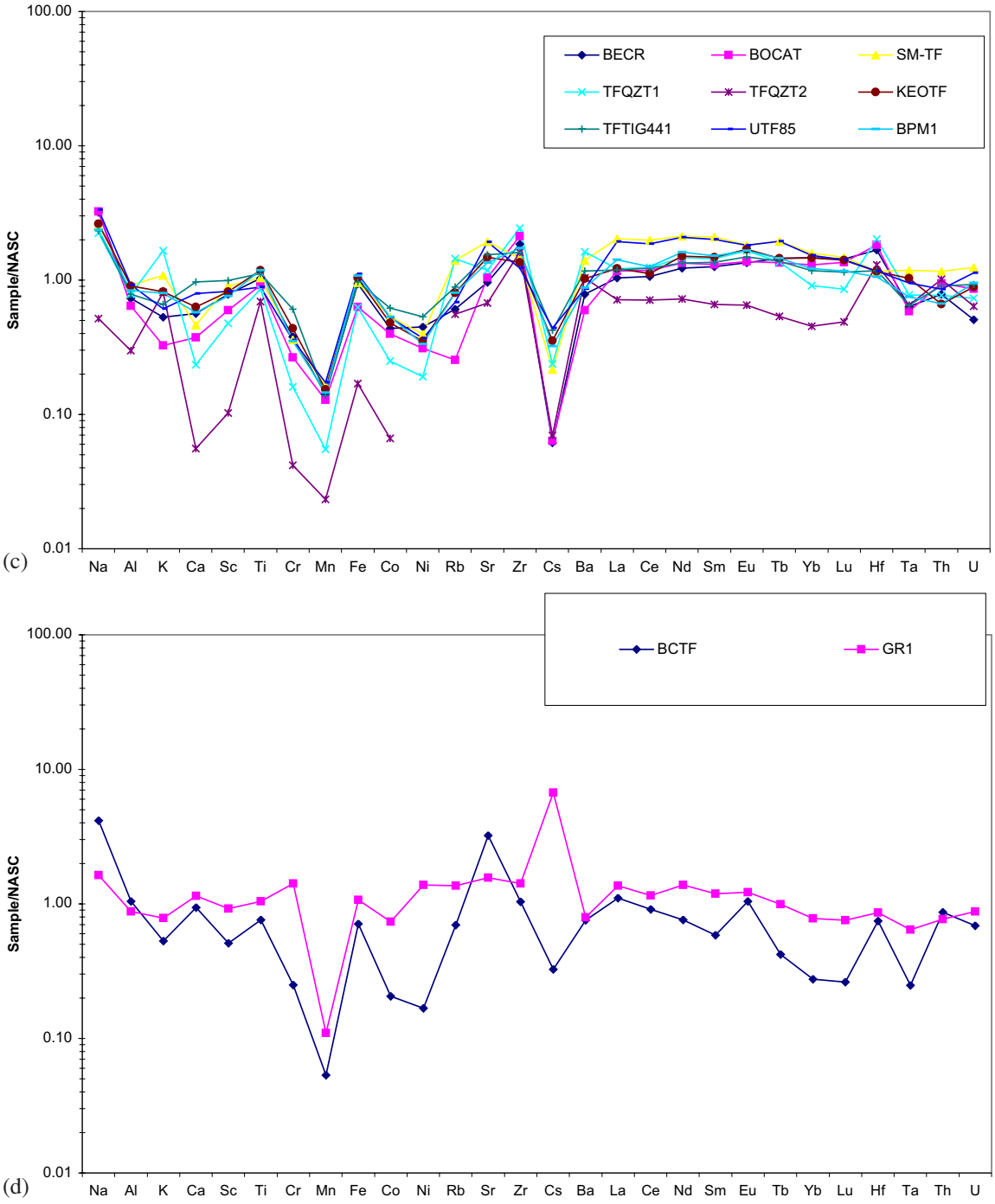

Figure 9. *continued*

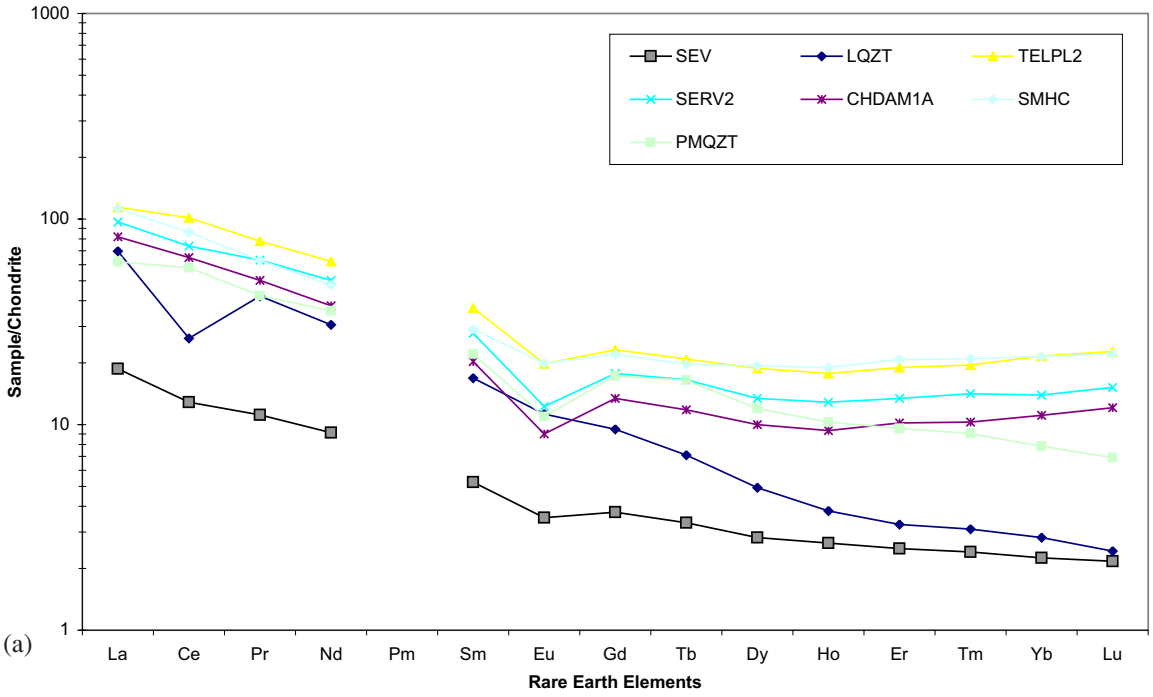

(a)

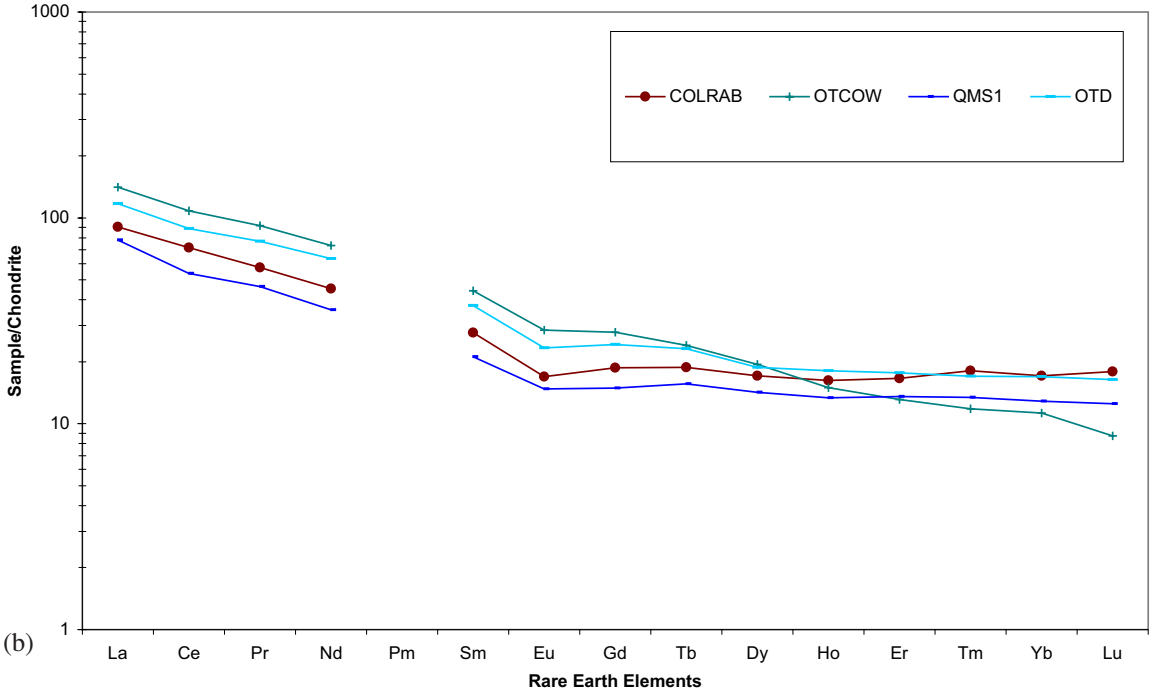

(b)

Figure 10. Chondrite normalized REE plot of (meta)sedimentary data. (a) Sevier Shale (Valley and Ridge), western Blue Ridge, and Sauratown Mountains window. (b) Central Blue Ridge. (c) Eastern Blue Ridge and western Inner Piedmont. (d) Eastern Inner Piedmont. (e) Blue Ridge Grenvillian basement data from Carrigan et al. (in press) and Hatcher et al. (in press). (f) Mars Hill terrane data from Carrigan et al. (in press) and Ownby et al. (in press).

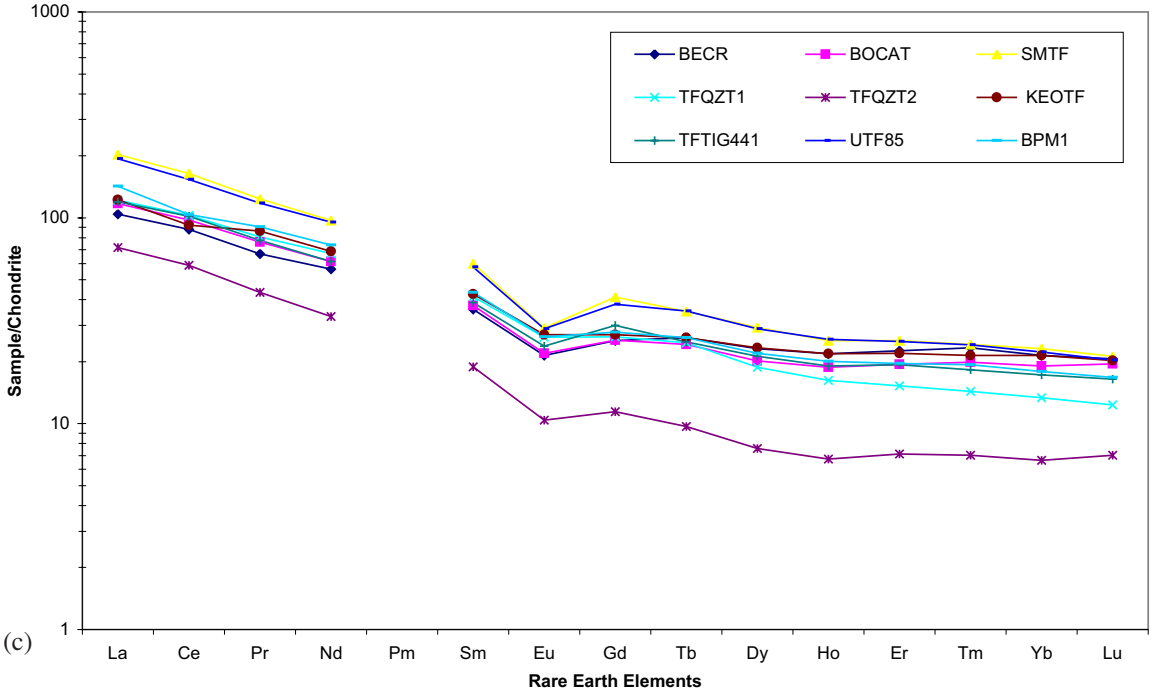

(c)

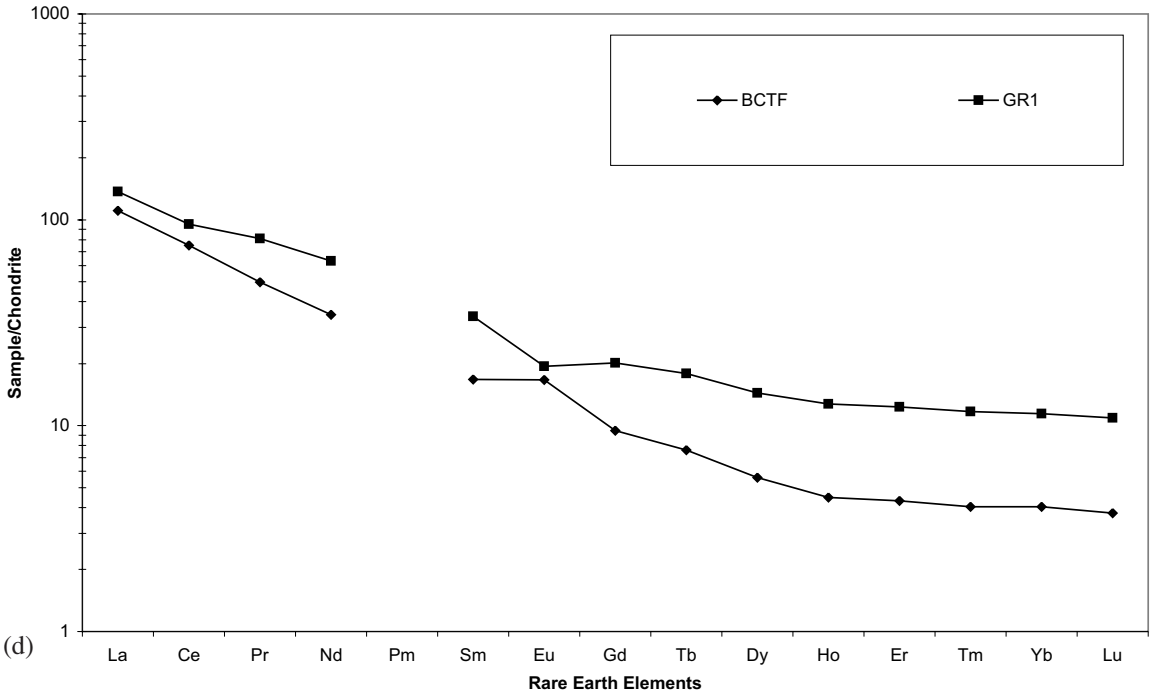

(d)

Figure 10. *continued*

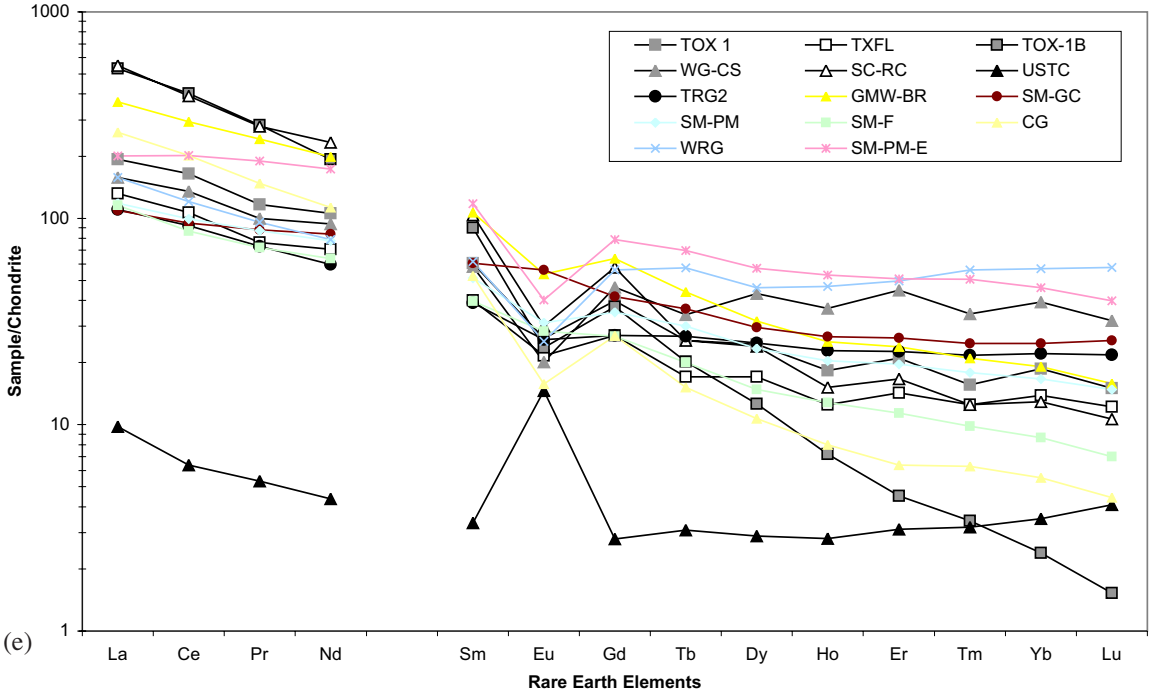

(e)

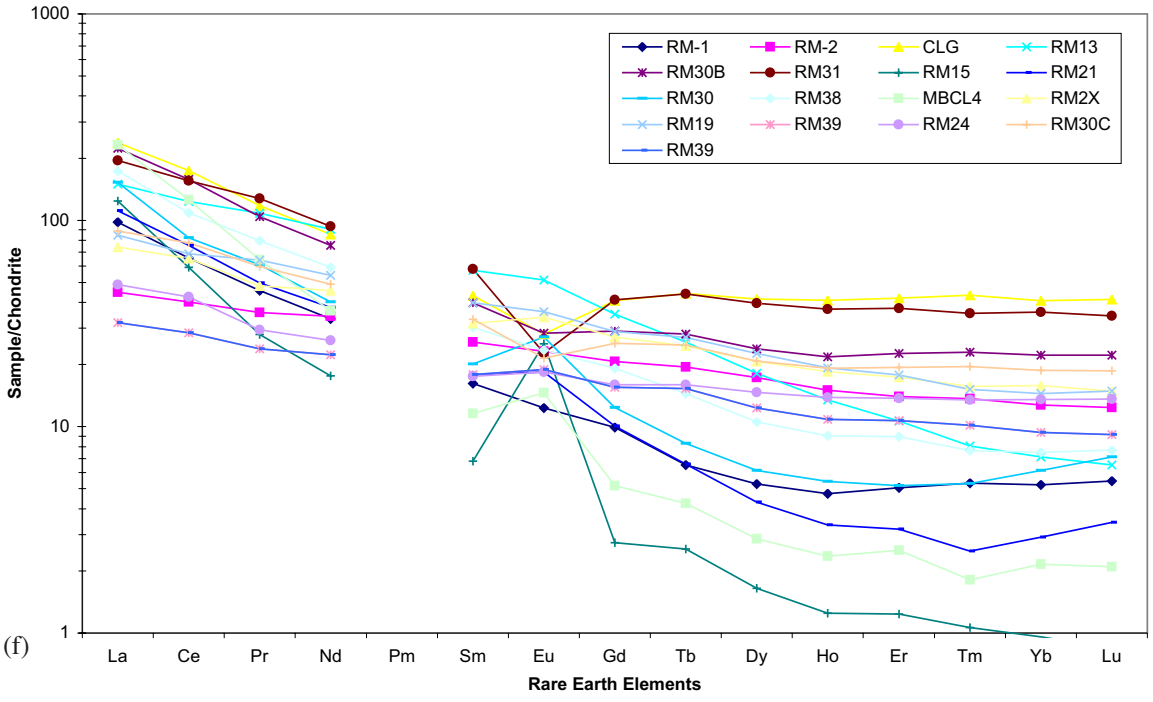

(f)

Figure 10. *continued*

comparison to Sc in igneous rocks and Zr is enriched during sedimentary recycling and sorting (McLennan et al., 1993). Southern Appalachian samples have Th/Sc ratios between 0.6 and 1.5, five samples are between 2 and 8.1, and Zr/Sc ratios between 15 and 532 with most less than 200. Similarly, La/Sc values are mostly between 2 and 6, but, four analyses have values between 10 and 31. Co/Th values are between 0.1 to 2.7, Cr/Th values are between 0.2-8.0 with two higher values of 13.4 and 18.6, Cr/V values are between 0.1 and 1.7, and V/Ni values for samples with detectable Ni are between 1.3 and 8.5. Comparison of Th/Sc versus Zr/Sc for data here with a model proposed for compositional variation and sediment recycling (Zr addition) in trailing edge and active margin turbidites (McLennan et al., 1990) suggests that sedimentary recycling occurred for some samples. The narrow range of Zr/Sc (most between 10 and 100) and Th/Sc (most between 0.7 and 1.1) favors derivation from a compositionally uniform source. Th/Sc, La/Sc, Co/Th, Cr/Th, Cr/V, and V/Ni values are comparable to those of post Archean average Australian shale (PAAS; 0.9 for Th/Sc; 2.4 for La/Sc; 1.6 for Co/Th; 7.5 for Cr/Th; 0.7 for Cr/V; 2.7 for V/Ni; Taylor and McLennan, 1985) (Table 7). Higher Th/Sc and La/Sc values are attributed to heavy mineral concentration during sedimentary processes. Tectonic discriminant diagrams (Bhatia and Crook, 1986) suggest a continental island arc or passive continental margin setting (Fig. 11).

Metaigneous

Sampled granitoids are felsic with SiO_2 greater than 70% in all samples except the Kennesaw granitoid (61%) (Table 8). Sr concentrations are low, between 80-305 ppm (Poor Mountain Quartzite sample has 4 ppm) (Table 9), like other Ordovician granitoids in the southern Appalachian crystalline core (e.g., Vinson, 1999). The samples are also LREE-enriched with moderate to pronounced negative Eu anomalies (Fig. 12) and have high concentrations of large-ion lithophile elements (LILE) and high field strength elements (HFSE) (Fig. 13). Notable exceptions include the Lenoir Quarry Migmatite

Table 7. Whole-rock trace element concentrations and ratios for (meta)sedimentary samples. nd-below detection limit. See Table 6 for abbreviations.

	Unit or Formation[†]	-na-	TF Fm	TF Fm	CR Fm	CR Fm	WC Gp	-na-	TF Fm	S Gp	O Fm	O Fm	PM Qtz	O Fm	WC Gp
	Sample ID	BCTF	BECR	BOCAT	BPM1	COLRAB	CHDAM	GR1	KEOTF	LQZT	OTCOW	OTD	PMQZT	QMS1	SERV2
	Tectonic belt[‡]	(eIP)	(eBR)	(eBR)	(wIP)	(cBR)	(wBR)	(eIP)	(wIP)	(wBR)	(Dgb)	(Dgb)	(SMW)	(Dgb)	(wBR)
	Detection Limit[#]														
Sc	0.01 ppm	7.60	11.70	8.91	11.30	7.92	4.60	13.70	12.20	0.70	16.70	12.90	1.91	10.00	2.20
V	5 ppm	82	72	54	70	70	35	105	78	7	171	84	11	82	17
Cr	0.5 ppm	31.1	47.2	33.1	43.8	37.4	15.8	176.0	54.4	0.6	81.3	49.0	5.9	39.4	8.3
Co	0.1 ppm	5.3	11.2	10.2	13.7	10.7	4.4	18.9	12.3	1.0	28.8	14.9	1.1	11.6	3.4
Ni	1 ppm	10	26	18	19	49	4	80	20	1	nd	20	nd	20	nd
As	1 ppm	nd	nd	nd	nd	1	2	98	nd	nd	nd	nd	nd	2	4
Br	0.5 ppm	nd	nd	nd	nd	nd	1.0	nd	nd	1.8	nd	nd	nd	nd	1.4
Rb	2 ppm	87	76	32	101	13	65	170	101	82	96	110	17	84	65
Sr	2 ppm	457	137	148	191	231	225	222	210	54	288	128	10	102	185
Y	1 ppm	9	42	37	42	32	19	26	41	7	28	38	21	29	27
Zr	1 ppm	208	371	425	345	378	473	283	271	93	356	285	159	394	1170
Nb	0.5 ppm	3.8	13.1	10.9	18.1	13.9	10.5	14.5	16.2	2.2	20.7	14.2	2.6	10.3	9.6
Cs	0.1 ppm	1.7	0.3	0.3	1.7	0.2	0.9	34.7	1.8	0.4	0.8	2.7	0.1	3.1	0.3
Ba	1 ppm	481	498	380	558	79	501	505	653	831	819	730	63	356	519
Hf	0.1 ppm	4.7	10.6	11.5	6.7	9.7	12.6	5.4	7.3	2.7	9.3	5.5	4.6	7.4	23.5
Ta	0.1 ppm	0.3	0.7	0.7	0.8	0.9	0.8	0.7	1.2	0.2	1.1	0.7	0.1	0.7	0.7
Pb	5 ppm	30	24	9	12	nd	7	nd	19	11	39	nd	nd	19	nd
Th	0.05 ppm	10.65	9.64	11.60	8.22	10.90	9.70	9.45	8.17	2.79	10.64	7.24	4.66	10.24	12.88
U	0.05 ppm	1.83	1.35	2.29	2.53	2.25	1.63	2.33	2.37	0.54	1.26	2.03	0.61	2.01	3.73
Cu	1 ppm	11	5	59	18	6	2	15	31	2	17	28	2	2	2
Zn	1 ppm	88	97	93	81	123	52	78	89	6	16	90	4	56	10
Tl	0.05 ppm	nd	0.51	0.19	0.68	0.06	0.41	1.66	0.64	0.26	0.40	0.91	nd	0.78	0.53
La	0.05 ppm	34.27	32.37	36.34	44.04	27.99	25.45	42.40	37.93	21.65	43.62	36.38	19.20	24.15	29.93
Ce	0.1 ppm	60.7	71.0	78.7	83.7	57.8	52.6	76.9	74.4	21.2	87.5	71.8	46.9	43.3	59.7
Pr	0.02 ppm	6.09	8.16	9.30	11.03	7.00	6.15	9.90	10.50	5.14	11.21	9.41	5.17	5.66	7.70
Nd	0.05 ppm	20.79	33.73	36.76	44.27	27.15	22.67	37.88	41.19	18.38	44.05	37.97	21.48	21.50	30.21
Sm	0.01 ppm	3.28	7.02	7.32	8.47	5.41	3.95	6.64	8.29	3.28	8.61	7.31	4.31	4.13	5.43
Eu	0.005 ppm	1.233	1.586	1.623	1.957	1.253	0.665	1.437	1.998	0.833	2.106	1.732	0.811	1.095	0.907
Gd	0.02 ppm	2.45	6.56	6.59	7.20	4.85	3.47	5.23	6.99	2.46	7.22	6.28	4.47	3.86	4.59
Tb	0.01 ppm	0.36	1.23	1.14	1.23	0.88	0.55	0.84	1.23	0.33	1.13	1.09	0.77	0.74	0.78
Dy	0.02 ppm	1.80	7.46	6.50	7.08	5.49	3.22	4.65	7.53	1.59	6.27	6.04	3.86	4.58	4.31
Ho	0.01 ppm	0.32	1.58	1.35	1.44	1.17	0.67	0.92	1.58	0.27	1.08	1.30	0.74	0.96	0.93
Er	0.01 ppm	0.91	4.76	4.07	4.12	3.49	2.14	2.59	4.60	0.69	2.75	3.72	2.02	2.84	2.81
Tm	0.005 ppm	0.129	0.748	0.636	0.617	0.578	0.330	0.375	0.688	0.099	0.378	0.544	0.290	0.430	0.452
Yb	0.01 ppm	0.84	4.49	3.98	3.74	3.57	2.32	2.39	4.48	0.59	2.36	3.55	1.64	2.69	2.91
Lu	0.002 ppm	0.121	0.662	0.624	0.537	0.574	0.387	0.349	0.648	0.078	0.280	0.523	0.221	0.401	0.486
Th/Sc		1.4	0.8	1.3	0.7	1.4	2.1	0.7	0.7	4.0	0.6	0.6	2.4	1.0	5.9
Zr/Sc		27.4	31.7	47.7	30.5	47.7	102.8	20.7	22.2	132.9	21.3	22.1	83.2	39.4	531.8
La/Sc		4.5	2.8	4.1	3.9	3.5	5.5	3.1	3.1	30.9	2.6	2.8	10.1	2.4	13.6
Co/Th		0.5	1.2	0.9	1.7	1.0	0.5	2.0	1.5	0.4	2.7	2.1	0.2	1.1	0.3
Cr/Th		2.9	4.9	2.9	5.3	3.4	1.6	18.6	6.7	0.2	7.6	6.8	1.3	3.8	0.6
Cr/V		0.4	0.7	0.6	0.6	0.5	0.5	1.7	0.7	0.1	0.5	0.6	0.5	0.5	0.5
V/Ni		8.5	2.8	3.0	3.6	1.4	8.3	1.3	3.8	6.3	—	4.2	—	4.0	—

Table 7. *continued*

	Unit or Formation†	S Fm	HC Fm	TF Fm	WC Gp	TF Fm	TF Fm	TF Fm	TF Fm	
	Sample ID	SEV	SM-HC	SM-TF	TELP2	TFQZT1	TFQZT2	TFTIG441	UTF85	PAAS
	Tectonic belt‡	(V&R)	(SMW)	(eBR)	(wBR)	(eBR)	(eBR)	(eBR)	(wIP)	
	Detection Limit#									
Sc	0.01 ppm	1.00	18.50	13.50	11.80	7.12	1.53	14.80	12.30	16
V	5 ppm	nd	110	69	78	38	17	91	60	150
Cr	0.5 ppm	4.1	178.0	44.8	45.2	20.0	5.2	75.6	44.5	110
Co	0.1 ppm	1.5	15.0	13.7	7.4	6.4	1.7	15.9	13.5	23
Ni	1 ppm	1	65	23	11	11	nd	31	21	55
As	1 ppm	1	nd	4	10	nd	nd	nd	nd	
Br	0.5 ppm	0.8	nd	nd	nd	nd	nd	nd	nd	
Rb	2 ppm	5	89	175	84	181	70	111	85	160
Sr	2 ppm	285	236	274	70	168	96	219	273	200
Y	1 ppm	7	37	49	34	30	13	36	51	27
Zr	1 ppm	51	270	290	766	487	322	321	246	210
Nb	0.5 ppm	1.7	15.7	19.8	19.0	12.9	9.5	9.0	11.6	1.9
Cs	0.1 ppm	nd	0.8	1.1	2.8	1.2	0.4	2.2	2.3	15
Ba	1 ppm	156	448	891	298	1033	659	743	547	650
Hf	0.1 ppm	1.4	7.2	7.4	20.2	12.7	8.2	7.4	7.3	5
Ta	0.1 ppm	nd	0.9	1.3	1.4	0.9	0.7	0.7	1.1	
Pb	5 ppm	9	14	24	6	31	17	11	17	
Th	0.05 ppm	1.07	13.29	14.30	12.95	9.46	12.42	11.16	10.55	14.6
U	0.05 ppm	0.59	1.69	3.30	3.62	1.95	1.70	2.47	3.02	3.1
Cu	1 ppm	1	7	16	6	3	2	4	14	50
Zn	1 ppm	nd	58	116	72	88	15	68	103	
Tl	0.05 ppm	nd	0.54	0.62	0.60	1.73	0.36	0.44	0.12	
La	0.05 ppm	5.79	34.91	63.05	35.38	37.78	22.22	37.03	60.11	38.2
Ce	0.1 ppm	10.4	69.8	132.6	81.8	83.1	47.5	82.1	123.9	79.6
Pr	0.02 ppm	1.36	7.67	15.07	9.52	9.85	5.29	9.48	14.39	8.83
Nd	0.05 ppm	5.49	28.71	58.27	37.34	40.18	19.88	36.79	57.06	33.9
Sm	0.01 ppm	1.02	5.68	11.69	7.23	8.06	3.68	7.56	11.22	5.55
Eu	0.005 ppm	0.261	1.469	2.158	1.462	1.948	0.770	1.761	2.142	1.08
Gd	0.02 ppm	0.97	5.69	10.69	5.99	6.84	2.96	7.76	9.87	4.66
Tb	0.01 ppm	0.16	0.92	1.65	0.98	1.16	0.46	1.17	1.65	0.77
Dy	0.02 ppm	0.91	6.22	9.45	6.05	6.06	2.44	6.83	9.30	4.68
Ho	0.01 ppm	0.19	1.36	1.82	1.28	1.17	0.48	1.37	1.85	0.99
Er	0.01 ppm	0.52	4.36	5.33	3.98	3.20	1.49	4.06	5.26	2.85
Tm	0.005 ppm	0.077	0.669	0.775	0.624	0.460	0.224	0.586	0.772	0.40
Yb	0.01 ppm	0.47	4.48	4.84	4.50	2.80	1.39	3.60	4.66	2.82
Lu	0.002 ppm	0.069	0.707	0.680	0.726	0.395	0.225	0.527	0.651	0.43
Th/Sc		1.1	0.7	1.1	1.1	1.3	8.1	0.8	0.9	0.9
Zr/Sc		51.0	14.6	21.5	64.9	68.4	210.5	21.7	20.0	13.1
La/Sc		5.8	1.9	4.7	3.0	5.3	14.5	2.5	4.9	2.4
Co/Th		1.4	1.1	1.0	0.6	0.7	0.1	1.4	1.3	1.6
Cr/Th		3.8	13.4	3.1	3.5	2.1	0.4	6.8	4.2	7.5
Cr/V		—	1.6	0.6	0.6	0.5	0.3	0.8	0.7	0.7
V/Ni		—	1.7	3.0	7.0	3.4	—	2.9	2.8	2.7

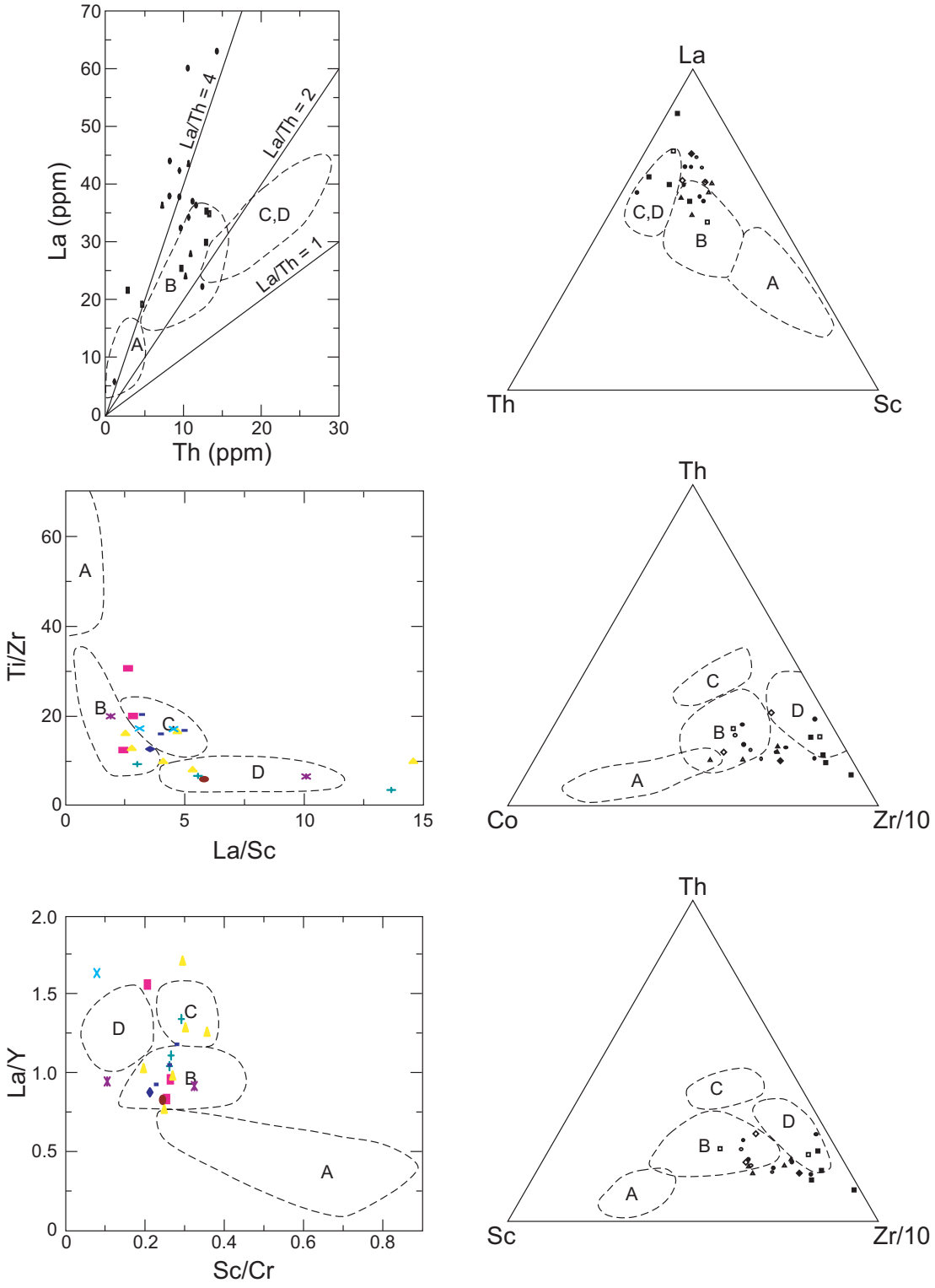

Figure 11. Tectonic discriminant plots for (meta)sedimentary data. Plots and oceanic island arc, continental island arc, active continental margin, and passive margin fields after Bhatia and Crook (1986). A-ocean island arcs. B-continental island arcs. C-active continental margin. D-passive continental margin.

Table 8. Whole-rock element granitoid chemistry with normative mineralogy. nd-below detection limit.

	Unit or Formation†		LL	LQM	PM Fm	T (IUGS)	DT	DT	DT	DT	CC (IUGS)
	Sample ID		KEN	LVQ1	POMTN	TOC1	G846	GL4	GL5	VM1782	WIMPY
	Tectonic belt§		(wIP)	(wIP)	(wIP)	(wIP)	(wIP)	(wIP)	(wIP)	(wIP)	(Dgb)
	Detection Limit#										
SiO_2	0.01	%	61.13	75.08	84.50	77.18	72.04	77.28	69.85	73.00	72.13
Al_2O_3	0.01	%	17.11	13.58	14.30	12.99	14.00	13.20	15.30	14.40	13.59
Fe_2O_3	0.01	%	5.95	1.83	0.05	0.81	2.57	1.45	3.71	3.12	3.70
MnO	0.01	%	0.11	0.03	nd	0.04	0.05	0.03	0.07	0.05	0.07
MgO	0.01	%	3.15	0.79	nd	0.17	0.67	0.36	1.02	0.62	0.92
CaO	0.01	%	6.52	3.31	0.01	0.94	2.69	1.73	3.86	3.66	3.78
Na_2O	0.01	%	3.40	3.82	0.12	4.10	3.79	5.34	3.62	3.84	3.32
K_2O	0.01	%	1.31	0.99	0.39	3.54	2.20	0.67	1.13	0.84	1.57
TiO_2	0.005 (0.001)	%	0.399	0.213	0.155	0.116	0.144	0.103	0.310	0.186	0.217
P_2O_5	0.01	%	0.10	0.03	0.02	0.03	0.04	0.02	0.07	0.03	0.05
LOI	0.01	%	0.60	0.74	0.72	0.32	1.16	0.30	1.16	0.40	0.93
	TOTAL	%	99.78	100.44	100.27	100.23	99.35	100.48	100.10	100.20	100.28
Ba	1 (20)	ppm	390	208	38	1350	603	241	205	193	356
Sr	2 (0.5)	ppm	303	130	4	88	101	127	119	128.0	84
Y	1	ppm	14	3	35	36	16	26	12	9	15
Zr	1 (2)	ppm	103	98	250	63	95	112	60	70	105
Be	1 (0.5)	ppm	2	1	nd	1	nd	nd	2	1.5	1
V	5 (2)	ppm	115	33	nd	nd	35	nd	67	43	50

† -na- = not assigned, TF Fm. = Tallulah Falls Fm.,

§ see Table 6 for abbreviations.

Values in parantheses are for sample VM1782 only (analyzed by XRAL).

Table 9. Whole-rock trace element concentrations for granitoid samples. nd-below detection limit.

	Unit or Formation†		LL	LQM	PM Fm	T	DT	DT	DT	DT	CC
	Sample ID		KEN	LVQ1	POMTN	TOC1	G846	GL4	GL5	VM1782	WIMPY
	Tectonic belt§		(wIP)	(wIP)	(wIP)	(wIP)	(wIP)	(wIP)	(wIP)	(wIP)	(Dgb)
	Detection Limit#										
Cs	0.1 (3)	ppm	0.6	0.8	nd	0.4	0.4	0.2	0.6	nd	0.5
Tl	0.05 (0.1)	ppm	0.33	0.23	0.08	0.56	0.13	0.07	0.22	0.3	0.18
Rb	2	ppm	52	43	6	97	42	14	41	41	51
Ba	1 (20)	ppm	390	208	38	1350	603	241	205	193	356
Th	0.05 (0.5)	ppm	3.59	4.53	16.25	8.90	2.94	3.12	2.40	1.0	6.00
U	0.05 (0.5)	ppm	0.69	0.49	2.72	2.16	0.62	1.05	0.69	0.70	1.91
Nb	0.5 (2)	ppm	4.9	3.2	14.7	7.9	1.9	1.8	2.4	5	5.4
Ta	0.1 (0.44)	ppm	0.3	0.3	1.3	0.7	0.2	0.2	0.2	0.5	0.5
Sr	2 (0.5)	ppm	303	130	4	88	101	127	119	128.0	84
Hf	0.1 (1)	ppm	2.9	2.6	7.7	2.3	2.8	3.8	1.5	2	2.8
Zr	1 (2)	ppm	103	98	250	63	95	112	60	70	105
Tb	0.01 (0.1)	ppm	0.50	0.12	0.73	0.78	0.36	0.61	0.37	0.2	0.38
La	0.05 (0.1)	ppm	13.87	10.98	16.06	27.76	7.77	11.30	5.66	2.5	16.51
Ce	0.1	ppm	29.6	20.7	16.5	52.1	19.6	23.3	42.1	8.5	30.6
Pr	0.02 (0.2)	ppm	3.67	2.34	1.80	6.26	2.06	2.97	1.83	0.7	3.36
Nd	0.05 (0.1)	ppm	14.93	8.36	7.54	23.02	7.67	12.13	7.38	3.5	11.79
Sm	0.01 (0.1)	ppm	3.38	1.37	2.60	4.45	1.71	2.87	2.03	0.9	2.19
Eu	0.005 (0.05)	ppm	0.842	0.361	0.714	0.688	0.408	0.382	0.578	0.40	0.525
Gd	0.02 (0.1)	ppm	3.25	0.95	3.04	4.10	1.72	3.04	1.53	1.0	2.00
Tb	0.01 (0.1)	ppm	0.50	0.12	0.73	0.78	0.36	0.61	0.37	0.2	0.38
Dy	0.02 (0.1)	ppm	2.77	0.61	5.56	4.99	2.39	3.95	2.28	1.5	2.46
Ho	0.01 (0.05)	ppm	0.54	0.11	1.43	1.14	0.54	0.91	0.48	0.30	0.55
Er	0.01 (0.1)	ppm	1.67	0.29	4.80	3.50	1.79	2.88	1.46	1.2	1.70
Tm	0.005 (0.1)	ppm	0.258	0.046	0.800	0.567	0.331	0.500	0.230	0.2	0.287
Yb	0.01 (0.1)	ppm	1.70	0.28	5.58	3.64	2.40	3.39	1.48	1.3	1.99
Lu	0.002 (0.05)	ppm	0.255	0.043	0.881	0.564	0.439	0.576	0.218	0.20	0.338

† -na- = not assigned, TF Fm. = Tallulah Falls Fm.,

§ see Table 6 for abbreviations.

sample (higher LREE-enrichment) and the Poor Mountain Quartzite (lower MREE with higher LREE values relative to the other samples).

Granitoid data presented here plot in the volcanic arc granite (or volcanic arc and syn-collisional granite) field on the tectonic discrimination diagrams of Pearce et al. (1984) (Fig. 14). The Poor Mountain Quartzite (metatuff?) sample plots close to or within the ocean ridge granite field on two of the diagrams and close to or within the within-plate granite field on the other two plots. Relative to most other samples in this study, the Poor Mountain Quartzite sample has a lower Rb concentration (6 ppm) and higher Yb (5.58 ppm), Nb (14.7 ppm), and Ta (1.3 ppm) concentrations (Table 9) resulting in the diversity of tectonic settings on these plots. Data from other central Blue Ridge (Spell and Norell, 1990; Settles, 2002), eastern Blue Ridge (Mapes, 2002), and Inner Piedmont (Vinson, 1999; Mapes, 2002) granitoids also cluster in the volcanic-arc granite field of Pearce et al. (1984).

SOUTHERN APPALACHIAN CRYSTALLINE CORE TECTONIC BOUNDARIES AND TERRANES

Tectonic Boundaries

Major tectonic boundaries of the southern Appalachians have been variably defined and correlated. The nature of these boundaries has been the subject of ongoing, sometimes vigorously contested, debates related to timing, kinematics, and crustal affinities of the blocks they bound. Several pre-Paleozoic boundaries have also been recognized including Grenvillian terrane boundaries between Adirondack-New England rocks and pre-Grenvillian Mars Hill terrane with Grenville crust in the Blue Ridge (e.g., Bartholomew and Lewis, 1988; Sinha and McLelland, 1999) and the 1.6 Ga eastern granite-rhyolite province interpreted from Nd model ages (Van Schmus et al., 1996).

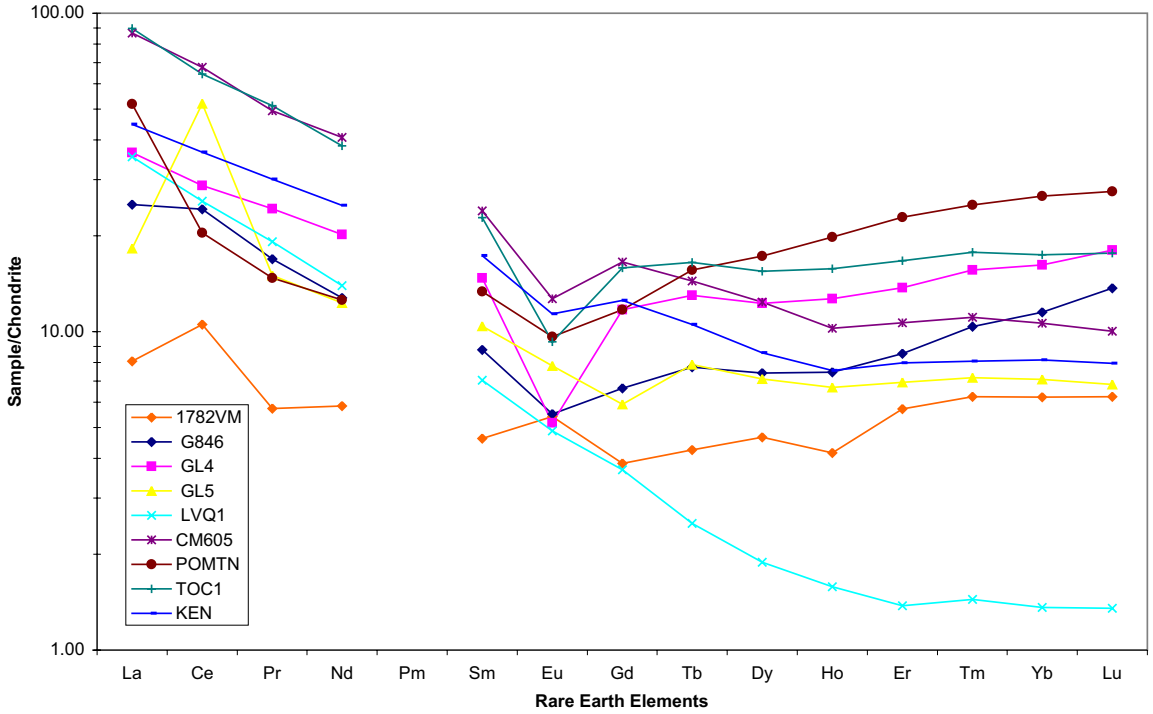

Figure 12. Chondrite normalized REE plot of granitoid data. Note that 1782VM, G846, GL4, GL5 are Dysartsville Tonalite samples.

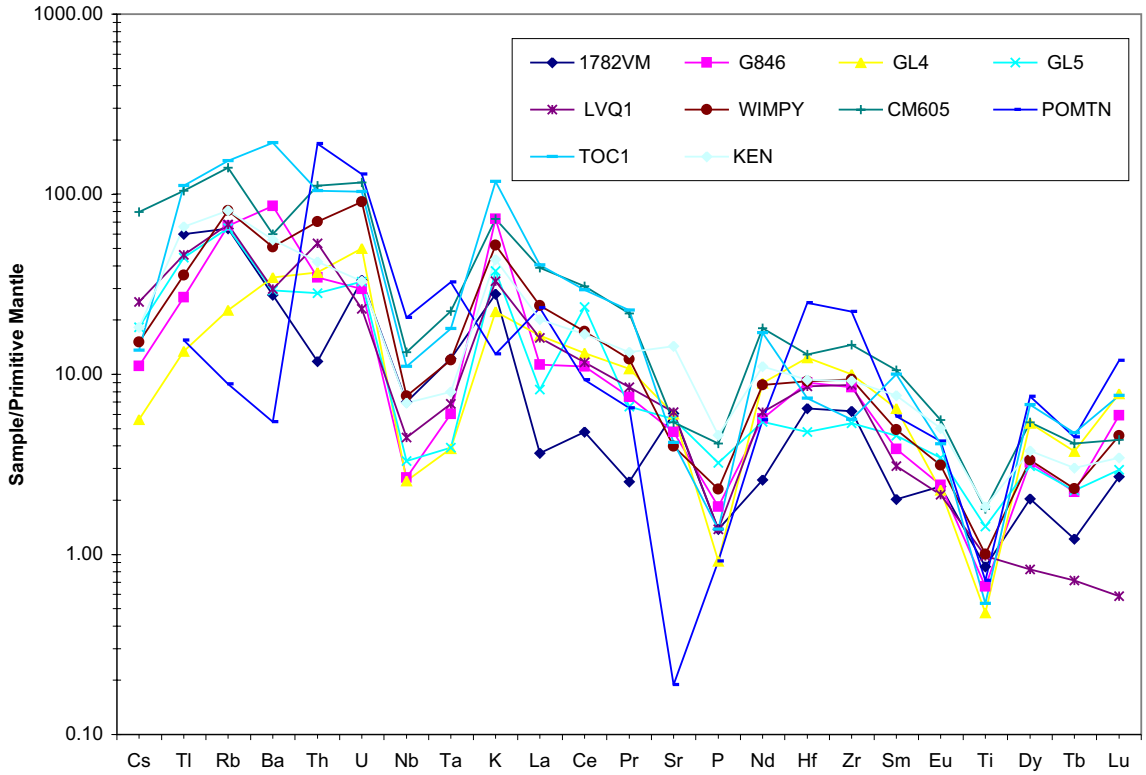

Figure 13. Element variance for granitoid data normalized to primitive mantle. Note that 1782VM, G846, GL4, GL5 are Dysartsville Tonalite samples.

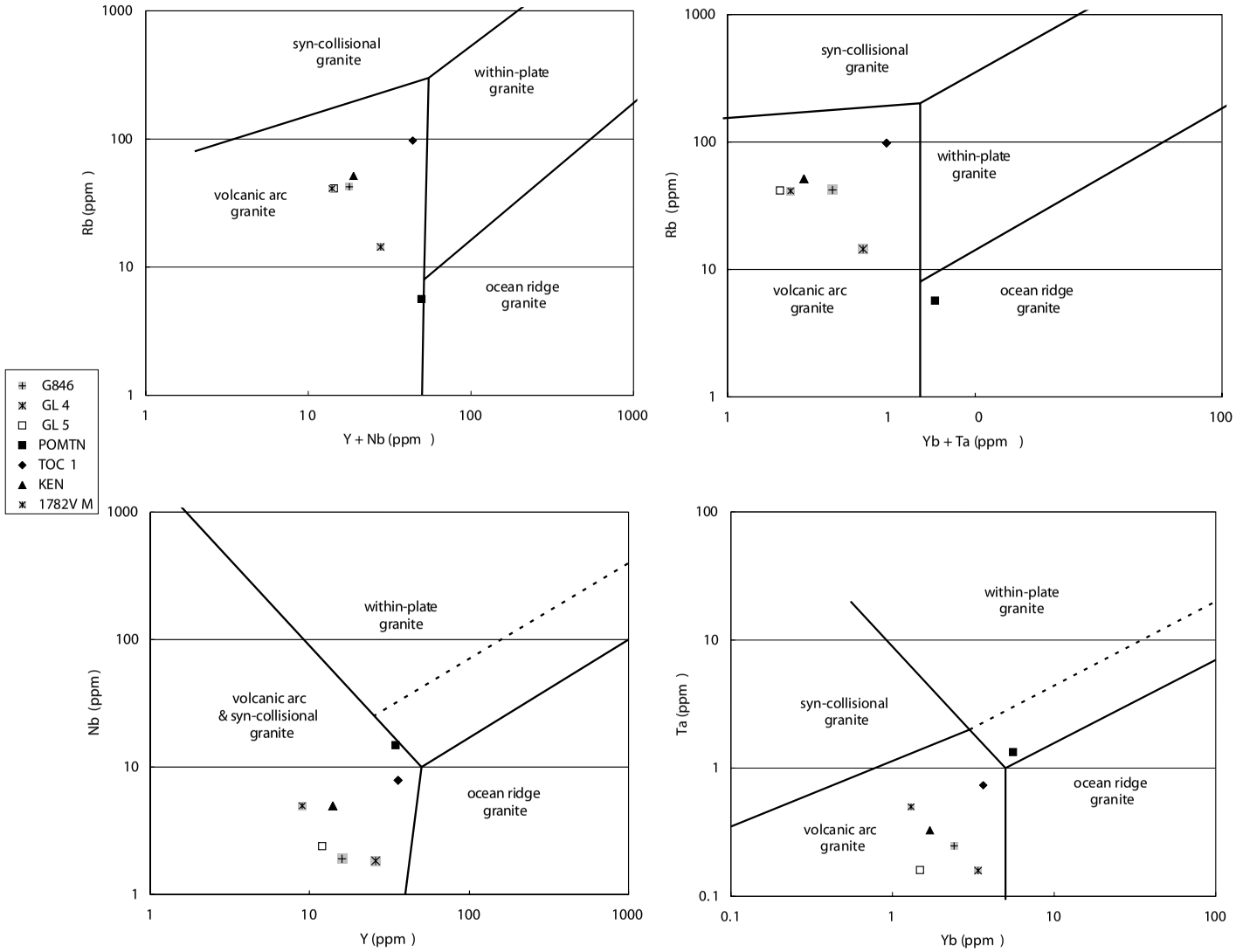

Figure 14. Tectonic discriminant plot for granitoids after Pearce et al. (1984).

Foreland-Blue Ridge

The southern Appalachian foreland is separated from the adjacent western Blue Ridge by a number of frontal Blue Ridge faults. This boundary represents the leading edge of the Alleghanian Blue Ridge-Inner Piedmont megathrust sheet, which drove Coulomb foreland fold-thrust belt development. In Alabama and Georgia this boundary is defined by the Talledega, Emerson, and Cartersville faults. In much of eastern Tennessee, the boundary is defined by the Great Smoky fault, but in NE Tennessee and at the Tennessee-Virginia border is defined by the Holston Mountain fault. The Great Smoky and Holston Mountain faults are bedding thrusts that transport Grenville basement and unmetamorphosed upper Walden Creek Group and Chilhowee Group rocks over the foreland. Outliers of this fault occur at Indian Mountain and Chocolocco Mountain in Georgia and Alabama. The Miller Cove-Alaculsy Valley-Cartersville-Emerson-Talladega faults transport previously cleaved, folded, and metamorphosed rocks and actually comprise the front of the crystalline megathrust sheet (Costello, 1984).

Western Blue Ridge-Central Blue Ridge/Dahlonega Gold Belt/Eastern Blue Ridge Assemblage

The western Blue Ridge is separated from adjacent rocks of the central and eastern Blue Ridge by a Taconic suture that represents the closure of a small forearc sea between the Laurentian margin and the Piedmont terrane obducting the Ordovician arc system onto the rifted Laurentian margin (e.g., Hatcher, 1978, 1989). Faults comprising this boundary in the southern Appalachians include the Hollins Line and Enitachopco (Alabama), Allatoona-Hayesville-Holland Mountain (Alabama, Georgia, and North Carolina), and Gossan Lead (North Carolina and Virginia) faults. This boundary is premetamorphic relative to the Taconic granulite facies event of the central Blue Ridge (Hatcher, 1978; Hatcher and Butler, 1979), but components in northeastern Georgia were reactivated during the Neoacadian tectonothermal event (Settles, 2002).

Central Blue Ridge/Dahlonega Gold Belt-Eastern Blue Ridge Assemblage

The central Blue Ridge terraneis separated from the eastern Blue Ridge by the Shope Fork and Chattahoochee faults. In Alabama and Georgia the Chattahoochee fault juxtaposes Tallulah Falls Formation rocks of the eastern Blue Ridge with Wedowee Group rocks in Alabama (Osborne et al., 1988) and Dahlonega gold belt-central Blue Ridge assemblages in Georgia and southernmost North Carolina The extent of the Chattahoochee farther north in North Carolina is not clear but it has to join the Holland Mountain fault (Wiener and Merschat, 1988; Quinn, 1990; Hatcher and Edelman, unpublished mapping in the Hazelwood 7.5-minute quadrangle). This fault is post-metamorphic (post-Neoacadian), and was later tightly folded, juxtaposing sillimanite grade eastern Blue Ridge rocks over lower- to middle-amphibolite grade Dahlonega gold belt rocks (Hopson et al., 1989; Hatcher and Goldberg, 1991). Timing of Chattahoochee fault displacement is delimited by the crystallization age of the deformed Rabun Granodiorite (375 Ma; C.F. Miller et al., 2000) indicating Acadian plutonism and Neoacadian deformation. A reported TIMS zircon age of 335 Ma for the Rabun Granodiorite (Miller and Stewart, 2002) indicates Alleghanian crystallization requiring much later (by 40 m.y.) movement of the Chattahoochee fault. Moreover, this age date requires penetrative deformation and metamorphism of the Rabun Granodiorite and enclosing Tallulah Falls Formation be post-335 Ma contradicting all other age dates, detailed geologic map relationships, and evidence from ion probe U-Pb zircon rim ages that indicate peak metamorphism and development of associated deformational fabrics occurred no later than ~350 Ma.

Eastern Blue Ridge-Western Inner Piedmont

Eastern Blue Ridge assemblages are separated from western Inner Piedmont assemblages by the Brevard fault zone, not considered a suture because of the presence of the same stratigraphic sequence (Tallulah Falls-Ashe Formation) in both the eastern

Blue Ridge and western Inner Piedmont. The Brevard fault zone is a major weak, multiply reactivated fault (Hatcher, 2001a). The Brevard fault zone extends from at least the Sauratown Mountains window area of North Carolina to the Coastal Plain in Alabama. Earliest movement on the Brevard fault was Neoacadian (Late Devonian to early Mississippian) with later movement occurring during the Alleghanian (Late Mississippian to Early Permian). Early movement was at amphibolite facies conditions whereas later movement on the Brevard fault zone was retrogressive at lower greenschist facies or lower grade (Hatcher, 2001a).

Western Inner Piedmont-Eastern Inner Piedmont

The Brindle Creek thrust fault, first recognized and named by Giorgis (1999) in the Dysartsville 7.5-minute quadrangle, juxtaposes a migmatitic biotite gneiss-pelitic schist assemblage and 366 ± 3 Ma Walker Top Granite (Giorgis et al., 2002; Mapes, 2002) in the hanging wall with intensely migmatitic Tallulah Falls and Poor Mountain Formations in the footwall. This fault separates older Ordovician granitoids in the footwall from younger Devonian to Mississippian granitoids in the hanging wall. This fault also juxtaposes paragneisses with distinct detrital zircon age ranges (see below), is a terrane boundary within the Inner Piedmont (Bream et al., 2001; Kalbas et al., 2002).

Eastern Inner Piedmont-Carolina terrane

The Central Piedmont suture (Hatcher and Zietz, 1980) separates the eastern Inner Piedmont from the exotic Panafrican Carolina terrane (Secor et al., 1983) based on field (McConnell, 1988; Hooper and Hatcher, 1992), isotopic (e.g., Samson et al., 1995; Fullagar et al., 1997), and geophysical criteria (Hatcher and Zietz, 1980; Thomas, 1983). This boundary probably formed during the Neoacadian and was partly reactivated during the Alleghanian (e.g., Hooper and Hatcher, 1988; Student and Sinha, 1992; Steltenphol and Kunk, 1993)

Revised Terranes

Early terrane models for the southern Appalachians identified the collage of terranes outboard of the western Blue Ridge as suspect (Williams and Hatcher, 1982; Rankin et al., 1989). This scenario is still favored by many who work in the southern Appalachians (e.g., Trupe et al., in review). "Suspect" terranes are fault-bounded crustal blocks with histories that contrast with those of adjacent blocks (Coney et al., 1980). They are recognized by contrasts in stratigraphy, structure, metamorphic and plutonic histories, faunas, mineral deposits, and/or paleomagnetic signatures (Williams and Hatcher, 1982). New geochronologic and isotopic data permit reevaluatation of southern Appalachian terranes. The terrane divisions discussed below attempt to revise the crustal subdivisions in the southern Appalachian crystalline core between western Blue Ridge Laurentian rocks and the peri-Gondwanan rocks of the Carolina terrane (Fig. 2).

Cartoogechaye and Cowrock

The central Blue Ridge Cartoogechaye terrane (Hatcher, 2001b), is separated from the western Blue Ridge by the Hayesville fault and from the Dahlonega gold belt by the Shope Fork (-Soque River) fault. It containes the Grenvillian Trimont Ridge basement massif overlain by a pelitic and quartzofeldspathic metasedimentary sequence that has been correlated with the Tallulah Falls Formation and Coweeta Group rocks (Eckert et al., 1989). It also contains the Taconian granulite facies metamorphic core (Hatcher and Butler, 1979; Absher and McSween, 1984; Eckert et al., 1989) and several mafic-ultramafic complexes (Hatcher et al., 1984; Hopson et al., 1989). The Cowrock terrane contains only Coweeta Group rocks and the Lake Chatuge mafic-ultramafic complex around the Brasstown Bald and Shooting Creek windows. It is in a lower thrust sheet bounded by the Hayesville fault to the west, the Soque River fault to the east, and the Chunky Gal Mountain-Shope Fork to the northeast (Fig. 2). No detrital zircon data or metasedimentary Nd data are presently available to confirm these subdivisions. Non-

Grenvillian detrital zircons in the Cartoogechaye sample include a small 2.7 Ga Archean component.

Dahlonega Gold Belt

The Dahlonega gold belt contains a metsedimentary assemblage of two-mica, two-feldspar metasandstone and aluminous schist, along with several arc-related mafic-ultramafic complexes (Hatcher, 1980, 1989; Hopson et al., 1989; Settles, 2002). It occurs beneath the Hayesville-Soque River and Chattahoochee thrust sheets. Hadley (1970) correlated these rocks with the Great Smoky Group, and others (e.g., Hatcher, 1988) have made a similar correlation. Dahlonega gold belt detrital zircon data; however, make such a correlation difficult. The western Blue Ridge samples from all Ocoee Supergroup units contain a consistent 1.1 to 1.5 Ga zircon suite whereas the Dahlonega gold belt metasandstones contain the same suite but with an older 1.8-2.0 Ga and Archean (2.7 and 2.9 Ga) suite. Data from these samples bear some similarity to the Cartoogechaye terrane sample, but differ in that several Late Proterozoic grains (632 ± 9, 712º± 7, and 819 ± 9; 1 sigma errors) were identified in two Dahlonega gold belt samples from near Otto (North Carolina) and Dahlonega (Georgia) (Bream et al., in press) suggesting that deposition of the Dahlonega gold belt metasedimentary assemblage is likely perhaps Ordovician like the dated mafic arc complexes (Thomas, 2001) and therefore younger than rocks in the adjacent higher Blue Ridge thrust sheets (terranes) (Settles, 2002).

Tugaloo

Unlike the western Blue Ridge, eastern Blue Ridge and western Inner Piedmont cover sequences (Tallulah Falls-Ashe Formation) were more distal slope-and-rise to oceanic sediments likely deposited on transitional or oceanic crust and small fragments of Grenvillian basement. The Tallulah Falls-Ashe Formation is the most areally

extensive lithologic package SE of the Chattahoochee fault and NW of the Brindle Creek fault. Detailed mapping in the Tugaloo terrane has identified all three subdivisions of the Tallulah Falls Formation in the eastern Blue Ridge (e.g., Hatcher, 1987) and the western Inner Piedmont (e.g., Hopson and Hatcher, 1988; Bier et al., 2002). The Tallulah Falls-Ashe Formation is present on both sides of the Brevard fault zone; thus the Brevard fault zone is *not* a terrane boundary or suture.

The western Inner Piedmont Poor Mountain MORB to arc volcanic sedimentary assemblage is stratigraphically below the Poor Mountain Quartzite which is ~445 Ma. Additionally, the Tugaloo terrane contains numerous Ordovician and Devonian plutons. Despite the absence of Grenvillian basement in the Inner Piedmont, the character of the sedimentary and plutonic assemblages links these tectonic divisions (Bream et al., in press). The Chopawamsic and Milton belts are probably northern equivalents of the Tugaloo terrane.

Cat Square

The Cat Square terrane(Hatcher, 2002) contains a mostly metapelitic and metapsammitic assemblage and mafic rocks and is devoid of Ordovician granitoids. In contrast, the western Inner Piedmont is dominated by metapsammitic material intruded by numerous Ordovician granitoids. The Cat Square terrane contains large Ordovician and minor Archean detrital zircon components absent in the adjacent Tugaloo terrane (Bream et al., in press). Additionally, the Cat Square terrane contains a detrital component between 500 and 600 Ma that was likely derived from the Carolina terrane, thus the sedimentary sequence here is interpreted to be derived from reworked Laurentian margin rocks and the accreting Carolina terrane.

SYNTHESIS OF MAJOR PALEOZOIC DEPOSITIONAL AND OROGENIC EVENTS IN THE SOUTHERN APPALACHIANS

Late Proterozoic to Early Paleozoic

Sedimentation

Despite issues raised by the possible non-Laurentian affinity of the southern Appalachian basement (e.g., Sinha and McLelland, 1999), detrital zircon and Nd isotopic data confirm that the cover sequence was largely derived from rocks similar in isotopic maturity and age to the Grenvillian massifs of the southern Appalachian basement (Bream et al., in press; Steltenpohl et al., in press). Sedimentation occurred in a large rift system that developed during the opening of the Iapetus ocean (e.g., Rast and Kohles, 1986; Thomas, 1991). Similar results have been reported for portions of the northern Appalachians and Newfoundland (e.g., Karabinos et al., 1990; Karabinos and Gromet, 1993; Cawood et al., 2001). Connections to Gondwanan sources are mostly limited to samples from within the exotic Avalon and Carolina terranes (Keppie et al., 1998), and samples that unconformably overlie the most distal of southern Appalachian Grenvillian rocks (Steltenpohl et al., in press).

Magmatism

Two major episodes of rift-related magmatism are documented in the Appalachians. The earliest unsuccessful 730-760 Ma rifting is Neoproterozoic (Goldberg et al., 1986; Su et al., 1994; Aleinikoff et al., 1995; Tollo and Aleinikoff, 1996; Miller, unpublished data) and successful 575-560 Ma rifting was latest Neoproterozoic to Early Cambrian (Badger and Sinha, 1988; Aleinikoff et al., 1995). Most of these rocks are rift-related bimodal volcanics.

Middle Ordovician

Sedimentation

Middle Ordovician sedimentation is widely documented in the Appalachian foreland (e.g., Colton, 1970; Drake et al., 1989). In the southern Appalachian foreland, the Sevier basin developed above the Middle Ordovician Knox unconformity in response to tectonic activity in the hinterland terminating the stable carbonate platform. Detrital zircons from the Sevier Shale were derived from southeastern sources that had previously been deposited during the rifting of Rodinia. Our results are similar to other foreland basin studies in the central and northern Appalachians (Gray and Zeitler, 1997; Cawood and Nemchin, 2001; McLennan et al., 2001; Eriksson et al., 2002). The near absence of a Paleozoic component in the detrital zircons suggests that the now-eroded equivalent of the western Blue Ridge served as a sedimentary barrier between the accreting Taconic arc and the foreland throughout most of the Appalachians (Eriksson et al., 2002). Provenance studies of later foreland clastic wedges demonstrate that this barrier was breached by the Acadian orogeny (Gray and Zeitler, 1997).

Hatcher (2002) noted a possible correlation with the Knox unconformity to the unconformity beneath the Poor Mountain Formation in the crystalline western Inner Piedmont. A nearly continuous outcrop belt of garnet-staurolite grade Poor Mountain Formation exists from South Carolina (and NE Georgia) to SW North Carolina; Poor Mountain rocks are then preserved at higher grade in synclines in the footwalls of major thrusts in the western Inner Piedmont farther north in North Carolina (Hatcher, 2002). Basal Poor Mountain Formation consists of finely laminated amphibolite formed in an oceanic setting overlain by and interlayered with quartz arenite, feldspathic sandstone, and clean limestone (in South Carolina), the Poor Mountain Quartzite-Marble. U-Pb zircon data from our Poor Mountain Quartzite sample require it be deposited later than 444 ± 4 Ma. Thus, the entire Poor Mountain sequence likely has a Middle to Late

Ordovician age. Stratigraphic, and likely nonconformable (Hatcher and Bream, 2002), deposition of the Poor Mountain Formation above probable Cambrian siliciclastics (and minor carbonate) of the Chauga River and Tallulah Falls Formation suggests a regional unconformity exists in the western Inner Piedmont.

Magmatism

The paucity of a subduction-related signature in most eastern Blue Ridge and western Inner Piedmont granitoids (Miller et al., 2000; McDowell et al., 2002) favors derivation from thickened, isotopically evolved crust, not subduction-related magmatic arc or continental margin arc as depicted in many tectonic models (e.g., Harper and Fullagar, 1981; Hatcher, 1989; Sinha et al., 1989; Hibbard, 2000). Larger intermediate plutons southwest of the rather small plutons in North Carolina and Georgia has prompted several workers to propose that a small ocean basin like the Sea of Okhotsk west of Kamchatka (Hatcher, 1978) or the Gulf of California (Thomas et al., 2001) may have opened and closed during the Ordovician (McDowell et al., 2002).

Nearly all of our granitoid sample data indicate the plutons are isotopically evolved and favor the interpretation of Mapes (2002) regarding the likelihood of deeper more juvenile sources for the eastern Blue Ridge plutons compared to Inner Piedmont plutons. Despite the felsic, nonintermediate composition of these samples, a volcanic-arc setting is possible. Given the tectonic setting outlined above, it is quite possible that Ordovician Tugaloo terrane plutons were produced in both continental and volcanic-arc settings. If the Poor Mountain Quartzite sample is metatuff, components of the Poor Mountain Formation might represent volcanic equivalents of the large granitoid belt in the western Inner Piedmont and eastern Blue Ridge, that could have been the source of K-bentonites in Middle and Upper Ordovician limestones of the Appalachian foreland.

Deformation and Metamorphism

A portion of the southern Appalachian central Blue Ridge records a Paleozoic granulite facies metamorphic event (Force, 1976; Hatcher and Butler, 1979; Eckert et al., 1989; Absher and McSween, 1984). Peak 470 Ma (Moecher and Miller, 2000) granulite facies conditions in the North Carolina eastern Blue Ridge require a minimum of 13-17 kbar between 625 ad 790°C (Willard and Adams, 1994). Proposed tectonic models place eclogite formation on oceanic crust subducted beneath the Inner Piedmont (e.g., Stewart et al., 1997; Trupe et al., in review).

Late Silurian

Sedimentation

Timing of deposition for the eastern Inner Piedmont samples is delimited by the age of the youngest detrital zircons in metapsammite samples from this terrane, 424 ± 11 Ma in the North Carolina sample and ~445 Ma in the South Carolina sample (1 sigma errors), and the oldest intrusive, ~380 Ma for the Toluca Granite (Mapes, 2002). These constraints favor Late Silurian (possibly Early Devonian) deposition almost immediately followed by burial, tectonic thickening, and magma generation. In addition to Silurian and Ordovician detrital grains, the eastern Inner Piedmont samples also contained 504 ± 5, 589 ± 7, and 590 ± 10 Ma detrital grains, ages not present in other samples except for a single 632 ± 9 Ma analysis from the Dahlonega gold belt. These ages best explained by a proximal Carolina terrane at the time of deposition, as Laurentian rocks within this age range have not been identified; magmatic rocks of this age, however, are present in the Carolina terrane (see Hibbard et al., 2002, for summary). The presence of these detrital components can be explained if the eastern Inner Piedmont sedimentary assemblage developed as an accretionary prism or ocean floor assemblage in front of the Carolina terrane. The reported age of 415 ± 3 Ma for the Anderson's Mill augen gneiss (Mapes, 2002) in the eastern Inner Piedmont remains difficult to explain, but it could be

located in the western Inner Piedmont (see maps by Curl, 1997a, 1997b).

Late Devonian-Early Carboniferous "Neoacadian"

Sedimentation

The lack of an Acadian clastic wedge is evidence against this orogeny in the southern Appalachians; however, there is evidence in the crystalline core and foreland for a Neoacadian event. This event is reflected in the foreland with the deposition of the Devonian-Mississippian Chattanooga Shale that thickens and becomes older to the north (into Ohio and West Virginia). A mixed silt- and sandstone sequence, lower Mississippian Grainger-Fort Payne Chert, overlies the Chattanooga Shale and overlying Fort Payne-Grainger Formation are interpreted to represent the Neoacadian clastic wedge in the southern Appalachians. Carbonate bank sedimentation (Newman Limestone) returned in the southern Appalachians after the Grainger was deposited. The upper Mississippian to Pennsylvanian siliciclastics of the southern Appalachian Cumberland Plateau represent the Alleghanian clastic wedge.

Magmatism

Magmatism occurred in both the Cat Square and Tugaloo terranes during this time frame. Although isotopic and zircon inheritance differences (Mapes, 2002) exist between the "Acadian" plutons of these terranes, the timing of crystallization is roughly the same: Cherryville is 351 (Kish, 1983), 355 ± 2 Ma (Mapes, 2002); Pelham is 364 ± 2 Ma (Mapes, 2002); Reedy River is 325 ± 2 Ma (Mapes, 2002); Toluca is 378 ± 4 Ma and 383 ± 2 Ma zircon, 380 ± 2 Ma monazite (Mapes, 2002); Walker Top is 366 ± 3 Ma (Mapes, 2002). Cat Square terrane granitoid chemistry resembles that of the enclosing metasedimentary assemblage (Mapes, 2002) thus melting of these granitoids likely occurred in a thickened stack of thrust sheets subducted beneath the overriding Carolina terrane. The timing of emplacement for the Zirconia pegmatites is roughly coeval with

emplacement of the Ben Hill, Stone Mountain, and Elberton granites in the Alleghanian plutonic arc of Sinha and Zietz (1982).

Deformation and Metamorphism

The metamorphic core in the southern Appalachians during this time interval is located in the Tugaloo terrane. A stack of crystalline thrust sheets formed at upper-amphibolite facies conditions. Buttressing against the primordial Brevard fault zone within the Tugaloo terrane occurred creating the complex structural patterns of the western Inner Piedmont (Hatcher, 2001a). Peak metamorphic grade was attained in the Cat Square terrane at the same time, locally sillimanite II conditions (Kish, 1997; Merschat and Kalbas, 2002), thus representing the first shared thermal event between the Laurentian margin and accreting exotic components (Dennis, 1995; Carrigan et al., 2001).

DISCUSSION

Many workers place the Iapetus suture of exotic accreted components onto the Laurentian margin at the southeastern boundary of the western Blue Ridge (e.g., Jefferson terrane of Rankin et al., 1989; Rankin, 1994, for summary). As noted by Rankin (1994), however, development of the accretionary wedge does not necessitate a non-Laurentian affinity for the rocks of the central and eastern Blue (Rankin's Jefferson terrane). Others workers contend that the ancestral (pre-Alleghanian) Brevard fault represents the boundary between the Piedmont terrane/belt/zone/island arc (Inner Piedmont) to the SE and an accretionary wedge named the Ashe metamorphic suite to the NE during the Taconic orogeny (e.g., Abbott and Raymond, 1984; Trupe et al., in review). These models require that the eastern Blue Ridge metasedimentary assemblage is younger than, and largely to entirely derived from, the western Inner Piedmont and have to discount strong field evidence that the *same* mappable sequence occurs in the

same order on *both* sides of the Brevard fault zone (e.g., Hatcher, 1978). Detrital zircon and Nd isotopic data strongly favor Laurentian derivation for all but the Cat Square terrane (Bream et al., in press;) thus dispelling interpretations favoring an exotic nature for these terranes.

CONCLUSIONS

(1) Latest Neoproterozoic to Early Cambrian sediments throughout the entire Blue Ridge and western Inner Piedmont are rift-and-drift facies deposited on the rifted Laurentian margin. Detrital zircon, evolved isotopic, and geochemical data favor derivation from existing Grenvillian crust similar to basement exposures in the Blue Ridge.

(2) Ordovician granitoids intruded the cover sequences of the eastern Blue Ridge, Dahlonega gold belt, and western Inner Piedmont. These intrusives (and extrusives) range in age from 440 to 480 Ma and were emplaced in both arc/MORB and within-plate settings. This suggests that the Taconic orogeny in the southern Appalachians closed a small ocean basin when the Piedmont terrane was accreted to the Laurentian margin.

(3) The eastern Inner Piedmont (Cat Square terrane) contrasts with Laurentian and reworked Laurentian rocks of the Blue Ridge and western Inner Piedmont. This assemblage of mostly metapelite and middle Paleozoic granitoids likely developed as an accretionary prism in front of the accreting Carolina terrane.

(4) Metamorphism in all but the central Blue Ridge is Neoacadian with a younger retrogressive Alleghanian event. Neoacadian metamorphism is attributed to docking of the Carolina terrane with later pegmatite and fluid influx related to Alleghanian overthrusting.

REFERENCES CITED

Abbott, R.N., Jr., and Raymond, L.A., 1984, The Ashe Metamorphic Suite, northwest North Carolina: Metamorphism and observations of geologic history: American Journal of Science, v. 284, p. 350-375.

Absher, B.S., and McSween, H.Y., Jr., 1985, Granulites at Winding Stair Gap, North Carolina; the thermal axis of Paleozoic metamorphism in the southern Appalachians: Geological Society of America Bulletin, v. 96, p. 588-599.

Aleinikoff, J.N., Zartman, R.E., Walter, M., Rankin, D.W., Lyttle, P.T., and Burton, W.C., 1995, U-Pb ages of metarhyolites of the Catoctin and Mount Rogers Formations, central and southern Appalachians: Evidence for two phases of Iapetian rifting: American Journal of Science, v. 295, p. 428-454.

Bacon, C.R., Persing, H.M., Wooden, J.L., and Ireland, T.R., 2000, Late Pleistocene granodiorite beneath Crater Lake caldera, Oregon, dated by ion microprobe: Geology, v. 28, p. 467-470.

Badger, R.L., and Sinha, A.K., 1988, Age and Sr isotopic signature of the Catoctin volcanic province: Implications for subcrustal mantle evolution: Geology, v. 16, p. 692-695.

Barker, F., 1979, Trondhjemite: Definition, environment and hypotheses of origin, *in* Barker, F., ed., Trondhjemites, dacites, and related rocks: New York, Elsevier Scientific Publishing Company, p. 1-12.

Bartholomew, M.J., and Lewis, S.E., 1984, Evolution of Grenville massifs in the Blue Ridge geologic province, southern and central Appalachians, *in* Bartholomew, M.J., ed., The Grenville event in the Appalachians and related topics: Geological Society of America Special Paper 194, p. 229-254.

Bartholomew, M.J., and Lewis, S.E., 1988, Peregrination of Middle Proterozoic massifs and terranes within the Appalachian orogen, eastern U.S.A., *in* Martinez-Garcia, E., ed., Geology of the Iberian Massif with communications presented at the International Conference on Iberian terranes and their regional correlation: Trabajos de Geologia, University of Oviedo, Spain, v. 17, p. 155-165.

Bartholomew, M.J., and Lewis, S.E., 1992, Appalachian Grenville massifs: Pre-Appalachian translational tectonics, *in* Mason, R., ed., Basement Tectonics 7: The Netherlands, Kluwer Academic Publishers, p. 363-374.

Bauluz, B., Mayayo, M.J., Fernandez-Nieto, C., Lopez, J.M.G., 2000, Geochemistry of Precambrian and Paleozoic siliciclastic rocks from the Iberian Range (NE Spain): Implications for source-area weathering, sorting, provenance, and tectonic setting: Chemical Geology, v. 168, p. 135-150.

Bhatia, M.R., and Crook, K.A.W., 1986, Trace element characteristics of graywackes and tectonic setting discrimination of sedimentary basins: Contributions to Mineralogy and Petrology, v. 92, p. 181-193.

Bier, S.E., Bream, B.R., and Giorgis, S.D., 2002, Inner Piedmont stratigraphy, metamorphism, and deformation in the Marion-South Mountains area, North Carolina, *in* Hatcher, R.D., Jr., and Bream, B.R., eds., Inner Piedmont geology in the

South Mountains-Blue Ridge Foothills and the southwestern Brushy Mountains, central-western North Carolina: North Carolina Geological Survey, Carolina Geological Society annual field trip guidebook, p. 65-99.
Bradley, D.C., 1989, Taconic plate kinematics as revealed by foredeep stratigraphy, Appalachian orogen: Tectonics, v. 8, p. 1037-1049.
Bream, B.R., 1999, Structural and stratigraphic relationships of ortho- and paragneisses southwest of Marion, North Carolina [M.S. thesis]: Knoxville, University of Tennessee, 162 p.
Bream, B.R., 2002, The southern Appalachian Inner Piedmont: new perspectives based on recent detailed geologic mapping, Nd isotopic evidence, and zircon geochronology, *in* Hatcher, R.D., Jr., and Bream, B.R., eds., Inner Piedmont geology in the South Mountains-Blue Ridge Foothills and the southwestern Brushy Mountains, central-western North Carolina: North Carolina Geological Survey, Carolina Geological Society annual field trip guidebook, p. 45-63.
Bream, B.R., Hatcher, R.D., Jr., Miller, C.F., and Fullagar, P.D., 2000, Paragneiss geochemistry and preliminary ion microprobe geochronology of detrital zircons from the southern Appalachian crystalline core: Geological Society of America Abstracts with Programs, v. 32, no. 7, p. 31.
Bream, B.R., Hatcher, R.D., Jr., Miller, C.F., and Fullagar, P.D., 2001, Geochemistry and provenance of Inner Piedmont paragneisses, NC and SC: Evidence for an internal terrane boundary?: Geological Society of America Abstracts with Programs, v. 33, no. 2, p. A-65.
Bream, B.R., Hatcher, R.D., Jr., Miller, C.F., and Fullagar, P.D., in press, Detrital zircon ages and Nd isotopic data from the southern Appalachian crystalline core, GA-SC-NC-TN: New provenance constraints for Laurentian margin paragneisses, *in* Tollo, R.P., Corriveau, L., McLelland, J., and Bartholomew, M.J., eds., Proterozoic evolution of the Grenville Orogen in North America: Boulder, Colorado, Geological Society of America Special Paper.
Brown, W.R., 1970, The Piedmont; investigations of the sedimentary record in the Piedmont and Blue Ridge of Virginia, *in* Fisher, G.W., Pettijohn, F.J., Reed, J.C., Jr., and Weaver, .N., eds., Studies of Appalachian geology, central and southern: new York, Interscience Publishers, p. 335-349.
Butler, J.R., 1991, Metamorphism, *in* Horton, J.W., Jr., and Zullo, V.A., eds., The Geology of the Carolinas: Knoxville, Tennessee, The University of Tennessee Press, p. 127-141.
Callahan, J.E., Stepp, J.D., Johnson, N.W., and Bream, B.R., 2002, Fluorescence and lack thereof in zircons from the Freeman zircon mine, Zirconia district, North Carolina: Geological Society of America Abstracts with Programs, v. 34, no. 2, p. 22.
Carrigan, C.W., Bream, B.R., Miller, C.F., and Hatcher, R.D., Jr., 2001, Ion microprobe analyses of zircon rims from the eastern Blue Ridge and Inner Piedmont, NC-SC-GA: Implications for the timing of Paleozoic metamorphism in the southern Appalachians: Geological Society of America Abstracts with Programs, v. 33, no. 2,

p. 7.
Carrigan, C.W., Miller, C.F., Fullagar, P.D., Bream, B.R., Hatcher, R.D., Jr., and Coath, C.D., in press, Ion microprobe age and geochemistry of southern Appalachian basement, with implications for Proterozoic and Paleozoic reconstructions: Precambrian Research.
Carter, M.W., 1994, Stratigraphy and structure of part of the western Blue Ridge Foothills, Polk and Monroe counties, Tennessee [M.S. thesis]: Knoxville, University of Tennessee, 233 p.
Carter, M.W., Geddes, D.J., Hatcher, R.D., Jr., and Martin, S.L., 1995, Stratigraphic and structural relationships in the western Blue Ridge foothills of southeastern Tennessee, *in* Driese, S.G., ed., Guidebook for field trip excursions, Southeastern Section Geological Society of America: Knoxville, University of Tennessee, Department of Geological Sciences Studies in Geology, v. 24, p. 91-128.
Cawood, P.A., and Nemchin, A.A., 2001, Paleogeographic development of the east Laurentian margin: Constraints from U-Pb dating of detrital zircons in the Newfoundland Appalachians: Geological Society of America Bulletin, v. 113, p. 1234-1246.
Cawood, P.A., McCausland, P.J.A., and Dunning, G.R., 2001, Opening Iapetus: Constraints from the Laurentian margin in Newfoundland: Geological Society of America Bulletin, v. 113, p. 443-453.
Colton, G.W., 1970, The Appalachian Basin–Its depositional sequences and their geological relationships, *in* Fisher, G.W., Pettijohn, F.J., Reed, J.C., Jr., and Weaver, K.N., eds., Studies of Appalachian geology: Central and southern: New York, Wiley Interscience, p. 5-47.
Coney, P.J., Jones, D.L., and Monger, J.W.H., 1980, Cordilleran suspect terranes: Nature, v. 288, p. 329-333.
Costello, J.O., 1984, Relationships between the Cartersville fault and Great Smoky fault in the southern Appalachians: A reinterpretation [M.S. thesis]: Columbia, University of South Carolina, 75 p.
Costello, J.O., and Hatcher, R.D., Jr., 1986, Contact relationships between the Walden Creek Group and Great Smoky Group in Ocoee Gorge, Tennessee: Implication for the regional extent of the Greenbrier fault: Geological Society of America Abstracts with Programs, v. 18, p. 216.
Cullers, R.L., 1994, The controls on the major and trace element variation of shales, siltstones, and sandstones of Pennsylvanian-Permian age from uplifted continental blocks in Colorado to platform sediment in Kansas: Geochimica et Cosmochimica Acta: v. 58, p. 4955-4972.
Curl, D.C., 1997a, Bedrock geologic map of the Reidville 7.5-minute quadrangle, Spartanburg and Laurens counties, South Carolina: South Carolina Department of Natural Resources, Geological Survey Open-file Report 94, 1:24,000 scale.
Curl, D.C., 1997b, Bedrock geologic map of the Wellford 7.5-minute quadrangle, Spartanburg County, South Carolina: South Carolina Department of Natural Resources, Geological Survey Open-file Report 95, 1:24,000 scale.

Dalla Salda, L.H., Cingolani, C.A., and Varela, L., 1992a, Early Paleozoic orogenic belt of the Andes in southwestern South America: Result of Laurentia-Gondwana collision?: Geology, v. 20, p. 616-620.

Dalla Salda, L.H., Dalziel, I.W.D., Cingolani, C.A., and Varela, L., 1992b, Did the Taconic Appalachians continue into South America?: Geology, v. 20, p. 1059-1062.

Dalziel, I.W.D., Dalla Salda, L.H., and Gahagan, L.M., 1994, Paleozoic Laurentia-Gondwana interaction and the origin of the Appalachian-Andean mountain system: Geological Society of America Bulletin, v. 106, p. 243-252.

Davis, T.L., 1993, Lithostratigraphy, structure, and metamorphism of a crystalline thrust terrane, western Inner Piedmont, North Carolina [Ph.D. dissertation]: Knoxville, University of Tennessee, 245 p.

Dennis, A.J., 1995, The Carolina terrane in northwestern South Carolina: Relative timing of events and recent tectonic models, *in* Hibbard, J.P., van Staal, C.R., and Cawood, P.A., eds., Current Perspectives in the Appalachian-Caledonian orogen: Stittsville, Ontario, Geological Association of Canada Special Paper 41, p. 173-189.

Dennis, A.J., and Wright, J.E., 1997, Middle and late Paleozoic monazite U-Pb ages, Inner Piedmont, South Carolina: Geological Society of America Abstracts with Programs, v. 29, no. 3, p. 12.

Drake, A.A., Jr., and Epstein, J.B., 1967, The Martinsburg Formation (Middle and Upper Ordovician) in the Delaware Valley, Pennsylvania-New Jersey: U.S. Geological Survey Bulletin 1244-H, 16 p.

Drake, A.A., Jr., Sinha, A.K., Laird, J., and Guy, R.E., 1989, The Taconic orogen, *in* Hatcher, R.D., Jr., Thomas, W.A., and Viele, G.W., eds., The Appalachian-Ouachita Orogen in the United States: Boulder, Colorado, Geological Society of America, The Geology of North America, v. F-2, p. 101–177.

Dypvik, H., and Harris, N.B., 2001, Geochemical facies analysis of fine-grained siliciclastics using Th/U, Zr/Rb and (Zr+Rb)/Sr ratios: Chemical Geology, v. 181, p. 131-146.

Eckert, J.O., Jr., Hatcher, R.D., Jr., and Mohr, D.W., 1989, The Wayah granulite-facies metamorphic core, southwestern North Carolina; high-grade culmination of Taconic metamorphism in the southern Blue Ridge: Geological Society of America Bulletin, v. 101, p. 1434-1437.

Eriksson, K.A., Campbell, I.H., Allen, C.M., and Palin, J.M., 2002, Sandstone petrography and detrital zircon geochronology of Neoproterozoic- through Pennsylvanian-age sandstones from the central Appalachians with implications for multiple recycling: Geological Society of America Abstracts with Programs, v. 34, no. 6, p. 208.

Fleet, A.J., 1984, Aqueous and sedimentary geochemistry of the rare earth elements, *in* Henderson, P., ed., Rare earth element geochemistry: Amsterdam, Elsevier, p. 343-373.

Force, E.R., 1976, Metamorphic source rocks of titanium placer deposits; a geochemical cycle: U.S. Geological Survey Professional Paper, p. B1-B16.

Fritz, W.J., Hatcher, R.D., Jr., and Hopson, J.L., 1989, Geology of the eastern Blue Ridge

of northeast Georgia and the adjacent Carolinas: Georgia Geological Society Guidebooks, v. 9, 199 p.

Fullagar, P.D., 2002, Evidence for Early Mesoproterozoic (and older?) crust in the southern and central Appalachians of North America: Gondwana Research, v. 5, p. 197-203.

Fullagar, P.D., and Butler, J.R., 1979, 325 to 265 m.y.-old granitic plutons in the Piedmont of the southeastern Appalachians: American Journal of Science, v. 279, p. 161-185.

Fullagar, P.D., Goldberg, S.A., and Butler, J.R., 1997, Nd and Sr isotopic characterization of crystalline rocks from the southern Appalachian Piedmont and Blue Ridge, North and South Carolina, *in* Sinha, A.K., Whalen, J.B., and Hogan, J.P., eds., The nature of magmatism in the Appalachian orogen: Boulder, Colorado, Geological Society of America Memoir 191, p. 165-179.

German, J.M., 1985, The geology of the northeastern portion of the Dahlonega gold belt: Georgia Geologic Survey Bulletin, v. 100, 41 p.

Giorgis, S.D., 1999, Geology of the northwestern South Mountains near Morganton, North Carolina [M.S. thesis]: Knoxville, University of Tennessee, 186 p.

Giorgis, S.D., Mapes, R.W., and Bream, B.R., 2002, The Walker Top Granite: Acadian granitoid or eastern Inner Piedmont basement?, *in* Hatcher, R.D., Jr., and Bream, B.R., eds., Inner Piedmont geology in the South Mountains-Blue Ridge Foothills and the southwestern Brushy Mountains, central-western North Carolina: North Carolina Geological Survey, Carolina Geological Society annual field trip guidebook, p. 33-43.

Goldberg, S.A., Butler, J.R., and Fullagar, P.D., 1986, The Bakersville dike swarm: Geochronology and petrogenesis of Late Proterozoic basaltic magmatism in the southern Appalachian Blue Ridge: American Journal of Science, v. 286, p. 403-430.

Goldsmith, R., Milton, D.J., and Horton, J.W., Jr., 1988, Geology of the Charlotte 1° x 2° quadrangle, North Carolina and South Carolina: U.S. Geological Survey Map I-1251-E, scale 1:250,000.

Götze, J., 1998, Geochemistry and provenance of the Altendorf feldspathic sandstone in the Middle Bunter of the Thuringian basin (Germany): Chemical Geology, v. 150, p. 43-61.

Gray, M.B., and Zeitler, P.K., 1997, Comparison of clastic wedge provenance in the Appalachian foreland using U/Pb ages of detrital zircons: Tectonics, v. 16, p. 151-160.

Gromet, L.P., Dymek, R.F., Haskin, L.A., and Korotex, R.L., 1984, The "North American Shale Composite": Its compilation, major and trace element characteristics: Geochimica et Cosmochimica Acta, v. 48, p. 2469-2482.

Hacker, B.R., Ratschbacher, L., Webb, L., Ireland, T., Walker, D., and Shuwen, D., 1998, U/Pb zircon ages constrain the architecture of the ultrahigh-pressure Qinling–Dabie Orogen, China: Earth and Planetary Science Letters, v. 161, p. 215-230.

Hadley, J.B., 1970, The Blue Ridge and the Reading Prong; the Ocoee series and its possible correlatives, *in* Fisher, G.W., Pettijohn, F.J., Reed, J.C., Jr., and Weaver,

K.N., eds., Studies of Appalachian geology, central and southern: New York, Interscience Publishing, p. 247-259.
Hardeman, 1966, Geologic map of Tennessee: State of Tennessee Department of Conservation Division of Geology: scale 1:250,000.
Harper, S.B., and Fullagar, P.D., 1981, Rb-Sr ages of granitic gneisses of the Inner Piedmont belt of northwestern North Carolina and southwestern South Carolina: Geological Society of America Bulletin, v. 92, p. 1864-1872.
Hatcher, R.D., Jr., 1969, Stratigraphy, petrology and structure of the low rank belt and part of the Blue Ridge of northwesternmost South Carolina: South Carolina Division of Geology, Geologic Notes, v. 13, p. 105-141.
Hatcher, R.D., Jr., 1978, Tectonics of the western Piedmont and Blue Ridge, southern Appalachians: Review and speculation: American Journal of Science, v. 278, p. 276-304.
Hatcher, R.D., Jr., 1979, The Coweeta Group and Coweeta syncline: Major feature of the North Carolina-Georgia Blue Ridge: Southeastern Geology, v. 21, p. 17-29.
Hatcher, R.D., Jr., 1980, Geologic map and mineral resources summary of the Prentiss quadrangle, North Carolina (scale 1:24,000), including geologic map of the Coweeta Hydrologic Laboratory (scale 1:14,400): North Carolina Department of Natural Resources and Community Development, GM 167-SW, MRS 167-SW, 10 p.
Hatcher, R.D., Jr., 1987, Tectonics of the southern and central Appalachian internides: Annual Review of Earth and Planetary Sciences, v. 15, p. 337-362.
Hatcher, R.D., Jr., 1988, Bedrock geology and regional geologic setting of Coweeta Hydrologic Laboratory in the eastern Blue Ridge, with some discussion of Quaternary deposits and structural controls of topography, *in* Swank, W.T., and Crossley, D.A., Jr., eds., Coweeta Symposium Volume 66: New York, Springer-Verlag, p. 81-92.
Hatcher, R.D., Jr., 1989, Tectonic synthesis of the U.S. Appalachians, *in* Hatcher, R.D., Jr., Thomas, W.A., and Viele, W.W., eds., The Appalachian-Ouachita Orogen in the United States: Boulder, Colorado, Geological Society of America, The Geology of North America, v. F-2, p. 511-535.
Hatcher, R.D., Jr., 2001a, Rheological partitioning during multiple reactivation of the Palaeozoic Brevard fault zone, southern Appalachians, USA: *in* Holdsworth, R.E., Strachan, R.A., Magloughlin, J.F., and Knipe, R.J., eds., The nature and tectonic significance of fault zone weakening: Geological Society, London, Special Publications, 186, p. 257-271.
Hatcher, R.D., Jr., 2001b, Terranes and terrane accretion in the southern Appalachians: An evolved working hypothesis: Geological Society of America Abstracts with Programs, v. 33, no. 2, p. A-65.
Hatcher, R.D., Jr., 2002, An Inner Piedmont primer, *in* Hatcher, R.D., Jr., and Bream, B.R., eds., Inner Piedmont geology in the South Mountains-Blue Ridge Foothills and the southwestern Brushy Mountains, central-western North Carolina: North Carolina Geological Survey, Carolina Geological Society annual field trip guidebook, p. 1-18.

Hatcher, R.D., Jr., and Acker, L.L., 1984, Geology of the Salem quadrangle, South Carolina: South Carolina Geological Survey MS-26, 23 p., 1:24,000 scale.
Hatcher, R.D., Jr., and Bream, B.R., eds., 2002, Inner Piedmont geology in the South Mountains-Blue Ridge Foothills and the southwestern Brushy Mountains, central-western North Carolina: North Carolina Geological Survey, Carolina Geological Society annual field trip guidebook, 145 p.
Hatcher, R.D., Jr., and Butler, J.R., 1979, Guidebook for southern Appalachian field trip in the Carolinas, Tennessee, and northeastern Georgia: International Geological Correlation Program Project 27, University of North Carolina, Chapel Hill, 117 p.
Hatcher, R.D., Jr., and Goldberg, S.A., 1991, The Blue Ridge geologic province, *in* Horton, J.W., Jr., and Zullo, V.A., eds., The geology of the Carolinas: Knoxville, University of Tennessee Press, p. 11-35.
Hatcher, R.D., Jr., and Williams, R.T., 1986, Mechanical model for single thrust sheets Part I: Taxonomy of crystalline thrust sheets and their relationships to the mechanical behavior of orogenic belts: Geological Society of America Bulletin, v. 97, p. 975-985.
Hatcher, R.D., Jr., and Zeitz, I., 1980, Tectonic implications of regional aeromagnetic and gravity data from the southern Appalachians, *in* Wones, D.R., eds., The Caledonides in the USA: Blacksburg, Virginia, Virginia Polytechnic Institute, Department of Geological Sciences, v. 2, p. 235-244.
Hatcher, R.D., Jr., Hooper, R.J., Petty, S.M., and Willis, J.D., 1984, Structure and chemical petrology of three southern Appalachian mafic-ultramafic complexes and their bearing upon the tectonics of emplacement and origin of Appalachian ultramafic bodies: American Journal of Science, v. 284, p. 484-505.
Hatcher, R.D., Jr., Hooper, R.J., McConnell, K.I., Heyn, T., and Costello, J.O., 1988, Geometric and time relationships between thrusts in the crystalline southern Appalachians, *in* Mitra, G. and Wojtal, S., eds., Appalachian thrusting: Geological Society of America Special Paper 222, p. 185-196.
Hatcher, R.D., Jr., Osberg, P.H., Drake, A.A., Jr., Robinson, P., and Thomas, W.A., 1990, Tectonic map of the U.S. Appalachians, *in* Hatcher, R.D., Jr., Thomas, W.A., and Viele, G.W., eds., The Appalachian–Ouachita Orogen in the United States: Boulder, Colorado, Geological Society of America, The Geology of North America, v. F-2, Plate 1, scale 1:2,000,000.
Hatcher, R.D., Jr., Bream, B.R., Hill, J.C., Giorgis, S.D., and Williams, S.T., 1999, Transect through the Acadian orogen in the Carolinas and northeast Georgia: Geological Society of America Abstracts with Programs, v. 31, no. 3, p. 19.
Hatcher, R.D., Jr., Bream, B.R., Miller, C.F., Eckert, J.O., Jr., Fullagar, P.D., and Carrigan, C.W., in press, Paleozoic structure of southern Appalachian Blue Ridge Grenvillian internal basement massifs, *in* Tollo, R.P., Corriveau, L., McLelland, J., and Bartholomew, M.J., eds., Proterozoic evolution of the Grenville Orogen in North America: Boulder, Colorado, Geological Society of America Memoir.
Heyn, T., 1984, Stratigraphic and structural relationships along the southwestern flank of the Sauratown Mountains anticlinorium [M.S. thesis]: Columbia, University of

South Carolina, 192 p.
Hibbard, J.P., 2000, Docking Carolina; mid-Paleozoic accretion in the southern Appalachians: Geology, v. 28, p. 127-130.
Hibbard, J.P., Stoddard, E.F., Secor, D.T., and Dennis, A.J., 2002, The Carolina Zone: Overview of Neoproterozoic to Early Paleozoic peri-Gondwanan terranes along the eastern flank of the southern Appalachians: Earth-Science Reviews, v. 57, p. 299-339.
Higgins, M.W., and McConnell, K.I., 1978, The Sandy Springs Group and related rocks of the Georgia Piedmont–nomenclature and stratigraphy, *in* Sohl, N.F., and Wright, W.B., eds., Changes in stratigraphic nomenclature by the U.S. Geological Survey, 1977: U.S. Geological Survey Bulletin 1457-A, p. A98-A105.
Hooper, R.J., and Hatcher, R.D., Jr., 1988, Pine Mountain Terrane, a complex window in the Georgia and Alabama Piedmont; evidence from the eastern termination: Geology, v. 16, p. 307-310.
Hooper, R.J., and Hatcher, R.D., Jr., 1992, The origin of the Pine Mountain Window; an internal basement massif within the Piedmont of Alabama Georgia, *in* Mason, R., ed., Basement Tectonics 7: The Netherlands, Kluwer Academic Publishers, p. 375-383.
Hopson, J.L., and Hatcher, R.D., Jr., 1988, Structural and stratigraphic setting of the Alto allochthon, northeast Georgia: Geological Society of America Bulletin, v. 100, p. 339-350.
Hopson, J. L., Hatcher, R. D., Jr., and Stieve, A. L., 1989, Geology of the eastern Blue Ridge, northeastern Georgia and the adjacent Carolinas, *in* Fritz, W. J., Hatcher, R. D., Jr., and Hopson, J. L., eds., Geology of the eastern Blue Ridge of northeast Georgia and the adjacent Carolinas: Georgia Geological Society Guidebooks, v. 9, p. 1-40.
Horton, J.W., Jr., and McConnell, K.I., 1991, The western Piedmont, *in* Horton, J.W., Jr., and Zullo, V.A., eds., The Geology of the Carolinas: Knoxville, Tennessee, The University of Tennessee Press, p. 36-58.
Horton, J.W., Jr., and Zullo, V.A., 1991, An introduction to the geology of the Carolinas, *in* Horton, J.W., Jr., and Zullo, V.A., eds., The geology of the Carolinas: Knoxville, Tennessee, The University of Tennessee Press, p. 1-10.
Horton, J.W., Jr., Drake, A.A., Jr., and Rankin, D.W., 1989, Tectonostratigraphic terranes and their Paleozoic boundaries in the central and southern Appalachians, *in* Dallmeyer, R.D., Jr., ed., Teranes in the Circum-Atlantic Paleozoic orogens: Geological Society of America Special Paper 230: Boulder, Colorado, p. 213-245.
Kalbas, J.L., 2003, Geology of part of the southwestern Brushy Mountains, Inner Piedmont, North Carolina, and the geochemistry of western Inner Piedmont migmatite [M.S. Thesis]: Knoxville, University of Tennessee, 206 p.
Kalbas, J.L., Bream, B.R., Hatcher, R.D., Jr., and Maybin, A.H., III, 2002, Evidence for mafic Ordovician magmatism and Acadian metamorphism in the Brushy Mountains, western Inner Piedmont of North Carolina: Geological Society of America Abstracts with Programs, v. 34, no. 2, p. 119.

Karabinos, P., and Gromet, L.P., 1993, Applications of single-grain zircon evaporation analyses to detrital grain studies and age discrimination in igneous suites: Geochimica et Cosmochimica Acta, v. 57, p. 4257-4267.
Karabinos, P., Aleinikoff, J.N., and Fanning, C.M., 1990, Distinguishing Grenvillian basement from pre-Taconian cover rocks in the northern Appalachians: American Journal of Science, v. 299, p. 502-515.
Keith, A., 1895, Description of the Knoxville sheet: U.S. Geological Survey Geologic Atlas, Folio 16, 6 p.
Keppie, J.D., Davis, D.W., and Krogh, T.E., 1998, U-Pb geochronological constraints on Precambrian stratified units in the Avalon Composite Terrane of Nova Scotia, Canada: Tectonic implications: Canadian Journal of Earth Science, v. 35, p. 222-236.
King, P.B., 1970, The Precambrian of the United States of America–Southeastern United States, *in* Rankama, K., ed., The geologic systems–The Precambrian, Volume 4: New York, Interscience, p. 1-71.
King, P.B., Hadley, J.B., Neuman, R.B., and Hamilton, W., 1958, Stratigraphy of the Ocoee Series, Great Smoky Mountains, Tennessee and North Carolina: Geological Society of America Bulletin, v. 69, p. 947-966.
King, P.B., Neuman, R.B., and Hadley, J.B., 1968, Geology of the Great Smoky Mountains National Park, Tennessee and North Carolina: U.S. Geological Survey Professional Paper 587, 23 p.
Kish, S.A., 1983, A geochronological study of deformation and metamorphism in the Blue Ridge and Piedmont of the Carolinas [Ph.D. thesis]: Chapel Hill, University of North Carolina, 220 p.
Kish, S.A., 1997, The Cat Square charnockite; a Paleozoic charnockite in the Inner Piedmont of North Carolina: Geological Society of America Abstracts with Programs, v. 29, no. 3, p. 28.
Kohn, M.J., 2001, Timing of arc accretion in the southern Appalachians: Perspectives from the Laurentian margin: Geological Society of America Abstracts with Programs, v. 33, no. 6, p. 262.
Larson, K. W., Hatcher, R. D., Jr., Neuman, R. B., and Finney, S. C., 1989, Structure of the Guess Creek fault and Fair Garden anticline, southeastern Tennessee: Relatives of the Great Smoky fault or unrelated structures?: Geological Society of America Abstracts with Programs, v. 21, no. 3, p. 46.
Loewy, S.L., Connelly, J.N., and Dalziel, I.W.D., 2002, Pb isotopes as a correlation tool to constrain Rodinia reconstruction: Geological Society of America Abstracts with Programs, v. 34, no. 6, p. 558.
Ludwig, K.R., 1991, ISOPLOT-a plotting and regression program for radiogenic-isotope data: Reston, Virginia, U.S. Geological Survey open file OF91-0445.
Ludwig, K.R., 1998, On the treatment of concordant uranium-lead ages: Geochimica et Cosmochimica Acta, v. 62, p. 665-676.
Ludwig, K.R., 2000, Decay constant errors in U-Pb concordia-intercept ages: Chemical Geology, v. 166, p. 315-318.
Ludwig, K.R., 2001a, Isoplot/Ex rev. 2.49: A geochronological toolkit for Microsoft

Excel: Berkeley Geochronology Center Special Publication No. 1a, 56 p.
Ludwig, K.R., 2001b, SQUID 1.02: A users manual: Berkeley Geochronology Center Special Publication No. 2, 19 p.
Mapes, R.W., 2002, Geochemistry and geochronology of mid-Paleozoic granitic plutonism in the southern Appalachian Piedmont terrane, North Carolina-South Carolina-Georgia [M.S. thesis]: Nashville, Vanderbilt University, 150 p.
McConnell, K.I., 1988, Geology of the Sauratown Mountains anticlinorium: Vienna and Pinnacle 7.5 minute quadrangles, *in* Hatcher, R.D., Jr., ed., Structure of the Sauratwon Mountains window, North Carolina: Carolina Geological Society Guidebook, p. 51-66.
McConnell, K.I., and Abrams, C.E., 1984, Geology of the greater Atlanta region: Georgia Geological Survey Bulletin 96, 127 p.
McDaniel, D.K., Sevigny, J.H., Hanson, G.N., and McLennan, S.M., 1997, Grenvillian provenance for the amphibolite-grade Trap Falls Formation: Implications for early Paleozoic tectonic history of New England: Canadian Journal of Earth Science, v. 34, p. 1286-1294.
McDowell, S.M., Miller, C.F., Fullagar, P.D., Bream, B.R., and Mapes, R.W., 2002, The Persimmon Creek Gneiss, eastern Blue Ridge, North Carolina-Georgia: Evidence for the missing Taconic arc?: Southeastern Geology, v. 41, p. 103-117.
McLennan, S.M., Taylor, S.R., Kroner, A., 1983, Geochemical evolution of Archean shales from South Africa: I. The Swaziland and Pongola Supergroups: Precambrian Research, v. 22, p. 93-124.
McLennan, S.M., Taylor, S.R., McCulloch, M.T., and Maynard, J.B., 1990, Geochemical and Nd-Sr isotopic composition of deep sea turbidites: Crustal evolution and plate tectonic association: Geochimica et Cosmochimica Acta: v. 54, p. 2015-2050.
McLennan, S.M., Hemming, S., McDaniel, D.K., and Hanson, G.N., 1993, Geochemical approaches to sedimentation, provenance, and tectonics, *in* Johnsson, M.J., and Basu, A., eds., Processes controlling the composition of clastic sediments: Boulder, Colorado, Geological Society of America Special Paper 284, p. 21-40.
McLennan, S.M., Bock, B., Compston, W., Hemming, S.R., and McDaniel, D.K., 2001, Detrital zircon geochronology of Taconian and Acadian foreland sedimentary rocks in New England: Journal of Sedimentary Research, v. 71, p. 305-317.
Merschat, A.J., and Kalbas, J.L., 2002, Geology of the southwestern Brushy Mountains, North Carolina Inner Piedmont: A summary and synthesis of recent studies, *in* Hatcher, R.D., Jr., and Bream, B.R., eds., Inner Piedmont geology in the South Mountains-Blue Ridge Foothills and the southwestern Brushy Mountains, central-western North Carolina: North Carolina Geological Survey, Carolina Geological Society annual field trip guidebook, p. 101-126.
Merschat, C.E., and Carter, M.W., 2002, Bedrock geologic map of the Bent Creek Research and Demonstration Forest, Southern Research Station, USDA Forest Service, including the North Carolina Arboretum and a portion of the Blue Ridge Parkway: North Carolina Geological Survey Geologic Map Series-9, 1:12,000 scale.
Meschter, S.M., Miller, C.F., Fullagar, P.D., Bream, B.R., and Mapes, R.W., 2002, The

Persimmon Creek Gneiss, eastern Blue Ridge, North Carolina-Georgia: Evidence for the missing Taconic arc?: Southeastern Geology, v. 41, p. 103-117.
Miller, B.V., and Stewart, K.G., 2002, Pluton ages in the eastern Blue Ridge province, North Carolina: Constraints on timing of tectonics and metamorphism in deep levels of an Ordovician accretionary wedge complex: Geological Society of America Abstracts with Programs, v. 34, no. 6, p. 41.
Miller, B.V., Stewart, K.G., Miller, C.F., and Thomas, C.W., 2000, U-Pb ages from the Bakersville, North Carolina eclogite; Taconian eclogite metamorphism followed by Acadian and Alleghanian cooling: Geological Society of America Abstracts with Programs, v. 32, no. 2, p. 62.
Miller, B.V., and Stewart, K.G., 2002, Pluton ages in the eastern Blue Ridge province, North Carolina: Constraints on timing of tectonics and metamorphism in deep levels of an Ordovician accretionary wedge complex: Geological Society of America Abstracts with Programs, v. 34, no. 6, p. 41.
Miller, C.F., Hatcher, R.D., Jr., Ayers, J.C., Coath, C.D., and Harrison, T.M., 2000, Age and zircon inheritance of eastern Blue Ridge plutons, southwestern North Carolina and northeastern Georgia, with implications for magma history and evolution of the southern Appalachian orogen: American Journal of Science, v. 300, p. 142-172.
Mirante, D.C., 2001, Monazite ages from the southern Appalachian Inner Piedmont-The Athens gneiss: Geological Society of America Abstracts with Programs, v. 33, no. 2, p. 3.
Mirante, D.C., and Patiño-Douce, A.E., 2000, Melting and migmatization in the southern Appalachian Inner Piedmont of northeast Georgia: The Athens gneiss: Geological Society of America Abstracts with Programs, v. 32, no. 7, p. 297.
Moecher, D.P., and Miller, C.F., 2000, Precise age for peak granulite facies metamorphism and melting in the eastern Blue Ridge from SHRIMP U-Pb analysis of zircon: Geological Society of America Abstracts with Programs, v. 32, no. 2, p. 63.
Moecher, D.P., Samson, S., and Miller, C.F., in review, Precise time and conditions of peak Taconian granulite facies metamorphism in the southern Blue Ridge: Geology.
Montes, C., and Hatcher, R.D., Jr., 1999, Documenting late Proterozoic rifting in the Ocoee Basin, western Blue Ridge, North Carolina: Southeastern Geology, v. 39, p. 37-50.
Muecke, G.K., Pride, C., and Sarkar, P., 1979, Rare-earth element geochemistry of regional metamorphic rocks, *in* Ahrens, L.H., ed., Origin and distribution of the elements, 2: Oxford, Pergamon, p. 449-464.
Mueller, P.A., Kozuch, M., Heatherinton, A.L., Wooden, J.L., Offield, T.W., Koeppen, R.P., Klein, T.L., and Nutman, A.P., 1996, Evidence for Mesoproterozoic basement in the Carolina terrane and speculations on its origin, *in* Nance, R.D., and Thompson, M.D., eds., Avalonian and related peri-Gondwanan terranes of the circum-North Atlantic: Boulder, Colorado, Geological Society of America Special Paper 304, p. 207-217.
Nelson, A.E., 1991, Geologic map of the Campbell Mountain quadrangle, Lumpkin

County, Georgia: U.S. Geological Survey Miscellaneous Field Studies Map MF-2148, 1:24,000 scale.
Nelson, A.E., and Gillon, K.A., 1985, Stratigraphic nomenclature in the Richard Russell and Helen thrust sheet, north Georgia, *in* Contributions to Stratigraphy, 1984: U.S. Geological Survey Bulletin No. 1605-A, p. A59-A62.
Nesbitt, H.W., and Young, G.M., 1982, Early Proterozoic climates and plate motions inferred from major element chemistry of lutites: Nature, v. 299, p. 715-717.
Neuman, R.B., 1955, Middle Ordovician rocks of the Tellico-Sevier belt eastern Tennessee: U.S. Geological Survey Professional Paper 274-F, 177 p.
Olson, J.C., 1952, Pegmatites of the Cashiers and Zirconia districts, North Carolina: North Carolina Department of Conservation and Development Bulletin 64, 32 p.
Osborne, W. E., Szabo, M.W., Neathery, T.L., and Copeland, C.W., Jr., 1988, Geologic map of Alabama, northeast sheet: Geologic Survey of Alabama Special Map 220: 1:250,000 scale.
Ownby, S.E., Miller, C.F., Berquist, P.J., Carrigan, C.W., and Fullagar, P.D., in press, Geochemistry and U-Pb geochronology of a portion of the Mars Hill terrane, North Carolina-Tennessee: Constraints on origin, history, and tectonic assembly, *in* Tollo, R.P., Corriveau, L., McLelland, J., and Bartholomew, M.J., eds., Proterozoic evolution of the Grenville orogen in North America: Boulder, Colorado, Geological Society of America Special Paper.
Paces, J.B., and Miller, J.D., 1993, Precise U-Pb age of Duluth complex and related mafic intrusions, northeastern Minnesota: Geochronological insights into physical, petrogenetic, paleomagnetic, and tectonomagmatic processes associated with the 1.1 Ga Mid-Continent rift system: Journal of Geophysical Research, v. 98, p. 13997-14103.
Pearce, J.A., Harris, N.B.W., and Tindle, A.G., 1984, Trace element discrimination for the tectonic interpretation of granitic rocks: Journal of Petrology, v. 25, p. 956-983.
Quidelleur, X., Grove, M., Lovera, O.M., Harrison, T.M., Yin, A., and Ryerson, F.J., 1997, Thermal evolution and slip history of the Renbu Zedong thrust, southeastern Tibet: Journal of Geophysical Research, v. 102, p. 2659-2679.
Quinlan, G.M., and Beaumont, C., 1983, Appalachian thrusting, lithospheric flexure, and the Paleozoic stratigraphy of the eastern interior of North America: Canadian Journal of Earth Sciences, v. 21, p. 973-996.
Quinn, M.J., 1990, Two lithotectonic boundaries in western North Carolina: Geologic interpretation of a region surrounding Sylva, Jackson County [M.S. thesis]: Knoxville, University of Tennessee, 223 p.
Rankin, D.W., 1970, Stratigraphy and structure of Precambrian rocks in northwestern North Carolina, *in* Fisher, G.W., Pettijohn, F.J., Reed, J.C., Jr., and Weaver, K.N., eds., Studies of Appalachian geology: Central and southern: New York, Interscience, p. 227-245.
Rankin, D.W., 1994, Continental margin of the eastern United States: Past and present: *in* Speed, R.C., ed., Phanerozoic evolution of North American continent-ocean transitions: Boulder, Colorado, Geological Society of America, DNAG Continent-

Ocean Transect Volume, p. 129-218.
Rankin, D.W., Drake, A.A., Jr., Glover, L., III, Goldsmith, R., Hall, L.M., Murray, D.P., Ratcliffe, N.M., Read, J.F., Secor, D.T., Jr., and Stanley, R.S., 1989, Pre-orogenic terranes, *in* Hatcher, R.D., Jr., Thomas, W.A., and Viele, G.W., eds., The Appalachian-Ouachita orogen in the United States: Boulder, Colorado, Geological Society of America, The Geology of North America, v. F-2, p. 7-100.
Ranson, W.A., Williams, I.S., and Garihan, J.M., 1999, SHRIMP zircon U-Pb ages of granitoids from the Inner Piedmont of South Carolina: Evidence for Ordovician magmatism involving Mid to Late Proterozoic crust: Geological Society of America Abstracts with Programs, v. 31, no. 7, p. 167.
Rast, N., and Kohles, K.M., 1986, The origin of the Ocoee Supergroup: American Journal of Science, v. 286, p. 593-616.
Roden, M.K., Elliot, W.C., Aronson, J.L., and Miller, D.S., 1993, A comparison of fission-track ages of apatite and zircon to the K/Ar ages of illite-smectite (I/S) from Ordovician K-bentonites, southern Appalachian basin: Journal of Geology, v. 101, p. 633-641.
Rodgers, J., 1953, Geologic map of East Tennessee with explanatory text: Tennessee Division of Geology Bulletin 58, Part II, 168 p.
Samson, S.D., Hibbard, J.P., and Wortman, G.L., 1995, Nd isotopic evidence for juvenile crust in the Carolina terrane, southern Appalachians: Contributions to Mineralogy and Petrology, v. 121, p. 171-184.
Secor, D.T., Jr., Samson, S.L., Snoke, A.W., and Palmer, A.R., 1983, Confirmation of the Carolina slate belt as an exotic terrane: Science, v. 221, p. 649-651.
Settles, D.J., 2002, Defining the Hayesville-Soque River and Allatoona faults and an Ordovician arc assemblage within the central Blue Ridge northwest of Dahlonega, Georgia [M.S. thesis]: Knoxville, University of Tennessee, 148 p.
Settles, D.J., Bream, B.R., and Hatcher, R.D., Jr., 2001, The Sally Free mafic complex and associated mafic rocks of the Dahlonega gold belt: Evidence of Ordovician arc volcanism and intrusion northwest of Dahlonega, Georgia: Geological Society of America Abstracts with Programs, v. 33, no. 6, p. A-262.
Shanmugam, G., and Lash, G.G., 1982, Analogous tectonic evolution of the Ordovician foredeeps, southern and central Appalachians: Geology, v. 10, p. 562-566.
Shanmugam, G., and Walker, K.R., 1978, Tectonic significance of distal turbidites in the Middle Ordovician Blockhouse and lower Sevier Formations in east Tennessee: American Journal of Science, v. 278, p. 551-578.
Shanmugam, G., and Walker, K.R., 1980, Sedimentation, subsidence, and evolution of a foredeep basin in the Middle Ordovician, southern Appalachians: American Journal of Science, v. 280, p. 479-496.
Sinha, A.K., and McLelland, J.M., 1999, Lead isotope mapping of crustal reservoirs within the Grenville superterrane: II. Adirondack massif, New York, *in* Sinha, A.K., ed., Basement Tectonics 13: Kluwer Academic Publishers, Dordrecht, The Netherlands, p. 297-312.
Sinha, A.K., and Zietz, I., 1982, Geophysical and geochemical evidence for a Hercynian

magmatic arc, Maryland to Georgia: Geology, v. 10, p. 593-596.
Sinha, A.K., Hund, E.A., and Hogan, J.P., 1989, Paleozoic accretionary history of the North American plate margin (central and southern Appalachians): Constraints from the age, origin, and distribution of granitic rocks, *in* Hillhouse, J., ed., Deep structure and past kinematics of accreted terranes: American Geophysical Union Monograph Series, p. 219-238.
Spell, T.L., and Norrell, G.T., 1990, The Ropes Creek assemblage: Petrology, geochemistry, and tectonic setting of an ophiolitic thrust sheet in the southern Appalachians: American Journal of Science, v. 290, p. 811-842.
Steltenphol, M.G., and Kunk, M.J., 1993, 40Ar/39Ar thermochronology and Alleghanian development of the southernmost Appalachian Piedmont, Alabama and southwest Georgia: Geological Society of America Bulletin, v. 105, p. 819-833.
Steltenpohl, M.G., Heatherington, A., and Mueller, P., in press, Current understanding of pre-Appalachian tectonic evolution in the southernmost Appalachians, Pine Mountain window, Alabama & Georgia, *in* Tollo, R.P., Corriveau, L., McLelland, J., and Bartholomew, M.J., eds., Proterozoic evolution of the Grenville Orogen in North America: Boulder, Colorado, Geological Society of America Special Paper.
Stewart, K.G., and Miller, B.V., 2001, The tectonic implications of 460 Ma eclogite along the Taconian Suture in the eastern Blue Ridge of North Carolina: Geological Society of America Abstracts with Programs, v. 33, no. 2, p.651.
Stewart, K.G., Adams, M.G., and Trupe, C.H., 1997, Paleozoic structural evolution of the Blue Ridge thrust complex, western North Carolina, *in* Stewart, K.G., Adams, M.G., and Trupe, C.H., eds., Paleozoic structure, metamorphism, and tectonics of the Blue Ridge of western North Carolina: North Carolina Geological Survey, Carolina Geological Society annual field trip guidebook, p. 21-31.
Student, J. J., and Sinha, A. K., 1992, Carboniferous U-Pb ages of zircons from the Box Ankle and Ocmulgee faults, central Georgia: Implications for accretionary models: Geological Society of America Abstracts with Programs, v. 24, no. 2, p. 69.
Su, Q., Goldberg, S.A., and Fullagar, P.D., 1994, Precise U-Pb zircon ages of Neoproterozoic plutons in the southern Appalachian Blue Ridge and their implications for the rifting of Laurentia: Precambrian Research, v. 68, p. 81-95.
Taylor, S.R., and McLennan, S.M., 1985, The continental crust: Its composition and evolution: Oxford, Blackwell's, 312 p.
Taylor, S.R., Rudnick, R.L., McLennan, S.M., and Eriksson, K.A., 1986, Rare earth element patterns in Archean high-grade metasediments and their tectonic significance: Geochimica et Cosmochimica Acta, v. 50, p. 2267-2279.
Thomas, C.W., 2001, Origins of mafic-ultramafic complexes of the eastern Blue Ridge province, southern Appalachians: Geochronological and geochemical constraints [M.S. thesis]: Nashville, Vanderbilt University, 154 p.
Thomas, M. D., 1983, Tectonic significance of paired gravity anomalies in the southern and central Appalachians, *in* Hatcher, R. D., Jr., Williams, H., and Zietz, Isidore, eds., Contributions to the tectonics and geophysics of mountain chains: Geological Society of America Memoir 158, p. 113-124.

Thomas, W.A., 1991, The Appalachian-Ouachita rifted margin of southeastern North America: Geological Society of America Bulletin, v. 103, p. 415-431.
Tollo, R.P., and Aleinikoff, J.N., 1996, Petrology and U-Pb geochronology of the Robertson River igneous suite, Blue Ridge Province, Virginia; evidence for multistage magmatism associated with an early episode of Laurentian rifting: American Journal of Science, v. 296, p. 1045-1090.
Unrug, R., and Unrug, S., 1990, Palontological evidence of Paleozoic age for the Walden Creek Group, Ocoee Supergroup, Tennessee: Geology, v. 18, p. 1041-1045.
Unrug, R., Ausich, W.I., Bednarczyk, J., Cuffey, R.J., Mamet, B.L., Palmes, S.L., and Unrug, S., 2000, Paleozoic age of the Walden Creek Group, Ocoee Supergroup, in the western Blue Ridge, southern Appalachians: Implications for evolution of the Appalachian margin of Laurentia: Geological Society of America Bulletin, v. 112, p. 982-996.
Van Schmus, W.R., Bickford, M.E., Turek, A., 1996, Proterozoic geology of the east-central midcontinent basement, *in* van der Pluijm, B.A., and Catacosinos, P.A., eds., Basement and basins of eastern North America: Geological Society of America Special paper 308, p. 7-32.
Vick, H.K., Channell, J.E.T., and Opdyke, N.D., 1987, Ordovician docking of the Carolina slate belt: Paleomagnetic data: Tectonics, V. 6, p. 573-583.
Vinson, S.B., 1999, Ion probe geochronology of granitoid gneisses of the Inner Piedmont, North Carolina and South Carolina [M.S. thesis]: Nashville, Vanderbilt University, 84 p.
Walker, D., Driese, S.G., and Hatcher, R.D., Jr., 1989, Paleotectonic significance of the quartzite of the Sauratown Mountains window, North Carolina: Geology, v. 17, p. 913-917.
Walker, K.R., Shanmugam, G., and Ruppel, S.C., 1983, A model for carbonate to terrigenous clastic sequences: Geological Society of America Bulletin, v. 94, p. 700-712.
Wiener and Merschat, 1988, Geology of the Sandymush and Canton quadrangles, North Carolina: North Carolina Geological Survey, 1:24,000 scale, 66 p.
Willard, R.A., and Adams, M.G., 1994, Newly discovered eclogite in the southern Appalachian orogen, northwestern North Carolina: Earth and Planetary Science Letters, v. 123, p. 61-70.
Williams, H., and Hatcher, R.D., Jr., 1982, Suspect terranes and accretionary history of the Appalachian orogen: Geology, v. 10, p. 530-536.
Williams, H., and Hiscott, R.N., 1987, Definition of the Iapetus rift-drift transition in western Newfoundland: Geology, v. 15, p. 1044-1047.
Wronkiewicz, D.J., and Condie, K.C., 1990, Geochemistry and mineralogy of sediments from the Ventersdorp and Transvaal Supergroup, South Africa: Cratonic evolution during the early Proterozoic: Geochimica et Cosmochimica Acta, v. 54, p. 343-354.
Yanagihara, G.M., 1994, Structure, stratigraphy, and metamorphism of a part of the Columbus Promontory, western Inner Piedmont, North Carolina [M.S. thesis]: Knoxville, University of Tennessee, 214 p.

PART III

The southern Appalachian Inner Piedmont: New perspectives based on recent detailed geologic mapping, Nd isotopic evidence, and zircon geochronology

This chapter is a slightly modified version of a paper that I wrote and was published in the 2002 Carolina Geological Society field trip guidebook:

> Bream, B.R., 2002, The southern Appalachian Inner Piedmont: New perspectives based on recent detailed geologic mapping, Nd isotopic evidence, and zircon geochronology, *in* Hatcher, R.D., Jr., and Bream, B.R., eds., Inner Piedmont geology in the South Mountains-Blue Ride Foothills and southwestern Brushy Mountains, central-western North Carolina: North Carolina Geological Survey, Carolina Geological Society annual field trip guidebook, p. 45-63.

INTRODUCTION

The objectives of this paper are to summarize geochemical and geochronologic data from the southern Appalachian crystalline core, to integrate and examine recent detailed mapping along strike from the Columbus Promontory, and to present several new or revised ideas and interpretations concerning the evolution of the southern Appalachian Inner Piedmont. Numerous contributions to our understanding of the Inner Piedmont have been made over the last ten years since the last University of Tennessee-affiliated CGS field trip. Because of the ongoing nature and volume of new Inner Piedmont research, any attempt to integrate and present this work is admittedly limited. Therefore, for the purpose of this guidebook and from a practical standpoint, this synthesis emphasizes new work in the North Carolina Inner Piedmont and highlights recent and/or pertinent work from other areas of the southern Appalachians where appropriate. This overview contains some information from UTK M.S. theses (Bream, 1999; Giorgis, 1999; Hill; 1999; Williams, 2000; Bier, 2001; Kalbas, in preparation; Merschat, in preparation), Vanderbilt M.S. theses (Vinson, 1999; Carrigan, 2000; Thomas, 2001; Mapes, 2002), and the work of several undergraduate students at both universities.

The traditional geologic and tectonic divisions of the southern Appalachians include the Cumberland-Allegheny Plateau, Valley and Ridge, western Blue Ridge, eastern Blue Ridge, Inner Piedmont, and Carolina composite terrane (Fig. 1). Together, the Blue

Ridge (exclusive of the frontal thrust sheet), Inner Piedmont, and portions of the Carolina composite terrane comprise the crystalline core of the southern Appalachians. Most of the Inner Piedmont has not been studied in detail partially due to the common misconception that this region lacks exposure and a recognizable stratigraphy. For these reasons, a large portion (~75 %) of Inner Piedmont remains unmapped; recent detailed mapping, however, has delineated coherent and extensive lithotectonic packages throughout much of the Inner Piedmont. As in most high-grade gneiss terranes, the rocks of the Inner Piedmont are varied, intensely deformed, and partially to intensely migmatitic. The dominant rock types of the Inner Piedmont include quartzofeldspathic gneiss, amphibolite, quartzite and pelitic schist with lesser amounts of amphibole gneiss, calc-silicate, and ultramafic rocks.

Current thinking regarding the Inner Piedmont is an extension of several pioneering researchers, namely Griffin (1967; 1969a; 1969b; 1971a; 1971b; 1974a; 1974b), Hatcher (1969; 1970; 1978), Bentley and Neathery (1970), and contributions included in the 1993 Carolina Geological Society Guidebook (Hatcher, 1993; Davis, 1993a; Yanagihara, 1993; Garihan et al., 1993; Clark, 1993; Hibbard, 1993; Grimes et al., 1993; Goldberg and Fullagar, 1993). Hatcher (1993), in particular, provided a more detailed summary of significant contributions prior to 1993. Many of the original ideas and concepts, or slightly modified versions, presented by these workers are the foundation on which nearly all subsequent Inner Piedmont work is built.

Tectonostratigraphic terranes within the crystalline core are based on the crustal affinity and tectonic history of the rocks present. The terrane boundaries within and bounding the crystalline core are variably interpreted and defined (e.g., Williams and Hatcher, 1983; Horton et al., 1989; Hibbard and Samson, 1995). The Inner Piedmont is often grouped with the adjacent Blue Ridge in tectonic maps and has been designated as the eastern part of the larger Piedmont terrane, Piedmont zone, or Tugaloo terrane

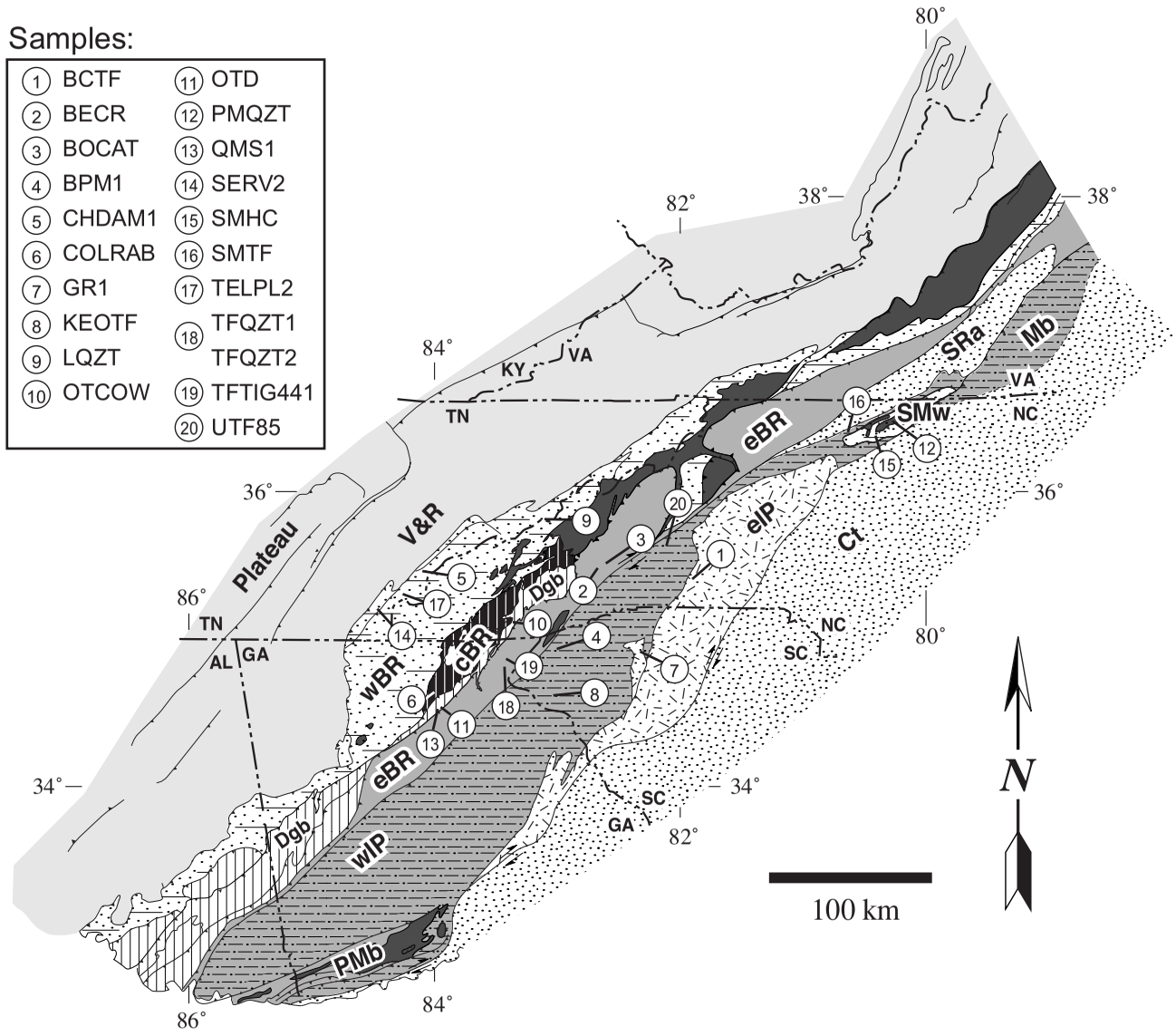

Figure 1. Tectonic map of the southern Appalachians modified from Hatcher et al. (1990) and Bream et al. (in review). cBR-central Blue Ridge; Ct-Carolina terrane; Dgb-Dahlonega gold belt; eBR-eastern Blue Ridge; eIP-central and eastern Inner Piedmont; Mb-Milton belt; PMb-Pine Mountain block; SMw-Sauratown Mountains window; SRa-Smith River allochthon; V&R-Valley and Ridge; wBR-western Blue Ridge; wIP-western Inner Piedmont. Sample locations and associated formations are provided in Table 1.

Table 1. Sample locations with formations keyed to Figure 1.

Sample	Figure 1 Location	Formation	7.5-minute quadrangle	County (State)
western Blue Ridge				
CHDAM1	5	Walden Creek Group (Ocoee Supergroup)	Tallassee	Blount (TN)
LQZT	9	Snowbird Group (Ocoee Supergroup)	Waterville	Cocke (TN)
SERV2	14	Walden Creek Group (Ocoee Supergroup)	McFarland	Polk (TN)
TELPL2	17	Great Smoky Group (Ocoee Supergroup)	Tellico Plains	Monroe (TN)
central Blue Ridge				
COLRAB	6	Coleman River Formation	Hightower Bald	Rabun (GA)
Dahlonega gold belt				
OTCOW	10	Otto Formation	Prentiss	Macon (NC)
OTD	11	Otto Formation	Campbell Mountain	Lumpkin (GA)
QMS1	13	Otto Formation	Campbell Mountain	Lumpkin (GA)
eastern Blue Ridge				
BECR	2	Tallulah Falls Formation-Ashe Formation (metagraywacke member)	Dunsmore Mountain	Buncombe (NC)
BOCAT	3	Tallulah Falls Formation-Ashe Formation (metagraywacke member)	Asheville	Buncombe (NC)
TFQZT1	18	Tallulah Falls Formation (quartzite member)	Tiger	Rabun (GA)
TFQZT2*	18	Tallulah Falls Formation (quartzite member)	Tallulah Falls	Rabun (GA)
TFTIG441	19	Tallulah Falls Formation-Ashe Formation (metagraywacke member)	Tiger	Rabun (GA)
Sauratown Mountains window				
SMHC	15	Hogan Creek Formation	Siloam	Surry (NC)
PMQZT	12	Pilot Mountain Quartzite	Pinnacle	Surry (NC)
western Inner Piedmont				
BPM1	4	Chauga River Formation (Brevard-Poor Mountain Transitional member)	Salem	Oconee (SC)
KEOTF	8	Tallulah Falls Formation-Ashe Formation (metagraywacke member)	Seneca	Oconee (SC)
SMTF	16	Tallulah Falls Formation-Ashe Formation (metagraywacke member)	Copeland	Surry (NC)
UTF85	20	Tallulah Falls Formation-Ashe Formation (metagraywacke member)	Marion East	McDowell (NC)
eastern Inner Piedmont				
BCTF	1	metagraywacke not presently assigned to a formation	Benn Knob	Rutherford (NC)
GR1	7	metagraywacke not presently assigned to a formation	Greer	Spartanburg (SC)

*Nd and Sr isotopic analysis only.

(Williams and Hatcher, 1983; Hibbard and Samson, 1995; Hatcher et al., 1999; respectively). This grouping favors interpretations that correlate sedimentary packages, and likely crustal affinity, across the Brevard fault zone. Other tectonic affinity interpretations for the North Carolina Inner Piedmont are varied: mélange complex (Goldsmith et al., 1988; Horton et al., 1989); accretionary wedge (Abbot and Raymond, 1984; Hatcher, 1987; Rankin, 1988); probable accreted exotic terrane (Dennis, 1991; Rankin et al., 1989; Rankin, 1994; Dennis and Wright, 1997). Incomplete detailed mapping and the paucity of geochemical and geochronologic data have exacerbated attempts to subdivide or correlate lithotectonic packages thus further obscuring relationships within the southern Appalachians and between the southern and northern Appalachians.

GEOLOGIC SETTING AND PREVIOUS WORK

Despite the highly enigmatic nature of the Inner Piedmont, several general observations can be made regarding its complex history; and are divided here into four

broad categories: stratigraphic, metamorphic, magmatic, and tectonic. The following sections focus on background information for the North Carolina Inner Piedmont and establishes the framework from which a revised perspective can be drawn based on new detailed geologic mapping, geochemistry, and geochronology.

Stratigraphic

The opening of the Iapetus ocean is temporally constrained by rift-related magmatism and deposition that suggests: (1) rifting separated west Gondwana cratons from Laurentia around 570 Ma, (2) the Iapetus ocean was developed before 550 Ma, and (3) this Early Cambrian rifting could have propagated along zones already weakened by earlier Neoproterozoic failed rifting ~760-700 Ma (e.g., Su et al., 1994; Aleinikoff et al., 1995; Cawood et al., 2001). Paragneisses within the Appalachian crystalline core are commonly interpreted as post-Grenvillian rift fill, possibly time-transgressive from west to east, from Late Proterozoic in the western Blue Ridge to as young as Silurian in the eastern Inner Piedmont (e.g., Bream et al., 2001a). Portions of the same lithologic packages, on the other hand, have been interpreted as large Ordovician accretionary wedges (Abbott and Raymond, 1984), Devonian transtensional basins (Unrug et al., 2000), and Grenville basement (Espenshade et al., 1975; Gillon, pers.comm., 2000).

A recognizable stratigraphy, traceable along strike into Georgia and across strike in several thrust sheets, has been identified throughout the North Carolina western Inner Piedmont. This stratigraphy consists of the following dominant rock types (from bottom to top): metagraywacke and amphibolite; aluminous schist; metagraywacke with minor amphibolite; metasiltstone and pelitic schist with minor carbonate; finely laminated amphibolite; quartzite, marble, feldspathic quartzite, and calcareous quartzite. Lithologies similar to the lower part of the sequence are present in the eastern Inner Piedmont, in the hanging wall of the Brindle Creek thrust, but show a considerable increase in the amount of metapelite relative to metagraywacke. Correlation of western

Inner Piedmont stratigraphy with the eastern Inner Piedmont lithologies is not made now because of new geochronologic data discussed later in this paper.

Tallulah Falls-Ashe Formation

The lowest part of the stratigraphic sequence, below the Poor Mountain amphibolite, is correlative with Davis' (1993a, 1993b) Mill Spring complex that includes the thick biotite gneiss unit recognized by Lemmon (1973) below his Sugarloaf Mountain group. The knotted biotite gneiss of Whisnant (1975, 1979) in the Sugar Hill 7.5-minute quadrangle is roughly correlative with the upper biotite gneiss unit in the stratigraphy whereas his porphyroclastic schist and gneiss unit contains portions of the upper and lower biotite gneiss units recognized in recent mapping (Bream, 1999; Hill, 1999). The Tryon formation and Mill Spring group of Conley and Drummond (unpublished) also contain a similar sequence of rock units. Within the Sugarloaf Mountain thrust sheet, this formation occurs discontinuously from at least the northeast edge of the Marion East quadrangle into South Carolina where Garihan (1999) has mapped it. Due to the remarkable similarity of the western Inner Piedmont stratigraphy to the Tallulah Falls and Ashe Formations of the eastern Blue Ridge, Hatcher (1978, 1987, 1989, this volume), Heyn (1984), Hopson and Hatcher (1988), Davis (1993b), and Hill (1999) have correlated the western Inner Piedmont psammitic-pelitic sequence with the Tallulah Falls-Ashe Formation. The name Tallulah Falls Formation is used here, therefore, to refer to the biotite paragneiss and aluminous schist units of the western Inner Piedmont and eastern Blue Ridge, or the Tugaloo terrane of Hatcher (this guidebook).

Poor Mountain Formation

The upper portion of the western Inner Piedmont stratigraphy can be correlated with the Poor Mountain sequence first described by Sloan (1907) northwest of Walhalla,

South Carolina. Shufflebarger (1961) first subdivided the Poor Mountain sequence and Hatcher (1969, 1970) subsequently correlated the Poor Mountain rocks with the Chauga River Formation in South Carolina. Hatcher (1969, 1970) also defined the Poor Mountain sequence as a formation and attributed lithologic differences between the Chauga River and Poor Mountain Formation to facies changes. Additionally, Hatcher (1969, 1970) defined the Brevard-Poor Mountain transitional member as the lowest part of the Poor Mountain Formation. The transitional unit is recognized from the Chauga belt in South Carolina along strike to as far north as the Columbus Promontory of North Carolina.

Metamorphic

Originally defined by King (1955) as a high-grade gneiss terrane, the Inner Piedmont is now widely regarded as the southern Appalachian Acadian metamorphic core (e.g., Osberg et al., 1989; Hatcher, 1993; Hatcher et al., 1999). Regional studies in the southern Appalachian crystalline core (e.g., Griffin, 1974a; Osberg et al., 1989; Butler, 1991; Hatcher and Goldberg, 1991) identify the southeast dipping kyanite-sillimanite isograd that places more migmatitic sillimanite grade assemblages over less migmatitic kyanite and lower grade assemblages in the western Inner Piedmont (Fig. 2). The internal Inner Piedmont is dominated by sillimanite-grade rocks almost entirely encompassed by relatively thin flanks of kyanite and/or kyanite + staurolite-grade (lower in South Carolina) rocks near its southeastern and northwestern boundaries.

The Inner Piedmont contains abundant evidence of polyphase deformation at or near middle- to upper-amphibolite facies conditions later superposed by brittle event(s). The presence of migmatite at all scales throughout most of the Inner Piedmont demonstrates that these rocks were at or near minimum melt conditions during prograde metamorphism. Based on textural and mapping evidence in the South Carolina Cashiers, Tamassee, and Satolah 7.5-minute quadrangles, Roper and Dunn (1973) defined two

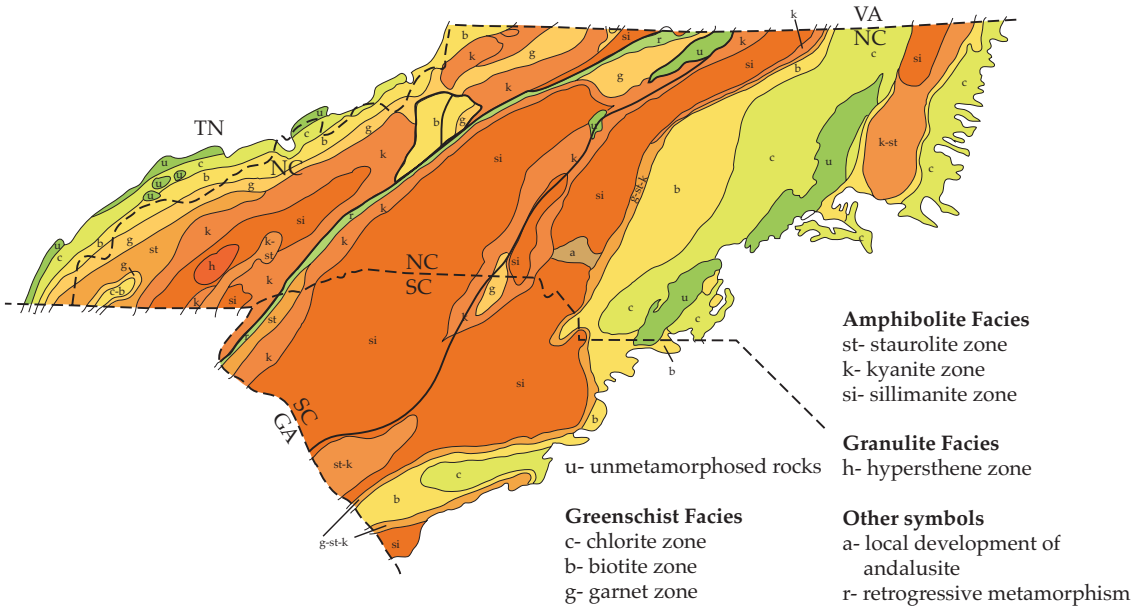

Figure 2. Metamorphic isograd map of North Carolina, South Carolina, and part of east Tennessee. Modified from Butler (1991) and Hatcher and Goldberg. (1991). Modified from a figure drafted by Scott D. Giorgis.

metamorphic events; an earlier amphibolite facies Taconic (?) event and a later greenschist facies Acadian (?) event that retrogressed some of the earlier prograde mineral assemblages. Lemmon (1973) proposed two prograde metamorphic events (possibly Taconic and Acadian equivalents) for the North Carolina Inner Piedmont, whereas Davis (1993a, 1993b) indicated only a single prograde Acadian metamorphic event occurred here.

Magmatic

The Inner Piedmont contains abundant outcrop- and map-scale granitoid bodies with small mafic and ultramafic bodies (with the notable exception of the Poor Mountain Amphibolite) (Hatcher, this guidebook, his Fig. 1). Sinha et al. (1989) suggested several magmatic phases affected the central and southern Appalachian Blue Ridge, Inner Piedmont, and Carolina terrane: a 520-490 Ma magmatic arc along the cratonic margin; 460-440 Ma high pressure magmas resulting from arc collapse followed by thrusting; Siluro-Devonian decompressional melting following the Taconic orogeny in the Blue

Ridge and Inner Piedmont; and extensive 330-270 Ma subduction related magma generation largely restricted to the Inner Piedmont and Carolina terrane. McSween et al., (1991) defined four distinct age groups for plutonic rocks: 1197-1005 Ma intrusions into Precambrian basement of the Blue Ridge and Sauratown Mountains window; 734-495 Ma for basaltic and peralkaline granitic magmas in the Blue Ridge and plutons of the slate belt; 436-375 Ma for the Blue Ridge Spruce Pine Plutonic Suite and western Inner Piedmont granitoids; and 340-385 Ma for granitoid-gabbro plutons of the central and eastern Piedmont. The nature and timing of granitoid genesis within the Inner Piedmont is now better constrained but regional perspectives are largely lacking and the distribution of many bodies are poorly delineated and several are likely unidentified. Harper and Fullagar (1981), Drake et al. (1989), Osberg et al. (1989), Horton and McConnell (1991), McSween et al. (1991), and Fullagar et al. (1997) provided more detailed regional accounts and interpretations of the igneous rocks in the southern Appalachians. The presentation here focuses on magmatic Inner Piedmont rocks that have been more thoroughly studied since the 1993 CGS field trip.

Henderson Gneiss

The Henderson Gneiss is one of the most areally extensive granitoids of the Appalachian orogen and is by far the largest (~5000 km^2) granitoid of the North and South Carolina Inner Piedmont. Spectacular Henderson Gneiss outcrops occur primarily in locations where the across-strike outcrop width of the main body is greatest (e.g., North Carolina Columbus Promontory). Keith (1905, 1907) first described the Henderson Gneiss and defined the type locality in Henderson County, North Carolina. Reed (1964) and Bryant and Reed (1970) restricted the Henderson Gneiss to a belt southeast of the Brevard fault zone. Citing the complex map pattern and compositional variability of the Henderson Gneiss in South Carolina, Hatcher (1970) proposed that the Henderson Gneiss and Poor Mountain Formation have sedimentary protoliths and are

Late Proterozoic to Early Cambrian. Lemmon (1973) concluded that the Henderson Gneiss has an igneous protolith based on zircon morphology. Numerous Rb-Sr whole-rock ages have been determined for the Henderson Gneiss: 509 Ma (Sinha et al., 1989) using a revised decay constant for Odom and Fullagar (1973) data; 460 ± 9 Ma (Harper and Fullagar, 1981) for lithologies initially mapped as Henderson Gneiss in Wilkes County, NC (Rankin et al., 1972); 438 ± 22 Ma for the large intrusive granitoid within the Henderson Gneiss (Odom and Russell, 1975); 356 and 387 Ma for mylonitic Henderson Gneiss in the Brevard fault zone (Odom and Fullagar, 1973; Bond and Fullagar, 1974, respectively). Using conventional U-Pb data from Henderson Gneiss zircon fractions, Sinha and Glover (1978) proposed a 593 Ma intrusive age for the protolith, 456 Ma age for Taconic metamorphism, and a 360-390(?) Ma age range for Acadian metamorphism.

Caesars Head Granite

The Caesars Head Granite, originally named the Caesars head Quartz Monzonite by Hadley and Nelson (1970), was renamed by Horton and McConnell (1991) and grouped with several smaller Inner Piedmont granitoids into the Table Rock Plutonic Suite. Geochronology for the Caesars Head Granite includes a 435 Ma $^{207}Pb/^{206}Pb$ zircon age (J.W. Horton and T.W. Stern, unpublished data) and a 409 Ma Rb-Sr whole-rock age (P.D. Fullagar, unpublished data). The Caesars Head Granite, as depicted on the Greenville 1˚ x 2˚ sheet (Nelson et al., 1998) and the preliminary South Carolina Blue Ridge and Piedmont map (Horton and Dicken, 2001), crosscuts at least two Paleozoic faults, implying that movement on these faults pre-dates intrusion.

Smaller Inner Piedmont Granitoids

Numerous smaller granitoids (relative to the Henderson Gneiss and Caesars Head Granite) are present in the Inner Piedmont. Several of these granitoids were included in

the Table Rock Plutonic Suite of Horton and McConnell (1991), which "consists mainly of gneissic biotite granitoids and granitoid gneisses of probably Late Ordovician to Early Silurian age." Granitoids that were included in the Table Rock Plutonic Suite include the Brooks Crossroads, NC (Harper and Fullagar, 1981), Dysartsville, NC (Goldsmith et al., 1988), Reedy River, SC (Wagener, 1977), and Toluca, NC (see Overstreet et al., 1963b) granitoids. Other Inner Piedmont granitoids, most fitting the criteria for the Table Rock Plutonic Suite, which will be mentioned here include the Anderson's Mill, SC (Curl, 1998); Call, NC (Rankin et al., 1972); Pelham, SC (Maybin, 1997); Sugarloaf Mountain, NC (Lemmon, 1973); Toccoa, GA (R.D. Hatcher Jr., unpublished mapping); and Walker Top, NC (possible less sheared shallow-level Henderson Gneiss of Goldsmith et al., 1988) granitoids. Granitoids that Horton and McConnell (1991) designated as Devonian and Early Carboniferous include the Cherryville, NC (Griffitts and Overstreet, 1952) and Gray Court, SC (Wagener, 1977). Several other granitoids have been recognized in the Inner Piedmont for which no new data exist. In North Carolina these include the Sandy Mush granite, less foliated (relative to the Henderson Gneiss) megacrystic granitoid southeast of the Brindle Creek fault, and unnamed granitoid and migmatitic granitoid gneisses (all delineated by Goldsmith et al., 1988). Based on new geochronologic, isotopic, and geochemical data, and as proposed by Mapes et al. (2002), division of the Inner Piedmont into eastern and western magmatic belts is appropriate.

Western Inner Piedmont magmatic belt

Goldsmith et al. (1988) mapped the Dysartsville Tonalite as granitoid gneiss (termed the Dysartsville pluton on the tectonic inset) and indicated that the unit continues northeastward along strike from near Dysartsville, NC. Bream (1999), Giorgis (1999), Hill (1999), and Williams (2000) remapped the Dysartsville Tonalite southeast of Marion, North Carolina; and Yanagihara (1994) noted that the Mill Spring complex (Tallulah Falls Formation equivalent) contains significant amounts of granitoid that are

likely correlative with the main Dysartsville Tonalite body. Several mafic and ultramafic bodies are present within the Dysartsville Tonalite in the Glenwood 7.5-minute quadrangle. Data for other western Inner Piedmont smaller granitoids is largely limited to a whole-rock Rb-Sr age, 427 ± 9 Ma, for the Brooks Crossroads pluton (Harper and Fullagar, 1981), originally mapped as Inner Piedmont granitic rock (Espenshade et al., 1975), and a whole-rock Rb-Sr age of 460 ± 9 Ma for granitoids originally mapped as Henderson Gneiss (Rankin et al., 1972) near Call, North Carolina.

Eastern Inner Piedmont magmatic belt

Several mappable megacrystic K-feldspar granitoids (first recognized by Goldsmith et al., 1988) are present in the South Mountains (Giorgis, 1999; Bier, 2001) and along strike in the Brushy Mountains (Merschat and Kalbas, this guidebook). They occur as discontinuous linear elongate bodies in the immediate hanging wall of the Brindle Creek thrust, and have been formally named the Walker Top Granite (Giorgis et al., this guidebook). A similar megacrystic K-feldspar augen gneiss was recognized by Curl (1998) near Spartanburg, South Carolina, and was informally named the Anderson's Mill gneiss. The Toluca Granite, named by Griffitts and Overstreet (1952) and first mapped in detail near Shelby (Griffitts and Overstreet, 1962; Griffitts et al., 1962; Yates and Overstreet, 1962; Yates, 1963; Overstreet et al., 1963a; compiled by Overstreet et al., 1963b), occurs as small- to moderate-sized bodies that parallel regional fabrics from at least the Brushy Mountains in North Carolina southwestward into northern Cherokee County, SC (Goldsmith et al., 1988). Davis et al. (1962) proposed that the Toluca Granite has a minimum age of 400 Ma and noted that zircon morphology favors a sedimentary origin.

The Cherryville granite is located along the Central Piedmont suture at the southeastern boundary of the Inner Piedmont. Griffitts and Overstreet (1952) also named this unit, which was subsequently included in work by Davis et al. (1962) and Kish

(1983). Kish (1983) determined younger Rb-Sr whole-rock isochron (351 Ma), Rb-Sr muscovite (311 Ma), and Rb-Sr biotite (277 Ma) ages than the Rb-Sr biotite (375 Ma) age determined by Davis et al. (1962).

Mafic and ultramafic rocks

Small (relative to the Poor Mountain Amphibolite) bodies of amphibolite and amphibole gneiss are present throughout the Inner Piedmont but have received little attention. This is partially due to the fact that many occur as boudins or small outcrops, which are not mappable at most scales; however, Goldsmith et al. (1988) delineated several large (up to 10 km length) amphibolite bodies near the southeastern edge of the North Carolina Inner Piedmont in the Charlotte 1:250,000-scale map. Most detailed accounts of mafic and ultramafic occurrences have focused on ultramafic or altered ultramafic outcrops (e.g., Misra and Keller, 1978; Misra and McSween, 1984; Butler 1989; Mittwede, 1989; Warner et al., 1989).

Tectonic

Fault relationships in the Inner Piedmont have been ascribed to tectonic slides (Griffin, 1974a), metamorphic gradients (Hatcher and Acker, 1984), fold-related Type-F thrusts (Hatcher and Hooper, 1992), and crustal-scale shear zones (Davis, 1993a, 1993b). Because detailed mapping in the Inner Piedmont is incomplete, regional correlations of thrust stacks, faults, structural trends, etc. remain somewhat speculative (see Hatcher this guidebook, his Fig. 1). As a result, major compilation efforts are unavoidably oversimplified and often support improper correlation of lithologies and tectonic features in the crystalline core.

The Inner Piedmont stack of crystalline thrust sheets represents the metamorphic core of middle Paleozoic orogenic events in the southern Appalachians (Davis, 1993a, 1993b; Hatcher, 1998). Penetrative deformation in the Inner Piedmont is attributed to

these events and was coeval with peak upper-amphibolite facies metamorphism. In the western Inner Piedmont, Type-F thrust sheets originated by shearing the common limb of ductile antiform-synform pairs and evolved as they cooled into more coherent Type-C thrust sheets (Hatcher and Hooper, 1992). Most transport indicators are parallel or sub-parallel to a strong mineral lineation and show a gradual change from NW-directed transport in the core of the Inner Piedmont to SW-direc-ted transport at the western flank (Davis, 1993a; Hatcher, 2001). Previous workers (Griffin, 1974a; Goldsmith, 1981) noted the mineral lineation trend but did not attribute it to regional flow or transport direction. Davis (1993a, 1993b) used this pattern and the partially mylonitic character of the dominant foliation to conclude that regionally extensive shear occurred parallel and oblique to the penetrative foliation surface, and that the entire western Inner Piedmont is a crustal-scale shear zone. This regional orogen-parallel and orogen-oblique heterogeneous simple shear produced the majority of near-metamorphic peak structures.

NEW PERSPECTIVES ON OLD PROBLEMS

Detailed geologic maps remain the fundamental reference frame, albeit incomplete, from which Inner Piedmont work is evaluated. Isotopic and geochronologic data greatly complement mapping and provide important temporal and chemical constraints not offered by geologic mapping alone. We now have more of the Inner Piedmont mapped in detail (most also within reasonable regional context) than ever before and, given the renewed interest and resurgence of isotopic and geochronologic work, can offer a new and improved conceptual framework for the evolution of the Inner Piedmont.

Stratigraphic

A significant amount of Nd and Sr isotopic data now exist for crystalline rocks (mainly granitoids) of the Blue Ridge, Inner Piedmont, and Carolina terrane. Nd isotopic data for metasedimentary rocks can provide an independent measure of crustal affinity

not afforded by U-Pb zircon data alone due to the robust nature of Sm/Nd ratios in sediments during sedimention (e.g., McCulloch and Wasserburg, 1978), the relative immobility of REE (e.g., Bernard-Griffiths et al., 1985), and similar behavior of Sm and Nd during metamorphism. Nd isotopic data from the metasedimentary rocks of the Blue Ridge and Inner Piedmont clearly overlap with the Grenville basement data of Carrigan et al. (in press) and to a lesser degree with data from the Mars Hill terrane (Ownby et al., in review), Chopawamsic (Wortman et al., 1996; Coler et al., 2000) (Fig. 3). Based on these data, it is possible that the sediments were derived from a combination of more isotopically evolved (relative to the Grenville basement) source(s) and less evolved more juvenile crustal source(s); or, more likely, directly derived from rocks similar in age and isotopic maturity to Blue Ridge and Sauratown Mountains window Grenville basement (Bream et al., in review).

The variety of proposed tectonic settings and crustal affinities (sometimes inferred) of the areally extensive metasedimentary packages within and surrounding the Inner Piedmont are undoubtedly related to our incomplete understanding of tectonic evolution in the southern Appalachian crystalline core. This is due to the intense deformation and metamorphism that obscure most primary relationships, a general lack of detailed mapping, and paucity of studies that integrate available geochronologic and geochemical constraints with existing or proposed tectonic models. With the exception of a few focused studies (mostly on granitoids), little analytical data (specifically U-Pb zircon data) are available for the Inner Piedmont; therefore, it is difficult to critically delimit tectonic models and the crustal affinity of most lithotectonic packages, which are dominated by metasedimentary rocks.

High-resolution ion microprobe analyses of detrital zircon separates can determine multiple source ages in sedimentary and metasedimentary rocks. For the southern Appalachian crystalline core paragneisses, this data (albeit preliminary) places important

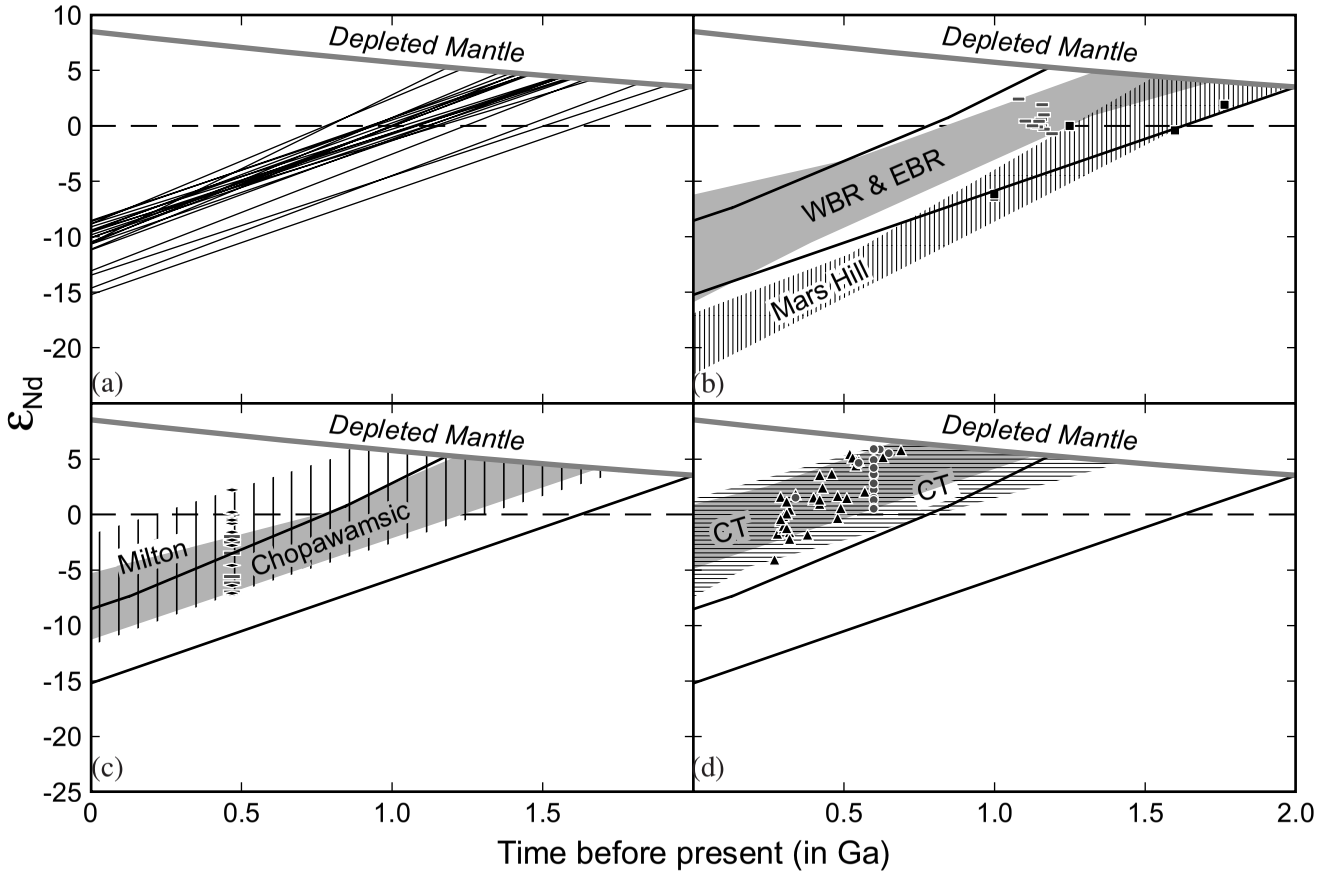

Figure 3. Epsilon Nd evolution over time for metasedimentary samples compared with data from Blue Ridge basement (Carrigan et al., in press; Ownby et al., in review), Carolina terrane (Samson et al., 1995; Fullagar et al., 1997), and Chopawamsic-Milton terranes (Wortman et al., 1996; Coler et al., 2000). (a) Metasedimentary sample data presented here showing evolution from present to intersection with the depleted mantle. (b) Metasedimentary data with fields defined for western and eastern Blue Ridge Grenvillian basement (WBR & EBR; gray field) and Mars Hill terrane (vertical lines). (c) Metasedimentary data with Chopawamsic (gray) and Milton belt (vertical lines) data. (d) Metasedimentary data with Carolina terrane data (CT; gray field defined by data of Samson et al., 1995; horizontal line field defined by data of Fullagar et al., 1997). Note evolution lines in (b-d) are defined by upper and lower boundaries of data in (a), symbols represent values at the estimated time of crystallization and/or deposition for the reference fields, and depleted mantle curve defined by DePaolo (1981). Figure modified from Bream et al., in review.

new constraints on the tectonic evolution of the entire orogen Composite probability age plots for southern Appalachian quartzofeldspathic and quartzite paragneiss samples presented by the traditional tectonic divisions of western Blue Ridge, eastern Blue Ridge, Dahlonega gold belt, western Inner Piedmont, and eastern Inner Piedmont reveal a significant Grenville component in each of the divisions and subtle differences (Fig. 4). For comparison, composite probability plots of detrital zircon ages can also be constructed for the Blue Ridge, Dahlonega gold belt, and the proposed crystalline core subdivisions of Hatcher (this volume): Cartoogechaye, Tugaloo, and Cat Square (Fig. 5). The summed probabilities should be viewed as "relative" abundances due to differences in number and types of samples; number of individual analyses for each division; separation and analytical bias; and the consolidation of samples in potentially artificial divisions. These plots illustrate the predominance of Grenville magmatic (~1000-1250 Ma) and metamorphic (~850-1000 Ma) ages in detrital zircons for most and suggest that the proposed crystalline core divisions of Hatcher (this volume) contain lithostratigraphic packages of similar crustal provenance.

The detrital zircon ages reveal a pre-Grenvillian component for most of the divisions, except for the eastern Blue Ridge and Sauratown Mountains window, which based on four and six samples respectively, contain only Grenvillian detrital zircons. Non-Grenvillian grains are broadly categorized as Middle Proterozoic (1.25-1.6 Ga), Early Proterozoic (1.6-2.1 Ga), and Late Archean (2.7-2.9 Ga). Exclusive of the eastern Blue Ridge and Sauratown Mountains window, Early Proterozoic peaks are discernable and the western and central Blue Ridge, Dahlonega gold belt, and eastern Inner Piedmont contain Late Archean zircons. Post-Grenvillian detrital zircons are also present in many of the samples. These ages are Late Proterozoic (570-850 Ma) and early Paleozoic (440-500 Ma) for detrital components with "Neoacadian" zircon rim age peaks. Overall, the data define several important age ranges and suggest that the Dahlonega gold belt, and

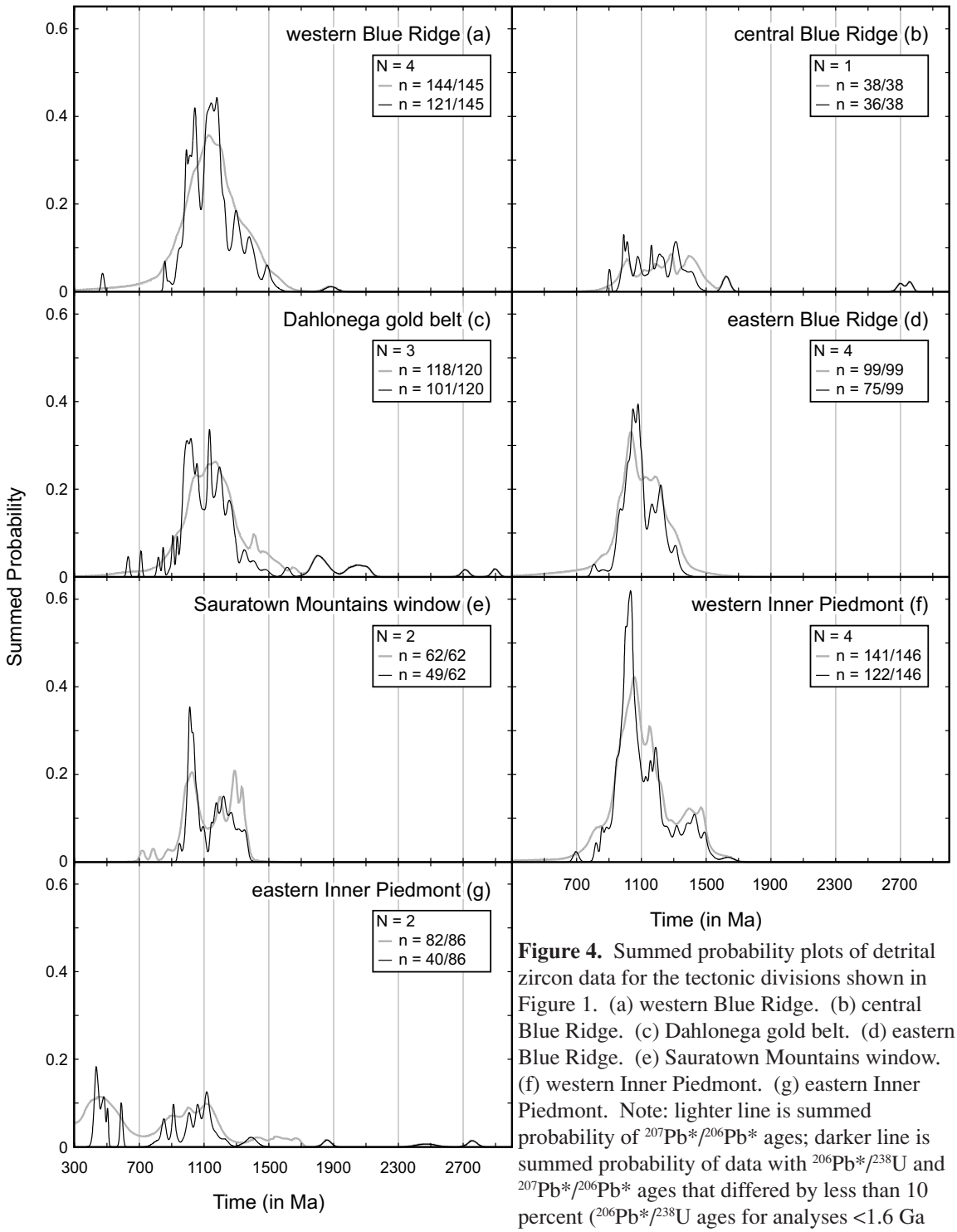

Figure 4. Summed probability plots of detrital zircon data for the tectonic divisions shown in Figure 1. (a) western Blue Ridge. (b) central Blue Ridge. (c) Dahlonega gold belt. (d) eastern Blue Ridge. (e) Sauratown Mountains window. (f) western Inner Piedmont. (g) eastern Inner Piedmont. Note: lighter line is summed probability of $^{207}Pb^*/^{206}Pb^*$ ages; darker line is summed probability of data with $^{206}Pb^*/^{238}U$ and $^{207}Pb^*/^{206}Pb^*$ ages that differed by less than 10 percent ($^{206}Pb^*/^{238}U$ ages for analyses <1.6 Ga and $^{207}Pb^*/^{206}Pb^*$ ages for analyses >1.6 Ga); N denotes number of samples, n denotes number of analyses plotted over total analyses. Figure modified from Bream et al., in review.

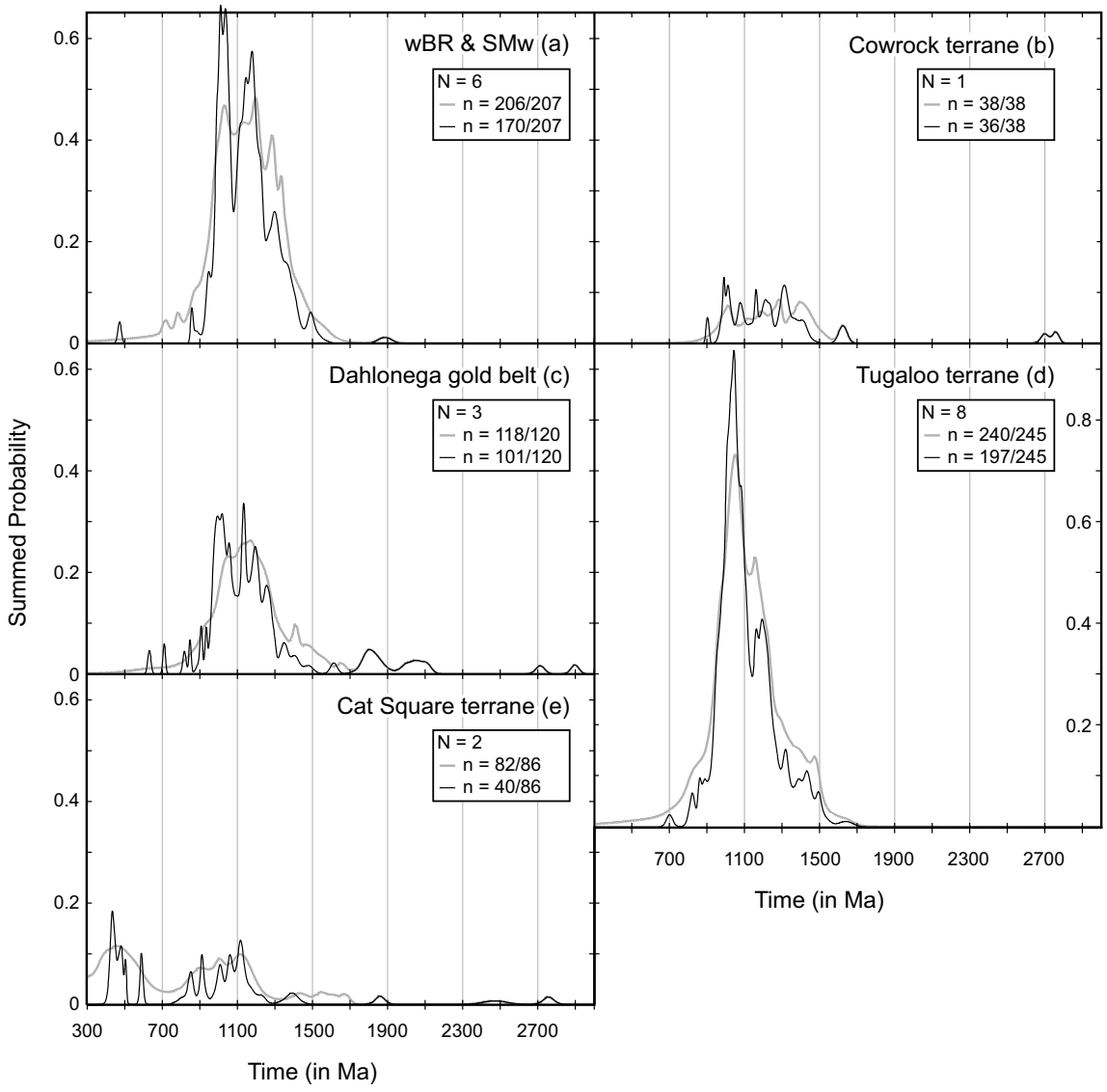

Figure 5. Summed probability plots of detrital zircon data for the tectonic divisions shown in Figure 1 and proposed divisions of Hatcher (this guidebook) for divisions southeast of the Hayesville fault. (a) western Blue Ridge (wBR) and Sauratown Mountains window (SMw). (b) Cowrock terrane (central Blue Ridge). (c) Dahlonega gold belt. (d) Tugaloo terrane (eastern Blue Ridge and western Inner Piedmont. (e) Cat Square terrane (eastern Inner Piedmont). Ages used and abbreviations same as Figure 4.

possibly central Blue Ridge, contains a greater proportion of sediment derived from Late Archean crust than the other divisions.

Grenvillian detrital zircons are clearly the dominant component for southern Appalachian paragneisses. These ages, however, have limited use for establishing distinct source(s) because of the numerous Grenvillian belts on the margins of pre-Grenvillian cratons that were near or adjacent to the Laurentian margin during the Rodinian break-up (e.g., Hoffman, 1991). Consequently, the ages that provide the best constraints on the provenance of the paragneisses have pre- and post-Grenvillian ages. Based on the presence of 2.2-2.4 and ~1.35 Ga detrital zircons in the Pine Mountain window of Alabama, Heatherington et al. (1997) and Steltenpohl et al. (2002) suggested that the Hollis Quartzite could have been derived from the Gondwanan Rio de la Plata, Kalahari, or Congo cratons and that the mixture of Laurentian (or South American Rondonian province) and probable Gondwanan detrital zircons favor deposition of the Hollis Quartzite roughly coeval with the separation of the Pine Mountain window from Gondwana. Miller et al. (2000) cited the lack of Early Proterozoic and presence of Late Archean inherited zircons in eastern Blue Ridge mid-Ordovician and mid-Devonian plutons, as evidence for one of the following scenarios: the presence of an unrecognized Archean component within southern Appalachian basement; southern Appalachian paragneisses contain detrital zircons derived from the Superior Province of Canada; or that the eastern Blue Ridge is exotic and contains detrital zircons from a non-Laurentian source (probably Gondwanan). As noted by Miller et al. (2000), a substantial amount of published ages for Archean detrital and inherited zircons within and to the east of the Appalachians are considered to be derived from Gondwanan or peri-Gondwanan crustal fragments. The data shown in Figures 5 and 6 do not preclude any of the aforementioned scenarios given that the age ranges reported by Miller et al. (2000), Heatherington et al. (1997), and Steltenpohl et al. (2002), except for the 2.2-2.4 Ga range, are also present.

The data differ from each, however, in that there is a minor Early Proterozoic component in most divisions. Based solely on the pre-Grenvillian detrital zircon ages, this allows for the possibility that the paragneisses of the southern Appalachian crystalline core (exclusive of the Cat Square terrane): (1) are entirely derived from Laurentian sources Hatcher (this guidebook); (2) are exotic to Laurentia and contain sediments derived from the Kalahari, Congo, and/or Amazonian cratons; or (3) contain a mixture of (1) and (2) as proposed by Heatherington et al. (1997) and Steltenpohl et al. (2002). The post-Grenvillian detrital zircon ages could represent sediment input from one or more of the following: pan-African crustal fragments (e.g., Carolina terrane), late Neoproterozoic rift-related igneous rocks (e.g., Crossnore pluton or Catoctin Formation equivalent?), or Ordovician magmatic rocks (eastern Inner Piedmont only).

A Laurentian crustal affinity for the paragneisses is favored here for all tectonic divisions, except the eastern Inner Piedmont (Cat Square terrane) based on the presence of similar North American cratonic ages and the lack of distinctly Gondwanan (2.2-2.4 Ga) detrital zircons. Samples from the eastern Inner Piedmont contain a unique suite of detrital zircons relative to the other tectonic subdivisions (Figs. 5 and 6). Most notably, a significant number of Ordovician and a smaller component of Neoproterozoic grains are present. Using the youngest detrital zircon age (~430 Ma) and the oldest zircon rim age (~400 Ma) we can establish a 30 Ma time interval in which the sediments of the eastern Inner Piedmont were deposited and metamorphosed to sillimanite grade. It is most likely that the Neoproterozoic grains from the eastern Inner Piedmont samples were shed from the approaching Carolina terrane as the Iapetus ocean closed. Ordovician detrital zircons most likely were eroded from exposed volcanic rocks in the immense magmatic belt in the eastern Tugaloo terrane. Based on these ages the eastern Inner Piedmont is distinct from the adjacent western Inner Piedmont and, as proposed by Bream et al. (2001b), the Brindle Creek fault is the boundary. In addition, Bream et al. (2001a) and Hatcher (this

guidebook) proposed that the entire sequence from the western Blue Ridge to the western Inner Piedmont could represent a time-transgressive sequence that reflects the opening of the Iapetus ocean and the younging of oceanic crust (and deposition) to the east. The Cat Square terrane is thus composed of an even more distal sequence that was still being deposited *after* Ordovician plutonism and volcanism in the Tugaloo terrane.

Metamorphic

Several southern Appalachian crystalline core workers have produced a significant amount of new evidence that supports the presence of one or more widespread thermal events between 360 and 320 Ma (e.g., Dennis and Wright, 1997; Bream et al., 2000; Mirante and Patino-Douce, 2000; Carrigan et al., 2001; Mirante, 2001; Kohn, 2001; Kalbas et al., 2002). This age range and lack of evidence for earlier metamorphism supports the single prograde Neoacadian event proposed by Davis (1993a, 1993b). Consequently, Inner Piedmont migmatization, upper amphibolite grade mineral assemblages, and penetrative deformation are likely related to Neoacadian and early Alleghanian orogenesis. These ages, interpreted to represent growth or recrystallization of monazite and zircon during peak metamorphic conditions, are similar to the 333-322 Ma hornblende cooling ages of Dallmeyer (1988) for the eastern Blue Ridge, Chauga belt, Walhalla thrust sheet, and the Six Mile thrust sheet. Other reported U-Pb zircon ages include conventional data of T.W. Stern (USGS) for the Chauga belt-Walhalla thrust assemblage and the eastern Six Mile thrust sheet, which, according to Nelson et al. (1998), record ~385 Ma and 391 to 365 Ma thermal events, respectively.

The ~350 Ma peak reported for southern Appalachian metamorphism does not correspond to ages for the northern Appalachian Acadian peak 384-402 Ma (e.g., Eusden and Barreiro, 1988) and ending by 355 Ma (Eusden et al., 2000). The Valley and Ridge foreland basin contains evidence of the Taconic orogenic events, but only minor evidence of Neoacadian orogenesis. As proposed by Rogers (1967), Acadian deformation may

have migrated southwestward over time, which favors oblique convergence, possibly providing an explanation for the younger southern Appalachian metamorphic ages. The 470 Ma metamorphic age reported by Moecher and Miller (2000) in the central Blue Ridge delimits the timing of granulite facies metamorphism there; this event, however, is either not present or not recorded by zircon and monazite in the eastern Blue Ridge and Inner Piedmont.

Evidence previously cited of the similarity and exact correlation of sequences on both sides of the Brevard fault is complicated by geochronologic data from granitoids of the eastern Blue Ridge and Inner Piedmont. Most notably, Paleozoic granitoids of the Inner Piedmont contain few Grenville and younger inherited zircon cores (e.g., Ranson et al., 1999; Mapes et al., 2002; Vinson, 1999) whereas similar age granitoids of the eastern Blue Ridge contain abundant Grenville and older inherited zircon cores (Miller et al., 2000). Additionally, the lack of Grenvillian basement in the Inner Piedmont represents another contrast across the Brevard fault zone. Although deposition of Inner Piedmont paragneisses on oceanic crust could explain the lack of Grenville basement in the Inner Piedmont and presence of small Grenville massifs within the adjacent eastern Blue Ridge, this basement distribution remains a major contrast across the Brevard fault zone. The peak at ~1.4 Ga for detrital zircons from the western Inner Piedmont and absence of pre-Grenvillian detrital zircons in the eastern Blue Ridge suggests a difference across the Brevard fault zone that could be real or related to sampling and/or statistical issues. Regardless, 1.4 Ga detrital zircons are also present in the western Blue Ridge so Laurentian derivation is not precluded.

Magmatic

Given the complex history of the southern Appalachian crystalline core, it is not surprising that whole-rock Rb-Sr and conventional U-Pb zircon ages are difficult to interpret. New ion microprobe U-Pb zircon data for several western Inner Piedmont

granitoids document a sizeable Middle Ordovician (dominantly between 460 and 470 Ma) magmatic complex (Ranson et al., 1999; Vinson, 1999) and several Late Silurian to Late Carboniferous (most are Late Devonian to Early Carboniferous, 375 to 325 Ma) granitoids (Mapes, 2002) in the eastern Inner Piedmont. Recent detailed mapping has further documented the occurrence of mafic and ultramafic rocks (many of which are associated with granitoids) in the western Inner Piedmont. Whole-rock geochemical data have also been collected from the South Carolina crystalline core (Maybin and Niewendorp, 1997); however, the petrogenesis and regional context of these mostly mafic rocks remain largely unexplored.

Vinson (1999) reported a range of U-Pb zircon ages from 350 to 490 Ma with clusters at 420, 445, 471, and 492 Ma for a Henderson Gneiss sample from the Vulcan Materials Company Hendersonville, NC, quarry. Unpublished data (Miller and Meschter McDowell) of another sample from the Moffitt Hill quadrangle revealed a similar age range with a single distinct Middle Ordovician grouping, interpreted to represent the magmatic age for the Henderson Gneiss. Recent U-Pb zircon ion microprobe data for augen and banded gneisses from near Caesars Head State Park yield Ordovician magmatic ages (Late Ordovician according to Ranson et al., 1999, their Table Rock gneiss; Middle Ordovician according to Vinson, 1999, his Caesars Head gneiss) with Mid to Late Proterozoic inheritance. Other recently dated Ordovician granitoids of the western Inner Piedmont include: 440-490 Ma Brooks Crossroads, NC (Vinson, 1999); ~465 Ma Dysartsville, NC (Bream, unpublished data); ~490 Ma Sugarloaf Mountain gneiss (Vinson, 1999); and ~460 Ma Toccoa, GA (Bream, unpublished data). Zircon separates from a sample of Poor Mountain Quartzite yielded a single Middle Ordovician age of ~460 Ma (Bream, unpublished data; Kalbas et al., 2002). This age is interpreted as a magmatic age, favoring the interpretation that the Poor Mountain Quartzite had a volcanic or immature volcaniclastic protolith. If this is a metatuff, components of the

Poor Mountain Formation might represent the volcanic equivalent of the large magmatic belt in the western Inner Piedmont. Tectonic discriminant diagrams indicate that the underlying and interlayered Poor Mountain Amphibolite has a probable oceanic affinity (Davis, 1993b; Yanigihara, 1994; Bream, 1999; Kalbas, in progress) suggesting a complex depositional and magmatic setting for the western Inner Piedmont during the Middle Ordovician. Recently dated eastern Inner Piedmont granitoids, ranging in age from Late Silurian to Pennsylvanian, include: ~415 Ma Anderson's Mill, SC (Mapes, 2002); ~357 Ma Gray Court, SC (Mapes, 2002); ~364 Ma Pelham, SC (Mapes, 2002); ~325 Ma Reedy River, SC (Mapes, 2002); ~380 Ma Toluca, NC (Mapes, 2002), and ~366 Ma Walker Top, NC (Vinson, 1999; Mapes, 2002). Based on these new granitoid crystallization ages and the clear distinction across the Brindle Creek fault as noted by Mapes et al., (2002), I propose that the name Table Rock Plutonic Suite (Horton and McConnell, 1991) either be restricted to western Inner Piedmont granitoids or dropped.

As noted by Vinson (1999), the chemistry of most western Inner Piedmont granitoids is likely the product of collisional or postcollisional crustal thickening, not the subduction related magmatic arc or continental margin arc as depicted in many tectonic models (e.g., Harper and Fullagar, 1981; Sinha et al., 1989; Hatcher, 1989; Hibbard, 2000). It has been proposed that a small ocean basin like the one between Kamchatka and the Okhotsk Sea (Hatcher, 1978) or the Gulf of California (Thomas et al., 2001) with an apex in what is now North Carolina could have developed or that the arc-related rocks are either eroded or deeply buried (Thomas et al., 2001). Fullagar et al. (1997) concluded that Inner Piedmont granitoids are isotopically intermediate between western Blue Ridge and Carolina terrane granitoids, perhaps reflecting the mixing of evolved Laurentian margin material with less evolved Pan-African material. Based on geochronology, isotopic evidence, and trace element concentrations, Mapes et al. (2002) proposed that the magmatic histories of the western and eastern Inner Piedmont are

distinct from one another both temporally and petrogenetically. Regional structural relationships support this conclusion (Hatcher, this guidebook, his Fig. 1b).

Despite a plethora of new mapping and geochemical work in the western Inner Piedmont, the relationships between the Henderson Gneiss and Table Rock Plutonic Suite remain somewhat enigmatic near the North and South Carolina border. For example, mapping in the Zirconia (Davis, 1993b; Garihan, 1999) and Standingstone Mountain (Garihan, 1999; Garihan, this volume) quadrangles reveals that both units occur in the footwall of the Sugarloaf Mountain thrust sheet as undifferentiated granitoids. Previous mapping in the Hendersonville (Lemmon, 1973), Bat Cave (Lemmon and Dunn, 1973a), and Fruitland (Lemmon and Dunn, 1973b) quadrangles however, did not delineate mappable granitoids fitting the Table Rock Plutonic Suite criteria in the footwall of the Sugarloaf Mountain thrust beyond the extent of the OSgg granitoid, which is completely enclosed in Henderson Gneiss. As discussed previously, similarity of zircon U-Pb ages (470-490 Ma) for the Henderson Gneiss and Caesars Head-Table Rock gneiss suggests these granitoids were emplaced during the same magmatic event. The true extent and nature of the contacts between each lithology remain problematic, and the tectonic setting for this major Ordovician magmatic event remains poorly constrained. Difficulties related to these suites are further complicated by the numerous unnamed or informally named granitoids that are not mapped in detail, incompletely portrayed, or loosely catalogued on regional compilations.

Tectonic

Recent detailed mapping by geologists from the University of Tennessee to the northeast and Furman University to the southwest of previous mapping in the Columbus Promontory permits correlation of several thrust stacks across the North and South Carolina border. The regional tectonic model of Davis (1993a, 1993b) remains unrefuted; new conclusions addressing the extent, nature, and displacement of several

major Inner Piedmont faults can now be considered (Fig. 7). The major faults of the central and southern North Carolina Inner Piedmont are discussed below in ascending order, from the Brevard fault zone southeastward.

While the correlation of major Inner Piedmont faults through the Carolinas allows us to ask questions concerning the nature, continuity, timing, and correlation of fault and lithologic units, it also brings into question some of the conclusions that previous workers have drawn for portions of these faults and lithotectonic packages. Correlation of the Mill Spring fault across a reconnaissance-mapped area to the Brushy Mountains of North Carolina and correlation of the Seneca (Six Mile) and Sugarloaf Mountain faults represents over 100 km of continuous faults. Although the Seneca fault represents a major lithologic break in South Carolina, displacement on the North Carolina equivalent (Sugarloaf Mountain fault) decreases to zero near Marion, North Carolina, and has possibly transferred motion up the thrust stack to the Mill Spring thrust (Merschat and Kalbas, this guidebook). The mapped truncations of major Paleozoic faults in the western Inner Piedmont by Ordovician granitoids (Nelson et al., 1998) could be incorrect but, if correct, suggest that faulting occurred prior to magma intrusion, penetrative deformation, and peak metamorphism in contrast to the new geochronologic and field data (Hatcher and Acker, 1984; Davis, 1993a, 1993b; Hatcher, in preparation) that strongly indicate faulting was post-Ordovician. Additional detailed mapping in North and South Carolina should better resolve the extent of Inner Piedmont faults.

Marion thrust sheet

The Marion thrust sheet, defined herein and by Merschat and Kalbas (this guidebook), is the structurally lowest thrust sheet in the North Carolina Inner Piedmont. The Marion thrust sheet includes the lithotectonic packages from the Brevard fault zone southeastward to the Mill Spring thrust in North Carolina. Correlation of this nappe in South Carolina is presently uncertain; however, it occurs in the same structural position

as the South Carolina Chauga belt, but the Chauga belt contains several additional thrust sheets (see Hatcher, this guidebook, his Fig. 3). Along the northwestern boundary of the Marion thrust sheet, western Inner Piedmont metasedimentary packages are juxtaposed with similar eastern Blue Ridge packages. Folded Tallulah Falls metasedimentary units of the Marion thrust sheet are truncated by the main Henderson Gneiss body and by numerous small elongate bodies. This contact is either intrusive or fault-defined (Tumblebug Creek fault of Davis 1993a, 1993b).

Tumblebug Creek thrust

The Tumblebug Creek thrust fault placed Henderson Gneiss over Tallulah Falls Formation in North Carolina (Davis, 1993a; 1993b). Fault emplacement for the Henderson Gneiss is favored over intrusive or unconformable relationships based on the truncation of footwall folds and the size reduction of K-feldspar augen in the Henderson Gneiss near the contact. Truncated contacts in the footwall of the Tumblebug Creek fault indicate that fault emplacement occurred subsequent to a folding event; however, the folded nature of the Tumblebug Creek fault and observations of mesoscopic isoclinal reclined folds and other fabric elements in the Henderson Gneiss (Bream, 1999) suggest that the Henderson Gneiss and Tallulah Falls Formation rocks of the Marion thrust sheet were juxtaposed prior to penetrative deformation.

Sugarloaf Mountain-Seneca thrust

Garihan (2001) has correlated the Seneca fault, renamed by Horton and McConnell (1991) from Griffin's (1969) Six Mile thrust, at the base of the Six Mile thrust sheet with the Sugarloaf Mountain fault of Davis (1993b). Thus, the Sugarloaf Mountain-Seneca fault placed Tallulah Falls and Poor Mountain Formation rocks over migmatitic Tallulah Falls Formation, metagrabbro amphibolite, ultramafic schist, and granitoids (various biotite gneisses and augen gneisses including the Caesars Head Granite) of the Walhalla

nappe in South Carolina and thrusts Tallulah Falls and Poor Mountain Formations over the Henderson Gneiss in North Carolina. Within the Sugar Hill 7.5-minute quadrangle, Bream (1999) noted that the Sugarloaf Mountain fault tips out and that the outcrop pattern of the Henderson Gneiss with the overlying Tallulah Falls Formation is related to reclined to recumbent isoclinal folding. As previously noted, Nelson et al., (1998) depicted the truncation of Paleozoic faults (including the Six Mile fault) in South Carolina by the Caesars Head Granite, suggesting that movement of this fault occurred before the Middle Ordovician. Klippes of Poor Mountain Formation rocks on Henderson Gneiss, windows of Henderson Gneiss to the southeast of the main body, and small linear elliptical bodies of Henderson Gneiss to the northeast suggest low-angle Type-F thrusting.

Mill Spring thrust

The Mill Spring thrust fault emplaced mid- to upper-Tallulah Falls Formation, migmatitic Poor Mountain Formation, and granitoids over Poor Mountain and upper Tallulah Falls Formations. The Mill Spring thrust was originally defined by work of Tabor (unpublished mapping) in the Mill Spring 7.5-minute quadrangle and subsequently delineated in the Cliffield Mountain 7.5-minute quadrangle by Davis (1993b). Because the Pea Ridge and Fingerville West 7.5-minute quadrangles remain unmapped, correlation of the fault into the Sugar Hill 7.5-minute quadrangle is based on Davis' (1993a, 1993b) thrust stack model (Yanagihara, 1994). Map relationships in the Brushy Mountains suggest that the Mill Spring fault is also likely present along strike from detailed work near Marion, NC (Bream, 1999; Hill, 1999). Although the Mill Spring fault is mapped to the North Carolina-South Carolina border, the recent report of its absence and the presence of Henderson Gneiss in the southern part of the Saluda quadrangle (Warlick et al., 2001) precludes correlation of this fault into South Carolina.

Brindle Creek thrust

The Brindle Creek thrust fault, first recognized and named by Giorgis (1999) in the Dysartsville quadrangle, thrusts a paragneiss sequence dominated by aluminous schist with Walker Top Granite over intensely migmatitic Tallulah Falls (?) and Poor Mountain Formations. This fault separates older Ordovician granitoids in the footwall from younger mainly Devonian granitoids in the hanging wall; the fault has not been mapped in detail along strike beyond, or between, the Brushy and South Mountains but, it can be extrapolated using the maps of Reed (1964), Rankin et al. (1972), Espenshade et al. (1975), and Goldsmith et al. (1988) (see Hatcher, this guidebook). Additionally, this fault may be present in South Carolina, but lack of detailed mapping near the border of both states permits only speculative extrapolation (Hatcher, this guidebook, his Fig. 1b). This fault juxtaposes paragneisses with distinct detrital zircon age ranges, represents a major crustal-scale boundary within the Inner Piedmont (Kalbas et al., 2002), and is possibly a terrane boundary as proposed by Bream et al. (2001b) and Bream and Hatcher (2002).

ACKNOWLEDGMENTS

This paper summarizes a portion of the author's Ph.D. dissertation at the University of Tennessee–Knoxville, under the direction of Robert D. Hatcher Jr. and Calvin F. Miller (Vanderbilt University). Paul D. Fullagar collected the Nd isotopic data presented in this paper and is acknowledged for interpretive assistance. Calvin Miller, Joe Wooden, Anders Meibom, Chris Coath, and Mark Harrison are gratefully acknowledged for assistance with the Stanford and UCLA ion microprobes. Much of this work has benefited from numerous conversations with members of the North Carolina Geological Survey (Leonard Wiener, Carl Merschat, and Mark Carter), South Carolina Geological Survey (Butch Maybin), faculty at Furman University (Jack Garihan and Bill Ranson),

UTK Inner Piedmont mappers (Joe Hill, Scott Giorgis, Scott Williams, Sara Bier, Jeff Riedel, Jay Kalbas, and Arthur Merschat) and Vanderbilt University students (Sam Vinson, Charles Carrigan, Susanne Meschter McDowell, Russ Mapes); however, any errors remain my responsibility. Detailed geologic mapping was funded by EDMAP grants 1434HQ97AG01720, 98HQAG2026, 99HQAG0026, 00HQAG0035, and 01HQAG0176 to R.D. Hatcher, Jr. from the National Cooperative Geologic Mapping Program (administered by U.S.G.S.). Ion microprobe work was funded by NSF grant EAR-9814800 to R.D. Hatcher, Jr. and NSF EAR-9814801 to C.F. Miller. Additional funding was provided by the UTK Science Alliance Center of Excellence.

REFERENCES CITED

Abbott, R.N., and Raymond, L.A., 1984, The Ashe metamorphic suite, northwest North Carolina: Metamorphism and observations on geologic history: American Journal of Science, v. 284, p. 350-375.

Aleinikoff, J.N., Zartman, R.E., Walter, M., Rankin, D.W., Lyttle, P.T., and Burton, W.C., 1995, U-Pb ages of metarhyolites of the Catoctin and Mount Rogers formations, central and southern Appalachians: Evidence for two phases of Iapetian rifting: American Journal of Science, v. 295, p. 428-454.

Bernard-Griffiths, J., Peucat, J.-J., Cornichet, J., Iglesias Ponce de Léon, M., and Gil Ibarguchi, J.I., 1985, U-Pb, Nd isotope and REE geochemistry in eclogites from the Cabo Ortegal Complex, Galicia, Spain: An example of REE immobility conserving MORB-like patterns during high-grade metamorphism, *in* Smith, D.C., and Vidal, Ph., eds., Isotope geochemistry and geochronology of eclogites: Chemical Geology, v. 52, p. 217-225.

Bond, P.A., and Fullagar, P.D., 1974, Origin and age of the Henderson augen gneiss and associated cataclastic rocks in southwestern North Carolina: Geological Society of America Abstracts with Programs, v. 6, no. 4, p. 336.

Bentley, R.D., and Neathery, T.N., 1970, Geology of the Brevard zone and related rocks of the Inner Piedmont of Alabama: Alabama Geological Society, Eighth annual field trip guidebook, 119 p.

Bier, S.E., 2001, Geology of the southeastern South Mountains, North Carolina [unpublished M.S. thesis]: Knoxville, University of Tennessee, 162 p.

Bream, B.R., 1999, Structural and stratigraphic relationships of ortho- and paragneisses southwest of Marion, North Carolina [M.S. thesis]: Knoxville, Tennessee, University of Tennessee, 155 p.

Bream, B.R., and Hatcher, R.D., Jr., 2002, Southern Appalachian terranes amended:

timing of accretion and delimiting provenance from new detrital zircon and Nd isotopic data: Geological Society of America Abstracts with Programs.

Bream, B.R., Hatcher, R.D., Jr., Miller, C.F., and Fullagar, P.D., 2000, Paragneiss geochemistry and preliminary ion microprobe geochronology of detrital zircons from the southern Appalachian crystalline core: Geological Society of America Abstracts with Programs, v. 32, p. 31.

Bream, B.R., Hatcher, R.D., Jr., Miller, C.F., Carrigan, C.W., and Fullagar, P.D., 2001a, Provenance and geochemistry of Late Proterozoic southern Appalachian crystalline core paragneisses, NC-SC-GA-TN: Geological Society of America Abstracts with Programs, v. 33, p. 29.

Bream, B.R., Hatcher, R.D., Jr., Miller, C.F., and Fullagar, P.D., 2001b, Geochemistry and provenance of Inner Piedmont paragneisses, NC and SC: Evidence for an internal terrane boundary?: Geological Society of America Abstracts with Programs, v. 33, p. 65.

Bream, B.R., Hatcher, R.D., Jr., Miller, C.F., and Fullagar, P.D., in review, Detrital zircon ages and Nd isotopic data from the southern Appalachian crystalline core, GA-SC-NC-TN: New provenance constraints for Laurentian margin paragneisses, *in* Tollo, R.P., Corriveau, L., McLelland, J., and Bartholomew, M.J., eds., Proterozoic evolution of the Grenville orogen in North America: Boulder, Colorado, Geological Society of America Special Paper.

Bryant, B., and Reed, J.C., Jr., 1970, Geology of the Grandfather Mountain window and vicinity, North Carolina and Tennessee: U.S. Geological Survey Professional Paper 614, 189 p.

Butler, J.R., 1989, Review and classification of ultramafic bodies in the Piedmont of the Carolinas, *in* Mittwede, S.K., and Stoddard, E.F., eds., Ultramafic rocks of the Appalachian Piedmont: Boulder, Colorado, Geological Society of America Special Paper 231, p. 19-31.

Butler, J.R., 1991, Metamorphism, *in* Horton, J.W., Jr., and Zullo, V.A., eds., The Geology of the Carolinas: Knoxville, Tennessee, The University of Tennessee Press, p.127-141.

Carrigan, C.W., 2000, Ion microprobe geochronology of Grenville and older basement in the southern Appalachians [M.S. thesis]: Nashville, Tennessee, Vanderbilt University, 101 p.

Carrigan, C.W., Bream, B.R., Miller, C.F., and Hatcher, R.D., Jr., 2001, Ion microprobe analyses of zircon rims from the eastern Blue Ridge and Inner Piedmont, NC-SC-GA: Implications for the timing of Paleozoic metamorphism in the southern Appalachians: Geological Society of America Abstracts with Programs, v. 33, p. 7.

Carrigan, C.W., Miller, C.F., Fullagar, P.D., Hatcher, R.D., Jr., Bream, B.R., and Coath, C.D., in press, Ion microprobe age and geochemistry of southern Appalachian basement, with implications for Proterozoic and Paleozoic reconstructions: Precambrian Research.

Cawood, P.A., and Nemchin, A.A., 2001, Paleogeographic development of the east Laurentian margin: constraints from U-Pb dating of detrital zircons in the

Newfoundland Appalachians: Geological Society of America Bulletin, v. 113, p. 1234-1246.
Cawood, P.A., McCausland, P.J.A., and Dunning, G.R., 2001, Opening Iapetus: Constraints from the Laurentian margin in Newfoundland: Geological Society of America Bulletin, v. 113, p. 443-453.
Clark, G.M., 1993, Quaternary geology and geomorphology of part of the Inner Piedmont of the southern Appalachians in the Columbus Promontory upland area, southwestern North Carolina and northwestern South Carolina, *in* Hatcher, R.D., Jr., and Davis, T.L., eds., Studies of Inner Piedmont geology with a focus on the Columbus Promontory: Carolina Geological Society annual field trip guidebook, p. 67-84.
Coler, D.G., Wortman, G.L., Samson, S.D., Hibbard, J.P., and Stern, R., 2000, U-Pb geochronologic, Nd isotopic, and geochemical evidence for the correlation of the Chopawamsic and Milton terranes, Piedmont Zone, southern Appalachian orogen: Journal of Geology, v. 108, p. 363-380.
Curl, D.C., 1998, Stratigraphy and structure of Wellford and Reidville quadrangles in part of the eastern Inner Piedmont, near Spartanburg South Carolina [M.S. thesis]: Knoxville, Tennessee, University of Tennessee, 129 p.
Dallmeyer, R.D., 1988, Late Paleozoic tectonothermal evolution of the western Piedmont and eastern Blue Ridge, Georgia: Controls on the chronology of terrane accretion and transport in the southern Appalachian orogen: Geological Society of America Bulletin, v. 100, p. 702-713.
Dalziel, I.W.D., 1997, Neoproterozoic-Paleozoic geography and tectonics: Review, hypothesis, environmental speculation: Geological Society of America Bulletin, v. 109, p. 16-42.
Dalziel, I.W.D., Mosher, S., and Gahagan, L.M., 1998, Laurentia-Kalahari collision and the assembly of Rodinia: Journal of Geology, v. 108, p. 499-513.
Davis, G.L., Tilton, G.R., and Wetherill, G.W., 1962, Mineral ages from the Appalachian province in North Carolina and Tennessee: Journal of Geophysical Research, v. 67, p. 1987-1996.
Davis, T.L., 1993a, Geology of the Columbus Promontory, western Piedmont, North Carolina, southern Appalachians, *in* Hatcher, R.D., Jr., and Davis, T.L., eds., Studies of Inner Piedmont geology with a focus on the Columbus Promontory: Carolina Geological Society annual field trip guidebook, p. 17-43.
Davis, T.L., 1993b, Lithostratigraphy, structure, and metamorphism of a crystalline thrust terrane, western Inner Piedmont, North Carolina [Ph.D. dissertation]: Knoxville, Tennessee, University of Tennessee, 245 p.
Dennis, A.J., 1991, Is the central Piedmont suture a low-angle normal fault?: Geology, v. 19, p. 1081-1084.
Dennis, A.J., and Wright, J.E., 1997, Middle and late Paleozoic monazite U-Pb ages, Inner Piedmont, South Carolina: Geological Society of America Abstracts with Programs, v. 29, p. 12.
DePaolo, D., 1981, Neodymium isotopes in the Colorado Front Range and crust-mantle

evolution in the Proterozoic: Nature, v. 291, p. 193-196.
Drake, A.A., Jr., Sinha, A.K., Laird, J., and Guy, R.E., 1989, The Taconic orogen, *in* Hatcher, R.D., Jr., Thomas, W.A., and Viele, G.W., eds., The Appalachian-Ouachita orogen in the United States: Boulder, Colorado, Geological Society of America, The Geology of North America, v. F-2, p. 101-177.
Espenshade, G.H., Rankin, D.W., Shaw, K.W., and Neuman, R.B., 1975, Geologic map of the east half of the Winston-Salem quadrangle, North Carolina-Virginia: U.S. Geological Survey Miscellaneous Geologic Investigations Map I-709B, scale 1:250,000.
Eusden, J.K., Jr., Guzofski, C.A., Robinson, A.C., and Tucker, R.D., 2000, Timing of the Acadian orogeny in northern New Hampshire: Journal of Geology, v. 108, p. 219-232.
Eusden J.K., Jr., and Barreiro, B., 1988, The timing of peak high-grade metamorphism in central-eastern New England: Maritime Sediments and Atlantic Geology, v. 24, p. 241-255.
Fullagar, P.D., Goldberg, S.A., and Butler, J.R., 1997, Nd and Sr isotopic characterization of crystalline rocks from the southern Appalachian Piedmont and Blue Ridge, North and South Carolina, *in* Sinha, A.K., Whalen, J.B., and Hogan, J.P., eds., The nature of magmatism in the Appalachian orogen: Boulder, Colorado, Geological Society of America Memoir 191, p. 165-179.
Garihan, J.E., 1999, The Sugarloaf Mountain thrust in the western Inner Piedmont between Zirconia, North Carolina, and Pumpkintown, South Carolina, *in* Hatcher, R.D., Jr., ed., Geotraverse across part of the Acadian orogen in the southern Appalachians: Southeastern Section Geological Society of America Field Trip Guidebook, p. 23-40.
Garihan, J.E., 2001, Observations of the Seneca fault and their implications for thrust sheet emplacement in the Inner Piedmont of the Carolinas: South Carolina Geology, v. 43, p. 1-13.
Garihan, J.M., Preddy, M.S., and Ranson, W.A., 1993, Summary of mid-Mesozoic brittle faulting in the Inner Piedmont and nearby Charlotte Belt of the Carolinas, *in* Hatcher, R.D., Jr., and Davis, T.L., eds., Studies of Inner Piedmont geology with a focus on the Columbus Promontory: Carolina Geological Society annual field trip guidebook, p. 55-65.
Giorgis, S.D., 1999, Geology of the northwestern South Mountains near Morganton, North Carolina [M.S. thesis]: Knoxville, Tennessee, University of Tennessee, 186 p.
Goldberg, S.A., and Fullagar, P.D., 1993, Alleghanian Rb-Sr mineral ages from the Inner Piedmont of southwestern North Carolina, *in* Hatcher, R.D., Jr., and Davis, T.L., eds., Studies of Inner Piedmont Geology with a focus on the Columbus Promontory: Carolina Geological Society annual field trip guidebook, p. 105-107.
Goldsmith, R., 1981, Structural patterns in the Inner Piedmont of the Charlotte and Winston-Salem 2-degree quadrangles, North Carolina and South Carolina, *in* Horton, J.W., Jr., Butler, J.R., and Milton, D.M., eds., Geological investigations of the Kings Mountain belt and adjacent areas in the Carolinas: Carolina Geological

Society Guidebook annual field trip guidebook, p. 19-27.
Goldsmith, R., Milton, D.J., and Horton, J.W., Jr., 1988, Geology of the Charlotte 1˚ X 2˚ quadrangle, North Carolina and South Carolina: U.S. Geological Survey Map I-1251-E, scale 1:250,000.
Gray, M.B., and Zeitler, P.K., 1997, Comparison of clastic wedge provenance in the Appalachian foreland using U/Pb ages of detrital zircons: Tectonics, v. 16, p. 151-160.
Griffin, V.S., Jr., 1967, Geology of the Six Mile quadrangle, South Carolina: South Carolina Division of Geology MS-14, scale 1:24,000.
Griffin, V.S., Jr., 1969a, Inner Piedmont tectonics in the vicinity of Walhalla, South Carolina: South Carolina Division of Geology, Geologic Notes, v. 14, p. 15-28.
Griffin, V.S., Jr., 1969b, Migmatitic Inner Piedmont belt of northwestern South Carolina: South Carolina Division of Geology, Geologic Notes, v. 13, p. 87-104.
Griffin, V.S., Jr., 1971a, The Inner Piedmont belt of the southern crystalline Appalachians: Geological Society of America Bulletin, v. 82, p. 1885-1898.
Griffin, V.S., Jr., 1971b, Stockwork tectonics in the Appalachian Piedmont of South Carolina: Geologische Rundschau, v. 60, p. 868-886.
Griffin, V.S., Jr., 1974a, Analysis of the Piedmont in northwest South Carolina: Geological Society of America Bulletin, v. 85, p. 1123-1138.
Griffin, V.S., Jr., 1974b, Geology of the Walhalla quadrangle, South Carolina: South Carolina Division of Geology MS-19, scale 1:24,000.
Griffin, V.S. Jr., 1974c, Progress report on a geologic study in Anderson County, South Carolina: South Carolina Division of Geology, Geologic Notes, v. 18, p. 13-23.
Griffitts, W.R., and Overstreet, W.C., 1952, Granitic rocks of the western Carolina Piedmont: American Journal of Science, v. 250, p. 777-789.
Griffitts, W.R., and Overstreet, W.C., 1962, Preliminary geologic map of the southeast quarter of the Shelby quadrangle, Cleveland County, North Carolina: U.S. Geological Survey Field Studies Map MF 250, scale 1:24,000.
Griffitts, W.R., Yates, R.G., and Overstreet, W.C., 1962, Preliminary geologic map of the southwest quarter of the Shelby quadrangle, Cleveland and Rutherford counties, North Carolina: U.S. Geological Survey Field Studies Map MF-252, scale 1:24,000.
Grimes, J.E., Steltenpohl, M.G., Cook, R.B., and Keefer, W.D., 1993, Geology of the southernmost Brevard fault zone, Alabama, and its implications for southern Appalachian tectonostratigraphy, *in* Hatcher, R.D., Jr., and Davis, T.L., eds., Studies of Inner Piedmont geology with a focus on the Columbus Promontory: Carolina Geological Society annual field trip Guidebook, p. 91-103.
Hadley, J.B., and Nelson, A.E., 1970, Caesars Head Quartz Monzonite in the western Carolina Piedmont, *in* Cohee, G.V., Bates, R.G., and Wright, W.B., eds., Changes in stratigraphic nomenclature by the U.S. Geological Survey, 1969: U.S. Geological Survey Bulletin 1324-A, p. 23-24.
Harper, S.B., and Fullagar, P.D., 1981, Rb-Sr ages of granitic gneisses of the Inner Piedmont belt of northwestern North Carolina and southwestern South Carolina: Geological Society of America Bulletin, v. 92, p. 864-872.

Hatcher, R.D., Jr., 1969, Stratigraphy, petrology, and structure of the low rank belt and part of the Blue Ridge of northwesternmost South Carolina: South Carolina Division of Geology, Geologic Notes, v. 13, p. 105-141.
Hatcher, R.D., Jr., 1970, Stratigraphy of the Brevard zone and Poor Mountain area, northwestern South Carolina: Geological Society of America Bulletin, v. 81, p. 933-940.
Hatcher, R.D., Jr., 1978, Tectonics of the western Piedmont and Blue Ridge: Review and speculation: American Journal of Science, v. 278, p. 276-304.
Hatcher, R.D., Jr., 1987, Tectonics of the southern and central Appalachian internides: Annual Review of Earth and Planetary Science, v. 15, p. 337-362.
Hatcher, R.D., Jr., 1989, Tectonic synthesis of the U.S. Appalachians, *in* Hatcher, R.D., Jr., Thomas, W.A., and Viele, G.W., eds., The Appalachian-Ouachita orogen in the United States: Boulder, Colorado, Geological Society of America, The Geology of North America, v. F-2, p. 511-535.
Hatcher, R.D., Jr., 1993, Perspective of the tectonics of the Inner Piedmont, southern Appalachians, *in* Hatcher, R.D., Jr., and Davis, T.L., eds., Studies of Inner Piedmont geology with a focus on the Columbus Promontory: Carolina Geological Society annual field trip guidebook, p. 1-16.
Hatcher, R.D., Jr., 1998, Structure of the Appalachian Inner Piedmont: Geological Society of America Abstracts with Programs, v. 30, p. 17.
Hatcher, R.D., Jr., and Acker, L.L., 1984, Geology of the Salem quadrangle, South Carolina: South Carolina Geological Survey, MS-26, 23 p., scale 1:24,000.
Hatcher, R.D., Jr., and Goldberg, S.A., 1991, The Blue Ridge geologic province, *in* Horton, J.W., Jr., and Zullo, V.A., eds., The Geology of the Carolinas: Knoxville, Tennessee, The University of Tennessee Press, p. 11-35.
Hatcher, R.D., Jr., and Hooper, R.J., 1992, Evolution of crystalline thrust sheets in the internal parts of mountain chains, *in* McClay, K.R., ed., Thrust tectonics: London, Chapman and Hall, p. 217-234.
Hatcher, R.D., Jr., Osberg, P.H., Drake, A.A., Jr., Robinson, P., and Thomas, W.A., 1990, Tectonic map of the U.S. Appalachians, *in* Hatcher, R.D., Jr., Thomas, W.A., and Viele, G.W., eds., The Appalachian-Ouachita orogen in the United States: Boulder, Colorado, Geological Society of America, The Geology of North America, v. F-2, Plate 1.
Hatcher, R.D., Jr., Bream, B.R., Hill, J.C., Giorgis, S.D., and Williams, S.T., 1999, Transect through the Acadian orogen in the Carolinas and northeast Georgia: Geological Society of America Abstracts with Programs, v. 31, p. 19.
Hatcher, R.D., Jr., Bream, B.R., Miller, C.F., Eckert, J.O., Jr., Fullagar, P.D., and Carrigan, C.W., in review, Paleozoic structure of southern Appalachian Blue Ridge Grenvillian internal basement massifs, *in* Tollo, R.P., Corriveau, L., McLelland, J., and Bartholomew, M.J., eds., Proterozoic evolution of the Grenville orogen in North America: Boulder, Colorado, Geological Society of America Special Paper.
Heatherington, A.L., Steltenpohl, M.G., Yokel, L.S., and Mueller, P.A., 1997, Ages of detrital zircons from the Pine Mountain and Inner Piedmont terranes and the Valley

and Ridge Province; implications for Neoproterozoic tectonics of the southern Laurentian margin: Geological Society of America Abstracts with Programs, v. 29, p. 432.

Hibbard, J., 1993, The Milton belt–Carolina slate belt boundary: the northern extension of the Central Piedmont suture?, *in* Hatcher, R.D., Jr., and Davis, T.L., eds., Studies of Inner Piedmont geology with a focus on the Columbus Promontory: Carolina Geological Society annual field trip guidebook, p. 85-89.

Hibbard, J., 2000, Docking Carolina: Mid-Paleozoic accretion in the southern Appalachians: Geology, v. 28, p. 127-130.

Hibbard, J.P., and Samson, S.D., 1995, Orogenesis exotic to the Iapetan cycle in the southern Appalachians, *in* Hibbard, J.P., van Staal, C.R., and Cawood, P.A., eds., Current Perspectives in the Appalachian-Caledonian orogen: Geological Association of Canada Special Paper 41, p. 191-205.

Hill, J.C., 1999, Stratigraphy, structure, and tectonics of the southern Appalachian Inner Piedmont, near Marion, North Carolina [M.S. thesis]: Knoxville, Tennessee, University of Tennessee, 188 p.

Hoffman, P.F., 1991, Did the breakout of Laurentia turn Gondwanaland inside-out?: Science, v. 252, p. 1409-1412.

Hopson, J.L., and Hatcher, R.D., Jr., 1988, Structural and stratigraphic setting of the Alto allochthon, northeast Georgia: Geological Society of America Bulletin, v. 100, p. 339-350.

Horton, J.W., Jr., and Dicken, C.L., 2001, Preliminary geologic map of the Appalachian Piedmont and Blue Ridge, South Carolina Segment: U.S. Geological Survey open-file report 01-298, scale 1:500,000.

Horton, J.W., Jr., and McConnell, K.I., 1991, The western Piedmont, *in* Horton, J.W., Jr., and Zullo, V.A., eds., The Geology of the Carolinas: Knoxville, Tennessee, The University of Tennessee Press, p. 36-58.

Horton, J.W., Jr., Drake, A.A., Jr., and Rankin, D.W., 1989, Tectonostratigraphic terranes and their Paleozoic boundaries in the central and southern Appalachians, *in* Dallmeyer, R.D., ed., Terranes in the circum-Atlantic Paleozoic orogens: Geological Society of America Special Paper 230, p. 213-245.

Kalbas, J.L., Bream, B.R., Hatcher, R.D., Jr., and Maybin, A.H., III, 2002, Evidence for mafic Ordovician magmatism and Acadian metamorphism in the Brushy Mountains, western Inner Piedmont, of North Carolina: Geological Society of America Abstracts with Programs, v. 34, p. 119.

Keith, A., 1905, Description of the Mount Mitchell quadrangle (North Carolina-Tennessee): U.S. Geological Survey Geologic Atlas, Folio 124, 10 p.

Keith, A., 1907, Description of the Pisgah quadrangle (North Carolina-Tennessee): U.S. Geological Survey Geologic Atlas, Folio 147, 8 p.

King, P.B., 1955, A geologic cross section across the southern Appalachians, an outline of the geology in the segment in Tennessee, North Carolina, and South Carolina, *in* Russell, R.J., ed., Guides to southeastern geology: Geological Society of America Annual Meeting, p. 332-373.

Kish, S.A., 1983, A geochronological study of deformation and metamorphism in the Blue Ridge and Piedmont of the Carolinas [Ph.D. dissertation]: Chapel Hill, University of North Carolina, 220 p.

Kohn, M.J., 2001, Timing of arc accretion in the southern Appalachians: Perspectives from the Laurentian margin: Geological Society of America Abstracts with Programs, v. 33, p. 262.

Lemmon, R.E., 1973, Geology of the Bat Cave and Fruitland quadrangles and the origin of the Henderson Gneiss, western North Carolina [Ph.D. dissertation]: Chapel Hill, University of North Carolina, 145 p.

Lemmon, R.E., and Dunn, D.E., 1973a, Geologic map and mineral resources of the Bat Cave quadrangle, North Carolina: North Carolina Department of Natural Resources and Community Development GM 202-NE, scale 1:24,000.

Lemmon, R.E., and Dunn, D.E., 1973b, Geologic map and mineral resources of the Fruitland quadrangle, North Carolina: North Carolina Deparment of Natural Resources and Community Development GM-202-NW, scale 1:24,000.

Mapes, R.W., Maybin, A.H., III, Miller, C.F., Fullagar, P.D., and Bream, B.R., 2002, Geochronology and geochemistry of mid Paleozoic granitic magmatism, central and eastern Inner Piedmont, NC & SC: Geological Society of America Abstracts with Programs, v. 34, p. 92.

Maybin, A.H., III, 1997, Bedrock geologic map of the Pelham 7.5-minute quadrangle, Greenville, Laurens and Spartanburg Counties South Carolina: South Carolina Department of Natural Resources, Geological Survey, Open-File Report 93, scale 1:24,000.

Maybin, A.H., III, and Niewendorp, C.A., 1997, Whole-rock geochemical analysis of samples from Abbeville, Greenville, Greenwood, Laurens, Newberry, Saluda, Spartanburg and Union Counties, South Carolina: South Carolina Geological Survey OFR-98, 16 p.

McCulloch, M.T., and Wasserburg, G.J., 1978, Sm-Nd and Rb-Sr chronology of continental crust formation: Science, v. 200, p. 1003-1011.

McSween, H.Y., Speer, J.A., and Fullagar, P.D., 1991, Plutonic rocks, *in* Horton, J.W., Jr., and Zullo, V.A., eds., The Geology of the Carolinas: Knoxville, Tennessee, The University of Tennessee Press, p. 109-126.

Miller, C.F., Hatcher, R.D., Jr., Ayers, J.C., Coath, C.D., and Harrison, T.M., 2000, Age and zircon inheritence of eastern Blue Ridge plutons, southwestern North Carolina and northeastern Georgia, with implications for magma history and evolution of the southern Appalachian orogen: American Journal of Science, v. 300, p. 142-172.

Mirante, D.C., 2001, Monazite ages from the southern Appalachian Inner Piedmont – The Athens gneiss: Geological Society of America Abstracts with Programs, v. 33, p. 3.

Mirante, D.C., and Patino-Douce, A.E., 2000, Melting and migmatization in the southern Appalachian Inner Piedmont of northeast Georgia; The Athens gneiss: Geological Society of America Abstracts with Programs, v. 32, p. 297.

Misra, K.C., and Keller, F.B., 1978, Ultramafic bodies in the southern Appalachians: A

review: American Journal of Science, v. 278, p. 389-418.
Misra, K.C., and McSween, H.Y., Jr., 1984, Mafic rocks of the southern Appalachians: A review: American Journal of Science, v. 284, p. 294-318.
Mittwede, S.K., 1989, The Hammett Grove Meta-igneous Suite; A possible ophiolite in the northwestern South Carolina Inner Piedmont, *in* Mittwede, S.K., and Stoddard, E.F., eds., Ultramafic rocks of the Appalachian Piedmont: Boulder, Colorado, Geological Society of America Special Paper 231, p. 45-62.
Moecher, D.P., and Miller, C.F., 2000, Precise age for peak granulite facies metamorphism and melting in the eastern Blue Ridge from SHRIMP U-Pb analysis of zircon: Geological Society of America Abstracts with Programs, v. 32, p. 63.
Nelson, A.E., Horton, J.W., Jr., and Clarke, J.W., 1998, Geologic map of the Greenville 1˚ X 2˚ quadrangle, Georgia, South Carolina, and North Carolina: U.S. Geological Survey Miscellaneous Investigations Series Map I-2175, scale 1:250,000, 2 sheets, 12 p. text.
Odom, A.L., and Fullagar, P.D., 1973, Geochronological and tectonic relationships between the Inner Piedmont, Brevard zone, and Blue Ridge belts, North Carolina: American Journal of Science, v. 273, p. 133-149.
Odom, A.L., and Russell, G.S., 1975, The time of regional metamorphism of the Inner Piedmont, North Carolina, and Smith River allochthon: Inference from whole-rock ages: Geological Society of America Abstracts with Programs, v. 7, p. 522-523.
Osberg, P.H., Tull, J.F., Robinson, P., Hon, R., and Butler, J.R., 1989, The Acadian orogen, *in* Hatcher, R.D., Jr., Thomas, W.A., and Viele, G.W., eds., The Appalachian-Ouachita orogen in the United States: Boulder, Colorado, Geological Society of America, The Geology of North America, v. F-2, p. 179-232.
Overstreet, W.C., Whitlow, J.W., White, A.W., and Griffitts, W.R., 1963a, Geologic map of the southern part of the Casar quadrangle, Cleveland, Lincoln, and Burke Counties, North Carolina: U.S. Geological Survey Field Studies Map MF-252, scale 1:24,000.
Overstreet, W.D., Yates, R.G., Griffitts, W.R., 1963b, Geologic map of the Shelby 15-minute quadrangle, North Carolina: U.S. Geological Survey Miscellaneous Geologic Investigations Map I-384, scale 1:62,500.
Ownby, S.E., Miller, C.F., Berquist, P.J., Carrigan, C.W., and Fullagar, P.D., in review, Geochemistry and U-Pb geochronology of a portion of the Mars Hill terrane, North Carolina-Tennessee: Constraints on origin, history, and tectonic assembly, *in* Tollo, R.P., Corriveau, L., McLelland, J., and Bartholomew, M.J., eds., Proterozoic evolution of the Grenville orogen in North America: Boulder, Colorado, Geological Society of America Special Paper.
Powell, C.M., Jones, D.L., Pisarevsky, S., and Wingate, M.T.D., 2001, Paleomagnetic constraints on the position of the Kalahari craton in Rodinia: Precambrian Research, v. 110, p. 33-46.
Rankin, D.W., 1988, The Jefferson terrane of the Blue Ridge tectonic province: An exotic accretionary prism: Geological Society of America Abstracts with Programs, v. 20, p. 310.

Rankin, D.W., 1994, Continental margin of the eastern United States: Past and present, *in* Speed, R.C., ed., Phanerozoic Evolution of North American continent-ocean transitions: Boulder, Colorado, Geological Society of America, DNAG continent-ocean transect volume, p. 129-218.

Rankin, D.W., Espenshade, G.H., and Neuman, R.B., 1972, Geologic map of the west half of the Winston-Salem quadrangle, North Carolina, Virginia, and Tennessee: U.S. Geological Survey Miscellaneous Geologic Investigations Map I-709A, scale 1:250,000.

Rankin, D.W., Chiarenzelli, J.R., Drake, A.A., Jr., Goldsmith, R., Hall, L.M., Hinze, W.J., Isachsen, Y.W., Lidiak, E.G., McLelland, J., Mosher, S., Ratcliffe, N.M., Secor, D.T., Jr., and Whitney, P.R., 1989, Proterozoic rocks east and southeast of the Grenville front, *in* Reed, J.C., Jr., Bickford, M.E., Houston, R.S., Link, P.K., Rankin, D.W., Sims, P.K., and Van Schmus, W.R., eds., Precambrian: Conterminous U.S.: Boulder, Colorado, Geological Society of America, The geology of North America, v. C-2, p. 335-461.

Ranson, W.A., Williams, I.S., and Garihan, J.M., 1999, SHRIMP zircon U-Pb ages of granitoids from the Inner Piedmont of South Carolina: evidence for Ordovician magmatism involving Mid to Late Protereozoic crust: Geological Society of America Abstracts with Programs, v. 31, p. 167.

Reed, J.C., Jr., 1964, Geology of the Linville Falls quadrangle North Carolina: U.S. Geological Survey Bulletin 1161-B, 53 p.

Rogers, J.J.W., 1967, Chronology of tectonic movements in the Appalachian region of eastern North America: American Journal of Science, v. 265, p. 408-427.

Roper, P.J., and Dunn, D.E., 1973, Superposed deformation and polymetamorphism, Brevard zone, South Carolina: Geological Society of America Bulletin, v. 84, p. 3373-3386.

Samson, S.D., Hibbard, J.P., and Wortman, G.L., 1995, Nd isotopic evidence for juvenile crust in the Carolina terrane, southern Appalachians: Contributions to Mineralogy and Petrology, v. 121, p. 171-184.

Shufflebarger, T.E., 1961, Notes on relationships of Piedmont sedimentary rocks with emphasis on the Poor Mountain-Chauga River area, Oconee County, South Carolina: South Carolina Division of Geology, Geologic Notes, v. 5, p. 31-38.

Sinha, A.K., and Glover, L., III, 1978, U/Pb systematics of zircons during dynamic metamorphism: Contributions to Mineralogy and Petrology, v. 66, p. 305-310.

Sinha, A.K., Hund, E.A., and Hogan, J.P., 1989, Paleozoic accretionary history of the North American plate margin (central and southern Appalachians): Constraints from the age, origin, and distribution of granitic rocks, *in* Hillhouse, J., ed., Deep structure and past kinematics of accreted terranes: American Geophysical Union Monograph Series, p. 219-238.

Sloan, E., 1907, Catalogue of the mineral localities of South Carolina: South Carolina Geological Survey Bulletin, v. 2, 4th series, 505 p.

Steltenpohl, M.G., Heatherington, A.L., Mueller, P.A., 2002, Our current understanding of the Grenville event in the southernmost Appalachians, Pine Mountain Window,

Alabama: Geological Society of America Abstracts with Programs, v. 33, p. 29.
Su, Q., Goldberg, S.A., and Fullagar, P.D., 1994, Precise U-Pb zircon ages of Neoproterozoic plutons in the southern Appalachian Blue Ridge and their implications for the initial rifting of Laurentia: Precambrian Research, v. 68, p. 81-95.
Tabor, J.R., unpublished, Geologic map of the Mill Spring quadrangle [unpublished mapping]: Knoxville, University of Tennessee, scale 1:24,000.
Thomas, C.W., 2001, Origins of mafic-ultramafic complexes of the eastern Blue Ridge province, southern Appalachians: Geochronological and geochemical constraints [M.S. thesis]: Nashville, Tennessee, Vanderbilt University, 154 p.
Thomas, C.W., Miller ,C.F., Fullagar, P.D., Meschter McDowell, S.M., Vinson, S.B., and Bream, B.R., 2001, Where is the arc? Discontinuities in the Taconian arc magmatism in the southern Appalachians: Geological Society of America Abstracts with Programs, v. 33, p. 262.
Unrug, R., Ausich, W.I., Bednarczyk, J., Cuffey, R.J., Mamaet, B.L., Palmes, S.L., and Unrug, S., 2000, Paleozoic age of the Walden Creek Group, Ocoee Supergroup, in the western Blue Ridge, southern Appalachians: Implications for evolution of the Appalachian margin of Laurentia: Geological Society of America Bulletin, v. 112, p. 982-996.
Vinson, S., 1999, Ion probe geochronology of granitoid gneisses of the Inner Piedmont, North Carolina and South Carolina [M.S. thesis]: Nashville, Tennessee, Vanderbilt University, 84 p.
Wagener, H.D., 1977, The granitic stone resources of South Carolina: Columbia, South Carolina Geological Survey, Mineral Resources Series 5, 65 p.
Warlick, C.M., Clendenin, C.W., and Castle, J.W., 2001, Geology of The Cliffs at Glassy development, southern Saluda 7.5-minute quadrangle, Greenville County, South Carolina, *in* Garihan, J.M., Ranson, W.A., and Clendenin, C.W., eds., Geology of the Inner Piedmont in the Caesars head and Table Rock state parks area, northwestern South Carolina: Carolina Geological Society annual field trip guidebook, p. 37-56.
Warner, R.D., Griffin, V.S., Steiner, J.C., Schmitt, R.A., and Bryan, J.G., 1989, Ultramafic chlorite-tremolite-olivine schists; Three bodies from the Inner Piedmont belt, South Carolina, *in* Mittwede, S.K., and Stoddard, E.F., eds., Ultramafic rocks of the Appalachian Piedmont: Boulder, Colorado, Geological Society of America Special Paper 231, p. 63-74.
Whisnant, J.S., 1975, Geology of the southeastern quarter of the Marion 15-minute quadrangle, North Carolina [M.S. thesis]: Chapel Hill, University of North Carolina, 50 p.
Whisnant, J.S., 1979, Geologic map of the SE 1/4 of the Marion quadrangle, North Carolina: North Carolina Geological Survey and Tennessee Valley Authority GM 210-SE, scale 1:24,000.
Williams, S.T., 2000, Structure, stratigraphy, and migmatization in the southwestern South Mountains, North Carolina [M.S. thesis]: Knoxville, Tennessee, University of Tennessee, 111 p.

Williams, H., and Hatcher, R.D., Jr., 1983, Suspect terranes: a new look at the Appalachian orogen, *in* Hatcher, R.D., Jr., Williams, H., and Zietz, I., eds., Contributions to the tectonics and geophysics of mountain chains: Geological Society of America Memoir 158, p. 33-54.

Yanagihara, G.M., 1993, Evolution of folds associated with D_2 and D_3 deformation and their relationship with shearing in a part of the Columbus Promontory, North Carolina, *in* Hatcher, R.D., Jr., and Davis, T.L., eds., Studies of Inner Piedmont Geology with a focus on the Columbus Promontory: Carolina Geological Society annual field trip guidebook, p. 45-65.

Yanagihara, G.M., 1994, Structure, stratigraphy, and metamorphism of a part of the Columbus Promontory, western Inner Piedmont, North Carolina [M.S. Thesis]: Knoxville, Tennessee, University of Tennessee, 214 p.

Yates, R.G., 1963, Preliminary geologic map of the northwest quarter of the Shelby quadrangle, Cleveland and Rutherford Counties, North Carolina: U.S. Geological Studies Map MF-258, scale 1:24,000.

Yates, R.G., and Overstreet, W.C., 1962, Preliminary geologic map of the northeast quarter of the Shelby quadrangle, Cleveland County, North Carolina: U.S. Geological Survey Field Studies Map MF-249, scale 1:24,000.

PART IV

Inner Piedmont stratigraphy, metamorphism, and deformation in the Marion-South Mountains area, North Carolina

This chapter is a slightly modified version of a paper that was published in the 2002 Carolina Geological Society field trip guidebook:

> Bier, S.E., Bream, B.R., and Giorgis, S.D., 2002, Inner Piedmont stratigraphy, metamorphism, and deformation in the Marion-South Mountains area, North Carolina, *in* Hatcher, R.D., Jr., and Bream, B.R., eds., Inner Piedmont geology in the South Mountains-Blue Ride Foothills and southwestern Brushy Mountains, central-western North Carolina: North Carolina Geological Survey, Carolina Geological Society annual field trip guidebook, p. 65-99.

My contributions to this paper are: (1) data used in the stratigraphy, metamorphism, and structure sections, (2) most of the electron microprobe work, and (3) formatting and revision. The use of "we" and "our" in the text refers to the co-authors and myself.

ABSTRACT

The western Inner Piedmont stratigraphy consists of Cambrian (?) metagraywacke, aluminous schist, and amphibolite of the Tallulah Falls Formation overlain by Middle Ordovician Poor Mountain Amphibolite and Poor Mountain Quartzite. This sequence is intruded by Middle Ordovician plutons (e.g., Dysartsville Tonalite) and is in thrust contact with Early Ordovician Henderson Gneiss. The eastern Inner Piedmont in the South Mountains contains mappable biotite gneiss and sillimanite schist units (Silurian to Early Devonian?) intruded by Devonian Walker Top and Toluca Granites. Pressure and temperature estimates with structural, geochronologic, and petrologic data for the North Carolina Inner Piedmont confirm the polydeformed nature of this terrane and delimit the timing and conditions of Paleozoic metamorphism. Peak metamorphic conditions are coeval with post-penetrative deformation and appear to postdate major displacement on the Mill Spring fault. Pressures of 5.1 and 5.3 (± 1) kbar were estimated for two samples from the kyanite + staurolite and sillimanite domains, respectively. Temperature estimates for six other samples, using these pressures, range from 520 to 670 ˚C. Deformational fabrics and temperature estimates do not appear to be offset by major

Inner Piedmont faults. Map relationships demonstrate that major displacement on the Mill spring fault postdates the ~465 Ma crystallization age of the Dysartsville Tonalite and that this displacement is pre- to syn-metamorphic peak. Metamorphic zircon and monazite growth, deformation fabrics, and crosscutting relationships indicate a single high-T peak metamorphic prograde event during the Neoacadian orogeny in this part of the Inner Piedmont. A portion of the North Carolina Inner Piedmont from the Brevard fault zone to the eastern Inner Piedmont is divisible into three fault-bounded domains and enables construction of a deformational framework that includes at least five episodes of deformation. The easternmost domain is further subdivided into five structurally homogeneous subdomains. Foliation (S_2) reflects a regional change in strike from NE-SW in the western flank to N-S in the eastern Inner Piedmont back to NE-SW in the southeastern part of the domains. Lineations are aligned NE-SW (orogen parallel) in the western Inner Piedmont and E-W in the eastern Inner Piedmont and probably indicate transport direction. Rare D_1 intrafolial folds and foliation are attributed to the Taconic orogeny. D_2 foliation, lineations, tight to isoclinal, recumbent to reclined folds, sheath folds and Type-F thrust faults represent penetrative Neoacadian deformation. D_3 folds and Type-C thrust faults probably constitute the latter portion of ductile Neoacadian deformation. D_4 broad open folds formed during the Alleghanian orogeny. D_5 fractures are a result of Mesozoic uplift and extension. The structural data and map patterns presented here are best explained by crustal flow during oblique collision.

INTRODUCTION

Rocks found in the internal portions of mountain chains reveal details about deep crustal processes. Despite decades of study, many important aspects of Paleozoic orogenesis in the central and southern Appalachians are unresolved. In particular, the

nature and timing of metamorphism and deformation in the southern Appalachian crystalline core remain poorly understood. This paper outlines the stratigraphy of North Carolina Inner Piedmont in the Marion and South Mountains area, summarizes preliminary P-T estimates, and presents a deformational framework that addresses the relative timing of regional structures. Documenting the metamorphic history of this part of the Appalachians and its relationship to the deformational history of the Inner Piedmont is a fundamental key to understanding southern Appalachian tectonics, Appalachian terrane accretion, and the process of medium- to high-grade Barrovian metamorphism.

The southern Appalachians have been divided into several lithotectonic units (Fig. 1). The Piedmont and Carolina terranes were accreted to Laurentia during Paleozoic orogenesis (Williams and Hatcher, 1983) and together comprise the southern Appalachian crystalline core. The Inner Piedmont is located between the eastern Blue Ridge and the Carolina terrane and extends from northern North Carolina to the Coastal Plain in Alabama. Rock types here are varied, multiply deformed, strongly migmatitic, and bear similarities to other high-grade gneiss terranes (e.g., Shuswaps and Scottish Grampians). The Inner Piedmont is characterized by middle to upper amphibolite facies mineral assemblages and contains some of the most intensely deformed and metamorphosed rocks in the Appalachians. Regardless of the largely migmatitic and polydeformed nature of this terrane, the relationships between primary lithostratigraphic sequences, granitoids, and other rock types are only partially obscured. The Inner Piedmont has been interpreted as a mélange complex (Goldsmith et al., 1988; Horton et al., 1989), part of the larger Piedmont terrane (Williams and Hatcher 1983) or Tugaloo and Cartoogechaye terranes (Hatcher et al., 1999; Hatcher, 2001), and an accreted exotic terrane (Dennis, 1991; Rankin, 1994; Dennis and Wright, 1997). It has generally been accepted that accretion of the Tugaloo terrane to Laurentia occurred during Ordovician

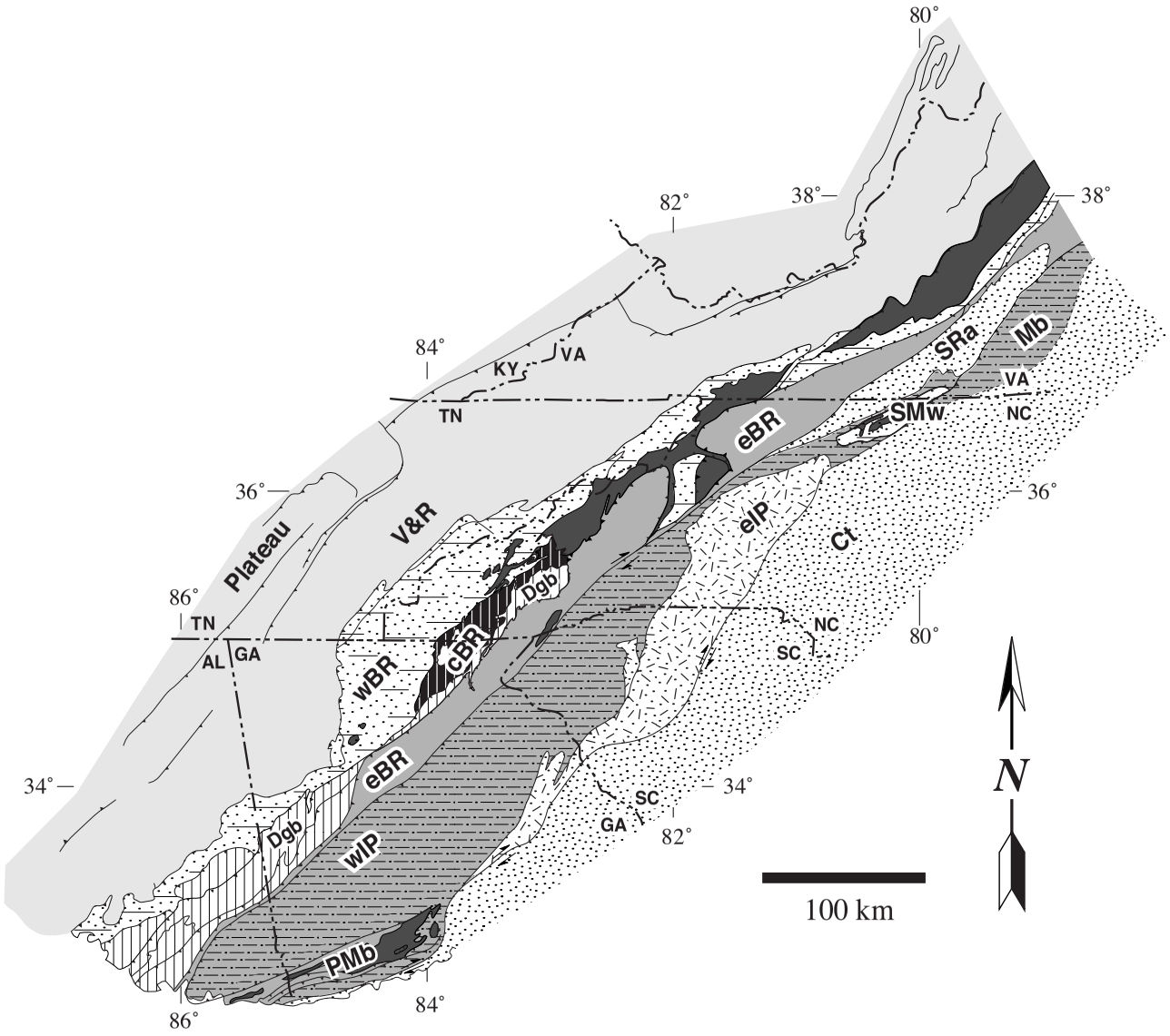

Figure 1. Tectonic map of the southern Appalachians modified from Hatcher et al. (1990) and Bream et al. (in review). cBR-central Blue Ridge; Ct-Carolina terrane; Dgb-Dahlonega gold belt; eBR-eastern Blue Ridge; eIP-central and eastern Inner Piedmont; Mb-Milton belt; PMb-Pine Mountain block; SMw-Sauratown Mountains window; SRa-Smith River Allochthon; V&R-Valley and Ridge; wBR-western Blue Ridge; wIP-western Inner Piedmont.

Taconian orogenesis (e.g., Hatcher, 1989; Horton et al., 1989). The timing of peak deformation and metamorphism within the Inner Piedmont, however, remains equivocal (e.g., Tull, 1980; Dallmeyer, 1988; Horton et al., 1989; Osberg et al., 1989; Hibbard, 2000). Only a small portion (~15%) of the Inner Piedmont has been mapped and studied in detail due to the complex nature of the terrane and the common misconception that this region lacks exposure and a recognizable stratigraphy. Our recent detailed mapping (1:12,000- and 1:24,000-scales) with accompanying structural analysis and geothermobarometric estimates define a mappable stratigraphy, key structures, and minimum peak metamorphic conditions for the study area.

GEOLOGIC SETTING

The Inner Piedmont consists of a stack of west- to southwest-vergent plastic thrust sheets rooted on the southeast flank of the belt. Transposition of earlier fabrics and map patterns reveal that penetrative deformation occurred at, or near, peak metamorphism with later superposition of brittle deformation and retrograde metamorphism. Mapping has identified the presence of a mostly orogen-parallel paragneiss sequence (Tallulah Falls/Ashe and Poor Mountain Formations) that is repeated in several thrust sheets across strike to the southeast. The area of recent detailed mapping is divisible into three fault-defined lithotectonic packages (Fig. 2). Each of the thrust sheets contains a portion of the western Inner Piedmont paragneiss stratigraphy except for the Tumblebug Creek thrust sheet, which contains only the Henderson Gneiss, and the Brindle Creek thrust, which thrusts a younger paragneiss sequence over the western Inner Piedmont.

Metapsammite and metapelite paragneisses of the western Inner Piedmont are generally considered to have a Late Proterozoic to Cambrian age (Hatcher, 1969, 1987; Drake et al. 1989); the eastern Inner Piedmont paragneiss sequence which is dominated by metapelite with lesser metapsammite was likely deposited from the Silurian to Early

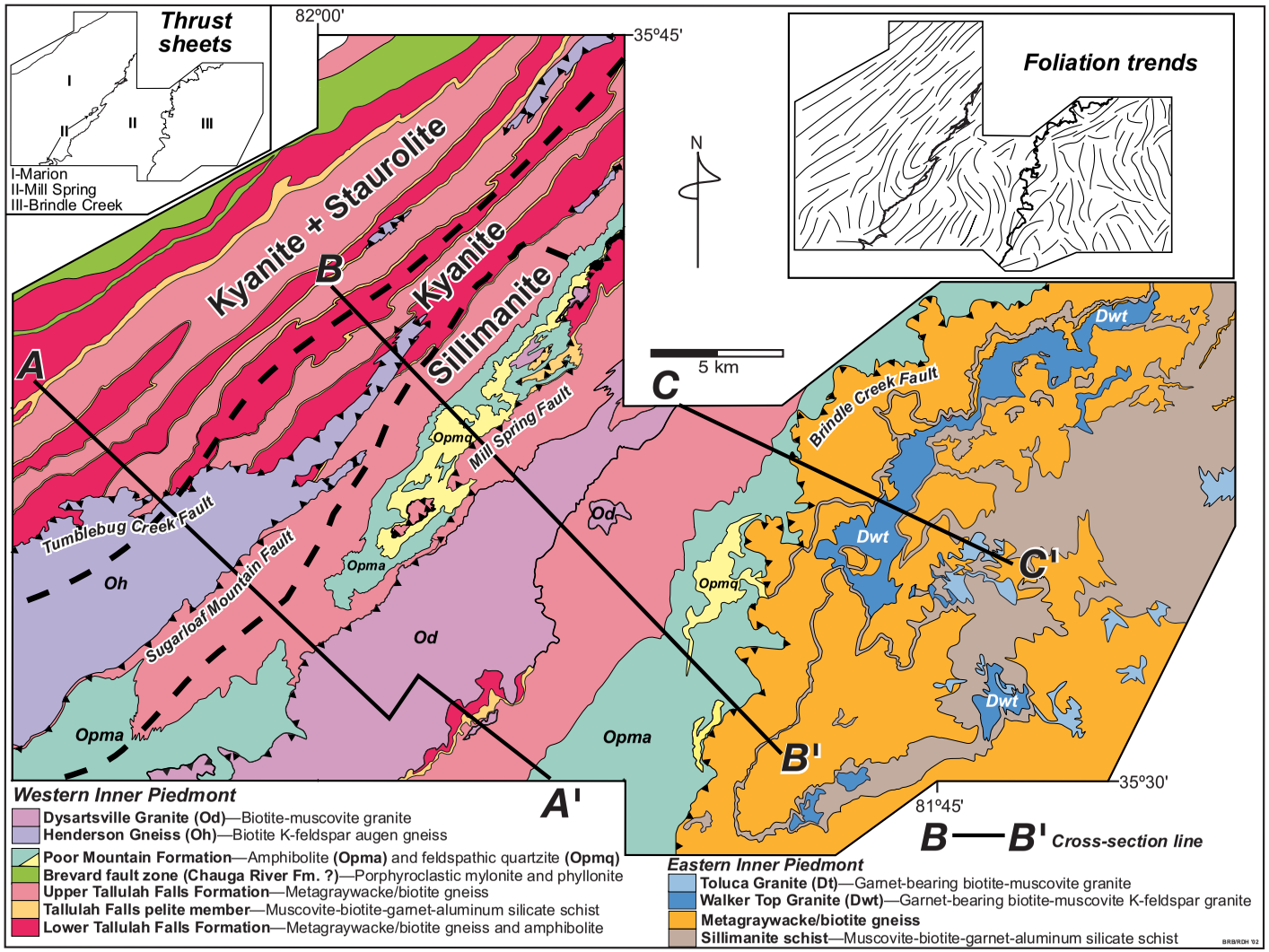

Figure 2. Geologic map of the Marion-South Mountains area. Compiled from detailed mapping of Whisnant (1975), Yanagihara (1994), Bream (1999), Giorgis (1999), Hill (1999), Williams (2000), and Bier (2001). Cross sections are in Figure 28.

Devonian (Bream et al., 2001, in review). Amphibole gneiss, amphibolite, quartzite, calc-silicate, and ultramafic rocks are also present. The quartzofeldspathic gneiss and aluminous schist portions of the western Inner Piedmont stratigraphy are interpreted to share a similar provenance to that of the eastern Blue Ridge Tallulah Falls/Ashe Formations over which they are thrust (Hatcher 1987). The finely laminated amphibolite and quartzite units are correlative with the South Carolina western Inner Piedmont Poor Mountain Formation of Hatcher (1969). Continuous portions of this stratigraphy occur parallel to and across strike from just southwest of the Sauratown Mountains window in North Carolina to Alabama. Numerous regional summaries (e.g., Griffin, 1974; Osberg et al., 1989; Butler, 1991; Hatcher and Goldberg, 1991) have identified the kyanite-sillimanite isograd that places migmatitic sillimanite-grade assemblages over kyanite-grade assemblages on the western flank of the Inner Piedmont. These prograde assemblages are overprinted within the Brevard fault zone by Alleghanian lower greenschist facies retrograde metamorphism (Reed and Bryant, 1964).

ROCK UNITS

Much of the Inner Piedmont has not been studied in detail partially because of a historical misconception that it contains an indecipherable high grade assemblage of gneiss, schist, migmatite, amphibolite, and granitoid (King, 1955), and a mappable stratigraphy is therefore not present. As in most high-grade gneiss terranes (Passchier et al., 1990), rocks of the Inner Piedmont *are* both lithologically and deformationally complex. A cursory look at this belt confirms the earlier misconception. Davis (1993), however, provided the first clues that the stratigraphic sequence in the Columbus Promontory of southwestern North Carolina is the same as that in the western Inner Piedmont and eastern Blue Ridge of South Carolina and northeastern Georgia (Hopson and Hatcher, 1988). New work by Hill (1999) and Bream (1999) reviewed during the

2002 CGS field trip has confirmed that the Tallulah Falls and Poor Mountain Formations stratigraphy does indeed exist between the Brindle Creek and pre-Alleghanian Brevard fault in the South Mountains and that it is readily mappable at the 1:12,000 and 1:24,000 scales employed for detailed mapping (Fig. 3).

Research by Giorgis (1999), Williams (2000), and Bier (2001) east of the Brindle Creek fault initially suggested Tallulah Falls Formation stratigraphy is present there as well but with large thickness changes in the aluminous schist member and the intervening metagraywacke. Detrital and igneous ion microprobe zircon studies (e.g., Mapes, 2002; Bream, this guidebook); however, indicate the paragneiss sequence east of the Brindle Creek fault may be as young as Early Devonian, whereas sequences west of the Brindle Creek fault are Middle Ordovician and older. Additionally, detailed and reconnaissance mapping (where available) has not delineated an eastern Inner Piedmont equivalent to the western Inner Piedmont Poor Mountain Formation. New stratigraphic and geochronologic data have thus resulted in delineation of a previously unrecognized terrane of younger rocks within the Inner Piedmont. The assemblage represented here may be analogous to the Siluro-Devonian sequence in the Merrimack synclinorium and

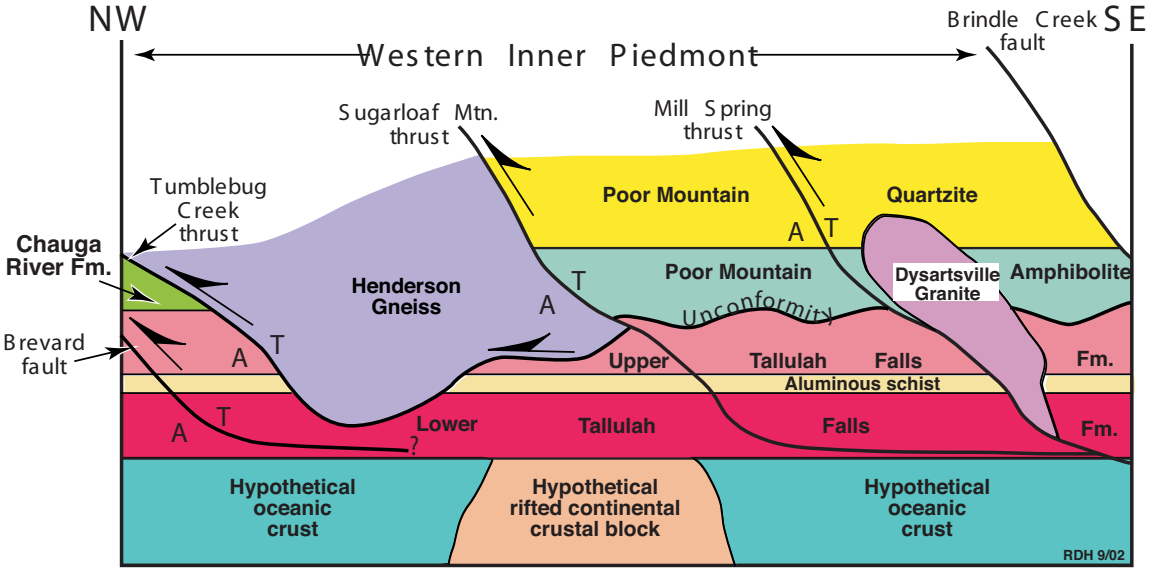

Figure 3. Western Inner Piedmont generalized stratigraphy with major faults. T-toward; A-away.

Bronson Hill anticlinorium in the New England Appalachians.

Western Inner Piedmont

Rock types present in the western Inner Piedmont near Marion, North Carolina, include quartzofeldspathic biotite gneiss, amphibole gneiss, amphibolite, quartzite, metatuff, pelitic and aluminous schist, calc-silicate, and ultramafic rocks. Protoliths for this assemblage consist of immature quartzofeldspathic psammite and pelite overlain by metabasalt and feldspathic sandstone interlayered with felsic tuff(?). Granitic and mafic orthogneisses later intruded this assemblage. Hatcher (1978, 1987, 1989), Hopson and Hatcher (1988), Davis (1993), Bream (1999), and Hill (1999) correlated the western Inner Piedmont stratigraphy with the Tallulah Falls Formation in the eastern Blue Ridge. In this area, the main body of Henderson Gneiss truncates all units of the Tallulah Falls Formation, and the contact is faulted (see Hatcher, this guidebook, his Fig. 4). The amphibolite-quartzite-metatuff (?) units are correlative with the Poor Mountain Amphibolite and Quartzite. See Bream (this guidebook) for a more detailed discussion of correlative map units in the North and South Carolina western Inner Piedmont.

Tallulah Falls Formation

In the Marion area, Tallulah Falls Formation occurs in each thrust sheet west of the Brindle Creek fault, except for the Tumblebug Creek thrust sheet that carries only Henderson Gneiss. A thin aluminous schist unit divides the formation within the study area. Mapped subdivisions (Fig. 2) are the result of careful identification of the aluminous schist and relative abundance of amphibolite/amphibole gneiss in the metagraywacke-biotite gneisses of the upper and lower Tallulah Falls Formation. Tallulah Falls amphibolite and amphibole gneiss occur as pods, layers, and boudins within the lower and upper metagraywacke-biotite gneisses. Compositional layering is commonly parallel to the dominant foliation. It was also noted by Davis (1993),

Yanagihara (1994), and Hill (1999) that the lower Tallulah Falls Formation is more migmatitic than the upper Tallulah Falls Formation. Bream (1999) noted, however, that both units are partially migmatitic and the metagraywacke-biotite gneiss of the upper Tallulah Falls appears more migmatitic than that of the lower Tallulah Falls. This is attributed mostly to the absence of the lower Tallulah Falls in the higher-grade thrust sheets above the Tumblebug Creek fault in the Marion area. Isoclinal folding in the lowest thrust sheet repeats the entire formation several times. The sillimanite isograd occurs at and immediately west of the Mill Spring thrust in the Marion area (Fig. 2).

Upper and lower Tallulah Falls metagraywacke-biotite gneiss and two-mica schist.

The lower Tallulah Falls Formation is a light- to dark-gray metagraywacke-biotite gneiss and two-mica schist unit that contains more amphibolite and amphibole gneiss than the upper Tallulah Falls graywacke-biotite gneiss unit (Fig. 4). Where mica content is high, the lithology is coarser grained and schistose. Modal analyses reveal that metagraywacke-bioite gneiss contains: 26-46 percent quartz, 28-46 percent plagioclase (An_{25-35}), 15-30 percent biotite, and 1-7 percent muscovite. Minor constituents present include epidote, microcline, chlorite, and opaque minerals. Trace zircon and sphene are also present. Quartz commonly exhibits high-angle grain boundaries, indicating complete recrystallization. Brown biotite is variably replaced by green biotite in thin sections. Metagraywacke is frequently porphyroclastic with 0.5- to 3-cm composite quartz and white or milky microcline or plagioclase grains. Porphyroclastic texture is present in both metagraywacke units and does not appear to be gradational or limited to the lower unit, as suggested by Davis (1993). Foliation is defined by parallel alignment of quartzofeldspathic material and micas in the metagraywacke and by biotite and muscovite in schist. Modal compositions of all metagraywackes plot as graywackes or arkoses using the modified Pettijohn (1949) sandstone classification (Fig. 5). Layer thicknesses vary from a few millimeters to several meters.

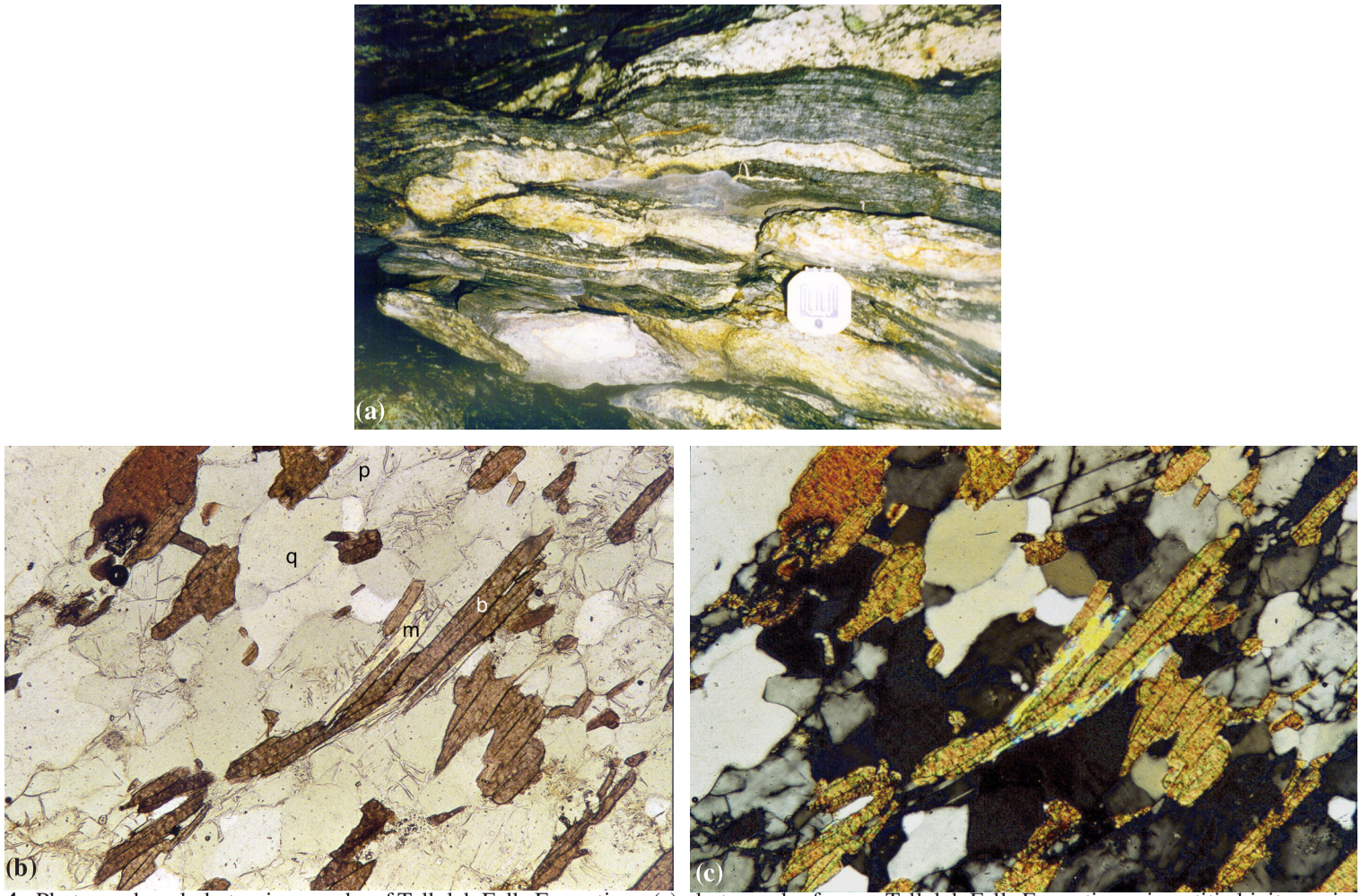

Figure 4. Photograph and photomicrographs of Tallulah Falls Formation. (a) photograph of upper Tallulah Falls Formation migmatitic bioite gneiss east of Pogue Mountain in the Glenwood 7.5-minute quadrangle. (b) Plane light photomicrograph of upper Tallulah Falls Formation from the Glenwood 7.5-minute quadrangle just south of Chestnut Mountain near the Tallulah Falls/Poor Mountain contact. Thin section was cut perpendicular to foliation and parallel to lineation. Abbreviations are as follows: q-quartz, p-plagioclase, b-biotite, m-muscovite. (c) Cross-polarized photomicrograph of same area in Figure 4b thin section. Width of field for (b) and (c) is 1.7 mm.

Tallulah Falls aluminous schist.

The presence of kyanite or sillimanite in this unit is the principal characteristic used to separate it from the much thicker metagraywacke-biotite gneiss units that lie above and below it. Fresh aluminous schist is silver or light- to dark-gray whereas saprolite is tan or reddish-purple. Because of the garnetiferous nature of this unit, it is frequently mapped based on the abundance of garnet "gravel" especially along trails and dirt roads or in fields (Fig. 6). Aluminous schist modal analyses exhibit wide variation in dominant minerals: 7-40 percent quartz, 4-30 percent plagioclase, 3-46 percent muscovite, 0-22 percent biotite, and 8-16 percent garnet. Garnets range from less than 0.5 cm to over 2 cm in diameter, are subhedral, and contain numerous inclusions. Large subhedral and euhedral kyanite, up to one cm, is often present in the aluminous schist. Fibrolitic sillimanite makes up approximately 15 percent of a thin section of a sample collected above the Mill Spring thrust (Fig. 6). The aluminous schist is typically no more than 80 m thick, although thickness varies locally. The relative increase in outcrop width of the most northwesterly aluminous schist is probably related to the shallow dip produced by later folding. Individual schist layers can be traced from terminations against the main body of Henderson Gneiss through the Marion West and Marion East quadrangles and beyond (Bream, 1999; Hill, 1999) (Fig. 2).

Previous work in the Sugar Hill quadrangle by Whisnant (1975) and in the Marion West quadrangle by Conley and Drummond (1981) conservatively projected the aluminous schist unit as a series of disconnected lenses. This is partially related to the weathering characteristics of the aluminous schist that make it difficult to identify where dirt roads, undeveloped trails, or farmland are not present. Where the aluminous schist unit is identifiable, it can usually be followed or projected along strike to other outcrops. Tabor (1990), Davis (1993), and Yanagihara (1994) did not delineate the aluminous schist as a separate map unit in the Columbus Promontory, which allowed the Tallulah

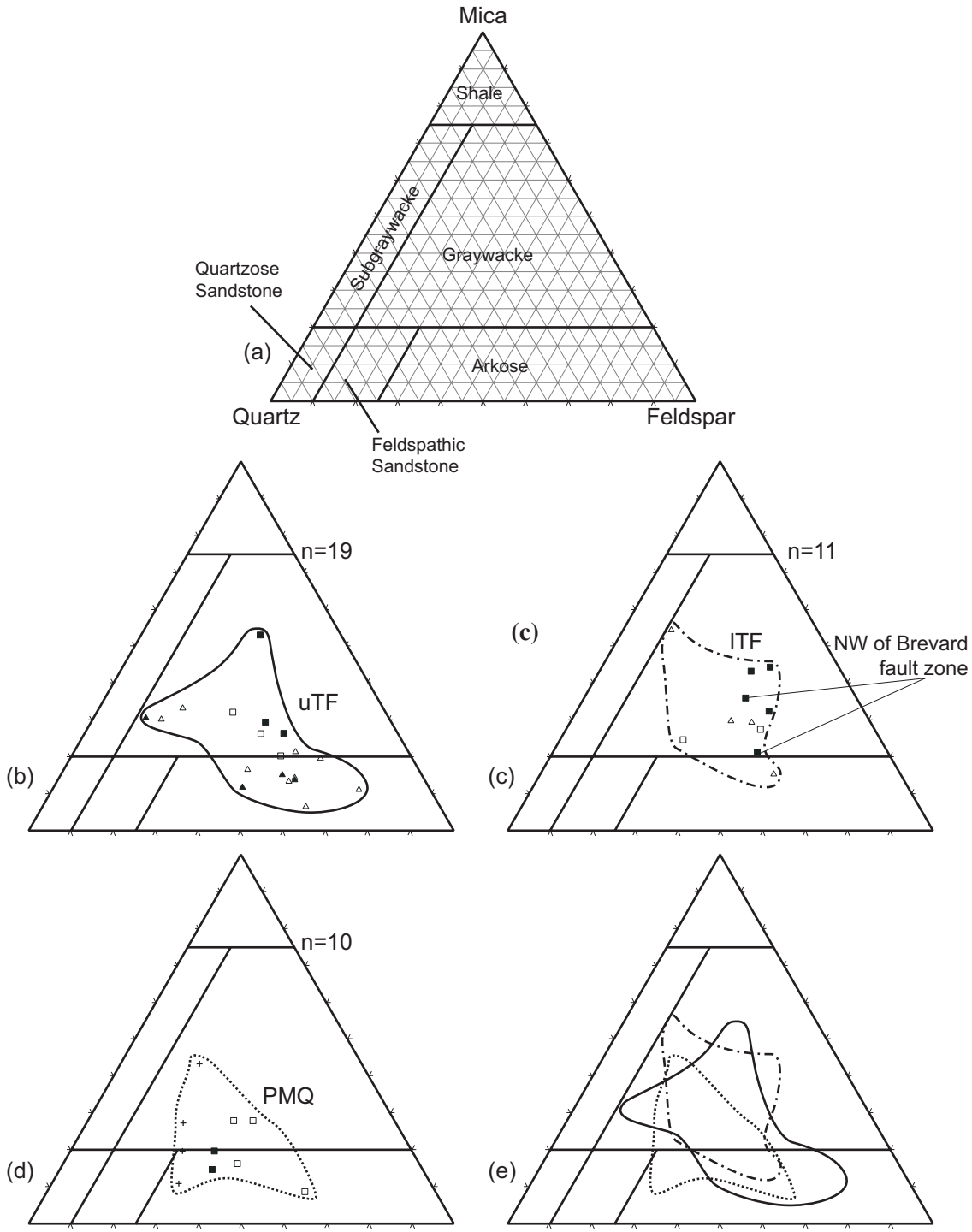

Figure 5. Quartz-feldspar-mica ternary diagram comparing the composition of the upper Tallulah Falls Formation, lower Tallulah Falls Formation, and Poor Mountain Quartzite. Filled triangles are data from Lemmon (1973), open triangles are data from Davis (1993), addition symbols are data from Yanagihara (1994), filled boxes are data from Hill (1999), and open boxes are from Bream (1999). (a) Modified sandstone classification from Pettijohn (1949). (b) uTF-upper Tallulah Falls Formation. (c) lTF-lower Tallulah Falls Formation. (d) PMQ-Poor Mountain Quartzite. (e) Composite field diagram of b, c, and d.

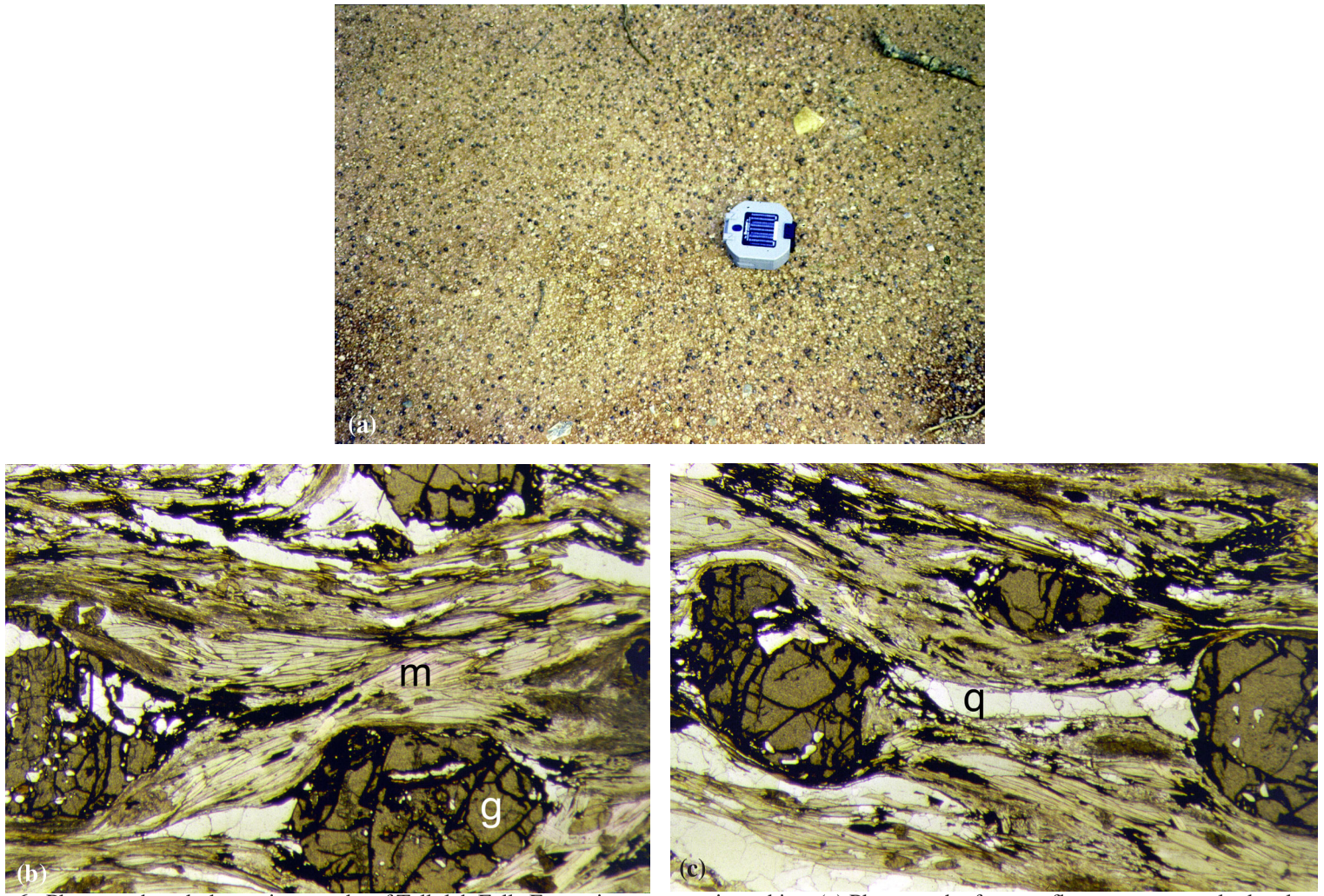

Figure 6. Photograph and photomicrographs of Tallulah Falls Formation garnet-mica schist. (a) Photograph of garnet float near a recently developed housing site north of Goose Creek Road in the Marion West 7.5-minute quadrangle. (b) and (c) Plane light photomicrographs of a garnet-mica schist sample thin section. Abbreviations are as follows: m-muscovite, g-garnet, q-quartz. (d) and (e) Crossed polarized photomicrographs of the same sample. Width of field for all photomicrographs is 11.1 mm. The thin section sample is from the Sugar Hill 7.5-minute quadrangle south of Goose Creek Road and

Falls Formation to be divided approximately only into upper (amphibolite-poor) and lower (amphibolite-rich) units. A single aluminous schist layer was noted by Whisnant (1975), who stated that the "lenses" are indistinguishable except where kyanite blades occur that are longer than 1 cm. We have been able to trace kyanite-bearing aluminous schist where size of kyanite is much smaller and sillimanite-bearing aluminous schist where sillimanite is identifiable only with a hand lens. The key to tracing this unit is first the location of abundant garnet accumulations on the surface or in saprolite, and then searching for the diagnostic aluminum silicate mineral.

Tallulah Falls-Poor Mountain Contact

Yanagihara (1994) noted that the contact between the upper Tallulah Falls Formation and Poor Mountain Amphibolite is sharp with limited interlayering. This contact remains sharp and is well exposed on Second Broad River just south of Spooky Hollow Road immediately west of U.S. 221 in the Glenwood 7 1/2-minute quadrangle (STOP 4, this guidebook). Based on the Second Broad River exposure, distinct lithologic differences, lack of evidence for faulting, and limited interlaying, this contact is best explained as an unconformity.

Muscovite schist occurs along the exposed Tallulah Falls-Poor Mountain Formation contact in the Second Broad River. It is coarser grained than muscovite-rich Poor Mountain Quartzite. Figure 7 is a photomicrograph of the thin section made from the contact unit. There is limited exposure of this unit and its extent along strike is unknown. Some interlayers of this material are also present in the basal Poor Mountain Amphibolite that is also exposed just above the contact. The unit was sampled stratigraphically above and attached to porphyroclastic upper Tallulah Falls Formation. This unit is white to gray and weathers to light and dark tans. A modal analysis of the single thin section showed the following proportions: 38 percent plagioclase (An_{24}), 33 percent muscovite, and 24 percent quartz. Clinozoisite, sphene, and opaques are each

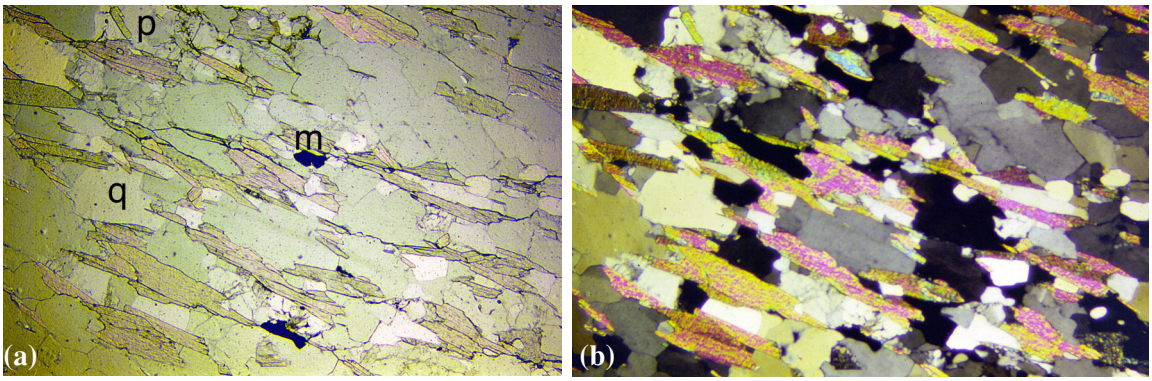

Figure 7. Photomicrographs of the unit at the contact between the upper Tallulah Falls Formation and the Poor Mountain Amphibolite. The sample is from the exposure in the Second Broad River south of Spooky Hollow Road in the Glenwood 7.5-minute quadrangle. (a) Plane light photomicrograph. Width of field is 4.25 mm. Abbreviations are as follows: p-plagioclase, m-muscovite, q-quartz. (b) Crossed polarized

present at less than 0.1 percent. Based on the mineralogy it is more likely that this unit represents the uppermost part of the Tallulah Falls Formation than the basal part of the Poor Mountain Formation or that it is a lens of Brevard-Poor Mountain transitional unit, which would further support the interpretation of this contact as an unconformity.

Poor Mountain Formation

The uppermost stratigraphic unit recognized to date in the western Inner Piedmont near Marion is correlative with the Poor Mountain sequence, first described by Sloan (1907) northwest of Walhalla, South Carolina. Shufflebarger (1961) first subdivided the Poor Mountain sequence into amphibolite and quartzite/marble units. Hatcher (1969, 1970) correlated the Poor Mountain rocks with the Chauga River Formation in northwestern South Carolina, redefined the Poor Mountain sequence as a formation (adding the lower Brevard-Poor Mountain transitional member), and attributed lithologic differences between the Chauga River and Poor Mountain Formations to facies changes. The transitional member has been recognized with certainty only from the Chauga belt in South Carolina to the Columbus Promontory of North Carolina. New geochronologic data (Bream, this guidebook) indicate the Poor Mountain and Chauga River Formations are not correlative, as Hatcher previously indicated, and the Chauga River Formation is

older than the Poor Mountain Formation but probably still younger than the Tallulah Falls Formation. See Hatcher (this guidebook, his Figs. 5, 6, and 7) for a revision of stratigraphic relationships based on a combination of Bream's geochronologic data and field relationships from the Marion, North Carolina, area to northeastern Georgia. Critical to this revision is Bream's (1999) recognition of the possible unconformable relationship between the Poor Mountain Formation and the rocks that occur beneath it at different places from northeast to southwest.

Lemmon (1973) observed that the amphibolite and hornblende gneiss on Chimney Rock in the Columbus Promontory is interlayered with feldspathic quartzite and muscovite schist. He also suggested that the amphibolite-hornblende gneiss unit thickens and undergoes a facies change southwestward from Chimney Rock in North Carolina. This relationship and a higher quartzofeldspathic granofels unit were described by Whisnant (1975) to the northeast in the Sugar Hill quadrangle. Based on relationships directly observed in the Glenwood quadrangle and the work of Yanagihara (1994) in the Sugar Hill quadrangle, the quartzofeldspathic granofels unit of Whisnant (1975) may actually be two units: Poor Mountain Quartzite and Dysartsville Tonalite. The contact between Dysartsville Tonalite and the Poor Mountain Formation rocks is interpreted as a fault most likely correlative with the Mill Spring fault of Davis (1993) and Yanagihara (1994). Whisnant (1975) also noted the presence of what appeared to be detrital garnets in his quartzofeldspathic granofels. Garnets with a detrital appearance were noted in the Poor Mountain Quartzite; only trace relict garnets, however, have been observed in Dysartsville Tonalite.

The Poor Mountain Formation is preserved in synclines in the eastern parts of the Sugarloaf Mountain and Mill Spring thrust sheets (Fig. 2). It comprises one of the most distinct rock units in the Marion area and consists of a basal amphibolite-rich (>70% amphibolite) unit that grades upward into a quartz-rich unit (>70% quartz + feldspar).

The Poor Mountain Formation also contains layers of pelitic schist, metagraywacke, and granitoid gneiss (metatuff?). The Poor Mountain Formation in the Marion area lacks the basal garnet mica schist metasiltstone unit mapped by Lemmon (1973) and Davis (1993) and correlated with the Brevard-Poor Mountain transitional unit of Hatcher (1970). Poor Mountain Amphibolite here rests directly on upper Tallulah Falls Formation. In the Marion area, the Poor Mountain Formation is divisible into two mappable units, the basal amphibolite and amphibolite gneiss (Poor Mountain Amphibolite) that grades upward into feldspathic quartzite and metatuff (Poor Mountain Quartzite) (Bream, 1999; Hill, 1999).

Preliminary geochronologic data (Kalbas et al., 2002; Bream, unpublished data), based on ion microprobe analyses of zircons interpreted to have an igneous origin, reveal that a metatuff (?) component in the Poor Mountain Quartzite from the Glenwood 7 1/2-minute quadrangle has an age of ~460 Ma. A similar U-Pb age was obtained on zircon cores from an intensely migmatitic sample, interpreted by Kalbas (in preparation) to have a major protolith component of Poor Mountain Formation, from the Vulcan Materials Company Lenoir Quarry (STOP 12) (Kalbas et al., 2002; Bream, unpublished data). The Middle Ordovician age of the Poor Mountain Formation also favors interpretation of the contact with the underlying Tallulah Falls Formation rocks as an unconformity.

Poor Mountain Amphibolite

Nonmigmatitic Poor Mountain Amphibolite is predominantly fine-laminated amphibolite and lesser amounts of thin to thick bands of amphibole gneiss interlayered with feldspathic quartzite near the contact (Fig. 8). Mineral lineations of the Poor Mountain Amphibolite is defined by parallel alignment of elongate hornblende grains. Layering in the laminated amphibolite varies from a few mm to approximately 30 cm thick. The interlayering in the laminated amphibolite and feldspathic quartzite is interpreted as a primary sedimentary/volcanic feature of the Poor Mountain Formation,

although transposition doubtlessly played a role here. Equivalents to this unit in the Columbus Promontory and in the Chauga belt of South Carolina are described as gray to black fine- to medium-grained amphibolite and amphibole gneiss interlayered with quartzite-marble-metatuff (?) (Hatcher, 1970; Davis, 1993; Yanagihara, 1994).

In the Marion area, the laminated amphibolite is mostly fine grained and rarely contains mesoscopic folding. This unit is dark- to medium-gray and weathers to an ochre-colored saprolite. Thin sections of laminated amphibolite from the Sugarloaf Mountain thrust sheet contain: 48-65 percent hornblende, 5-45 percent plagioclase (An_{25-32}), 0-28 percent epidote/clinozoisite, and 0-6 percent quartz. Trace and accessory minerals include biotite, sphene, zircon, and opaque minerals. Epidote and clinozoisite are found mostly in quartzofeldspathic layers, as products of either hydrous alteration or the prograde metamorphic reactions involving originally calcareous components with quartz. Recrystallized quartz occurs in the laminated amphibolite but is more common in the amphibole gneiss and quartzite layers. The hornblende is prismatic and has strong green pleochroism. Nematoblastic and sometimes poikiloblastic textures are found in this unit.

Chemical analyses of nonmigmatitic Poor Mountain Amphibolite agree well with the geochemical results of Davis (1993) and Yanagihara (1994) who interpreted it as metamorphosed tholeiitic normal mid-oceanic basalt (N–MORB). Tectonic discriminant diagrams containing all of the available geochemical data for nonmigmatitic Poor Mountain Amphibolite are summarized by Hatcher (this guidebook, his Figs. 5, 6, and 7). Previous and current detailed geologic mapping, similarity and order of the stratigraphic sequence, and bulk chemical analyses confirm the occurrence of this unit throughout the western Inner Piedmont in the Carolinas and northeastern Georgia. The bulk chemistry and normative mineralogy of the Poor Mountain Amphibolite samples from this study show that the unit contains 45-52 percent SiO_2 and is mostly olivine-normative. The

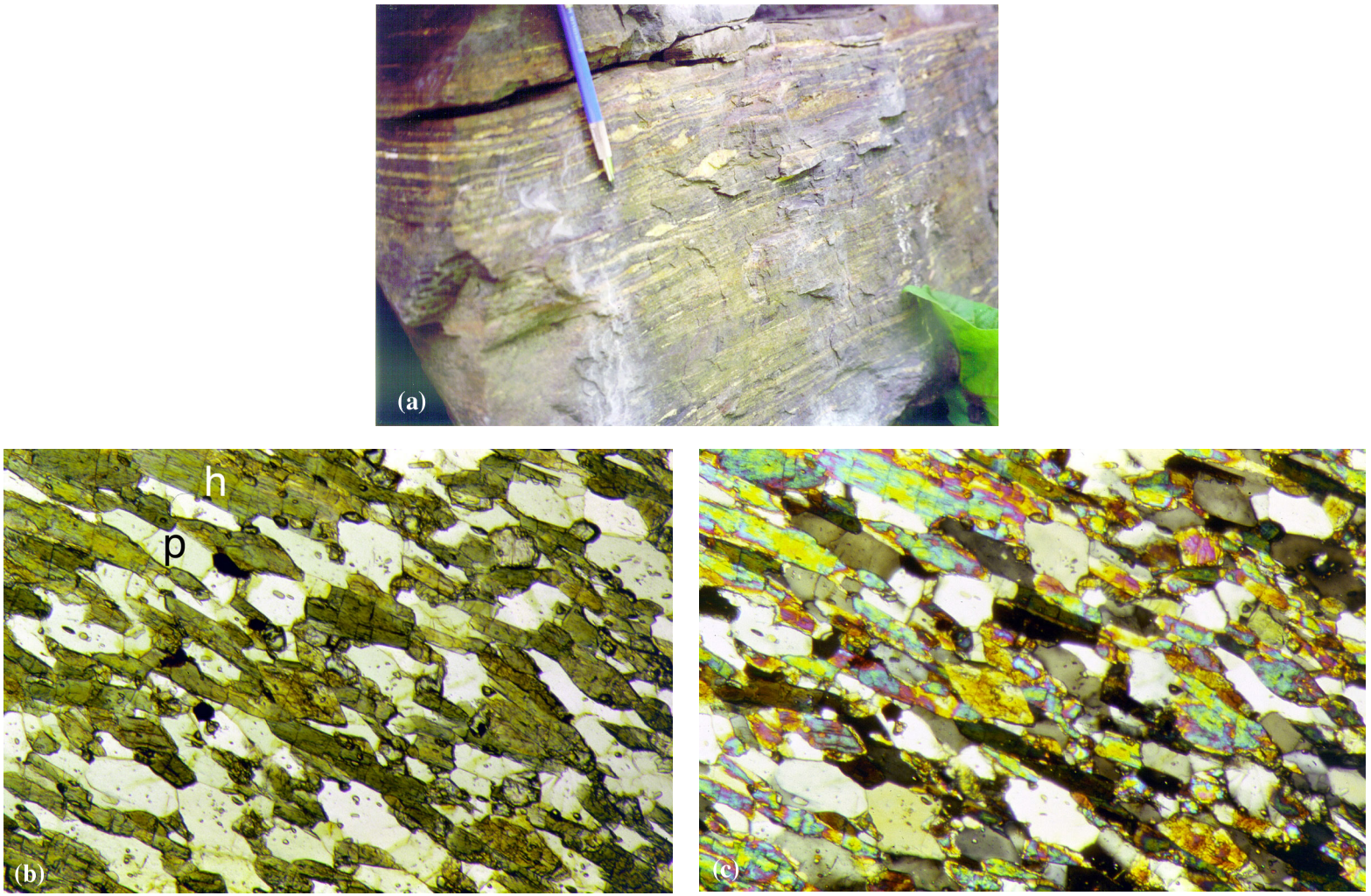

Figure 8. Photograph and photomicrographs of Poor Mountain Amphibolite. (a) Photograph of typical Poor Mountain Amphibolite outcrop along U.S. 221. (b) Plane light photomicrograph of a Poor Mountain Amphibolite sample from the Glenwood 7.5-minute quadrangle. Abbreviations are as follows: p-plagioclase, h-hornblende. (c) Crossed polarized photomicrograph of the same area in thin section as shown in (b). Width of field for (b) and (c) is 1.7 mm.

primary goal in the presentation of the chemical data is to show the strong agreement between samples collected as part of this study and those collected southwest of the study area. Amphibolites and amphibole gneisses of the Tallulah Falls Formation and Dysartsville Tonalite from the study area are plotted on all figures for comparison. Niggli *mg-c-*(*al-alk*) plots (Fig.9) of nonmigmatitic Poor Mountain Amphibolite samples define a trend that is at a high-angle to the proposed sedimentary trend of Leake (1964). This trend favors an igneous origin for the unit. The samples also indicate a tholeiitic source (Figs. 10 and 11) based on the fields of Irvine and Baragar (1971). The tectonomagmatic discriminant diagrams of Shervais (1982) and Meschede (1986) reconfirm the dominant mid-oceanic ridge basalt (MORB) chemistry of most samples. Based on this data set and plots on other tectonic discriminant diagrams (see Hatcher, this guidebook, his Figs. 5, 6, and 7) Poor Mountain Amphibolite most likely developed in an oceanic setting, possibly in an extensive deep-water basin along the Laurentian margin as suggested by Davis (1993). Presence of marble and clean quartzite farther southwest in South Carolina (Shufflebarger, 1961; Hatcher, 1969) remain difficult to explain if parts of the Poor Mountain Formation accumulated in deep water.

Migmatitic Poor Mountain Amphibolite (and Quartzite) occurs in synclines in the southeastern part of the exposed Mill Spring thrust sheet (immediate Brindle Creek footwall) in the South Mountains (Giorgis, 1999; Williams, 2000). Migmatization and metamorphic differentiation exploited the felsic layers in the amphibolite to enhance the layered character of the amphibolite, producing layered (stromatic) migmatite (STOP 9, this guidebook). Migmatization is sufficiently intense in places that layering is totally disrupted and only blocks of amphibolite remain in a more uniform matrix of totally homogenized granodioritic neosome-forming agmatite (Williams, 2000) (STOP 7, this guidebook). Similar relationships are present in the same structural position in the southwestern Brushy Mountains (Merschat and Kalbas, this guidebook).

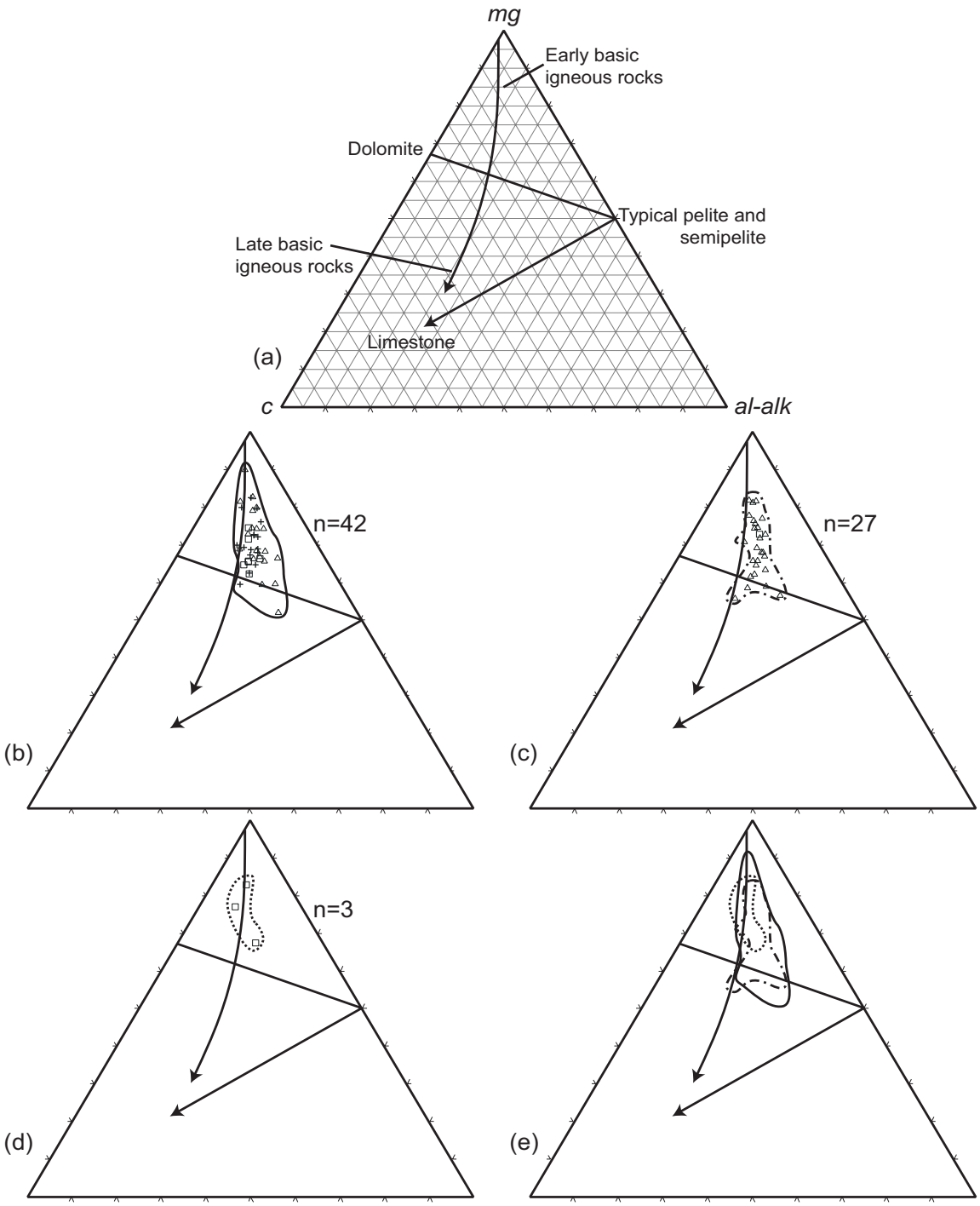

Figure 9. Ortho- and para-amphibolite discriminant diagram comparing amphibolites and amphibole gneisses of the Poor Mountain Formation, Tallulah Falls Formation, and Dysartsville Tonalite. Open triangles are data from Davis (1993), addition signs are data from Yanagihara (1994), and open boxes are data from Bream (1999). (a) *mg, c, al-alk* ternary diagram with igneous and sedimentary trends of Leake (1964). *mg* = 100*(MgO/(FeO + MnO + $2Fe_2O_3$)); *c* = CaO; *al-alk* = Al_2O_3-(K_2O + Na_2O), all in weight percent. Note that FeO and Fe_2O_3 were calculated assuming $Fe^{3+}/Fe^{2+} = 0.1$. (b) Poor Mountain Amphibolite. (c) Tallulah Falls Formation amphibolite and amphibole gneiss. (d) Dysartsville Tonalite amphibolite and amphibole gneiss. (e) composite field diagram of b, c, and d.

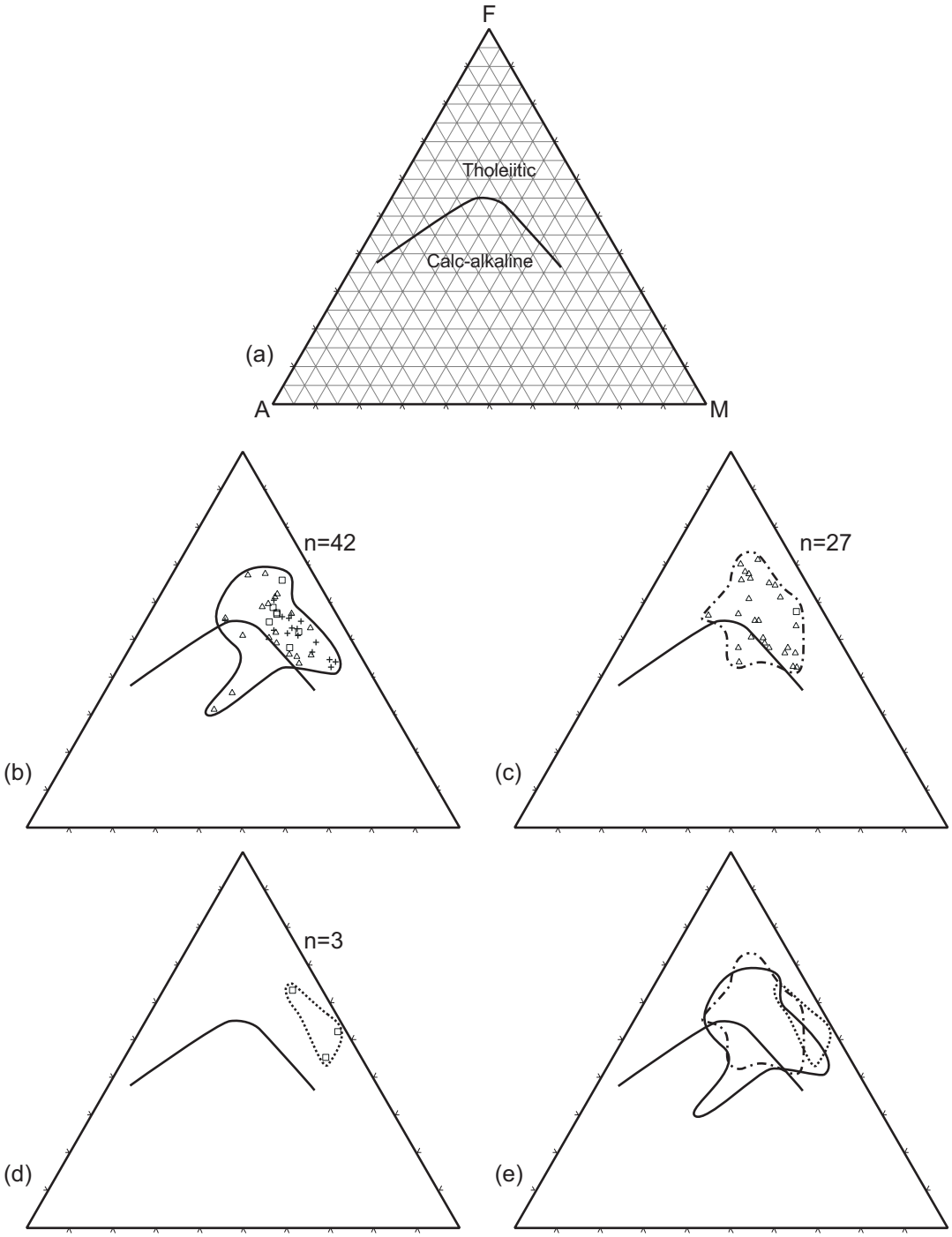

Figure 10. AFM diagram comparing amphibolites and amphibole gneisses of the Poor Mountain Formation, Tallulah Falls Formation, and Dysartsville Tonalite. Open triangles are data from Davis (1993), addition signs are data from Yanagihara (1994), and open boxes are data from Bream (1999). (a) AFM ternary diagram with the tholeiitic and calc-alkaline fields of Irvine and Baragar (1971). A = $Na_2O + K_2O$; F = FeO + 0.8998 Fe_2O_3; M = MgO, all in weight percent. Note that FeO and Fe_2O_3 were calculated assuming $Fe^{3+}/Fe^{2+} = 0.1$. (b) Poor Mountain Amphibolite. (c) Tallulah Falls Formation amphibolite and amphibole gneiss. (d) Dysartsville Tonalite amphibolite and amphibole gneiss. (e) Composite field diagram of b, c, and d.

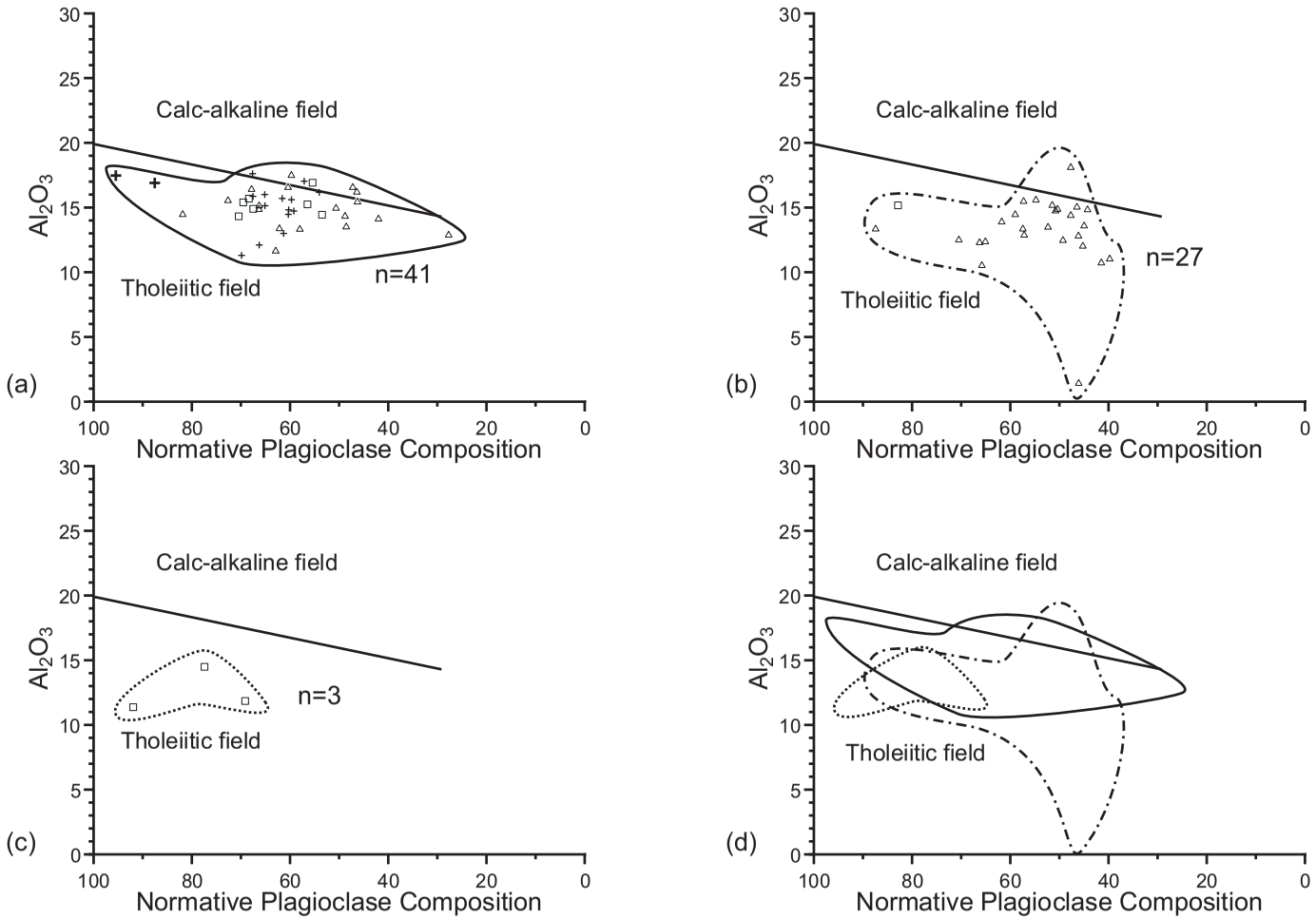

Figure 11. Plots of wt % Al_2O_3 versus normative plagioclase composition (P = 100*An/(An + Ab)) comparing amphibolites and amphibole gneisses of the Poor Mountain Formation, Tallulah Falls Formation, and Dysartsville Tonalite. The dividing line for the calc-alkaline and tholeiitic fields is from Irvine and Baragar (1971). All samples were plotted regardless of the MgO + CaO value. Open triangles are data from Davis (1993), addition symbols are data from Yanagihara (1994), and open boxes are data from Bream (1999). (a) Poor Mountain Amphbolite. (b) Tallulah Falls Formation amphibolite and amphibole gneiss. (c) Dysartsville Tonalite amphibolite and amphibole gneiss. (d) Composite field diagram of a, b, and c.

Poor Mountain Quartzite

Poor Mountain Quartzite in the Marion area consists of massive to layered feldspathic micaceous quartzite and metatuff (Fig. 12) interlayered near its base with laminated amphibolite. Layering in Poor Mountain Quartzite is considerably thicker (up to several m) than that in Poor Mountain Amphibolite. Parallel alignment of micas in Poor Mountain Quartzite defines a foliation and less commonly a lineation. Muscovite-rich outcrops of Poor Mountain Quartzite may be strongly schistose. Protolith of the quartzite component is graywacke or arkose (Fig. 5). The Poor Mountain Quartzite is white to light tan to light gray. Modal analyses of quartzite from the Marion area contain 30-60 percent plagioclase (An_{25-30}), 30-43 percent quartz, 0-20 percent biotite, 0-8 percent muscovite, 0-5 percent chlorite, and 0-2 percent microcline. Accessory minerals include garnet, epidote/clinozoisite, and opaque minerals. As first noted by Yanagihara (1994), two generations of muscovite appear in thin section. The first is most likely synmetamorphic and the second is probably retrograde as indicated by the random orientation of the coarser-grained set.

Ordovician Granitoids

Two granitoids were mapped in the Marion area: the Dysartsville Tonalite and the

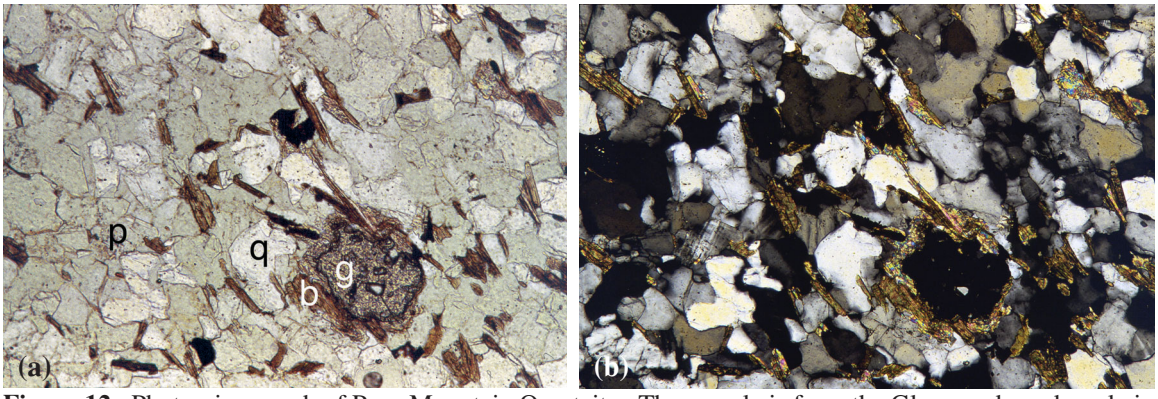

Figure 12. Photomicrograph of Poor Mountain Quartzite. The sample is from the Glenwood quadrangle in the Huntsville Branch of Stanfords Creek and is cut perpendicular to foliation and parallel to lineation. (a) Plane light photomicrograph. Note the rounded (detrital?) appearance of the garnet grain. Width of field is 1.7 mm. Abbreviations are as follows: g-garnet, q-quartz, p-plagioclase, b-biotite, m-muscovite. (b) Photomicrograph with polarizers crossed of the same area in thin section. Width of field is 1.7 mm.

Henderson Gneiss (Fig. 2). The structural relationship of the Henderson Gneiss to the Tallulah Falls Formation in the footwall of the Tumblebug Creek fault had previously not been mapped in the same detail or in the context provided by the western Inner Piedmont stratigraphy. Although not as extensive as the Henderson Gneiss, the Dysartsville Tonalite is significant both stratigraphically and structurally. Williams (2000) investigated the southeast contact of the Dysartsville Tonalite in the Glenwood 7 1/2-minute quadrangle. The contact of the Dysartsville Tonalite with the underlying Poor Mountain Amphibolite in the Sugar Hill quadrangle is the approximate contact between the "migmatitic" and "paragneiss and schist" units, respectively, of Hadley and Nelson (1971). Farther southwest in the Columbus Promontory the "migmatitic" unit of Hadley and Nelson (1971) also includes the lower part of the Tallulah Falls Formation. The two mappable granitoids are markedly dissimilar despite similar map patterns in the Marion area. The Henderson Gneiss is noted for its large feldspar augen, mostly microcline, and its unique augen texture. The Dysartsville Tonalite contains only trace amounts of microcline and is fine to medium grained.

Chemical analyses of the two units show that the Dysartsville Tonalite contains much less K_2O (0.65-1.71%) than other Inner Piedmont granitoids. Bulk chemical data from the Sugarloaf Mountain gneiss (Lemmon, 1973), the 438 Ma intrusive granitic gneiss (Lemmon, 1973), the Henderson Gneiss (Lemmon, 1973; Yanagihara, 1994; Bream, 1999), and the Devonian Walker Top Granite (Giorgis, this guidebook) have K_2O values ranging from 3.0 percent to 6.3 percent. Another difference found in the Dysartsville Tonalite is the much higher SiO_2 content (up to 82%). In addition to field observations during detailed mapping, the major element discriminant diagram of Werner (1987) further suggests that these units have igneous protoliths (Fig. 13). Sinha *et al.* (1989) divided southern and central Appalachian plutons into five age groups based primarily on geochronologic criteria: Late Proterozoic to Early Cambrian, Late

Cambrian to Early Ordovician, Middle to Late Ordovician, Silurian-Devonian, and Permian-Carboniferous. The Henderson Gneiss was included in the Late Cambrian to Early Ordovician group based on a 509 Ma whole rock Rb-Sr age and despite older U-Pb ages (Sinha and Glover, 1978). Based on new ion microprobe U-Pb zircon analyses, the Henderson has an age of ~470 Ma (Vinson, 1999; Vinson and Miller, 1999). Modally and chemically the Dysartsville Tonalite is most similar to the granitoids in the Late Cambrian to Early Ordovician group or those in the Silurian-Devonian group. We now know, however, that the Dysartsville Tonalite has a Middle Ordovician ~465 Ma high resolution ion microprobe age (Bream, unpublished data).

Dysartsville Tonalite

Structurally, this unit occurs within the highest thrust sheet of the Marion area and is in contact only with the Tallulah Falls Formation. The type area for the Dysartsville

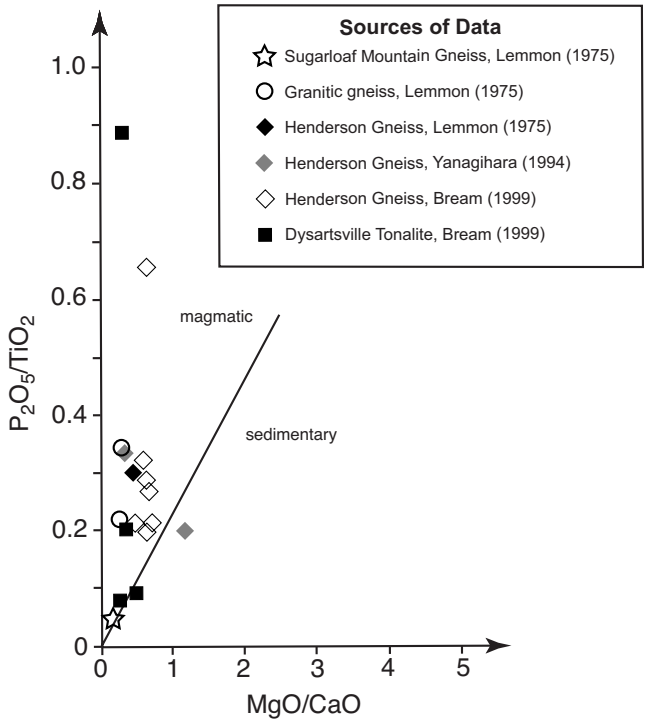

Figure 13. Major element discrimination diagram for distinguishing ortho- and paragneisses in metamorphic terranes. Plotted samples are from the western Inner Piedmont. Diagram after Werner (1987).

Tonalite is located in the Glenwood 7 1/2-minute quadrangle roughly parallel to Vein Mountain Road with excellent road exposures on U.S. 221 and in the CSX railroad cuts near and through Vein Mountain and Fero (all within the Glenwood 7 1/2-minute quadrangle). Goldsmith et al. (1988) mapped the Dysartsville Tonalite in the Charlotte 1° x 2° sheet as granitoid gneiss (termed the Dysartsville pluton on the tectonic map) and indicated the unit continues along strike to the northeast. Horton and McConnell (1991) compiled an exaggerated version of this unit and also used the Dysartsville pluton label. Adjacent to and southwest of the Marion area, Yanagihara (1994) noted that the upper Mill Spring complex contains abundant granitoid gneiss that is complexly folded with biotite gneiss, amphibolite, and minor pelitic schist and quartzite. Yanagihara (1994) mapped this as undifferentiated upper Mill Spring complex in the Sugar Hill and Shingle Hollow quadrangles southwest of Bream's (1999) mapping. The Dysartsville Tonalite mapped by Bream (1999) is probably related to Yanagihara's granitoid gneiss and is so depicted in our regional compilations. As previously noted, the quartzofeldspathic granofels unit of Whisnant (1975) in the Sugar Hill quadrangle has been separated into two units, one being Dysartsville Tonalite in the southeast corner of the quadrangle.

Dysartsville Tonalite is massive to foliated, fine to medium grained, and leucocratic (Fig. 14). Several amphibolite bodies, one containing an altered ultramafic body, have been mapped in the Dysartsville Tonalite (Bream, 1999; Williams, 2000). Smaller lenses and layers of amphibolite are also present but are not mappable. The Dysartsville Tonalite is locally called "blue granite." Limited gold production has been associated with veins and placer deposits in and near the body. Several small tourist gold panning camps and a larger failed gold mine are located in the Dysartsville Tonalite near Vein Mountain in the Glenwood quadrangle. The Dysartsville Tonalite plots as tona-lite on the IUGS igneous classification of Streckeisen (1976) and mostly as a tonalite in the normative Ab-Or-An diagram (Fig. 15) of Barker (1979). Normative corundum for the

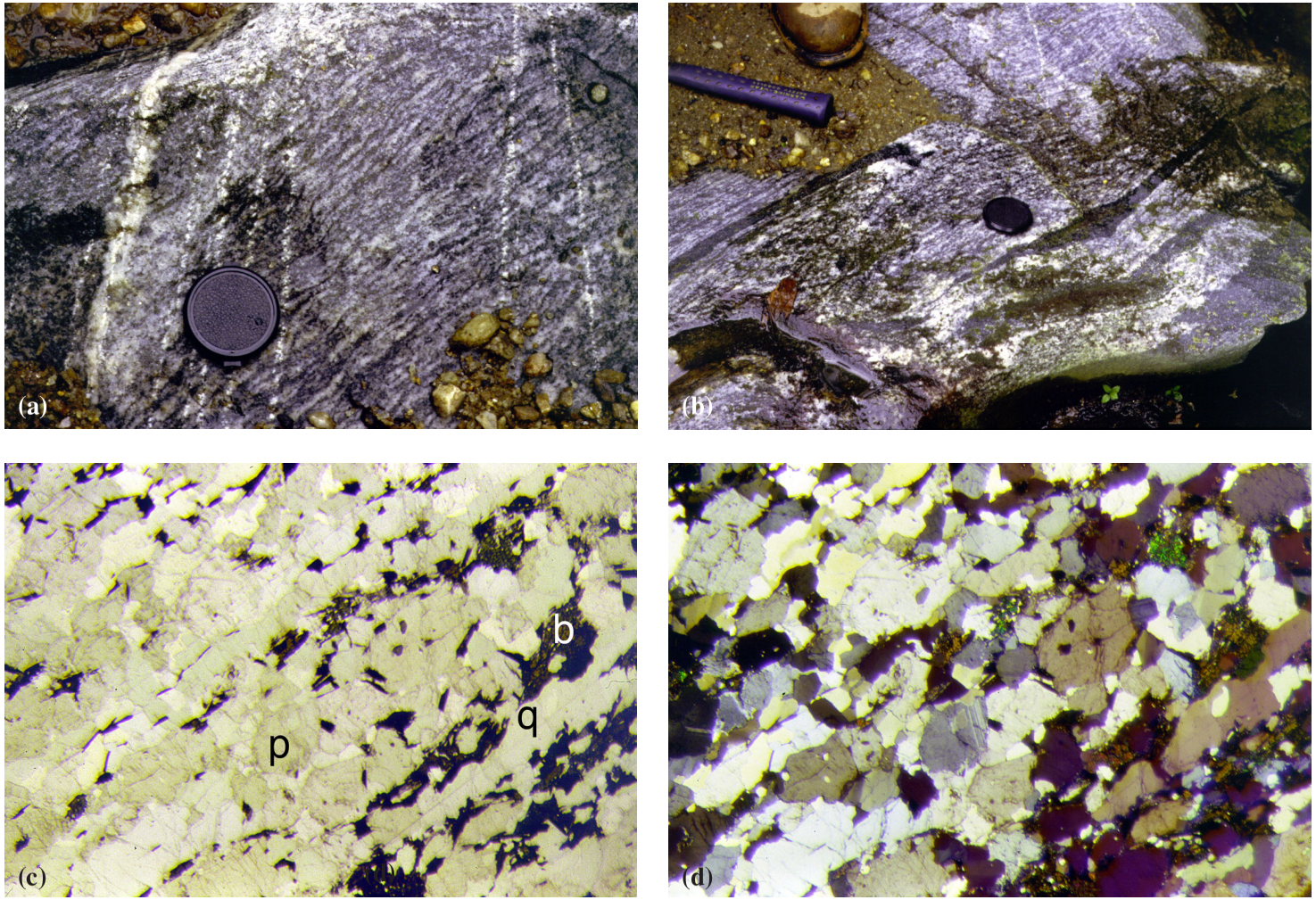

Figure 14. Photographs and photomicrographs of the Dysartsville Tonalite. (a) and (b) Typical outcrops of Dysartsville Tonalite. Photographs were taken north of Vein Mountain Road in South Muddy Creek. Note the amphibolite layers in (b). (c) Plane light photomicrograph of a Dysartsville Tonalite thin section. Abbreviations are as follows: b-biotite, p-plagioclase, q-quartz. Width of field is 11.1 mm. (d) Photomicrograph with polarizers crossed. Width of field is 11.1 mm. The sample is from the Glenwood quadrangle along U.S. 221 west of Wolf Mountain.

Dysartsville Tonalite is high, from 1.14 to 3.15 percent, and the $K_2O/(K_2O + Na_2O)$ ratios are low, ranging from 0.16 to 0.30. The modal composition of Dysartsville Tonalite is: 40-55 percent plagioclase (An_{20-25}), 30-43 percent quartz, 4-15 percent biotite, and 0-10 percent muscovite. Muscovite, where it is abundant, is coarse-bladed and overgrown by biotite. Biotite is present as subhedral and euhedral pleochroic grains from 0.1 to 1 cm long that define the foliation. Epidote is colorless, commonly present as aggregates, and often forms bands with biotite and other accessory minerals along the foliation. Common accessory minerals are magnetite, pyrite, sphene, zircon, apatite, and allanite. Outcrops of this unit typically contain both granoblastic and lepidoblastic textures, often in the same outcrop.

Henderson Gneiss

The Henderson Gneiss has an outcrop area of ~5,000 km^2 in the North and South Carolina Inner Piedmont. Usually in locations where the Henderson Gneiss is widest in outcrop, it forms spectacular cliffs such as those in the Columbus Promontory at Chimney Rock. Henderson Gneiss underlies Hickorynut Mountain (elevation 976 m or 3,200 ft) in the Sugar Hill quadrangle, one of the highest points in the greater Marion area. Henderson Gneiss occurs only in the hanging wall of the Tumblebug Creek and Stumphouse Mountain faults. It is likely that the Henderson Gneiss was emplaced as a single large thrust sheet, consistent with the interpretations of Liu (1991) and Davis (1993). Explanation of the current distribution of Henderson Gneiss as a product of southwest-directed sheath folding was entertained by Bream (1999) and Hatcher (this guidebook). Goldsmith et al. (1988) identified several bodies to the east and southeast of the Marion area as a possible shallow-level, less sheared phase of Henderson Gneiss. Giorgis (1999), Williams (2000), and Bier (2001) concluded this is a separate unit, now called Walker Top Granite (Giorgis et al., this guidebook). See Bream (this guidebook) for a review of Henderson Gneiss geochronology and interpretations.

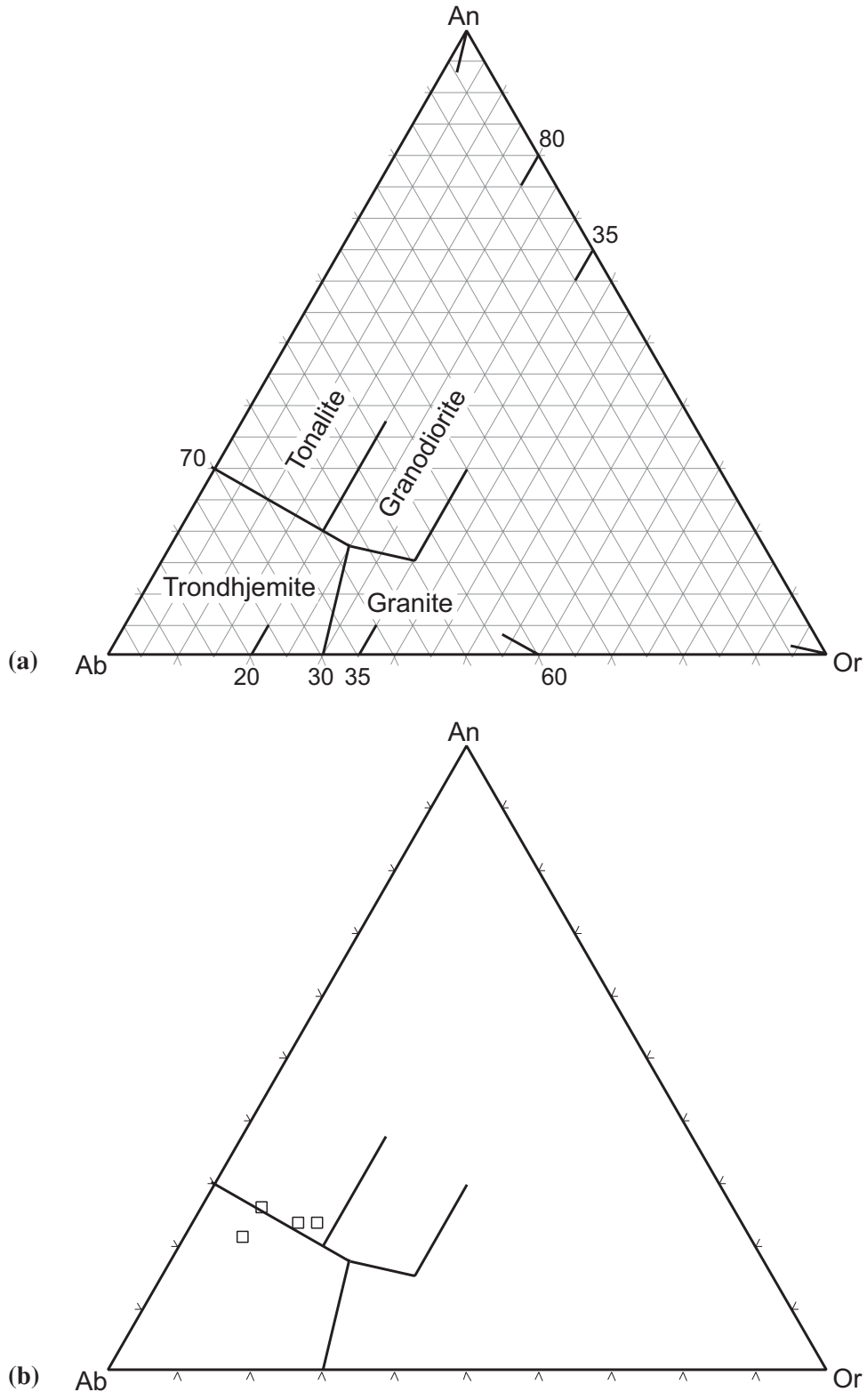

Figure 15. Anorthite (An)-Orthoclase (Or)-Albite (Ab) normative feldspar ternary diagram. Data are from Bream (1999). (a) Normative ternary diagram after Barker (1979). (b) Dysartsville Tonalite samples.

Using the IUGS classification (Streckeisen, 1976), the Henderson Gneiss is mostly monzogranite, but a few samples plot in the granodiorite, tonalite, and quartz monzodiorite fields (Fig. 16). The distinctive 1- to 3-cm augen in the Henderson Gneiss (Fig. 17) are mostly individual crystals or clots of microcline and less frequently plagioclase. Myrmekite commonly comprises the rims of most of the augen. Based on textural evidence and the definitions provided by Shelley (1964), Lemmon (1973) concluded that the myrmekitic texture in the Henderson Gneiss is either syn- or post-tectonic. Lemmon (1973) also concluded that the groundmass quartz, microcline, and plagioclase surrounding the augen clearly prove that the augen are porphyroclasts. Henderson Gneiss thin sections contain 30-40 percent plagioclase (An_{15-22}), 18-28 percent quartz, 13-21 percent biotite, and 17-26 percent microcline. Accessory allanite and sphene occur in all samples.

Other Rock Units

Altered ultramafic bodies, small granitoids, pegmatite, vein quartz, and Quaternary deposits also occur in the western Inner Piedmont in the Marion area. Ultramafic bodies are small and often occur in or near the Dysartsville Tonalite. The small granitoid bodies are mostly unmappable. Whisnant (1975) delineated five granodiorite intrusions in the Sugar Hill quadrangle that are mineralogically similar to those in the Glenwood quadrangle. Pegmatites are present in most units and are likely related to a post-peak metamorphic intrusive event as suggested by Yanagihara (1994), but there is also an earlier deformed suite. Vein quartz is also present in most units but is especially abundant in both Henderson Gneiss and Dysartsville Tonalite. Quaternary alluvium is also present throughout the western (and eastern) Inner Piedmont. Other Quaternary units that are present but mostly not large enough to map include colluvium, stream terraces, debris flows, talus, and landslides.

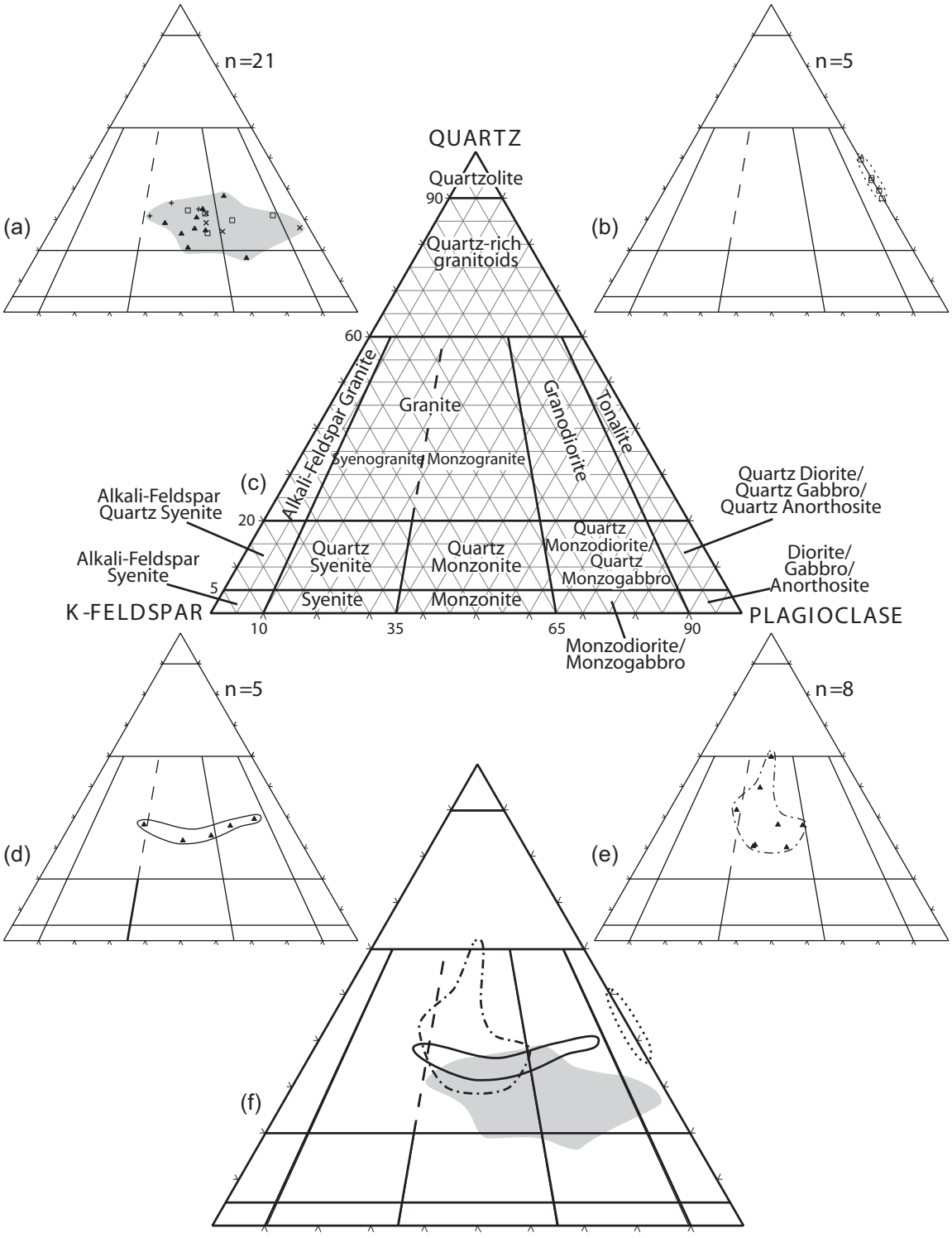

Figure 16. IUGS modal classification of granitoid units of the western Inner Piedmont. Triangles are data from Lemmon (1973), addition signs are data from Yanagihara (1994), crosses are data from Whisnant (1975) and open boxes are from Bream (1999). (a) Henderson Gneiss. (b) Dysartsville Tonalite. (c) IUGS igneous classification after Streckeisen (1979). (d) Granitic gneiss within Henderson Gneiss. (e) Sugarloaf Mountain Gneiss. (f) Composite field diagram of a, b, d, and e.

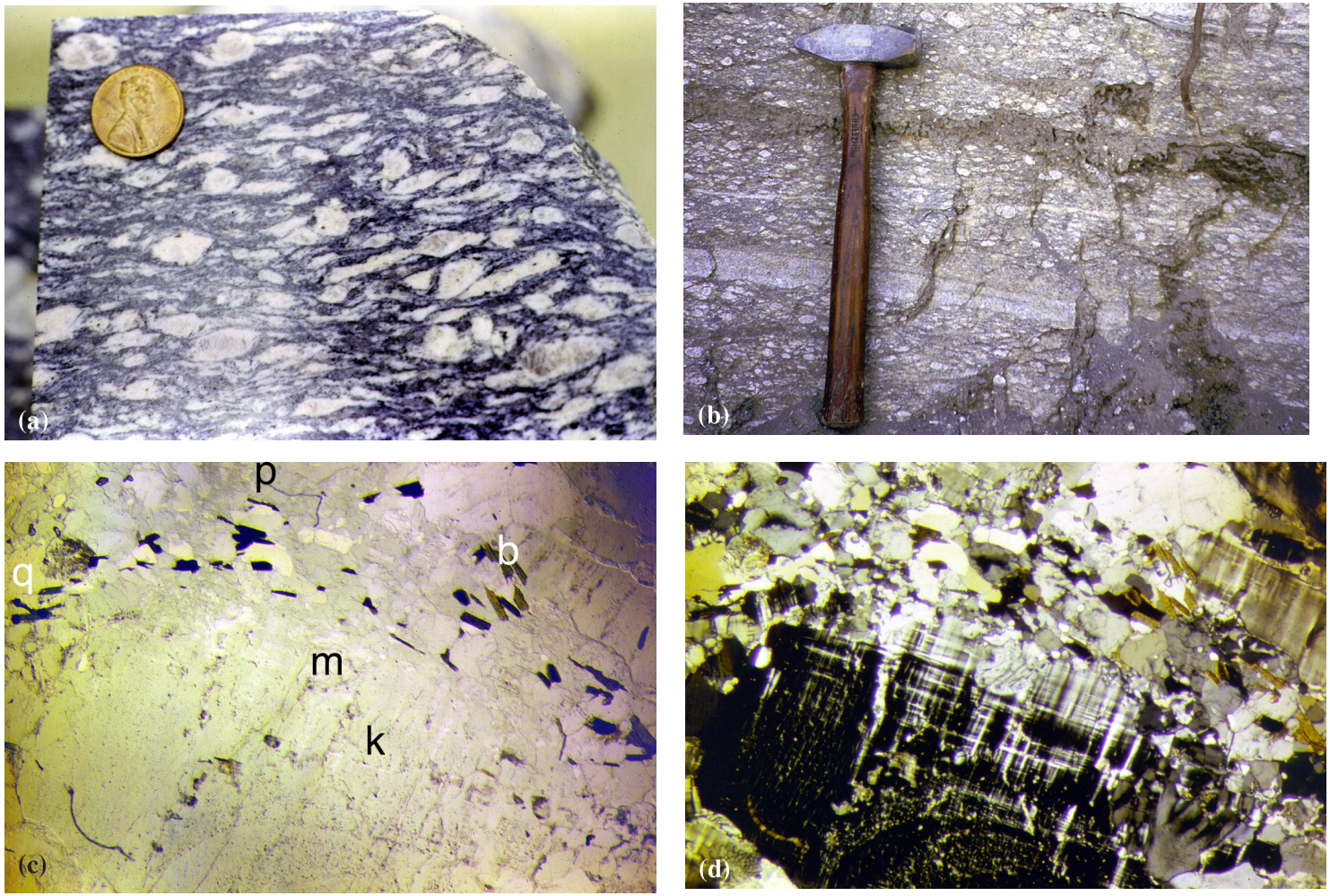

Figure 17. Photographs and photomicrographs of the Henderson Gneiss. (a) Polished hand sample from the Hendersonville quarry. (b) Typical saprolite outcrop of Henderson Gneiss near Heddrick Knob in the Sugar Hill 7.5-minute quadrangle. (c) Plane light photomicrograph. Abbreviations are as follows: b-biotite, k-K-feldspar, m-myrmekite, p-plagioclase, q-quartz. Width of field is 4.25 mm. (d) Photomicrograph with polarizers crossed. Width of field is 4.25 mm. The sample is from the Sugar Hill quadrangle on the ridge south of the Second Broad River and north of Mud Cut Road.

Eastern Inner Piedmont—Brindle Creek Thrust Sheet

Lithologies present in the South Mountains include metagraywacke/biotite gneiss and aluminous schist. Goldsmith et al. (1988) mapped biotite gneiss and large amphibolite bodies to the east and northeast of the South Mountains. Walker Top and Toluca Granites occur as mappable plutons and disseminated pods throughout the hanging wall of the Brindle Creek thrust sheet.

Aluminous schist-Metagraywacke assemblage

The sedimentary sequence throughout the eastern Inner Piedmont is dominated by metapelite (aluminous schist) with a minor metapsammite (metagraywacke) component (~25%).

Metapelite

The aluminous schist unit thickens dramatically in the hanging wall of the Brindle Creek thrust (Giorgis, 1999; Bier, 2001). This thickness increase could be related to an original depositional thickness change or to complex folding. The aluminous schist unit contains sillimanite schist and sillimanite gneiss in the South Mountains. Fresh sillimanite schist and gneiss are gray to grayish-brown purple and weather to tan, yellow ochre, and purple-brown saprolite (Fig. 18). The well-developed foliation is defined by parallel alignment of micas—predominantly muscovite—sillimanite, and quartz. Sillimanite (up to 5 cm) occurs in foliation-concordant mats, rarely displaying a strong lineation. Modal analyses of aluminous schist reveal a mineral assemblage of muscovite + quartz + plagioclase (An_{20-35}) + sillimanite + biotite + garnet ± tourmaline. Accessory chlorite and epidote occur as retrograde alterations of biotite and plagioclase, along with trace zircon, apatite, and opaque minerals. Muscovite occurs both as large grains (1-3 mm) and as fine-grained (0.2 mm) alterations within sillimanite mats. Both fibrolitic and prismatic sillimanite were recognized in thin sections. Fibrolite is commonly associated with muscovite layers, while prismatic sillimanite occurs throughout the sections.

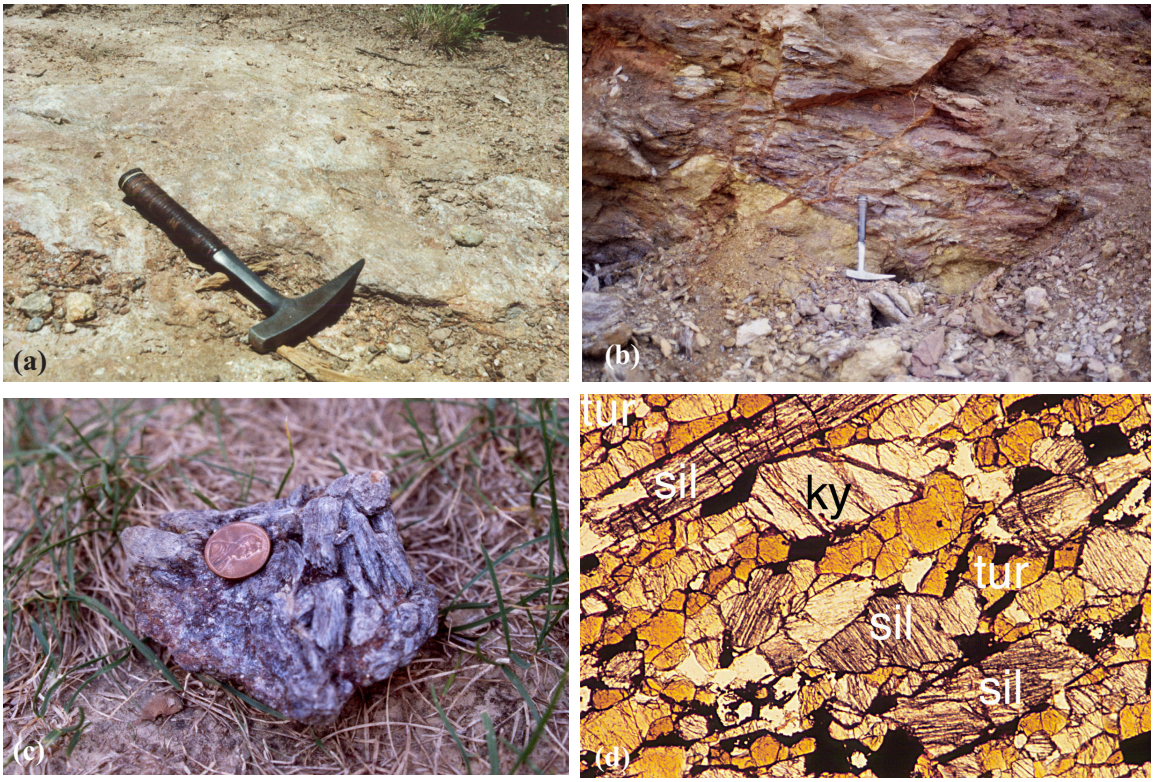

Figure 18. Photographs and photomicrograph of eastern Inner Piedmont sillimanite schist. (a) Sillimanite schist outcrop near Horse Ridge. (b) Sillimanite schist saprolite near Dogwood Stamp Mountain, Benn Knob 7.5-minute quadrangle. (c) Hand specimen from Benn Knob 7.5-minute quadrangle. Sillimanite pseudomorphs after kyanite. (d) Thin section from Huckleberry Mountain, Benn Knob quadrangle. Prismatic sillimanite (sil), kyanite (ky), and anhedral tourmaline (tur). Field of view is 1.7 mm.

Metapsammite

In outcrop, the metagraywacke-biotite gneiss is gray; composed of quartz, plagioclase, and biotite; and contains migmatitic quartzofeldspathic leucosome. It is interlayered with biotite-muscovite schist (Fig. 19). Calc-silicate pods and layers are rare and were observed as float. The well-developed foliation is defined by the alignment of biotite, muscovite, and quartz. Alternating quartzofeldspathic and biotite-muscovite schist layers from one centimeter to several meters thick define compositional banding. Modal analyses of metagraywacke reveal a mineral assemblage of plagioclase (An_{20-30}) + quartz + biotite + muscovite $\pm$ sillimanite ± garnet. Zircon and chlorite occur as accessory or trace minerals. Biotite (0.5-3 mm) and muscovite (0.25-1.5 mm) define the foliation and are segregated into layers that alternate with quartz (0.1-2 mm) and plagioclase (An_{20-30}) layers 0.2 to 3 mm thick. Biotite frequently defines microscale structures.

Granitoids

Two granitoids are recognized in this part of the eastern Inner Piedmont: Toluca and Walker Top Granites.

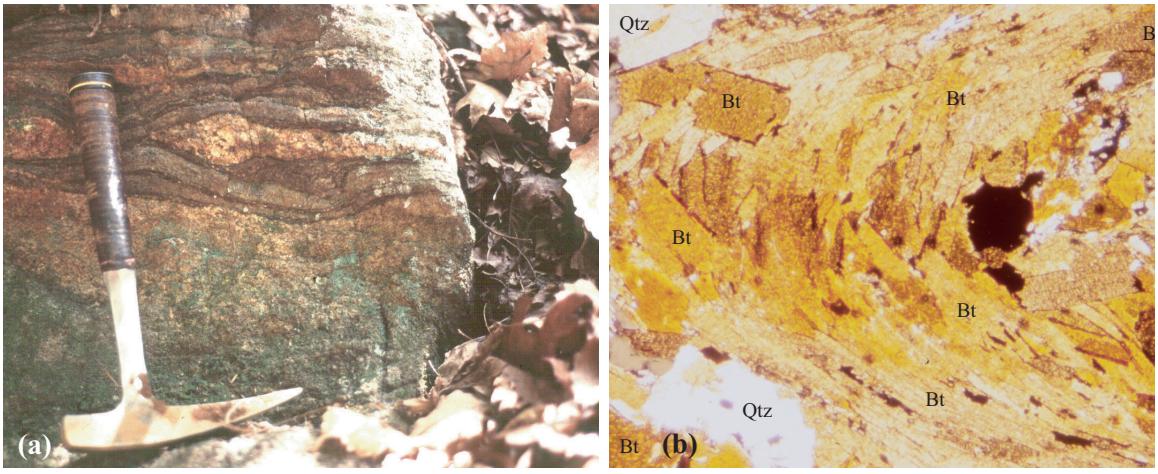

Figure 19. Photograph and photomicrograph of eastern Inner Piedmont metagraywacke. (a) Migmatitic metagraywacke near Gibbs Gap, Benn Knob 7.5-minute quadrangle. (b) Photomicrograph of a sample from Shinny Creek, Benn Knob 7.5-minute quadrangle. Microfold defined by biotite. Field of view is 4.25 mm. Qtz-quartz, Bt-biotite.

Toluca Granite

Keith and Sterrett (1931) originally recognized the Toluca Granite (Goldsmith et al., 1988) and called it the Whiteside Granite. Griffitts and Overstreet (1952) subdivided the Whiteside Granite into the Toluca Quartz Monzonite and the Cherryville Quartz Monzonite. The Toluca Quartz Monzonite was renamed Toluca Granite by Goldsmith et al. (1988) to adhere to Streckeisen's (1976) IUGS classification (Fig. 20). Preliminary ion microprobe analyses yield zircon and monazite ages ranging from 370 to 385 Ma for the Toluca Granite (Mapes, 2002). Griffitts and Overstreet (1952) noted that individual Toluca Granite bodies range from cm to hundreds of meters thick, and from a few meters to kilometers long. The size of bodies mapped in the South Mountains is also widely variable, possibly indicating deformed sills rather than one large contiguous pluton. Toluca Granite is medium gray and weathers to light gray and tan saprolite. The unit is weakly to moderately foliated (Fig. 21), and, although bodies parallel the foliation of the enclosing aluminous schist and paragneiss, the foliation within the Toluca Granite does not always parallel the contacts. This may be the product of folding, incomplete transposition, relict magmatic foliation, or rheological differences between granite and country rock. Foliation is defined by parallel alignment of muscovite, biotite, and quartz.

Modal analyses of Toluca Granite reveal a mineral assemblage plagioclase (An_{25-35}) + microcline + quartz + muscovite + biotite + garnet. Accessory or trace minerals include sillimanite, zircon, monazite, xenotime, apatite, and opaque minerals. The Toluca Granite is medium- to coarse-grained (1-4 mm) and usually equigranular but sometimes is porphyritic with megacrysts of either garnet or K-spar. Myrmekite forms rims around some microcline megacrysts. Bulk energy dispersive X-ray fluorescence analyses, with major elements plotted on Werner's (1987) tectonic discrimination diagram, supports the interpretation of Toluca Granite having an igneous protolith (Fig. 22).

Walker Top Granite

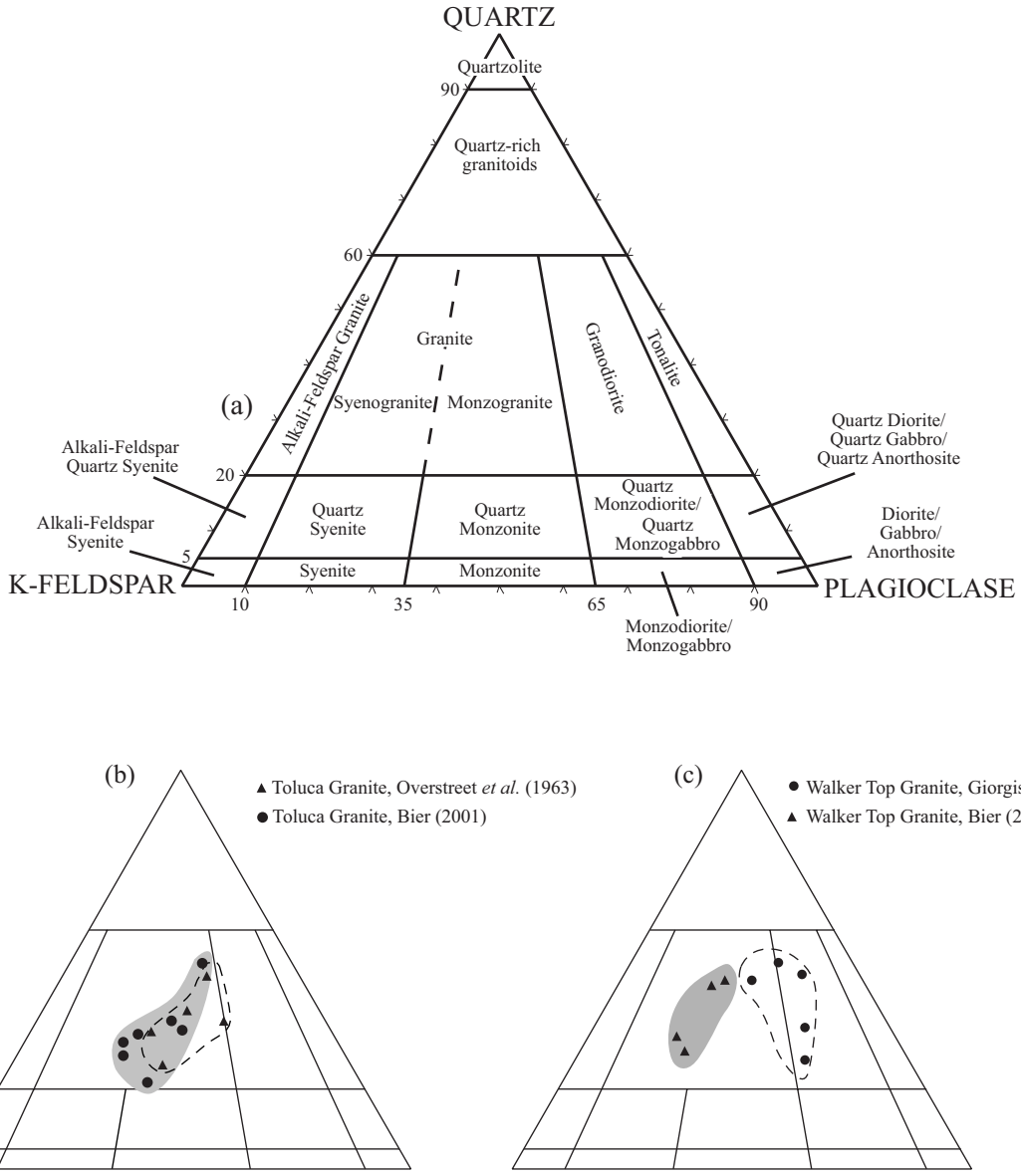

Figure 20. IUGS modal classification of Toluca Granite and Walker Top Granite. (a) IUGS igneous classification after Streckeisen (1976). (b) Toluca Granite. Dashed line encloses data from Overstreet et al. (1963b). (c) Walker Top Granite. Dashed line encloses data from Giorgis (1999). The difference in data sets is attributed to different point-counting techniques (Giorgis, 1999; Bier, 2001).

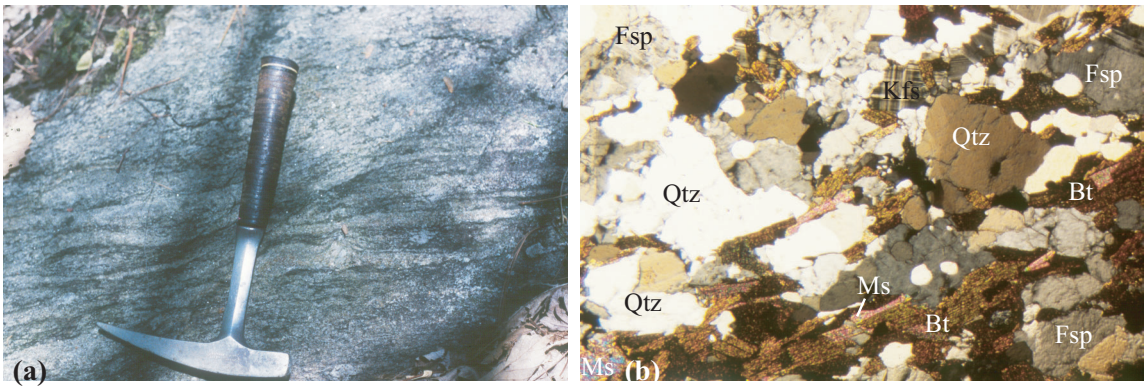

Figure 21. Photograph and photomicrograph of the Toluca Granite. (a) Toluca Granite near Black Mountain, Benn Knob 7.5-minute quadrangle. (b) Photomicrograph of a Toluca Granite sample thin section. Field of view is 1.7 mm. Fsp-feldspar (plagioclase), Kfs-Kfeldspar (microcline), Qtz-quartz, Ms-muscovite, Bt-biotite.

The Walker Top Granite was mapped by Goldsmith et al. (1988) as medium to dark gray, less foliated, less sheared, garnetiferous Henderson Gneiss. The Walker Top Granite and Henderson Gneiss both contain large dominantly microcline with some plagioclase (An_{20-30}) megacrysts surrounded by a coarse-grained equigranular groundmass of biotite, two feldspars, and quartz. Walker Top Granite was first recognized as a separate unit from Henderson Gneiss by spatial and textural differences. Feldspar megacrysts in the Henderson Gneiss are mostly lenticular (as part of an S-C fabric), whereas the feldspar megacrysts in Walker Top Granite are euhedral to subhedral (Fig. 23). Bulk chemical analyses suggest a strong genetic correlation between the Henderson Gneiss and the Walker Top Granite (Giorgis, 1999; Giorgis et al., this guidebook). A new high resolution ion microprobe $^{238}U/^{206}Pb$ age for Walker Top Granite is 366 ± 3 Ma (Mapes, 2002; Giorgis et al., this guidebook).

Megacrysts in Walker Top Granite are oriented parallel to the regional foliation (Merschat and Kalbas, this guidebook), but Goldsmith et al. (1988) concluded the foliation resembles a flow pattern rather than deformational foliation. The weak foliation in the groundmass is defined by parallel alignment of biotite (1-3 mm), muscovite (0.5-2 mm), quartz (0.5-3 mm), and plagioclase (0.5-2 mm). The mineral assemblage in Walker Top Granite is microcline + plagioclase (An_{20-30}) + quartz + biotite + muscovite, with

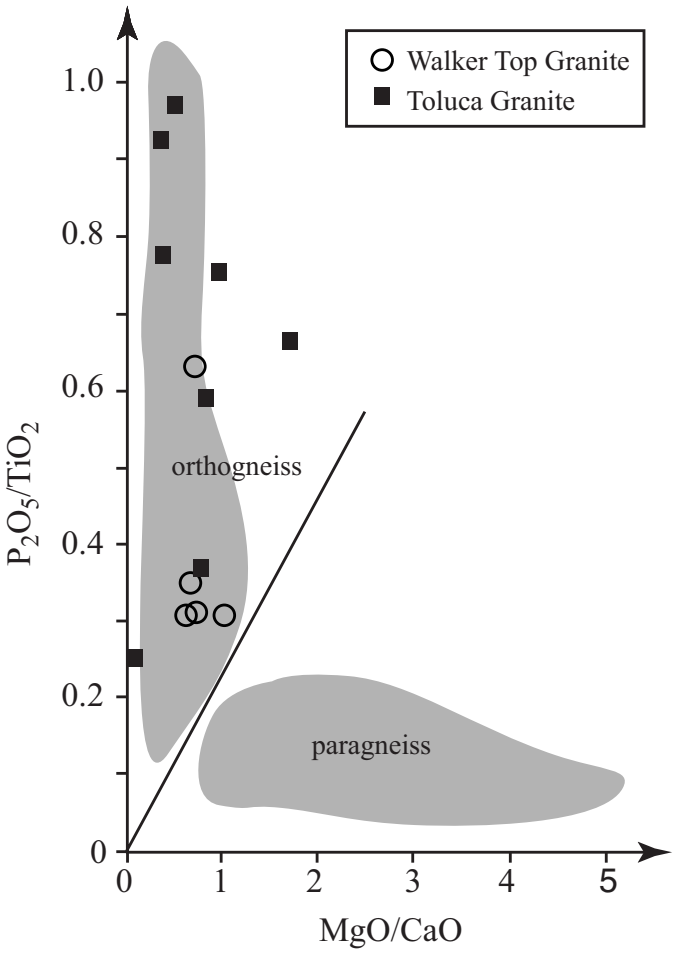

Figure 22. Major element discrimination diagram distinguishing ortho- and paragneisses in metamorphic terranes. Shaded areas are data from the Saxonian granulite massif used to construct the diagram. Diagram and fields from Werner (1987).

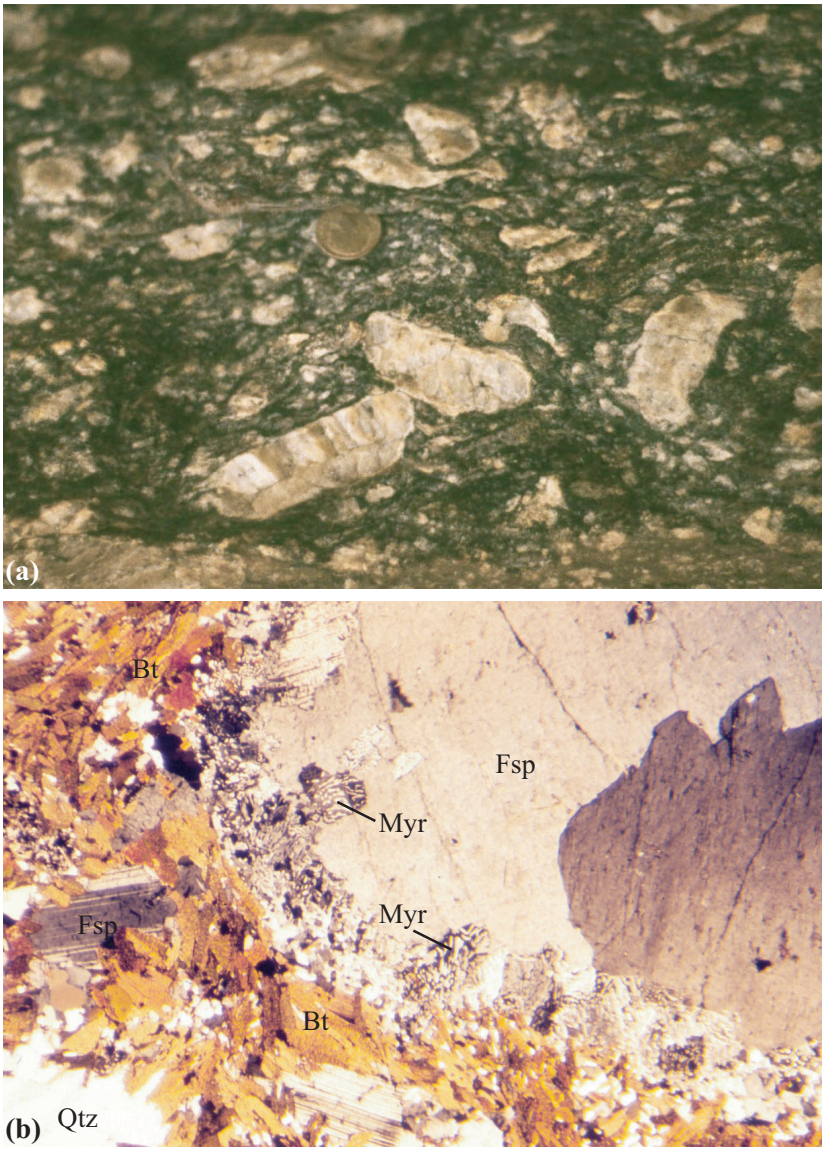

Figure 23. Photograph and photomicrograph of Walker Top Granite. (a) Walker Top Granite near Richland Mountain, Benn Knob 7.5-minute quadrangle. (b) Photomicrograph of a sample thin section obtained near Camp Knob, Benn Knob 7.5-minute quadrangle. Microcline megacryst with myrmekitic rim in a matrix of plagioclase (An_{20-30}), quartz, and biotite. Field of view is 11.1 mm. Bt-biotite, Fsp-feldspar, Myr-myrmekite, Qtz-quartz.

trace zircon, apatite, epidote-clinozoisite, and opaque minerals. Microcline and plagioclase occur both as megacrysts and part of the coarse-grained groundmass. Microcline megacrysts (2-6 cm), which are much larger than plagioclase megacryts (1-4 cm), are rimmed by myrmekite. Modal analyses reveal that the Walker Top Granite ranges from granodiorite to granite (Fig. 20). Major elements from bulk X-ray fluorescence analyses of Walker Top Granite, when plotted on Werner's (1987) major element discrimination diagram (Fig. 22), support a magmatic origin for Walker Top Granite.

METAMORPHISM

Electron microprobe (EMP) analyses were performed on seven garnet-mica schist samples from the Marion and South Mountains area (Fig. 2). The metapelite and metapsammite samples chosen for EMP analysis are fine- to medium-grained (<0.25-1 mm), except for garnet (up to 2 cm diameter) and kyanite (up to 1 cm), and have a well-developed foliation. The following mineral assemblage is present: muscovite + biotite + garnet + quartz + plagioclase (An_{20}) + staurolite (NW of the ky-sill isograd only) + kyanite and/or sillimanite + ilmenite + magnetite. Garnets are dark red, mostly almandine (~80%), partially fractured, and contain minor chlorite alteration. Garnets occur as euhedral to subhedral porphyroblasts and commonly contain inclusions of biotite, ilmenite, magnetite, chlorite, and quartz. Accessory minerals include zircon, apatite, and allanite. Biotite and garnet chemistries are similar to analyses from other amphibolite-grade terranes. Samples containing sillimanite lack significant amounts of K-feldspar, placing the assemblage below the second sillimanite isograd of Chatterjee and Johannes (1974). Textural evidence suggests that staurolite was consumed, partially in rocks NW of our staurolite + kyanite-kyanite isograd and completely SE of this isograd, by terminal staurolite reactions (e.g., Pigage and Greenwood, 1982; Dutrow and

Holdaway, 1989). The presence of mostly mesoscale migmatites above the middle kyanite zone demonstrates that much of this area was at or near minimum melt conditions. The presence of kyanite and sillimanite pseudomorphs after kyanite suggests that kyanite formed before sillimanite where both are present. The location of the staurolite + kyanite-kyanite isograd in the footwall of the Mill Spring fault is defined by the first appearance of prismatic kyanite, commonly at high angles to the dominant foliation.

The location of the kyanite-sillimanite isograd was determined by the first occurrence of fibrolitic sillimanite in aluminous schist. Where kyanite or sillimanite is the dominant prograde phase, growth does not reveal a preferred orientation with regard to the local structures; smaller and partially resorbed kyanite, however, is typically oriented parallel to regional foliation and lineation. Sillimanite is present in the Mill Spring fault hanging wall either as unoriented mats in proximity to the kyanite-sillimanite isograds or prismatic rhombs near the core of the Inner Piedmont. The lack of consistent orientation of sillimanite needles with respect to dominant mineral lineation, the presence of kyanite oriented at high angles to smaller partially resorbed kyanite grains, and the penetrative foliation suggest that growth of these minerals occurred toward the end of major penetrative deformation (D_2). Most garnets here are zoned and relatively inclusion-poor at the rims, whereas the cores commonly contain numerous small inclusions. Lemmon (1973) suggested that this textural relationship, in addition to the presence of small euhedral inclusion-poor garnets, indicates two prograde metamorphic events. Zoning profiles of garnet are relatively flat for the interiors with increasing almandine and spessartine content and decreasing grossular content toward the rims, suggesting a single event of diffusional growth and equilibrium (Spear, 1993) for garnets from both the staurolite-kyanite and sillimanite zones. Considering the zoning profiles, the textures and morphologies are more likely the result of

decompressional post-thermal peak reequilibration, as noted by Spear et al. (1990) in southwest New Hampshire and suggested by Davis (1993) for metapelite samples from the Sugarloaf Mountain thrust sheet in the North Carolina Columbus Promontory area.

A single garnet-amphibolite from the Tallulah Falls Formation in the Mill Spring fault footwall was chosen for analysis. This lithology is not abundant in the study area and differs in mineral assembage from other amphibolites associated with the Tallulah Falls Formation. The mineral assemblage for this sample is hornblende + garnet + quartz + ilmenite + biotite + plagioclase (An_{25}) + magnetite. The foliation, defined by hornblende and quartz (both between 0.5 and 2 mm long), wraps subhedral to euhedral garnet porphyroblasts (3-5 mm in diameter). The garnets are dark red, mostly almandine (55-65%) with up to 30 percent grossular component, highly fractured, and inclusion-rich. Quartz, biotite, apatite, magnetite, and ilmenite inclusions are present within the garnets and are commonly oriented at high angles to the dominant foliation. Zoning in garnets of the garnet-amphibolite is characterized by an increase in the spessartine end-member toward the rims and suggests diffusional growth in response to net transfer reactions most likely with amphibole.

Analytical Methods

Detailed chemical analyses of garnet, biotite, hornblende, and plagioclase were performed using the four-spectrometer CAMECA SX-50 EMP at the University of Tennessee–Knoxville. An acceleration voltage of 15 kV and a beam current of 20 nA were used for all analyses. Beam size was varied depending on the mineral phase analyzed: a 5 μm beam was used for biotite, hornblende, and plagioclase; and a 2 μm beam was used for garnet. A peak counting time of 20 seconds was used for all analyses, except for Fe in plagioclase and Na in garnet where a counting time of 30 seconds was used. Some garnet cation totals indicated the presence of Fe^{3+}, but all iron was calculated as Fe^{2+} due to uncertainty in Fe^{3+} electron microprobe calculations (Sobolev et al., 1999).

Analyses chosen for pressure and temperature estimates were obtained from 5-point line traverses across grain boundaries. The points were selected based on proximity to the rim boundaries, cation totals, and weight percent totals. In all cases, analyses were within 6 μm of the grain boundary and mineral pairs used for the PT estimates were no more than 10 μm apart.

Pressure and Temperature Estimates

The mineral assemblages present in the paragneisses delimit the pressure and temperature conditions to the stable staurolite, kyanite, and sillimanite fields of the aluminum silicate phase diagram (Holdaway, 1971) and KFMASH (SiO_2-Al_2O_3-MgO-FeO-K_2O-H_2O) system. To further constrain the fields for the footwall and hanging wall in the area, temperature estimates were calculated using EMP analyses of garnet and biotite pairs in the garnet-mica schist samples. Due to the presence of Mn and Ca, the Berman (1990) modification of the Ferry and Spear (1978) temperature estimate model was chosen for the paragneiss samples. Fe-Mg exchange between garnet and hornblende is also commonly used to estimate temperatures for mafic schists (e.g., Ghent et al., 1983; Labotka, 1987). Temperatures in the garnet-amphibolite were estimated using the model of Perchuk et al. (1985). The modified GASP pressure estimate of Koziol (1989) was used for two samples with garnet, plagioclase, and biotite in contact with one another. Equilibrium conditions of 520 ± 25˚C and 5.1 ± 1 kbar and 645 ± 25˚C and 5.3 ± 1 kbar were determined for samples ME658 and BK959, respectively (the intersection of the median temperature and pressure was used for ME658). These pressures fall within the mid- to upper ranges of estimates for the western Inner Piedmont: 3.5-5.2 kbar for metapelite from the Sugarloaf Mountain thrust sheet in North Carolina (Davis, 1993) and 4.5-5.7 kbar for Alto allochthon metapelite in Georgia (Schumann, 1988). The estimated pressure for ME658 was assumed for the garnet-amphibolite sample in the kyanite field and the estimated pressure for BK959 was assumed for the remaining

samples in the sillimanite field lacking plagioclase in contact with the phases necessary to estimate pressures. Core temperature estimates obtained for biotite inclusions within garnet for the footwall metapelite are ~480˚C whereas rim temperature estimates for the same garnet are ~520˚C. This relationship indicates that the rim compositions reflect minimum prograde metamorphic conditions without complete retrograde or diffusional overprint. Mean temperature estimates for the samples range from 580 to 670 ˚C (Table 1). The variability in temperature estimates for individual samples is most likely a reflection of disequilibrium or net transfer between individual garnet-biotite and garnet-hornblende pairs rather than a temporal expression of metamorphic conditions or the pressures that were assumed for the footwall and hanging wall. If diffusion is a significant process at garnet rims, the kyanite zone temperature estimates from metapelite samples are underestimated, likely less varied than reported, and do not display a significant temperature gradient or necessitate a large amount of telescoping by post-metamorphic thrusting as suggested by Dallmeyer (1988) and Hopson and Hatcher (1988) for the Alto allochthon in Georgia.

Timing of Metamorphism and Deformation

The timing of deformation for the Inner Piedmont may be constrained using granitoid crystallization ages, monazite ages, zircon rim ages, and the crosscutting relationships of fabrics. The paucity of geochemical and geochronologic work in the North Carolina Inner Piedmont makes regional comparisons difficult; detailed work in the adjacent North Carolina eastern Blue Ridge, however, is abundant. Our timing and minimum metamorphic conditions correspond to the M3 event outlined by Abbott and Raymond (1984) for the Ashe metamorphic suite in northwest North Carolina. Based on our work, the peak Taconian event, M2 event of Abbott and Raymond (1984), is not preserved in garnet-biotite and garnet-amphibole rim compositions or zircon rim growth in North Carolina Inner Piedmont paragneisses. Minimum pressure and temperature

Table 1. Pressure and temperature estimates from a garnet amphibolite sample and several pelitic schist samples from the Marion-South Mountains area.

Sample	Temperature in °C	n	Pressure in kbar	n
ME658-core	480 (14)*	5		
ME658-rim	517 (21)*	8	5.1 (0.1)§	4
SH340	610 (26)†	6		
D255	657 (41)*	4		
D537	583 (55)*	3		
GW1	669*	1		
GW230	599 (12)*	2		
DY36	669 (83)*	6		
BK959	645*	1	5.3§	1

*Temperatures calculated using the Berman (1990) for model and 5.1 kbar footwall samples and 5.3 kbar for hanging wall samples.
†Temperatures calculated using Perchuk et al. (1985).
§Pressures calculated using Koziol (1989).

estimates are best explained with a single prograde event synchronous with zircon rim and monazite growth in and nearby the study area at ~350 Ma (Neoacadian; Dennis and Wright, 1997; Bream et al., 2001; Carrigan et al., 2001).

Discussion

Temperature and pressure estimates for garnet-biotite and garnet-amphibole rims in the Marion and South Mountains areas do not reveal systematic northwest to southeast increases across the kyanite-sillimanite isograd, Mill Spring fault, or Brindle Creek fault. We suspect that additional geothermobarometric work will also reveal modest pressure and temperature differences across the kyanite-sillimanite isograd and other plastic faults in the Inner Piedmont. The faults do not offset the gradual change in fabric orientation from the core of the Inner Piedmont to the highly aligned zone along the western flank, indicating that movement on the Mill Spring fault either predates or is coeval with major penetrative deformation and metamorphism. The conditions at which major displacement occurred on both faults likely approach the minimum conditions estimated for peak metamorphism. The temperature estimates in the study area do not show

appreciable telescoping by the Mill Spring fault, which implies that peak metamorphism also predates movement on the fault. The ~460 Ma crystallization age of the Dysartsville Tonalite (Bream, this guidebook) thus delimits the timing of metamorphism and displacement on the Mill Spring fault. The Dysartsville Tonalite is truncated by the Mill Spring fault and therefore must have crystallized prior to final movement on the fault. Taconian granulite facies metamorphism within the central Blue Ridge (Moecher and Miller, 2000) may not extend eastward into the Tugaloo terrane. The crystallization age of the Dysartsville Tonalite alone does not preclude Taconic deformation or metamorphism; however, recent geochronologic data (e.g., Dennis and Wright, 1997; Bream et al., 2001) indicate that there was significant thermal activity within the Tugaloo terrane during the Neoacadian.

STRUCTURAL GEOLOGY

Inner Piedmont rocks have been subjected to a complex deformational history, recording multiple episodes of folding and faulting. This section presents a deformational framework for the Inner Piedmont that addresses the relative timing of regional structures, using mesoscale and macroscale data. The analyzed area extends from the Brevard fault zone to the eastern Inner Piedmont and contains distinct changes in style, structural orientation, and displacement direction (Davis, 1993). Granitoid crystallization ages and U-Pb ages of monazite and zircon separates from the eastern Blue Ridge and Inner Piedmont help to delimit the timing of deformation. See Bream (this guidebook) for a summary of Inner Piedmont granitoid geochronology.

Structures parallel, normal, and oblique to the orogen have been recognized in the Inner Piedmont for decades (e.g., Reed and Bryant, 1964; Hatcher, 1972; Roper and Dunn, 1973; Griffin, 1974). Davis (1993) suggested that this structural pattern was a result of a “thrust-wrench partitioned deformation . . . and is a manifestation of an early

oblique convergence within the southern Appalachians." The deformational framework outlined by Davis (1993) and subsequently modified by Yanagihara (1994), Bream (1999), Giorgis (1999), Hill (1999), and Williams (2000) identifies five deformational events. Compilation of recent detailed mapping from the above workers along with that of Overstreet et al. (1963a, 1963b) also supports five deformational events, although slightly modified (Table 2).

This compilation has been divided into three domains for structural analysis using thrust sheets as primary tectonic units (Fig. 24). The Brevard fault zone bounds Domain I to the northwest and the Mill Spring thrust forms the southeast boundary. The Mill Spring thrust to the west and the Brindle Creek thrust to the east form the boundary of Domain II. Domain III is composed of the Brindle Creek thrust sheet hanging wall. Due to the heterogeneity of structural fabrics and orientations, Domain III is additionally subdivided into 5 subdomains (IIIa, IIIb, IIIc, IIId, and IIIe). Structures will be discussed in chronological order of deformation events (D_1-D_5).

Deformation Events

D_1 Deformation

The D_1 deformation event occurred prior to the main phase of recrystallization (Davis, 1993) and because of later transposition, evidence of the D_1 is rare. Hopson and Hatcher (1988) recognized D_1 in the Alto allochthon, Georgia, represented by F_1 folds that produced the S_1 axial planar foliation. Hatcher (1995) recognized five or more deformations in the same rocks at Woodall Shoals (easternmost Blue Ridge) on the South Carolina-Georgia line in the Chattahoochee thrust sheet (still in the Tugaloo terrane). In the Columbus Promontory, Davis (1993) recognized compositional layering in the Poor Mountain Formation preserved in F_1 folds in a small window within the Tumblebug Creek thrust sheet.

Table 2. Deformational framework and related events for the Inner Piedmont, North Carolina.*

DEFORMATION EVENTS		STRUCTURES			OROGENIC EVENTS
		FABRICS	FOLDS	FAULTS	
D_5		joints	———	———	Mesozoic Uplift and Extension
D_4	b	joints	F_{4b} open, upright; trend NW	———	Alleghanian
	a	joints	F_{4a} open, upright; trend N to NE	———	
D_3		S_3	F_3 tight reclined to upright trend N to NE	final movement of faults as Type-C thrusts	Neoacadian
D_2	b	S_2 L_2	F_{2b} tight to isoclinal, reclined to recumbent; sheath folds	initial movement on the SMT, MST, and BCT as Type-F thrusts	
	a	S_2	F_{2a} upright folds	TCT	
D_1		S_1	F_1 intrafolial folds, map scale in TCT footwall and BCT hanging wall	———	Taconian(?) or Neoacadian

prograde metamorphism

*Modified from Davis (1993), Yanagihara (1994), Bream (1999), Giorgis (1999), and Williams, 2000). BCT-Brindle Creek thrust. MST-Mill Spring thrust; TCT-Tumblebug Creek thrust. SMT-Sugarloaf Mountain thrust.

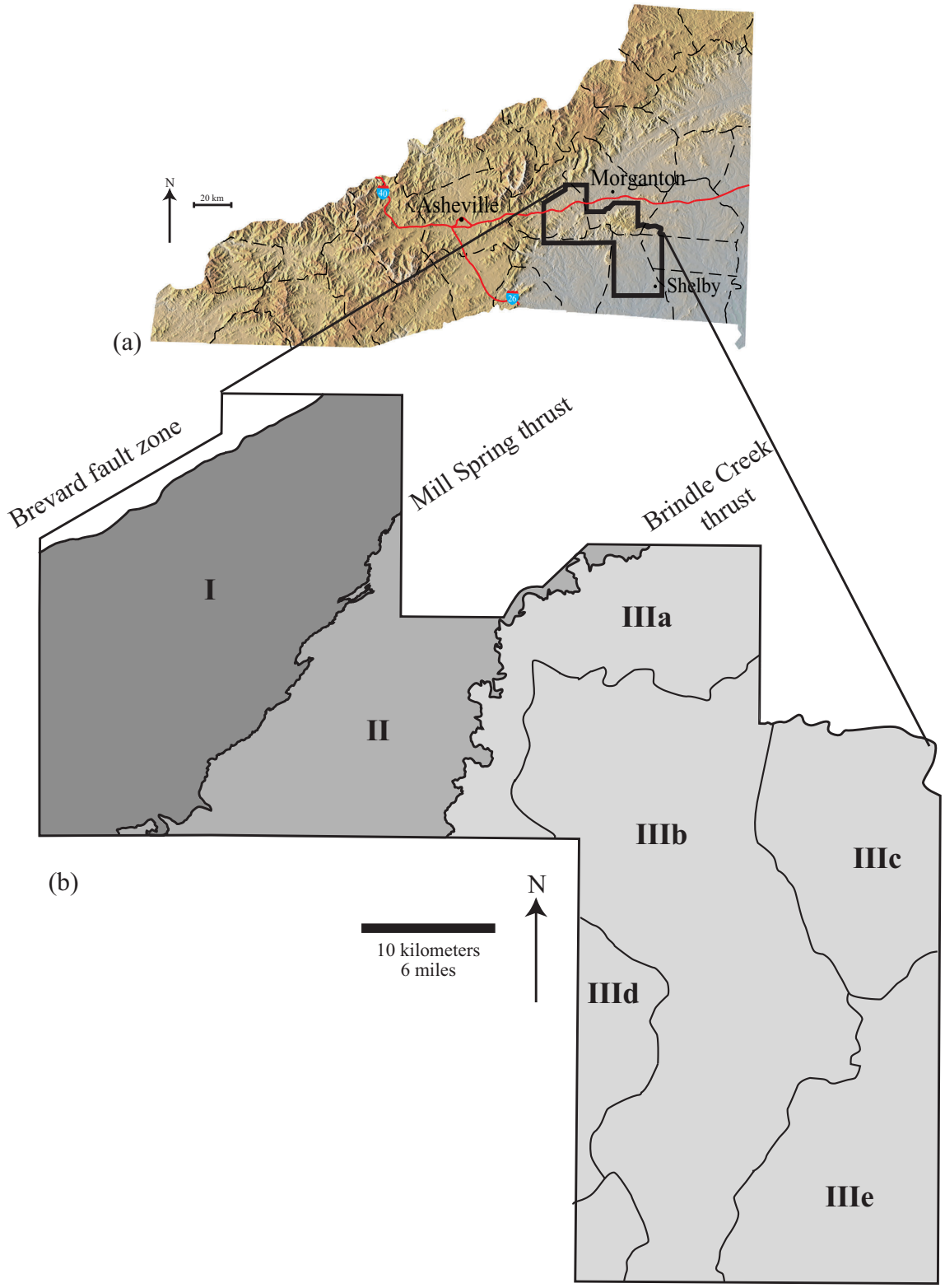

Figure 24. Domain map for a portion of the North Carolina Inner Piedmont. (a) Geographic location of the area. (b) Domains within the area. See text for details.

As discussed earlier, truncated folds in the footwall of the Tumblebug Creek thrust provide macroscale evidence of D_1 (Bream, 1999). A regional recumbent antiform in the hanging wall of the Brindle Creek thrust also resulted from this early episode of deformation. Stratigraphic constraints necessitate the existence of this early folding episode. A regional scale F_1 antiform occurs in the eastern South Mountains. The antiform trends SW-NE, verges northwest, and comprises the hanging wall of the Brindle Creek thrust. Devonian Walker Top Granite may be localized in the core of the fold that abuts the Brindle Creek thrust. Mesoscale evidence of D_1 deformation in the Marion-South Mountains area (Domains I, II, and III) includes truncated folds and foliation within amphibolite boudins and rootless, intrafolial folds. These have been recognized as the most defining mesoscale criteria for D_1 deformation (Hopson and Hatcher, 1988; Davis, 1993; Yanagihara, 1994; Curl, 1998; Bream, 1999; Giorgis, 1999; Hill, 1999; Williams, 2000). Based on the younger depositional age of eastern Inner Piedmont sediments, it is unlikely that D_1 is preserved SE of the Brindle Creek fault.

D_2 Deformation

D_2 is the most pervasive deformation event in the Inner Piedmont, a penetrative polyphase event at or near peak metamorphism (e.g., Davis, 1993; Bream, 1999; Hill, 1999). This event formed the dominant foliation (S_2); the most prominent mineral lineation; reclined to recumbent, tight to isoclinal folds; sheath folds; and Type-F thrust faults. D_2 is interpreted to be "a progressive episode, in which heterogeneous and slightly diachronous deformation occurred as a continuum" (Hill, 1999). Equal-area fabric diagrams of over 10,000 foliations are presented in Figure 25. Southeast of the Brevard fault zone, S_2 strikes parallel to the fault zone and dips moderately (~40˚) to the southeast. S_2 in Domain I is roughly orogen-parallel and strikes N41E and dips 25˚ SE. The average foliation in the Mill Spring thrust sheet strikes N19E and dips 22˚ SE. In the Brindle Creek thrust sheet, the mean foliation in Domain IIIa strikes N10E and dips

11˚ SE. Domains IIIb, IIIc, and IIId strike NE-SW and dip shallowly to the southeast. Domain IIId is dominated by a later (D_5) open fold in the eastern portions of the Polkville and Boiling Springs 7.5-minute quadrangles (Overstreet et al., 1963b). The foliations reflect a regional change in strike from NE-SW in the western flank to N-S in the eastern Inner Piedmont back to NE-SW in the southeastern part of the South Mountains.

In the western Inner Piedmont, mineral lineations were interpreted to be stretching lineations (e.g., Davis, 1993; Giorgis, 1999) based on the orientation of independent kinematic indicators (snowball garnets, asymmetric folds, winged porphyroclasts, boudinage, etc.) parallel to the lineation (Davis, 1993). L_2 lineations are defined by elongate and rodded quartz, micas, amphiboles, and feldspars in the western Inner Piedmont (Domains I and II) and by elongate micas, quartz rods, and sillimanite needles in the eastern Inner Piedmont. Lineations in Domain I and II trend NE-SW, roughly parallel to the trend of F_2 fold axes (Fig. 26). Whisnant (1975) observed the parallel nature of isoclinal fold axes and lineations in the western Inner Piedmont and interpreted isoclinal folding and lineation formation to be synchronous. An alternative explanation for the lineation trends in the Marion-South Mountains area involves transport parallel to axes of regional sheath folds (Bream, 1999). Structural data and map patterns here support a genetic association between mesoscopic sheath folds and lineations (Fig.26).

Davis (1993) was able to distinguish D_{2a} folds and D_{2b} folds based on truncated footwall structures, transposition of D_{2a} folds into S_2 and the abrupt structural and metamorphic relationships across D_{2b} folds. This division is supported by initial folding of the Tumblebug Creek thrust (a D_{2a} fault) in a Type-F thrust relationship that is then truncated by the Sugarloaf Mountain thrust, a D_{2b} fault (Bream, 1999). D_{2a} is characterized by upright isoclinal folds (Davis, 1993) and pre-peak metamorphism emplacement of the Henderson Gneiss by the Tumblebug Creek thrust. Timing of displacement on the Tumblebug Creek thrust (and later deformation) is constrained by

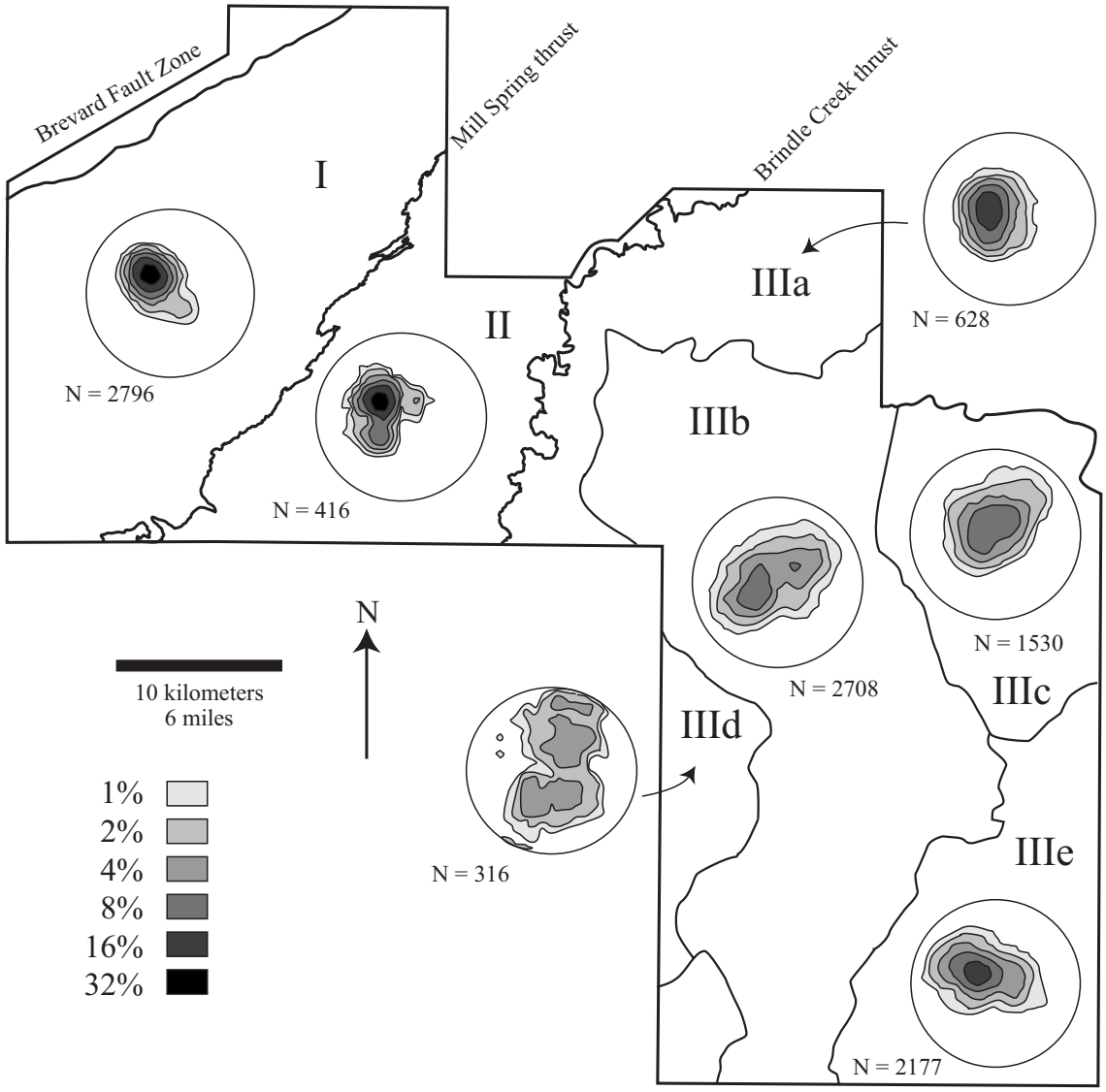

Figure 25. Lower hemisphere, equal-area contoured diagrams of poles to foliation for theMarion-South Mountains area.

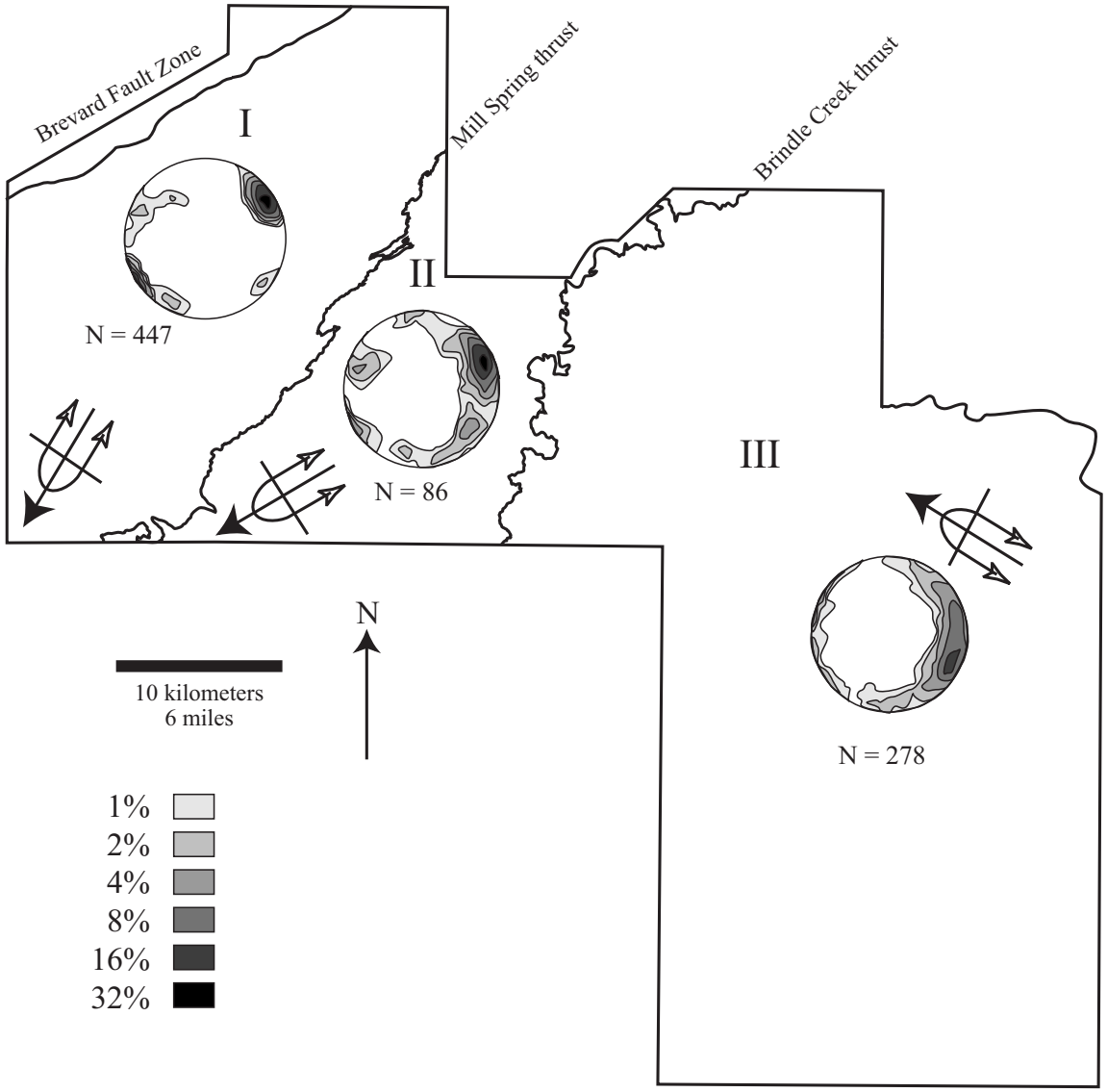

Figure 26. Lower hemisphere, equal-area contoured diagrams of lineations and directions of regional scale sheath fold axes in the Marion-South Mountains area.

the ~470 Ma age of the Henderson Gneiss (Vinson, 1999). Therefore, the most intense deformation and metamorphic conditions occurred after 470 Ma.

Mesoscopic and macroscopic sheath folds recognized throughout the South Mountains are attributed to D_{2b}. At the outcrop scale, these are identified by their characteristic eye or anvil shape (Davis, 1993). Bream (1999) recognized regional-scale sheath folding within the Henderson Gneiss because of the map pattern at both southeast and northeast terminations of the main outcrop body. The outcrop pattern can be explained by northwest-directed thrusting on the Tumblebug Creek thrust prior to later southwest-directed sheath folding. Convincing structural evidence in support of large-scale sheath folds is the strong NE-SW-oriented mineral stretching lineation (Bream, 1999). Map-scale sheath folds are recognized in each of the thrust sheets in the Marion-South Mountains area. Hinges of these sheath folds are nearly parallel to the lineation trends in the respective domains. Map patterns and fabric diagrams support a transport direction that is NE-SW in the western Inner Piedmont that becomes more E-W in the central and eastern Inner Piedmont, which is consistent with the tectonic models proposed by Davis (1993) and Hill (1999). The spread in the lineations in Domains II and III may be related to later D_3 and D_4 folding. A conspicuous northwest-directed lineation in the study area may be the result of D_3 thrust emplacement.

Equal-area stereonets of fold axes (F_1-F_4) are presented in Figure 27. Due to the dominant D_2 deformation at both the meso- and macroscales, trends in the stereonets are primarily attributed to F_2. The most common folds indicative of D_{2b} deformation are tight to isoclinal, reclined to recumbent folds with west vergence. F_{2b} folds in Domain III show a wide variety of orientations. Regional map patterns reflect a strong N-NW trend of tight to isoclinal, reclined to recumbent F_{2b} folds. F_{2b} folds in the western portion of Domain III (IIIa) trend E-W, but become NW-SE in Domains IIIb, IIIc, IIId, and N-S in Domain IIIe. F_{2b} folds are tight to isoclinal, reclined to recumbent, and trend NE, parallel

to the orogen. At the outcrop scale, F_{2b} folds have thickened hinges and attenuated limbs indicative of flexural flow to passive flow folding. The Mill Spring thrust, Sugarloaf Mountain thrust, and Brindle Creek thrust are examples of Type-F thrust faults that formed when the common limb of an F_{2b} antiform-synform pair is removed, and the fault then accommodates displacement. Initial movement on these faults is interpreted to have occurred late during D_{2b}.

D_3 Deformation

D_3 deformation occurred after peak metamorphism, but prior to complete cooling of the rocks (Hopson and Hatcher, 1988). D_3 structures are oriented parallel and subparallel to D_2 structures in Domains I and II. Davis (1993) noted that F_3 folds are common in the western Inner Piedmont but are not penetrative. These folds include outcrop-scale undulations that locally produce crenulation cleavage (Davis, 1993). Bream (1999) observed that F_3 folds have moderately inclined axial surfaces and maintain constant thickness in the limbs and hinges. F_3 folds are not conspicuous in Domain III, and may not be parallel to NW-SE- and W-E-oriented D_2 structures. Final emplacement of coherent thrust sheets took place during D_3. Earlier F_2 folds are truncated by each of these thrusts (Sugarloaf Mountain, Mill Spring, and Brindle Creek thrusts). D_3 deformation likely marks the end of the Neoacadian event or beginning of the Alleghanian.

D_4 Deformation

D_4 produced open, upright folds that overprinted earlier (F_1-F_3) folds resulting in map-scale folds and dome-and-basin interference patterns. F_{4a} folds trend NE and are orogen-parallel while F_{4b} folds trend NW, perpendicular to earlier structures. Bream (1999) suggested that D_{4a} may be the terminal event of D_3 probably as a result of the Alleghanian orogeny. The brittle nature and style of these open folds suggest they formed in the same deformational event. The perpendicular nature of these two fold sets

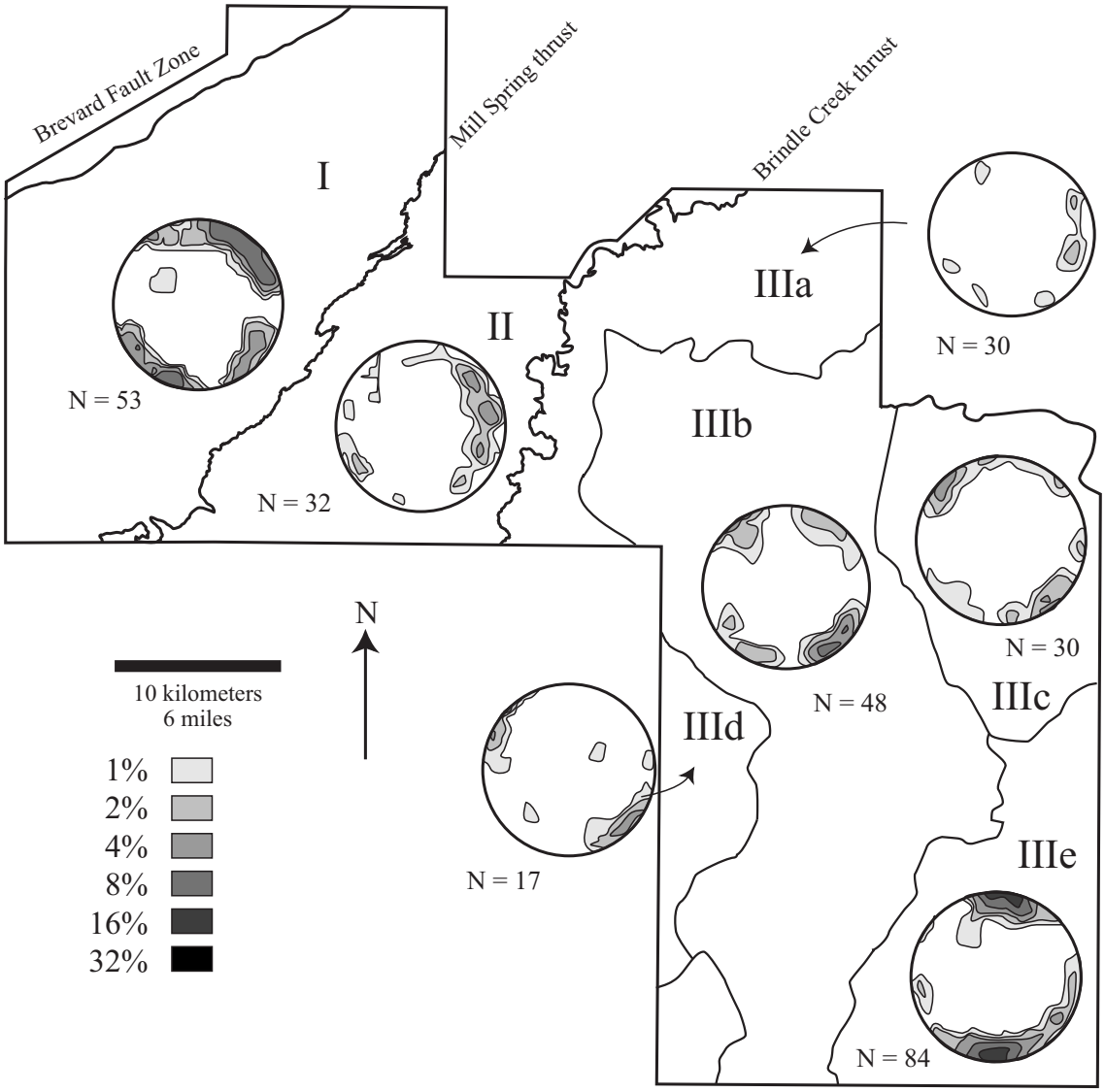

Figure 27. Lower hemisphere, equal-area contoured diagrams of fold axes in the area.

can be explained by a spasmodic episode of deformation (Whitten, 1966). D_4 is coeval with or predates joint formation.

D_5 Deformation

Several major joint sets have been recognized in the Inner Piedmont. Unfilled fractures are typically planar with small apertures. Garihan et al. (1993) and Curl (1998) associated these fractures with later (Mesozoic) brittle faulting in the southern Appalachians. One joint set parallels to N50°-N70° fault system that produced the Marietta-Tryon graben in South Carolina (Garihan et al., 1993).

Cross Sections

Locations of sections A-A', B-B', and C-C' (Fig. 2) were chosen for continuity with sections constructed earlier by Bream (1999), Giorgis (1999), and Williams (2000). Section D-D' was drawn perpendicular to major structures in the Shelby 15-minute quadrangle.

Section A-A'

Section A-A' is located in the Glenwood, Sugar Hill, and Dysartsville quadrangles and illustrates the subsurface geometry of the Tumblebug Creek, the Sugarloaf Mountain, and the Mill Spring thrusts (Fig 28). In this cross section, folds in the footwall of the Tumblebug Creek thrust represent the earliest episode of deformation (D_1). The Tumblebug Creek thrust emplaced the Henderson Gneiss over the Tallulah Falls Formation during D_{2a}. The Mill Spring thrust was active during D_{2b} as a Type-F (Hatcher and Hooper, 1992) thrust and then evolved into a Type-C thrust. The Sugarloaf Mountain thrust truncates the Tumblebug Creek thrust and is also attributed to D_{2b} deformation. The contact between Dysartsville Tonalite and Tallulah Falls Formation is interpreted as concordant because the contact at the surface mostly parallels foliation. The open folding of tight-to-isoclinal folds and faults in the section is a result of D_4

deformation.

Section B-B'

Section B-B', also located in the Sugar Hill, Glenwood, and Dysartsville quadrangles, depicts the subsurface geometry of the Tumblebug Creek, Mill Spring, and the Brindle Creek faults (Fig. 28). This section portrays the northeast termination of the Henderson Gneiss and bounding Tumblebug Creek thrust, possibly the distal end of a regional sheath fold. The Sugarloaf Mountain thrust dies out between section lines A-A' and B-B'. Erosion of the Mill Spring thrust formed a klippe (projected into the section) that is folded into an F_4 synform. Truncation of the main body of Middle Ordovician Dysartsville Tonalite by the Mill Spring thrust indicates emplacement prior to faulting. Like the Sugarloaf Mountain thrust, the Mill Spring thrust cuts up section to the southwest. The Brindle Creek thrust placed Siluro-Devonian bioite gneiss, sillimanite schist, and Devonian-Mississippian granitoids onto footwall Poor Mountain and Tallulah Falls Formation. Displacement on the Brindle Creek thrust was originally interpreted to be < 5 km (Giorgis, 1999), but because of stratigraphic and isotopic contrasts across the fault, displacement is probably much greater (Bream et al., 2001; Mershcat and Kalbas, this guidebook).

Section C-C'

Section C-C' is located in Dysartsville, Benn Knob, and Casar quadrangles and illustrates structural contrasts from the Brindle Creek hanging wall and footwall (Fig. 28). Isoclinal reclined folds (F_{2b}) in the footwall have been refolded by open, upright F_4 folds. Superposed and sheath folds complicate the structural geometry in the Brindle Creek hanging wall. F_2 macroscale boudinage segmented the F_1 regional antiform. The hook-shaped elliptical bodies of biotite gneiss and sillimanite schist represent sheath folds. The isolated occurrence of Walker Top Granite enclosed by the biotite gneiss and

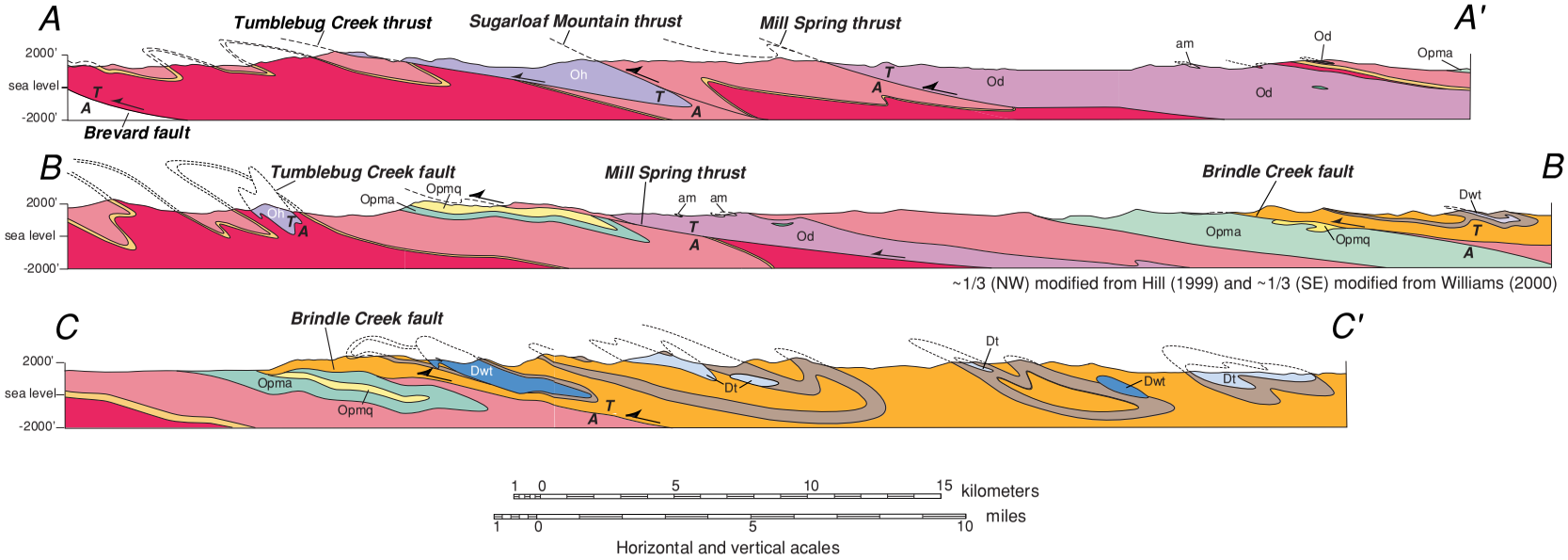

Figure 28. Cross sections. See Figure 2 for locations and explanation of symbols.

sillimanite schist may also represent parts of a sheath fold. Toluca and Walker Top Granites are consistently associated with the aluminous schist in the South Mountains. This relationship is less prevalent in the Brushy Mountains (Merschat and Kalbas, this guidebook).

Deformational synthesis and tectonic summary

Several tectonic models have been proposed for the Inner Piedmont and the crystalline southern Appalachians including regional scale nappes (Hatcher, 1972; Griffin, 1974), stockwork tectonics and tectonic slides (Griffin, 1971, 1974), and oblique convergence (Davis, 1993; Hill, 1999). Portions of each of these models are applicable to this portion of the North Carolina Inner Piedmont. In South Carolina, Griffin (1971) characterized the migmatitic Inner Piedmont as the infrastructure in his stockwork tectonics model. He initially recognized two major nappes (the Six Mile nappe and the Walhalla nappe) and a deep synformal structure (the nonmigmatitic belt, Hatcher's 1972 Chauga belt) in the South Carolina Inner Piedmont. Griffin (1974) recognized early plastic and late brittle folds in the Inner Piedmont, and attributed them to only two deformational events. The change in outcrop pattern and structural style between the nonmigmatitic belt (western Inner Piedmont) and the Walhalla and Six Mile nappes (eastern Inner Piedmont) was cited as evidence of a tectonic slide boundary (Griffin, 1974). In his model, the infrastructure is the Inner Piedmont, the Carolina slate belt (eastern Carolina terrane) is the suprastructure, and the nonmigmatitic Chauga belt represents an infolded *abscherung* or detachment zone, based on the concepts originally formulated by Wegmann (1935) and Haller (1956).

Hatcher (1972, 1978) recognized that nappes in the Inner Piedmont were formed during D_2. Hatcher (1978) stated that structures in the Inner Piedmont did not form in a single deformational episode as Griffin's (1971) stockwork-tectonics model suggests. The boundary between the Chauga belt and the Inner Piedmont was originally thought to

be a fault (Hatcher, 1969; Griffin, 1971). Hatcher (1972) suggested that it is a metamorphic gradient across an antiform synform pair, rather than a tectonic boundary or detachment zone, but more recently realized that it is partly faulted, as indicated in the compilation by Nelson et al. (1998). In the Columbus Promontory, Davis (1993) recognized a change in displacement direction within the western Inner Piedmont from W-directed in the core of the Inner Piedmont to SW-directed in the western Inner Piedmont. The variations in structural orientation result from polyphase deformation, deformation partitioning during a single event, or ductile flow. The progressive change of orientation and similar metamorphic assemblages and textures across the western Inner Piedmont suggest that the structures formed from a single deformation event during amphibolite facies metamorphic conditions (Davis, 1993; Yanagihara, 1994). Davis (1993) argued that the E-W and NE-SW structures resulted from orogen-oblique to orogen-normal displacement of thrusts in the central Inner Piedmont that became orogen-parallel southeast of the Brevard fault zone. The pervasiveness of S_2 and its control of western Inner Piedmont D_2 and D_3 structures suggest that the western Inner Piedmont is a crustal-scale shear zone (Davis, 1993). "The S_2 mylonitic foliation was the common décollement that linked SW-directed transcurrent movement along the primordial Brevard fault zone with E-W contractional movement of Inner Piedmont thrust sheets" (Davis, 1993). Hatcher (1998) expanded on this crustal flow model by recognizing the NW-directed transport in the eastern Inner Piedmont in addition to W- and SW-directed transport in the western Inner Piedmont. Oblique collision and buttressing of ductile Inner Piedmont thrusts against the primordial Brevard fault zone caused this change in transport direction (Davis, 1993; Hatcher, 1998, 2001; Hill, 1999)

Hill (1999) proposed a two-stage oblique collision during the Acadian orogeny produced the map patterns and kinematic indicators in the North Carolina Inner Piedmont. Mineral stretching lineations and significant ductile extension subparallel to

cylindrical and sheath fold axes and the orogen in the footwall are associated with first-phase structures, while the second phase starts with underthrusting towards the foreland (Ellis and Watkinson, 1987). "First-phase structures develop parallel to the orogen and later deformation in the hanging wall reflects isostatically driven emergence normal to the orogen" (Hill, 1999). First-phase structures (D_2 here) include mineral stretching lineations, sheath fold axes, and isoclinal folds. The stack of westward-vergent thrust sheets (D_{2b} and D_3) characteristic of both the South and North Carolina Inner Piedmont can be thought of as the imbricating blocks in the Ellis and Watkinson (1987) model. The map pattern in the eastern Inner Piedmont is complicated and disharmonic, indicative of progressively disharmonic deformation of the hanging wall during the second phase.

The detailed geologic map (Fig 27) illustrates map patterns that support portions of the above tectonic models. The Mill Spring and Brindle Creek thrust sheets resemble Griffin's (1974) Walhalla and Six Mile nappes in South Carolina, but Griffin (1974) failed to recognize multiple plastic deformation episodes. The lineation trends (NE-SW, E-W, and NW-SE) and sheath fold axes support Davis' (1993) and Hatcher's (1998) crustal flow model for the Inner Piedmont. Evidence of disharmonic deformation in the Brindle Creek hanging wall support Hill's (1999) two-stage oblique collisional model. Macroscopic evidence of a polyphase deformation includes the truncation of F_1 and F_2 folds by the Sugarloaf Mountain, Mill Spring, and Brindle Creek thrusts. Mineral stretching lineations and sheath fold axes support a crustal flow model (Davis, 1993; Hatcher, 1998), whereas map patterns provide additional support for Hill's (1999) two-stage oblique collisional model. Therefore, this portion of the Inner Piedmont experienced a polyphase deformational history that included crustal flow during oblique collision.

SUMMARY

The Inner Piedmont was influenced by a high-temperature event at ~350 Ma, which is coeval with penetrative deformation and postdates major faulting and crystallization of deformed Ordovician plutons in the southern Appalachian crystalline core. Within the South Mountains, these events are documented by penetrative fabrics, P-T estimates of prograde mineral assemblages, zircon rim ages, and deformed Henderson, Walker Top, Toluca, and Dysartsville granitoids. Based on existing geochronology, zircon zoning, observed mineral assemblages, garnet morphologies, and garnet zoning profiles, we conclude that the Inner Piedmont was affected by a single prograde Late Devonian-early Mississippian event.

Because of the rarity of D_1 evidence and the penetrative nature of later deformations, D_1 must have occurred early and may be either a vestige of the Taconic orogeny or the relicts of the earliest stages of the Neoacadian event. We interpret D_2 to represent the Neoacadian orogeny because it represents peak metamorphic conditions. D_3 structures resulted from either late Neocadian deformation or early Alleghanian. Because of its brittle overprinting nature, D_4 is likely a result of late Alleghanian deformation. D_5 structures resulted from Mesozoic and younger crustal extension.

ACKNOWLEDGMENTS

Mapping contributions of Jack Whisnant, Greg Yanagihara, Scott Williams, and Joseph Hill in the Marion area are also acknowledged. We thank Ted Labotka, Larry Taylor, and Allen Patchen for assistance with interpretation of the EMP data. Any errors in this paper remain the responsibility of the authors. Detailed geologic mapping was funded by contracts 1434HQ97AG01720 and 98HQAG2026, 99HQAG0026 and 00HQAG0035 from the National Cooperative Geologic Mapping Program EDMAP component (administered by the U.S. Geological Survey) to RDH. Electron microprobe

work at UTK was funded by NSF grant EAR-9814800 (to RDH) and by the UTK Science Alliance Center of Excellence Distinguished Scientist Stipend.

REFERENCES CITED

Abbott, R. N., and Raymond, L. A., 1984, The Ashe metamorphic suite, northwest North Carolina: Metamorphism and observations on geologic history: American Journal of Science, v. 284, p. 350-375.

Barker, F., 1979, Trondhjemite: Definition, environment and hypotheses of origin, *in* Barker, F., ed., Trondhjemites, Dacites, and Related Rocks: New York, Elsevier Scientific Publishing Company, p. 1-12.

Berman, R. G., 1990, Mixing properties of Ca-Mg-Fe-Mn garnets: American Mineralogist, v. 75, p. 328-334.

Bier, S. E., 2001, Geology of the southeastern South Mountains, North Carolina [unpublished M.S. thesis]: Knoxville, University of Tennessee, 162 p.

Bream, B. R., 1999, Structural and stratigraphic relationships of ortho- and paragneisses southwest of Marion, North Carolina [unpublished M.S. thesis]: Knoxville, University of Tennessee, 155 p.

Bream, B. R., Hatcher, R. D., Jr., Miller, C. F., and Fullagar, P. D., 2001, Geochemistry and provenance of Inner Piedmont paragneisses, NC and SC: Evidence for an internal terrane boundary?: Geological Society of America Abstracts with Programs, v. 33, p. 65.

Bream, B. R., Hatcher, R. D., Jr., Miller, C. F., and Fullagar, P. D., in review, Detrital zircon ages and Nd isotopic data from the southern Appalachian crystalline core, GA-SC-NC-TN: New provenance constraints for Laurentian margin paragneisses, *in* Tollo, R. P., Corriveau, L., McLelland, J., and Bartholomew, M. J., eds., Proterozoic evolution of the Grenville Orogen in North America: Boulder, Colorado, Geological Society of America Special Paper.

Butler, J. R., 1991, Chapter 8, Metamorphism, *in* Horton, J. W., Jr., and Zullo, V. A., eds., The geology of the Carolinas, Carolina Geological Society Fiftieth Anniversary Volume: Knoxville, University of Tennessee Press, p. 127-142.

Carrigan, C. W., Bream, B. R., Miller, C. F., and Hatcher, R. D., Jr., 2001, Ion microprobe analyses of zircon rims from the eastern Blue Ridge and Inner Piedmont, NC-SC-GA: Implications for the timing of Paleozoic metamorphism in the southern Appalachians: Geological Society of America Abstracts with Programs, v. 33, p. 7.

Chatterjee, N. D., and Johannes, W., 1974, Thermal stability and standard thermodynamic properties of synthetic 2M1 muscovite, $KAl_2AlSi_3O_{10}(OH)_2$: Contributions to Mineralogy and Petrology, v. 48, p. 89-114.

Conley, J. F., and Drummond, K. M., 1981, Geologic map and mineral resources summary of the northeast 1/4 Marion quadrangle, North Carolina: North Carolina Department of Natural Resources and Community Development and Tennessee

Valley Authority GM 210–NE, scale 1:24,000.
Curl, D. C., 1998, Stratigraphy and structure of Wellford and Reidville quadrangles in part of the eastern Inner Piedmont, near Spartanburg, South Carolina [unpublished M.S. thesis]: Knoxville, University of Tennessee, 129 p.
Dallmeyer, R. D., 1988, Late Paleozoic tectonothermal evolution of the western Piedmont and eastern Blue Ridge, Georgia: controls on the chronology of terrane accretion and transport in the southern Appalachian orogen: Geological Socie-ty of America Bulletin, v. 100, p. 702-713.
Davis, T. L., 1993, Lithostratigraphy, structure, and metamorphism of a crystalline thrust terrane, western Inner Piedmont, North Carolina [unpublished Ph.D. dissertation]: Knoxville, University of Tennessee, 245 p.
Dennis, A. J., 1991, Is the central Piedmont suture a low-angle normal fault?: Geology, v. 19, p. 1081-1084.
Dennis, A. J., and Wright, J. E., 1997, Middle and Late Proterozoic monazite U-Pb ages, Inner Piedmont, South Carolina: Geological Society of America Abstracts with Programs, v. 29, p. 12.
Drake, A. A., Jr., Sinha, A. K., Laird, J., and Guy, R. E., 1989, The Taconic orogen, *in* Hatcher, R. D., Jr., Thomas, W. A., and Viele, G. W., eds., The Appalachian–Ouachita orogen in the United States: Boulder, Colorado, Geological Society of America, The Geology of North America, v. F–2, p. 101-177.
Dutrow, B. L., and Holdaway, M. J., 1989, Experimental determination of the upper thermal stability of Fe-staurolite + quartz at medium pressures: Journal of Petrology, v. 30, p. 229-248.
Ellis, M., and Watkinson, A. J., 1987, Orogen-parallel extension and oblique tectonics: The relation between stretching lineations and relative plate motions: Geology, v. 15, p. 1022-1026.
Ferry, J. M., and Spear, F. S., 1978, Experimental calibration of the partitioning of Fe and Mg between biotite and garnet: Contributions to Mineralogy and Petrology, v. 66, p. 113-117.
Garihan, J. E., Preddy, M. S., and Ranson, W. A., 1993, Summary of Mid-Mesozoic brittle faulting in the Inner Piedmont and nearby Charlotte belt of the Carolinas, *in* Hatcher, R. D., Jr., and Davis, T. L., eds., Studies of the Inner Piedmont geology with a focus on the Columbus Promontory: Carolina Geological Society Guidebook, p. 55-65.
Ghent, E. D., Stout, M. V., and Raeside, R. P., 1983, Plagioclase-clinopyroxene-garnet-quartz equilibria and the geobarometry and geothermometry of garnet amphibolites from Mica Creek, British Columbia: Canadian Journal of Earth Science, v. 20, p. 699-706.
Giorgis, S. D., 1999, Geology of the northwestern South Mountains near Morganton, North Carolina [unpublished M.S. thesis]: Knoxville, University of Tennessee, 186 p.
Goldsmith, R., Milton, D. J., and Horton, J. W., Jr., 1988, Geology of the Charlotte 1° x 2° quadrangle, North Carolina and South Carolina: U.S. Geological Survey Map I–

1251–E, scale 1:250,000.
Griffin, V. S., Jr., 1971, The Inner Piedmont belt of the southern crystalline Appalachians: Geological Society of America Bulletin, v. 82, p. 1885-1898.
Griffin, V. S., 1974, Analysis of the Piedmont in northwest South Carolina: Geological Society of America Bulletin, v. 85, p. 1123-1138.
Griffitts, W. C., and Overstreet, W. C., 1952, Granitic rocks of the western Carolina Piedmont: American Journal of Science, v. 250, p. 777-789.
Hadley, J. B., and Nelson, A. E., 1971, Geologic map of the Knoxville quadrangle, North Carolina, Tennessee, and South Carolina: U.S. Geological Survey Miscellaneous Geologic Investigations Map I-654, scale 1:250,000.
Haller, J., 1956, Problee der tiefentectonik: Bauformen in Migmatit-Stockwerk der ostgronlandischen Kaledoniden: Geologische Rundschau, v. 45, p. 159-167.
Hatcher, R. D., Jr., 1969, Stratigraphy, petrology, and structure of the low rank belt and part of the Blue Ridge of northwesternmost South Carolina: South Carolina Division of Geology, Geologic Notes, v. 13, p. 105-141.
Hatcher, R. D., Jr., 1970, Stratigraphy of the Brevard zone and Poor Mountain area, northwestern South Carolina: Geological Society of America Bulletin, v. 81, p. 933-940.
Hatcher, R. D., Jr., 1972, Developmental model for the southern Appalachians: Geological Society of America Bulletin, v. 83, p. 2735-2760.
Hatcher, R. D., Jr., 1978, Tectonics of the western Piedmont and Blue Ridge: Review and speculation: American Journal of Science, v. 278, p. 276-304.
Hatcher, R. D., Jr., 1987, Tectonics of the southern and central Appalachian internides: Annual Review of Earth and Planetary Science, v. 15, p. 337-362.
Hatcher, R. D., Jr., 1989, Tectonic synthesis of the U.S. Appalachians, *in* Hatcher, R. D., Jr., Thomas, W. A., and Viele, G. W., eds., The Appalachian-Ouachita orogen in the United States: Boulder, Colorado, Geological Society of America, The Geology of North America, v. F-2, p. 511-535.
Hatcher, R. D., Jr., Miller, C. F., and Lamb, D. D., 1995, Deformation processes related to emplacement of the Rabun Granite in the eastern Blue Ridge, Georgia and North Carolina, *in* Driese, S. G., ed., Guidebook for field trip excursions, Southeastern Section, GSA: Knoxville, Tennessee, University of Tennessee, Department of Geological Sciences, Studies in Geology 24, p. 39–56.
Hatcher, R. D., Jr., 1998, Structure of the Appalachian Inner Piedmont: Geological Society of America Abstracts with Programs, v. 30, p. 17.
Hatcher, R. D., Jr., 2001, Terranes and terrane accretion in the southern Appalachians: an evolved working hypothesis: Geological Society of America Abstracts with Programs, v. 33, p. 65.
Hatcher, R. D., Jr., and Goldberg, S. A., 1991, Blue Ridge Geologic Province, *in* Horton, J. W., Jr., and Zullo, V. A., eds., The geology of the Carolinas, Carolina Geological Society Fiftieth Anniversary Volume: Knoxville, University of Tennessee Press, p. 11-35.
Hatcher, R. D., Jr., and Hooper, R. J., 1992, Evolution of crystalline thrust sheets in the

internal parts of mountain chains, *in* McClay, K. R., ed., Thrust tectonics: London, Chapman and Hall, p. 217-234.
Hatcher, R. D., Jr., Bream, B. R., Hill, J. C., Giorgis, S. D., and Williams, S. D., 1999, Transect through the Acadian orogen in the Carolinas and northeast Georgia: Geological Society of America Abstracts with Programs, v. 31, p. 19.
Hibbard, J., 2000, Docking Carolina: Mid-Paleozoic accretion in the southern Appalachians: Geology, v. 28, p.127-130.
Hill, J. C., 1999, Stratigraphy, structure, and tectonics of part of the southern Appalachian Inner Piedmont, near Marion, North Carolina [unpublished M.S. thesis]: Knoxville, University of Tennessee, 188 p.
Holdaway, M. J., 1971, Stability of andalusite and the aluminum silicate phase diagram: American Journal of Science, v. 271, p. 97-131.
Hopson, J. L., and Hatcher, R. D., Jr., 1988, Structural and stratigraphic setting of the Alto allochthon, northeast Georgia: Geological Society of America Bulletin, v. 100, p. 339-350.
Horton, J. W., Jr., and McConnell, K. I., 1991, The Western Piedmont, Chapter 3, *in* Horton, J. W., Jr., and Zullo, V. A., eds., The geology of the Carolinas, Carolina Geologic Society Fiftieth Anniversary Volume: Knoxville, Tennessee, The University of Tennessee Press, p. 36-58.
Horton, J. W., Jr., Drake, A., and Rankin, D., 1989, Tectonostratigraphic terranes and their Paleozoic boundaries in the central and southern Appalachians, *in* Dallmeyer, R. D., ed., Terranes in the circum-Atlantic Paleozoic orogens: Geological Society of America Special Paper 230, p. 213-245.
Irvine, T. N., and Baragar, W. R. A., 1971, A guide to the chemical classification of common rocks: Canadian Journal of Earth Science, v. 8, p. 523-548.
Kalbas, J. L., Bream, B. R., Hatcher, R. D., Jr., and Maybin, A. H., 2002, Evidence for mafic Ordovician magmatism in the Brushy Mountains, western Inner Piedmont of North Carolina: Geological Society of America Abstracts with Programs, v. 34, p. 119.
Keith, A., and Sterrett, D. B., 1931, Description of the Gaffney and Kings Mountain quadrangles, S. C.-N. C.: U. S. Geological Survey Folio 222, 18 p.
King, P. B., 1955, A geologic cross-section across the southern Appalachians, an outline of the geology in the segment in Tennessee, North Carolina, and South Carolina, *in* Russell, R. J., ed., Guides to southeastern geology: Geological Society of America Annual Meeting, p. 332-373.
Koziol, A. M., 1989, Recalibration of the garnet-plagioclase-Al_2SiO_5-quartz (GASP) geobarometer and applications for natural parageneses: EOS, v. 70, p. 493.
Labotka, T. C., 1987, The garnet + hornblende isograd in calcic schists from an andalusite-type regional metamorphic terrain, Panamint Mountains, California: Journal of Petrology, v. 28, p. 323-354.
Leake, B. E., 1964, The chemical distinction between ortho- and para-amphibolites: Journal of Petrology, v. 5, p. 238-254.
Lemmon, R. E., 1973, Geology of the Bat Cave and Fruitland quadrangles and the origin

of the Henderson Gneiss, western North Carolina [unpublished Ph.D. dissertation]: Chapel Hill, University of North Carolina, 145 p.
Liu, A., 1991, Structural geology and deformation history of the Brevard fault zone, Chauga belt, and Inner Piedmont, northwestern South Carolina and adjacent areas [Ph.D. dissertation]: Knoxville, Tennessee, University of Tennessee, 200 p.
Mapes, R. W., 2002, Geochemistry and geochronology of mid-Paleozoic granitic plutonism in the southern Appalachian Piedmont terrane, North Carolina-South Carolina-Georgia [unpublished M.S. thesis]: Nashville, Vanderbilt University, 150 p.
Meschede, M., 1986, A method of discriminating between different types of mid-oceanic ridge basalts and continental tholeiites with the Nb-Zr-Y diagram: Chemical Geology, v. 56, p. 207-218.
Moecher, D. P., and Miller, C. F., 2000, Precise age for peak granulite facies metamorphism and melting in the eastern Blue Ridge from SHRIMP U-Pb analysis of zircon: Geological Society of America Abstracts with Programs, v. 32, p. 63.
Nelson, A. E., Horton, J. W., Jr., and Clarke, J. W., 1998, Geologic map of the Greenville 1° x 2° quadrangle, Georgia, South Carolina, and North Carolina: U.S. Geological Survey Miscellaneous Investigations Series Map I–2175, scale 1:250,000.
Osberg, P. H., Tull, J. F., Robinson, P., Hon, R., and Butler, J. R., 1989, The Acadian orogen, Chapter 4, *in* Hatcher, R. D., Jr., Thomas, W. A., and Viele, G. W., eds., The Appalachian-Ouachita orogen in the United States: Boulder, Colorado, Geological Society of America, The Geology of North America, v. F-2, p. 179-232.
Overstreet, W. C., Whitlow, J.W., White, A. W., and Griffits, W. R., 1963a, Geologic map of the southern part of the Casar quadrangle, Cleveland, Lincoln, and Burke Counties, North Carolina: United States Geological Survey Field Studies Map MF-252, scale 1:24,000.
Overstreet, W. C., Yates, R. G., Griffits, W. R., 1963b, Geologic map of the Shelby 15-minute quadrangle, North Carolina: United States Geological Survey Miscellaneous Geologic Investigations Map 1-384, scale 1:62,500.
Passchier, C. W., Myers, J. S., and Kroner, A., 1990, Field geology of high-grade gneiss terrains: New York, Springer-Verlag, 150 p.
Perchuk, L. L., Aranovich, L. Y., Podlesskii, K. K., Lavrant'eva, I. V., Gerasimov, V. Y., Fed'kin, V. V., Kitsul, V. I., Karsakov, L. P., and Berdnikov, N. V., 1985, Precambrian granulites of the Aldan shield, eastern Siberia, USSR: Journal of Metamorphic Geology, v. 3, p. 265-310.
Pettijohn, F. J., 1949, Sedimentary rocks: New York, Harper and Brothers, 526 p.
Pigage, L. C. and Greenwood, H. J., 1982, Internally consistent estimates of pressure and temperature; the staurolite problem: American Journal of Science, v. 282, p. 943-969.
Rankin, D. W., 1994, Continental margin of the eastern United States: Past and present, *in* Speed, R. C., ed., Phanerozoic evolution of North American continent-ocean transitions: Boulder, Colorado, Geological Society of America, Decade of North American Geology Continent-Ocean Transect Volume, p. 129-218.
Reed, J. D., and Bryant, B., 1964, Evidence for strike-slip faulting along the Brevard

zone in North Carolina: Geological Society of America Bulletin, v. 75, p. 1177-1196.
Roper, P. J., and Dunn, D. E., 1973, Superposed deformation and polymetamorphism, Brevard zone, South Carolina: Geological Society of America Bulletin, v. 84, p. 3373-3386.
Schumann, P. L., 1988, Metamorphic history of the Alto allochthon and petrology of the adjacent Chauga Belt, Ayersville Quadrangle, Georgia [unpublished M.S. thesis]: Knoxville, University of Tennessee, 95 p.
Shelley, D., 1964, On myrmekite: American Mineralogist, v. 49, p. 41-52.
Shervais, J. W., 1982, Ti-V plots and the petrogenesis of modern and ophiolitic lavas: Earth and Planetary Science Letters, v. 59, p. 101-118.
Shufflebarger, T. E., 1961, Notes on relationships of Piedmont sedimentary rocks with emphasis on the Poor Mountain-Chauga River area, Oconee County, South Carolina: South Carolina Division of Geology, Geologic Notes, v. 5, p. 31-38.
Sinha, A. K., and Glover, L., III, 1978, U/Pb systematics of zircons during dynamic metamorphism: Contributions to Mineralogy and Petrology, v. 66, p. 305-310.
Sinha, A. K., Hund, E. A., and Hogan, J. P., 1989, Paleozoic accretionary history of the North American plate margin (central and southern Appalachians): Constraints from the age, origin, and distribution of granitic rocks, *in* Hillhouse, J., ed., Deep structure and past kinematics of accreted terranes: American Geophysical Union Monograph Series, p. 219-238.
Sloan, E., 1907, Catalogue of the mineral localities of South Carolina: South Carolina Geological Survey Bulletin, v. 2, 4th series, 505 p.
Sobolev, V. N., McCammon, C. A., Taylor, L. A., Snyder, G. A., and Sobolev, N. V., 1999, Precise Mössbauer milliprobe determination of ferric iron in rock-forming minerals and limitations of electron microprobe analysis: American Mineralogist, v. 84, p. 78-85.
Spear, F. S., 1993, Metamorphic phase equilibria and pressure-temperature-time paths: Chelsea, Michigan, Book Crafters, Inc., 799 p.
Spear, F. S., Hickmott, D. D., and Selverstone, J., 1990, Metamorphic consequences of thrust emplacement, Fall Mountain, New Hampshire: Geological Society of America Bulletin, v. 102, p. 1344-1360.
Streckeisen, A. L., 1976, To each plutonic rock its proper name: Earth Science Reviews, v. 12, p. 1-33.
Tabor, J. R., 1990, Geologic map of the Mill Spring quadrangle [unpublished mapping]: Knoxville, University of Tennessee, scale 1:24,000.
Tull, J. F., 1980, Overview of the sequence and timing of deformational events in the southern Appalachians: evidence from the crystalline rocks, North Carolina to Alabama, *in* Wones, D. R., ed., The Caledonides in the U.S.A.: Virginia Polytechnic Institute Department of Geological Sciences Memoir, no. 2, p. 167-177.
Vinson, S. B., 1999, Ion probe geochronology of granitoid gneisses of the Inner Piedmont, North Carolina and South Carolina [unpublished M.S. thesis]: Nashville, Vanderbilt, 84 p.

Vinson, S. B, and Miller, C. F., 1999, Constraints on timing of Inner Piedmont plutonism, N.C.-S.C., from ion microprobe U-Pb zircon analysis: Geological Society of America Abstracts with Programs, v. 31, p. A77.

Wegmann, C. E., 1935, Zur Deutung der Migmatite: Geologische Rundschau, v. 26, p. 303-350.

Werner, C. D., 1987, Saxonian granulites—Igneous or lithogenous. A contribution to the geochemical diagnosis of the original rocks in high-metamorphic complexes, *in* Gerstenberger, H., ed., Contributions to the geology of the Saxonian granulite massif: Leipzig, Akademie der Wissenschaften der DDR Zentralinstitut für Isotopen- und Strahlenforschung, p. 221-250.

Whisnant, J. S., 1975, Geology of the southeastern quarter of the Marion 15-minute quadrangle, North Carolina [unpublished M.S. thesis]: Chapel Hill, University of North Carolina, 50 p.

Whitten, E. H. T., 1966, Structural geology of folded rocks: Chicago, Rand McNally and Company, 663 p.

Williams, H., and Hatcher, R. D., Jr., 1983, Appalachian suspect terranes, *in* Hatcher, R. D., Jr., Williams, H., and Zietz, I., eds., Contributions to the tectonics and geophysics of mountain chains: Geological Society of America Memoir 158, p. 33-53.

Williams, S. T., 2000, Geology, structure, and migmatization in the Inner Piedmont near Morganton, North Carolina [unpublished M.S. thesis]: Knoxville, University of Tennessee, 111 p.

Yanagihara, G. M., 1994, Structure, stratigraphy, and metamorphism of a part of the Columbus Promontory, western Inner Piedmont, North Carolina [unpublished M.S. thesis]: Knoxville, University of Tennessee, 214 p.

PART V

Ion microprobe age of Malanjkhand granitoids, Central India

This chapter is an excerpt from a manuscript submitted for publication in Precambrian Research:

> Panigrahi, M.K., Bream, B.R., Misra, K.C., and Naik, R.K., *in review*, Petrogenesis and ion microprobe age of Malanjkhand granitoids, Central India: Deviations from typical copper-porphyry deposits.

My contributions to this paper are: (1) zircon separation of both samples, (3) collection and interpretation of the ion microprobe data, and (3) review and revision of the text. The use of "we" and "our" in the text refers to the co-authors and myself.

INTRODUCTION

Granitoids located near and within Malanjkhand, Central India, are key components to the Precambrian and Phanerozoic crustal evolution of the Bhandara craton. The Malanjkhand and Dongargarh granites are located near volcanics of the Nandgaon and Khairagarh group (together known as the Dongargarh volcanics), rocks of the Sausar and Sakoli metamorphic belts, the Chatishgarh sediments and Phanerozoic rock successions, and unclassified gneisses. Two granitoids, the regionally dominant grey granite (Gr-II) and pink granite (Gr-III) are the focus of this research. The pink granite is largely confined to the mineralized (copper and molybdenum) zone and occurs as pods within the grey granite (Fig. 1).

SHRIMP RG METHODOLOGY

Fresh, representative samples (~2 kg) of each rock unit were collected and standard mineral separation techniques were used to isolate the heaviest non-ferromagnetic phases. Approximately 60 zircon grains per sample were hand-picked, mounted in epoxy with zircon standard AS57 (1099 Ma; Paces and Miller, 1993), and polished to the approximate center (equal reflected and transmitted light dimensions). The grain mount was photographed using a combination of transmitted and reflected light in order to

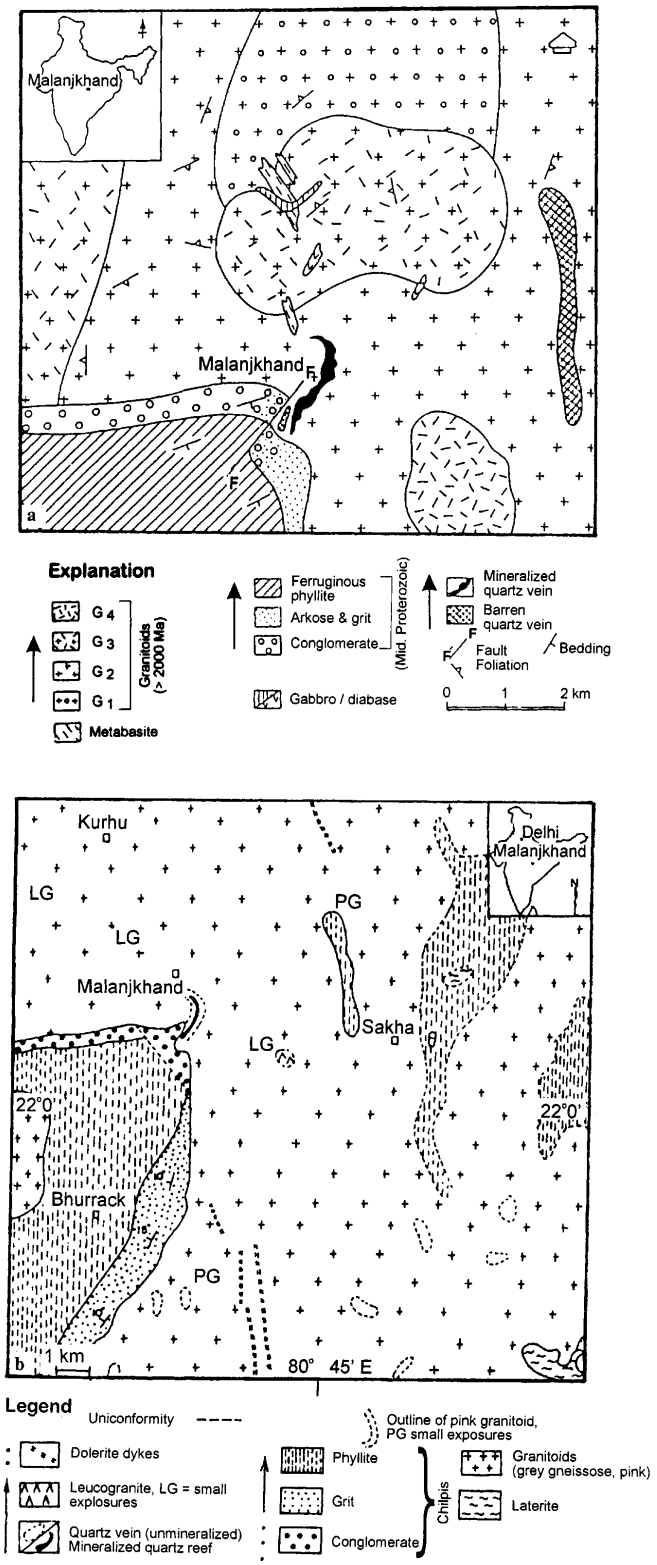

Figure 1. Regional geologic maps of the Malanjkhand area. (a) Granitoid extent and classification scheme of Sarkar et al., 1996. (b) Generalized geology of around Malanjkhand showing the extent of the sampled granites. Composite figure is taken from Sikka and Nehru (1998).

identify surface and internal features. Cathodoluminescence (CL) images were also obtained to identify zoning and locate inclusions using the Stanford JEOL JSM5600 SEM equipped with a Hamamatsu photo multiplier tube for CL imaging. Prior to SHRIMP RG analysis, the mount was cleaned in a 1M HCl solution, thoroughly rinsed with deionized water, baked in a slow oven (at ~60˚C for 30 min), and gold-coated (~10 nm thickness). Routine analytical techniques and operating conditions for SHRIMP RG zircon analyses (e.g., Bacon et al., 2000) were followed and are briefly summarized here. A primary ion beam (at ~8 nA) produced ~1 μm deep and ~25 μm by ~30 μm wide analysis pits. Before each analysis, the area surrounding, and including, the targeted spot was rastered with the primary beam for 90 seconds to remove the gold coat and surface contamination. Five scans of $^{90}Zr_2O$, ^{204}Pb, ^{206}Pb, ^{207}Pb, ^{208}Pb, ^{238}U, $^{232}Th^{16}O$, and 238U16O peaks were collected for each spot. Zircon standard SL13 was analyzed at the beginning of the session to calibrate U concentrations and sample isotopic data was referenced to zircon standard AS57, which was analyzed every four to five analyses during the session. Analyzed grains were re-imaged (backscatter electron and CL) with a Cameca SX-50 electron microprobe at the University of Tennessee–Knoxville to confirm the location and dimensions of SHRIMP RG analytical spots. Most unknown analyses contained minor amounts of common Pb (four analyses had <99% radiogenic ^{206}Pb) corresponding to low ^{204}Pb count rates, which resulted in modest common Pb corrections. Corrections for common Pb were made using the Stacey and Kramers (1975) model to predict the Pb isotopic compositions for each unknown at its $^{207}Pb^*/^{206}Pb^*$ age. Analytical results (corrected for common Pb) were plotted on Tera-Wasserburg and conventional Concordia diagrams. Concordia ages were determined using ISOPLOT (Ludwig, 1991; Ludwig, 1998). We chose to exclude unknown analyses with $^{206}Pb^*/^{238}U$ and $^{207}Pb^*/^{206}Pb^*$ ages that differed by more than 5 percent in order to increase the likelihood that the pooled analyses represent reliable magmatic ages; however, all

analyses (with the exception of a single anslysis) yielded comparable ages. This arbitrary rejection of data reduced the number of pooled analyses for the grey and pink granites from 14 to 10 and 10 to 8, respectively. Most of the excluded analyses had increased common Pb corrections, relative to the pooled analyses, and contained greater concentrations of U and Th. We prefer the $^{207}Pb^*/^{206}Pb^*$ ages for the grey and pink granites due to the equivalence (within error) of the $^{207}Pb^*/^{206}Pb^*$, $^{206}Pb^*/^{238}U$, and Concordia ages for the pooled analyses; resistance of $^{207}Pb^*/^{206}Pb^*$ ages to Pb loss; and the increased precision of $^{207}Pb^*/^{206}Pb^*$ ages for Early Proterozoic U-Pb data. SHRIMP RG data is provided in Table 1.

ZIRCON U-Pb DATING

The mounted zircon separates from the grey and pink granites range in size from ~125 μm to ~450 μm and ~75 μm to ~300 μm (longest dimension), respectively. Most grains are between 125 μm and 150 μm in the longest dimension and are generally composed of more luminescent (CL) euhedral oscillatory zoned interiors with relatively low U concentrations surrounded by les luminescent (CL) coarsely zoned exteriors with higher U concentrations (Fig. 2 and Table 1). Zoning of the type present within the zircon interiors is extensively documented (e.g., Vavra, 1990; Hanchar and Miller, 1993) and most commonly recognized as magmatic growth. Because this research is focused on determining the magmatic age of the granites, our analyses favored inclusion-free unfractured interior zones; however, several analyses within, or overlapping with, the exterior zones were also obtained. These exterior zone analyses did not produce statistically dissimilar ages and were therefore included in the magmatic age determination. Uranium and thorium concentrations for the analyses are ~205 ppm and ~160 ppm, respectively, with Th/U ratios between 0.3 and 1.2 with an average value of 0.75 (typical for igneous zircons). Although there is a correlation between the exterior

Table 1. Ion microprobe (SHRIMP RG) data for zircons from the grey and pink granites.

Analysis	Concentration in ppm				^{204}Pb/		Total ^{238}U/		^{207}Pb/		Radiogenic Ratios[1] ^{238}U/		^{207}Pb/		^{207}Pb/		^{206}Pb/		error	Ages (in Ma)[1] ^{206}Pb/		^{207}Pb/		%
Label	^{206}Pb*	U	Th	Th/U	^{206}Pb	f206%[2]	^{206}Pb	± 1σ	^{206}Pb	± 1σ	^{206}Pb	± 1σ	^{206}Pb	± 1σ	^{235}U	± 1σ	^{238}U	± 1σ	corr	^{238}U	± 1σ	^{206}Pb	± 1σ	Conc
PINK-1.1	92	223	134	0.60	0.000037	0.0527	2.08	0.09	0.1615	0.0007	2.08	0.09	0.1610	0.0008	10.663	0.444	0.480	0.020	0.993	2529	87	2466	8	103
PINK-2.1	53	132	104	0.78	<0.000001	<0.0001	2.14	0.08	0.1632	0.0010	2.14	0.08	0.1632	0.0010	10.541	0.404	0.468	0.018	0.988	2476	78	2490	10	99
PINK-3.1	73	204	240	1.18	<0.000001	<0.0001	2.39	0.09	0.1636	0.0010	2.39	0.09	0.1636	0.0010	9.419	0.361	0.418	0.016	0.988	2249	72	2493	10	90
PINK-4.1	51	127	86	0.68	<0.000001	<0.0001	2.15	0.08	0.1609	0.0011	2.15	0.08	0.1609	0.0011	10.334	0.397	0.466	0.018	0.984	2466	77	2465	12	100
PINK-5.1	80	205	222	1.09	0.000110	0.1547	2.18	0.08	0.1643	0.0008	2.19	0.08	0.1629	0.0009	10.269	0.392	0.457	0.017	0.990	2427	77	2486	9	98
PINK-6.1	56	137	89	0.65	0.000014	0.0203	2.09	0.08	0.1625	0.0011	2.09	0.08	0.1623	0.0011	10.688	0.411	0.478	0.018	0.984	2517	79	2480	12	101
PINK-7.1	31	78	48	0.62	0.000146	0.2067	2.18	0.08	0.1643	0.0027	2.19	0.08	0.1625	0.0028	10.251	0.429	0.458	0.017	0.913	2429	77	2481	29	98
PINK-8.1	46	112	67	0.60	<0.000001	<0.0001	2.11	0.08	0.1608	0.0013	2.11	0.08	0.1608	0.0013	10.515	0.409	0.474	0.018	0.977	2502	79	2465	14	102
PINK-9.1	52	128	133	1.04	0.000017	0.0239	2.12	0.08	0.1626	0.0010	2.12	0.08	0.1624	0.0011	10.577	0.419	0.472	0.018	0.986	2493	81	2481	11	100
PINK-10.1	76	215	138	0.64	0.000024	0.0346	2.43	0.10	0.1600	0.0010	2.43	0.10	0.1597	0.0010	9.070	0.395	0.412	0.018	0.990	2224	81	2452	10	91
GREY-1.1	91	215	243	1.13	0.000008	0.0107	2.03	0.08	0.1621	0.0007	2.04	0.08	0.1620	0.0007	10.978	0.417	0.491	0.019	0.994	2577	80	2477	7	104
GREY-2.1	81	201	92	0.46	0.000010	0.0142	2.14	0.08	0.1630	0.0008	2.14	0.08	0.1628	0.0008	10.490	0.404	0.467	0.018	0.992	2471	78	2485	8	99
GREY-3.1	30	75	38	0.51	<0.000001	<0.0001	2.11	0.08	0.1595	0.0017	2.11	0.08	0.1595	0.0017	10.431	0.418	0.474	0.018	0.966	2502	80	2451	18	102
GREY-3.2	232	555	274	0.49	<0.000001	<0.0001	2.05	0.08	0.1620	0.0008	2.05	0.08	0.1620	0.0008	10.872	0.419	0.487	0.019	0.991	2556	81	2477	9	103
GREY-4.1	91	235	254	1.08	0.000021	0.0294	2.22	0.08	0.1618	0.0008	2.22	0.08	0.1615	0.0008	10.049	0.385	0.451	0.017	0.992	2401	76	2472	8	97
GREY-5.1	48	122	80	0.65	<0.000001	<0.0001	2.20	0.08	0.1621	0.0016	2.20	0.08	0.1621	0.0016	10.135	0.396	0.454	0.017	0.967	2411	76	2477	17	97
GREY-6.1	161	433	413	0.95	0.000096	0.1351	2.31	0.09	0.1647	0.0007	2.31	0.09	0.1635	0.0008	9.745	0.372	0.432	0.016	0.992	2316	74	2492	8	93
GREY-7.1	51	101	81	0.80	0.001589	2.2968	1.70	0.06	0.1696	0.0011	1.74	0.07	0.1492	0.0032	11.847	0.521	0.576	0.022	0.873	2932	90	2337	37	125
GREY-8.1	158	391	164	0.42	<0.000001	<0.0001	2.12	0.08	0.1619	0.0006	2.12	0.08	0.1619	0.0006	10.514	0.397	0.471	0.018	0.995	2488	78	2475	6	101
GREY-9.1	218	1427	472	0.33	0.003089	4.7958	5.64	0.21	0.1532	0.0018	5.92	0.22	0.1114	0.0040	2.595	0.135	0.169	0.006	0.726	1006	35	1822	65	55
GREY-10.1	51	131	85	0.65	0.000138	0.1949	2.20	0.09	0.1638	0.0019	2.20	0.09	0.1621	0.0021	10.144	0.417	0.454	0.018	0.948	2412	78	2478	22	97
GREY-11.1	41	100	103	1.02	0.002943	4.2078	2.08	0.08	0.1931	0.0066	2.17	0.08	0.1556	0.0095	9.867	0.711	0.460	0.018	0.538	2439	79	2409	103	101
GREY-12.1	88	218	212	0.98	0.000044	0.0624	2.12	0.08	0.1623	0.0019	2.12	0.08	0.1618	0.0019	10.528	0.416	0.472	0.018	0.954	2492	78	2474	20	101
GREY-13.1	28	80	56	0.70	0.000988	1.4099	2.48	0.14	0.1694	0.0019	2.52	0.14	0.1568	0.0034	8.582	0.520	0.397	0.022	0.933	2155	103	2422	37	89

Notes: Pb* denotes radiogenic Pb.
(1) Common Pb corrected using measured ^{204}Pb.
(2) f206% denotes the percentage of ^{206}Pb that is common Pb.

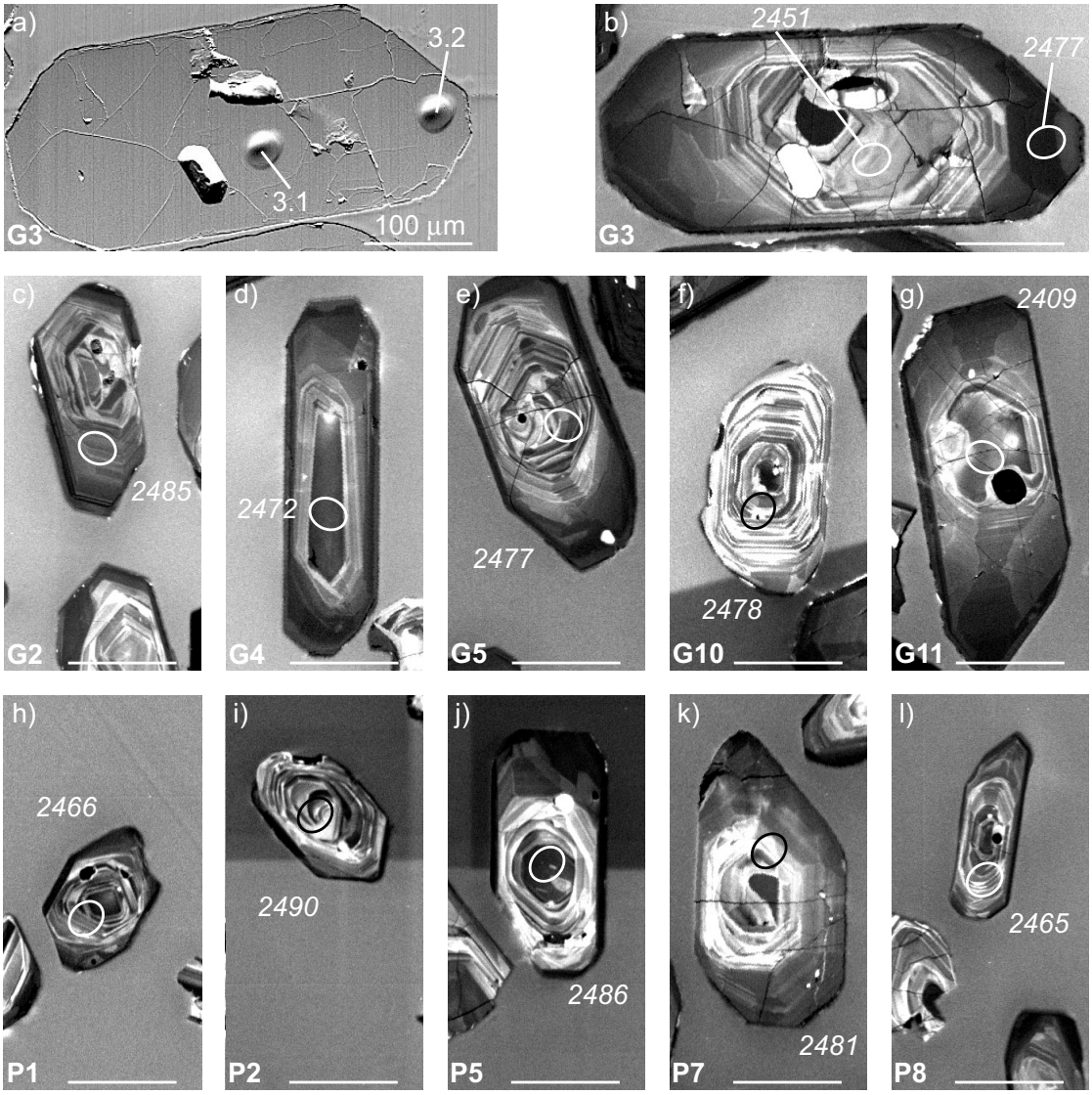

Figure 2. Images of representative zircon grains from the grey and pink granites. Analytical spots with $^{207}Pb^*/^{206}Pb^*$ ages are highlighted in the cathodoluminescence (CL) images, scale bar in each image is 100 µm, and lower left hand corner labels refer to the analysis labels in Table 1. (a) Backscatter electron image of grain 3 from the grey granite showing the location of SHRIMP RG analytical spots. (b) through (g) CL images of grey zircon grains. (h) through (l) CL images of pink granite zircon grains.

portions of the grains and higher U concentration, the age data suggest that the exterior zones did not crystallize/recrystallize during a separate event. Our preferred ages, $^{207}Pb^*/^{206}Pb^*$, of the grey and pink granites are 2476 ± 7 (2s error, mswd = 0.5, n = 10 of 14 total spots) and 2477 ± 8 Ma (2s error, mswd = 0.9, n = 8 of 10 total spots), respectively. A summary of ages with associated statistics is provided in Table 2. Concordia diagrams and summed probability plots of $^{207}Pb^*/^{206}Pb^*$ ages are shown in Figure 3. In agreement with previous work (Ghosh et al., 1986; Panigrahi et al., 1993), this data provides compelling evidence that the granites are the product of the same magmatic pulse ca. 2.47 Ga.

CONCLUSIONS

- Subtle disparities in the Malanjkhand granite led to a division of the same to two dominant groups - a more gneissic, regionally extensive grey granite (Gr-II) and a massive pink granite (Gr-III) mainly found enveloping a rich copper mineralization in a fracture zone. The visual disparities are however not supported by petrographic and chemical characteristics. Earlier attemps at dating these two types were largely unsuccessful though comparable ages for the two were suspected.
- SHRIMP RG U-Pb zircon age dating resulted in identical magmatic ages of 2476 Ma for both granite types, thus resolving the issue of age relationship an improved basis for evaluating the metallogenesis associated with these granites.
- The chemical characteristics of the granites indicate amphibole fractionation and possible derivation from an amphibolite of low crustal residence.
- The granites crystallized at a pressure of about 4.5 kb and the initial water solubility limit can be fixed at 6.5 wt%.
- Hydrothermal alterations caused deuteric alterations, mild in Gr-II and extensive in Gr-III resulting in microclinization and silicification that has redistributed chemical

Table 2. Summary of zircon ages.

	All Data[1]			95% - 105% Concordant[2]		
Sample	$^{206}Pb^*/^{238}U$ Age	$^{207}Pb^*/^{206}Pb^*$ Age	Concordia Age[3]	$^{206}Pb^*/^{238}U$ Age	$^{207}Pb^*/^{206}Pb^*$ Age	Concordia Age[3]
GREY	2472 ± 45	2477 ± 6	2478 ± 6[4]	2465 ± 50	2476 ± 7	2476 ± 7[4]
	n = 13	n = 13	n = 12	n = 10	n = 10	n = 10
	mswd = 3.0	mswd = 2.0	equivalence[5] = 0.26	mswd = 0.6	mswd = 0.5	equivalence[5] = 0.95
			(mswd = 1.2)			(mswd = 0.6)
			concordance[6] = 0.57			concordance[6] = 0.98
PINK	2427 ± 50	2476 ± 7	2479 ± 7[4]	2478 ± 56	2477 ± 8	2477 ± 8[4]
	n = 10	n = 10	n = 9	n = 8	n = 8	n = 8
	mswd = 1.9	mswd = 1.6	equivalence[5] = 0.32	mswd = 0.3	mswd = 0.9	equivalence[5] = 0.89
			(mswd = 1.1)			(mswd = 0.6)
			concordance[6] = 0.61			concordance[6] = 0.95

Notes: Common Pb corrected using measured ^{204}Pb.
Ages are in Ma and reported errors are 2σ, except Concordia Age errors see (4).
(1) All SHRIMP analytical data, some spots auto-rejected for Concordia Age, a single younger outlier (Grey 9.1) was also removed.
(2) Where % Conc. = [($^{206}Pb/^{238}U$ Age)/($^{207}Pb/^{206}Pb$ Age)] * 100, 100% denotes a concordant analysis.
(3) Most probable age for grouped analyses assuming that the true age lies on concordia, some analyses were arbitrarily rejected (Ludwig, 1998). Determined using Squid (version 1.02; Ludwig, 2001).
(4) Concordia Age error is 95% confidence level.
(5) Probability that analyses are equivalent (with associated mswd).
(6) Probability that the Concordia Age is concordant.

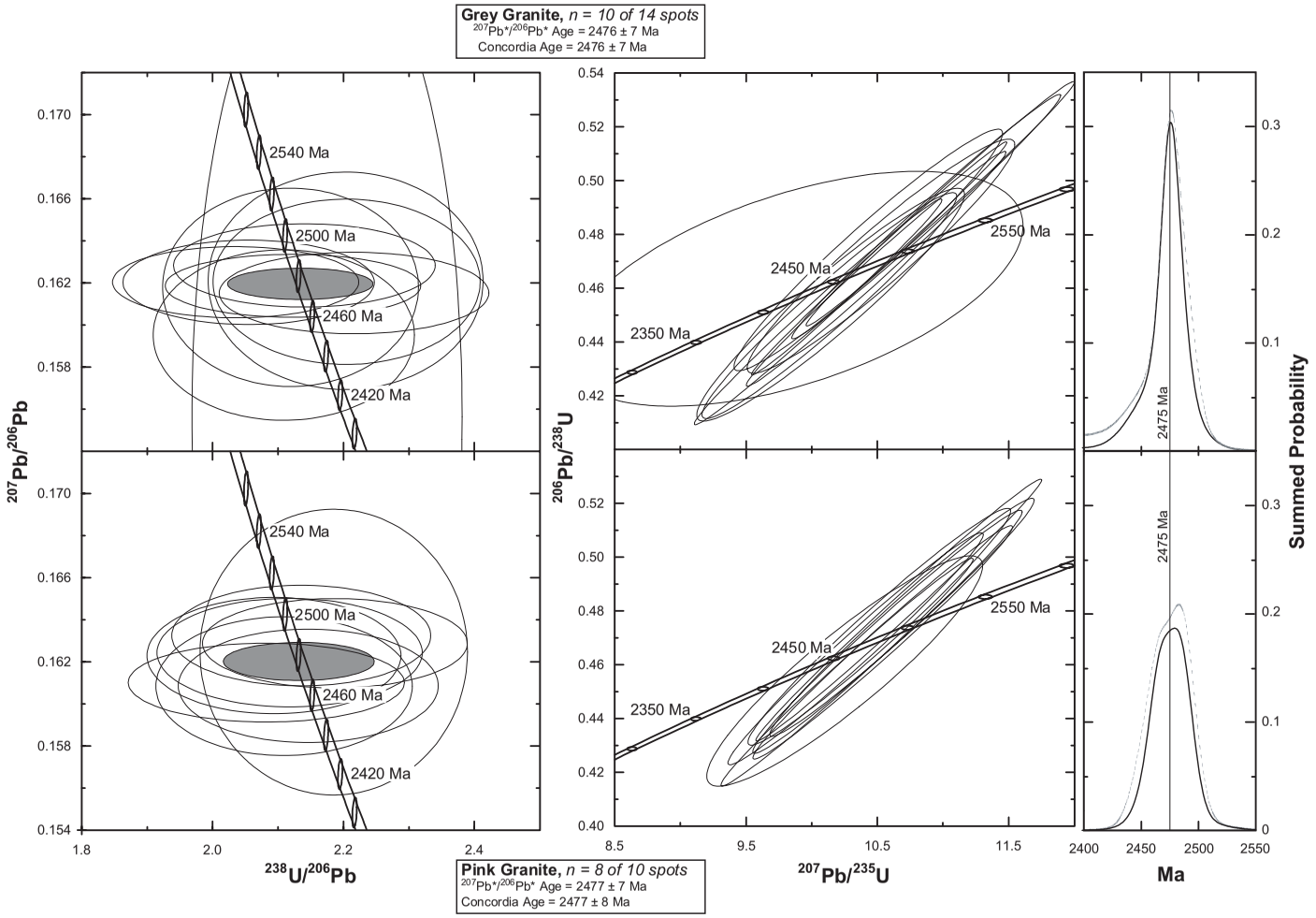

Figure 3. Tera-Wasserburg concordia diagrams, conventional concordia diagrams, and summed probability plots of SHRIMP RG data for the pink and grey granites. Shaded ellips in Tera-Wasserburg concordia diagrams is the Concordia age. Probability plots show the summed probability for all data (dashed gray line) and for 95 to 105 percent concordant spots (solid black line). NOTE: all errors are 2 sigma except the Concordia age, which was determined at a 95 percent confidence level, probability plot is the summed probability for analyses at million year intervals assuming Gaussian distribution of uncertainties after Deino and Potts (1992).

species, altered REE signatures, and disturbed the Rb-Sr isotopic system.

REFERENCES CITED

Bacon, C.R., Persing, H.M., Wooden, J.L., and Ireland, T.R., 2000, Late Pleistocene granodiorite beneath Crater Lake caldera, Oregon, dated by ion microprobe: Geology, v. 28, p. 467-470.

Deino, A., and Potts, R., 1992, Age-probability spectra for examinations of single-crystal $^{40}Ar/^{39}Ar$ dating results; examples from Olorgesailie, southern Kenya Rift, *in* Westgate, J.A., Walter, R.C., and Naeser, N., eds., Tephrochronology; stratigraphic applications of tephra: Oxford, United Kingdom, Quaternary International, p. 47-53.

Ghosh, P.K., Chandy, K.C., Bishui, P.K., and Prasad, R., 1986, Rb-Sr age of granite gneiss in Malanjkhand area, Balaghat District, Madhya Pradesh, India: Indian Minerals, v. 40, p. 1-8.

Hanchar, J.M., and Miller, C.F., 1993, Zircon zonation patterns as revealed by cathodoluminescence and backscattered electron images; implications for interpretation of complex crustal histories: Chemical Geology, v. 110, p. 1-13.

Ludwig, K.R., 1991, ISOPLOT-a plotting and regression program for radiogenic-isotope data: Reston, Virginia, U.S. Geological Survey open file OF91-0445.

Ludwig, K.R., 1998, On the treatment of concordant uranium-lead ages: Geochimica et Cosmochimica Acta, v. 62, p. 665-575.

Ludwig, K.R., 2001, SQUID 1.02: A users manual: Berkeley Geochronology Center Special Publication No. 2, 19 p.

Paces, J.B., and Miller, J.D., Jr., 1993, Precise U-Pb ages of Dulth Complex and related mafic intrusions, northeastern Minnesota; geochronological insight to physical, petrogenetic, paleomagnetic, and tectonomagnetic processes associated with the 1.1 Ga Midcontinent Rift System: Journal of Geophysical Research, B, Solid Earth and Planets, v. 98, p. 13,997-14,013.

Panigrahi, M.K., Mookherjee, A., Pantulu, G.V.C., and Gopalan, K., 1993, Granitoids around the Malanjkhand copper deposit: Types and age relationship: Proceedings of the Indian Academy of Science (Earth and Planetary Science), v. 102, p. 399-403.

Sarkar, S.C., Kabiraj, S., Bhattacharya, S., Das, S., and Pal, A.B., 1996, Nature, origin and evolution of the granitoid-hosted early Proterozoic copper-molybdenum mineralization at Malanjkhand, Central India: Mineralium Deposita, v. 31, p. 419-431.

Sikka, D.B., and Nehru, C.E., 1998, Comments on the article by S.C. Sarkar, S. Kabiraj, S. Bhattacharya, A.B. Pal: Nature, origin and evolution of the granitoid-hosted early Proterozoic copper-molybdenum mineralization at Malanjkhand, Central India: Mineralium Deposita, v. 31, p. 524-530.

Stacey, J.S., and Kramers, J.D., 1975, Approximation of terrestrial lead isotope evolution by a two-stage model: Earth and Planetary Science Letters, v. 26, p. 207-221.

Vavra, G., 1990, On the kinematics of zircon growth and its petrogenetic significance; a

cathodoluminescence study: Contributions to Mineralogy and Petrology, v. 106, p. 90-99.

APPENDICES

APPENDIX I

This appendix contains topographic maps with localities for samples referenced in Parts I and II. The maps are reduced versions of 1:24,000 and 1:100,000 scale topographic quadrangle maps (note scale bars).

Walden Creek Group (CHDAM1), Tallassee 7.5-minute quadrangle, Tennessee (Blount County)

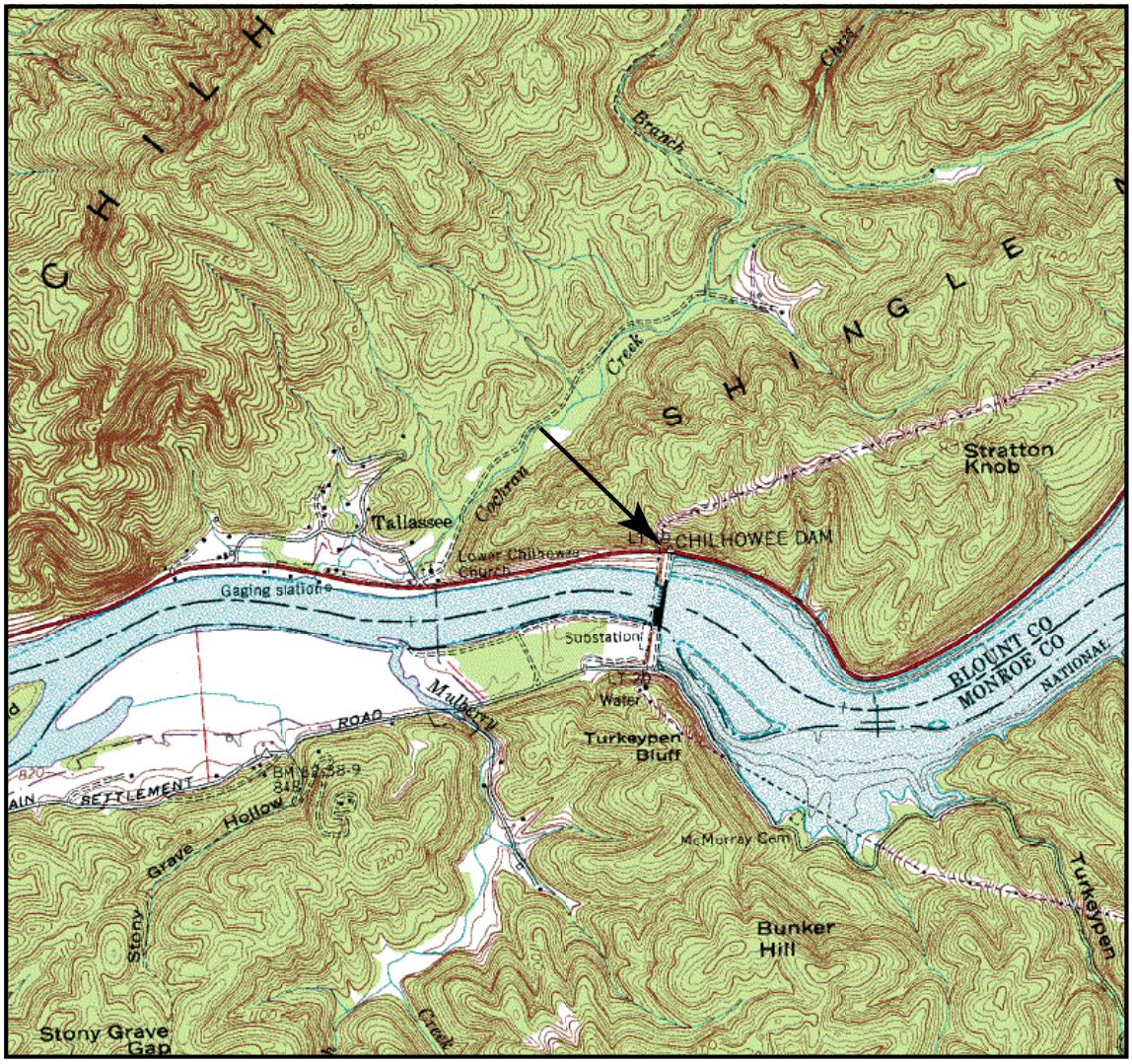

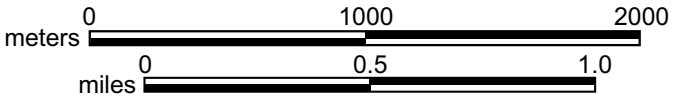

Longarm Quartzite (LQZT), Cove Creek Gap 7.5-minute quadrangle, North Carolina (Haywood County)

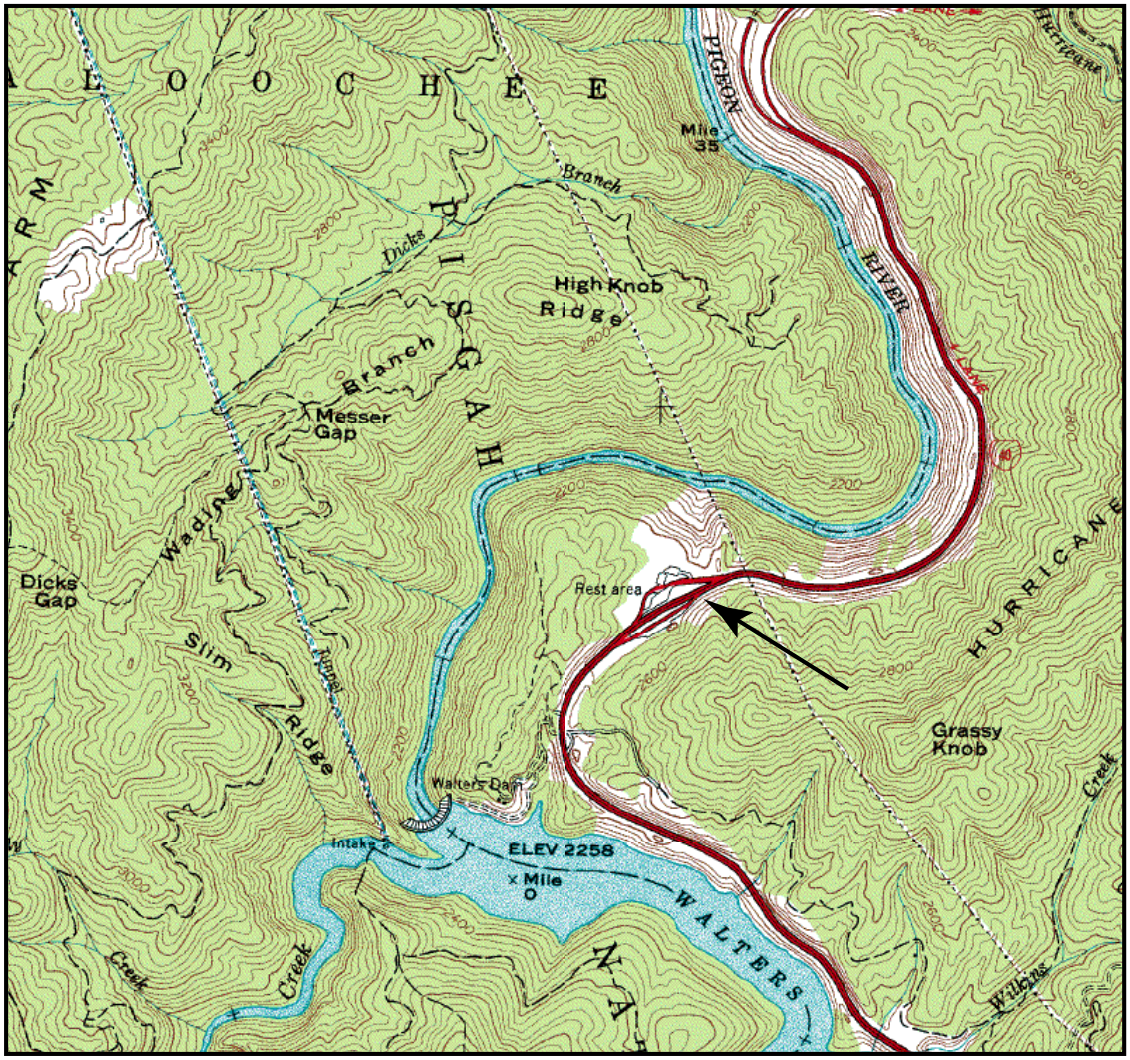

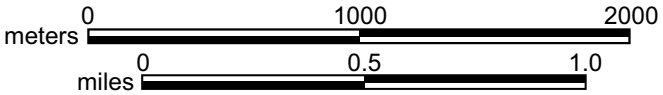

Sandsuck Formation (SERV2), McFarland 7.5-minute quadrangle, Tennessee (Polk County)

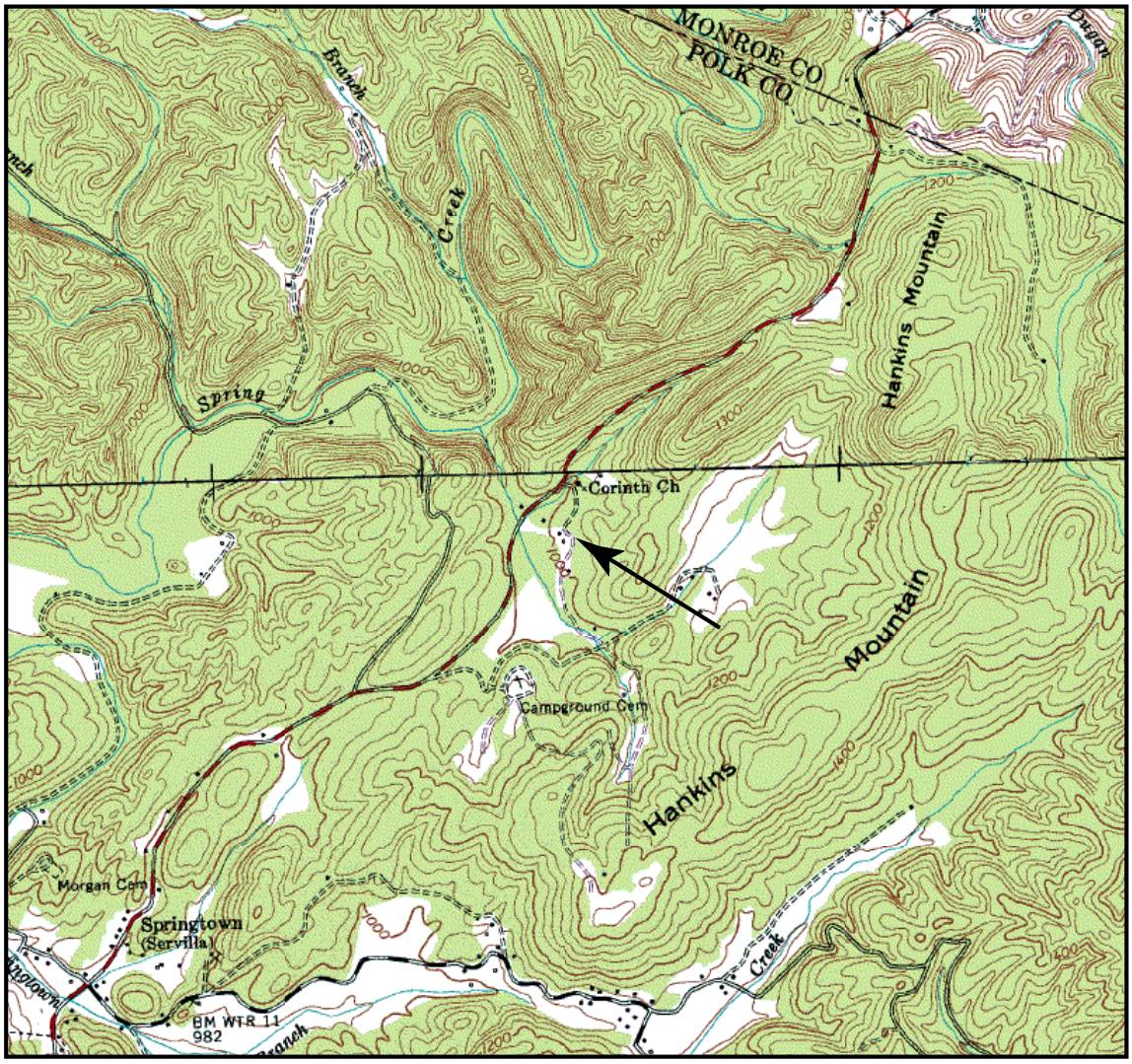

Dean Formation (TELP2), Tellico Plains 7.5-minute quadrangle, Tennessee (Monroe County)

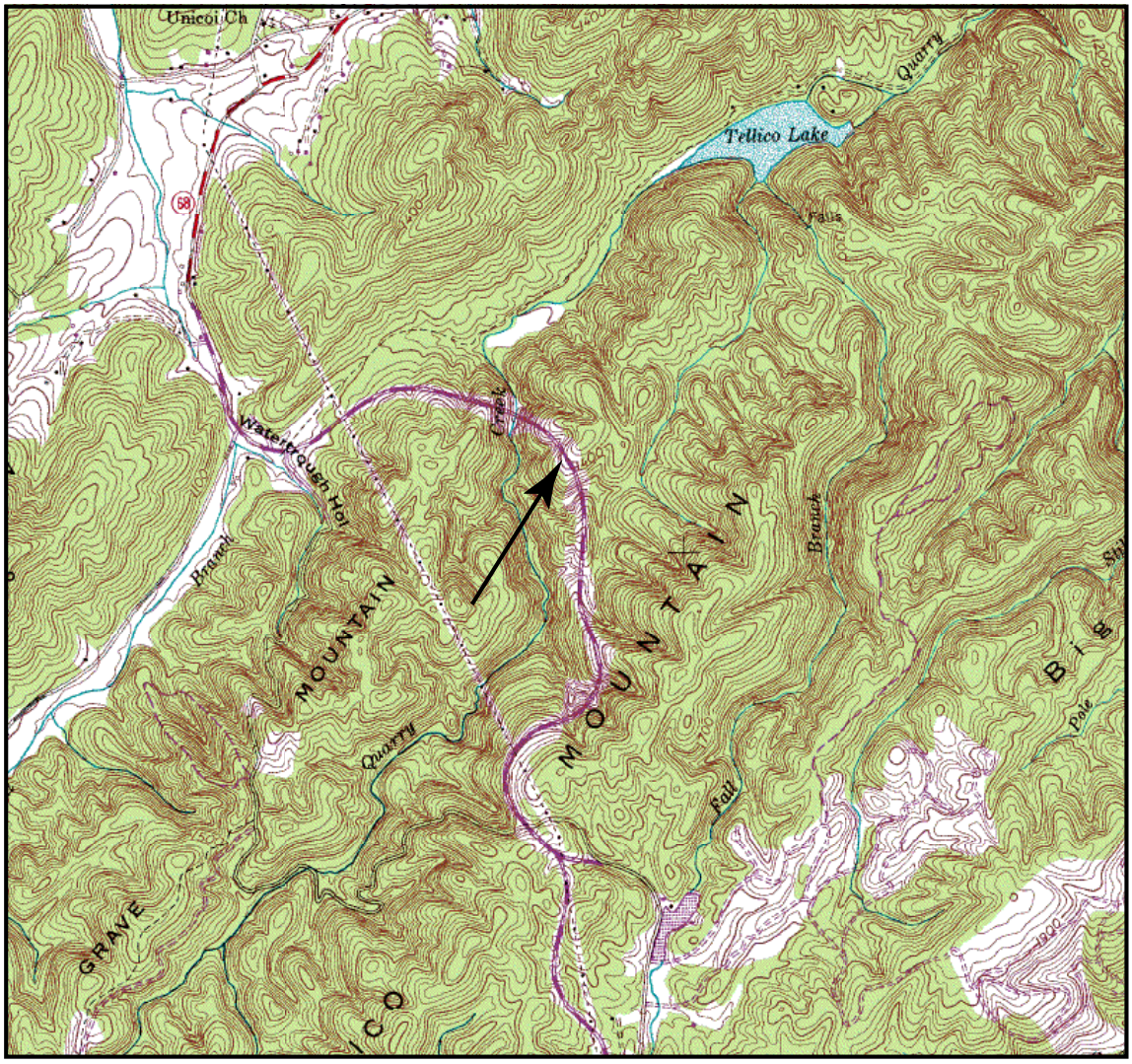

Coleman River Formation (COLRAB), Hightower Bald 7.5-minute quadrangle, Georgia (Rabun County)

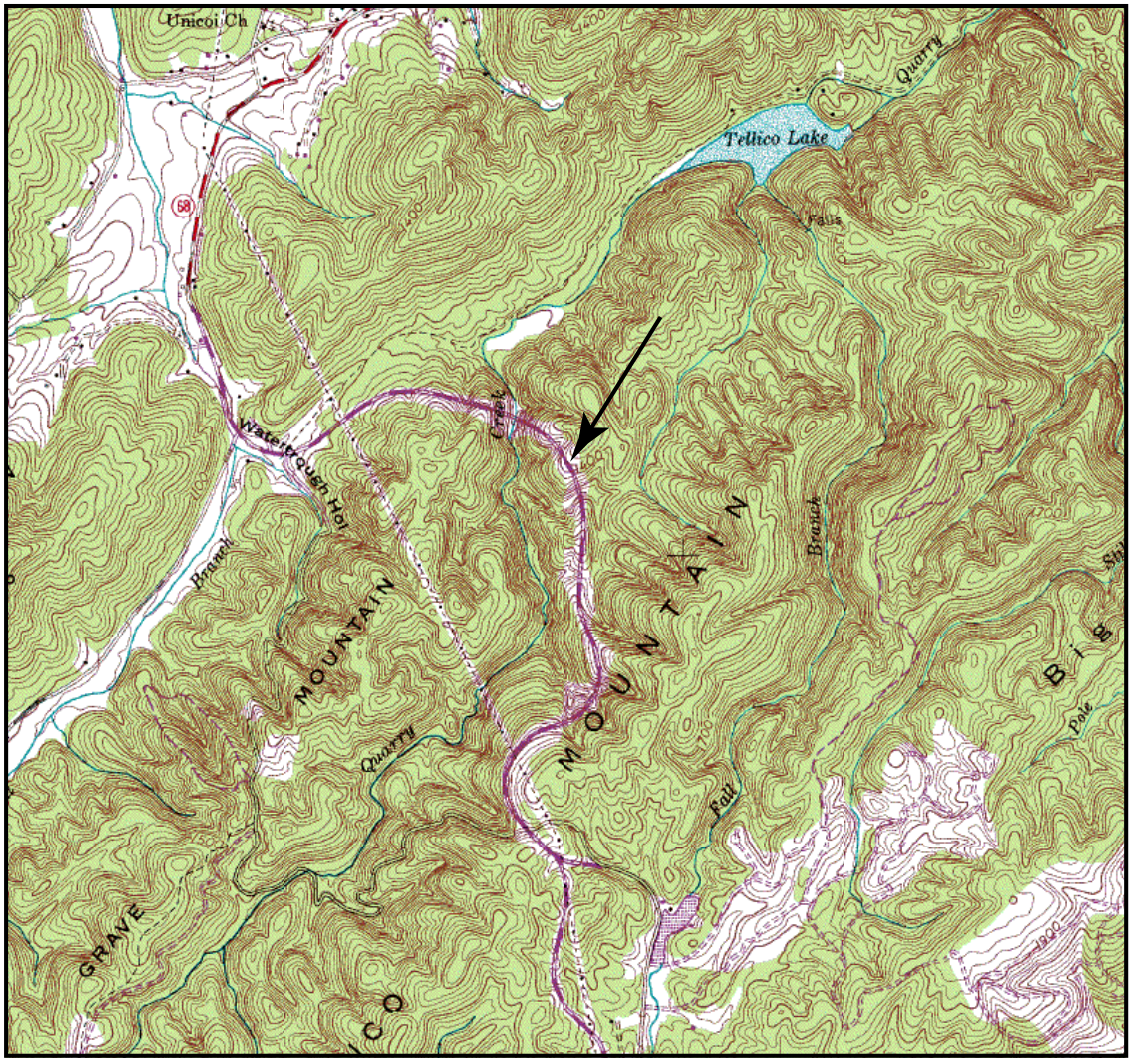

Otto Formation (OTCOW), Prentiss 7.5-minute quadrangle, North Carolina (Macon County)

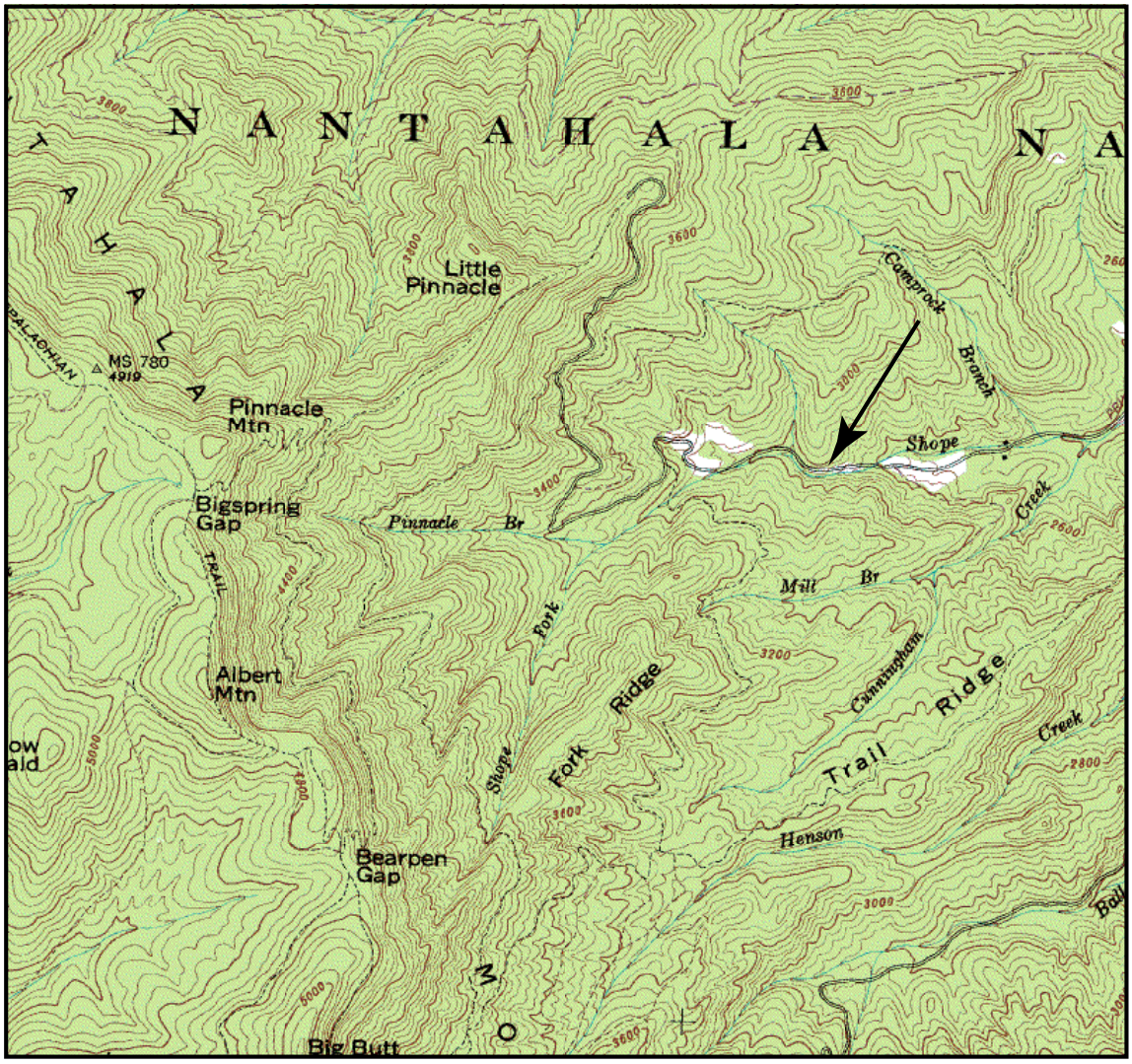

Otto Formation (OTD), Campbell Mountain 7.5-minute quadrangle, Georgia (Lumpkin County)

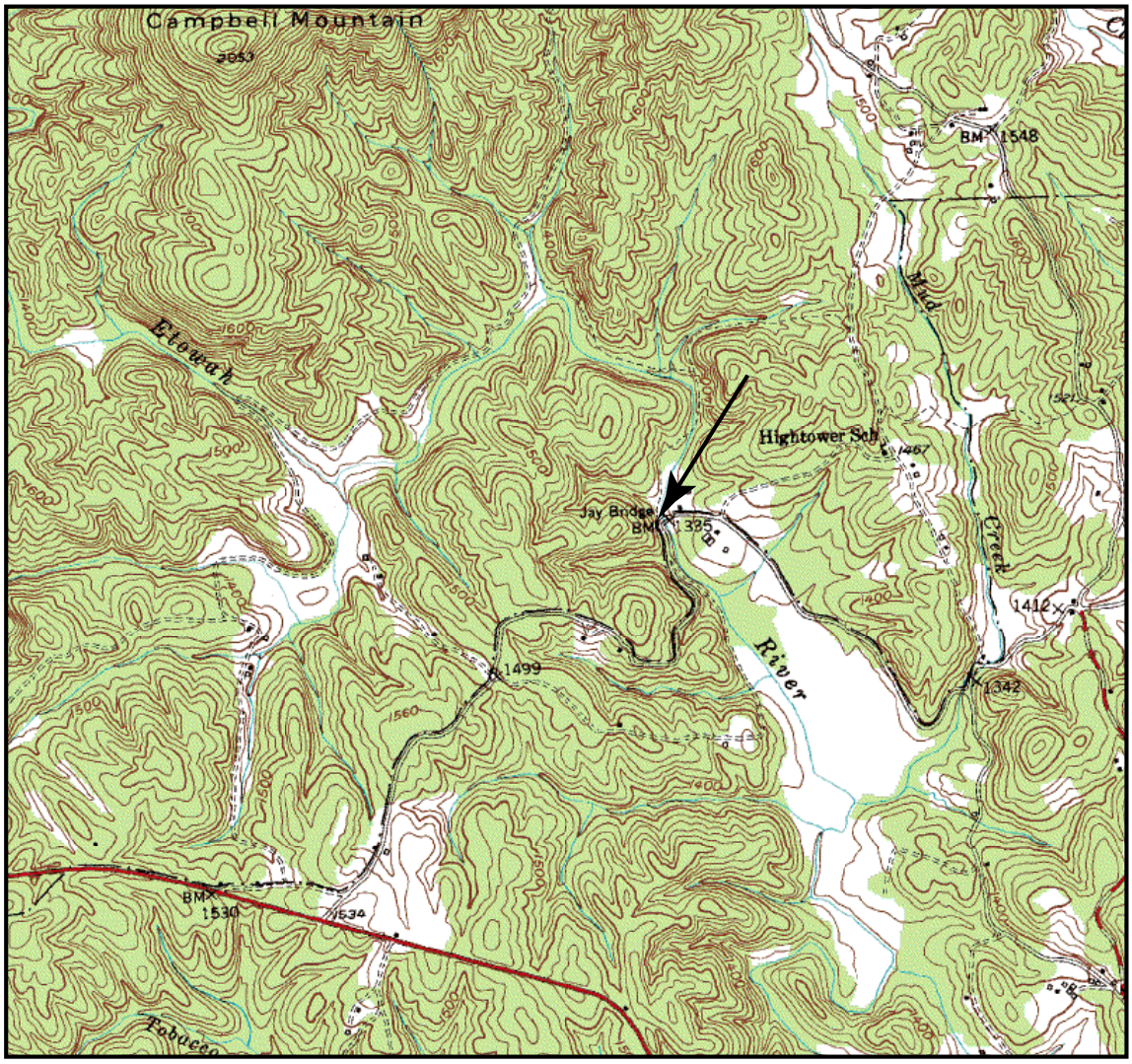

0 1000 2000
meters

0 0.5 1.0
miles

Otto Formation (QMS1), Campbell Mountain 7.5-minute quadrangle, Georgia (Lumpkin County)

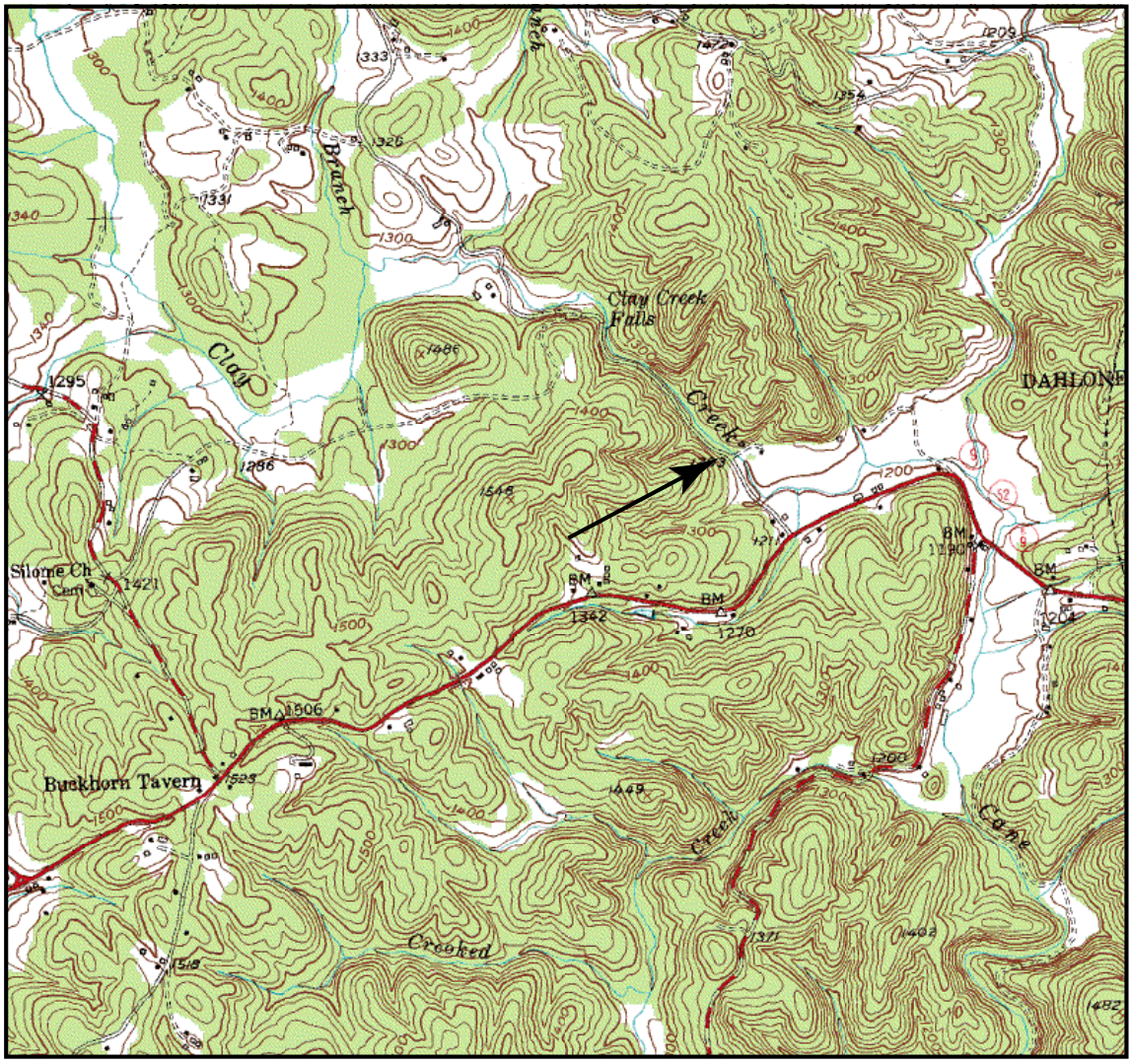

Tallulah Falls Formation (BECR), Dunsmore Mountain 7.5-minute quadrangle, North Carolina (Buncombe County)

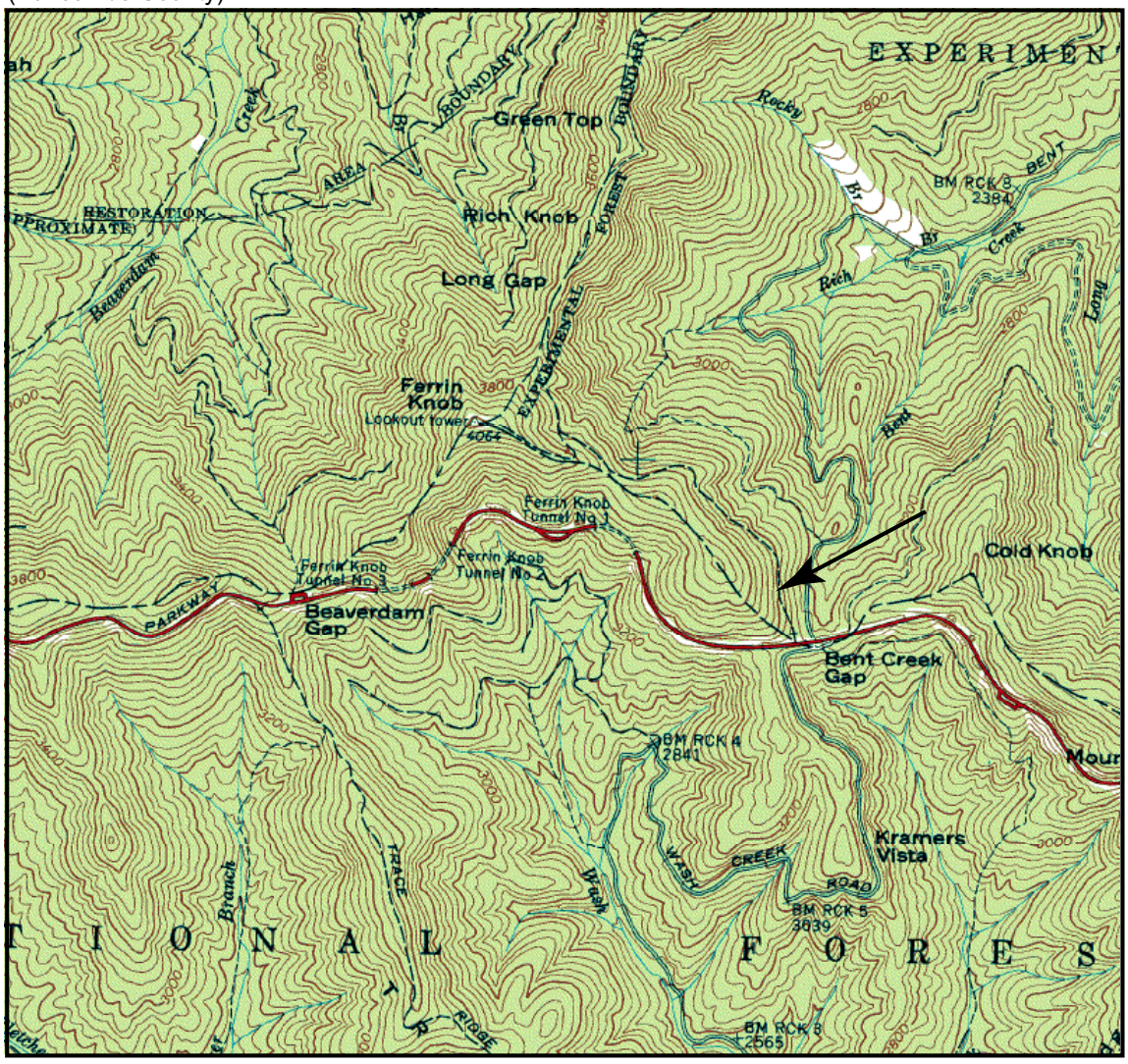

Tallulah Falls Formation (BOCAT), Asheville 7.5-minute quadrangle, North Carolina (Buncombe County)

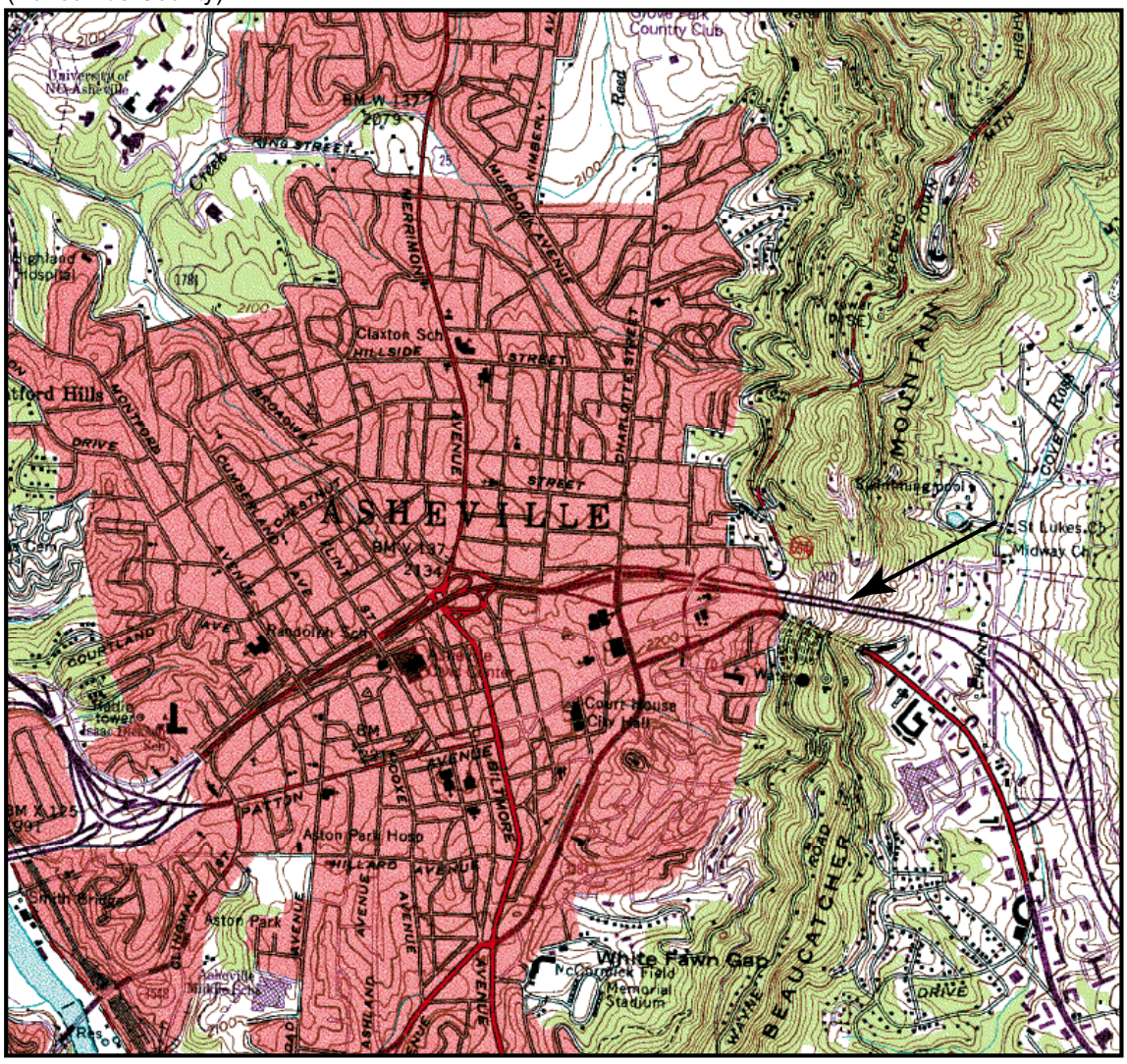

Tallulah Falls Quartzite (TFQZT1), Tiger 7.5-minute quadrangle, Georgia (Rabun County)

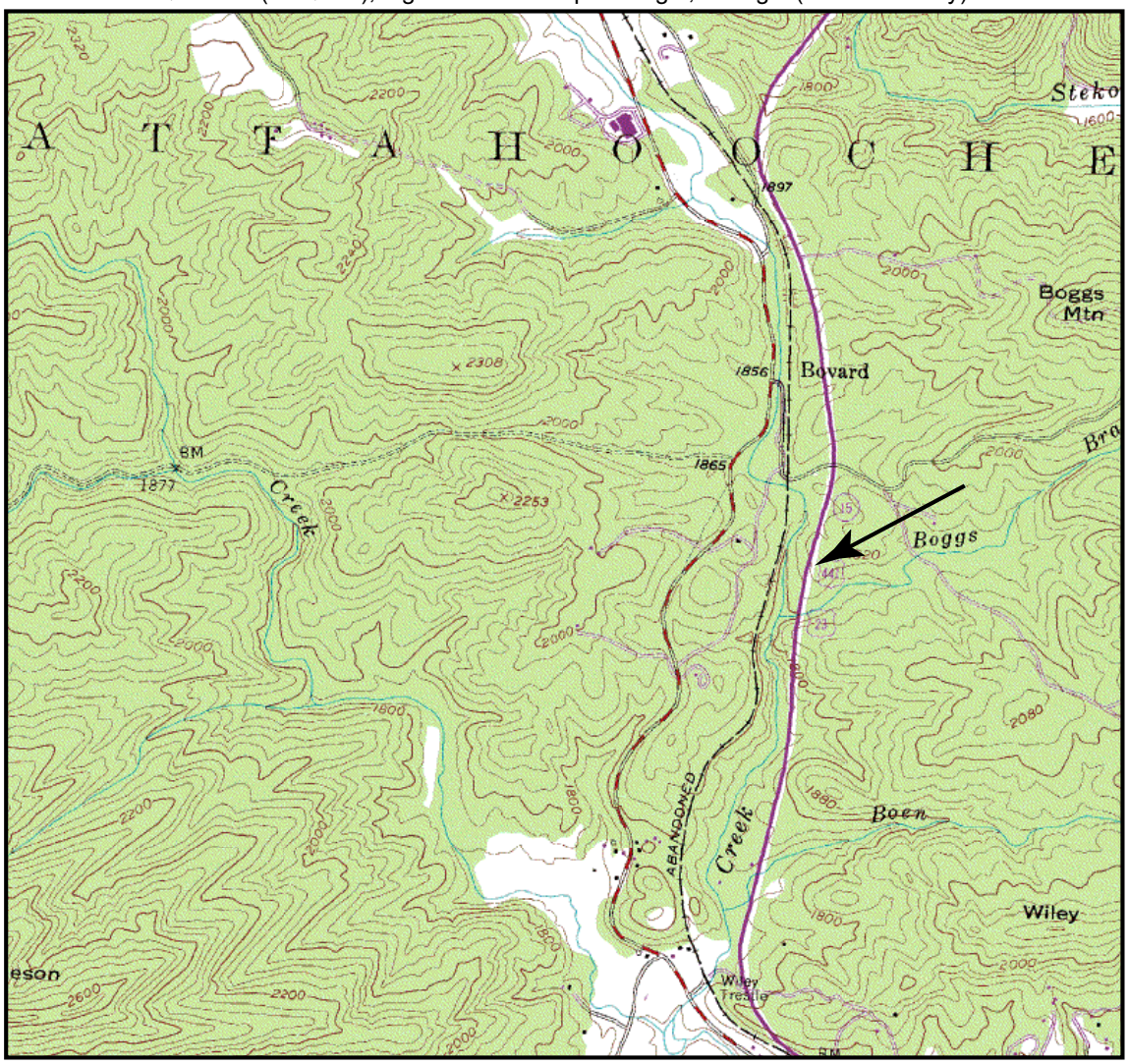

Tallulah Falls Quartzite (TFQZT2), Tallulah Falls 7.5-minute quadrangle, Georgia (Rabun County)

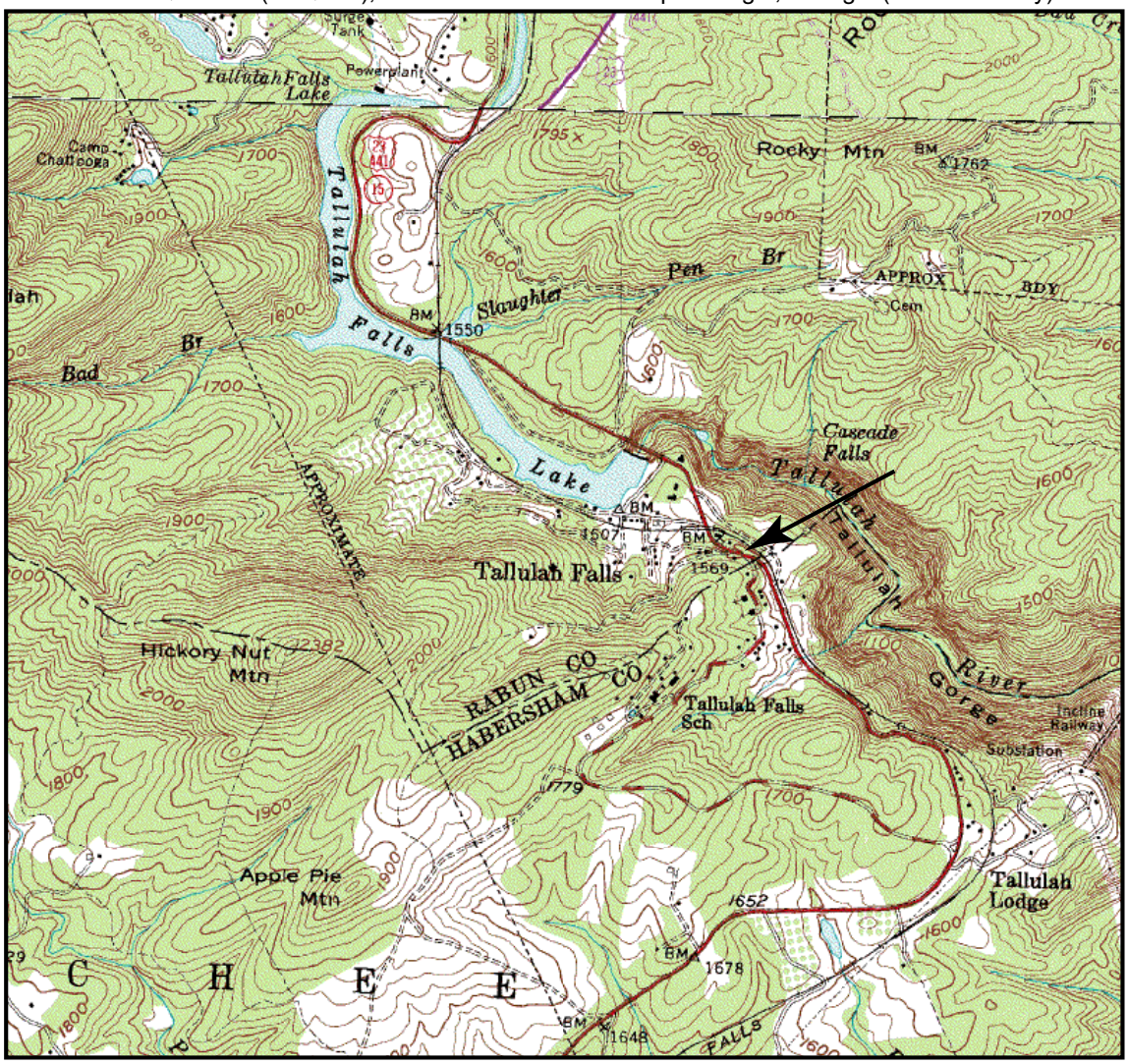

Tallulah Falls Formation (TFTIG441), Tiger 7.5-minute quadrangle, Georgia (Rabun County)

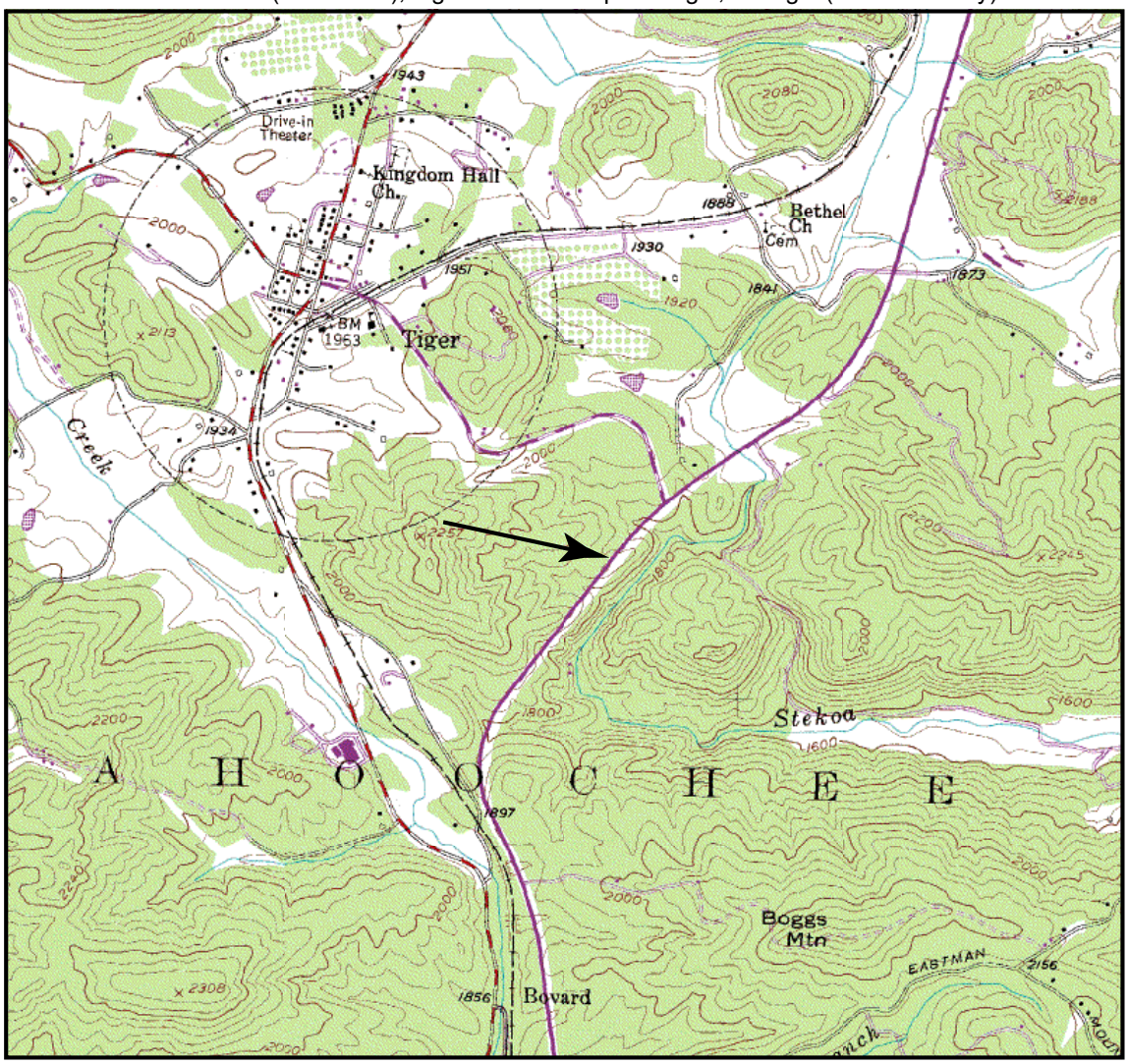

Hogan Creek Formation (SMHC), Siloam 7.5-minute quadrangle, North Carolina (Surry County)

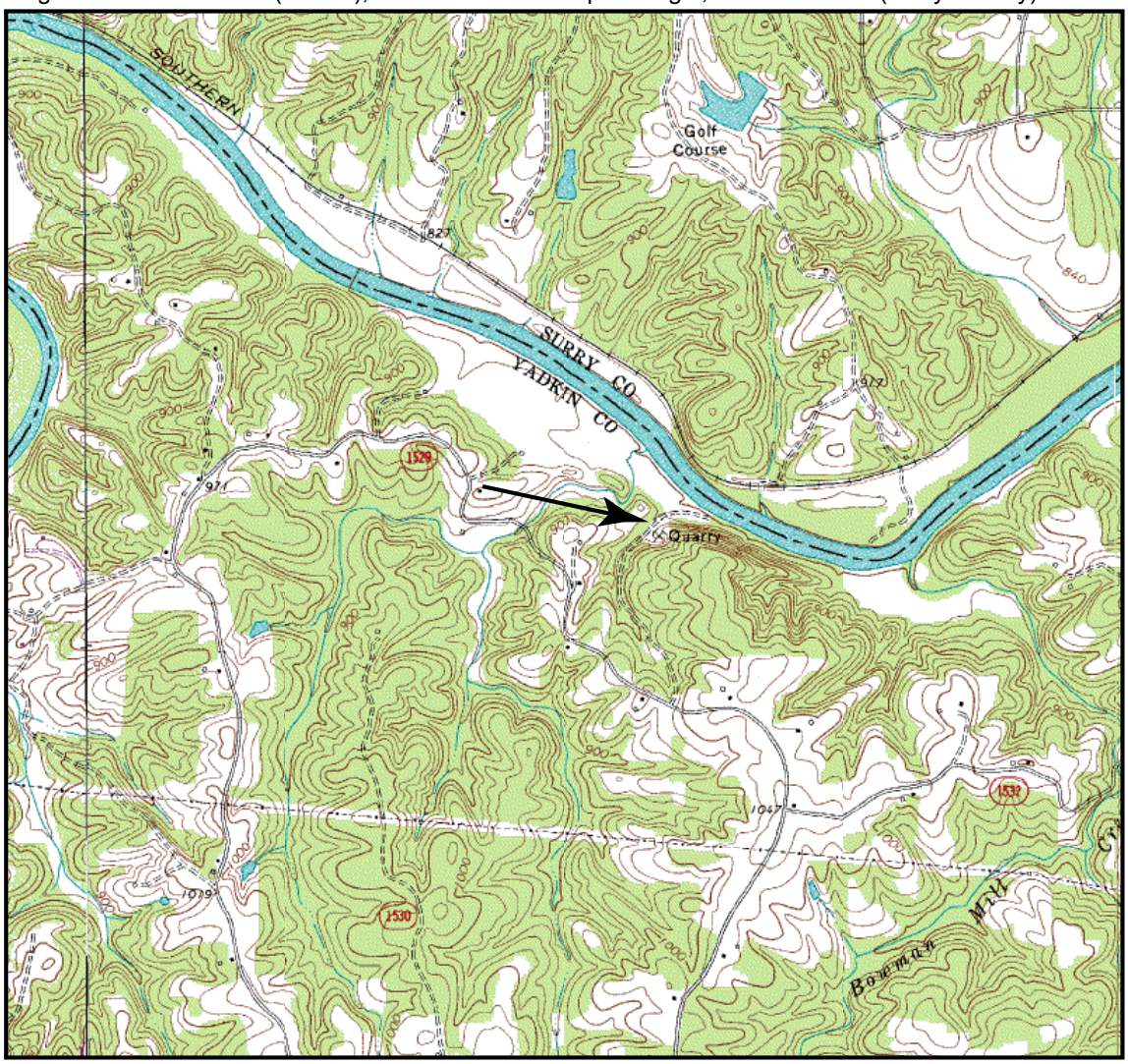

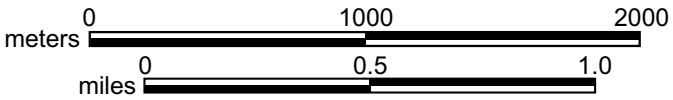

Pilot Mountain Quartzite (PMQZT), Pinnacle 7.5-minute quadrangle, North Carolina (Surry County)

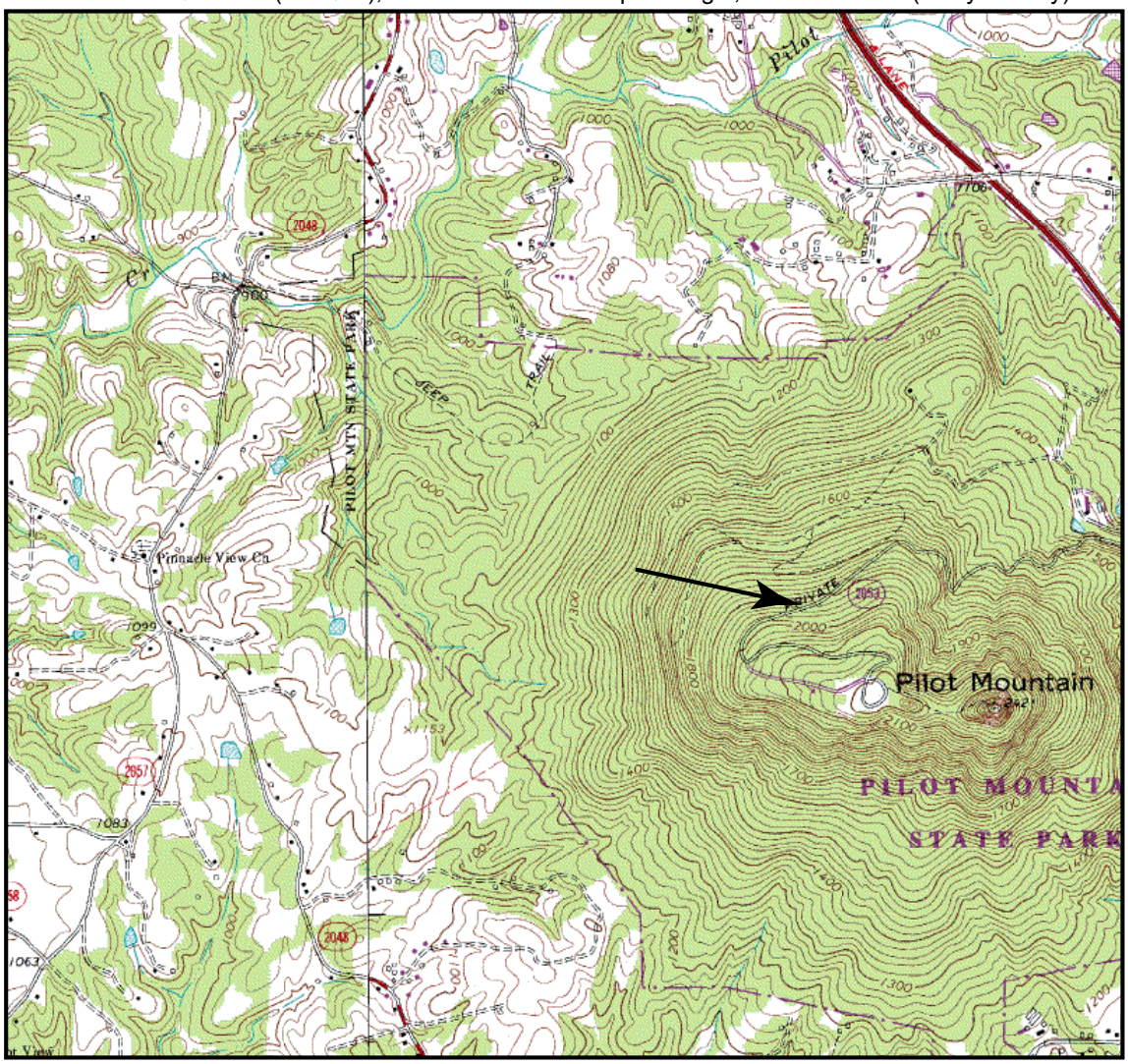

Chauga River Formation (BPM1), Salem 7.5-minute quadrangle, South Carolina (Oconee County)

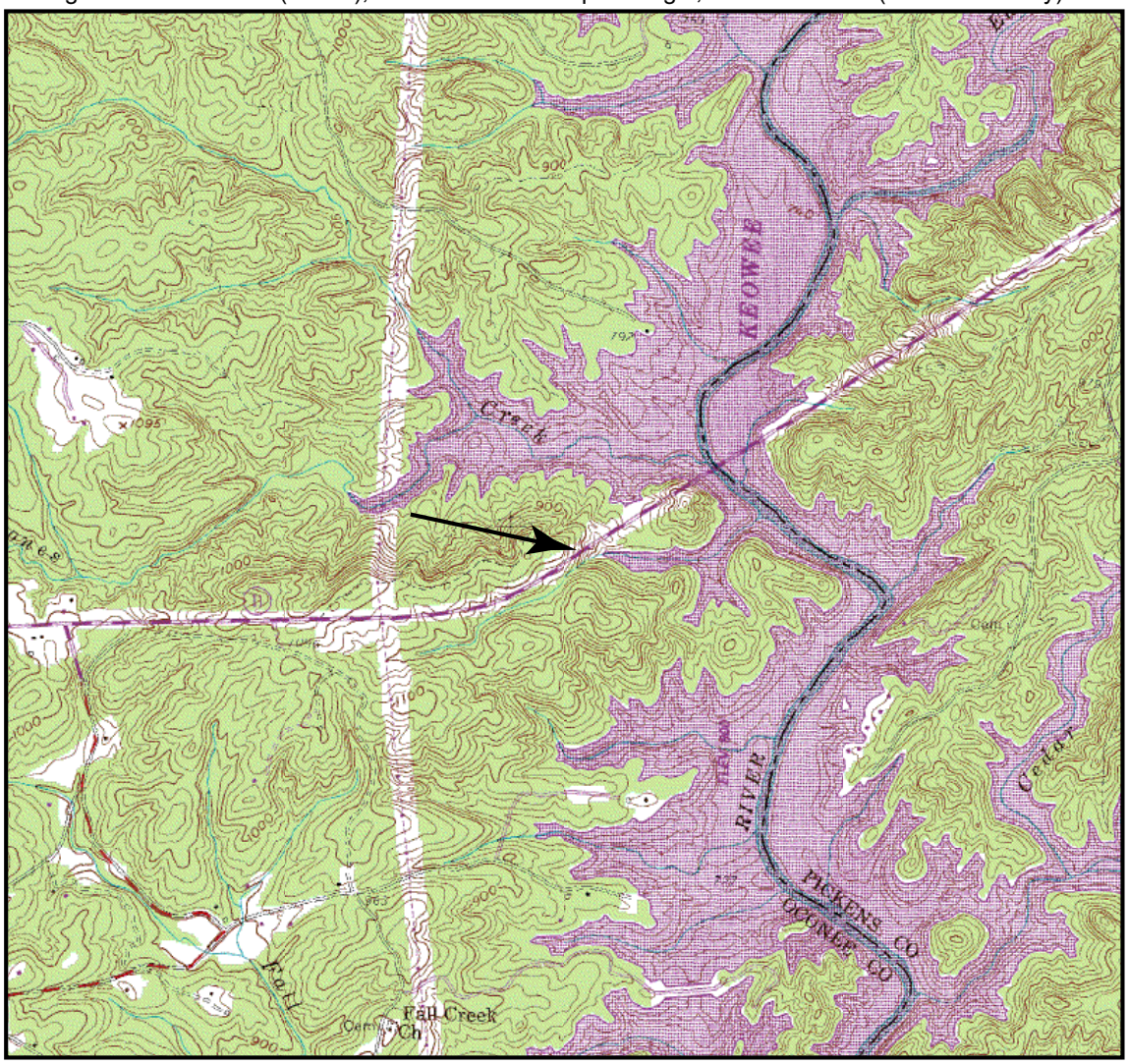

Tallulah Falls Formation (KEOTF), Seneca 7.5-minute quadrangle, South Carolina (Oconee County)

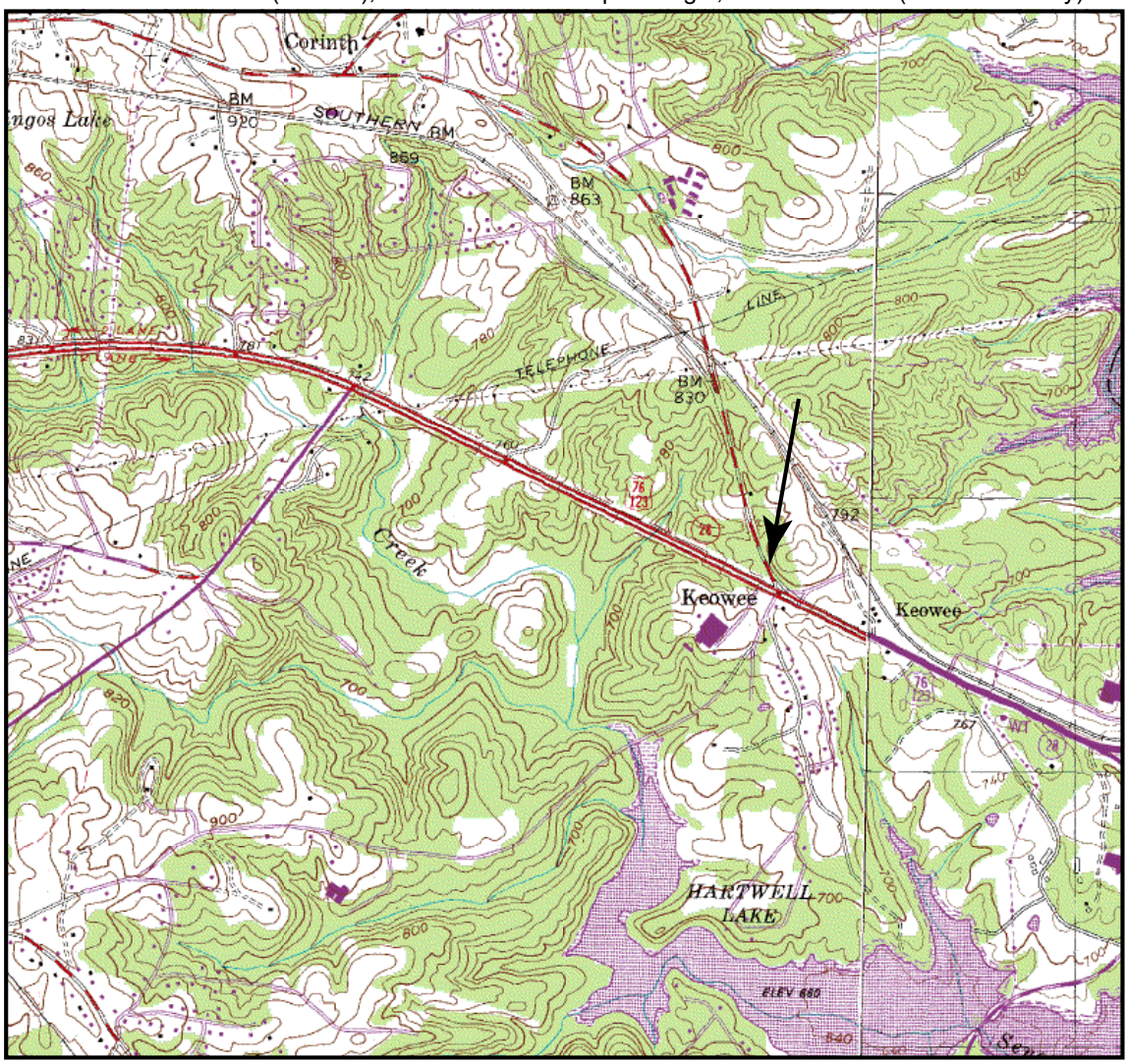

Tallulah Falls Formation (SMTF), Copeland 7.5-minute quadrangle, North Carolina (Surry County)

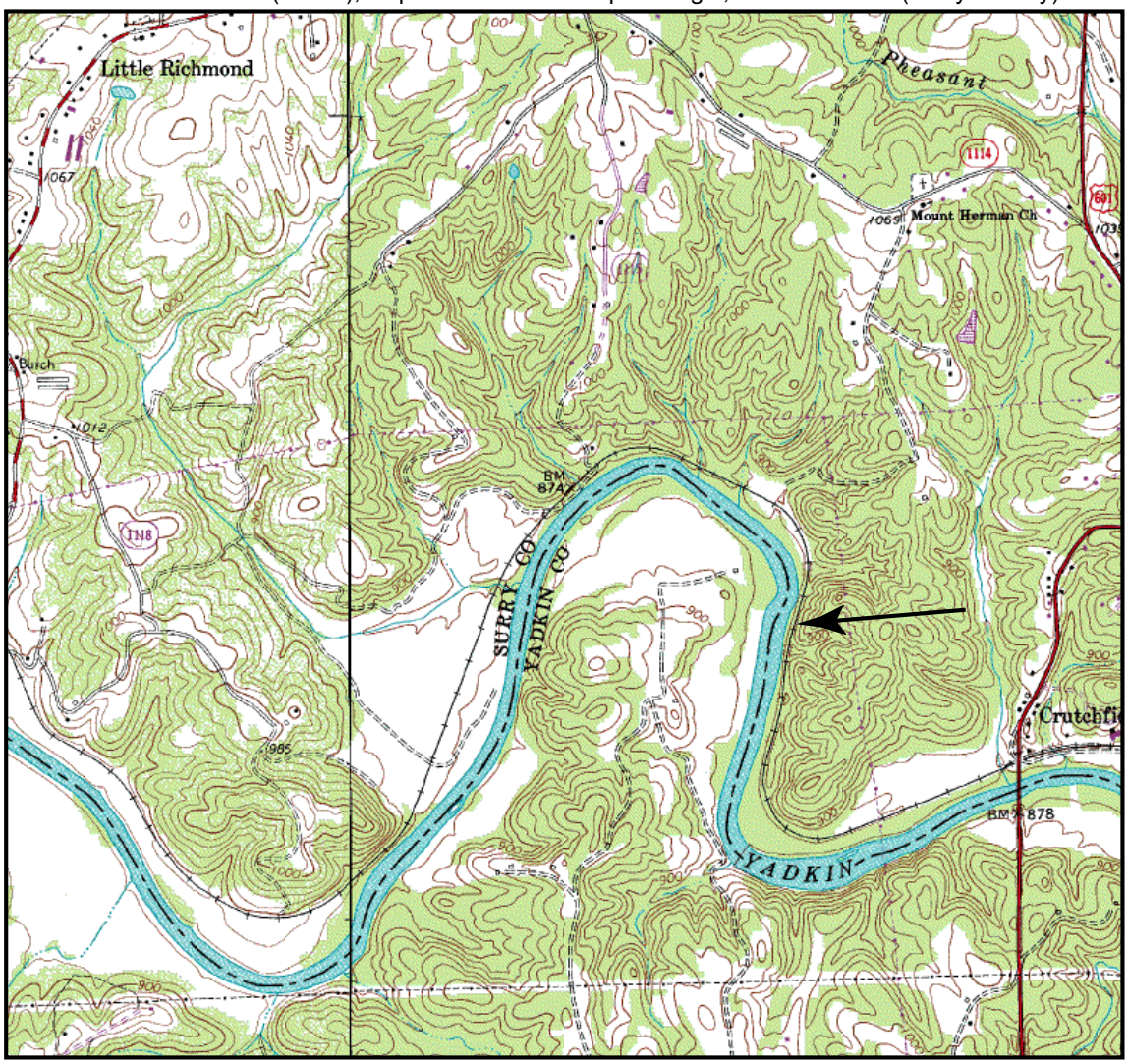

Unnamed metagraywacke (BCTF), Benn Knob 7.5-minute quadrangle, North Carolina
(Rutherford County)

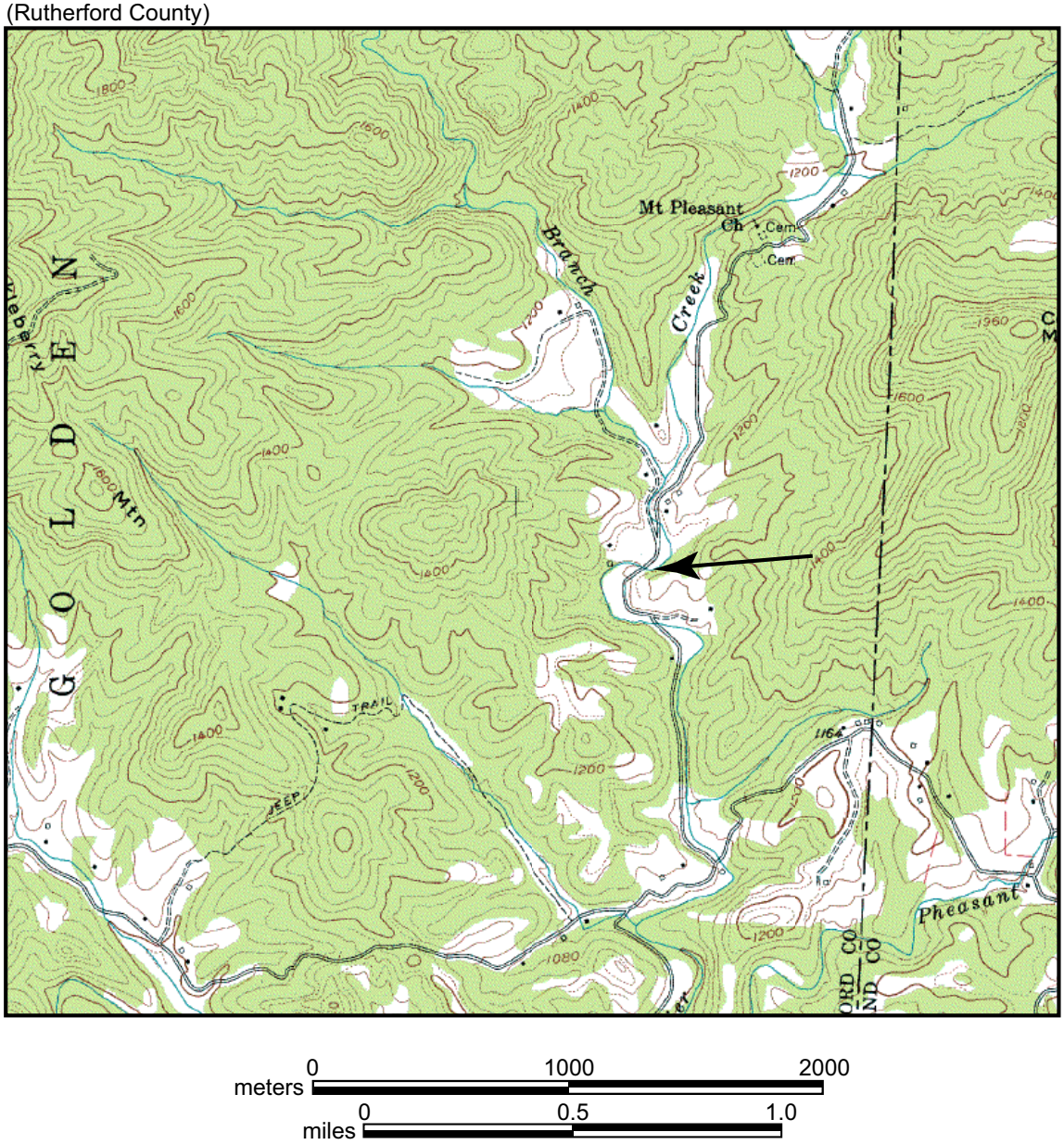

0 1000 2000
meters

0 0.5 1.0
miles

Unnamed metagraywacke (GR1), Greer 7.5-minute quadrangle, South Carolina (Spartanburg County)

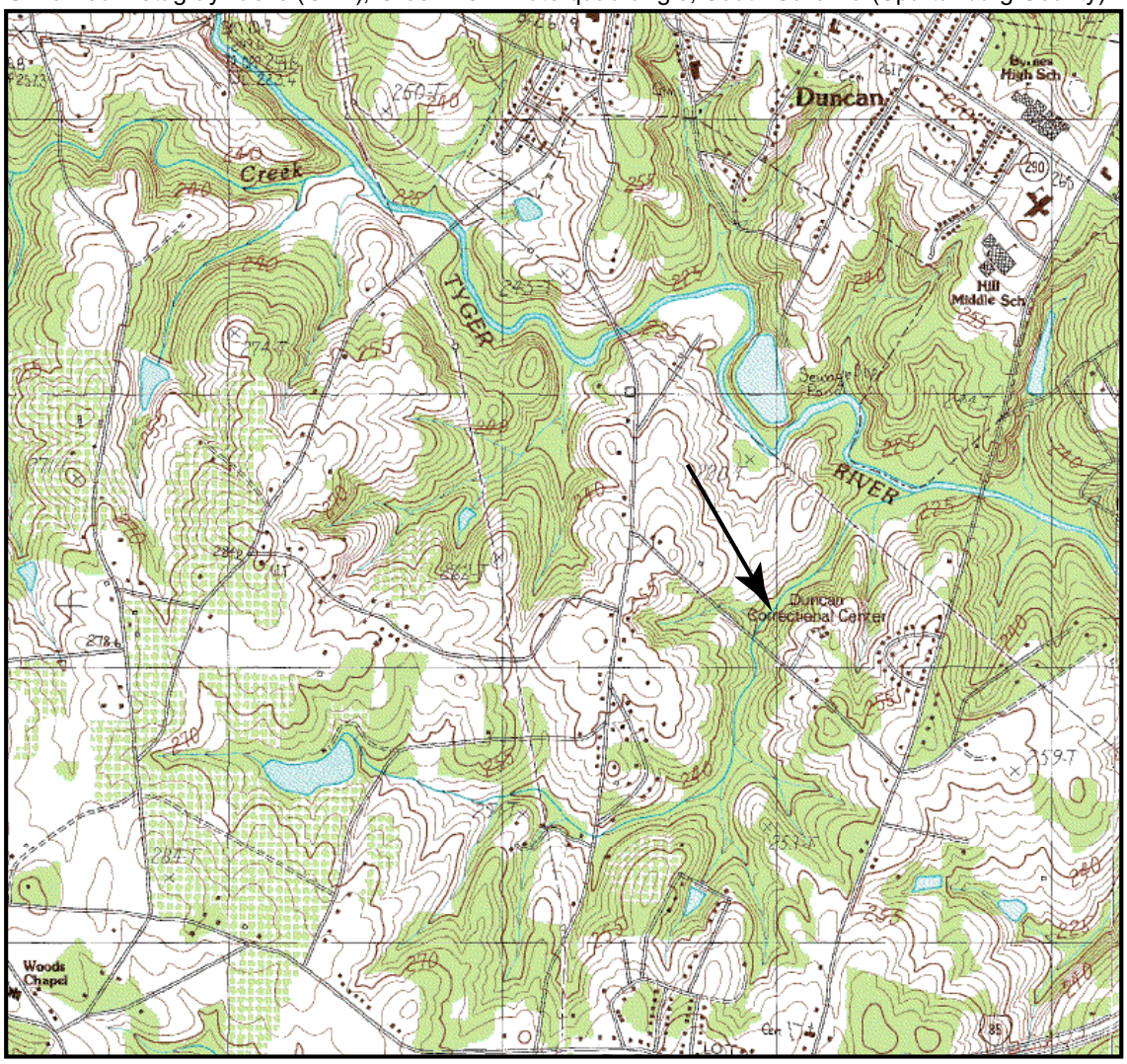

Sevier Shale (SEV), Kinzel Springs 7.5-minute quadrangle, Tennessee (Blount County)

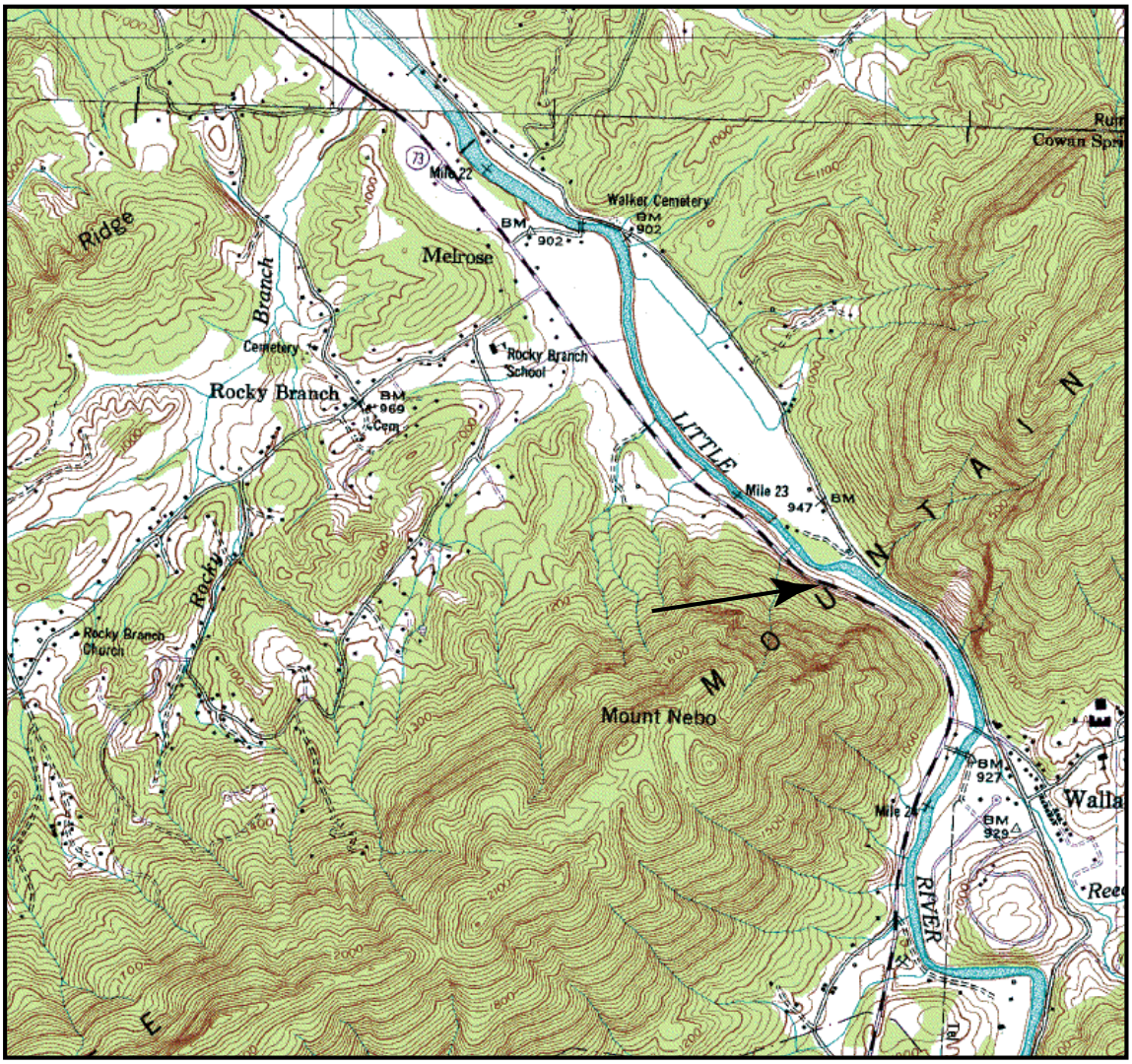

Cane Creek felsic gneiss (WIMPY), Campbell Mountain 7.5-minute quadrangle, Georgia (Lumpkin County)

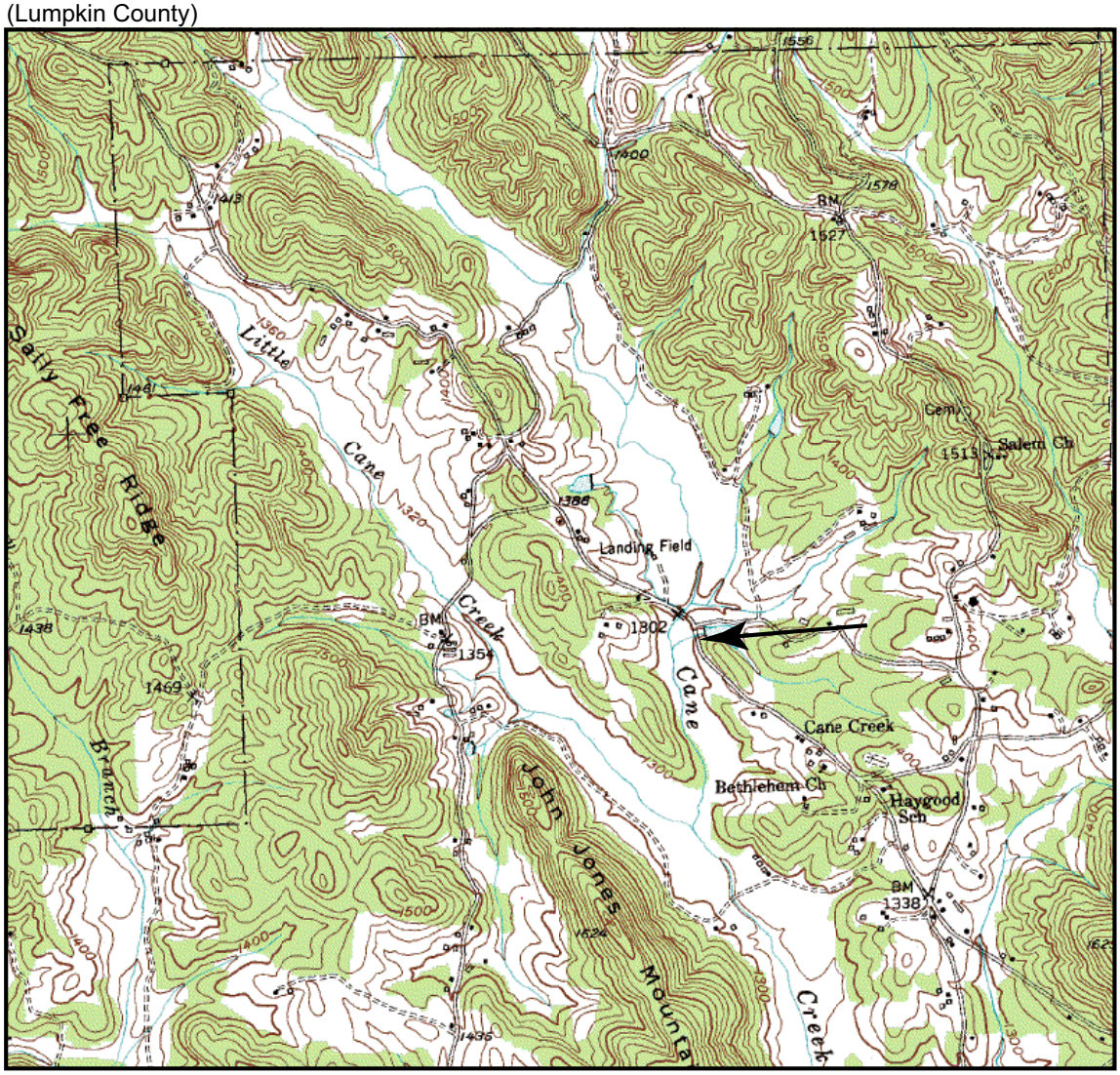

0 1000 2000
meters

0 0.5 1.0
miles

Kennesaw granitoid (KEN), Kennesaw 7.5-minute quadrangle, Georgia (Cobb County)

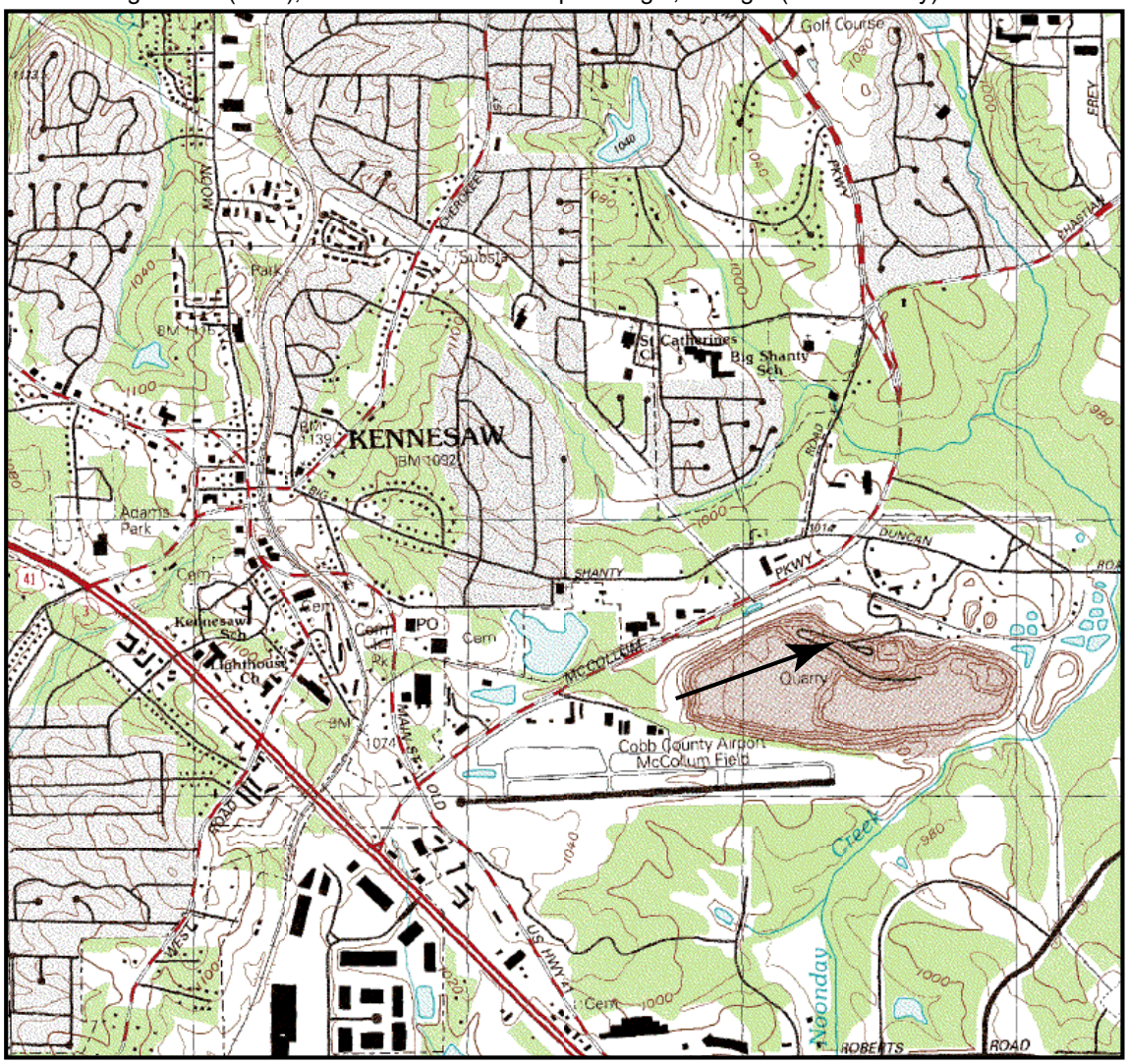

Dysartsville Tonalite (VM1782), Glenwood 7.5-minute quadrangle, North Carolina (McDowell County)

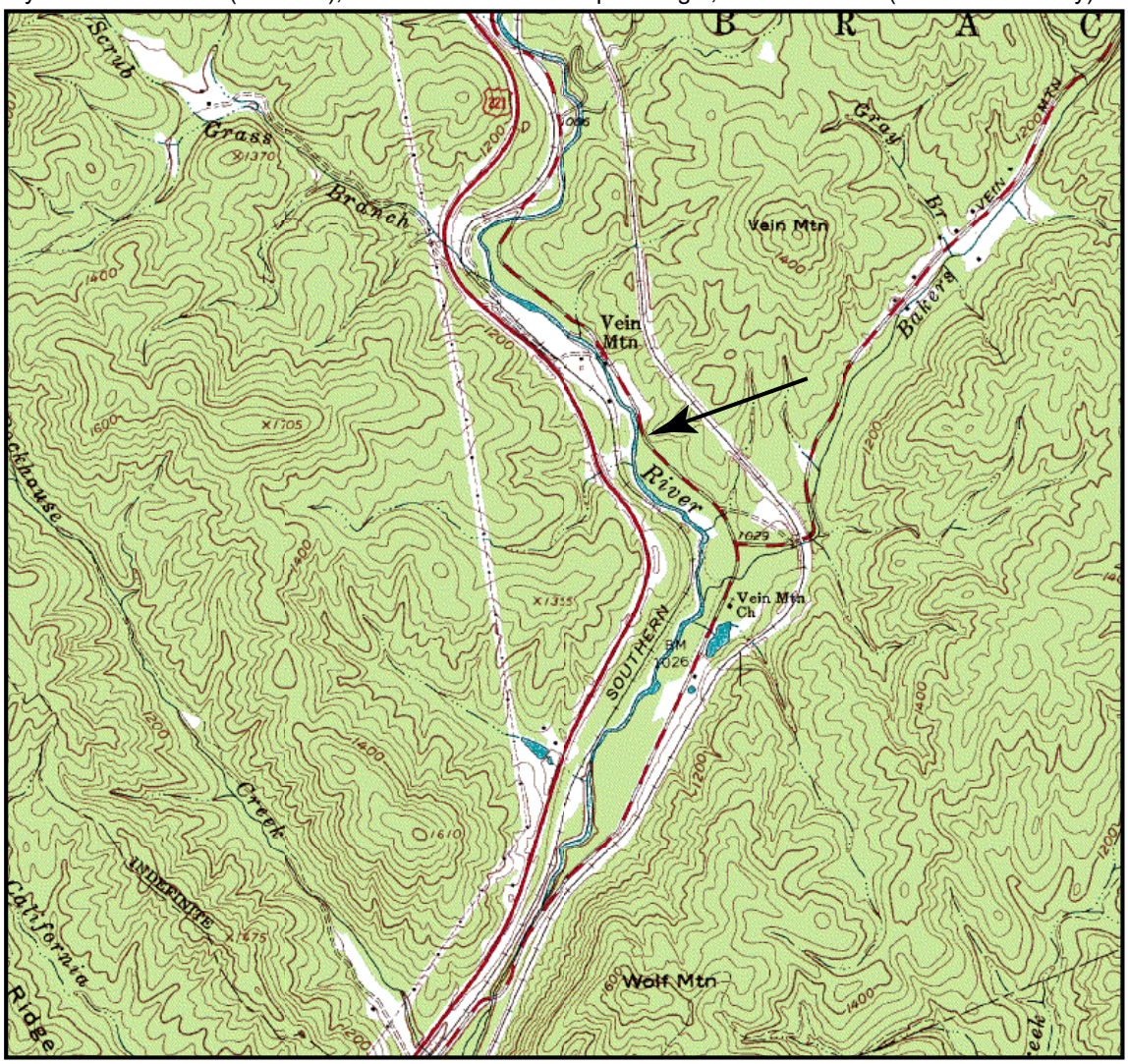

Lenoir Quarry migmatite (LVQ1), Kings Creek 7.5-minute quadrangle, North Carolina (Caldwell County)

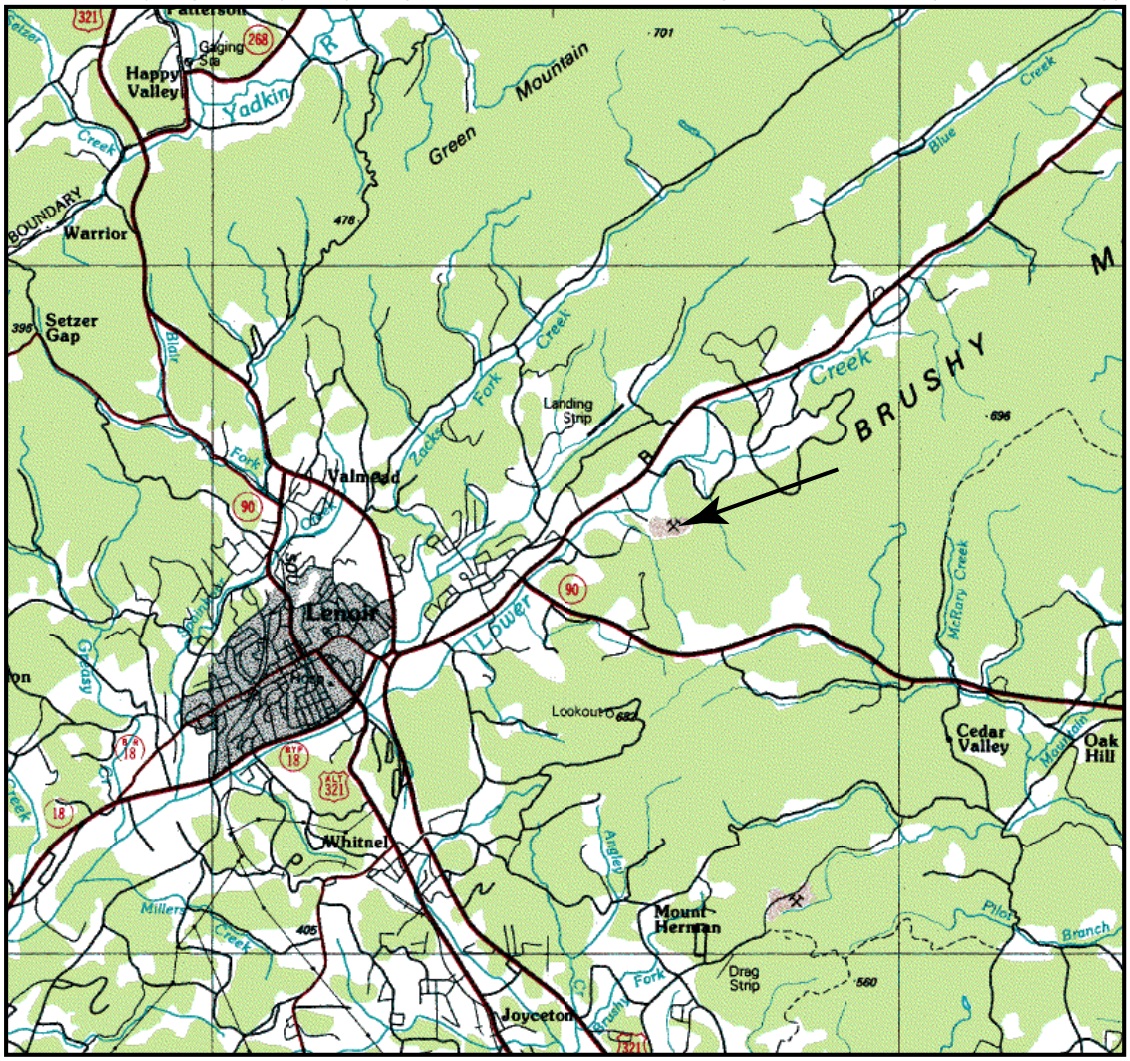

meters 0 4000 8000

miles 0 2.0 4.0

Poor Mountain Quartzite (POMTN), Glenwood 7.5-minute quadrangle, North Carolina (McDowell County)

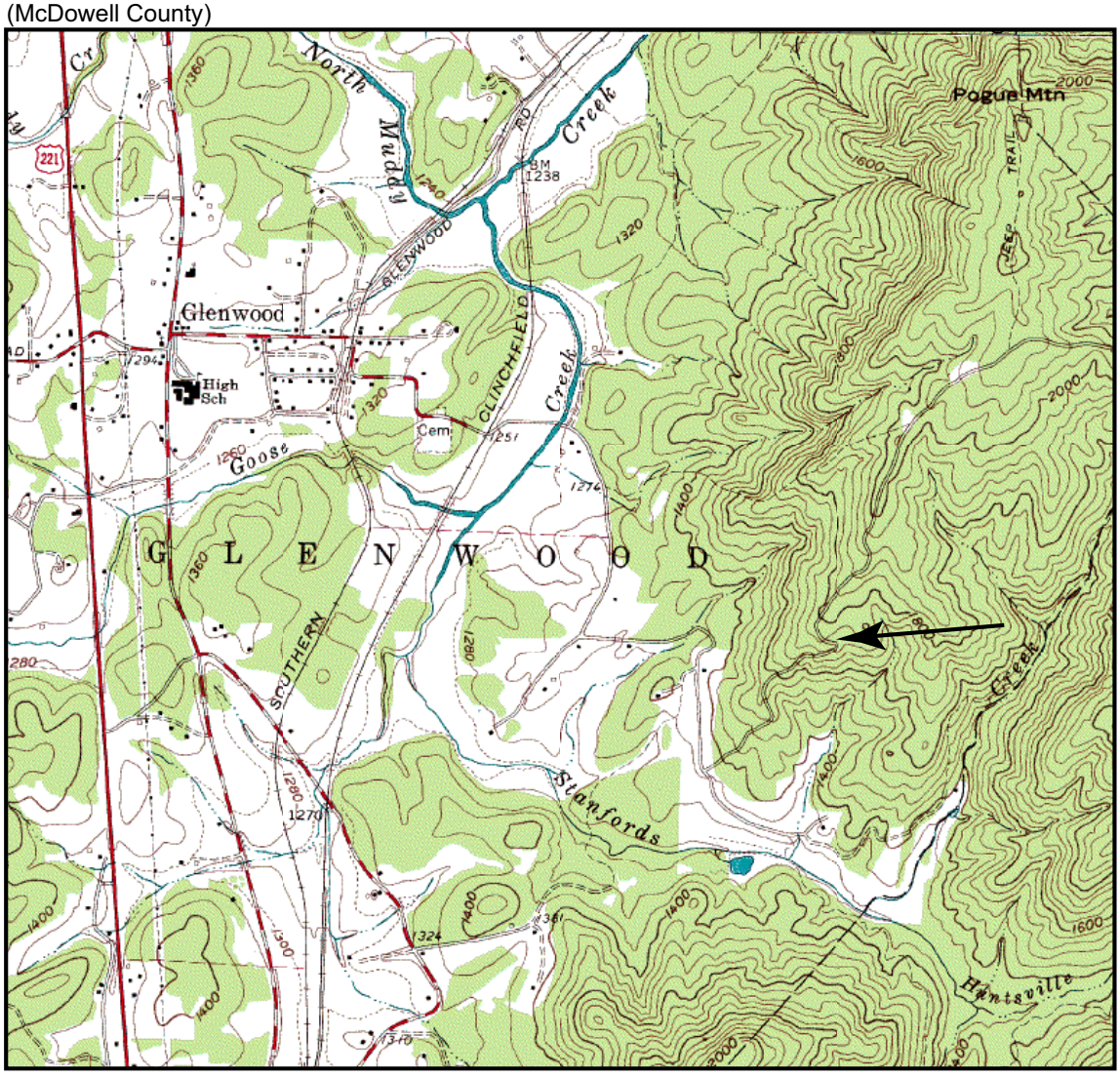

Zirconia Pegmatite (ZIRCONIA), Zirconia 7.5-minute quadrangle, North Carolina (Henderson County)

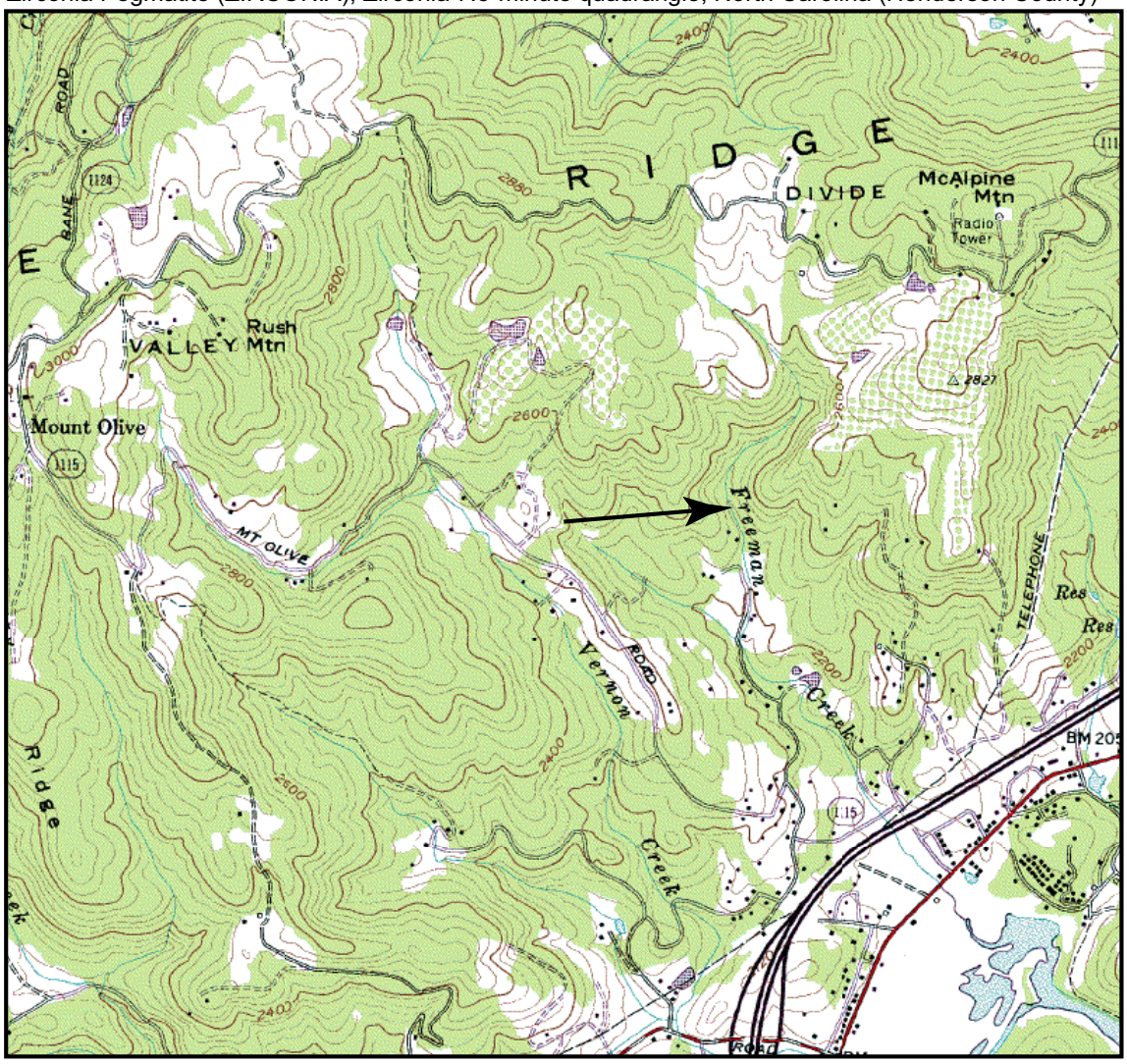

APPENDIX II

This appendix contains ion microprobe U-Pb detrital zircon data collected at Stanford University. All detrital zircon data collected at UCLA and Stanford University is available from the Geological Society of America as a Data

Analysis		U	Th		$^{204}Pb/$			Total $^{238}U/$		$^{207}Pb/$		Radiogenic Ratios[1] $^{238}U/$		$^{207}Pb/$		$^{207}Pb/$		$^{206}Pb/$		error	Ages (in Ma)[1] $^{206}Pb/$		$^{207}Pb/$		$^{207}Pb/$		%
Label	Zone	(in ppm)		Th/U	^{206}Pb	± 1σ	f206%[2]	^{206}Pb	± 1σ	^{206}Pb	± 1σ	^{206}Pb	± 1σ	^{206}Pb	± 1σ	^{235}U	± 1σ	^{238}U	± 1σ	corr.	^{238}U	± 1σ	^{235}U	± 1σ	^{206}Pb	± 1σ	Conc
BCTF-1 (sq)		750.1	91.1	0.12	<0.000001	<0.000001	0.0000	3.86	0.14	0.1029	0.0012	3.86	0.14	0.1029	0.0012	3.674	0.145	0.259	0.010	0.952	1484	50			1678	22	88
BCTF-2 (sq)	R	1129.6	5.6	0.00	<0.000001	<0.000001	0.0000	16.33	0.61	0.0519	0.0015	16.33	0.61	0.0519	0.0015	0.439	0.021	0.061	0.002	0.800	383	14			283	65	135
BCTF-3 (sq)		249.0	283.7	1.14	0.000924	0.000379	1.6594	13.40	0.63	0.0644	0.0027	13.62	0.65	0.0509	0.0063	0.515	0.068	0.073	0.003	0.358	457	21			236	286	194
BCTF-4 (sq)	R	3134.9	157.0	0.05	0.000092	0.000045	0.1645	16.34	0.61	0.0556	0.0007	16.37	0.61	0.0543	0.0010	0.457	0.019	0.061	0.002	0.901	382	14			383	40	100
BCTF-5 (sq)		180.3	62.8	0.35	<0.000001	<0.000001	0.0000	11.59	0.48	0.0660	0.0028	11.59	0.48	0.0660	0.0028	0.785	0.046	0.086	0.004	0.693	533	21			806	89	66
BCTF-6 (sq)		395.8	441.8	1.12	0.000798	0.000270	1.4327	17.40	0.68	0.0626	0.0022	17.65	0.69	0.0509	0.0047	0.397	0.040	0.057	0.002	0.394	355	14			236	211	150
BCTF-7 (sq)	R	1368.5	6.4	0.00	<0.000001	<0.000001	0.0000	16.84	0.64	0.0548	0.0011	16.84	0.64	0.0548	0.0011	0.449	0.019	0.059	0.002	0.884	372	14			405	45	92
BCTF-8 (sq)		998.7	81.4	0.08	0.000073	0.000048	0.1316	13.23	0.50	0.0550	0.0012	13.24	0.50	0.0540	0.0014	0.562	0.025	0.076	0.003	0.832	469	17			370	57	127
BCTF-9 (sq)		319.1	211.2	0.66	<0.000001	<0.000001	0.0000	13.23	0.52	0.0565	0.0021	13.23	0.52	0.0565	0.0021	0.589	0.032	0.076	0.003	0.732	470	18			472	81	99
BCTF-10 (sq)		380.4	251.5	0.66	<0.000001	<0.000001	0.0000	14.47	0.57	0.0549	0.0022	14.47	0.57	0.0549	0.0022	0.523	0.030	0.069	0.003	0.690	431	16			408	92	105
BCTF-11 (sq)		624.8	575.8	0.92	<0.000001	<0.000001	0.0000	13.38	0.52	0.0559	0.0017	13.38	0.52	0.0559	0.0017	0.576	0.029	0.075	0.003	0.783	465	17			450	69	103
BCTF-12 (sq)		67.7	67.4	0.99	<0.000001	<0.000001	0.0000	5.88	0.24	0.0796	0.0036	5.88	0.24	0.0796	0.0036	1.865	0.115	0.170	0.007	0.672	1012	39			1187	90	85
BCTF-13 (sq)	R	1417.2	9.5	0.01	<0.000001	<0.000001	0.0000	16.76	0.64	0.0535	0.0015	16.76	0.64	0.0535	0.0015	0.440	0.021	0.060	0.002	0.799	374	14			351	65	107
BCTF-14 (sq)		1378.6	1155.4	0.84	0.001194	0.000349	2.1426	15.79	0.60	0.0765	0.0047	16.14	0.62	0.0592	0.0071	0.506	0.064	0.062	0.002	0.302	388	14			574	262	68
BCTF-15 (sq)		489.4	239.5	0.49	0.000066	0.000042	0.1178	5.42	0.20	0.0794	0.0013	5.43	0.20	0.0784	0.0015	1.992	0.084	0.184	0.007	0.895	1090	38			1158	37	94
BCTF-16 (sq)		1110.5	515.0	0.46	<0.000001	<0.000001	0.0000	13.32	0.51	0.0588	0.0016	13.32	0.51	0.0588	0.0016	0.608	0.028	0.075	0.003	0.820	467	17			559	58	83
BCTF-17 (sq)		72.5	46.9	0.65	<0.000001	<0.000001	0.0000	12.83	0.58	0.0611	0.0048	12.83	0.58	0.0611	0.0048	0.656	0.059	0.078	0.004	0.498	484	21			642	169	75
BCTF-18 (sq)		355.5	109.4	0.31	<0.000001	<0.000001	0.0000	7.45	0.29	0.0691	0.0017	7.45	0.29	0.0691	0.0017	1.280	0.058	0.134	0.005	0.843	812	29			903	51	90
BCTF-19 (sq)		660.9	236.8	0.36	0.000000	<0.000001	0.0000	6.78	0.26	0.0763	0.0013	6.78	0.26	0.0763	0.0013	1.552	0.064	0.147	0.006	0.907	887	31			1104	35	80
BCTF-19-2 (sq)		438.4	123.0	0.28	0.000191	0.000073	0.3431	8.81	0.34	0.0705	0.0018	8.84	0.34	0.0678	0.0021	1.057	0.052	0.113	0.004	0.775	691	25			861	65	80
BCTF-21 (sq)	R	1340.7	31.8	0.02	<0.000001	<0.000001	0.0000	17.77	0.67	0.0540	0.0012	17.77	0.67	0.0540	0.0012	0.419	0.018	0.056	0.002	0.867	353	13			369	49	96
KEO-1.1		41.1	21.6	0.52	0.000010	0.000000	0.0002					6.02	0.15	0.0757	0.0027	1.732	0.078	0.166	0.004		990	23	1021	29	1086	72	91
KEO-2.1		36.1	26.2	0.73	0.000087	0.000126	0.0014					4.62	0.13	0.0857	0.0030	2.561	0.124	0.217	0.006		1264	33	1290	36	1332	70	95
KEO-3.1		210.7	42.9	0.20	0.000152	0.000093	0.0027					13.96	0.30	0.0645	0.0020	0.637	0.026	0.072	0.002		446	9	500	16	758	68	59
KEO-4.1		57.1	49.6	0.87	0.000055	0.000122	0.0009					6.27	0.19	0.0712	0.0029	1.565	0.083	0.159	0.005		953	27	956	33	964	84	99
KEO-4.2		369.3	107.1	0.29	0.000091	0.000056	0.0016					7.37	0.10	0.0679	0.0019	1.270	0.041	0.136	0.002		820	10	832	18	866	58	95
KEO-5.1		171.4	20.7	0.12	0.000010	0.000000	0.0002					5.57	0.07	0.0793	0.0010	1.963	0.037	0.180	0.002		1064	12	1103	13	1180	26	90
KEO-6.1		47.5	3.1	0.07	0.000261	0.000166	0.0045					5.87	0.12	0.0686	0.0033	1.611	0.087	0.170	0.003		1013	19	974	34	887	102	114
KEO-6.2	R	1778.4	15.5	0.01	0.000007	0.000008	0.0001					18.16	0.13	0.0521	0.0005	0.396	0.005	0.055	0.000		346	2	338	4	290	23	119
KEO-7.1		230.9	64.5	0.28	0.000010	0.000000	0.0002					5.08	0.06	0.0787	0.0015	2.136	0.049	0.197	0.002		1159	12	1161	16	1165	38	99
KEO-8.1		58.7	21.3	0.36	0.000010	0.000000	0.0002					4.47	0.09	0.0828	0.0026	2.554	0.102	0.224	0.005		1301	25	1288	30	1265	62	103
KEO-9.1		425.1	126.4	0.30	0.000010	0.000012	0.0002					5.21	0.05	0.0782	0.0008	2.069	0.031	0.192	0.002		1131	11	1139	10	1153	20	98
KEO-10.1		100.2	34.1	0.34	0.000038	0.000073	0.0006					5.95	0.10	0.0699	0.0017	1.620	0.052	0.168	0.003		1002	16	978	20	925	52	108
KEO-11.1		79.3	30.9	0.39	-0.000031	0.000060	-0.0005					5.19	0.13	0.0801	0.0018	2.128	0.075	0.193	0.005		1136	26	1158	25	1200	44	95
KEO-12.1		510.1	46.2	0.09	0.000005	0.000010	0.0001					5.75	0.04	0.0757	0.0006	1.814	0.020	0.174	0.001		1033	6	1050	7	1086	17	95
KEO13.1		73.9	43.5	0.59	0.000064	0.000093	0.0011					6.45	0.20	0.0722	0.0022	1.542	0.070	0.155	0.005		928	26	947	28	992	62	94
KEO14.1		102.9	30.4	0.29	0.000042	0.000110	0.0007					4.96	0.10	0.0779	0.0025	2.167	0.087	0.202	0.004		1185	22	1171	28	1144	66	104
KEO15.1		309.0	28.2	0.09	0.000010	0.000010	0.0002					5.03	0.09	0.0858	0.0010	2.352	0.051	0.199	0.003		1169	19	1228	16	1333	22	88
KEO16.1		37.7	47.3	1.26	0.000010	0.000000	0.0002					5.77	0.22	0.0735	0.0035	1.756	0.114	0.173	0.007		1030	37	1029	43	1027	99	100
KEO17.1		605.9	58.0	0.10	-0.000009	0.000019	-0.0002					5.95	0.04	0.0736	0.0006	1.705	0.020	0.168	0.001		1001	6	1011	7	1031	17	97
KEO-18.1		116.0	150.0	1.29	0.000010	0.000000	0.0002					4.03	0.06	0.0913	0.0021	3.128	0.091	0.248	0.004		1430	19	1440	23	1453	44	98
KEO-19.1		344.9	81.0	0.23	0.000082	0.000040	0.0014					5.79	0.19	0.0701	0.0013	1.669	0.067	0.173	0.006		1027	32	997	26	931	38	110
KEO-20.1		60.9	49.9	0.82	0.000010	0.000000	0.0002					5.74	0.11	0.0722	0.0017	1.733	0.054	0.174	0.003		1035	18	1021	20	991	47	104
KEO-21.1		46.1	21.9	0.47	0.000010	0.000000	0.0002					5.41	0.15	0.0774	0.0022	1.975	0.082	0.185	0.005		1094	27	1107	28	1132	57	97
KEO-22.1		222.9	141.0	0.63	0.000010	0.000000	0.0002					4.04	0.05	0.0924	0.0009	3.150	0.051	0.247	0.003		1425	16	1445	13	1475	17	97
KEO-23.1		228.2	49.4	0.22	0.000034	0.000040	0.0006					6.19	0.11	0.0730	0.0020	1.626	0.057	0.162	0.003		966	16	980	22	1013	58	95
KEO-24.1		97.2	69.3	0.71	-0.000044	0.000063	-0.0008					5.88	0.08	0.0743	0.0017	1.741	0.049	0.170	0.002		1012	13	1024	18	1049	46	96
KEO-25.1		410.7	271.3	0.66	0.000031	0.000027	0.0005					4.86	0.05	0.0812	0.0008	2.301	0.034	0.206	0.002		1205	11	1213	10	1226	20	98
KEO-26.1		155.4	75.5	0.49	0.000054	0.000052	0.0009					4.18	0.07	0.0891	0.0018	2.937	0.084	0.239	0.004		1381	21	1392	22	1407	40	98
KEO-27.1		62.8	22.8	0.36	-0.000073	0.000070	-0.0012					4.88	0.10	0.0810	0.0038	2.287	0.124	0.205	0.004		1201	23	1208	39	1221	96	98
KEO-28.1		368.7	90.8	0.25	-0.000007	0.000007	-0.0001					5.24	0.05	0.0775	0.0007	2.038	0.029	0.191	0.002		1125	10	1128	10	1133	19	99
KEO-29.1		169.2	50.6	0.30	0.000010	0.000019	0.0002					6.42	0.14	0.0730	0.0015	1.568	0.050	0.156	0.003		933	19	958	20	1015	42	92
KEO-30.1		9.5	4.1	0.43	0.000553	0.000618	0.0095					6.47	0.63	0.0727	0.0118	1.550	0.310	0.155	0.015		927	85	950	131	1006	371	92
KEO-31.1		268.8	70.8	0.26	0.000009	0.000021	0.0002					4.91	0.07	0.0787	0.0011	2.210	0.047	0.204	0.003		1195	16	1184	15	1165	27	103
KEO-32.1		383.4	202.9	0.53	0.000012	0.000018	0.0002					6.11	0.06	0.0720	0.0007	1.625	0.024	0.164	0.002		978	9	980	10	985	21	99
KEO-33.1		628.6	64.7	0.10	0.000192	0.000039	0.0033					5.82	0.04	0.0736	0.0010	1.743	0.028	0.172	0.001		1022	7	1025	10	1031	28	99
KEO-34.1		97.4	53.3	0.55	0.000010	0.000000	0.0002					3.82	0.09	0.0941	0.0014	3.401	0.098	0.262	0.006		1501	31	1505	23	1510	28	99
KEO-35.1		1069.8	255.8	0.24	0.000014	0.000032	0.0002					5.71	0.04	0.0730	0.0008	1.764	0.024	0.175	0.001		1041	6	1032	9	1014	23	103
KEO-36.1		82.4	74.2	0.90	0.000145	0.000124	0.0025					5.59	0.09	0.0733	0.0024	1.809	0.069	0.179	0.003		1062	16	1049	25	1022	68	104
KEO-37.1		149.1	32.3	0.22	0.000010	0.000000	0.0002					5.72	0.08	0.0748	0.0015	1.804	0.047	0.175	0.002		1039	13	1047	17	1063	41	98
KEO-38.1		59.3	27.9	0.47	0.000500	0.000725	0.0085					5.79	0.17	0.0660	0.0117	1.572	0.288	0.173	0.005		1027	29	959	121	807	422	127
KEO-39.1		381.0	114.5	0.30	0.000010	0.000011	0.0002					5.33	0.06	0.0747	0.0009	1.934	0.033	0.188	0.002		1109	12	1093	12	1061	23	104
KEO-40.1		827.8	201.6	0.24	0.000016	0.000013	0.0003					6.80	0.10	0.0743	0.0013	1.508	0.037	0.147	0.002		885	12	933	15	1050	37	84
BECR-1.1		410.9	219.2	0.53	0.000012	0.000011	0.0002					5.12	0.07	0.0845	0.0012	2.276	0.047	0.195	0.003		1151	14	1205	15	1304	28	88
BECR-2.1		142.1	164.5	1.16	0.000013	0.000034	0.0002					5.22	0.50	0.0783	0.0044	2.069	0.240	0.192	0.018		1130	99	1139	83	1155	115	98
BECR-2.2		406.5	87.8	0.22	0.000005	0.000011	0.0001					6.26	0.11	0.0718	0.0017	1.581	0.049	0.160	0.003		955	16	963	19	981	48	97
BECR-3.1		97.6	56.1	0.57	0.000028	0.000062	0.0005					5.87	0.14	0.0736	0.0019	1.729	0.065	0.171	0.004		1015	23	1019	24	1029	53	99
BECR-4.1		242.5	189.6	0.78	0.000041	0.000026	0.0007					5.34	0.07	0.0777	0.0018	2.006	0.056	0.187	0.002		1106	13	1118	19	1140	46	97
BECR-5.1		98.5	38.1	0.39	0.000010	0.000000	0.0002					6.21	0.11	0.0747	0.0024	1.659	0.065	0.161	0.003		963	16	993	25	1061	67	91
BECR-6.1		129.3	47.7	0.37	0.000010	0.000000	0.0002					5.68	0.10	0.0735	0.0015	1.785	0.051	0.176	0.003		1046	17	1040	19	1027	41	102
BECR-6.2		117.0	46.2	0.39	0.000025	0.000052	0.0004					7.51	0.14	0.0663	0.0036	1.218	0.073	0.133	0.003		806	14	809	34	816	119	99
BECR-7.1		180.4	52.9	0.29	0.000081	0.000124	0.0014					5.70	0.18	0.0823	0.0024	1.990	0.091	0.175	0.006		1042	30	1112	31	1252	59	83
BECR-8.1		168.5	37.8	0.22	0.000014	0.000032	0.0002					5.04	0.08	0.0806	0.0022	2.203	0.075	0.198	0.003		1167	17	1182	24	1210	55	96
BECR-9.1		541.8	41.6	0.08	0.000025	0.000025	0.0004					7.40	0.10	0.0734	0.0014	1.368	0.034	0.135	0.002		817	11	875	15	1026	38	80
BECR-10.1		163.6	192.5	1.18	0.000046	0.000049	0.0008					4.43	0.05	0.0826	0.0013	2.571	0.052	0.226	0.002		1313	13	1292	15	1259	32	104
BECR-11.1		366.3	113.1	0.31	0.000006	0.000013	0.0001					5.92	0.07	0.0800	0.0013	1.862	0.039	0.169	0.002		1006	11	1068	14	1196	32	84

Analysis		U	Th		$^{204}Pb/$			Total $^{238}U/$		$^{207}Pb/$		Radiogenic Ratios[1] $^{238}U/$		$^{207}Pb/$		$^{207}Pb/$		$^{206}Pb/$		error	Ages (in Ma)[1] $^{206}Pb/$		$^{207}Pb/$		$^{207}Pb/$		%
Label	Zone	(in ppm)		Th/U	^{206}Pb	± 1σ	f206%[2]	^{206}Pb	± 1σ	^{206}Pb	± 1σ	^{206}Pb	± 1σ	^{206}Pb	± 1σ	^{235}U	± 1σ	^{238}U	± 1σ	corr.	^{238}U	± 1σ	^{235}U	± 1σ	^{206}Pb	± 1σ	Conc
BECR-12.1		142.1	66.4	0.47	0.000021	0.000044	0.0004					7.82	0.22	0.0707	0.0016	1.246	0.047	0.128	0.004		776	21	822	22	948	46	82
BECR-13.1		220.3	355.9	1.62	0.000010	0.000000	0.0002					4.46	0.12	0.0856	0.0016	2.647	0.092	0.224	0.006		1305	32	1314	26	1329	36	98
BECR-14.1		325.7	106.2	0.33	0.000010	0.000000	0.0002					5.46	0.06	0.0774	0.0012	1.954	0.039	0.183	0.002		1084	11	1100	14	1131	31	96
BECR-15.1		130.5	35.3	0.27	-0.000034	0.000076	-0.0006					5.25	0.13	0.0795	0.0020	2.088	0.078	0.191	0.005		1124	25	1145	26	1184	50	95
BECR-16.1		96.8	40.0	0.41	0.000010	0.000018	0.0002					6.61	0.14	0.0739	0.0023	1.542	0.061	0.151	0.003		908	18	947	25	1040	65	87
BECR-17.1		315.7	112.3	0.36	0.007120	0.001125	0.1246					7.94	0.20	0.0595	0.0206	1.034	0.362	0.126	0.003		765	18	721	199	587	1009	130
BECR-17.2		275.3	67.3	0.24	0.000073	0.000033	0.0012					4.86	0.06	0.0789	0.0014	2.241	0.052	0.206	0.003		1207	14	1194	17	1171	36	103
BECR-18.1		364.3	200.6	0.55	0.000010	0.000015	0.0002					4.77	0.05	0.0798	0.0012	2.305	0.045	0.209	0.002		1226	12	1214	14	1192	30	103
BECR-19.1		344.2	156.7	0.46	0.000071	0.000047	0.0012					5.35	0.04	0.0799	0.0010	2.058	0.033	0.187	0.002		1104	8	1135	11	1194	25	92
BECR-20.1		200.8	63.6	0.32	0.000010	0.000000	0.0002					5.61	0.07	0.0768	0.0011	1.887	0.038	0.178	0.002		1058	12	1077	13	1115	29	95
BECR-21.1		210.0	74.5	0.35	0.000010	0.000000	0.0002					5.38	0.10	0.0763	0.0019	1.955	0.065	0.186	0.003		1098	19	1100	23	1104	51	100
BECR-21.2		494.1	163.7	0.33	0.000024	0.000055	0.0004					7.34	0.14	0.0719	0.0014	1.350	0.038	0.136	0.003		823	14	868	16	984	39	84
BECR-22.1		153.4	68.3	0.45	0.000040	0.000094	0.0007					5.87	0.15	0.0713	0.0018	1.672	0.063	0.170	0.004		1013	24	998	24	965	53	105
BECR-23.1		171.8	73.8	0.43	0.002723	0.000304	0.0460					5.42	0.12	0.0829	0.0054	2.107	0.150	0.184	0.004		1091	23	1151	50	1266	132	86
BECR-24.1		325.0	94.6	0.29	0.000029	0.000041	0.0005					5.48	0.07	0.0750	0.0016	1.887	0.048	0.183	0.002		1081	12	1077	17	1068	43	101
BECR-25.1		125.2	28.5	0.23	0.000021	0.000046	0.0004					4.82	0.08	0.0818	0.0019	2.340	0.069	0.207	0.003		1215	18	1225	21	1241	45	98
BECR-26.1		182.4	108.2	0.59	0.000012	0.000024	0.0002					4.79	0.05	0.0781	0.0013	2.249	0.048	0.209	0.002		1223	12	1196	15	1149	34	106
BECR-27.1		41.0	25.4	0.62	-0.000077	0.000160	-0.0013					5.63	0.27	0.0723	0.0035	1.771	0.128	0.178	0.009		1055	47	1035	48	994	102	106
BECR-28.1		350.0	150.7	0.43	0.000010	0.000000	0.0002					4.77	0.13	0.0808	0.0019	2.333	0.088	0.209	0.006		1226	30	1223	27	1216	47	101
BECR-29.1		173.0	76.5	0.44	0.000044	0.000037	0.0007					4.68	0.06	0.0802	0.0014	2.364	0.054	0.214	0.003		1249	14	1232	16	1201	35	104
BECR-30.1		50.4	55.3	1.10	0.000048	0.000101	0.0008					5.72	0.17	0.0760	0.0032	1.832	0.099	0.175	0.005		1039	29	1057	36	1095	86	95
BECR-31.1		56.3	28.9	0.51	0.000010	0.000000	0.0002					4.73	0.11	0.0818	0.0021	2.384	0.089	0.211	0.005		1236	27	1238	27	1240	52	100
BECR-32.1		75.6	4.1	0.05	-0.000032	0.000065	-0.0005					4.55	0.14	0.0821	0.0027	2.486	0.118	0.220	0.007		1280	36	1268	35	1248	65	103
BECR-33.1		167.4	59.9	0.36	0.000016	0.000034	0.0003					6.23	0.15	0.0714	0.0019	1.581	0.059	0.161	0.004		960	21	963	24	968	55	99
BECR-34.1		69.2	25.3	0.37	0.000365	0.000174	0.0061					4.82	0.11	0.0822	0.0045	2.350	0.147	0.207	0.005		1215	26	1227	46	1249	112	97
BECR-35.1		199.2	80.3	0.40	0.000013	0.000029	0.0002					4.91	0.09	0.0766	0.0014	2.149	0.059	0.203	0.004		1194	20	1165	19	1111	36	108
BECR-36.1		105.5	50.6	0.48	0.000010	0.000000	0.0002					5.02	0.11	0.0822	0.0015	2.257	0.069	0.199	0.004		1170	24	1199	22	1251	37	94
BECR-37.1		127.8	57.5	0.45	0.000033	0.000078	0.0006					5.38	0.09	0.0784	0.0021	2.011	0.067	0.186	0.003		1100	18	1119	23	1157	53	95
PMQ-1.1		116.6	71.1	0.61	0.00001	0.00000	0.0002					4.83	0.13	0.0845	0.0019	2.410	0.089	0.207	0.005		1213	29	1246	27	1304	45	93
PMQ-2.1		97.7	18.9	0.19	0.00001	0.00001	0.0002					5.65	0.07	0.0740	0.0013	1.806	0.041	0.177	0.002		1051	13	1048	15	1042	35	101
PMQ-3.1		143.8	62.0	0.43	0.00004	0.00005	0.0007					5.89	0.06	0.0747	0.0017	1.748	0.045	0.170	0.002		1011	10	1026	17	1059	45	95
PMQ-4.1		650.3	9.4	0.01	0.00001	0.00001	0.0002					5.74	0.04	0.0737	0.0005	1.772	0.019	0.174	0.001		1036	7	1035	7	1034	14	100
PMQ-5.1		75.9	27.7	0.36	0.00001	0.00002	0.0002					5.89	0.12	0.0718	0.0017	1.681	0.055	0.170	0.003		1011	19	1001	21	979	49	103
PMQ-6.1		221.6	46.0	0.21	0.00003	0.00005	0.0006					5.73	0.09	0.0774	0.0023	1.864	0.065	0.175	0.003		1038	14	1068	23	1132	61	92
PMQ-7.1		235.6	196.2	0.83	0.00002	0.00002	0.0003					5.41	0.07	0.0766	0.0012	1.953	0.043	0.185	0.002		1094	14	1100	15	1110	31	99
PMQ-8.1		206.6	53.9	0.26	0.00001	0.00000	0.0002					6.31	0.07	0.0737	0.0011	1.610	0.032	0.158	0.002		948	10	974	12	1034	31	92
PMQ-8.2		277.1	56.1	0.20	0.00001	0.00000	0.0002					6.87	0.07	0.0722	0.0011	1.449	0.028	0.146	0.001		877	8	910	12	991	32	88
PMQ-9.1		87.2	40.1	0.46	0.00012	0.00007	0.0020					5.63	0.09	0.0731	0.0022	1.791	0.064	0.178	0.003		1055	16	1042	24	1016	61	104
PMQ-10.1		514.4	85.8	0.17	0.00018	0.00006	0.0030					5.96	0.08	0.0737	0.0015	1.706	0.044	0.168	0.002		1000	13	1011	17	1034	42	97
PMQ-11.1		302.7	99.3	0.33	0.00001	0.00000	0.0002					5.05	0.06	0.0817	0.0026	2.233	0.078	0.198	0.002		1165	13	1192	25	1239	63	94
PMQ-12.1		102.7	38.4	0.37	0.00003	0.00006	0.0005					5.91	0.11	0.0747	0.0016	1.741	0.053	0.169	0.003		1007	18	1024	20	1060	44	95
PMQ-13.1		104.6	53.4	0.51	0.00001	0.00003	0.0002					5.81	0.09	0.0742	0.0021	1.762	0.061	0.172	0.003		1024	15	1032	23	1048	59	98
PMQ-14.1		1045.1	103.6	0.10	0.00000	0.00001	0.0000					5.58	0.05	0.0748	0.0009	1.848	0.028	0.179	0.001		1062	8	1063	10	1064	23	100
PMQ-15.1		227.4	35.2	0.15	0.00001	0.00000	0.0002					5.79	0.06	0.0763	0.0021	1.817	0.055	0.173	0.002		1027	10	1052	20	1103	55	93
PMQ-16.1		140.2	21.8	0.16	0.00001	0.00000	0.0002					5.88	0.10	0.0726	0.0017	1.701	0.053	0.170	0.003		1012	16	1009	20	1002	49	101
PMQ-17.1		162.3	137.7	0.85	0.00139	0.00041	0.0240					6.45	0.09	0.0776	0.0068	1.660	0.151	0.155	0.002		930	13	993	59	1137	185	82
PMQ-18.1		246.9	47.1	0.19	0.00002	0.00002	0.0003					4.80	0.05	0.0803	0.0015	2.310	0.051	0.209	0.002		1221	11	1215	16	1205	37	101
PMQ-19.1		79.1	49.0	0.62	0.00001	0.00000	0.0002					5.71	0.09	0.0701	0.0017	1.693	0.053	0.175	0.003		1040	15	1006	20	932	52	112
PMQ-20.1		143.4	55.3	0.39	0.00001	0.00000	0.0002					5.72	0.09	0.0727	0.0015	1.753	0.047	0.175	0.003		1039	14	1028	18	1005	43	103
PMQ-21.1		114.2	36.9	0.32	0.00001	0.00000	0.0002					5.66	0.14	0.0742	0.0013	1.808	0.058	0.177	0.004		1049	24	1048	21	1048	36	100
PMQ-22.1		212.2	48.7	0.23	0.00001	0.00000	0.0002					5.89	0.07	0.0725	0.0011	1.699	0.035	0.170	0.002		1011	12	1008	13	1001	30	101
PMQ-23.1		262.9	69.0	0.26	0.00001	0.00000	0.0002					5.77	0.10	0.0724	0.0010	1.729	0.041	0.173	0.003		1030	17	1020	15	997	28	103
PMQ-24.1		216.6	89.5	0.41	0.00004	0.00004	0.0006					5.40	0.10	0.0793	0.0011	2.025	0.051	0.185	0.004		1095	19	1124	17	1181	29	93
PMQ-25.1		57.7	43.1	0.75	0.00131	0.00049	0.0222					5.62	0.11	0.0691	0.0083	1.695	0.210	0.178	0.004		1055	20	1007	83	902	269	117
PMQ-26.1		52.7	13.4	0.25	-0.00005	0.00002	-0.0008					4.70	0.12	0.0794	0.0035	2.327	0.126	0.213	0.006		1243	30	1221	39	1181	90	105
PMQ-27.1		330.9	92.5	0.28	0.00002	0.00002	0.0003					5.39	0.08	0.0774	0.0020	1.982	0.063	0.186	0.003		1098	15	1109	22	1132	53	97
PMQ-28.1		101.1	71.7	0.71	0.00001	0.00000	0.0002					4.98	0.07	0.0822	0.0012	2.275	0.047	0.201	0.003		1180	14	1205	15	1249	29	94
PMQ-28.2		571.5	86.6	0.15	0.00001	0.00001	0.0001					5.15	0.04	0.0793	0.0011	2.122	0.037	0.194	0.002		1143	8	1156	12	1180	29	97
PMQ-29.1		256.5	57.3	0.22	0.00001	0.00000	0.0002					4.26	0.04	0.0851	0.0008	2.753	0.041	0.235	0.002		1358	13	1343	11	1319	18	103
PMQ-30.1		255.2	46.0	0.18	0.00004	0.00007	0.0007					5.87	0.07	0.0720	0.0015	1.691	0.042	0.170	0.002		1014	12	1005	16	987	42	103
PMQ-31.1		242.5	783.6	3.23	0.00019	0.00010	0.0033					7.45	0.11	0.0781	0.0018	1.446	0.042	0.134	0.002		812	11	908	17	1150	47	71
PMQ-31.2		611.3	133.5	0.22	0.00001	0.00002	0.0002					5.89	0.04	0.0729	0.0008	1.706	0.022	0.170	0.001		1010	6	1011	8	1012	21	100
PMQ-32.1		111.1	73.6	0.66	0.00005	0.00005	0.0008					5.11	0.07	0.0785	0.0014	2.118	0.050	0.196	0.003		1152	14	1155	16	1159	36	99
PMQ-33.1		67.8	9.4	0.14	0.00003	0.00006	0.0006					4.46	0.26	0.0850	0.0056	2.626	0.243	0.224	0.013		1304	68	1308	70	1315	133	99
PMQ-34.1		216.6	137.0	0.63	0.00001	0.00002	0.0002					4.44	0.07	0.0865	0.0011	2.686	0.056	0.225	0.003		1309	18	1325	16	1350	25	97
PMQ-33.2		183.1	36.2	0.20	0.00003	0.00005	0.0005					4.81	0.08	0.0813	0.0012	2.329	0.054	0.208	0.003		1217	18	1221	17	1228	29	99
PMQ-35.1		113.9	86.9	0.76	0.00001	0.00000	0.0002					6.05	0.10	0.0729	0.0011	1.662	0.039	0.165	0.003		986	15	994	15	1011	31	98
COLRAB-1.1		141.2	62.3	0.44	0.00001	0.00000	0.0002					5.52	0.07	0.0758	0.0013	1.894	0.043	0.181	0.002		1074	13	1079	15	1089	35	99
COLRAB-2.1		283.4	116.5	0.41	0.00001	0.00000	0.0002					4.83	0.10	0.0822	0.0011	2.345	0.062	0.207	0.004		1213	24	1226	19	1250	25	97
COLRAB-3.1		92.1	35.9	0.39	0.00004	0.00003	0.0007					4.07	0.06	0.0909	0.0013	3.076	0.067	0.245	0.004		1415	19	1427	17	1444	27	98
COLRAB-4.1		193.8	56.7	0.29	-0.00002	0.00002	-0.0004					4.72	0.04	0.0830	0.0009	2.423	0.036	0.212	0.002		1238	11	1249	11	1269	20	98
COLRAB-4.2		1072.1	44.1	0.04	0.00001	0.00000	0.0002					6.65	0.06	0.0721	0.0006	1.495	0.020	0.150	0.001		903	8	928	8	988	17	91
COLRAB-5.1		87.2	49.1	0.56	0.00003	0.00006	0.0005					6.08	0.12	0.0711	0.0018	1.613	0.054	0.164	0.003		982	17	975	21	961	52	102
COLRAB-6.1		158.9	158.4	1.00	0.00003	0.00002	0.0006					4.14	0.09	0.0909	0.0017	3.025	0.093	0.241	0.005		1393	28	1414	24	1445	35	96
COLRAB-7.1		520.6	331.1	0.64	0.00001	0.00000	0.0002					5.06	0.03	0.0839	0.0005	2.283	0.021	0.197	0.001		1162	6	1207	7	1290	12	90
COLRAB-8.1		122.4	33.7	0.28	0.00120	0.00031	0.0200					4.67	0.09	0.0823	0.0054	2.430	0.171	0.214	0.004		1250	23	1252	52	1254	133	100
COLRAB-9.1		105.9	63.9	0.60	0.00004	0.00004	0.0007					5.71	0.10	0.0729	0.0021	1.762	0.062	0.175	0.003		1041	16	1032	23	1011	59	103

Analysis		U	Th		$^{204}Pb/$			Total $^{238}U/$		$^{207}Pb/$		Radiogenic Ratios[1] $^{238}U/$		$^{207}Pb/$		$^{206}Pb/$			error	Ages (in Ma)[1] $^{206}Pb/$		$^{207}Pb/$		$^{207}Pb/$		%
Label	Zone	(in ppm)		Th/U	^{206}Pb	± 1σ	f206%[2]	^{206}Pb	± 1σ	^{206}Pb	± 1σ	^{206}Pb	± 1σ	^{206}Pb	± 1σ	^{238}U	± 1σ		corr.	^{238}U	± 1σ	^{235}U	± 1σ	^{206}Pb	± 1σ	Conc
COLRAB-10.1		52.3	20.4	0.39	-0.00005	0.00004	-0.0008					5.07	0.10	0.0822	0.0018	2.238	0.071	0.197	0.004		1161	22	1193	23	1251	44	93
COLRAB-11.1		128.8	214.8	1.67	-0.00001	0.00001	-0.0002					3.66	0.05	0.1001	0.0012	3.766	0.074	0.273	0.004		1556	20	1586	16	1625	22	96
COLRAB-11.2		234.6	128.8	0.55	0.00001	0.00000	0.0002					4.21	0.07	0.0948	0.0016	3.102	0.075	0.237	0.004		1373	19	1433	19	1524	32	90
COLRAB-12.1		146.3	60.8	0.42	-0.00005	0.00005	-0.0009					6.06	0.09	0.0715	0.0013	1.626	0.039	0.165	0.002		984	13	980	15	971	37	101
COLRAB-13.1		241.8	101.6	0.42	0.00001	0.00000	0.0002					5.82	0.07	0.0737	0.0008	1.746	0.031	0.172	0.002		1022	12	1026	11	1033	22	99
COLRAB-14.1		253.7	66.2	0.26	0.00001	0.00002	0.0002					5.48	0.08	0.0800	0.0009	2.013	0.040	0.183	0.003		1081	14	1120	13	1197	23	90
COLRAB-15.1		965.6	124.5	0.13	0.00001	0.00002	0.0002					5.90	0.05	0.0770	0.0010	1.801	0.029	0.170	0.002		1010	8	1046	11	1122	25	90
COLRAB-15.2		66.8	23.4	0.35	0.00007	0.00006	0.0012					5.80	0.11	0.0793	0.0024	1.886	0.072	0.172	0.003		1025	19	1076	26	1181	61	87
COLRAB-16.1		179.4	61.8	0.34	0.00001	0.00000	0.0002					4.42	0.07	0.0879	0.0008	2.742	0.052	0.226	0.003		1315	18	1340	14	1380	18	95
COLRAB-17.1		154.7	45.5	0.29	0.00001	0.00000	0.0002					4.83	0.05	0.0795	0.0010	2.268	0.040	0.207	0.002		1213	13	1203	13	1184	25	102
COLRAB-17.2		511.4	4.4	0.01	0.00001	0.00000	0.0002					14.47	0.14	0.0566	0.0014	0.539	0.015	0.069	0.001		431	4	438	10	475	54	91
COLRAB-18.1		38.0	27.6	0.73	-0.00003	0.00005	-0.0004					1.92	0.05	0.1918	0.0021	13.758	0.423	0.520	0.014		2701	61	2733	30	2757	18	98
COLRAB-18.2		33.1	11.5	0.35	0.00003	0.00005	0.0004					1.82	0.05	0.1850	0.0024	14.030	0.479	0.550	0.017		2825	69	2752	33	2699	21	105
COLRAB-19.1		149.0	100.3	0.67	0.00001	0.00003	0.0002					4.42	0.07	0.0890	0.0013	2.776	0.063	0.226	0.004		1315	19	1349	17	1404	28	94
COLRAB-20.1		115.7	33.5	0.29	0.00001	0.00000	0.0002					4.54	0.06	0.0881	0.0017	2.677	0.068	0.220	0.003		1284	17	1322	19	1385	37	93
COLRAB-21.1		126.0	51.5	0.41	0.00001	0.00002	0.0002					4.45	0.06	0.0885	0.0015	2.745	0.065	0.225	0.003		1308	17	1341	18	1394	33	94
COLRAB-22.1		867.9	49.8	0.06	0.00001	0.00001	0.0002					6.02	0.04	0.0731	0.0005	1.674	0.016	0.166	0.001		991	6	999	6	1016	14	98
COLRAB-23.1		100.5	58.6	0.58	0.00003	0.00003	0.0005					4.46	0.05	0.0843	0.0014	2.604	0.058	0.224	0.003		1304	14	1302	16	1299	33	100
COLRAB-24.1		236.3	200.2	0.85	0.00001	0.00001	0.0001					3.67	0.03	0.0999	0.0012	3.755	0.061	0.273	0.002		1554	13	1583	13	1623	23	96
COLRAB-25.1		105.2	26.6	0.25	0.00002	0.00003	0.0004					5.16	0.12	0.0807	0.0022	2.154	0.081	0.194	0.004		1141	24	1166	26	1214	54	94
COLRAB-26.1		146.5	35.3	0.24	0.00894	0.00052	0.1512					5.41	0.12	0.0748	0.0091	1.906	0.241	0.185	0.004		1093	22	1083	88	1063	267	103
COLRAB-27.1		172.0	80.7	0.47	-0.00001	0.00000	-0.0002					4.94	0.09	0.0780	0.0017	2.178	0.065	0.203	0.004		1189	20	1174	21	1146	43	104
COLRAB-28.1		39.7	21.1	0.53	-0.00004	0.00000	-0.0007					4.84	0.09	0.0839	0.0017	2.388	0.070	0.206	0.004		1210	20	1239	21	1290	41	94
COLRAB-29.1		77.0	36.5	0.47	-0.00002	0.00000	-0.0003					4.29	0.06	0.0890	0.0012	2.862	0.059	0.233	0.003		1351	17	1372	16	1405	26	96
COLRAB-30.1		63.2	26.4	0.42	0.00004	0.00010	0.0007					5.30	0.16	0.0761	0.0023	1.981	0.088	0.189	0.006		1115	30	1109	31	1098	62	102
COLRAB-31.1		112.9	65.0	0.58	0.00004	0.00003	0.0006					5.87	0.08	0.0700	0.0025	1.644	0.064	0.170	0.002		1014	13	987	25	929	74	109
COLRAB-32.1		388.3	118.5	0.31	0.00004	0.00002	0.0008					5.56	0.04	0.0862	0.0007	2.139	0.024	0.180	0.001		1067	6	1161	8	1343	16	79
COLRAB-33.1		468.1	218.7	0.47	0.00000	0.00001	0.0001					4.04	0.12	0.0925	0.0016	3.159	0.111	0.248	0.007		1427	37	1447	27	1477	32	97
COLRAB-34.1		219.6	123.8	0.56	0.00007	0.00005	0.0012					4.38	0.05	0.0907	0.0017	2.856	0.067	0.228	0.003		1326	14	1370	18	1441	36	92
OTCOW-1.1		92.7	74.2	0.80	0.00206	0.00027	0.0336					4.10	0.08	0.0913	0.0049	3.069	0.182	0.244	0.005		1407	25	1425	47	1453	106	97
OTCOW-2.1		98.6	81.5	0.83	0.00004	0.00010	0.0007					5.09	0.09	0.0819	0.0032	2.217	0.100	0.196	0.003		1156	18	1187	32	1244	80	93
OTCOW-3.1		243.5	134.0	0.55	-0.00001	0.00003	-0.0002					3.51	0.05	0.0975	0.0014	3.825	0.080	0.285	0.004		1614	19	1598	17	1576	28	102
OTCOW-4.1		942.8	218.3	0.23	0.00003	0.00003	0.0005					7.70	0.08	0.0701	0.0007	1.255	0.020	0.130	0.001		787	8	825	9	931	22	84
OTCOW-1.2		102.7	64.2	0.62	0.00001	0.00000	0.0002					5.01	0.07	0.0866	0.0021	2.384	0.070	0.200	0.003		1174	15	1238	21	1351	47	87
OTCOW-1.2		224.6	126.8	0.56	0.00001	0.00000	0.0002					4.66	0.05	0.0828	0.0014	2.452	0.051	0.215	0.002		1254	13	1258	15	1264	32	99
OTCOW-6.1		454.7	199.2	0.44	0.00002	0.00002	0.0003					5.60	0.07	0.0748	0.0008	1.840	0.032	0.178	0.002		1059	12	1060	12	1063	22	100
OTCOW-7.1		441.9	149.7	0.34	0.00002	0.00002	0.0004					6.03	0.09	0.0744	0.0011	1.700	0.037	0.166	0.002		989	13	1009	14	1051	30	94
OTCOW-8.1		613.1	44.5	0.07	0.00001	0.00001	0.0002					5.17	0.04	0.0823	0.0013	2.193	0.040	0.193	0.001		1140	7	1179	13	1252	31	91
OTCOW-9.1		474.4	179.6	0.38	0.00002	0.00003	0.0003					4.34	0.05	0.1018	0.0013	3.233	0.058	0.230	0.003		1337	14	1465	14	1656	24	81
OTCOW-10.1		360.3	101.0	0.28	0.00001	0.00001	0.0002					4.92	0.05	0.0793	0.0009	2.222	0.035	0.203	0.002		1192	11	1188	11	1180	22	101
OTCOW-10.2		372.6	46.0	0.12	0.00130	0.00017	0.0229					8.56	0.09	0.0636	0.0034	1.023	0.057	0.117	0.001		712	7	715	29	727	117	98
OTCOW-11.1		82.9	24.5	0.30	-0.00003	0.00003	-0.0005					5.47	0.15	0.0787	0.0016	1.982	0.073	0.183	0.005		1082	28	1110	25	1164	41	93
OTCOW-12.1		930.8	30.8	0.03	0.00009	0.00004	0.0015					6.61	0.04	0.0702	0.0011	1.466	0.026	0.151	0.001		909	6	917	11	935	33	97
OTCOW-13.1		83.9	46.8	0.56	-0.00004	0.00002	-0.0007					3.88	0.07	0.0934	0.0016	3.322	0.089	0.258	0.005		1480	25	1486	21	1495	32	99
OTCOW-14.1		119.7	44.6	0.37	0.00001	0.00000	0.0002					4.67	0.06	0.0839	0.0012	2.478	0.051	0.214	0.003		1251	16	1266	15	1290	27	97
OTCOW-15.1		72.9	40.3	0.55	-0.00004	0.00002	-0.0007					4.67	0.10	0.0868	0.0018	2.561	0.080	0.214	0.004		1251	24	1290	23	1355	41	92
OTCOW-16.1		510.3	246.5	0.48	0.00001	0.00000	0.0002					5.25	0.05	0.0788	0.0009	2.068	0.032	0.190	0.002		1124	10	1138	11	1166	22	96
OTCOW-17.1		518.3	259.0	0.50	0.00001	0.00001	0.0002					5.20	0.04	0.0792	0.0015	2.101	0.045	0.192	0.001		1134	8	1149	15	1178	38	96
OTCOW-18.1		92.5	45.3	0.49	0.00002	0.00004	0.0004					4.92	0.08	0.0804	0.0017	2.255	0.062	0.203	0.003		1193	17	1198	20	1208	41	99
OTCOW-19.1		118.3	35.5	0.30	0.00001	0.00000	0.0002					5.86	0.10	0.0771	0.0022	1.814	0.064	0.171	0.003		1016	16	1051	23	1124	58	90
OTCOW-20.1		88.6	42.3	0.48	0.00003	0.00007	0.0006					5.96	0.09	0.0747	0.0019	1.729	0.054	0.168	0.003		1001	14	1019	20	1060	52	94
OTCOW-21.1		57.4	16.3	0.28	0.00006	0.00011	0.0010					5.54	0.22	0.0779	0.0026	1.941	0.106	0.181	0.007		1070	39	1095	37	1145	67	93
OTCOW-22.1		301.3	155.3	0.52	0.00001	0.00001	0.0001					5.20	0.04	0.0816	0.0014	2.165	0.043	0.192	0.002		1134	8	1170	14	1237	35	92
OTCOW-23.1		121.8	87.8	0.72	0.00001	0.00004	0.0002					4.84	0.07	0.0780	0.0013	2.223	0.051	0.207	0.003		1211	15	1188	16	1148	33	105
OTCOW-23.1		57.2	25.2	0.44	0.00001	0.00000	0.0002					5.00	0.13	0.0800	0.0017	2.208	0.079	0.200	0.005		1176	28	1184	25	1197	43	98
OTCOW-25.1		236.7	74.8	0.32	0.00001	0.00000	0.0002					5.45	0.06	0.0767	0.0011	1.941	0.038	0.184	0.002		1086	12	1095	13	1114	29	98
OTCOW-26.1		221.9	107.2	0.48	0.00009	0.00004	0.0015					4.28	0.06	0.0858	0.0014	2.765	0.063	0.234	0.003		1355	16	1346	17	1332	33	102
OTCOW-27.1		63.5	26.6	0.42	0.00012	0.00011	0.0020					4.93	0.10	0.0769	0.0024	2.152	0.086	0.203	0.004		1191	23	1166	28	1119	65	106
OTCOW-28.1		161.8	135.6	0.84	0.00093	0.00016	0.0158					5.87	0.11	0.0699	0.0032	1.643	0.084	0.170	0.003		1014	18	987	33	926	96	110
OTCOW-28.2		241.7	91.8	0.38	0.00001	0.00003	0.0003					7.38	0.08	0.0682	0.0012	1.275	0.029	0.136	0.002		819	9	834	13	874	38	94
OTCOW-29.1		139.1	57.7	0.41	0.00002	0.00004	0.0003					5.95	0.08	0.0729	0.0014	1.688	0.041	0.168	0.002		1001	13	1004	16	1010	38	99
OTCOW-30.1		143.1	119.9	0.84	0.00001	0.00000	0.0002					5.40	0.10	0.0759	0.0015	1.938	0.057	0.185	0.004		1096	19	1094	20	1092	41	100
OTCOW-31.1		57.2	32.3	0.56	0.00001	0.00000	0.0002					4.95	0.11	0.0760	0.0036	2.117	0.117	0.202	0.005		1186	24	1154	39	1096	98	108
OTCOW-32.1		84.7	48.3	0.57	0.00001	0.00000	0.0002					5.94	0.08	0.0693	0.0025	1.609	0.064	0.168	0.002		1003	13	974	25	908	75	110
OTCOW-33.1		81.1	48.7	0.60	0.00001	0.00000	0.0002					5.59	0.08	0.0758	0.0022	1.871	0.063	0.179	0.003		1062	15	1071	23	1090	58	97
OTCOW-34.1		845.4	185.1	0.22	0.00001	0.00001	0.0002					5.37	0.05	0.0767	0.0009	1.971	0.032	0.186	0.002		1102	10	1106	11	1114	24	99
OTCOW-35.1		63.2	38.9	0.61	0.00011	0.00007	0.0017					3.15	0.06	0.1118	0.0022	4.894	0.139	0.318	0.006		1778	29	1801	24	1828	36	97
OTCOW-36.1		128.3	21.5	0.17	0.00001	0.00000	0.0002					5.74	0.06	0.0748	0.0011	1.796	0.036	0.174	0.002		1036	11	1044	13	1062	31	98
OTCOW-36.2		567.2	51.6	0.09	0.00007	0.00006	0.0012					6.90	0.07	0.0719	0.0012	1.438	0.029	0.145	0.001		873	8	905	12	984	34	89
OTCOW-37.1		153.0	53.3	0.35	0.00001	0.00003	0.0003					5.74	0.06	0.0738	0.0019	1.774	0.051	0.174	0.002		1036	10	1036	19	1036	52	100
TFQ1-1.1		192.0	66.4	0.35	0.00002	0.00004	0.0003					6.17	0.07	0.0720	0.0017	1.611	0.045	0.162	0.002		969	11	974	18	987	49	98
TFQ1-2.1		280.4	111.2	0.40	0.00001	0.00002	0.0002					5.40	0.08	0.0753	0.0010	1.924	0.041	0.185	0.003		1096	16	1089	14	1077	26	102
TFQ1-3.1		162.3	66.7	0.41	0.00001	0.00000	0.0002					5.53	0.07	0.0730	0.0010	1.821	0.036	0.181	0.002		1072	12	1053	13	1014	29	106
TFQ1-3.2		632.5	104.6	0.17	0.00003	0.00002	0.0005					5.48	0.05	0.0737	0.0007	1.854	0.026	0.182	0.002		1081	9	1065	9	1033	19	105
TFQ1-4.1		128.5	60.1	0.47	0.00008	0.00013	0.0013					5.93	0.10	0.0712	0.0024	1.655	0.066	0.169	0.003		1004	16	991	26	963	71	104
TFQ1-5.1		131.5	52.8	0.40	0.00002	0.00005	0.0004					5.95	0.08	0.0720	0.0018	1.668	0.049	0.168	0.002		1002	13	997	19	985	50	102
TFQ1-6.1		378.6	78.3	0.21	0.00001	0.00001	0.0001					5.85	0.06	0.0739	0.0008	1.742	0.028	0.171	0.002		1017	10	1024	10	1040	21	98

Analysis		U	Th		$^{204}Pb/$			Total $^{238}U/$		$^{207}Pb/$		Radiogenic Ratios[1] $^{238}U/$		$^{207}Pb/$		$^{207}Pb/$		$^{206}Pb/$		error	Ages (in Ma)[1] $^{206}Pb/$		$^{207}Pb/$		$^{207}Pb/$		%
Label	Zone	(in ppm)		Th/U	^{206}Pb	± 1σ	f206%[2]	^{206}Pb	± 1σ	^{206}Pb	± 1σ	^{206}Pb	± 1σ	^{206}Pb	± 1σ	^{235}U	± 1σ	^{238}U	± 1σ	corr.	^{238}U	± 1σ	^{235}U	± 1σ	^{206}Pb	± 1σ	Conc
TFQ1-7.1		53.4	19.1	0.36	0.00001	0.00001	0.0002					5.06	0.10	0.0781	0.0017	2.126	0.065	0.197	0.004		1162	21	1157	21	1150	43	101
TFQ1-8.1		103.4	66.1	0.64	0.00063	0.00035	0.0106					4.91	0.09	0.0886	0.0067	2.488	0.199	0.204	0.004		1195	19	1269	60	1396	153	86
TFQ1-9.1		53.9	25.9	0.48	0.00005	0.00011	0.0009					5.76	0.15	0.0723	0.0026	1.731	0.080	0.174	0.004		1033	24	1020	30	993	74	104
TFQ1-9.2		233.6	65.9	0.28	0.00002	0.00002	0.0004					5.58	0.06	0.0733	0.0011	1.810	0.036	0.179	0.002		1063	10	1049	13	1021	31	104
TFQ1-10.1		316.1	89.3	0.28	0.00003	0.00004	0.0005					5.48	0.04	0.0734	0.0011	1.847	0.033	0.183	0.001		1081	7	1062	12	1025	32	105
TFQ1-11.1		541.8	158.2	0.29	0.00001	0.00000	0.0002					5.67	0.05	0.0740	0.0009	1.802	0.028	0.176	0.002		1048	8	1046	10	1042	24	101
TFQ1-12.1		132.2	50.8	0.38	0.00001	0.00002	0.0002					5.57	0.09	0.0735	0.0012	1.820	0.044	0.180	0.003		1065	16	1053	16	1028	33	104
TFQ1-13.1		247.4	126.9	0.51	0.00001	0.00000	0.0002					4.81	0.09	0.0802	0.0012	2.300	0.057	0.208	0.004		1218	20	1212	18	1203	29	101
TFQ1-14.1		55.0	39.7	0.72	0.00010	0.00011	0.0017					5.76	0.15	0.0720	0.0024	1.724	0.078	0.174	0.005		1032	25	1018	29	987	70	105
TFQ1-15.1		241.2	186.1	0.77	0.00004	0.00004	0.0007					5.70	0.05	0.0740	0.0012	1.789	0.035	0.175	0.002		1042	9	1041	13	1040	33	100
TFQ1-16.1		172.3	51.1	0.30	-0.00002	0.00002	-0.0003					5.66	0.09	0.0750	0.0015	1.827	0.050	0.177	0.003		1049	15	1055	18	1069	42	98
TFQ1-17.1		419.4	88.6	0.21	0.00001	0.00001	0.0002					5.61	0.07	0.0741	0.0008	1.822	0.033	0.178	0.002		1057	13	1053	12	1045	22	101
TFQ1-18.1		66.5	27.1	0.41	0.00001	0.00000	0.0002					5.73	0.09	0.0784	0.0017	1.887	0.053	0.175	0.003		1037	15	1077	19	1157	43	90
BPM-1		225.5	221.6	0.98	0.00012	0.00011	0.0021					6.08	0.09	0.0738	0.0025	1.674	0.065	0.164	0.003		982	14	999	25	1037	70	95
BPM-2.1		378.8	185.4	0.49	0.00005	0.00005	0.0008					5.98	0.08	0.0751	0.0022	1.731	0.059	0.167	0.002		997	12	1020	22	1071	61	93
BPM-3.1		1382.5	67.9	0.05	0.00003	0.00003	0.0006					6.25	0.09	0.0746	0.0007	1.646	0.029	0.160	0.002		957	12	988	11	1056	19	91
BPM-4.1		247.7	98.9	0.40	0.00185	0.00025	0.0310					5.04	0.18	0.0833	0.0042	2.279	0.148	0.198	0.007		1167	38	1206	47	1275	101	92
BPM-4.1		926.0	285.6	0.31	0.00236	0.00018	0.0411					7.37	0.07	0.0855	0.0035	1.601	0.070	0.136	0.001		821	8	971	28	1328	82	62
BPM-5.1		578.8	332.9	0.58	0.00001	0.00000	0.0002					5.19	0.06	0.0791	0.0009	2.100	0.038	0.193	0.002		1135	13	1149	12	1175	23	97
BPM-6.1		373.4	145.9	0.39	-0.00001	0.00002	-0.0002					4.96	0.04	0.0775	0.0021	2.154	0.063	0.202	0.002		1184	9	1167	21	1133	55	105
BPM-7.1		1438.9	134.9	0.09	0.00001	0.00002	0.0002					5.10	0.04	0.0791	0.0007	2.139	0.025	0.196	0.001		1154	8	1161	8	1175	16	98
BPM-8.1		228.1	76.8	0.34	0.00004	0.00006	0.0007					5.78	0.10	0.0741	0.0028	1.769	0.077	0.173	0.003		1029	16	1034	29	1044	79	99
BPM-9.1		162.3	173.7	1.07	0.00014	0.00009	0.0024					5.70	0.12	0.0729	0.0028	1.766	0.081	0.176	0.004		1043	20	1033	30	1012	80	103
BPM-10.1		159.3	73.5	0.46	0.00011	0.00010	0.0018					3.78	0.10	0.0890	0.0027	3.245	0.139	0.264	0.007		1513	36	1468	34	1404	59	108
BPM-11.1		214.0	81.9	0.38	0.00019	0.00019	0.0032					4.91	0.10	0.0824	0.0043	2.311	0.135	0.204	0.004		1194	22	1216	42	1254	106	95
BPM-12.1		686.2	266.0	0.39	0.00033	0.00011	0.0055					4.76	0.04	0.0894	0.0023	2.589	0.074	0.210	0.002		1229	10	1298	21	1412	51	87
BPM-13.1		502.6	255.0	0.51	0.00013	0.00005	0.0021					5.38	0.06	0.0786	0.0018	2.015	0.052	0.186	0.002		1100	11	1121	18	1161	45	95
BPM-14.1		332.1	114.9	0.35	-0.00003	0.00006	-0.0005					5.77	0.07	0.0752	0.0023	1.796	0.061	0.173	0.002		1030	12	1044	22	1073	62	96
BPM-15.1		91.5	86.0	0.94	0.00012	0.00014	0.0020					4.04	0.06	0.0912	0.0036	3.110	0.135	0.247	0.004		1425	19	1435	34	1451	77	98
BPM-16.1		987.1	11.9	0.01	0.00000	0.00000	0.0001					5.83	0.08	0.0751	0.0009	1.777	0.035	0.172	0.002		1021	13	1037	13	1071	25	95
BPM-17.1		214.6	121.1	0.56	-0.00003	0.00003	-0.0004					4.96	0.06	0.0828	0.0019	2.303	0.062	0.202	0.002		1184	12	1213	19	1265	46	94
BPM-18.1		202.3	87.1	0.43	-0.00011	0.00012	-0.0019					5.31	0.15	0.0792	0.0036	2.057	0.115	0.188	0.005		1112	28	1135	39	1178	92	94
BPM-19.1		89.2	29.9	0.34	0.00005	0.00006	0.0009					4.34	0.08	0.0851	0.0031	2.705	0.117	0.230	0.004		1337	23	1330	33	1319	72	101
BPM-20.1		335.8	160.6	0.48	0.00001	0.00004	0.0002					4.41	0.05	0.0882	0.0011	2.756	0.049	0.227	0.002		1317	12	1344	13	1387	25	95
BPM-21.1		227.3	22.4	0.10	0.00001	0.00000	0.0002					5.96	0.07	0.0697	0.0027	1.612	0.067	0.168	0.002		1000	11	975	27	919	81	109
BPM-22.1		133.8	131.0	0.98	0.00001	0.00006	0.0002					3.91	0.07	0.0912	0.0019	3.216	0.096	0.256	0.005		1468	25	1461	23	1451	40	101
BPM-23.1		786.4	200.0	0.25	-0.00002	0.00005	-0.0003					5.47	0.09	0.0729	0.0010	1.838	0.040	0.183	0.003		1082	16	1059	14	1012	27	107
BPM-24.1		69.3	45.9	0.66	0.00001	0.00000	0.0002					5.77	0.20	0.0765	0.0056	1.828	0.155	0.173	0.006		1030	33	1055	57	1108	154	93
BPM-25.1		509.7	243.2	0.48	0.00009	0.00005	0.0015					3.84	0.03	0.0969	0.0018	3.474	0.074	0.260	0.002		1491	12	1521	17	1564	34	95
BPM-26.1		150.4	93.5	0.62	0.00029	0.00025	0.0049					5.66	0.31	0.0717	0.0045	1.746	0.155	0.177	0.010		1048	53	1026	59	978	134	107
BPM-27.1		668.6	418.5	0.63	0.00026	0.00006	0.0043					4.59	0.05	0.0909	0.0021	2.727	0.071	0.218	0.002		1269	12	1336	20	1444	44	88
BPM-28.1		543.2	221.9	0.41	0.00011	0.00005	0.0018					5.46	0.05	0.0793	0.0012	2.003	0.039	0.183	0.002		1084	10	1117	13	1180	31	92
BPM-29.1		213.5	60.6	0.28	-0.00004	0.00002	-0.0006					5.89	0.10	0.0746	0.0018	1.744	0.056	0.170	0.003		1010	16	1025	21	1057	50	96
BPM-29.2		170.1	56.0	0.33	0.00018	0.00011	0.0030					5.81	0.09	0.0711	0.0030	1.689	0.079	0.172	0.003		1024	15	1004	30	962	88	107
BPM-30.1		13.0	7.3	0.56	0.00004	0.00004	-0.0001					0.40	4.74	0.0633	0.0104	21.936	262.160	2.515	30.006		8104	14537	3181	3181	717	393	1131
BPM-30.2		155.6	48.7	0.31	0.00005	0.00008	0.0009					4.30	0.07	0.0876	0.0031	2.810	0.117	0.233	0.004		1348	21	1358	32	1374	71	98
BPM-31.1		151.1	49.4	0.33	0.00001	0.00000	0.0002					4.03	0.09	0.0918	0.0017	3.139	0.098	0.248	0.006		1429	30	1442	24	1462	35	98
BPM-32.1		600.6	52.2	0.09	0.00002	0.00002	0.0003					5.92	0.16	0.0763	0.0009	1.776	0.056	0.169	0.005		1006	26	1037	21	1102	24	91
BPM-33.1		326.4	238.5	0.73	0.00012	0.00005	0.0020					4.17	0.05	0.0890	0.0016	2.941	0.068	0.240	0.003		1385	16	1392	18	1404	35	99
BPM-34.1		213.4	106.5	0.50	0.00016	0.00007	0.0026					3.99	0.07	0.0910	0.0018	3.146	0.087	0.251	0.004		1442	22	1444	22	1447	38	100
BPM-35.1		213.7	55.7	0.26	0.00011	0.00021	0.0018					5.05	0.13	0.0767	0.0043	2.096	0.137	0.198	0.005		1166	29	1148	46	1114	117	105
BPM-36.1		159.6	90.6	0.57	0.00176	0.00372	0.0298					5.67	0.38	0.0772	0.0609	1.879	1.502	0.176	0.012		1048	66	1074	749	1127	4764	93
BPM-36.2		248.7	75.0	0.30	-0.00003	0.00005	-0.0004					5.75	0.09	0.0756	0.0028	1.811	0.076	0.174	0.003		1033	15	1049	28	1083	76	95
BPM-37.1		839.0	192.6	0.23	0.00001	0.00001	0.0002					4.17	0.06	0.0925	0.0009	3.060	0.057	0.240	0.004		1387	19	1423	14	1477	17	94
BPM-38.1		241.2	163.8	0.68	0.00002	0.00004	0.0003					3.60	0.05	0.1005	0.0020	3.846	0.102	0.277	0.004		1579	21	1602	22	1634	38	97
BPM-39.1		171.5	206.1	1.20	0.00001	0.00000	0.0002					5.42	0.12	0.0756	0.0016	1.922	0.063	0.185	0.004		1092	22	1089	22	1083	44	101
BPM-40.1		407.1	138.7	0.34	0.00026	0.00012	0.0044					5.92	0.09	0.0736	0.0024	1.713	0.064	0.169	0.002		1006	13	1013	24	1030	68	98
BPM-41.1		127.3	65.4	0.51	0.00030	0.00041	0.0054					8.77	0.22	0.0619	0.0069	0.973	0.114	0.114	0.003		696	17	690	61	669	259	104
BPM-41.2		66.8	32.6	0.49	0.00069	0.00050	0.0122					8.94	0.36	0.0537	0.0085	0.829	0.139	0.112	0.004		684	26	613	80	360	359	190
BPM-42.1		171.5	85.1	0.50	0.00001	0.00000	0.0002					4.96	0.12	0.0782	0.0017	2.176	0.073	0.202	0.005		1185	26	1174	24	1153	43	103
BPM-43.1		162.8	67.6	0.42	0.00011	0.00018	0.0019					5.06	0.07	0.0785	0.0032	2.139	0.093	0.198	0.003		1162	14	1162	31	1161	82	100
BPM-44.1		165.4	248.0	1.50	0.00007	0.00007	0.0011					5.56	0.07	0.0783	0.0019	1.943	0.057	0.180	0.002		1067	13	1096	20	1154	49	92
SERV-30.1		335.4	275.2	0.82	-0.00004	0.00005	-0.0008					5.11	0.10	0.0803	0.0023	2.165	0.080	0.196	0.004		1151	20	1170	26	1205	58	96
SERV-31.1		96.8	37.8	0.39	0.00001	0.00005	0.0002					5.02	0.09	0.0776	0.0025	2.133	0.082	0.199	0.004		1172	19	1159	27	1137	66	103
SERV-32.1		137.5	75.6	0.55	-0.00014	0.00020	-0.0023					5.47	0.09	0.0808	0.0043	2.036	0.118	0.183	0.003		1082	16	1128	40	1217	109	89
SERV-33.1		616.3	123.9	0.20	-0.00002	0.00002	-0.0003					4.97	0.09	0.0833	0.0015	2.313	0.064	0.201	0.004		1182	20	1216	20	1277	36	93
SERV-34.1		60.0	28.7	0.48	0.00001	0.00014	0.0002					4.89	0.10	0.0826	0.0050	2.328	0.154	0.204	0.004		1199	23	1221	48	1259	122	95
SERV-35.1		208.3	76.2	0.37	-0.00006	0.00012	-0.0010					5.09	0.08	0.0790	0.0026	2.142	0.081	0.197	0.003		1157	17	1162	27	1172	65	99
SERV-1.1		179.4	98.1	0.55	0.000110	0.000062	0.0019					5.17	0.14	0.0806	0.0023	2.148	0.089	0.193	0.005		1139	28	1165	29	1212	58	94
SERV-2.1		259.4	88.7	0.34	0.000010	0.000000	0.0002					6.03	0.06	0.0738	0.0014	1.686	0.038	0.166	0.002		988	9	1003	14	1036	39	95
SERV-3.1		342.6	88.4	0.26	0.000043	0.000040	0.0007					5.35	0.07	0.0752	0.0012	1.939	0.044	0.187	0.003		1105	14	1095	15	1074	33	103
SERV-4.1		238.3	155.1	0.65	-0.000026	0.000024	-0.0004					3.15	0.04	0.1154	0.0022	5.054	0.121	0.318	0.004		1779	20	1828	21	1885	34	94
SERV-5.1		188.2	37.0	0.20	0.000199	0.000127	0.0034					5.93	0.12	0.0714	0.0034	1.661	0.090	0.169	0.003		1005	18	994	35	968	101	104
SERV-6.1		190.5	63.2	0.33	0.000010	0.000061	0.0002					4.24	0.07	0.0908	0.0018	2.950	0.077	0.236	0.004		1364	19	1395	20	1442	37	95
SERV-7.1		70.5	37.8	0.54	0.000010	0.000062	0.0002					5.30	0.13	0.0814	0.0042	2.116	0.127	0.189	0.005		1114	25	1154	42	1231	105	90
SERV-8.1		282.1	72.3	0.26	0.000010	0.000000	0.0002					5.89	0.07	0.0737	0.0019	1.726	0.050	0.170	0.002		1012	11	1018	19	1033	52	98

Analysis		U	Th		$^{204}Pb/$			Total $^{238}U/$		$^{207}Pb/$		Radiogenic Ratios[1] $^{238}U/$		$^{207}Pb/$		$^{207}Pb/$		$^{206}Pb/$		error	Ages (in Ma)[1] $^{206}Pb/$		$^{207}Pb/$		$^{207}Pb/$		%
Label	Zone	(in ppm)		Th/U	^{206}Pb	± 1σ	f206%[2]	^{206}Pb	± 1σ	^{206}Pb	± 1σ	^{206}Pb	± 1σ	^{206}Pb	± 1σ	^{235}U	± 1σ	^{238}U	± 1σ	corr.	^{238}U	± 1σ	^{235}U	± 1σ	^{206}Pb	± 1σ	Conc
SERV-9.1		373.4	213.3	0.57	0.000044	0.000102	0.0007					4.50	0.08	0.0884	0.0020	2.709	0.080	0.222	0.004		1293	20	1331	22	1392	43	93
SERV-10.1		277.3	163.3	0.59	0.000029	0.000020	0.0005					4.44	0.05	0.0883	0.0014	2.742	0.054	0.225	0.002		1310	13	1340	15	1388	30	94
SERV-11.1		365.6	113.3	0.31	-0.000040	0.000069	-0.0007					5.60	0.09	0.0749	0.0028	1.842	0.078	0.179	0.003		1059	16	1061	28	1065	76	99
SERV-12.1		112.5	34.0	0.30	0.000357	0.000222	0.0060					5.13	0.16	0.0749	0.0046	2.015	0.144	0.195	0.006		1149	33	1121	50	1067	128	108
SERV-13.1		81.8	47.6	0.58	0.000301	0.000351	0.0052					6.30	0.14	0.0726	0.0065	1.589	0.152	0.159	0.004		950	20	966	61	1002	195	95
SERV-14.1		109.2	35.4	0.32	0.000218	0.000139	0.0036					4.33	0.11	0.0874	0.0047	2.787	0.172	0.231	0.006		1340	29	1352	47	1370	107	98
SERV-15.1		222.3	90.8	0.41	-0.000090	0.000173	-0.0015					4.91	0.06	0.0788	0.0030	2.212	0.091	0.204	0.002		1195	13	1185	29	1168	77	102
SERV-16.1		1203.3	986.3	0.82	0.000566	0.000158	0.0098					6.57	0.06	0.0830	0.0027	1.741	0.060	0.152	0.001		913	8	1024	22	1268	64	72
SERV-17.1		181.4	74.8	0.41	0.000114	0.000069	0.0019					4.93	0.10	0.0782	0.0018	2.184	0.073	0.203	0.004		1190	23	1176	24	1151	47	103
SERV-18.1		555.3	190.2	0.34	0.000466	0.000297	0.0079					5.62	0.16	0.0684	0.0048	1.679	0.133	0.178	0.005		1055	28	1001	52	882	153	120
SERV-19.1		1165.2	30.6	0.03	0.000076	0.000028	0.0013					6.01	0.03	0.0749	0.0014	1.719	0.035	0.166	0.001		992	5	1016	13	1067	38	93
SERV-20.1		83.7	36.6	0.44	0.000010	0.000005	0.0002					5.74	0.13	0.0759	0.0030	1.824	0.087	0.174	0.004		1036	21	1054	32	1093	81	95
SERV-21.1		54.3	27.6	0.51	0.000123	0.000269	0.0021					5.03	0.18	0.0785	0.0059	2.152	0.189	0.199	0.007		1169	39	1166	63	1159	158	101
SERV-21.2		207.3	101.2	0.49	0.002094	0.000969	0.0372					10.12	0.25	0.0693	0.0158	0.943	0.219	0.099	0.002		607	14	675	121	906	556	67
SERV-22.1		709.4	59.2	0.08	0.000031	0.000029	0.0005					5.63	0.09	0.0770	0.0011	1.887	0.043	0.178	0.003		1054	16	1076	15	1122	28	94
SERV-23.1		404.3	268.8	0.67	0.000115	0.000094	0.0020					5.71	0.06	0.0765	0.0022	1.847	0.060	0.175	0.002		1040	11	1062	22	1108	59	94
SERV-24.1		350.4	181.7	0.52	0.000255	0.000176	0.0043					5.34	0.11	0.0780	0.0031	2.014	0.094	0.187	0.004		1106	21	1120	32	1148	80	96
SERV-25.1		115.9	42.3	0.36	-0.000058	0.000040	-0.0010					4.15	0.07	0.0914	0.0034	3.037	0.129	0.241	0.004		1392	21	1417	33	1456	72	96
SERV-26.1		609.2	223.2	0.37	-0.000020	0.000017	-0.0003					5.67	0.05	0.0752	0.0010	1.828	0.031	0.176	0.002		1047	8	1056	11	1073	28	98
SERV-27.1		2736.9	577.6	0.21	0.001346	0.000229	0.0237					8.41	0.06	0.0789	0.0038	1.292	0.064	0.119	0.001		724	5	842	29	1168	99	62
SERV-28.1		228.4	79.0	0.35	0.001327	0.000376	0.0227					6.13	0.13	0.0678	0.0063	1.525	0.149	0.163	0.003		974	19	940	62	862	206	113
SERV-29.1		92.4	34.9	0.38	0.000010	0.000041	0.0002					5.72	0.14	0.0726	0.0030	1.751	0.088	0.175	0.004		1039	23	1027	33	1002	86	104
OTD-1.1		83.9	65.0	0.77	0.000079	0.000068	0.0011					2.10	0.06	0.1867	0.0027	12.268	0.436	0.477	0.015		2512	64	2625	34	2713	24	93
OTD-2.1		138.6	98.5	0.71	-0.000168	0.000144	-0.0029					6.10	0.16	0.0759	0.0030	1.714	0.085	0.164	0.004		978	24	1014	32	1092	81	90
OTD-3.1		175.2	48.3	0.28	0.000175	0.000093	0.0029					4.79	1.55	0.0770	0.0035	2.215	0.738	0.209	0.068		1222	372	1186	265	1120	94	109
OTD-4.1		385.9	104.1	0.27	0.000127	0.000057	0.0021					4.55	0.03	0.0873	0.0022	2.646	0.070	0.220	0.002		1281	9	1313	20	1367	48	94
OTD-5.1		258.9	85.7	0.33	0.000020	0.000040	0.0003					4.37	0.07	0.0922	0.0021	2.910	0.087	0.229	0.004		1330	20	1385	23	1470	45	90
OTD-6.1		184.8	103.2	0.56	0.000010	0.000000	0.0002					6.17	0.09	0.0736	0.0018	1.643	0.049	0.162	0.002		968	13	987	19	1030	51	94
OTD-6.1		1227.8	385.4	0.31	0.000021	0.000035	0.0004					5.61	0.04	0.0772	0.0008	1.898	0.026	0.178	0.001		1058	7	1080	9	1127	22	94
OTD-8.1		457.0	140.7	0.31	0.000079	0.000087	0.0013					5.22	0.08	0.0781	0.0019	2.064	0.063	0.192	0.003		1130	16	1137	21	1150	50	98
OTD-8.2		175.1	74.2	0.42	0.000153	0.000157	0.0026					5.39	0.11	0.0789	0.0031	2.020	0.094	0.186	0.004		1098	21	1122	32	1170	80	94
OTD-7.1		109.3	26.4	0.24	0.000092	0.000108	0.0016					6.66	0.13	0.0706	0.0027	1.462	0.066	0.150	0.003		902	17	915	28	946	80	95
OTD-8.1		1215.8	165.8	0.14	0.000316	0.000132	0.0055					7.10	0.05	0.0698	0.0023	1.355	0.048	0.141	0.001		849	6	870	21	922	71	92
OTD-9.1		61.4	23.0	0.37	0.000010	0.000117	0.0002					5.04	0.17	0.0780	0.0035	2.133	0.125	0.198	0.007		1166	35	1160	41	1148	91	102
OTD-10.1		85.8	46.4	0.54	-0.000008	0.000005	-0.0001					5.20	0.15	0.0830	0.0024	2.199	0.095	0.192	0.006		1133	30	1181	31	1269	57	89
OTD-11.1		893.9	739.8	0.83	0.000015	0.000010	0.0003					4.28	0.06	0.0895	0.0008	2.881	0.052	0.234	0.004		1353	18	1377	14	1415	16	96
OTD-12.1		102.7	39.8	0.39	0.000046	0.000093	0.0008					4.62	0.10	0.0808	0.0022	2.410	0.089	0.216	0.005		1262	25	1246	27	1217	54	104
OTD-13.1		455.5	10.1	0.02	0.002256	0.000980	0.0384					5.75	0.15	0.0747	0.0173	1.790	0.422	0.174	0.004		1034	24	1042	167	1060	553	98
OTD-14.1		306.7	69.1	0.23	0.000281	0.000095	0.0047					5.29	0.09	0.0741	0.0020	1.932	0.065	0.189	0.003		1116	17	1092	23	1045	56	107
OTD-15.1		1271.3	172.3	0.14	0.000003	0.000008	0.0001					6.77	0.12	0.0736	0.0008	1.499	0.033	0.148	0.003		888	15	930	13	1031	21	86
OTD-16.1		127.9	41.8	0.33	0.000213	0.000200	0.0036					6.23	0.19	0.0683	0.0038	1.512	0.100	0.161	0.005		960	27	935	41	877	118	109
OTD-17.1		117.8	47.4	0.40	0.000219	0.000112	0.0036					4.69	0.09	0.0775	0.0024	2.278	0.086	0.213	0.004		1246	22	1206	27	1133	62	110
OTD-18.1		963.3	126.0	0.13	0.001328	0.000165	0.0234					8.86	0.22	0.0515	0.0030	0.801	0.052	0.113	0.003		690	16	597	30	261	137	264
OTD-19.1		490.9	198.1	0.40	0.000142	0.000042	0.0024					5.23	0.06	0.0782	0.0013	2.060	0.043	0.191	0.002		1127	11	1136	14	1152	33	98
OTD-20.1		182.4	105.6	0.58	0.000110	0.000067	0.0019					6.12	0.12	0.0741	0.0034	1.669	0.086	0.163	0.003		976	17	997	33	1044	95	93
OTD-20.2		713.9	1.7	0.00	0.000355	0.000464	0.0064					15.17	0.67	0.0653	0.0089	0.593	0.088	0.066	0.003		412	18	473	58	782	317	53
OTD-21.1		302.7	135.6	0.45	0.001058	0.000248	0.0180					5.80	0.10	0.0737	0.0043	1.754	0.111	0.172	0.003		1026	17	1029	42	1034	123	99
OTD-22.1		323.3	160.6	0.50	0.000167	0.000091	0.0028					5.52	0.06	0.0727	0.0023	1.815	0.063	0.181	0.002		1073	11	1051	23	1006	65	107
OTD-23.1		281.7	110.3	0.39	0.000630	0.000345	0.0105					4.64	0.07	0.0834	0.0058	2.475	0.180	0.215	0.003		1257	18	1265	54	1278	142	98
OTD-24.1		253.6	121.7	0.48	0.000064	0.000160	0.0011					5.85	0.08	0.0757	0.0034	1.785	0.087	0.171	0.002		1018	13	1040	32	1087	92	94
OTD-25.1		685.4	132.1	0.19	0.000010	0.000000	0.0002					4.48	0.03	0.0893	0.0007	2.745	0.030	0.223	0.002		1298	9	1341	8	1410	14	92
OTD-26.1		301.1	167.6	0.56	0.000010	0.000018	0.0002					4.10	0.07	0.0920	0.0014	3.093	0.075	0.244	0.004		1406	22	1431	19	1468	28	96
OTD-27.1		166.1	170.9	1.03	0.000181	0.000098	0.0031					5.65	0.08	0.0748	0.0022	1.828	0.062	0.177	0.002		1051	14	1056	22	1064	60	99
OTD-28.1		379.1	137.1	0.36	-0.000017	0.000009	-0.0003					5.17	0.06	0.0801	0.0014	2.138	0.048	0.194	0.002		1141	13	1161	16	1200	35	95
OTD-29.1		180.5	55.6	0.31	0.000453	0.000266	0.0077					5.59	0.12	0.0741	0.0054	1.828	0.144	0.179	0.004		1061	21	1056	53	1044	154	102
OTD-30.1		406.0	118.5	0.29	0.000294	0.000308	0.0050					6.12	0.08	0.0705	0.0051	1.588	0.119	0.163	0.002		975	12	965	48	943	155	103
OTD-31.1		492.8	361.3	0.73	0.000254	0.000075	0.0043					5.83	0.05	0.0771	0.0016	1.824	0.043	0.172	0.001		1021	8	1054	15	1124	42	91
OTD-32.1		45.8	17.2	0.38	-0.000210	0.000190	-0.0036					5.75	0.24	0.0810	0.0053	1.941	0.158	0.174	0.007		1033	40	1096	56	1222	134	85
OTD-33.1		1444.0	63.5	0.04	0.000115	0.000039	0.0020					6.40	0.04	0.0735	0.0008	1.582	0.021	0.156	0.001		935	6	963	8	1027	23	91
OTD-34.1		104.0	37.1	0.36	0.000415	0.000309	0.0071					5.94	0.14	0.0729	0.0052	1.692	0.133	0.168	0.004		1003	22	1006	51	1011	153	99
OTD-35.1		674.8	13.6	0.02	0.000349	0.000159	0.0060					6.07	0.10	0.0770	0.0029	1.749	0.074	0.165	0.003		983	14	1027	28	1121	77	88
OTD-36.1		133.1	52.8	0.40	0.001526	0.000312	0.0255					4.87	0.11	0.0945	0.0059	2.675	0.184	0.205	0.005		1203	25	1322	52	1519	122	79
SEV-1.1		179.4	170.8	0.95	0.000165	0.000142	0.0028					5.14	0.13	0.0851	0.0034	2.279	0.114	0.194	0.005		1145	26	1206	36	1317	80	87
SEV-2.1		133.9	119.2	0.89	0.000206	0.000146	0.0035					5.71	0.12	0.0693	0.0036	1.674	0.099	0.175	0.004		1040	21	999	38	909	112	114
SEV-2.1		201.1	63.3	0.31	0.000343	0.000172	0.0058					5.45	0.07	0.0748	0.0030	1.893	0.083	0.184	0.002		1086	13	1079	30	1063	83	102
SEV-4.1		481.6	318.4	0.66	0.000240	0.000064	0.0040					5.15	0.05	0.0881	0.0015	2.358	0.047	0.194	0.002		1144	9	1230	14	1384	33	83
SEV-5.1		111.3	71.1	0.64	0.000974	0.000495	0.0174					11.60	0.32	0.0440	0.0086	0.523	0.105	0.086	0.002		533	14	427	73	0	0	#DIV/0!
SEV-6.1		61.4	25.7	0.42	-0.000146	0.000133	-0.0025					5.51	0.12	0.0778	0.0045	1.947	0.123	0.181	0.004		1075	21	1097	43	1142	118	94
SEV-6.1		235.3	4.2	0.02	0.000073	0.000055	0.0012					5.58	0.06	0.0739	0.0023	1.827	0.064	0.179	0.002		1063	11	1055	23	1039	65	102
SEV-7.1		139.9	82.9	0.59	0.000061	0.000153	0.0010					5.50	0.13	0.0807	0.0039	2.024	0.114	0.182	0.004		1078	23	1124	39	1213	99	89
SEV-8.1		90.7	62.4	0.69	0.000232	0.000351	0.0039					5.19	0.14	0.0836	0.0064	2.222	0.187	0.193	0.005		1136	28	1188	61	1284	157	88
SEV-9.1		272.9	152.2	0.56	0.000919	0.000343	0.0165					12.51	0.32	0.0479	0.0058	0.528	0.067	0.080	0.002		496	12	430	46	95	266	523
SEV-10.1		156.1	77.9	0.50	0.000338	0.000153	0.0056					4.82	0.10	0.0854	0.0040	2.446	0.131	0.208	0.004		1216	23	1256	39	1326	93	92
SEV-11.1		140.4	57.0	0.41	0.000010	0.000000	0.0002					3.95	0.09	0.0929	0.0024	3.242	0.116	0.253	0.005		1454	28	1467	28	1486	49	98
SEV-12.1		62.3	36.5	0.59	0.000141	0.000207	0.0023					4.37	0.10	0.0851	0.0040	2.688	0.149	0.229	0.005		1330	28	1325	42	1318	95	101
SEV-13.1		326.1	104.3	0.32	0.000065	0.000063	0.0011					5.08	0.06	0.0792	0.0017	2.148	0.056	0.197	0.002		1157	13	1164	18	1177	44	98

Analysis		U	Th		$^{204}Pb/$			Total $^{238}U/$		$^{207}Pb/$		Radiogenic Ratios[1] $^{238}U/$		$^{207}Pb/$		$^{207}Pb/$		$^{206}Pb/$		error	Ages (in Ma)[1] $^{206}Pb/$		$^{207}Pb/$		$^{207}Pb/$		%
Label	Zone	(in ppm)		Th/U	^{206}Pb	± 1σ	f206%[2]	^{206}Pb	± 1σ	^{206}Pb	± 1σ	^{206}Pb	± 1σ	^{206}Pb	± 1σ	^{235}U	± 1σ	^{238}U	± 1σ	corr.	^{238}U	± 1σ	^{235}U	± 1σ	^{206}Pb	± 1σ	Conc
SEV-14.1		39.0	20.5	0.53	0.000105	0.000091	0.0018					4.94	0.18	0.0855	0.0045	2.388	0.161	0.203	0.007		1189	40	1239	49	1327	105	90
CHD-1.1		113.4	60.4	0.53	0.000045	0.000099	0.0007					4.37	0.06	0.0873	0.0030	2.752	0.108	0.229	0.003		1328	17	1343	30	1367	68	97
CHD-2.1		51.8	36.3	0.70	0.000085	0.000095	0.0014					4.93	0.10	0.0840	0.0028	2.348	0.099	0.203	0.004		1190	23	1227	30	1293	67	92
CHD-2.2		273.6	82.7	0.30	0.000016	0.000031	0.0003					5.06	0.08	0.0789	0.0013	2.152	0.052	0.198	0.003		1163	17	1166	17	1171	33	99
CHD-3.1		193.1	61.1	0.32	0.000010	0.000036	0.0002					4.47	0.08	0.0850	0.0022	2.618	0.085	0.224	0.004		1300	20	1306	24	1315	51	99
CHD-4.1		54.4	44.4	0.82	0.000513	0.000651	0.0088					5.95	0.17	0.0671	0.0112	1.553	0.270	0.168	0.005		1001	27	952	113	840	394	119
CHD-5.1		155.2	83.8	0.54	0.000053	0.000078	0.0009					5.37	0.14	0.0802	0.0026	2.057	0.089	0.186	0.005		1100	26	1135	30	1201	64	92
CHD-6.1		128.2	58.5	0.46	0.000041	0.000126	0.0007					5.26	0.14	0.0764	0.0028	2.001	0.096	0.190	0.005		1121	27	1116	33	1105	76	101
CHD-7.1		68.7	23.1	0.34	-0.000101	0.000313	-0.0017					5.01	0.14	0.0808	0.0057	2.222	0.177	0.200	0.006		1173	31	1188	57	1215	146	97
CHD-8.1		165.3	98.4	0.59	0.000207	0.000121	0.0035					4.96	0.06	0.0761	0.0033	2.116	0.097	0.202	0.002		1185	12	1154	32	1097	89	108
CHD-9.1		69.9	46.3	0.66	-0.000196	0.000115	-0.0033					4.97	0.10	0.0798	0.0036	2.216	0.114	0.201	0.004		1182	22	1186	37	1193	91	99
CHD-10.1		69.8	35.7	0.51	0.000702	0.000294	0.0118					5.03	0.07	0.0737	0.0066	2.020	0.186	0.199	0.003		1169	16	1122	65	1032	192	113
CHD-11.1		58.4	27.2	0.47	0.000771	0.000349	0.0132					6.01	0.15	0.0616	0.0065	1.414	0.157	0.166	0.004		992	23	895	68	661	243	150
CHD-12.1		129.7	57.5	0.44	0.000021	0.000048	0.0004					5.83	0.13	0.0738	0.0019	1.746	0.062	0.172	0.004		1021	21	1026	23	1035	52	99
CHD-13.1		151.6	52.5	0.35	0.000904	0.000400	0.0154					5.84	0.09	0.0771	0.0065	1.819	0.160	0.171	0.003		1018	15	1052	59	1124	179	91
CHD-14.1		159.2	60.2	0.38	0.000037	0.000081	0.0006					5.30	0.08	0.0787	0.0026	2.048	0.078	0.189	0.003		1115	16	1132	26	1164	66	96
CHD-15.1		256.3	144.6	0.56	0.000023	0.000026	0.0004					4.00	0.23	0.0944	0.0028	3.253	0.220	0.250	0.014		1438	75	1470	54	1516	56	95
CHD-16.1		122.7	39.7	0.32	0.001892	0.000462	0.0318					5.16	0.10	0.0750	0.0076	2.006	0.212	0.194	0.004		1143	21	1118	74	1069	218	107
CHD-18.1		487.3	127.5	0.26	0.000679	0.000158	0.0111					4.18	0.05	0.0885	0.0032	2.921	0.116	0.239	0.003		1383	15	1387	31	1394	72	99
QMS-1.1		264.1	268.1	1.01	0.000136	0.000160	0.0023					5.93	0.13	0.0734	0.0030	1.707	0.083	0.169	0.004		1004	21	1011	32	1026	85	98
QMS-2.1		126.2	112.8	0.89	0.000045	0.000091	0.0008					4.97	0.10	0.0820	0.0039	2.277	0.123	0.201	0.004		1183	22	1205	39	1246	96	95
QMS-3.1		172.7	135.9	0.79	0.000010	0.000015	0.0002					4.34	0.07	0.0954	0.0015	3.027	0.070	0.230	0.004		1336	19	1415	18	1535	29	87
QMS-4.1		556.4	213.4	0.38	0.000321	0.000103	0.0053					4.64	0.06	0.0915	0.0019	2.718	0.068	0.216	0.003		1258	14	1333	19	1456	39	86
QMS-5.1		115.3	118.4	1.03	0.000010	0.000000	0.0002					3.20	0.06	0.1098	0.0032	4.733	0.177	0.313	0.006		1754	30	1773	32	1796	54	98
QMS-6.1		379.9	187.2	0.49	0.000031	0.000030	0.0005					4.81	0.07	0.0798	0.0018	2.286	0.066	0.208	0.003		1217	17	1208	21	1192	45	102
QMS-7.1		156.7	110.4	0.70	0.000120	0.000147	0.0020					5.09	0.09	0.0796	0.0033	2.156	0.100	0.196	0.003		1156	18	1167	33	1187	83	97
QMS-8.1		190.0	208.1	1.10	0.000280	0.000140	0.0048					5.79	0.07	0.0715	0.0026	1.703	0.067	0.173	0.002		1027	11	1010	26	972	76	106
QMS-9.1		1269.3	365.5	0.29	0.000393	0.000146	0.0067					6.30	0.07	0.0811	0.0024	1.774	0.058	0.159	0.002		950	10	1036	22	1223	59	78
QMS-10.1		104.3	97.9	0.94	-0.000182	0.000068	-0.0031					6.71	0.17	0.0742	0.0028	1.524	0.072	0.149	0.004		895	21	940	30	1047	78	85
QMS-11.1		136.9	64.3	0.47	-0.000176	0.000385	-0.0029					4.86	0.10	0.0887	0.0072	2.514	0.217	0.206	0.004		1206	22	1276	65	1397	165	86
QMS-12.1		486.6	300.0	0.62	0.000057	0.000040	0.0010					5.09	0.07	0.0817	0.0013	2.213	0.050	0.196	0.003		1156	14	1185	16	1239	33	93
QMS-13.1		530.1	138.2	0.26	0.000052	0.000045	0.0008					3.29	0.04	0.1094	0.0015	4.579	0.089	0.304	0.004		1709	19	1745	16	1789	25	96
QMS-14.1		159.8	96.2	0.60	-0.000010	0.000009	-0.0001					2.72	0.03	0.1277	0.0025	6.470	0.158	0.368	0.004		2018	21	2042	22	2066	35	98
QMS-14.2		207.5	121.1	0.58	0.000031	0.000037	0.0005					2.74	0.05	0.1264	0.0020	6.370	0.155	0.366	0.006		2009	29	2028	22	2048	28	98
QMS-15.1		307.7	173.3	0.56	0.000049	0.000032	0.0008					4.59	0.04	0.0824	0.0013	2.474	0.048	0.218	0.002		1271	11	1264	14	1254	31	101
QMS-16.1		145.1	96.5	0.66	0.000010	0.000000	0.0002					2.59	0.04	0.1310	0.0018	6.983	0.147	0.387	0.005		2107	25	2109	19	2111	25	100
QMS-18.1		692.6	268.9	0.39	0.000034	0.000032	0.0006					6.04	0.08	0.0728	0.0011	1.662	0.035	0.166	0.002		988	12	994	13	1008	30	98
QMS-19.1		311.6	123.0	0.39	0.000025	0.000029	0.0004					4.93	0.07	0.0797	0.0011	2.232	0.049	0.203	0.003		1192	16	1191	15	1190	28	100
QMS-20.1		118.6	72.7	0.61	0.000031	0.000035	0.0005					6.03	0.11	0.0748	0.0020	1.711	0.058	0.166	0.003		990	16	1013	22	1063	54	93
QMS-21.1		657.9	160.2	0.24	0.000010	0.000006	0.0002					6.10	0.08	0.0757	0.0015	1.713	0.043	0.164	0.002		979	13	1013	16	1088	40	90
QMS-22.1		72.2	112.1	1.55	-0.000245	0.000360	-0.0044					11.99	0.51	0.0595	0.0066	0.684	0.085	0.083	0.004		516	21	529	53	584	263	88
QMS-23.1		168.1	86.5	0.51	0.000061	0.000034	0.0008					1.81	0.03	0.2090	0.0028	15.942	0.332	0.553	0.008		2838	33	2873	20	2898	22	98
QMS-24.1		154.9	121.6	0.79	-0.000080	0.000045	-0.0014					5.97	0.14	0.0758	0.0021	1.751	0.067	0.168	0.004		999	21	1028	25	1089	57	92
QMS-25.1		503.3	41.7	0.08	0.000031	0.000080	0.0005					5.61	0.08	0.0773	0.0026	1.900	0.073	0.178	0.003		1057	14	1081	26	1130	69	94
QMS-27.1		108.9	111.5	1.02	0.000010	0.000000	0.0002					4.88	0.09	0.0825	0.0023	2.329	0.082	0.205	0.004		1201	20	1221	25	1257	55	96
QMS-28.2		505.1	58.8	0.12	0.000055	0.000080	0.0009					4.85	0.05	0.0797	0.0020	2.268	0.064	0.206	0.002		1210	12	1202	20	1190	50	102
QMS-28.3		389.8	245.8	0.63	0.000023	0.000033	0.0004					2.86	0.05	0.1226	0.0018	5.910	0.147	0.350	0.006		1932	31	1963	22	1995	26	97
QMS-29.1		105.2	208.9	1.99	0.000132	0.000087	0.0020					3.08	0.07	0.1105	0.0030	4.942	0.185	0.324	0.007		1810	36	1809	32	1808	51	100
QMS-30.1		284.9	219.0	0.77	0.000098	0.000096	0.0018					9.70	0.14	0.0607	0.0024	0.863	0.037	0.103	0.001		633	9	632	21	629	87	101
QMS-31.1		106.7	77.4	0.73	0.000067	0.000175	0.0010					2.92	0.07	0.1152	0.0037	5.437	0.237	0.342	0.009		1898	42	1891	38	1883	59	101
QMS-32.1		205.2	109.5	0.53	0.000070	0.000063	0.0011					3.08	0.05	0.1119	0.0025	5.009	0.146	0.325	0.005		1813	25	1821	25	1830	42	99
QMS-33.1		232.8	100.6	0.43	0.000219	0.000137	0.0037					5.40	0.11	0.0818	0.0032	2.090	0.096	0.185	0.004		1096	20	1145	32	1241	78	88
QMS-34.1		1085.0	46.2	0.04	0.000013	0.000011	0.0002					5.05	0.22	0.0815	0.0016	2.225	0.110	0.198	0.009		1165	47	1189	35	1232	38	95
QMS-35.1		249.5	138.3	0.55	0.000052	0.000074	0.0009					4.66	0.09	0.0870	0.0025	2.574	0.094	0.215	0.004		1253	22	1293	27	1361	56	92
QMS-36.1		1067.9	67.2	0.06	0.000037	0.000066	0.0006					4.72	0.39	0.0831	0.0034	2.429	0.236	0.212	0.018		1239	94	1251	72	1272	82	97
QMS-36.2		333.6	305.6	0.92	0.000010	0.000011	0.0002					5.01	0.10	0.0821	0.0014	2.258	0.064	0.200	0.004		1173	22	1199	20	1247	34	94
QMS-37.1		80.9	47.5	0.59	0.003108	0.001083	0.0539					7.05	0.24	0.0237	0.0179	0.464	0.352	0.142	0.005		855	27	387	279	0	0	#DIV/0!
QMS-38.1		147.2	45.6	0.31	0.000018	0.000024	0.0003					4.86	0.18	0.0825	0.0025	2.341	0.119	0.206	0.008		1206	41	1225	37	1258	61	96
TELP-1.1		143.6	50.4	0.35	0.000103	0.000090	0.0017					5.29	0.10	0.0787	0.0022	2.054	0.072	0.189	0.004		1117	19	1134	24	1166	55	96
TELP-2.1		216.5	453.0	2.09	0.000010	0.000036	0.0002					5.57	0.21	0.0738	0.0032	1.829	0.113	0.180	0.007		1065	38	1056	41	1037	91	103
TELP-3.1		124.2	48.0	0.39	0.000010	0.000025	0.0002					4.47	0.08	0.0878	0.0026	2.710	0.099	0.224	0.004		1302	22	1331	28	1379	57	94
TELP-4.1		478.5	147.9	0.31	0.000740	0.000428	0.0125					5.22	0.11	0.0825	0.0078	2.181	0.217	0.192	0.004		1131	21	1175	72	1258	197	90
TEL-5.1		383.9	189.5	0.49	0.000076	0.000066	0.0013					5.47	0.15	0.0784	0.0026	1.979	0.090	0.183	0.005		1083	28	1108	31	1158	66	94
TEL-6.1		556.1	333.2	0.60	0.000309	0.000117	0.0054					8.62	0.25	0.0798	0.0023	1.275	0.055	0.116	0.003		707	19	835	25	1191	58	59
TELP-7.1		1423.9	362.0	0.25	0.000690	0.000125	0.0119					6.59	0.13	0.0745	0.0021	1.559	0.058	0.152	0.003		911	17	954	23	1056	59	86
TELP-8.1		251.4	101.7	0.40	0.000575	0.000175	0.0099					6.25	0.17	0.0705	0.0041	1.556	0.104	0.160	0.004		957	24	953	42	942	124	102
TELP-9.1		145.0	55.2	0.38	0.000148	0.000208	0.0024					4.09	0.11	0.0883	0.0039	2.978	0.162	0.245	0.006		1411	34	1402	42	1388	88	102
TELP-10.1		132.5	58.3	0.44	0.000203	0.000167	0.0034					5.07	0.16	0.0779	0.0058	2.120	0.178	0.197	0.006		1161	33	1155	60	1145	156	101
TELP-11.1		121.1	152.9	1.26	0.000256	0.000594	0.0044					6.81	0.14	0.0718	0.0100	1.452	0.208	0.147	0.003		883	17	911	90	979	314	90
TELP-12.1		359.2	175.8	0.49	-0.000036	0.000078	-0.0006					4.21	0.04	0.0894	0.0026	2.929	0.094	0.237	0.002		1374	13	1389	25	1414	56	97
TELP-13.1		4740.7	309.4	0.07	0.003638	0.000428	0.0655					13.04	0.27	0.0571	0.0144	0.603	0.154	0.077	0.002		476	9	479	103	494	494	96
TELP-14.1		183.3	142.6	0.78	0.000095	0.000106	0.0016					5.07	0.10	0.0851	0.0041	2.313	0.125	0.197	0.004		1160	21	1216	39	1317	95	88
TELP-15.1		630.2	385.6	0.61	0.000075	0.000037	0.0013					4.80	0.07	0.0866	0.0013	2.487	0.054	0.208	0.003		1220	16	1268	16	1351	29	90
TELP-16.1		548.1	359.9	0.66	0.000037	0.000023	0.0006					4.92	0.32	0.0814	0.0021	2.283	0.167	0.203	0.013		1194	72	1207	53	1231	50	97
TELP-17.1		721.0	715.6	0.99	0.000040	0.000036	0.0007					5.59	0.06	0.0777	0.0010	1.919	0.035	0.179	0.002		1062	11	1088	12	1140	27	93

Analysis		U	Th		$^{204}Pb/$			Total $^{238}U/$		$^{207}Pb/$		Radiogenic Ratios[1] $^{238}U/$		$^{207}Pb/$		$^{207}Pb/$		$^{206}Pb/$		error	Ages (in Ma)[1] $^{206}Pb/$		$^{207}Pb/$		$^{207}Pb/$		%
Label	Zone	(in ppm)		Th/U	^{206}Pb	± 1σ	f206%[2]	^{206}Pb	± 1σ	^{206}Pb	± 1σ	^{206}Pb	± 1σ	^{206}Pb	± 1σ	^{235}U	± 1σ	^{238}U	± 1σ	corr.	^{238}U	± 1σ	^{235}U	± 1σ	^{206}Pb	± 1σ	Conc
TELP-17.2		455.4	363.1	0.80	0.000302	0.000236	0.0053					8.85	0.13	0.0758	0.0047	1.181	0.077	0.113	0.002		690	10	792	36	1090	128	63
TELP-18.1		342.6	207.5	0.61	0.000010	0.000004	0.0002					5.09	0.13	0.0775	0.0014	2.097	0.067	0.196	0.005		1156	26	1148	22	1133	35	102
TELP-19.1		110.4	59.0	0.53	0.000530	0.000423	0.0091					6.27	0.23	0.0663	0.0070	1.460	0.169	0.160	0.006		954	33	914	72	817	237	117
TELP-20.1		594.3	144.4	0.24	0.000082	0.000071	0.0014					5.94	0.10	0.0724	0.0024	1.682	0.066	0.168	0.003		1004	15	1002	25	997	70	101
TELP-21.1		373.3	86.3	0.23	0.000190	0.000205	0.0032					5.24	0.13	0.0824	0.0034	2.169	0.110	0.191	0.005		1127	26	1171	36	1254	82	90
TELP-22.1		271.8	154.6	0.57	0.000233	0.000083	0.0039					4.61	0.20	0.0854	0.0023	2.555	0.138	0.217	0.009		1266	50	1288	40	1325	54	95
TELP-23.1		167.1	58.7	0.35	0.000010	0.000011	0.0002					5.40	0.17	0.0781	0.0052	1.993	0.154	0.185	0.006		1095	32	1113	53	1149	138	95
TELP-23.2		574.9	14.1	0.02	0.000077	0.000038	0.0013					5.83	0.10	0.0737	0.0015	1.743	0.050	0.171	0.003		1020	17	1024	19	1034	42	99
TELP-24.1		192.7	136.6	0.71	-0.000011	0.000026	-0.0002					6.30	0.19	0.0715	0.0015	1.566	0.060	0.159	0.005		950	27	957	24	971	42	98
TELP-25.1		175.6	54.2	0.31	0.000063	0.000121	0.0011					4.91	0.10	0.0792	0.0027	2.224	0.093	0.204	0.004		1195	23	1189	30	1177	68	102
TELP-26.1		172.1	124.0	0.72	-0.000060	0.000130	-0.0010					5.27	0.09	0.0801	0.0033	2.097	0.098	0.190	0.003		1121	18	1148	33	1199	84	93
TELP-27.1		68.8	69.1	1.00	0.000368	0.000275	0.0063					5.72	0.13	0.0736	0.0051	1.774	0.133	0.175	0.004		1038	22	1036	50	1031	145	101
TELP-28.1		143.3	80.1	0.56	0.000121	0.000152	0.0021					5.59	0.14	0.0756	0.0044	1.866	0.122	0.179	0.004		1062	24	1069	44	1084	120	98
TELP-29.1		1073.4	1000.0	0.93	0.000549	0.000150	0.0092					4.86	0.06	0.0881	0.0026	2.499	0.085	0.206	0.003		1205	15	1272	25	1385	59	87
TELP-30.1		143.5	71.3	0.50	0.000178	0.000109	0.0030					5.19	0.09	0.0764	0.0029	2.030	0.087	0.193	0.003		1136	18	1125	30	1106	77	103
TELP-31.1		174.5	76.7	0.44	0.000095	0.000069	0.0016					5.13	0.06	0.0778	0.0017	2.091	0.054	0.195	0.002		1148	13	1146	18	1142	44	101
TELP-31.2		465.0	326.3	0.70	0.000107	0.000221	0.0018					5.80	0.14	0.0727	0.0038	1.730	0.105	0.173	0.004		1026	23	1020	40	1006	111	102
TELP-32.1		224.2	126.6	0.56	0.000139	0.000122	0.0023					4.47	0.08	0.0833	0.0023	2.569	0.089	0.224	0.004		1301	21	1292	26	1276	55	102
TELP-33.1		136.1	73.5	0.54	0.000062	0.000076	0.0011					6.01	0.14	0.0745	0.0021	1.708	0.066	0.166	0.004		992	21	1012	25	1054	58	94
TELP-34.1		640.4	237.8	0.37	0.000082	0.000105	0.0014					4.50	0.04	0.0868	0.0021	2.659	0.072	0.222	0.002		1294	10	1317	20	1355	48	96
TELP-34.2		283.3	91.3	0.32	0.000055	0.000048	0.0009					4.59	0.09	0.0845	0.0016	2.540	0.073	0.218	0.004		1272	22	1284	21	1304	38	98
TELP-35.1		82.1	41.9	0.51	0.000076	0.000147	0.0012					4.11	0.08	0.0943	0.0056	3.168	0.204	0.244	0.005		1405	24	1449	51	1515	116	93
TELP-36.1		93.5	30.2	0.32	0.000065	0.000143	0.0011					5.26	0.07	0.0807	0.0033	2.116	0.095	0.190	0.003		1122	15	1154	31	1215	82	92
TELP-37.1		98.2	52.8	0.54	0.000017	0.000015	0.0003					4.99	0.12	0.0768	0.0020	2.122	0.079	0.200	0.005		1177	26	1156	26	1117	53	105
TELP-38.1		15.2	2433.0	#####	0.000165	0.000046	0.9900					0.00	4.00	0.0000	0.0000	0.000	0.000	0.000	0.000		0	0	0	0	0	0	#DIV/0!
TELP-38.2		371.4	186.9	0.50	0.000276	0.000092	0.0046					4.69	0.48	0.0802	0.0027	2.359	0.266	0.213	0.022		1247	118	1230	84	1202	68	104
TELP-39.1		757.1	344.5	0.45	0.000017	0.000040	0.0003					4.94	0.13	0.0741	0.0023	2.068	0.090	0.202	0.005		1188	29	1138	30	1044	64	114
GR1-1 (sq)		97.0	34.7	0.36	0.000000	0.000000	0.0000	4.19	0.16	0.0950	0.0026	4.19	0.16	0.0950	0.0026	3.124	0.150	0.239	0.009	0.815	1379	49			1528	52	90
GR1-2.1 (sq)		4262.0	732.9	0.17	0.000788	0.000135	1.4138	15.26	0.57	0.0685	0.0008	15.48	0.58	0.0570	0.0022	0.508	0.027	0.065	0.002	0.694	404	15			491	85	82
GR1-3 (sq)		50.0	42.1	0.84	0.000000	0.000000	0.0000	9.80	0.44	0.0743	0.0052	9.80	0.44	0.0743	0.0052	1.045	0.087	0.102	0.005	0.541	626	27			1049	141	60
GR1-4.1 (sq)		241.9	107.2	0.44	0.000244	0.000159	0.4387	5.12	0.20	0.0927	0.0020	5.15	0.20	0.0893	0.0030	2.392	0.122	0.194	0.007	0.750	1145	40			1410	65	81
CHDAM-1 (sq)		56.914	32.3776	0.57	0.000000	0.000000	0.0000	4.88	0.20	0.0815	0.0035	4.88	0.20	0.0815	0.0035	2.306	0.136	0.205	0.008	0.695	1203	45			1235	83	97
CHDAM-2 (sq)		177.52	97.2857	0.55	0.000000	0.000000	0.0000	5.09	0.20	0.0800	0.0019	5.09	0.20	0.0800	0.0019	2.166	0.098	0.196	0.008	0.846	1156	41			1197	48	97
CHDAM-3 (sq)		633.79	312.352	0.49	0.000000	0.000000	0.0000	4.52	0.17	0.0829	0.0010	4.52	0.17	0.0829	0.0010	2.530	0.099	0.221	0.008	0.956	1289	44			1267	22	102
CHDAM-4 (sq)		219.85	112.77	0.51	0.000082	0.000052	0.1470	4.02	0.15	0.0974	0.0020	4.03	0.15	0.0963	0.0022	3.295	0.145	0.248	0.009	0.862	1429	49			1554	42	92
CHDAM-5 (sq)		156.58	43.0632	0.28	0.000575	0.000132	1.0324	5.67	0.22	0.0768	0.0022	5.72	0.23	0.0685	0.0030	1.650	0.097	0.175	0.007	0.669	1038	38			884	91	117
CHDAM-7 (sq)		150.77	111.48	0.74	0.000000	0.000000	0.0000	5.28	0.20	0.0810	0.0022	5.28	0.20	0.0810	0.0022	2.116	0.101	0.190	0.007	0.815	1119	40			1221	54	92
CHDAM-8A (sq)		332.98	531.131	1.60	0.000000	0.000000	0.0000	5.09	0.19	0.0775	0.0015	5.09	0.19	0.0775	0.0015	2.098	0.090	0.196	0.007	0.888	1156	40			1134	39	102
CHDAM-8B (sq)		147.75	98.506	0.67	0.000000	0.000000	0.0000	5.18	0.20	0.0812	0.0023	5.18	0.20	0.0812	0.0023	2.162	0.104	0.193	0.007	0.810	1138	40			1226	55	93
CHDAM-9 (sq)		144.38	32.2368	0.22	0.000000	0.000000	0.0000	4.92	0.19	0.0810	0.0023	4.92	0.19	0.0810	0.0023	2.269	0.109	0.203	0.008	0.808	1193	42			1221	56	98
CHDAM-10 (sq)		112.27	65.735	0.59	0.000166	0.000108	0.2983	3.90	0.15	0.0792	0.0023	3.91	0.16	0.0768	0.0028	2.706	0.146	0.255	0.010	0.736	1467	52			1116	73	131
CHDAM-11 (sq)		272.08	83.448	0.31	0.000000	0.000000	0.0000	4.76	0.18	0.0819	0.0016	4.76	0.18	0.0819	0.0016	2.372	0.101	0.210	0.008	0.889	1229	42			1243	38	99
CHDAM-12 (sq)		107.07	46.1034	0.43	0.000000	0.000000	0.0000	5.09	0.21	0.0795	0.0029	5.09	0.21	0.0795	0.0029	2.156	0.117	0.197	0.008	0.749	1157	43			1185	71	98
CHDAM-13 (sq)		168.99	62.3777	0.37	0.000000	0.000000	0.0000	5.83	0.23	0.0751	0.0021	5.83	0.23	0.0751	0.0021	1.777	0.085	0.172	0.007	0.805	1021	37			1072	57	95
GR1-1.1		168.2	144.0	0.86	0.000055	0.000065	0.0008					2.45	0.06	0.2459	0.0052	13.866	0.467	0.409	0.010		2210	45	2741	32	3159	34	70
GR1-2.1		95.7	35.7	0.37	0.000010	0.000000	0.0002					14.34	0.37	0.0587	0.0021	0.564	0.026	0.070	0.002		434	11	454	17	554	78	78
GR1-2.1		70.3	34.3	0.49	0.000010	0.000000	0.0002					5.19	0.16	0.0793	0.0019	2.107	0.087	0.193	0.006		1135	32	1151	29	1181	49	96
GR1-4.1		112.2	54.3	0.48	0.000048	0.000095	0.0009					13.92	0.24	0.0596	0.0035	0.590	0.037	0.072	0.001		447	8	471	24	587	131	76
GR1-5.1		77.2	68.4	0.89	0.000146	0.000208	0.0025					6.57	0.14	0.0719	0.0045	1.508	0.103	0.152	0.003		913	19	933	43	982	132	93
GR1-6.1		1780.2	47.7	0.03	0.000094	0.000042	0.0017					18.27	0.27	0.0559	0.0014	0.422	0.013	0.055	0.001		344	5	357	9	447	58	77
GR1-7.1		94.3	78.5	0.83	0.000059	0.000054	0.0010					5.33	0.12	0.0750	0.0015	1.941	0.062	0.188	0.004		1109	23	1095	21	1069	40	104
GR1-7.2		646.2	66.4	0.10	0.000017	0.000020	0.0003					9.59	0.12	0.0681	0.0014	0.979	0.025	0.104	0.001		639	8	693	13	871	44	73
GR1-8.1		69.8	17.1	0.24	0.000010	0.000000	0.0002					5.00	0.09	0.0785	0.0016	2.163	0.063	0.200	0.004		1175	20	1169	20	1159	40	101
GR1-9.1		613.2	505.1	0.82	0.000027	0.000032	0.0005					14.48	0.20	0.0573	0.0015	0.546	0.017	0.069	0.001		431	6	442	11	503	57	86
GR1-10.1		683.7	434.3	0.64	0.000029	0.000032	0.0005					13.95	0.23	0.0563	0.0015	0.556	0.018	0.072	0.001		446	7	449	12	464	59	96
GR1-11.1		472.8	149.8	0.32	0.000010	0.000000	0.0002					5.30	0.06	0.0773	0.0018	2.013	0.055	0.189	0.002		1115	12	1120	19	1129	48	99
GR1-12.1		255.8	145.7	0.57	0.000097	0.000067	0.0017					13.82	0.79	0.0571	0.0029	0.570	0.046	0.072	0.004		450	25	458	30	496	118	91
GR1-12.1		101.1	59.6	0.59	0.000010	0.000031	0.0002					14.12	0.25	0.0576	0.0022	0.563	0.024	0.071	0.001		441	8	453	16	514	85	86
GR1-14.1		50.2	26.3	0.52	0.000115	0.000170	0.0019					5.20	0.11	0.0762	0.0039	2.022	0.117	0.192	0.004		1135	22	1123	40	1100	106	103
GR1-15.1		71.5	73.1	1.02	0.000108	0.000236	0.0019					13.12	0.28	0.0562	0.0043	0.590	0.048	0.076	0.002		473	10	471	31	459	179	103
GR1-16.1		109.0	44.4	0.41	0.000010	0.000000	0.0002					5.33	0.12	0.0773	0.0028	2.000	0.090	0.188	0.004		1109	23	1115	31	1128	74	98
GR1-15.2		63.1	38.1	0.60	0.001206	0.000541	0.0219					15.11	0.38	0.0479	0.0093	0.437	0.087	0.066	0.002		413	10	368	63	93	538	444
GR1-17.1		153.3	50.0	0.33	0.000063	0.000059	0.0011					6.65	0.11	0.0729	0.0019	1.511	0.049	0.150	0.003		903	14	935	20	1012	53	89
GR1-18.1		81.3	88.5	1.09	0.000058	0.000064	0.0010					5.92	0.09	0.0747	0.0019	1.741	0.055	0.169	0.003		1006	14	1024	21	1062	53	95
GR1-19.1		105.5	25.5	0.24	0.000007	0.000015	0.0001					3.02	0.05	0.1137	0.0016	5.200	0.123	0.332	0.006		1846	28	1853	20	1860	25	99
GR1-20.1		78.7	36.5	0.46	0.000010	0.000000	0.0002					5.75	0.12	0.0776	0.0014	1.861	0.053	0.174	0.004		1033	19	1067	19	1138	35	91
GR1-20.1		260.3	117.0	0.45	0.000206	0.000177	0.0038					17.07	0.82	0.0596	0.0037	0.481	0.040	0.059	0.003		367	17	399	28	588	140	62
GR1-22.1		162.5	208.5	1.28	0.000032	0.000023	0.0005					4.03	0.09	0.0996	0.0014	3.405	0.099	0.248	0.006		1427	30	1506	23	1617	27	88
GR1-23.1		14.1	6.5	0.46	-0.000648	0.000467	-0.0117					13.62	0.79	0.0733	0.0091	0.742	0.106	0.073	0.004		457	26	563	64	1021	273	45
GR1-24.1		81.6	11.7	0.14	0.000010	0.000022	0.0001					2.07	0.05	0.1918	0.0033	12.765	0.377	0.483	0.011		2539	47	2663	28	2758	28	92
GR1-25.1		205.7	50.9	0.25	-0.000041	0.000052	-0.0008					14.84	0.22	0.0572	0.0012	0.531	0.014	0.067	0.001		420	6	433	10	499	47	84
GR1-26.1		689.2	356.5	0.52	0.000022	0.000018	0.0004					18.75	0.23	0.0555	0.0010	0.408	0.010	0.053	0.001		335	4	348	7	434	42	77
GR1-27.1		107.5	58.0	0.54	0.000037	0.000054	0.0006					7.06	0.11	0.0704	0.0016	1.373	0.040	0.142	0.002		853	12	878	17	939	47	91
GR1-28.1		210.0	240.4	1.14	0.000012	0.000024	0.0002					5.62	0.07	0.0963	0.0014	2.361	0.050	0.178	0.002		1055	13	1231	15	1553	28	68
GR1-29.1		464.4	155.2	0.33	0.000263	0.000110	0.0048					16.00	0.31	0.0558	0.0021	0.481	0.021	0.063	0.001		391	7	398	15	442	85	88

Analysis		U	Th		$^{204}Pb/$			Total $^{238}U/$		$^{207}Pb/$		Radiogenic Ratios[1] $^{238}U/$		$^{207}Pb/$		$^{207}Pb/$		$^{206}Pb/$		error	Ages (in Ma)[1] $^{206}Pb/$		$^{207}Pb/$		$^{207}Pb/$		%
Label	Zone	(in ppm)		Th/U	^{206}Pb	± 1σ	f206%[2]	^{206}Pb	± 1σ	^{206}Pb	± 1σ	^{206}Pb	± 1σ	^{206}Pb	± 1σ	^{235}U	± 1σ	^{238}U	± 1σ	corr.	^{238}U	± 1σ	^{235}U	± 1σ	^{206}Pb	± 1σ	Conc
GR1-30.1		313.2	41.5	0.13	0.000009	0.000017	0.0002					7.05	0.46	0.0819	0.0070	1.601	0.182	0.142	0.009		855	52	971	74	1244	177	69
GR1-30.1		16.4	22.3	1.36	0.000010	0.000000	0.0002					2.41	0.07	0.1616	0.0056	9.262	0.430	0.416	0.011		2241	52	2364	43	2473	59	91
GR1-32.1		236.3	85.7	0.36	0.000086	0.000117	0.0016					16.36	0.71	0.0561	0.0023	0.472	0.030	0.061	0.003		382	16	393	21	455	95	84
GR1-16.2		396.1	6.4	0.02	0.000238	0.000132	0.0043					17.75	0.63	0.0517	0.0032	0.402	0.030	0.056	0.002		353	12	343	22	274	150	129
GR1-17.2		384.6	4.6	0.01	0.000317	0.000092	0.0058					18.87	0.35	0.0511	0.0022	0.373	0.018	0.053	0.001		333	6	322	14	246	103	135

APPENDIX III

This appendix is a table with the whole-rock geochemical analyses from ACTLABS and XRAL. The elements are arranged in the order, by analytical technique, provided by ACTLABS. NOTE: nd denotes value below the detection limit, -- denotes element not analyzed.

	Detection Limit		SMHC	SMTF	SMTF (2)	TFTIG441	TFTIG441 (2)	BCTF	BECR	BOCAT	LQZT
Major Element Fusion ICP											
SiO_2	0.01	%	68.19	63.73		68.76		65.67	71.34	77.15	89.18
Al_2O_3	0.01	%	12.68	15.46		13.28		17.70	12.37	10.85	5.69
Fe_2O_3	0.01	%	7.69	5.40		5.50		4.02	5.33	3.57	0.45
MnO	0.01	%	0.18	0.10		0.08		0.03	0.09	0.08	nd
MgO	0.01	%	1.93	2.11		2.51		1.62	1.79	1.18	0.10
CaO	0.01	%	2.17	1.57		3.30		3.20	1.92	1.27	0.02
Na_2O	0.01	%	2.23	2.60		2.35		4.19	3.22	3.26	0.47
K_2O	0.01	%	2.07	4.12		2.51		2.01	2.02	1.24	3.63
TiO_2	0.005	%	0.901	0.809		0.874		0.595	0.803	0.714	0.067
P_2O_5	0.01	%	0.05	0.18		0.20		0.11	0.16	0.10	0.04
LOI	0.01	%	0.68	2.48		0.85		1.14	0.94	0.88	0.52
TOTAL		%	98.77	98.56		100.22		100.29	99.98	100.29	100.17
Ba	1	ppm	448	891		743		481	498	380	831
Sr	2	ppm	236	274		219		457	137	148	54
Y	1	ppm	37	49		36		9	42	37	7
Zr	1	ppm	270	290		321		208	371	425	93
Be	1	ppm	2	3		2		2	1	nd	nd
V	5	ppm	110	69		91		82	72	54	7
Trace Element Fusion ICP-MS											
V	0.1	ppm	--	--	--	--		82.8	74.8	57.2	6.6
Ga	1	ppm	14	21	21	19		11	17	14	7
Ge	0.5	ppm	1.8	nd	0.5	2.5		nd	0.6	nd	nd
Rb	2	ppm	89	175	173	111		87	76	32	82
Nb	0.5	ppm	15.7	19.8	19.9	9.0		3.8	13.1	10.9	2.2
Mo	0.1	ppb	--	--	--	--		nd	nd	nd	nd
In	0.1	ppm	nd	nd	nd	nd		nd	nd	nd	nd
Sn	1	ppm	nd	2	2	1		nd	nd	nd	nd
Cs	0.1	ppm	0.8	1.1	1.1	2.2		1.7	0.3	0.3	0.4
Ba	1	ppm	428	855	848	692		--	--	--	--
La	0.05	ppm	34.91	63.05	64.02	37.03		34.27	32.37	36.34	21.65
Ce	0.1	ppm	69.8	132.6	135.3	82.1		60.7	71.0	78.7	21.2
Pr	0.02	ppm	7.67	15.07	15.10	9.48		6.09	8.16	9.30	5.14
Nd	0.05	ppm	28.71	58.27	57.45	36.79		20.79	33.73	36.76	18.38
Sm	0.01	ppm	5.68	11.69	11.39	7.56		3.28	7.02	7.32	3.28
Eu	0.005	ppm	1.469	2.158	2.145	1.761		1.233	1.586	1.623	0.833
Gd	0.02	ppm	5.69	10.69	10.72	7.76		2.45	6.56	6.59	2.46
Tb	0.01	ppm	0.92	1.65	1.61	1.17		0.36	1.23	1.14	0.33
Dy	0.02	ppm	6.22	9.45	9.35	6.83		1.80	7.46	6.50	1.59
Ho	0.01	ppm	1.36	1.82	1.81	1.37		0.32	1.58	1.35	0.27
Er	0.01	ppm	4.36	5.33	5.30	4.06		0.91	4.76	4.07	0.69
Tm	0.005	ppm	0.669	0.775	0.753	0.586		0.129	0.748	0.636	0.099
Pb	5	ppm	--	--	--	--		nd	53	28	9
Trace Element Fusion ICP-MS Research Add-On											
Zr	1	ppm	--	--	--	--		--	--	--	--
Yb	0.01	ppm	4.48	4.84	4.75	3.60		0.84	4.49	3.98	0.59
Lu	0.002	ppm	0.707	0.680	0.682	0.527		0.121	0.662	0.624	0.078
Hf	0.1	ppm	7.2	7.4	7.2	7.4		4.7	10.6	11.5	2.7
Ta	0.1	ppm	0.9	1.3	1.4	0.7		0.3	0.7	0.7	0.2
W	1	ppm	nd	nd	nd	nd		nd	nd	nd	nd
Tl	0.05	ppm	0.54	0.62	0.62	0.44		nd	0.51	0.19	0.26
Bi	0.06	ppm	nd	nd	nd	nd		nd	nd	nd	nd
Th	0.05	ppm	13.29	14.30	14.13	11.16		10.65	9.64	11.60	2.79
U	0.05	ppm	1.69	3.30	3.25	2.47		1.83	1.35	2.29	0.54
"Near Total" Digestion ICP											
Cu	1	ppm	7	16		4	4	11	5	59	2
Pb	5	ppm	14	24		11	11	30	24	9	11
Zn	1	ppm	58	116		68	69	88	97	93	6
Ag	0.5	ppm	nd	nd		nd	nd	nd	nd	nd	nd
Ni	1	ppm	65	23		31	30	10	26	18	1
Cd	0.5	ppm	nd	nd		nd	nd	nd	nd	nd	nd
Bi	0.06	ppm	nd	nd		nd	nd	nd	nd	nd	nd
S	0.001	%	--	--		--	--	--	--	--	--
INAA											
Au	1	ppb	nd	nd		nd		nd	nd	6	nd
As	1	ppm	nd	4		nd		nd	nd	nd	nd
Br	0.5	ppm	nd	nd		nd		nd	nd	nd	1.8
Co	0.1	ppm	15.0	13.7		15.9		5.3	11.2	10.2	1.0
Cr	0.5	ppm	178.0	44.8		75.6		31.1	47.2	33.1	0.6
Hg	5	ppm	nd	nd		nd		nd	nd	nd	nd
Ir	1	ppb	nd	nd		nd		nd	nd	nd	nd
Mo	2	ppm	nd	nd		nd		--	--	--	--
Sb	0.1	ppm	nd	nd		nd		0.1	nd	nd	nd
Sc	0.01	ppm	18.50	13.50		14.80		7.60	11.70	8.91	0.70
Se	0.5	ppm	nd	nd		nd		nd	nd	nd	nd
W	1	ppm	--	--	--	--	--	--	--	--	--
Mass	0.001	g	1.804	1.684		1.442		1.537	1.555	1.547	1.507

	Detection Limit		PMQZT	TFQZT1	TFQZT2	UTF85	KEOTF	OTCOW	COLRAB	CHDAM1A	TELPL2
Major Element Fusion ICP											
SiO_2	0.01	%	95.71	71.50	88.98	65.82	66.65	61.36	72.61	75.93	69.76
Al_2O_3	0.01	%	2.80	13.30	5.05	15.62	15.26	14.56	11.40	7.36	14.71
Fe_2O_3	0.01	%	0.27	3.54	0.96	6.29	5.89	9.84	4.28	4.17	4.58
MnO	0.01	%	nd	0.03	0.01	0.10	0.09	0.07	0.22	0.09	0.03
MgO	0.01	%	0.09	0.96	0.27	1.92	1.76	2.71	0.83	0.90	1.06
CaO	0.01	%	nd	0.80	0.19	2.70	2.15	2.53	7.65	2.74	1.03
Na_2O	0.01	%	0.05	2.26	0.52	3.37	2.65	2.50	0.83	1.17	1.91
K_2O	0.01	%	0.80	6.31	3.08	2.32	3.12	2.89	0.37	2.40	2.26
TiO_2	0.005	%	0.175	0.669	0.542	0.692	0.922	1.821	0.801	0.531	1.194
P_2O_5	0.01	%	0.03	0.15	0.03	0.22	0.17	0.22	0.20	0.12	0.16
LOI	0.01	%	0.55	0.78	0.53	1.18	1.84	1.55	1.14	4.97	3.05
TOTAL		%	100.47	100.30	100.17	100.24	100.50	100.06	100.34	100.39	99.75
Ba	1	ppm	63	1033	659	547	653	819	79	501	298
Sr	2	ppm	10	168	96	273	210	288	231	225	70
Y	1	ppm	21	30	13	51	41	28	32	19	34
Zr	1	ppm	159	487	322	246	271	356	378	473	766
Be	1	ppm	nd	2	nd	3	2	1	2	1	2
V	5	ppm	11	38	17	60	78	171	70	35	78
Trace Element Fusion ICP-MS											
V	0.1	ppm	13.7	39.0	16.7	57.2	--	--	--	--	--
Ga	1	ppm	3	20	6	14	21	22	16	11	23
Ge	0.5	ppm	nd	0.8	nd	nd	1.8	1.4	1.9	1.0	1.7
Rb	2	ppm	17	181	70	85	101	96	13	65	84
Nb	0.5	ppm	2.6	12.9	9.5	11.6	16.2	20.7	13.9	10.5	19.0
Mo	0.1	ppb	nd	nd	nd	nd	--	--	--	--	--
In	0.1	ppm	nd	nd	nd	nd	nd	nd	nd	nd	nd
Sn	1	ppm	nd	1	nd	1	4	4	5	2	4
Cs	0.1	ppm	0.1	1.2	0.4	2.3	1.8	0.8	0.2	0.9	2.8
Ba	1	ppm	--	--	--	--	--	--	--	--	--
La	0.05	ppm	19.20	37.78	22.22	60.11	37.93	43.62	27.99	25.45	35.38
Ce	0.1	ppm	46.9	83.1	47.5	123.9	74.4	87.5	57.8	52.6	81.8
Pr	0.02	ppm	5.17	9.85	5.29	14.39	10.50	11.21	7.00	6.15	9.52
Nd	0.05	ppm	21.48	40.18	19.88	57.06	41.19	44.05	27.15	22.67	37.34
Sm	0.01	ppm	4.31	8.06	3.68	11.22	8.29	8.61	5.41	3.95	7.23
Eu	0.005	ppm	0.811	1.948	0.770	2.142	1.998	2.106	1.253	0.665	1.462
Gd	0.02	ppm	4.47	6.84	2.96	9.87	6.99	7.22	4.85	3.47	5.99
Tb	0.01	ppm	0.77	1.16	0.46	1.65	1.23	1.13	0.88	0.55	0.98
Dy	0.02	ppm	3.86	6.06	2.44	9.30	7.53	6.27	5.49	3.22	6.05
Ho	0.01	ppm	0.74	1.17	0.48	1.85	1.58	1.08	1.17	0.67	1.28
Er	0.01	ppm	2.02	3.20	1.49	5.26	4.60	2.75	3.49	2.14	3.98
Tm	0.005	ppm	0.290	0.460	0.224	0.772	0.688	0.378	0.578	0.330	0.624
Pb	5	ppm	7	94	32	nd	--	--	--	--	--
Trace Element Fusion ICP-MS Resear											
Zr	1	ppm	--	--	--	--	278	361	371	493	773
Yb	0.01	ppm	1.64	2.80	1.39	4.66	4.48	2.36	3.57	2.32	4.50
Lu	0.002	ppm	0.221	0.395	0.225	0.651	0.648	0.280	0.574	0.387	0.726
Hf	0.1	ppm	4.6	12.7	8.2	7.3	7.3	9.3	9.7	12.6	20.2
Ta	0.1	ppm	0.1	0.9	0.7	1.1	1.2	1.1	0.9	0.8	1.4
W	1	ppm	nd	nd	1	nd	--	--	--	--	--
Tl	0.05	ppm	nd	1.73	0.36	0.12	0.64	0.40	0.06	0.41	0.60
Bi	0.06	ppm	nd	0.42	nd	nd	nd	nd	2.70	nd	nd
Th	0.05	ppm	4.66	9.46	12.42	10.55	8.17	10.64	10.90	9.70	12.95
U	0.05	ppm	0.61	1.95	1.70	3.02	2.37	1.26	2.25	1.63	3.62
"Near Total" Digestion ICP											
Cu	1	ppm	2	3	2	14	31	17	6	2	6
Pb	5	ppm	nd	31	17	17	19	39	nd	7	6
Zn	1	ppm	4	88	15	103	89	16	123	52	72
Ag	0.5	ppm	nd	nd	nd	nd	nd	nd	nd	nd	nd
Ni	1	ppm	nd	11	nd	21	20	nd	49	4	11
Cd	0.5	ppm	nd	nd	nd	nd	nd	nd	nd	nd	nd
Bi	0.06	ppm	nd	nd	nd	nd	nd	nd	nd	nd	nd
S	0.001	%	--	--	--	--	0.012	0.009	0.009	0.004	0.019
INAA											
Au	1	ppb	nd	nd	nd	4	nd	2	2	10	nd
As	1	ppm	nd	nd	nd	nd	nd	nd	1	2	10
Br	0.5	ppm	nd	nd	nd	nd	nd	nd	nd	1.0	nd
Co	0.1	ppm	1.1	6.4	1.7	13.5	12.3	28.8	10.7	4.4	7.4
Cr	0.5	ppm	5.9	20.0	5.2	44.5	54.4	81.3	37.4	15.8	45.2
Hg	5	ppm	nd	nd	nd	nd	nd	nd	nd	nd	nd
Ir	1	ppb	nd	nd	nd	nd	nd	nd	nd	--	--
Mo	2	ppm	--	--	--	--	nd	nd	2	nd	nd
Sb	0.1	ppm	nd	nd	nd	nd	nd	nd	nd	0.4	0.3
Sc	0.01	ppm	1.91	7.12	1.53	12.30	12.20	16.70	7.92	4.60	11.80
Se	0.5	ppm	nd	nd	nd	nd	nd	nd	nd	nd	nd
W	1	ppm	--	--	--	--	nd	nd	nd	--	--
Mass	0.001	g	1.582	1.592	1.544	1.563	1.338	1.174	1.420	1.811	1.420

	Detection Limit		BPM1	GR1	OTD	QMS1	QMS1 rep	SERV2	SEV	TOL1
Major Element Fusion ICP										
SiO_2	0.01	%	68.30	64.08	65.20	77.44	77.91	79.77	20.62	73.14
Al_2O_3	0.01	%	14.09	14.87	15.56	10.35	10.23	6.54	1.27	15.04
Fe_2O_3	0.01	%	6.08	6.05	6.27	4.14	4.10	1.98	0.55	2.10
MnO	0.01	%	0.09	0.07	0.09	0.05	0.05	0.05	0.02	0.04
MgO	0.01	%	1.58	4.27	2.14	1.23	1.20	0.61	1.74	0.26
CaO	0.01	%	1.96	3.89	2.25	0.71	0.69	2.36	41.49	2.22
Na_2O	0.01	%	2.38	1.65	2.45	1.61	1.56	1.27	0.41	3.56
K_2O	0.01	%	3.03	2.98	3.37	2.17	2.11	2.84	0.19	3.63
TiO_2	0.005	%	0.925	0.816	0.954	0.820	0.815	0.701	0.051	0.117
P_2O_5	0.01	%	0.17	0.16	0.16	0.15	0.15	0.08	0.04	0.03
LOI	0.01	%	1.60	1.38	1.72	1.65	1.65	4.05	34.13	0.26
TOTAL		%	100.20	100.21	100.17	100.32	100.45	100.25	100.49	100.39
Ba	1	ppm	558	505	730	356	352	519	156	661
Sr	2	ppm	191	222	128	102	101	185	285	199
Y	1	ppm	42	26	38	29	28	27	7	8
Zr	1	ppm	345	283	285	394	369	1170	51	126
Be	1	ppm	2	3	2	2	2	nd	nd	2
V	5	ppm	70	105	84	82	82	17	nd	8
Trace Element Fusion ICP-MS										
V	0.1	ppm	--	--	--	--	--	--	--	9.9
Ga	1	ppm	20	20	22	13	13	7	1	16
Ge	0.5	ppm	1.2	1.5	1.3	1.4	1.5	0.8	nd	0.8
Rb	2	ppm	101	170	110	84	87	65	5	102
Nb	0.5	ppm	18.1	14.5	14.2	10.3	10.1	9.6	1.7	4.2
Mo	0.1	ppb	--	--	--	--	--	--	--	nd
In	0.1	ppm	nd	nd	nd	nd	nd	nd	nd	nd
Sn	1	ppm	2	5	2	2	2	1	nd	nd
Cs	0.1	ppm	1.7	34.7	2.7	3.1	3.2	0.3	nd	0.8
Ba	1	ppm	--	--	--	--	--	--	--	--
La	0.05	ppm	44.04	42.40	36.38	24.15	23.80	29.93	5.79	28.78
Ce	0.1	ppm	83.7	76.9	71.8	43.3	44.1	59.7	10.4	57.9
Pr	0.02	ppm	11.03	9.90	9.41	5.66	5.75	7.70	1.36	6.36
Nd	0.05	ppm	44.27	37.88	37.97	21.50	21.69	30.21	5.49	24.12
Sm	0.01	ppm	8.47	6.64	7.31	4.13	4.28	5.43	1.02	4.21
Eu	0.005	ppm	1.957	1.437	1.732	1.095	1.094	0.907	0.261	1.474
Gd	0.02	ppm	7.20	5.23	6.28	3.86	3.97	4.59	0.97	2.89
Tb	0.01	ppm	1.23	0.84	1.09	0.74	0.75	0.78	0.16	0.39
Dy	0.02	ppm	7.08	4.65	6.04	4.58	4.58	4.31	0.91	1.74
Ho	0.01	ppm	1.44	0.92	1.30	0.96	0.99	0.93	0.19	0.28
Er	0.01	ppm	4.12	2.59	3.72	2.84	2.91	2.81	0.52	0.73
Tm	0.005	ppm	0.617	0.375	0.544	0.430	0.432	0.452	0.077	0.090
Pb	5	ppm	--	--	--	--	--	--	--	89
Trace Element Fusion ICP-MS Resear										
Zr	1	ppm	249	206	207	282	269	1120	87	--
Yb	0.01	ppm	3.74	2.39	3.55	2.69	2.66	2.91	0.47	0.61
Lu	0.002	ppm	0.537	0.349	0.523	0.401	0.407	0.486	0.069	0.079
Hf	0.1	ppm	6.7	5.4	5.5	7.4	7.1	23.5	1.4	4.2
Ta	0.1	ppm	0.8	0.7	0.7	0.7	0.7	0.7	nd	nd
W	1	ppm	--	--	--	--	--	--	--	nd
Tl	0.05	ppm	0.68	1.66	0.91	0.78	0.71	0.53	nd	0.49
Bi	0.06	ppm	nd	nd	nd	0.11	0.17	nd	nd	nd
Th	0.05	ppm	8.22	9.45	7.24	10.24	10.56	12.88	1.07	10.63
U	0.05	ppm	2.53	2.33	2.03	2.01	2.03	3.73	0.59	0.95
"Near Total" Digestion ICP										
Cu	1	ppm	18	15	28	2		2	1	nd
Pb	5	ppm	12	nd	nd	19		nd	9	29
Zn	1	ppm	81	78	90	56		10	nd	31
Ag	0.5	ppm	nd	nd	nd	nd		nd	nd	nd
Ni	1	ppm	19	80	20	20		nd	1	2
Cd	0.5	ppm	0.6	nd	nd	nd		nd	nd	nd
Bi	0.06	ppm	nd	nd	nd	nd		nd	nd	nd
S	0.001	%	0.134	0.242	0.139	nd		0.125	0.146	--
INAA										
Au	1	ppb	3	nd	2	2		3	7	nd
As	1	ppm	nd	98	nd	2		4	1	nd
Br	0.5	ppm	nd	nd	nd	nd		1.4	0.8	nd
Co	0.1	ppm	13.7	18.9	14.9	11.6		3.4	1.5	1.8
Cr	0.5	ppm	43.8	176.0	49.0	39.4		8.3	4.1	0.5
Hg	5	ppm	nd	nd	nd	nd		nd	nd	nd
Ir	1	ppb	nd	nd	nd	nd		nd	nd	nd
Mo	2	ppm	nd	nd	nd	nd		nd	nd	--
Sb	0.1	ppm	nd	0.4	0.1	0.1		0.4	nd	nd
Sc	0.01	ppm	11.30	13.70	12.90	10.00		2.20	1.00	3.47
Se	0.5	ppm	nd	nd	nd	nd		nd	nd	nd
W	1	ppm	2	nd	1	2		2	nd	--
Mass	0.001	g	1.310	1.452	1.326	1.759		1.218	1.576	1.522

	Detection Limit		G846	GL4	GL5	LVQ1	OSGG2	WIMPY	CM605	TRG2	FI1
Major Element Fusion ICP											
SiO_2	0.01	%	72.04	77.28	69.85	75.08	74.52	72.13	71.20	68.76	60.70
Al_2O_3	0.01	%	14.00	13.20	15.30	13.58	14.24	13.59	13.95	15.06	17.52
Fe_2O_3	0.01	%	2.57	1.45	3.71	1.83	0.64	3.70	3.83	6.34	6.23
MnO	0.01	%	0.05	0.03	0.07	0.03	0.01	0.07	0.08	0.11	0.13
MgO	0.01	%	0.67	0.36	1.02	0.79	0.18	0.92	1.13	1.87	2.46
CaO	0.01	%	2.69	1.73	3.86	3.31	0.92	3.78	3.18	1.62	5.16
Na_2O	0.01	%	3.79	5.34	3.62	3.82	2.91	3.32	2.47	4.15	3.11
K_2O	0.01	%	2.20	0.67	1.13	0.99	5.58	1.57	2.20	1.20	2.21
TiO_2	0.005	%	0.144	0.103	0.310	0.213	0.131	0.217	0.388	0.773	0.740
P_2O_5	0.01	%	0.04	0.02	0.07	0.03	0.10	0.05	0.09	0.18	0.16
LOI	0.01	%	1.16	0.30	1.16	0.74	1.25	0.93	1.41	nd	1.30
TOTAL		%	99.35	100.48	100.10	100.44	100.50	100.28	99.92	100.04	99.73
Ba	1	ppm	603	241	205	208	467	356	419	133	335
Sr	2	ppm	101	127	119	130	129	84	114	177	215
Y	1	ppm	16	26	12	3	6	15	23	44	44
Zr	1	ppm	95	112	60	98	94	105	163	328	190
Be	1	ppm	nd	nd	2	1	2	1	2	2	2
V	5	ppm	35	nd	67	33	8	50	58	73	102
Trace Element Fusion ICP-MS											
V	0.1	ppm	--	--	--	--	--	--	--	--	--
Ga	1	ppm	13	12	16	12	16	12	14	20	21
Ge	0.5	ppm	1.3	1.1	1.2	1.1	1.4	1.3	2.4	1.2	1.4
Rb	2	ppm	42	14	41	43	136	51	89	25	130
Nb	0.5	ppm	1.9	1.8	2.4	3.2	11.8	5.4	9.5	14.4	10.6
Mo	0.1	ppb	--	--	--	--	--	--	--	--	--
In	0.1	ppm	nd	nd	nd	nd	nd	nd	nd	nd	nd
Sn	1	ppm	3	2	2	2	3	1	3	nd	3
Cs	0.1	ppm	0.4	0.2	0.6	0.8	0.5	0.5	2.5	nd	4.4
Ba	1	ppm	--	--	--	--	--	--	--	--	--
La	0.05	ppm	7.77	11.30	5.66	10.98	18.51	16.51	26.88	34.18	20.26
Ce	0.1	ppm	19.6	23.3	42.1	20.7	44.9	30.6	54.7	74.5	34.8
Pr	0.02	ppm	2.06	2.97	1.83	2.34	3.36	3.36	6.02	8.92	6.02
Nd	0.05	ppm	7.67	12.13	7.38	8.36	11.26	11.79	24.48	35.85	26.92
Sm	0.01	ppm	1.71	2.87	2.03	1.37	2.01	2.19	4.68	7.59	6.57
Eu	0.005	ppm	0.408	0.382	0.578	0.361	0.584	0.525	0.940	1.913	1.596
Gd	0.02	ppm	1.72	3.04	1.53	0.95	1.42	2.00	4.29	7.02	6.44
Tb	0.01	ppm	0.36	0.61	0.37	0.12	0.25	0.38	0.68	1.26	1.19
Dy	0.02	ppm	2.39	3.95	2.28	0.61	1.32	2.46	3.99	8.00	7.14
Ho	0.01	ppm	0.54	0.91	0.48	0.11	0.24	0.55	0.74	1.65	1.52
Er	0.01	ppm	1.79	2.88	1.46	0.29	0.68	1.70	2.24	4.75	4.47
Tm	0.005	ppm	0.331	0.500	0.230	0.046	0.118	0.287	0.355	0.695	0.680
Pb	5	ppm	--	--	--	--	--	--	--	--	--
Trace Element Fusion ICP-MS Resear											
Zr	1	ppm	93	110	50	93	83	107	160	330	151
Yb	0.01	ppm	2.40	3.39	1.48	0.28	0.79	1.99	2.22	4.63	4.15
Lu	0.002	ppm	0.439	0.576	0.218	0.043	0.117	0.338	0.321	0.697	0.600
Hf	0.1	ppm	2.8	3.8	1.5	2.6	2.9	2.8	4.0	8.9	4.0
Ta	0.1	ppm	0.2	0.2	0.2	0.3	1.5	0.5	0.9	1.0	0.5
W	1	ppm	--	--	--	--	--	--	--	--	--
Tl	0.05	ppm	0.13	0.07	0.22	0.23	0.46	0.18	0.52	0.10	1.21
Bi	0.06	ppm	nd	nd	nd	nd	nd	nd	0.14	nd	0.15
Th	0.05	ppm	2.94	3.12	2.40	4.53	10.66	6.00	9.48	9.80	3.43
U	0.05	ppm	0.62	1.05	0.69	0.49	2.41	1.91	2.44	2.50	1.26
"Near Total" Digestion ICP											
Cu	1	ppm	49	12	13	8	8	32	12	7	1
Pb	5	ppm	12	10	nd	11	15	7	20	5	nd
Zn	1	ppm	28	19	47	26	26	38	52	52	72
Ag	0.5	ppm	nd	nd	nd	nd	nd	nd	nd	nd	nd
Ni	1	ppm	1	1	nd	4	3	16	8	18	5
Cd	0.5	ppm	nd	nd	nd	nd	nd	nd	nd	nd	nd
Bi	0.06	ppm	nd	nd	nd	nd	nd	nd	--	nd	nd
S	0.001	%	0.009	0.011	0.005	0.009	0.011	0.071	0.002	0.001	0.004
INAA											
Au	1	ppb	nd	16	nd	nd	nd	nd	nd	nd	nd
As	1	ppm	nd	nd	nd	nd	nd	nd	nd	nd	1
Br	0.5	ppm	nd	nd	nd	nd	nd	nd	nd	nd	nd
Co	0.1	ppm	6.3	2.4	7.3	4.5	3.8	8.3	8.7	12.7	15.2
Cr	0.5	ppm	nd	nd	3.0	6.0	4.0	4.1	14.1	39.2	11.5
Hg	5	ppm	nd	nd	nd	nd	nd	nd	nd	nd	nd
Ir	1	ppb	nd	nd	nd	nd	nd	nd	nd	--	nd
Mo	2	ppm	nd	nd	nd	3	nd	3	3	nd	nd
Sb	0.1	ppm	nd	nd	nd	0.1	nd	nd	0.1	0.1	nd
Sc	0.01	ppm	9.30	5.22	13.70	2.43	2.84	12.40	14.90	12.50	13.70
Se	0.5	ppm	nd	nd	nd	nd	nd	nd	nd	nd	nd
W	1	ppm	nd	nd	nd	nd	nd	nd	nd	--	nd
Mass	0.001	g	1.070	1.599	1.420	1.265	1.151	1.555	1.399	1.879	1.299

	Detection Limit		FI2	GR2	PEL1	PEL1 rep	POMTN	TOC1	KEN
Major Element Fusion ICP									
SiO_2	0.01	%	58.59	52.59	65.85		84.50	77.18	61.13
Al_2O_3	0.01	%	16.40	19.29	17.03		14.30	12.99	17.11
Fe_2O_3	0.01	%	6.54	8.25	4.60		0.05	0.81	5.95
MnO	0.01	%	0.12	0.15	0.05		nd	0.04	0.11
MgO	0.01	%	3.99	4.09	1.23		nd	0.17	3.15
CaO	0.01	%	4.95	6.53	3.38		0.01	0.94	6.52
Na_2O	0.01	%	3.38	3.69	4.00		0.12	4.10	3.40
K_2O	0.01	%	3.09	2.69	2.57		0.39	3.54	1.31
TiO_2	0.005	%	1.100	1.561	0.750		0.155	0.116	0.399
P_2O_5	0.01	%	0.53	0.47	0.23		0.02	0.03	0.10
LOI	0.01	%	1.58	1.13	0.68		0.72	0.32	0.60
TOTAL		%	100.25	100.44	100.37		100.27	100.23	99.78
Ba	1	ppm	865	644	588		38	1350	390
Sr	2	ppm	887	561	270		4	88	303
Y	1	ppm	18	41	20		35	36	14
Zr	1	ppm	261	268	347		250	63	103
Be	1	ppm	3	5	3		nd	1	2
V	5	ppm	129	185	53		nd	nd	115
Trace Element Fusion ICP-MS									
V	0.1	ppm	--	--	--		--	--	--
Ga	1	ppm	23	26	23		19	13	17
Ge	0.5	ppm	1.2	1.4	1.2		2.3	1.2	1.5
Rb	2	ppm	168	161	136		6	97	52
Nb	0.5	ppm	13.9	17.1	14.4		14.7	7.9	4.9
Mo	0.1	ppb	--	--	--		--	--	nd
In	0.1	ppm	nd	nd	nd		nd	nd	nd
Sn	1	ppm	3	7	2		4	nd	nd
Cs	0.1	ppm	4.0	13.6	4.6		nd	0.4	0.6
Ba	1	ppm	--	--	--		--	--	--
La	0.05	ppm	67.65	35.35	40.32		16.06	27.76	13.87
Ce	0.1	ppm	128.2	80.3	73.0		16.5	52.1	29.6
Pr	0.02	ppm	16.22	11.57	8.59		1.80	6.26	3.67
Nd	0.05	ppm	60.90	51.22	32.41		7.54	23.02	14.93
Sm	0.01	ppm	8.64	10.36	5.87		2.60	4.45	3.38
Eu	0.005	ppm	2.191	3.003	1.663		0.714	0.688	0.842
Gd	0.02	ppm	5.71	8.29	4.93		3.04	4.10	3.25
Tb	0.01	ppm	0.70	1.33	0.75		0.73	0.78	0.50
Dy	0.02	ppm	3.26	7.12	3.78		5.56	4.99	2.77
Ho	0.01	ppm	0.58	1.38	0.71		1.43	1.14	0.54
Er	0.01	ppm	1.59	3.88	1.82		4.80	3.50	1.67
Tm	0.005	ppm	0.210	0.555	0.241		0.800	0.567	0.258
Pb	5	ppm	--	--	--		--	--	--
Trace Element Fusion ICP-MS Resear									
Zr	1	ppm	176	185	213		183	69	112
Yb	0.01	ppm	1.27	3.46	1.50		5.58	3.64	1.70
Lu	0.002	ppm	0.188	0.491	0.232		0.881	0.564	0.255
Hf	0.1	ppm	3.9	4.5	5.5		7.7	2.3	2.9
Ta	0.1	ppm	0.5	1.1	0.7		1.3	0.7	0.3
W	1	ppm	--	--	--		--	--	--
Tl	0.05	ppm	1.48	1.48	0.95		0.08	0.56	0.33
Bi	0.06	ppm	nd	0.20	nd		nd	nd	nd
Th	0.05	ppm	11.56	7.08	6.61		16.25	8.90	3.59
U	0.05	ppm	3.48	5.00	1.96		2.72	2.16	0.69
"Near Total" Digestion ICP									
Cu	1	ppm	4	11	3	3	nd	nd	20
Pb	5	ppm	6	nd	nd	nd	nd	8	9
Zn	1	ppm	117	90	62	67	4	7	57
Ag	0.5	ppm	nd	nd	nd	nd	nd	nd	nd
Ni	1	ppm	59	23	4	3	nd	nd	13
Cd	0.5	ppm	nd	0.6	nd	nd	nd	nd	nd
Bi	0.06	ppm	nd	nd	nd	nd	nd	nd	nd
S	0.001	%	0.008	0.020	0.019	0.021	0.002	0.008	0.018
INAA									
Au	1	ppb	2	nd	2		2	9	nd
As	1	ppm	nd	2	nd		nd	nd	nd
Br	0.5	ppm	nd	nd	nd		nd	nd	nd
Co	0.1	ppm	20.1	19.6	8.0		1.0	1.4	17.3
Cr	0.5	ppm	89.7	28.2	10.4		nd	nd	41.2
Hg	5	ppm	nd	nd	nd		nd	nd	nd
Ir	1	ppb	nd	nd	nd		nd	nd	nd
Mo	2	ppm	nd	nd	3		nd	nd	nd
Sb	0.1	ppm	nd	0.2	nd		0.1	0.1	nd
Sc	0.01	ppm	11.90	19.40	9.80		8.90	5.00	19.20
Se	0.5	ppm	nd	nd	nd		nd	nd	nd
W	1	ppm	nd	nd	nd		2	nd	nd
Mass	0.001	g	1.113	1.538	1.452		1.394	1.349	1.639

	Detection Limit				1782VM
Major Element Fusion ICP			XRAL	Detection Limit	
SiO_2	0.01	%	MERXRF	0.01 %	73.00
Al_2O_3	0.01	%	MERXRF	0.01 %	14.40
Fe_2O_3	0.01	%	MERXRF	0.01 %	3.12
MnO	0.01	%	MERXRF	0.01 %	0.05
MgO	0.01	%	MERXRF	0.01 %	0.62
CaO	0.01	%	MERXRF	0.01 %	3.66
Na_2O	0.01	%	MERXRF	0.01 %	3.84
K_2O	0.01	%	MERXRF	0.01 %	0.84
TiO_2	0.005	%	MERXRF	0.001 %	0.186
P_2O_5	0.01	%	MERXRF	0.01 %	0.03
LOI	0.01	%	MERXRF	0.01 %	0.40
TOTAL		%	MERXRF	0.01 %	100.20
Ba	1	ppm	MERXRF	20 ppm	193
Sr	2	ppm	MERICP	0.5 ppm	128.0
Y	1	ppm	MERMS	1 ppm	9
Zr	1	ppm	MERXRF	2 ppm	70
Be	1	ppm	MERICP	0.5 ppm	1.5
V	5	ppm			
Trace Element Fusion ICP-MS					
V	0.1	ppm	MERICP	2 ppm	43
Ga	1	ppm	MERMS	1 ppm	14
Ge	0.5	ppm	MERICP	10 ppm	nd
Rb	2	ppm	MERXRF	2 ppm	41
Nb	0.5	ppm	MERXRF	2 ppm	5
Mo	0.1	ppb			
In	0.1	ppm	MERMS	0.5 ppm	nd
Sn	1	ppm	MERXRP	2 ppm	4
Cs	0.1	ppm	MERNA	3 ppm	nd
Ba	1	ppm			--
La	0.05	ppm	MERMS	0.1 ppm	2.5
Ce	0.1	ppm	MERMS	0.1 ppm	8.5
Pr	0.02	ppm	MERMS	0.2 ppm	0.7
Nd	0.05	ppm	MERMS	0.1 ppm	3.5
Sm	0.01	ppm	MERMS	0.1 ppm	0.9
Eu	0.005	ppm	MERMS	0.05 ppm	0.40
Gd	0.02	ppm	MERMS	0.1 ppm	1.0
Tb	0.01	ppm	MERMS	0.1 ppm	0.2
Dy	0.02	ppm	MERMS	0.1 ppm	1.5
Ho	0.01	ppm	MERMS	0.05 ppm	0.30
Er	0.01	ppm	MERMS	0.1 ppm	1.2
Tm	0.005	ppm	MERMS	0.1 ppm	0.2
Pb	5	ppm	MERICP	2 ppm	nd
Trace Element Fusion ICP-MS Resear					
Zr	1	ppm			--
Yb	0.01	ppm	MERMS	0.1 ppm	1.3
Lu	0.002	ppm	MERMS	0.05 ppm	0.2
Hf	0.1	ppm	MERNA	1 ppm	2.0
Ta	0.1	ppm	MERNA	0.44 ppm	0.5
W	1	ppm	MERNA	4 ppm	nd
Tl	0.05	ppm	MERMS	0.1 ppm	0.3
Bi	0.06	ppm	MERMS	0.5 ppm	nd
Th	0.05	ppm	MERNA	0.5 ppm	1.0
U	0.05	ppm	MERNA	0.5 ppm	0.7
"Near Total" Digestion ICP					
Cu	1	ppm	MERICP	0.5 ppm	5.2
Pb	5	ppm			--
Zn	1	ppm	MERICP	0.5 ppm	42.4
Ag	0.5	ppm	MERICP	0.2 ppm	nd
Ni	1	ppm	MERICP	1 ppm	4
Cd	0.5	ppm	MERMS	0.2 ppm	nd
Bi	0.06	ppm			--
S	0.001	%	MERLEC	0.01 %	nd
INAA					
Au	1	ppb	MERNA	2 ppb	5
As	1	ppm	MERNA	2 ppm	nd
Br	0.5	ppm			--
Co	0.1	ppm	MERICP	1 ppm	5
Cr	0.5	ppm	MERNA	2 ppm	5
Hg	5	ppm	MERWET	5 ppb	nd
Ir	1	ppb			--
Mo	2	ppm	MERICP	1 ppm	1
Sb	0.1	ppm	MERNA	0.2 ppm	nd
Sc	0.01	ppm	MERICP	0.5 ppm	9.0
Se	0.5	ppm	MERNA	5 ppm	nd
W	1	ppm			--
Mass	0.001	g			--

VITA

Brendan Richardson Bream was born in Santa Rosa, California and raised in Visalia, California. He graduated from Redwood High School in June 1990 and attended the University of California–Santa Barbara through the summer of 1995. In 1995, he received a B.A. in Environmental Studies and a B.S. in Geology. After spending a year as a K-12 substitute teacher and 7th grade girls basketball coach in Visalia, he enrolled at the University of Tennessee to pursue his M.S. in Geology. He received his M.S. in December, 1999, was married to Katy Dodd, and chose to stay at UT for his Ph.D. with Prof. Robert D. Hatcher, Jr. as his advisor. He received his Ph.D. in May, 2003.